TMRC-02-01

MDOT Research Report RC-1415

Evaluation of the Dynamic Fracture Characteristics of Aggregate in PCC Pavements

Final Report

Submitted to the
Michigan Department of Transportation

By
Stanley J. Vitton, Ph.D., P.E. - Principal Investigator
Ghatu Subhash, Ph.D. - Co-Principal Investigator
George Dewey, Ph.D., P.E. - Co-Principal Investigator

Transportation Materials Research Center
Institute for Aggregate Research
Dept. of Civil and Environmental Engineering
Dept. of Mechanical Engineering and Engineering Mechanics

Michigan Technological University
1400 Townsend Drive
Houghton, MI 49931

December 2002

Technical Report Documentation Page

1. Report No. RC1415	2. Government Accession No.	3. MDOT Project Manager David Smiley
4. Title and Subtitle Evaluation of the Dynamic Fracture Characteristics of Aggregate in PCC Pavements		5. Report Date: October 31, 2002
7. Authors: Stanley J. Vitton, Ghatu Subhash and George Dewey		6. Performing Organization Code
9. Performing Organization Name and Address Michigan Technological University Department of Civil & Environmental Engineering 1400 Townsend Drive Houghton, Michigan 49931-1295		8. Performing Org Report No.
12. Sponsoring Agency Name and Address Michigan Department of Transportation Construction and Technology Division P.O. Box 30049 Lansing, MI 48909		10. Work Unit No. (TRAIS)
		11. Contract Number: 96-5434
		11(a). Authorization Number: 98-MTU-2-1
15. Supplementary Notes		13. Type of Report & Period Covered
		14. Sponsoring Agency Code

16. Abstract

One area that has received limited investigation is the dynamic fracture of concrete and in particular coarse aggregate. Research has shown that many materials increase their strength and stiffness as the strain rate increases. This behavior is known as rate sensitivity and is generally defined as the ratio of the dynamic strength to static strength (D/S). This report investigated the rate sensitivity of aggregate, mortar, and concrete. In addition, the report investigated aggregate interlock since it can be viewed as a dynamic loading process. The results of the investigation indicated that aggregate, mortar and concrete are all rate sensitive. In addition to the D/S ratio, a strain rate parameter λ was defined as the difference between dynamic and static strength divided by the difference in the respective strain rates at failure. The research results indicate that the D/S ratio appears to be primarily a function of the material's microstructure while the λ appears to be a function of the microstructural grain-to-grain strength. The D/S ratio also provided an interesting differentiation between limestone and dolomites suggesting variations in their respective microstructures. The D/S ratio for concrete was strongly controlled by the microstructure of the mortar and that there was a significant difference between dry and moist concrete suggesting that the dynamic strength is affected by moisture in the air-void system. The strain rate parameter λ provided a relatively broad variation in aggregate types and in particular the carbonate aggregates. An aggregate interlock test system was constructed to investigate the effect of the coarse aggregate strength on the efficiency of concrete joint performance. The system was design and constructed using a closed loop servo-hydraulic control system. The response of the testing system to aggregate interlock was found to be a function of the stiffness of the joint interface and the coarse aggregate strength. Although hydraulic and control problems limited the number of successful tests conducted, the results indicate that at close joint spacing aggregate interlock was very efficient regardless of coarse aggregate type. However, at larger joint spacing the strength of the coarse aggregate became important for joint efficiency.

17. Key Words: static strength, dynamic strength, uniaxial compressive strength, indirect tensile strength, aggregate interlock, rate sensitivity		18. Distribution Statement No restrictions. This document is available to the public through the Michigan Department of Transportation.	
19. Security Classification (report) Unclassified	20. Security Classification (Page) Unclassified	21. No of Pages 493	22. Price

Executive Summary

Traditionally, strength is one of the primary performance criteria used to assess the quality of concrete used in pavements. For most pavements, concrete strength is determined by the uniaxial compressive strength test and in some cases the indirect tensile strength test. However, a factor in determining concrete's strength is the loading rate at which the concrete is tested. ASTM testing standards, therefore, narrowly limit the loading rate that can be applied to a concrete specimen in determining its strength. In general, the allowable loading rate is relatively slow and is considered to be quasi-static (static). For many materials, though, as the loading rate increases the strength and stiffness of the material also increases. Materials that exhibit this behavior are considered to be rate sensitive. To determine a material's rate sensitivity the material is dynamically loaded to failure at very high strain rates on the order of 100 strain (in/in)/second and then compared to its quasi-static failure strength, which is tested at approximately 10^{-7} strain/second. Research on the dynamic strength of concrete has shown that it is also rate sensitive. The main explanation for concrete's rate sensitivity is that at quasi-static loading rates concrete's larger defects such as shrinkage cracks tend to dominate the fracture process. At dynamic strain rates the fracture strength is associated with microstructural inhomogenieties such as pores, micro-cracks, and impurities that exists along grain boundaries as opposed to the larger macrostructural defects. Although the strength of the grain boundaries are involved in the overall fracture process of brittle materials, the resistance to crack growth from microstructural inhomogenieties varies with strain rate. Therefore, during quasi-static loading the macrostructural defects dominate the fracture strength while at dynamic loading rates the microstructural grain boundary defects dominate the fracture strength. This is mainly due to the dynamic loading pulse moving through the material at a rate in which the larger defects do not have time to respond, thereby allowing the microstructural strength of the grain boundaries to control the material's strength and stiffness. Rate sensitivity is generally defined as the ratio of a material's dynamic strength to its static strength (D/S) and is sometimes referred to as the dynamic increase factor. An additional rate sensitivity measure that was developed in this research is the strain rate parameter λ, which is defined as the difference in the dynamic and static strength divided by the difference in the respective strain rates at failure. While the dynamic strength of concrete is important for design considerations involving dynamic loading,

it also provides a unique way of better characterizing concrete, which is a very complex material involving a porous solid structure and with, in many cases, fluid inclusions. It is able to characterize a material's fracture strength as a function of the grain boundary strength, which is unique to each material type.

The primary objective of this research was to investigate the dynamic fracture characteristics of coarse aggregate, mortar, and Portland Cement Concrete (PCC) and how the strength of the coarse aggregate affects overall PCC strength. Additionally, the relationship between coarse aggregate strength and the efficiency of aggregate interlock in concrete joint performance at various joint or crack widths was also investigated. The final objective was to assess if the dynamic properties of aggregate can be used as a classification system to better predict concrete pavements performance. In this research the following four coarse aggregate types were investigated: igneous, carbonate, blast furnace slag and natural gravel.

All of the coarse aggregates investigated in this research were found to be rate sensitive with an increase in the dynamic to static strength ratio of 1.9 to 2.7. The D/S ratio was found to closely correspond to the aggregate's crystalline structure. The igneous and blast furnace slag aggregates had similar D/S ratios in both dry and moist states. The carbonates, however, had a noticeable difference in D/S ratio - but were unaffected by moisture content. The difference in the D/S ratio between limestone and dolomite was believed to be due to the differences in geologic formation of the two carbonates. It is generally understood that limestone develops as a primary precipitate while dolomite forms as a secondary replacement product of limestone. This occurs when migrating ground waters moving through limestone replace calcium with magnesium in the limestone, thus forming dolomite. It is hypothesized that the replacement process disrupts the limestone's crystalline microstructure producing larger grain sizes but developing weaker grain boundaries, thus decreasing the dynamic strength of dolomite from that of limestone. However, it is also possible that the replacement process also heals the larger microstructural defects in the dolomite, thus improving its static strength. In fact, the strength results show that dolomite has a higher static strength than the limestone - but the opposite occurs in dynamic strength with limestone having a significantly higher dynamic strength than dolomite. The results of the aggregate's strain rate parameter λ revealed a very wide range of values from a low of 1.2 for blast furnace slag to a high of 31.30 for the igneous aggregates. The carbonates ranged from a low of 4.52 to a high of 25.52. The average λ for dolomite was 8.6

while the average for limestone was 16.4. Inspection of the microstructure of the carbonates indicated that for limestone the dynamic strength increased with decreasing grain size and for the dolomites the dynamic strength increased with increasing grain size.

Mortar blocks were cast, cored and tested over an eighteen-week period (once a week) to investigate the mortar's rate sensitivity. The mortar was found to be rate sensitive with the D/S ratio ranging from 1.5 to 3.0. However, the mortar strength and D/S ratio were also found to vary over the testing period with two maximums strength peaks and corresponding minimums occurring. Interestingly, the first maximum strength peak occurred during the fourth week or around the 28-day strength.

PCC specimens were prepared with the coarse aggregate the only variable in the mix. In addition to fresh PCC (30-day), existing (aged) PCC specimens were also tested. The static and uniaxial compression testing of the fresh PCC indicated that all PCC mixes had adequate strength and that there was no statistical correlation between coarse aggregate strength and PCC strength at either static or dynamic strain rates. The testing confirmed the generally held belief that the mortar controls the primary strength of PCC while the shape and surface texture appears to be a secondary control. However, the D/S ratio and λ values for the PCC showed a significant difference between dry and moist (30-day cure) conditions with the moist values higher than the dry values. Clearly, moisture in the air-void system affects the dynamic response of the PCC. Interestingly, both the dry D/S ratio and λ results were surprisingly consistent for all PCC tested. However, for the moist D/S ratio and λ results there was one PCC mix that was noticeably lower then the rest. It was believed that this mix had been improperly made. While the slump and air content values were within established limits for this PCC, it was the dynamic response that clearly indicated that the mix had a problem. It is speculated that the microstructure of the concrete's mortar and its corresponding air-void system responded differently to the dynamic loading resulting in a lower D/S ratio and λ values than the other concrete mixes tested.

The λ results of the aggregates were also compared to the LA abrasion and freeze-thaw durability index values. There was a general linear correlation of λ with LA abrasion, although the correlation was not strong, and the carbonates appear to be somewhat counter to the correlation. However, there appeared to be a relatively strong correlation with λ and the freeze-thaw durability index for the carbonates when separating the carbonate aggregates into high and low groups based on their strain rate parameters λ.

An aggregate interlock system was designed, constructed and tested to determine how coarse aggregate type affects the performance of concrete joints and to determine if the dynamic strength of the coarse aggregate is a factor in the joint performance since the loading of a joint can be viewed as dynamic event. The system tested nine by nine by 18-inch PCC blocks, which were fractured using a pure tension fracture device. The PCC blocks were fractured after 18-hours of curing and then additionally cured for a minimum of two months prior to testing. The initial aggregate interlock tests used a compressive load without a corresponding uplift load. While the tests were successfully completed it was realized that the loading did not replicate realistic field loading conditions. Consequently, a compressive load followed by a tension uplift load was applied to the PCC specimens to better simulate joint aggregate interlock. However, the frequency of the loading and difficultly in the hydraulic closed loop control system caused significant problems in the testing. In addition, it was realized after the testing was completed that a significant factor in the response of the hydraulic testing system was the stiffness of the concrete joint interface itself. Although these problems limited the results of the interlock research, it was found that at larger joint widths, the interface stiffness was clearly a function of the coarse aggregate strength and stiffness.

For the closed-loop testing system to function properly the digital control system's auto feedback system, termed the PID settings, had to be adjusted for the PCC joint interface stiffness. That is, at least one PID setting would be needed for very stiff PCC joint interfaces and a significantly different PID setting for relatively limited PCC joint interface stiffness. However, to maintain consistency between tests, a single PID setting was used in this research assuming that the difference between PCC joints would not be that large and that a single PID setting would be sufficient. Consequently, the PID setting selected was based on the least stiff PCC joint interface, which was PCC made with blast furnace slag as the coarse aggregate. While the blast furnace slag PCC joint interlock tests ran well, the higher stiffness PCC interface joint tests did not. For the higher stiffness PCC interface joint tests it was very difficult to maintain the stability of the hydraulic system when testing. In fact, a number of test blocks became unstable during testing resulting in a premature failure of the aggregate interlock. The higher stiffness joints consisted of the higher strength coarse aggregates. Therefore, due to system control and hydraulic problems only a limited number of tests were successfully completed. The results, while not conclusive, indicate that aggregate interlock at a 0.028-inch joint (crack) width was very efficient regardless of coarse aggregate type. However, at larger crack widths (0.035-inch and greater) the efficiency of the aggregate interlock becomes a function of the coarse aggregate strength and stiffness. These results were consistent with a recently completed aggregate interlock study at the University of Illinois where three coarse aggregate types (basalt, natural gravel, and limestone) were tested. The University of Illinois test results indicate that at larger crack widths the basalt coarse aggregate was the most efficient in aggregate interlock followed by the natural gravel while the limestone coarse aggregate had relatively poor aggregate interlock. The LA abrasion test was used to differentiate the coarse aggregate types in regards to an existing performance criterion.

The development of an aggregate classification system was not accomplished in this research. However, the results of this research strongly suggest that the dynamic strength of aggregate, mortar, and concrete as measured by the D/S and λ parameters, indicate unique material properties that can be used to better understand their performance and subsequently used as a classification system for aggregate and concrete. Additional research is highly recommended to continue the research into the dynamic properties of these materials and their relationship to field performance.

Table of Contents

SECTION 4 *CONCRETE MIXING, CURING AND UNIAXIAL COMPRESSION AND SPLIT TENSILE TESTING*

SECTION 5 *DYNAMIC AND QUASI-STATIC STRENGTH TESTING*

SECTION 7 *AGGREGATE INTERLOCK TESTING*

SECTION 1

Introduction and Background

1.1 Introduction

There are significant costs associated with premature distress to PCC pavements, including increased maintenance and repair costs, increased vehicle wear and tear, and the loss of use during maintenance and replacement. While many factors affect the performance of PCC pavements, such as the design and construction procedures used, one of the most important factors is the material quality of the PCC pavement itself. Consequently, the economic viability of PCC pavements depends on selecting quality materials that will consistently produce durable and long-lasting PCC. However, a major challenge in selecting quality materials is having available laboratory tests that successfully predict field performance.

In general, strength has been a key criteria used in determining the suitability of PCC for pavement structures. The strength of PCC in turn has been primarily considered a function of the water-to-cement ratio of the paste. While the quality of water, cement and to a lesser degree the fine aggregate can be relatively well controlled through selection and processing, the remaining component of PCC coarse aggregate has generally not been as well controlled. Consequently, the coarse aggregate, which is considered a filler material, is selected from a wide variety of materials, ranging from naturally occurring earth materials to industrially derived materials. Since coarse aggregate is considered a filler material, less emphasis has been placed on developing quality tests for coarse aggregate. The main reason for this lack of emphasis is that when fracture occurs in PCC it has been assumed that the primary fracture process is for cracks to propagate around the coarse aggregate and through the cement matrix. Consequently, the strength of PCC is largely controlled by the strength of the cement matrix. For high-strength PCC, however, the fracture process is for cracks to go through both the coarse aggregate and the cement matrix since the strength of the matrix may be as high as the coarse aggregate strength. Accordingly, for high strength concrete the strength of the aggregate does plays an important role in the overall strength of the PCC. However, strength testing of the coarse aggregate is generally not conducted for either normal strength PCC or high strength PCC. Currently, the most common tests conducted on coarse aggregate that are related to strength are the LA Abrasion test; freeze-thaw testing and aggregate wear index (AWI) testing. Although the LA abrasion test and to some degree the AWI are related to the aggregate strength, it is at best only an indirect measure of strength.

In addition to PCC strength a unique feature of PCC pavements is that it also experiences continuous dynamic vehicle loading. The majority of research on the dynamic loading of PCC has been is in the area of earthquake engineering and in military applications of the effects of explosives on structures while only limited research has been conducted on the dynamic characteristics of PCC used in pavements. It is known, however, that PCC is a rate dependent material. That is, the strength and stiffness of PCC are a function of the rate of loading and in general, the faster the rate of loading, the higher the PCC strength and stiffness. It is also known that some materials do not exhibit rate dependency. The practical issues of rate sensitivity will be further addressed later in the report.

An additional area of interest is the response of cracks in PCC to dynamic loading. Since cracks are an integral part of PCC structures, their ability to transmit shear and compressive loading becomes important and must be considered in analyzing and designing the structures for dynamic loading. This is especially important in earthquake engineering where research has been conducted to model and predict the response of cracks to dynamic loading. In general, this research should be directly related to the performance of pavement cracks and particularly construction and expansion joints in PCC pavements. However, a significant difference between earthquake engineering and the loading of PCC pavements is in the width of the crack itself. In earthquake engineering the cracks are generally tightly closed or are held closely together through reinforcement. In PCC pavements, however, the joint widths are significantly wider with the joint opening being a function of temperature as well as to long-term loading. As cracks and precut joint form in PCC, the ability of the crack to efficiently transmit shear loading is a function of the crack width with small openings having good load transfer capability and larger openings with poorer load carrying ability. At larger crack widths it is generally believed that the coarse aggregate plays an important role in transmitting loads across the crack. When the load transfer across a crack is maintained by the coarse aggregate the load transfer mechanism is referred to as *aggregate interlock.*

In considering the dynamic behavior of cracks, an additional consideration is the magnitude and rate at which strains develop and diminish at the points of contact between the surfaces of the crack during loading. When the surfaces of the crack are relatively smooth and close together there is significant surface area contact and thus for a given shear load a minimum strain on the contact points, with the points of contact being between the coarse aggregate, cement matrix or a combination of the two materials. However, as the crack width increases the contact surface area decreases and for the same shear load the strain levels will significantly increase. It can be further assumed that as the strain levels increase with larger crack openings that coarse aggregate and cement matrix crushing will occur resulting in load transfer to other contact points at the joint interface. This effect, the transfer of shear load at the contact points between the surfaces, will ultimately result abrasion and breakage that leads to an increase in displacement or faulting of the PCC pavement. Consequently, the strength of the coarse aggregate may also play an important role in maintaining the performance of a joint - especially for PCC pavements that experience large crack width openings.

1.2 Research Program

This research presented in this report was initiated in November of 1997 under the title *Evaluation of the Dynamic Fracture of Aggregates in PCC Pavements* and completed in December of 2001. The primary focus of the research was three-fold. The first focus area was to investigate the static and dynamic strength of the materials used in PCC materials focusing primarily on the coarse aggregate. The second focus area was to develop an aggregate interlock test system and to conduct aggregate interlock tests on PCC made with various types of coarse aggregate. The third focus area was to assess whether the strength of the coarse aggregate on PCC strength and aggregate interlock and if so whether strength testing of aggregate can be used as an index test for the performance of PCC pavements.

Based on these focus areas the following four objectives were developed for this research:

1) The first objective was to test the static and dynamic strength of the coarse aggregate, cement matrix, and PCC. The difference in the static and dynamic

strength in turn determines the rate sensitivity of the PCC materials. The rate sensitivity as well as the static and dynamic strength of the coarse aggregate was then compared to the 28-day uniaxial compressive strength and the indirect tensile strength of the PCC and the aggregate interlock tests.

2) The second objective was to develop an aggregate interlock testing system to investigate the performance of the PCC made with different types of coarse aggregate. A key part of this objective was to simulate (as close as possible) true aggregate interlock, but to also develop a system that would be efficient to use with a minimum amount of specimen set up time.
3) The third objective was to conduct aggregate interlock tests investigating different coarse aggregate types.
4) The fourth objective was to determine if the dynamic properties of coarse aggregate could be used as a selection criterion for coarse aggregate.

The remainder of this chapter provides background information used in this investigation as well as the format of the report.

1.3 Research Program Background

1.3.1 Aggregate Tests for PCC

There has been a significant amount of research conducted on PCC. However, due to the large variation in material properties used in PCC and lack of follow up studies there has not been good correlation of laboratory tests with field performance. This is particular true for aggregates. An evaluation of aggregate tests related to the performance of PCC was recently conducted by the National Cooperative Highway Research Program (NCHRP) and reported by Meininger (1998). While the report provided a comprehensive study of aggregate tests used for PCC, it did not provide an evaluation on how these tests are related to field performance. The report, however, provides the following recommendation: " A laboratory study is proposed to evaluate selected aggregates tests and to verify the relationship between the selected aggregate test and concrete performance. Then, the next step is to validate the set of tests and performance relationships with laboratory concrete research and PCC pavements performance in the field." Meininger cites a significant need to validate either current aggregate tests or to develop new tests to better predict PCC field performance since it is unclear how existing laboratory testing of aggregate relate to field performance.

The Meininger report also cited carbonate aggregate for special consideration. According to Meininger, "a better understanding of carbonate aggregates for use in concrete is needed." He states a number of questions such as why do many weaker, absorptive carbonates perform better than expected both in strength, while some do not. Or why do some carbonates with high absorption values have good durability, while some do not. Currently, there are no tests available that provide an indication as to how carbonates will behave. This is an important question for Michigan, since a significant amount of carbonate aggregates are used in the state.

According to Meininger (1998) the following four properties are currently investigated to evaluate aggregates used in PCC: physical, mechanical, petrographic, and chemical. Below are the specific tests used to investigate each of the four properties. Unfortunately, to date there is only limited information on how these specific tests are related to PCC field performance.

Physical Properties

Gradation and Minus #200 Determination
Characteristics of Minus No. 200 Material
Fine Particle Shape and Angularity
Coarse Aggregate Particle Shape and Angularity
Absorption, Porosity, and Specific Gravity
Pore Properties: Pore Size Distribution, Surface Area, Pore Volume
Coarse Aggregate Durability and Soundness
Thermal Coefficient of Aggregate
Coarse Aggregate Drying Shrinkage

Mechanical Properties

Fine Aggregate Breakdown and Slaking in Wet Attrition
Coarse Aggregate Breakdown and Slaking in Wet Attrition
Coarse Aggregate Breakdown in Dry Impact, Attrition, and Abrasion
Coarse Aggregate-Mortar Bond
Stress-Strain Response of CA, Modulus of Elasticity, Creep, and Impact
Strength of Coarse Aggregate

Petrographic/Chemical Properties of Aggregate

Mineral Structure of Coarse Aggregate and Fine Aggregate
Elements Present in Aggregate
Compounds Present in Aggregate
Fine Aggregate Mica Content
Organic Impurities
Chlorides in Aggregate
Reactivity with Alkalis in Concrete

1.3.2 Characteristic of Dynamic Problems

In general, dynamic problems are characterized when forces are applied to an object in a very short period of time resulting in very high strain per unit of time. Although the loading on PCC can be described as dynamic, strength testing of the PCC is conducted using static tests such as the uniaxial compression test, which tests the material at slow loading rates. In fact, the ASTM standard for uniaxial compression testing recognizes the problem of varying loading rates for concrete and requires that the loading rate be conducted within a narrow quasi-static range. A distinguishing feature in many dynamics problems, such as in wave propagation, is the relatively small strain levels considered. For example, dynamic strain level as low as 10^{-6} (e.g., in/in) would be disregarded in conventional material testing but when the strain level is dynamic the inertial forces that are generated must be considered. According to Ishihara (1996) inertia forces play an increasing significant role when the deformation occurs over a short period of time. Further, when considering sinusoidal loading, the inertia force increases in proportion to the square of the frequency at which soils deform. Consequently, even at very low levels of strain, the inertia forces become significantly larger with increasing speed of loading.

The rates of loading for various engineering applications are shown in Figure 1.1. The data presented in Figure 1.1 separate the time of loading into dynamic and static problems as well as by shock, wave, vibration, and fatigue. It can be seen that traffic loading is considered a dynamic problem as well as a wave and fatigue problem. However, this is considering only the loading rate from wheel loads traveling over smooth pavement. When wheel loads encounter bumps or cross an uneven joint the loading on the pavement can better be described as a shock loading. This is especially true for a concrete joint where the nature of the rough interface can result in high levels of localized strain as well as transfer of loading from one interface contact to another during dynamic loading.

In reviewing test results from dynamic testing it is common to use the units of strain per unit time as opposed to load per unit time. The primary reason for this is that loading does not provide a measure of material deformation, which is important in characterizing material behavior. Since strain is defined as deformation over total length, both of which are in units of length, strain is a dimensionless quantity, e.g., in/in. Consequently, the units used to report dynamic test results are commonly given as strain/second, e.g., 10^{-5}/sec and referred to as the strain rate. For example, a strain rate of 10^{-3}/sec would be a dynamic load that caused an average 10^{-3} strain per second in the material. As mentioned previously the uniaxial testing of concrete cylinders is generally a quasi-static test. Knowing the loading rate of a test the strain rate of the test can be determined. For example, assume that the minimum loading rate of a conventional ASTM uniaxial compressive test is 34,000 lbs/min, while the time to failure for a 12-inch long by six-inch diameter specimen is 5.3 minutes and that the failure load is 180,000 lbs. Further, assuming that the total vertical deformation of specimen prior to failure was 0.0315 inches (0.8 mm), the total strain at failure was 0.0315 in/12 in or 2.6^{-3} in/in. The average strain rate of this test is 2.6^{-3}/5.3 min or 8.8^{-6}/sec, which is a very slow strain rate and considered a quasi-static test. All of the quasi-static tests conducted in this research were conducted at strain rates of 10^{-5}/sec or slower, while the dynamic tests were conducted at strain rates of 10^{2}/sec or higher.

The main feature of dynamic testing, as discussed above, is that the load is applied over an extremely short period of time. In general, most dynamic testing of materials use loading duration of 100 to 400 microseconds, which is sufficient to fail most material. Failure loads (at a given strain rate) from the dynamic testing are then compared to the static failure strength to determine whether the material is rate sensitive. For many materials higher strain rates result in higher strength and stiffness. Although the fracture process is very complicated, a practical aspect of dynamic testing is that due to the velocity at which the loading is applied the larger material defects, which typically control failure (and subsequently compressive strength), do not have time to fail. Thus, more of the material experiences the loading, resulting (for rate sensitive materials) in higher strength and stiffness since more material can distribute the loading.

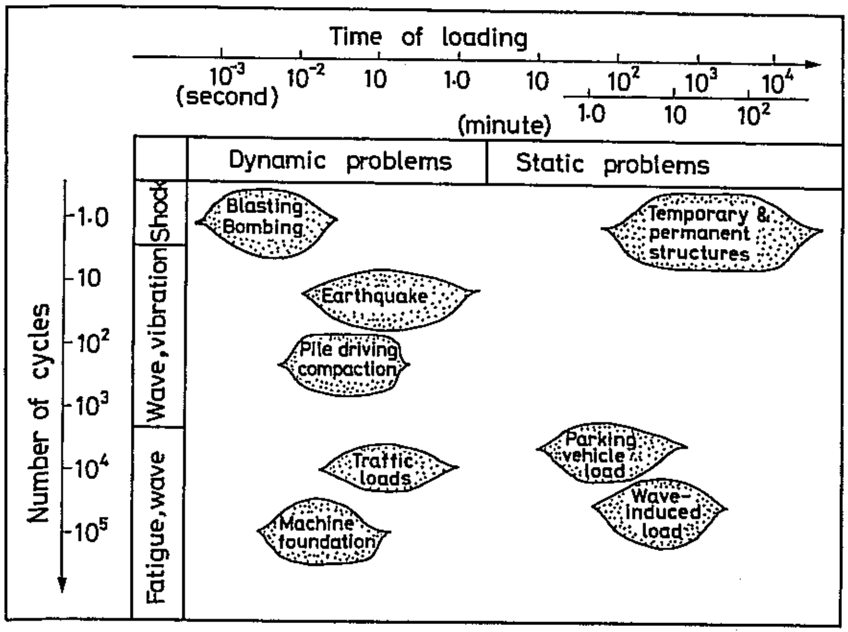

Figure 1.1 Classification of dynamic problems (Ishihara, 1996).

1.4 Report Format

The main objectives of this research were to investigate the dynamic strength of the coarse aggregate, mortar, and PCC and its relationship to aggregate interlock load transfer in PCC joint/crack performance. The research described in this research report is divided into seven sections. Section One provides the background and introduction into the research, while Section Two provides a summary of the research including the conclusions and recommendations of the research. A description of the aggregate types used in the research, which include the geologic properties of the aggregates, is provided in Section Three. Due to the importance of concrete mixing, Section Four details the concrete mixing procedures used in the research as well as the initial unconfined compression and indirect tension results for concrete with different aggregate types. Following this section, Section Five provides the results and discussion of the dynamic and quasi-static testing of the aggregate, cement matrix, and PCC. Sections Six and Seven details the aggregate interlock research with Section Six providing the details of the development, construction and initial testing of the aggregate interlock test device. The final section in the report, Section Seven, which details the test results and discussion of the aggregate interlock research. Section's four, six, and seven are based upon a graduate master thesis's and report work and follow the general outline of a master's thesis. However, each section is formatted into chapters so the number system adopted will be to start each chapter in a section as chapter one, proceeding to two and so on. References are provided at the end of each section.

1.5 References

Ishihara, K., *Soil Behavior in Earthquake Geotechniques*, Oxford Science Publications, Oxford, England, 1996, p.350.

Meininger, R.C., "Aggregate Tests Related to Performance of Portland Cement Concrete Pavement," National Cooperative Highway Research Program, Transportation Research Board, National Research Council, Report 4-20A, 1998, p.84.

SECTION 2

Major Conclusions and Recommendations

1 Major Conclusions and Observations

The research conducted in this report was initiated in November 1997 under the project title *Evaluation of the Dynamic Fracture of Aggregates in PCC Pavements* and completed in December 2001. The research project, which investigated the dynamic strength of Portland Cement Concrete (PCC) and its components as well as aggregate interlock, had four overall objectives. The first objective was to determine the static and dynamic strength of coarse aggregate, mortar and concrete. The static and dynamic strengths in turn provided a measure of the rate sensitivity of these materials. The rate sensitivity was then investigated to determine its relationship with existing performance tests for concrete and to assess whether it can be used for a possible classification system. Since concrete joint behavior is a significant dynamic loading event, the dynamic performance of the coarse aggregate was also investigated in regards to aggregate interlock, which is an important load transfer mechanism in jointed concrete pavement. The second objective, therefore, was to develop an aggregate interlock testing system that simulated, as closely as possible, actual field loading conditions. After completing this objective the third objective was to conduct aggregate interlock tests of PCC with different coarse aggregate strengths. Finally, the fourth objective was to assess the research results to determine whether dynamic testing might provide a means to better classify coarse aggregates for use in PCC and to possibly provide performance criteria for concrete pavements.

The major conclusions and observations developed from this research are summarized in the following three sections. The first section provides the conclusions and observations for the preparation of the PCC along with the standard strength testing to determine the effect of varying the coarse aggregate type. The second summarizes the results of the dynamic and static strength of the coarse aggregate and PCC, where the results of this research were then used to determine the coarse aggregate types to investigate in the aggregate interlock research. The third section presents the major conclusions and observations for the aggregate interlock research.

1.1 PCC Preparation and Static Strength Results

An important aspect of this research was to prepare PCC with uniform properties. Therefore, a concerted effort was made to properly utilize the MDOT mortar voids method in preparing the concrete tested in this research. The ability to prepare concrete was necessary to observe possible strength variations when different coarse aggregate types were investigated. All of the concrete in this research was prepared following the MDOT P1 mix design keeping the components as consistent as possible while only varying the coarse aggregate. For this phase of the research three different coarse aggregate types were used; basalt, gravel, and blast furnace slag. These three coarse aggregates provided a broad range of aggregate characteristics such as texture, specific gravity and strength. The following conclusions and observations from this phase of the research are summarized below.

(1) Automated test methods were used to determine the coarse aggregate's apparent specific gravity, bulk dry specific gravity and absorption. The results had excellent agreement with the standard ASTM test methods for the basalt and gravel aggregates. However, there was significant variation in the blast furnace slag aggregate values. It is believed that the conventional method of determining apparent specific gravity does not provide an accurate measure for the aggregates solid volume due to the inability of the water to fully penetrate the aggregate's void system. On the other hand, the helium gas, which was used by the automated method using a helium pycnometer, better penetrates the aggregate's void system providing a more accurate measure of the aggregate's true solid volume, which is needed to calculate the apparent specific gravity.

(2) All P1 mixes generated adequate (static) strength independent of coarse aggregate type compared to the design strength of 24 MPa (3500 psi) at 28 days.

(3) There were, however, strength variations up to 10% for uniaxial compression tests and 12% for indirect tension with the blast furnace slag PCC having the highest strength and the basalt PCC the lowest in both compression and tension while the gravel PCC fell in between these two.

(4) It was observed that the surface of the slag aggregate had significantly more surface voids that allowed mortar to penetrate into the particles. It was also observed in the *yield data* that the slag PCC had an overall decrease in volume per batch. It is believed that the capacity of the mortar to penetrate into the blast furnace slag coarse aggregate provided the increase in strength observed in the slag PCC over the other PCC tested. This is, the pores provide a better interlock with the mortar.

(5) The strength test results suggest that the overall strength of PCC is controlled primarily by the mortar's strength while the coarse aggregate's shape and texture has a secondary influence.

1.2 Static and Dynamic Strength of Aggregate, Mortar and PCC

As discussed in the Introduction, strength testing of aggregates and PCC is conducted at a relatively slow loading rate based on ASTM and AASHTO standards and is considered in the dynamic testing literature as being a static or quasi-static test. Further, a material's static strength is controlled by the presence of larger defects within the materials such as cracks, bedding planes or weak zones, while during dynamic loading the loading pulse travels through the material at a rate in which the macroscale defects do not have time to react subjecting the entire material to full loading prior to failure. As a result, the material's microstructure has a greater control over its dynamic strength. Consequently, materials where the dynamic strength and stiffness are greater than its static strength and stiffness are considered to be rate sensitive, which is the focus of this section.

The following three sections, therefore, provide the major conclusions and observations of the results of the static and dynamic testing of the aggregate, mortar and PCC tested in this research. To provide a better understanding of these conclusions and results, some of the research results, e.g., presented in figures and tables, which are more fully described and discussed in the following chapters, are repeated in the following sections. However, not all of the research details describing these results are provided and therefore the reader is advised to consult the following chapters for more detailed information concerning the research results presented in these sections.

1.2.1 Aggregates

Uniaxial compression testing was conducted on the following aggregate types: (1) three blast furnace slags, (2) three limestones, (3) four dolomites and (4) two igneous aggregate for a total of 12 aggregate types tested. Both static and dynamic testing was conducted under dry and moist conditions; with the dynamic tests being conducted on a one-half-inch split Hopkinson pressure. While the aggregates were placed in water for approximately two days prior to testing, they were not vacuum saturated and therefore were not considered fully saturated when tested. The conclusions and observations, based on the static and dynamic uniaxial compression test results, are summarized as follows.

(1) The static uniaxial compression results for the igneous and carbonates had excellent agreement with the commonly used Deere & Miller rock strength classification system, verifying the static uniaxial compression testing procedures used in this research. The Deere & Miller classification system along with the test results is shown in Figure 2.1.

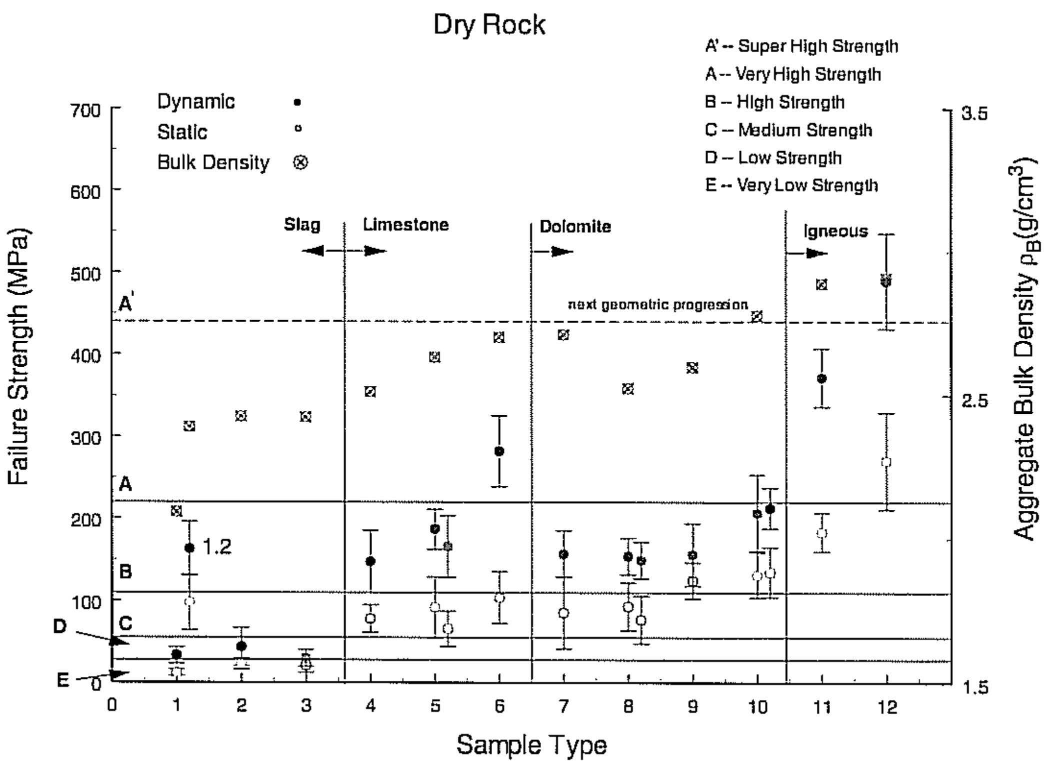

Figure 2.1 The Deere & Miller Strength Classification System along with the test results.

a. The mafic igneous aggregates had the highest uniaxial compressive strength under static loading conditions and are rated as "high strength" (Category A) according to the Deere and Miller Rock Classification System. The carbonate aggregates had average strength and are rated as "medium strength" (Category C), although two of the dolomites carbonates are in the next higher category "high strength" (Category B). The blast furnace slag's tested had the lowest strength and are rated as "very low strength" (Category E). However, the dense portion of the air-cooled slag (specimen 1.2) had significantly higher strength and is rated as "medium strength" (Category C). This strength was just below the "high strength" boundary and very close to the strength of dolomites.

b. In general, the dynamic strength for most of the aggregates increased by one strength category on the Deere & Miller Rock Strength Classification System over the aggregate's static strength. Since the static strength of the Specimen 12 (Bruce Mines aggregate, 95-010) was already in the "high strength category," an additional strength category needed to be added to the Deer & Miller classification system following the geometric progression used to generate the existing categories. The new category is termed "super high strength" (Category A') and is the category where the dynamic strength of the Bruce Mine aggregate (95-010) is in.

c. The majority of the carbonate aggregates are in the medium strength Category C with the exception of two dolomites, which are in the high strength Category B. In general, the *static* strength of the dolomites is higher than average *static* strength of the limestones, which is typically reported in the literature. However, the reverse occurs for the dynamic strengths in which the limestones have a higher average strength than the dolomites.

d. Specimens 1 (Algoma, 95-006), which was air-cooled, and 2 (Algoma, 95-006) and specimen 3 (Levy, 82-019), which were water-quenched, had the lowest aggregate strength and are rated as "Very Low Strength." However, the dense portion of the

Algoma air-cooled slag (specimen 1.2) is significantly stronger and is two strength categories higher at "Medium Strength" (Category B) and is approximately equivalent to the carbonate aggregate strength. It was also observed that even at a very low bulk density of 2.09 g/cm^3 the porous air-cooled slag had strength equal to the water-quenched slag, which had a significantly higher bulk density at 2.40 g/cm^3. It is speculated that the early crushing of the water-quenched slag may result in a more rapid cooling of the slag reducing the slag's strength.

e. There is a very good correlation with dynamic strength and bulk density for the limestone aggregate and similarly for the dolomites with the exception of the Cedarville dolomite. It appears that the random and non-uniform grain size distribution of the Cedarville dolomite (specimen 7 in Figure 2.1), which is believed due to the partial secondary replacement nature of dolomite, may account for this discrepancy.

(2) All of the aggregates tested were rate sensitive. Two measures of rate sensitivity were used in this research. The first measure was the dynamic to static strength ratio (*D/S*), which is also known as the dynamic increase factor (DIF). The second measure was the strain rate sensitivity parameter λ that provides a measure of the dynamic strength increase as an inverse function of the difference in the dynamic and static strain rate at failure. Functionally, the two parameters are described as follows:

$$\frac{D}{S} = \frac{\sigma_d}{\sigma_s} \qquad 2.1$$

$$\lambda = \frac{d\sigma_f}{d\left(\log \dot{\varepsilon}\right)} = \frac{\sigma_d - \sigma_s}{\log\left(\frac{\dot{\varepsilon}_d}{\dot{\varepsilon}_s}\right)} \qquad 2.2$$

where σ_d = Dynamic uniaxial compressive strength
σ_s = Static uniaxial compressive strength
$\dot{\varepsilon}_d$ = Dynamic uniaxial strain rate at failure
$\dot{\varepsilon}_s$ = Static uniaxial strain rate at failure

(3) The dynamic to static strengths ratios (D/S) ranged between 1.33 and 2.68 for the aggregates tested. There was a noticeable increase in the average D/S value between moist and dry conditions for the blast furnace slag and the mafic igneous aggregate with an average of 1.86 and 2.62 respectively. However, there was no noticeable difference in the carbonate aggregates between moist and dry conditions. There was, though, a significant difference in the D/S between limestones and dolomites at 2.27 and 1.74, respectively. This represents a 40% difference in the total range in the D/S of the aggregates tested. The D/S ratios obtained in this research are provided in Table 2.1. Note that the numbers listed under "ID No." correlate to those in Figure 2.1.

Table 2.1 Dynamic to static strength ratios.

			Compressive Fracture Strength Dynamic/Static Strength (D/S) Ratio			
ID No. Pit ID	**Aggregate/ (Quarry)**	**Orientation and Batch**	**Dry**	**Aggregate Average**	**Saturated**	**Aggregate Average**
1 95-006	AC Slag (Algoma)	Batch 1 Batch 1.2	2.74 1.67	**Slag**	2.42	**Slag**
2 95-006	WC Slag (Algoma)	Batch 2.0 Batch 2.1	1.90	1.93	2.75 3.49	2.68
3 82-019	WC Slag (Levy)	Random	1.42		2.05	
4 71-047	Limestone (Presque Isle)	Random	1.90	**Limestone**	2.67	**Limestone**
5 06-008	Limestone (Bay Co.)	Normal Parallel	2.04 2.54	2.30	1.88 2.30	2.23
6 75-005	Limestone (Port Inland)	Random	2.72		2.05	
7 49-065	Dolomite (Cedarville)	Random	1.84	**Dolomite**	2.15	**Dolomite**
8 58-009	Dolomite (Denniston)	Normal Parallel	1.66 1.95	1.64	1.55 2.05	1.83
9 58-008	Dolomite (Rockwood)	Normal Parallel	1.25		1.82	
10 93-003	Dolomite (France St.)	Normal Parallel	1.58 1.58		1.42	
11 31-076	Basalt (Moyle)	Random	2.03	**Igneous**	2.91	**Igneous**
12 95-010	Diabase (Ontario)	Water Cut Oil Cut	1.81 1.51	1.78	2.18	2.55

(4) A strain rate sensitivity parameter λ defined above takes into account the difference in static and dynamic strength and normalizes it to the difference in strain rate between the static and dynamic loading rates. The λ parameters obtained in this research are provided in Table 2.2. The slag aggregates have the lowest λ, ranging from 1.17 to 3.00 for the water quenched slag, but 9.29 for the dense air-cooled slag (specimen 1.2) for an overall average of 4.2. The carbonates have the intermediate values ranging from 4.52 to 25.52, with an average of 11.9. The high strength igneous aggregates have the highest λ, ranging from 26.90 to 31.30, with an average of 29.1. Based on the rate sensitivity parameter λ the trend in highest to lowest rate sensitivity was as follows: diabase > basalt > limestone > dolomite > slag. In addition, there was a significant range in the λ values for the aggregate such that they can be clearly differentiated, which might potentially be used for a classification system.

Table 2.2 Strain rate sensitivity λ values

ID Number	Strain Rate Sensitivity, λ Aggregate	λ	λ Average
1.0	Algoma air cooled blast furnace slag – porous section	3.00	
1.2	Algoma air-cooled blast furnace slag – dense section	9.81	
2	Algoma water-quenched blast furnace slag	2.93	4.2
3	Levy water-quenched blast furnace slag	1.27	
4	Limestone, Presque Isle	9.97	
5	Limestone, Bay County	13.59	16.4
6	Limestone, Port Inland	25.52	
7	Dolomite, Cedarville	10.27	
8	Dolomite, Denniston	8.77	
9	Dolomite, Rockwood	4.52	8.6
10	Dolomite, France Stone	10.81	
11	Basalt, Portage Lake Lava Series, Moyle	26.90	
12	Diabase, Ontario Traprock	31.30	29.1

(5) For the aggregates tested there is a general increase in the strain rate parameter λ with increasing bulk density with a linear correlation coefficient of 0.61. This correlation, however, did not include the slag aggregates since there did not appear to be a relationship between λ and bulk density for the slag. A correlation coefficient to 0.74 was found for the limestone, but the dolomite correlation coefficient was only 0.42.

(6) There was a significant difference in the average strain rate sensitivity parameter λ between the dense air-cool slag (specimen 1.2) at 9.8 and the remaining three slags at 2.4. The rate sensitivity of the air-cooled slag was even higher than the average rate sensitivity of the dolomite aggregates at 8.6.

(7) The dynamic testing results D/S and rate sensitivity parameter λ between limestones and dolomites is relatively large compared the range of all the aggregates tested. The limestone and dolomites had a D/S of 2.30 and 1.64, respectively, while the average rate sensitivity parameter λ for limestone and dolomite was 16.4 and 8.6, respectively. Inspecting the carbonate's microstructure indicates that for limestone the rate sensitivity increases (both in D/S and λ) with decreasing grain size while the opposite occurred for dolomite where the D/S and λ decreased with decreasing grain size. It is hypothesized that the limestone and dolomite's geologic formation may help explain this difference. Basically, limestones form as a primary sedimentary rock while dolomite forms by chemically altering the structure of the original limestone. This includes recrystallizing and replacing calcium with heavier magnesium and iron ions. It is highly probable that this replacement process results in a weakening of the dolomite's grain boundaries and thus results in lower dynamic strength. However, it is also possible that the higher *static* strength of dolomite versus limestone might result from a healing process during replacement, where some of the larger defects are repaired.

(8) The D/S ratios for the igneous and slag aggregates were approximately equal indicating similar microstructures, but with significantly different strain rate parameter values (4.2 versus 29.1) indicating that the grain boundary strength was significantly different between the igneous and slag aggregate. It is suggested that the D/S ratio provides an indication of microstructure characteristics, while the rate sensitivity parameter provides a measure of microstructural strength.

(9) The rate sensitivity parameter λ was compared to the freeze/thaw (F/T) susceptibility dilation and durability index values for all the aggregates tested. While there was considerable scatter in the data, the aggregates were separated into two clearly

identifiable groups; those with rate sensitivity parameters greater than 25 and those less than 15. When correlating the carbonate aggregates, which had rate sensitivity parameters less than 15, but excluding the Bay County limestone, there was an excellent agreement between rate sensitivity and the F/T index values dilation and durability with a linear correlation coefficient of 0.98. The Bay County limestone was excluded because it appeared to have contradictory performance vales, e.g., LA abrasion, F/T.

(10) There was a general linear inverse relationship between the LA abrasion index values and the static and dynamic compressive strength results. The dynamic strength results had a somewhat better correlation with a linear correlation coefficient of 0.77 versus 0.66 for the static strength results. In addition, the slope of the dynamic strength versus LA abrasion results was steeper providing a broader separation of dynamic strength and LA abrasion data.

(11) There was also a general inverse relationship between the strain rate sensitivity parameter λ and LA abrasion values, with a linear correlation coefficient of 0.74 for all aggregates. However, this relationship does not necessarily hold for the carbonate aggregate. For the carbonates, it appears that the relationship is reversed with the LA abrasion values increasing with increasing rate sensitivity.

1.2.2 Mortar

The mortar was prepared in two batches at an air content of 9 to 10%. Static and dynamic tests were conducted under dry and moist conditions using the one-half-inch split Hopkinson pressure bar located in the Department of Mechanical Engineering and Engineering Mechanics. The mortar was tested over an 18-week period with testing once a week. The conclusions and observations, based on the static and dynamic uniaxial compression test results, are summarized as follows.

(1) The mortar was found to be rate sensitive with the dynamic to static strength ratio (D/S) ratio range between 1.5 and 3.5 over the 18-week testing period.

(2) The mortar's static and dynamic strength varied over the 18-week testing period with two increases followed by decreases. Interestingly, a high strength period where the D/S was approximately 3 occurred at the 28-day testing period followed by a decrease to a D/S of 1.5 in week nine.

(3) The D/S changes may indicate that the development of the mortar's microstructure during the curing process may not be constant. However, it is possible that testing procedures may have also played a role in the increase and decrease in strength over the 18-week period.

1.2.3 Portland Cement Concrete

Two separate batches of PCC were prepared for each coarse aggregate type tested. The first batch was prepared for the static and dynamic indirect tension and compressive strength testing, while the second batch was prepared for the aggregate interlock testing. The following five coarse aggregate types were tested:

Coarse Aggregate Type	**MDOT Pit Number**
Bruce Mines, Diabase	95-010
Port Inland #1, Limestone	75-005
Presque Isle Stone, Limestone	71-047
Superior Sand & Gravel	31-045
Levy Steel Dix #1, Slag	82-019

In addition, aged concrete from existing highway pavement sections were cored and tested. The PCC specimens were tested under static and dynamic loading conditions in both uniaxial compression and indirect tension. The static tests were conducted using a 55 kip MTS system with a TestStar II digital controller, while the high strain rate tests were conducted using a three-inch diameter Split Hopkinson Pressure Bar (SHPB) located in the Concrete Testing Laboratory at Michigan Tech shown in Figure 2.2. The system functions in basically the same way as the half-inch diameter system but had not been modified for single load testing. The conclusions and observations of the testing are presented in the following two sections.

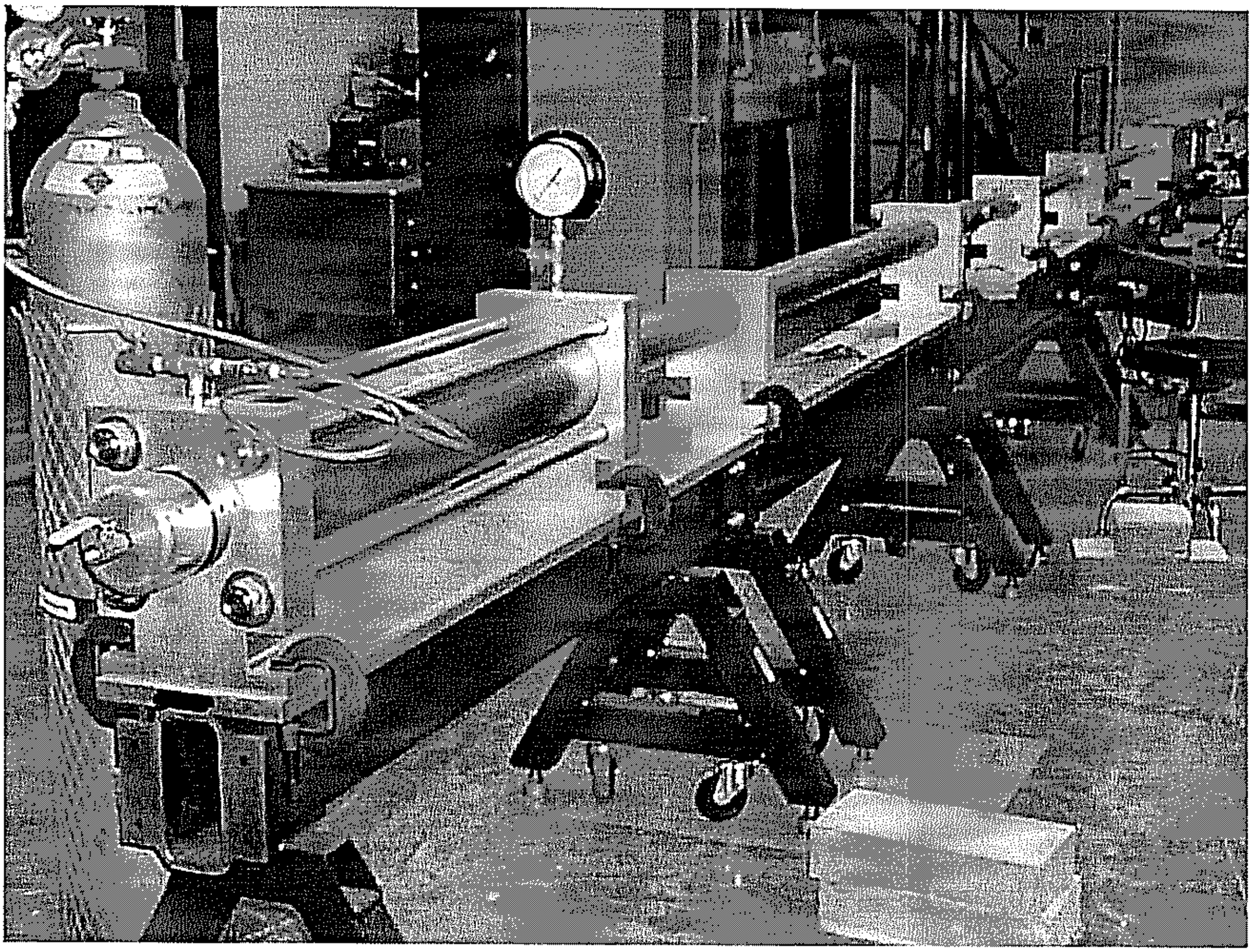

Figure 2.2 Three-inch split Hopkinson pressure bar.

1.2.3.1 Indirect Tension Test Results

(1) The PCC was found to be only slightly rate sensitive in tension. The dynamic to static strength ratio (D/S) ranged between 1 and 1.3. In addition, there was no statistical correlation between PCC strength and coarse aggregate type in either the static or dynamic indirect tension testing.

(2) The results of the indirect tension did not correlate with the results from other US researchers who found a 6 to 8 D/S ratio. However, similar research in Europe developed

a model known as the CEB model. According to the CEB model the concrete's rate sensitivity in tension at the strain rate tested in this research would have had a D/S ratio of approximately 2.2, somewhat closer to the results in this research.

(3) It is believed, however, that the results of the indirect tension testing might not have been properly conducted although the reasons for this remain unclear since other researchers used the same procedures that were used in this research. It is suspected that one reason for the lower results may be attributed to not having proper alignment of the specimen in the split Hopkinson pressure bar device.

1.2.3.2 Uniaxial Compression Test Results

(1) All of the 30-day[1] cured PCC tested in uniaxial compression was rate sensitive. In general, the PCC had an average static compressive strength of 45 MPa (6,525 psi), while the dynamic compressive strength was approximately 67 MPa (9,720 psi). The dynamic to static strength ratio (D/S) ranged between 1.4 and 1.9, which agrees extremely well with the results from other researchers.

(2) The aged pavement concrete (40 years old) was also found to be rate sensitive. The natural aggregate PCC had a static compressive strength at 80 MPa (11,600 psi), which was higher than all of the 30-day cured PCC tested, while its dynamic strength was significantly higher at 120 MPa (17,400 psi). On the other hand, the aged slag coarse aggregate PCC (25 years old) had a static compressive strength of 45 MPa (6,525 psi), which was close to the average strength of the 30-day cured PCC, while its dynamic strength was 78 MPa (11,300 psi), which was approximately equal to the static strength of the aged PCC, but somewhat higher than the dynamic strength of the 30-day cured PCC.

(3) There was generally good agreement between the six-inch diameter specimens and the three-inch diameter specimens tested in static loading conditions with a 6% difference for

[1] The PCC was tested at 30 days instead of the traditional 28-day due to a longer sample preparation time.

the Bruce Mines PCC, 2% for the Presque Isle PCC, and 2% for the Port Inland PCC. However, the Levy slag and Superior Sand & Gravel PCC had a 15% and 14% difference, respectively.

(4) There was no statistical correlation found between either the static and dynamic strength of the coarse aggregate in the PCC and the static or dynamic strength of the concrete. This suggests that the mortar controls the primary strength of concrete in both static and dynamic loading, while the coarse aggregate plays a secondary role.

(5) The dynamic strength of fresh concrete was greater than concrete that was oven dried.

(6) The results of the dynamic to static strength ratios (D/S) for the fresh (moist) and oven dried PCC are presented in Table 2.3. The results indicate that the dry PCC was relatively consistent with an average D/S of 1.41 for coarse aggregate types tested, while the moist PCC had an average D/S of 1.78. However, the average was 1.82 when excluding the Port Inland PCC. It was suspected that the Port Inland PCC might have been improperly prepared. While the D/S ratio for dry Port Inland PCC was similar to the other PCC, its moist D/S at 1.59 was well below the other moist D/S values. This is an interesting result since the air content, slump, and dry D/S ratio did not indicate any problems with the Port Inland PCC.

Table 2.3 Ratio of dynamic to static strength tests for uniaxial compression

PCC Type		Oven Dry Dynamic/Static	Fresh (moist) Dynamic/Static
Bruce Mines	(95-101)	1.50	1.86
Levy Slag	(82-019)	1.38	1.80
Port Inland	(75-005)	1.38	1.59
Presque Isle	(71-047)	1.40	1.84
Superior Sand & Gravel	(31-045)	1.40	1.79
Natural Aggregate:	Aged (40 yr)	1.50	Not Tested
Slag Aggregate:	Aged (25 yr)	1.73	Not Tested

(7) Since a material's rate sensitivity, as defined by the D/S ratio, has been found to originate from microstructural inhomogenieties such as pores, cracks and impurities that exist along the grain boundaries, the PCC D/S ratio results are believed to be a function of the concrete's microstructure and in particular the mortar. In addition, it has been shown that the presence of water in the pore space (Conclusion 5) also affects the rate sensitivity of concrete. Consequently, the D/S values for concrete may be a means by which the concrete's microstructure and air void system may be better quantified.

(8) The results of the rate sensitivity parameter λ for concrete were similar to the D/S ratio results showing a significant difference between dry and moist conditions as shown in Table 2.4. In addition, it also indicates that there was a problem with the Port Inland PCC, which had a significantly lower moist λ value than the other PCC tested. However, a significant difference between the D/S ratio and the λ values was in the strain rate parameter values between fresh (30-day cured) and aged concrete in dry conditions with an average 2.7 and 5.6, respectively. This suggests that the λ is sensitive to the concrete's maturity while the D/S ratio appears to be more a function of the concrete's microstructure. However, it is unclear at this point regarding the relationship between the D/S ratio and the λ and why the λ is sensitive to the maturity of a concrete while the D/S ratio is not. It appears, though, that both the D/S ratio and λ may provide significant information to better predict the performance of concrete.

Table 2.4 Rate sensitivity parameter λ for dry and moist conditions.

PCC Type		Dry Dynamic/Static	Moist Dynamic/Static
Bruce Mines	(95-101)	3.3	5.3
Levy Slag	(82-019)	2.8	5.2
Port Inland	(75-005)	2.3	3.6
Presque Isle	(71-047)	2.4	5.4
Superior Sand & Gravel	(31-045)	2.7	5.1
Natural Aggregate	Aged (40 yr)	6.2	Not Tested
Slag Aggregate	Aged (25 yr)	5.1	Not Tested

1.3 Aggregate Interlock

A critical component in the long-term performance of PCC pavements is the ability of joints and cracks to effectively transfer vehicle shear loading across the joint or crack interface. A key component in aggregate interlock is the joint width or crack width and the strength of the coarse aggregate. Recent research at the University of Illinois has found that the strength of the aggregate dramatically affects aggregate interlock. The Illinois research, which was conducted for the Federal Aviation Administration, constructed an aggregate interlock test system and investigated three coarse aggregate types; basalt, carbonate and a natural aggregate. A total of 34 tests were conducted over a range of crack widths. The primary finding of this study was that the coarse aggregate type dramatically affected aggregate interlock at large crack widths. The test showed that the basalt had the best results, followed by the natural aggregate, with the carbonates having the poorest results.

The first objective of the aggregate interlock research was to design and construct an aggregate interlock test system that was relatively easy to use, where tests could be set up in a minimum of time and where the tests could be very accurately controlled. The second objective was to conduct aggregate interlock tests on concrete using different coarse aggregate types with a range of static and dynamic strengths. The third objective was to determine how different coarse aggregates strengths affect aggregate interlock and if the dynamic strength of the aggregate could be used as a classification system to predict PCC long-term field performance. The conclusions and observations from the aggregate interlock research are divided into two sections. The first section is the development of the aggregate interlock system while the second section provides the conclusions and observations on the aggregate interlock test results.

1.3.1 Aggregate Interlock Test Equipment Development Conclusions

(1) The design, fabrication and construction of the structural frame and sample holders functioned well for their intended purpose, providing a frame that was structurally sound and adaptable for other research requirements. In addition, the sample holders performed very well, securely restraining the concrete blocks in place during testing. It was also found that the utilization of the holders, such as inserting the concrete blocks and

alignment could be accomplished in an efficient manner. A picture of the test system is shown in Figure 2.3.

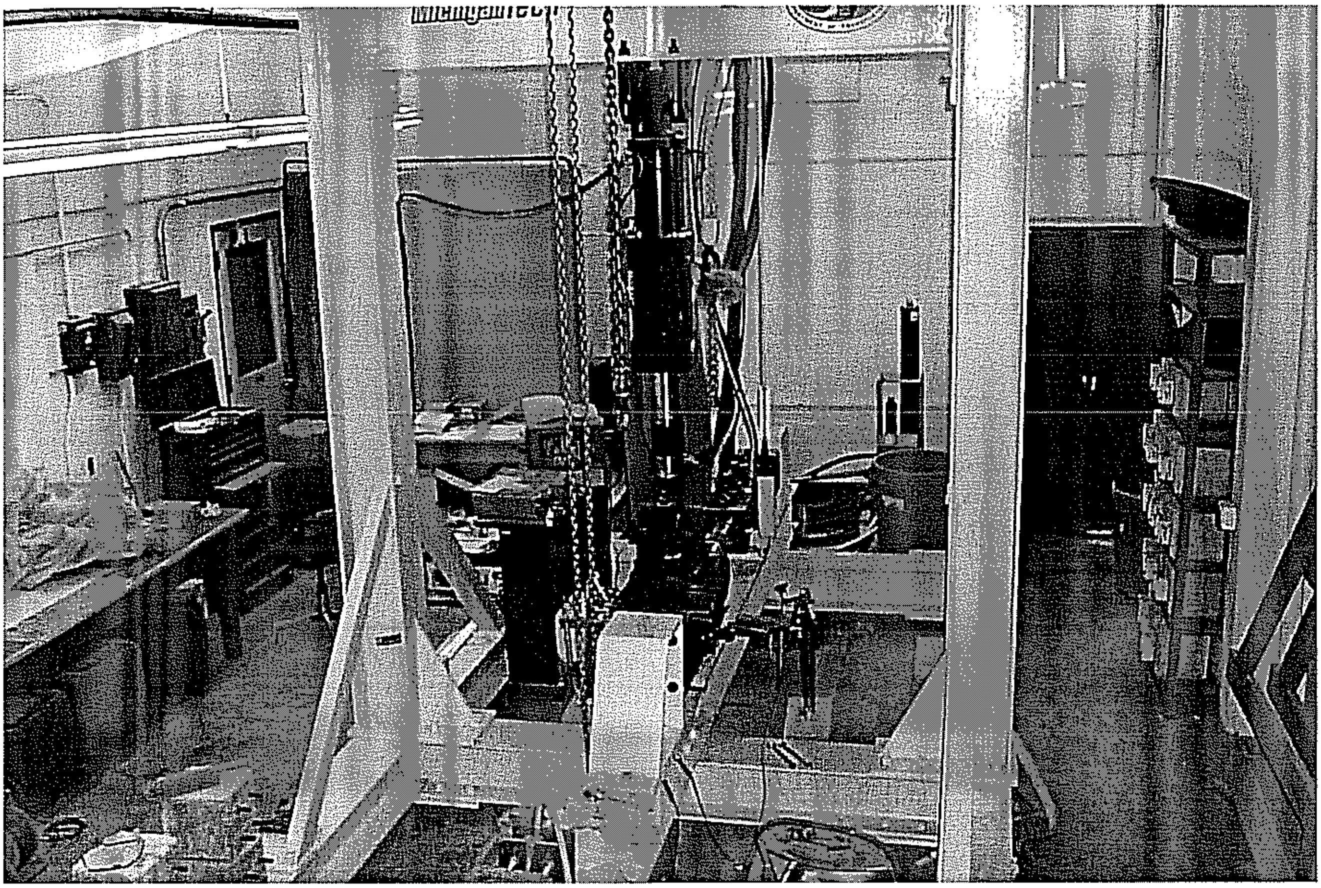

Figure 2.3 Aggregate interlock test system.

(2) The concrete fracturing device shown in Figure 2.4 performed moderately well in the initial development of the system. During later testing, however, a torque wrench was used to place a constant tension load on the threaded rods, which were secured in the concrete, prior and during sample fracture. In addition, anchor nuts were repositioned to the ends of the embedded threaded rods to provide better anchorage. These changes improved the performance of the sample fracture device, produced accurate data, and effectively produced cracks in all of the test blocks.

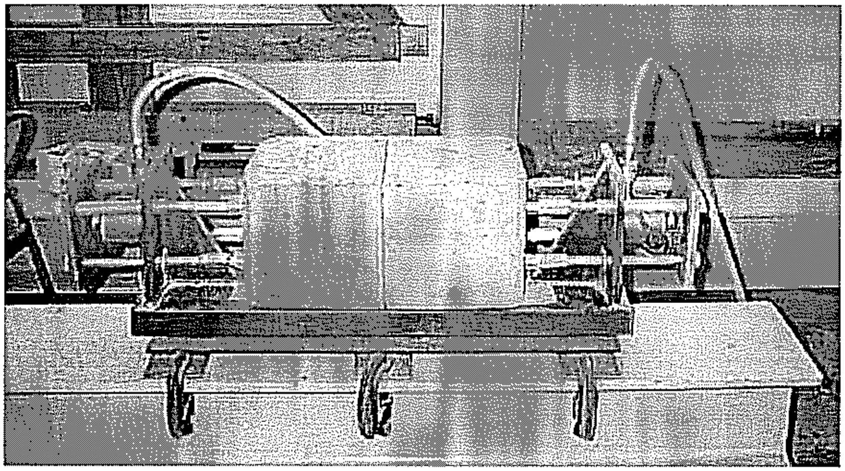

Figure 2.4 Concrete fracture device.

(3) Initially, a half sine wave in compression was applied to the concrete sample interface at a 9 kip load over a 0.1 second loading period as shown in Figure 2.4. However, it was clear from the initial test results that the nine kip load was too high for the concrete block size used. In addition, applying only a compressive load did not correctly simulate aggregate interlock. To better replicate aggregate interlock a sine-loading wave in both compression and tension was used as shown in Figure 2.5. Also, stress calculation indicated that a 3 kip load was more realistic for the concrete blocks being tested than the original 9 kips. However, the rest period between the sine wave load pulses was very difficult to control with the closed-loop control systems used in this research. After a number of attempts at trying to produce the pulse with a delay in the test sequence shown in Figure 2.5 a continuous sine-loading wave, without a rest period was used.

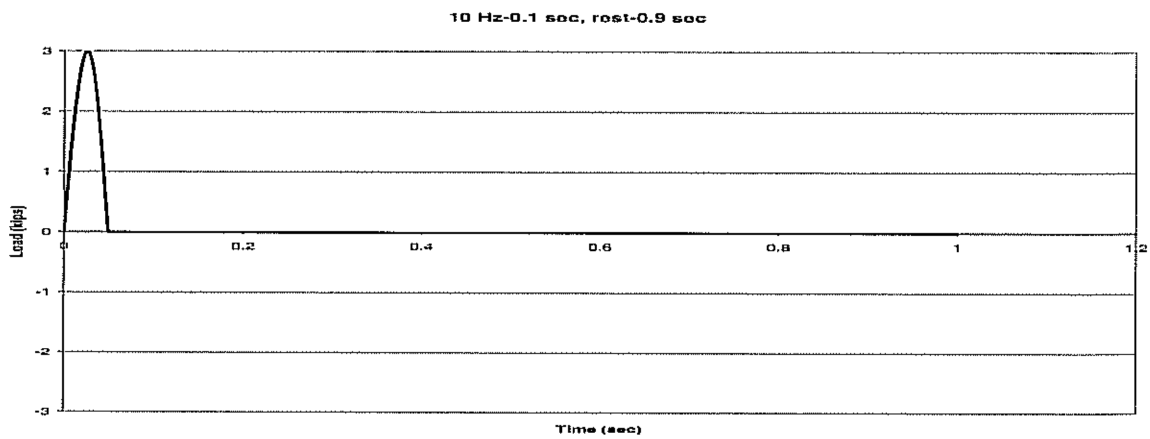

Figure 2.4 Compressive loading signal.

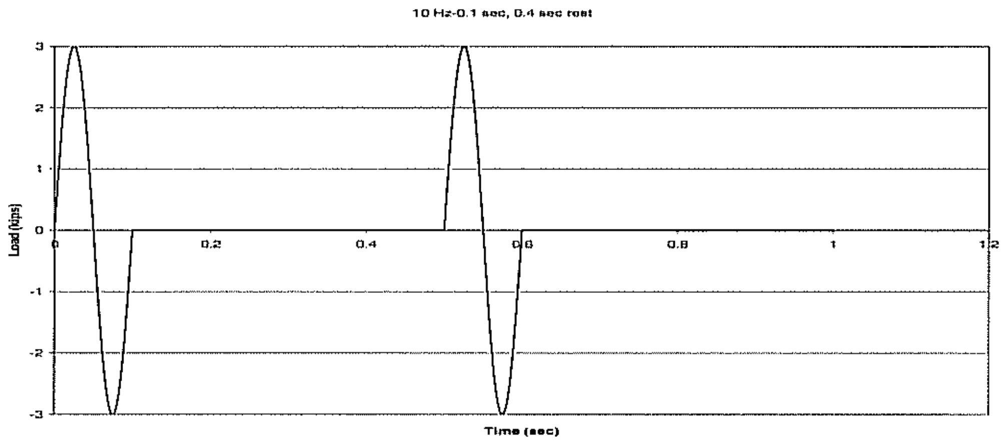

Figure 2.5 Compressive and tensile loading signal.

(4) A CNC mill with a LVDT displacement gauge was used to measure the surface texture of the concrete both before and after interlock testing. The results of this work were only partly successful. The main obstacle was in collection and analysis of the data. However, surfaces analyzed indicated, both visually and numerically, that the difference in roughness was a function of the coarse aggregate's strength with the stronger aggregate showing less wear than the weaker aggregates after testing.

1.3.2 Aggregate Interlock Testing Results

As discussed in the development of the aggregate interlock testing system, it became clear that the applied load was too large and that the method of loading needed to provide both a compressive load to the interface, as well as a tension load, to better simulate aggregate interlock. While lowering the applied load was straightforward, the application of a cyclical load between compression and tension was more difficult for the hydraulic and control system to handle. In addition, a significant factor in the close-loop control of the test was the stiffness of the joint interface itself. Basically, the stiffer the interface the easier it is for a close-loop control system to control the test. On the other hand, when the interface is not stiff it becomes more difficult to control, since more displacement is required for a given load and subsequently more hydraulic fluid is required to move the hydraulic piston. It was found that two significant factors controlled the concrete's joint stiffness; (1) the joint or crack width and (2) the coarse aggregate type at larger crack widths. All of the tests conducted at narrow crack widths of 0.028 inches performed well. However, when the crack width was increased the system had difficulty controlling the test for some of the PCC tested. The main problem in many of the tests was that the hydraulic system was back pressuring the return lines causing the hydraulic fluid to cavitate, i.e., gas bubbles forming in the fluid, causing the hydraulic system's emergency shut off system to stop the test. Unfortunately, this problem was not discovered until after the testing was complete and significant delays had been incurred. A second factor in the aggregate interlock testing was that the stiffness of the interface was controlled by the strength and stiffness of the coarse aggregate at larger crack widths. It was learned in the initial testing that the stronger coarse aggregate provided the stiffest interface while the weaker coarse aggregate provided the lower stiffness interface. Consequently, the control system was "fine-tuned" using the weaker coarse aggregate concrete, i.e., the closed-loop control response or ability to control the test was based on a the lower stiffness interface. A result of this is that all of the tests on the lower stiffness interface concrete worked well, while the higher stiffness interface concrete the system was unable to control the test due in part to the cavitation of the hydraulic fluid in the return line; but also in some cases the control system became so unstable the interface was damaged the resulting in premature failure. This can be observed in Figure 2.6 where the test results for the following three coarse aggregates are provided: (1) blast furnace slag, (2) limestone and (3) basalt. These tests were conducted at a crack width of 0.035 inches. All three aggregates types performed well between 1 and 100 cycles. Between 100 and 10,000 cycles the blast furnace slag develops significant displacement, while the limestone and basalt remain relatively constant. However, at approximately 10,000 cycles the basalt specimen started to have significant vertical displacement between the two PCC blocks indicating a rapid degradation of the aggregate interlock and ultimately resulting in premature failure of the specimen. Failure was selected as a maximum displacement of 0.5 inches between the two specimen blocks. The limestone, which was less stiff, became unstable after 50,000 cycles.

Although not all of the aggregate interlock tests were successfully completed, a number of conclusions and observations were still obtained from the successful tests. These conclusions and observations are provided as follows:

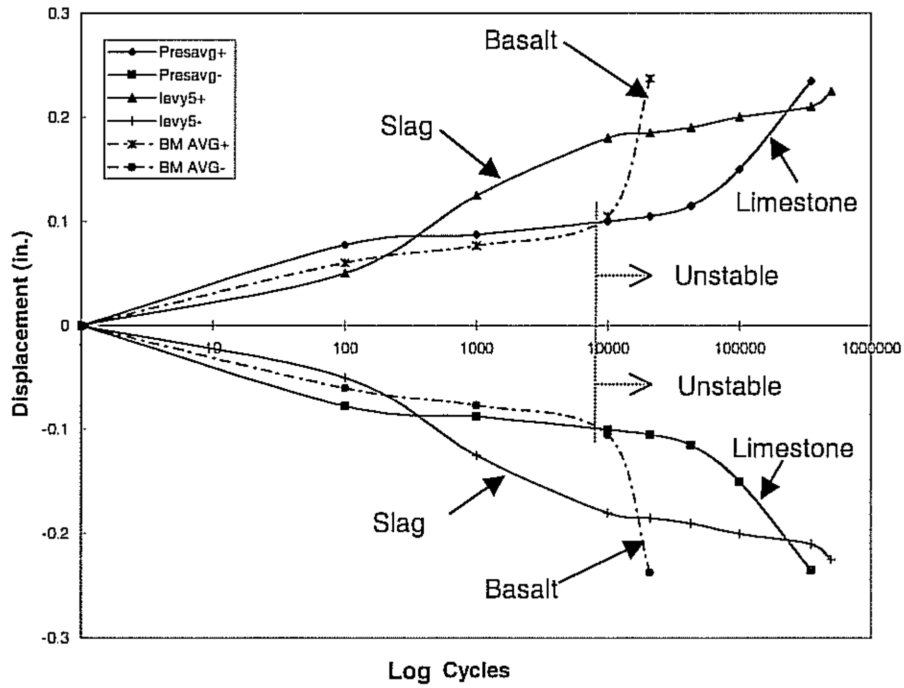

Figure 2.6 Aggregate interlock test results at 0.035 inch crack width.

(1) The aggregate interlock testing in this research was conducted under pure aggregate interlock since no base reaction was provided.

(2) It is believed that the aggregate interlock test system developed in this research, while experiencing some problems, is an effective system for testing aggregate interlock. Successful aggregate interlock testing can be accomplished provided the following changes are made.

a. First, the cavitation problem with the hydraulic return line must be eliminated. This can be accomplished by reducing the length of the supply and return hoses as well as slowing down the test frequency to one hertz (as opposed to two hertz). While changing the frequency will double the time for testing, it should also improve the test results.

b. Second, a different controller should be used to control the vertical (shear loading) actuator. A MTS TestStar controller (or equivalent) is recommended to accomplish this task.

c. Third, one concrete specimen per coarse aggregate type should be used to determine the system response and digital control settings. It should be noted, however, that this specimen once used for control setting would probably not be useful for further testing. The main reason for this is that significant degradation occurs in the early stages of loading. Consequently, it is likely that during the control setting that erratic behavior may occur, which will render the specimens as unusable.

(3) The aggregate interlock tests at a crack width of 0.024 inches indicated that this is an effective joint and crack width regardless of the aggregate type. However, it is speculated that stronger coarse aggregate concrete under very high vehicle loading may experience more degradation due to the gouging of the cement paste by the coarse aggregate. However, these higher deflections would be unrealistic given existing load limits on roads.

(4) It was apparent in the test results as well as in the literature that aggregate interlock stiffness varies significantly between aggregate concrete types at crack widths greater than 0.035 inches. Consequently, at large crack widths the coarse aggregate's strength and stiffness determines the degradation rate of the aggregate interlock, with the stronger aggregate providing better aggregate interlock over time. This was demonstrated in the Illinois research and in the two tests conducted at crack widths of 0.050 inches in this research.

(5) It appears that the coarse aggregate type also affects the morphology or texture of the concrete fracture surface. While the method used to quantify surface morphology was not as successful as anticipated, it did reveal to some extent that the stronger aggregate generated a rougher surface than the weaker aggregate.

(6) Tension fracturing of the concrete into specimen blocks was conducted at 18-hours. It was observed after fracture that coarse aggregate strength played a role in the overall tensile strength of the concrete at failure. For example, the Levy slag concrete always required higher pressure (tension load) to fracture the concrete compared to the other coarse aggregate concrete tested. It is speculated that the higher pressure, i.e., tension force required to fracture the concrete, was generated by the fracture surface going through the coarse aggregate as opposed to around the aggregate (pullout failure) resulting in smoother fractured surfaces. On the other hand, PCC with stronger coarse aggregate required lower pressure to fracture the PCC and produced rougher surfaces since less coarse aggregate fractured.

(7) The strength of the PCC specimens, as opposed to the strength of the coarse aggregate, does not appear to be a significant factor in aggregate interlock performance at large crack widths. This may be an important fact for future testing since it suggests that testing specimens at significantly different times in relation to their 28-day strength may not be important. That is, concrete may be tested anytime after a 28-day cure.

(8) The aggregate interlock test system was able to maintain an exceedingly constant crack width during testing. Since the horizontal actuator is used to accomplish this, it is relatively straightforward to adjust the crack width to any width desired. In addition, it would be possible to vary the crack width to simulate warm (small crack width) and cold weather (large crack widths) effects during a single test if desired.

(9) The aggregate interlock test set is relatively easy to use and can be set up in a short period of time. It is estimated that a test specimen (cured and ready for testing) can be set up in approximately two hours. As a comparison, in personal communications with the personnel at the University of Illinois it was stated that it took approximately two days to set up a test sample.

2 Recommendations for Further Research

The research investigated the novel use of a split Hopkinson pressure bar to investigate the dynamic properties of aggregate, mortar and concrete, as well as the development and use of an aggregate interlock test system. The research results strongly suggest that both dynamic testing and aggregate interlock research have significant potential. While the dynamic properties of concrete have been studied for military applications, there have not been studies for concrete pavements. The results of this research indicate that not only does dynamic testing describe the dynamic response of concrete, but it also may provide a means to quantify the properties of concrete, which may be related better to the performance of concrete than do traditional test such as the 28-day compression strength test. In addition, the aggregate interlock test system can provide a relatively efficient means to study the response of joints at various crack widths and in particular how the joint response varies with coarse aggregates strengths. Based on the results of this research, a number of recommendations are provided. These recommendations are divided into two areas; those involving dynamic testing and those involving the aggregate interlock testing.

2.1 Dynamic Testing Recommendations

The following research areas involving the dynamic response of aggregate, mortar and concrete are recommended for further study:

(1) The development of an aggregate database, which would include the dynamic to static ratio (D/S) and the strain rate parameter λ for aggregates used in Michigan. The database would consist of cross-section of aggregate such as metaphoric, igneous, sedimentary, including sandstone, limestone, dolomite, shale and industrial products such as blast furnace slag. Suggested specific research areas concerning the dynamic properties of aggregate are as follows:

- A detailed study of the dynamic properties of limestone and dolomite aggregate, since there was considerable difference between these two aggregate types. This would also include comparing the results of the dynamic parameters with the aggregate's microstructure. For example, the research showed an extremely high $\lambda = 25.5$ for the Port Inland limestone, near the level of igneous aggregate, while the Rockwood dolomite had a very low $\lambda = 4.5$ value. Yet, the Rockwood dolomite had a higher static strength than the Port Inland limestone. The microstructure analysis may provide insight into the reasons for this difference and to what extent grain size, fossil content and in the case of dolomites, whether the secondary replacement process has an effect on aggregate performance.

- Study the vertical variations in aggregate properties within quarries, e.g., various ledge formations in carbonate quarries.
- When freeze-thaw tests are conducted on concrete determine whether a correlation exists between the strain rate parameter λ and the freeze-thaw durability index.
- Investigate possible correlation of the dynamic parameters with aggregate wear, since aggregate wear is also a dynamic process.
- Further investigate the relationship between an aggregate's dynamic strength and its ability to function in aggregate interlock over the expected life of a pavement.
- Investigate why the dense portion of the air-cooled blast furnace slag had such good mechanical properties, as opposed to the water-quenched slag.

(2) The results of the dynamic parameters suggest that they could also be used to quantify the behavior of concrete in cases where traditional tests such as the 28-day strength, air content and slump may not. Therefore, the following recommendations concerning the concrete dynamic testing are suggested:

- It is recommended that research be conducted on the relationship between the D/S and λ values and the concrete microstructure. If a relationship can be established, then the dynamic testing might provide an inexpensive means to determine the long-term performance of the concrete without having to conduct more time-consuming microstructural characterization.
- A study of the effects of moisture on the D/S and λ parameters for concrete and the concrete's air-void system. Tests should also be conducted under fully saturated

conditions to study the effect of the loss of capillary stresses and its effect on the D/S and λ parameters, which may provide additional information on the nature of the air-void system.

- It is recommended that additional indirect tension testing be continued since the literature is indicating that a concrete might be better characterized by tensile strength as opposed to compressive strength. This might even be more important for the dynamic strength results.

2.2 Aggregate Interlock Recommendations

It is believed that the aggregate interlock test system developed in this research can be effectively utilized to conduct further aggregate interlock research. It is recommended that following research issues be considered:

- Correlation with the strain rate parameter λ: Additional aggregate interlock testing should be conducted to establish the relationship between λ and the rate of interface degradation at a constant crack width.
- Multiple tests at various constant crack widths: Develop a better understanding of the mechanism of shear transfer across various crack width settings. The crack width of 0.024 inches appears to be a very efficient crack width regardless of coarse aggregate type. However, aggregate interlock testing at larger crack widths would provide a measure of efficiency for aggregate interlock with different coarse aggregate types and crack widths.
- Changing crack widths during test: A specific joint/crack in the pavement does not maintain a constant width throughout its life. During the year the pavement goes through expansion and contraction cycles due to temperature change. Therefore, there are times that the pavement joint opening may be at 0.024 inches and other times, most likely in the winter months, that the crack width is much larger. With the capabilities of the dual actuators in the system, a scaled version of this cycle could be replicated. While the vertical actuator is administering the shear loading the horizontal actuator could change the crack width during the testing sequence.

For instance, if the frequency of the shear loading was kept at 1 Hz then the crack width could open and close over a range of 0.024-0.06 inches within a time period of 24 hours. This may better replicate the conditions in the field between summer and winter temperatures.

- Surface morphology: The surface morphology of the concrete interface should be measured using stereographic imagery, which would allow a better characterization of the concrete surfaces before and after testing. In addition, the effect of coarse aggregate type can also be examined as to how it affects the interface morphology after initial fracturing. This would also be very important in investigating the change in surface morphology with variations in crack width during loading. This information could be entered into a mathematical model to determine a relationship of surface texture to crack width. This is important to show that at larger crack widths, there is less surface area to generate the required load transfer. It could also be used to develop guidelines for crack width in the field.
- Aggregate Base: The effect of aggregate base and subgrade support for PCC pavements in aggregate interlock was not studied in this research. However, further research should be conducted to investigate the interaction of base material and the aggregate interlock load transfer mechanism. This has been anticipated in the design of the aggregate interlock system and can be accomplished by placing stiff springs between the fixed end holder and the steel frame base. The stiffness of the springs can be matched to various base stiffness or resilient modulus values. The system can then be modified to produce a load transfer mechanism that represents the base and sub-base material load transfer capabilities.

2.3 Automated Testing Recommendations

The automated specific gravity devices show excellent promise in quickly and accurately determining an aggregate's apparent specific gravity, bulk dry specific gravity and the maximum absorption. However, it is recommended that additional testing be considered to determine if the variation in test results with the blast furnace slag is due to the ASTM test method, which uses water to penetrate the aggregate, or with the helium pycnometer, which uses helium gas to penetrate the aggregate.

SECTION 3

Aggregate Selection and Characterization

1.1 Aggregate Selection

The aggregates used in this research were obtained from eight sources in Michigan, two in Ontario, Canada and one in Ohio. The location of each source is shown in Figure 1.1 while Table 1.1 lists the quarry, location and the MDOT aggregate source identification numbers. With the exception of the blast furnace slag, all of the aggregate samples were obtained from an active quarry soon after a production blast and prior to crushing and sizing. The blast furnace slag was obtained from steel mills in Ste. Sault Marie, Ontario and Detroit, Michigan.

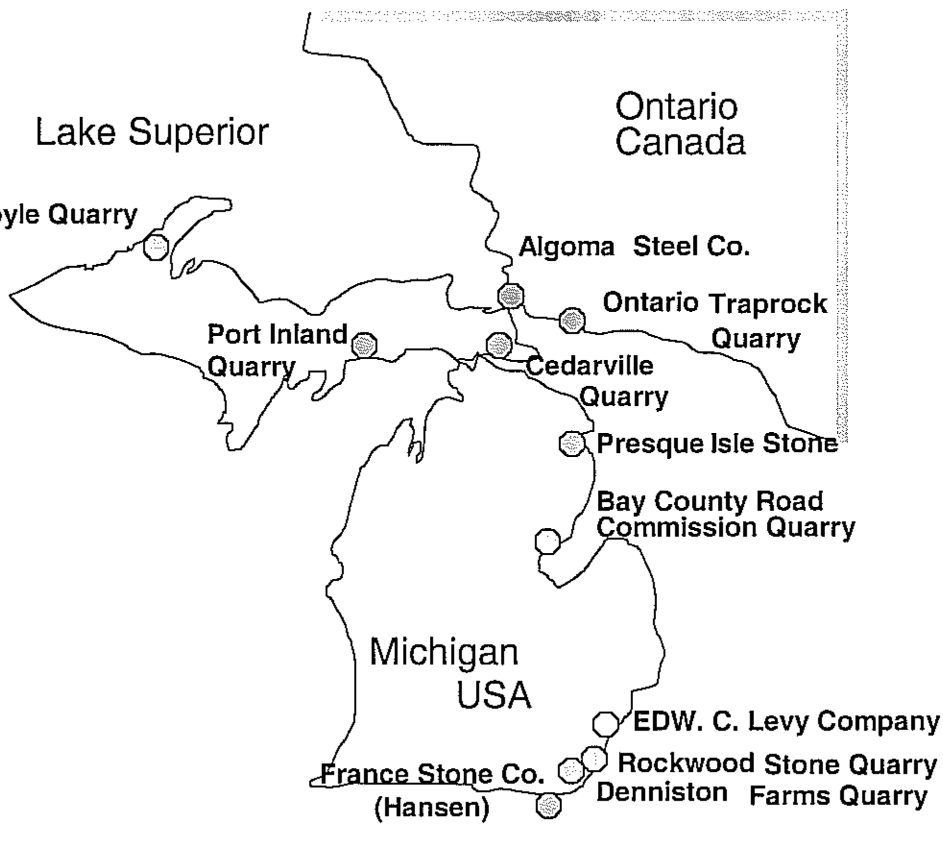

Figure 1.1 Aggregate sources locations.

Table 1.1 Aggregate Source Information

No.	Quarry	Aggregate Type	Location	MDOT Pit ID No.
1	Algoma	Air Cooled	Ste. Sault Marie, Ontario, Canada	95-006
2	Algoma	Water Quenched	Ste. Sault Marie, Ontario, Canada	95-006
3	Levy	Water Quenched	Detroit, MI	82-019
4	Presque Isle	Limestone	Rogers City, MI	71-047
5	Bay County	Limestone	Au Gres, MI	06-008
6	Port Inland	Limestone	Manistique, MI	75-005
7	Cedarville	Dolomite	Cedarville, MI	49-065
8	Denniston Farms	Dolomite	Monroe, MI	58-009
9	Rockwood	Dolomite	Newport, MI	58-008
10	France Stone (Hanson)	Dolomite	Sylvania, OH	93-003
11	Moyle	Basalt	Houghton, MI	31-076
12	Ontario Traprock	Diabase	Bruce Mines, Ontario, Canada	95-010

1.2 Aggregate Geology

1.2.1 Slag

Slag is a manufactured aggregate produced as a by-product in the production of pig iron and contains mainly silicates and calcium. During the making of pig iron the lighter slag material floats to the top of the blast furnace while the heavier pig iron sinks to the bottom where access doors are located to extract both materials. Consequently, the pig iron is released first followed by the slag. Generally, the pig iron is placed in containers and transported to a steel making facility while the slag is either sold or stockpiled, depending on its commercial value. Prior to slag being used commercially, it was simply disposed of in large slag piles generally located near the steel mills. The disposal was typically conducted using large buckets where the molten slag was placed and transported to the disposal area and dumped forming large slag piles. Significant tonnage of slag still exists at some blast furnace facilities. Later, when slag became a commercial product the slag was allowed to flow into trenches adjacent to the blast furnace building where it formed into a layer approximately a few feet thick. As the molten slag flows into the trench, water is sprayed onto the slag to induce thermal cracking in the slag allowing the slag to cool faster. However, the thermal mass of water is insufficient to appreciably cool the slag and so the slag is considered "air-cooled". After approximately 24 hours the slag is broken up by a front-end loader, transported to a crusher area, crushed and placed in stockpiles. However, to differentiate between the two types of slag the older technique of disposing of the slag in dumps will be referred to as "air-cooled" slag while the later method of placing the molten slag in trenches while spraying water on the slag will be referred to as "water-quenched" slag.

Thin-sections of the aggregates used in this research are provided in Appendix 3A, where each thin-section is provided with both a positive and negative image. However, only one thin-section was made from each aggregate and therefore they may not be representative of all of the aggregates tested in this research.

The air-cooled slag is shown in Figure A.1 while the water-quenched slag is shown in Figure A.2. Both the rate of cooling and method of deposition contribute to the crystalline nature of the slag. Comparing Figures A.1 for air-cooled slag and Figure A.2 for the water-quenched slag it can be seen that air-cooled slag has significantly smaller, splinter-like crystals while the water-quenched slag has a larger crystalline texture. Since the cooling rates are more than likely relatively similar, one possible explanation for the difference in the crystalline texture of the slag may be the method of deposition. As previously mentioned the air-cooled slag was deposited in large disposal areas where it was typically transported to the top of a pile and discharged over the slope. The molten slag would then flow down slopes of the piles forming along the slope of the pile. The water-quenched slag on the other hand was placed in shallow trenches where it spread out in the trench in a relatively uniform manner. Stratification of the slag with the heavier and darker mineral sinking towards the bottom, while the lighter minerals moves towards the top is clearly event in the slag. For the air-cooled slag it may be possible that the mixing action of the steep slope may allow better association of elements to form more nucleation sites for crystal growth in addition to generating the more splinter-like crystals. However, less crystal nucleation sites may develop in the slag deposited in trenches and as a consequence fewer but larger crystals form in the water-quenched slag. Nonetheless, there are a number of other possibilities that may contribute to the formation of the crystalline nature of the slag. In the study of material fracture, however, one of the primary controls of the fracture process is the crystalline nature of the material. Consequently, understanding the processes that contribute to the formation of an aggregate may also provide a better understanding of it strength and other performance related issues.

1.2.2 Carbonates

Figure 1.2 illustrates the stratigraphic sequence of the natural aggregates studied in this research. The carbonate aggregates were all mined in the Michigan Basin and are of Paleozoic age, ranging from 300 to 425 million years old. Figure 1.3 illustrates the unique geology of the Michigan Basin presented by Dorr and Eschman (1970) with the the seven carbonate aggregate source locations superimposed on the figure. One source is of Mississippian age (310 to 345 million years old), three sources are Devonian age (345 to 405 million years old), while three sources are of the older Silurian age (405 to 425 million years old). In general, the Michigan Basin consists of sedimentary rocks ranging from sandstones, shales, limestones, dolomites and evaporites (salts). Economically, the carbonates and salt deposits are the dominant materials mined in the Michigan Basin. The carbonates form as a chemical precipitate from an ancient ocean in which most of the sedmintary rocks in the basin were formed. Carbonate rocks can form either with a clastic texture, i.e., a collection of carbonate fragments, or in a crystalline form directly from a precipitate. The clastic textured carbonates go through a lithification process by which the unconsolidated materals are converted into rock. Lithification generally results from the pressure overlying rock and geothermal heat flow. In general, the greater the lithification (measured in both time, pressure and temperature) the more consolidated the rock is and theoretically stronger. However, studies conducted to relate strength, for example, to the degree of consolidation have not been successful at proving this point. If this were the case, the older more deeply buried carbonates would possess greater strength than the younger shallower carbonates. A complicating factor in this generalization is the texture of the carbonate. It may be reasonable to assume that the strength of clastically formed carbonates may be more a function of the lithification process than the crystalline formed carbonates. However, other contributing factors may affect carbonate strength, such as the amount of noncarbonate materials, mircostructure defects, pore structure, fossil content, or depositional environment. Thin sections of the carbonates are presented in Appendix A in Figures A.3 through A.9.

The limestones aggregates are composed primarily of calcium carbonate ($CaCo^3$) and have a fairly consistent specific gravity of 2.68. The three limestones studied were from the Presque Isle, Bay County and Port Inland quarries. It can be seen in Figures A.3 through A.5 that the texture of the three limestones vary from a larger crystalline texture in the Presque Isle to a smaller crystalline texture with fossils for the Bay County and Port Inland limestone. Note that the scale for the Presque Isle limestone is 500 μm while the other two thin sections are at a 250 μm scale, thus showning a fairly large crystalline texture size for the Presque Isle limestone.

The four dolomites tested were from the Cedarville, Denniston, Rockwood, and France Stone quarries. Dolomite is a carbonate composed primarily of calcium and magnesium, $CaMg(CO_3)^2$. Due to the presence of magnesium the specific gravity of dolomite is higher generally around 2.85. However, there is generally greater variability in specific gravity for dolomites than limestones due to the varying percent of magnesium. Thin sections of the dolomites can be seen in Figures A.6 through A.9 in Appendix 3A. The France Stone and Cedarville dolomites appear to have a clastic structure while the Dennison and Rockwood appear to have a crystalline texture. However, additional testing and analysis would have to be performed to verify these observationsconcerning whether the carboantes are crystalline or clastic. The grain size of the Cedarville dolomite is noteably larger than the France stone while the texture of the Dennison and Rockwood dolomites appear to be similar with the exception that there appears to be more larger size material, possibly silica grains in the Rockwood dolomite. It can also be seen that the crystalline texture of the two dolomites are larger than the crystalline structure of the limestone and that there appears to be less quartz grains in the limestone as opposed to the dolomite.

1.2.3 Igneous

The two igneous sources used in this research are Precambrian in age (over 600 millions old). Two mafic igneous rocks, both of Keweenawan age, were tested: a Nippissing Diabase from Bruce Mines, Ontario and a Portage Lake Volcanic basalt from Moyle Quarry, Houghton, Michigan. The Nippissing diabase is also known as a traprock since it was formed at depth in a trap environment. The trap environment allowed a slower cooling of the rock and thus a longer time for crystals to form during the cooling process. The Portage Lake volcanic basalt formational environment was that of a flood basalt, i.e., the basalt flowed onto the surface of the earth cooling in place at atmospheric conditions. Due to this type of formation and quick cooling the basalt has a less crystalline structure than the diabase. In addition, due to the more rapid cooling, significant gas bubbles, which are known as amyadoles, are trapped in the basalt. In most cases the gas bubbles have been filled with quartz, epidote, or native copper. Figure A.10 and A.11 in Appendix A illustrate thin sections of the Moyle and Ontario Traprock aggregates, respectively. The crystalline structure of the igneous rocks can easily be seen in the thin sections in addition, to the larger crystal size of the diabase.

1.3 Aggregate Characterization

1.3.1 Density

Measurement of the aggregate's apparent and bulk density was conducted using an automated Micromeritic's 1330 Accupyc helium pycnometer, which is shown in Figure 1.4, and a Micromeritic's 1360 Geopyc envelope density analyzer, which is shown in Figure 1.5. From data collected with these instruments the effective porosity, absorption, and bulk density SSD were then estimated. The automated testing methods are described in a paper by Vitton, Lehman and Van Dam, (1998), which was published in an ASTM special technical publication. The paper describes the use of the instruments and the calculation of the density parameters and density measurements for three Michigan aggregates.

In this research the apparent specific gravity, G_{ab}, and the bulk specific gravity, G_B, were measured while the bulk specific gravity, $G_{b,SSD}$ and the porosity, n, were calculated. The apparent specific gravity, G_{ab}, is equivalent to the specific gravity of soils, G_S, since both methods measure only the solid portion and not the volume of voids when calculating the volume of the material. The bulk specific gravity, G_B, however, includes the volume of voids when estimating the volume of the aggregate. This volume is sometimes referred to as the envelope volume. The difference between the two bulk specific gravity definitions is that the bulk specific gravity measurement is conducted when the voids are dry (oven-dried) and the bulk specific gravity (SSD) is conducted when the voids are water saturated but have dry surfaces, thus the designation saturated-surface dry or SSD. The AASHTO procedures to determine specific gravity depend on the ability of water to absorb into the soil and aggregate saturating the material. Current AASHTO test methods require that the soil or aggregate be saturated for 24 hours to satisfy most of the absorption potential of the material. However, it is recognized that for some materials not all of the effective pore space may be saturated after 24 hours. Helium gas, on the other hand, can more easily and effectively absorb into a material's effective pore space. This, coupled with recent advances in instrumentation and sensors, has led to the development of a helium pycnometer. This device uses the ideal gas law to determine the volume of a material based on pressure measurements of helium gas. By knowing the dry mass of a soil or aggregate its specific gravity, G_S, can be determined.

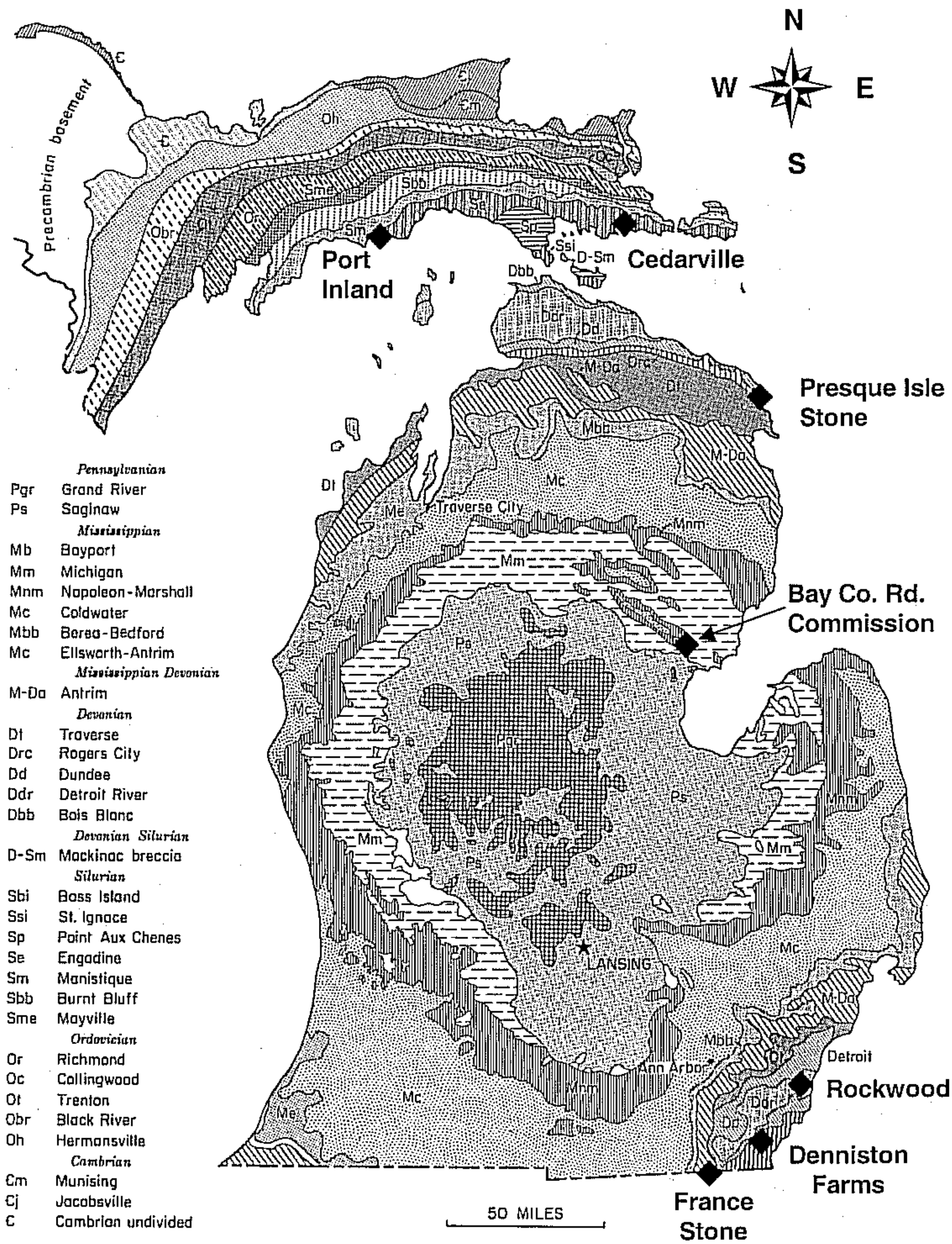

Figure 1.2 Geology of the Michigan Basin (Dorr and Eschman, 1970).

Geologic Period			Formation	Geologic Time Million Years
Cenozoic			Sand and Gravel Deposits	63
Mesozoic				230
Paleozoic	Permian			280
Paleozoic	Carbon-iferous	Pennsylvanian		310
Paleozoic	Carbon-iferous	Mississippian	Bayport Limestone (Bay Co.)	345
Paleozoic	Devonian		Lucas Dolomite (Denniston) Lucas Dolomite (Rockwood) Rogers City Limestone (Presque Isle)	405
Paleozoic	Silurian		Raisin River Dolomite (France Stone) Engadine Dolomite (Cedarville) Fiborn Limestone (Port Inland)	425
Paleozoic	Ordovician			500
Paleozoic	Cambrian			600
Precambrian	Proterozic	Keweenawan	Portage Lake Volcanics (Moyle) Nippissin Diabase (Ontario Traprock)	1,600
Precambrian	Proterozic	Huronian		

Figure 1.3 Geologic formation and age of aggregates.

Figure 1.4 Micromeritics 1330 helium pycnometer.

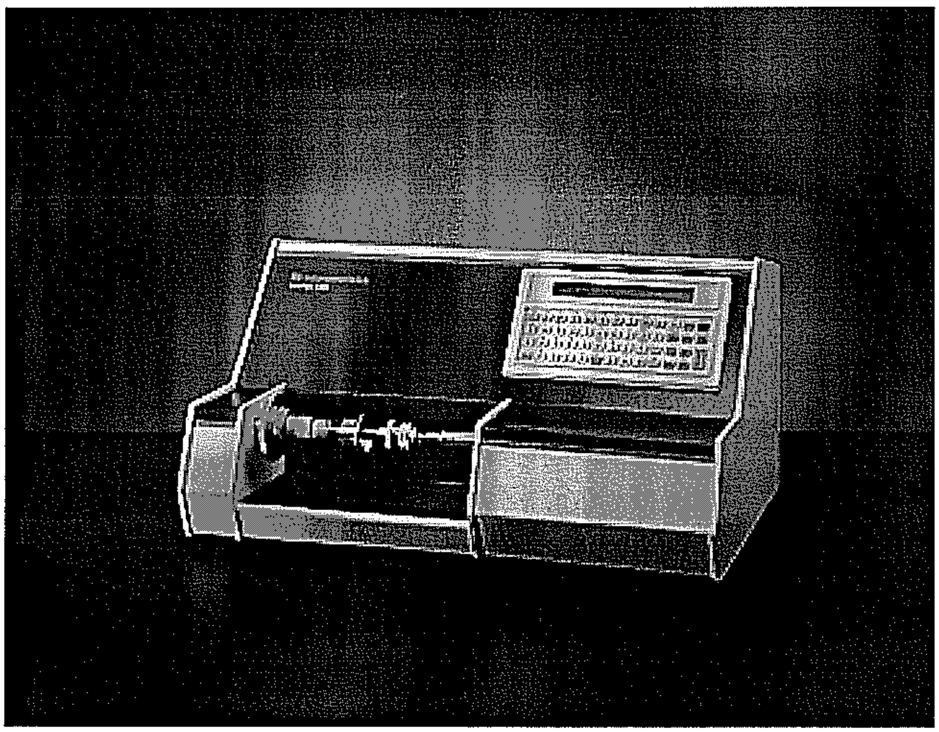

Figure 1.5 Micromertic's 1360 bulk density analyzer.

The bulk specific gravity of a material, G_B, can be determined using the Micromeritic's 1360 automated envelope density analyzer. This device determines the bulk volume or envelope volume of a sample by measuring the volume of a fine-grained material in a cylinder and then again measuring the volume of the fine-grained material plus the sample. By determining the difference in volume between the two measurements, the bulk volume of the sample can be calculated and the bulk specific gravity determined. If the apparent specific gravity, G_S, and bulk specific gravity, G_B, of the soil or aggregate is known, the effective porosity of a material, n, can also be determined by the following relationship:

$$n = \left[1 - \frac{G_B}{G_S}\right] x \ 100 \qquad \textbf{1.1}$$

Assuming that the bulk specific gravity, G_B, measurement is accurate, then the measured effective porosity, n, will be a function of the effectiveness of the fluid or gas used to permeate into the pore structure of the aggregate. When saturating the aggregate with water, the increase in the weight of the aggregate due to water in the pores, but not including water adhering to the outside surface, is referred to as the aggregate's absorption, A. While the ASTM standard is based on 24-hour saturation, it is possible that not all of the effective porosity, n, will be filled with water. However, if it is assumed that the aggregate is completely saturated (100% of the effective pores are filled with water), the aggregate's maximum absorption can be determined as a function of the bulk specific gravity and the effective porosity as follows:

$$A = \frac{n}{G_B} \qquad \textbf{1.2}$$

By knowing the effective porosity of a material an estimate of the bulk specific gravity (SSD), $G_{B,SSD}$, can also be made assuming that the material's effective pore structure is completely filled with water (specific gravity = G_{water} = G_w). This relationship is as follows:

$$G_{B,SSD} = G_B + nG_w \qquad \textbf{1.3}$$

The results of the density testing conducted in this research are presented in Table 1.2.

Table 1.2 Aggregate Type and Specific Gravity

No.	Source (MDOT ID)	Material Type	Orientation to Bedding	G_{ab}	G_B	$G_{B,SSD}$	Porosity (%)
1.0	Algoma Steel	Air-Cooled Blast	Porous Region	2.973	2.09	2.41	30
1.2	(95-006)	Furnace Slag	Dense Region	2.888	2.40	2.57	17
2	Algoma Steel (95-006)	Water Quenched Blast Furnace Slag	Random	2.942	2.43	2.61	17
3	Levy Co. (82-019)	Water Quenched Blast Furnace Slag	Random	2.985	2.42	2.61	19
4	Presque Isle Stone (71-047)	Limestone	Random	2.687	2.51	2.58	6
5	Bay County (06-008)	Limestone	Perpendicular	2.697	2.63	2.68	2
6	Port Inland (75-005)	Limestone	Random	2.69	2.68	2.68	<1
7	Cedarville (49-065)	Dolomite	Random	2.770	2.71	2.75	2
8	Denniston (58-009)	Dolomite	Perpendicular	2.828	2.48	2.65	12
9	Rockwood (58-008)	Dolomite	Parallel	2.836	2.49	2.63	12
			Perpendicular	2.834	2.60	2.70	8
10	France Stone (Hansen) (93-003)	Dolomite	Perpendicular	2.818	2.78	2.82	1
11	Moyle (31-076)	Flood Basalt	Random	2.938	2.89	2.91	1.6
12	Ontario Traprock (95-010)	Diabase	Random	2.931	2.91	2.92	<1

1.3.2 Drill Quality Index Test (DQI)

The initial dynamic and static strength testing for this research required that the aggregate be cored using a 3/8 inch diamond core bit. A six-inch direct drive drill was obtained to core the block aggregate samples. In addition, a precision cut-off saw was used to cut the core to length as well as produce parallel ends. During coring, the core bit was drilled approximately six inches into the aggregate block. With some aggregate types that are highly intact most, if not all of a six-inch core were obtained. However, it was found that some aggregate types tended to break up into a number of pieces while being cored. To quantify this core breakage a drill quality index (DQI) was developed based on a rock quality designation (RQD) used in the mining industry (Deere and Deere, 1988). This DQI index is based on the following formula

$$DCI = \frac{\frac{L_C}{L_D} + \frac{D}{3}}{N \times D} \qquad 1.4$$

where:
L_C = Length of core obtained from the core barrel
L_D = Length of block cored
D = Diameter of core
N = Number of pieces core broke into

A numerical rating system for the DQI was then developed and is presented in Table 1.2.

Table 1.2 Drill Quality Index (DQI) rating system

DQI	Rating	Designation
1.5 or higher	Highly Intact	1
1.00 - 1.50	Intact	2
0.70 – 1.00	Moderately Intact	3
0.70 – 0.44	Moderately Broken	4
0.44 – 0.33	Broken	5
0.33 – 0	Highly Broken	6

The DQI is highly dependent on both the microstructure of the aggregate as well as the macrostructure. The macrostructure, such as large fractures and fissures, will result in breakage of the core. Consequently, the DQI will include both effects, with highly fractured aggregates having high DQI values, while relatively intact aggregate blocks will have lower DQI numbers. Therefore, the DQI is a very relative measure of an aggregate intactness and will vary from block to block. A record was kept of all core lengths and their calculated DQI's. Table 1.3 provides the DQI values. Representative samples of the drilled aggregate core are provided in Appendix 3B.

Table 1.3 Drill Quality Index (DQI) values.

	Quarry	Pit ID	DQI Block 1, 2, 3	DQI Block Average	Average DQI Rating
1	Algoma Steel (air-cooled)	95-006	1[1], 4[2], 1[1]	2	Intact
2	Algoma (water-quenched)	95-006	4, 2	3	Moderately Intact
3	Levy Steel (water-quenched)	82-022	5, 4, NR[3], 4	5	Broken
4	Presque Isle Stone	71-047	1	1	Highly Intact
5	Bay County	06-008	4, 1, 4	3	Moderately Intact
6	Port Inland	75-005	2	2	Intact
7	Cedarville	49-065	1, 1, 1	1	Highly Intact
8	Denniston Farms	58-009	2, 4, 1, 1	2	Intact
9	Rockwood	58-008	1	1	Highly Intact
10	France Stone	93-003	1, 1, 3	2	Intact
11	Moyle	31-045	1	1	Highly Intact
12	Ontario Traprock	95-010	1	1	Highly Intact

[1] Dense dark region (specimen 1.2)

[2] Porous light colored region (specimen 1.0)

[3] NR: No core recovered, i.e., coring did not provide length long enough for testing. A value of 6 is given a NR core.

APPENDIX 3A

AGGREGATE THIN SECTIONS

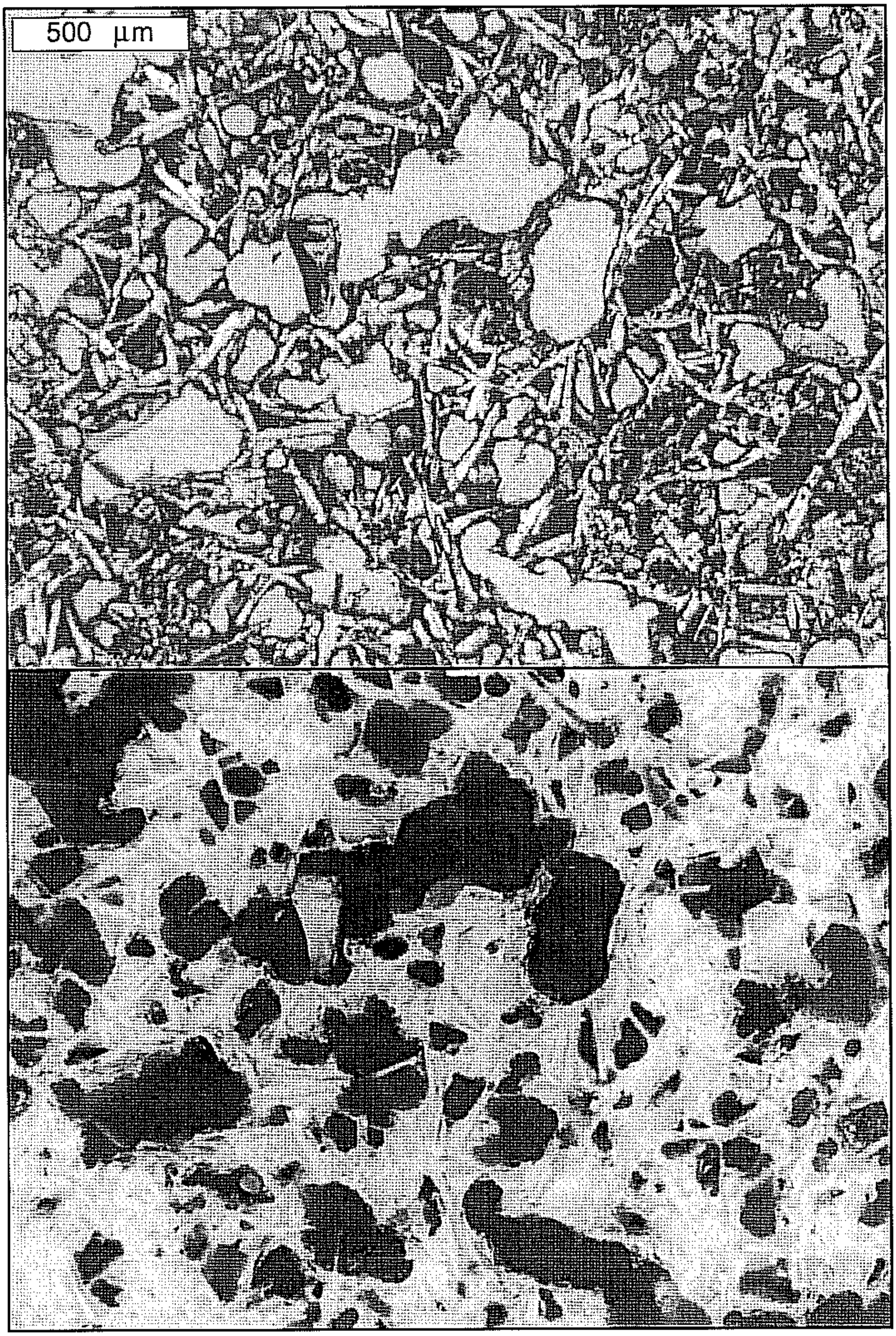

Figure A.1 Thin section of Algoma air-cooled slag (96-006).

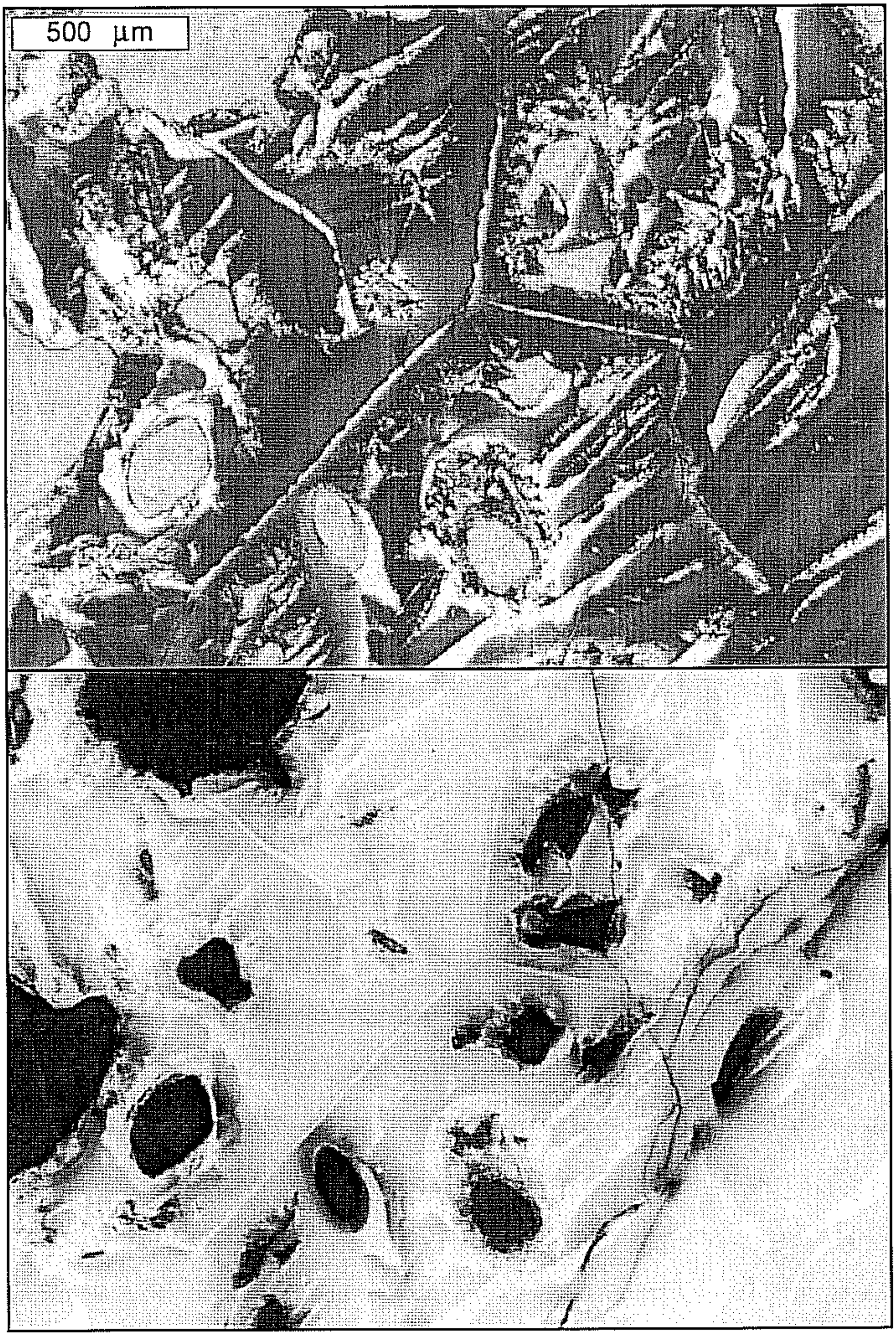

Figure A.2 Thin section of water-quenched Levy slag (82-019).

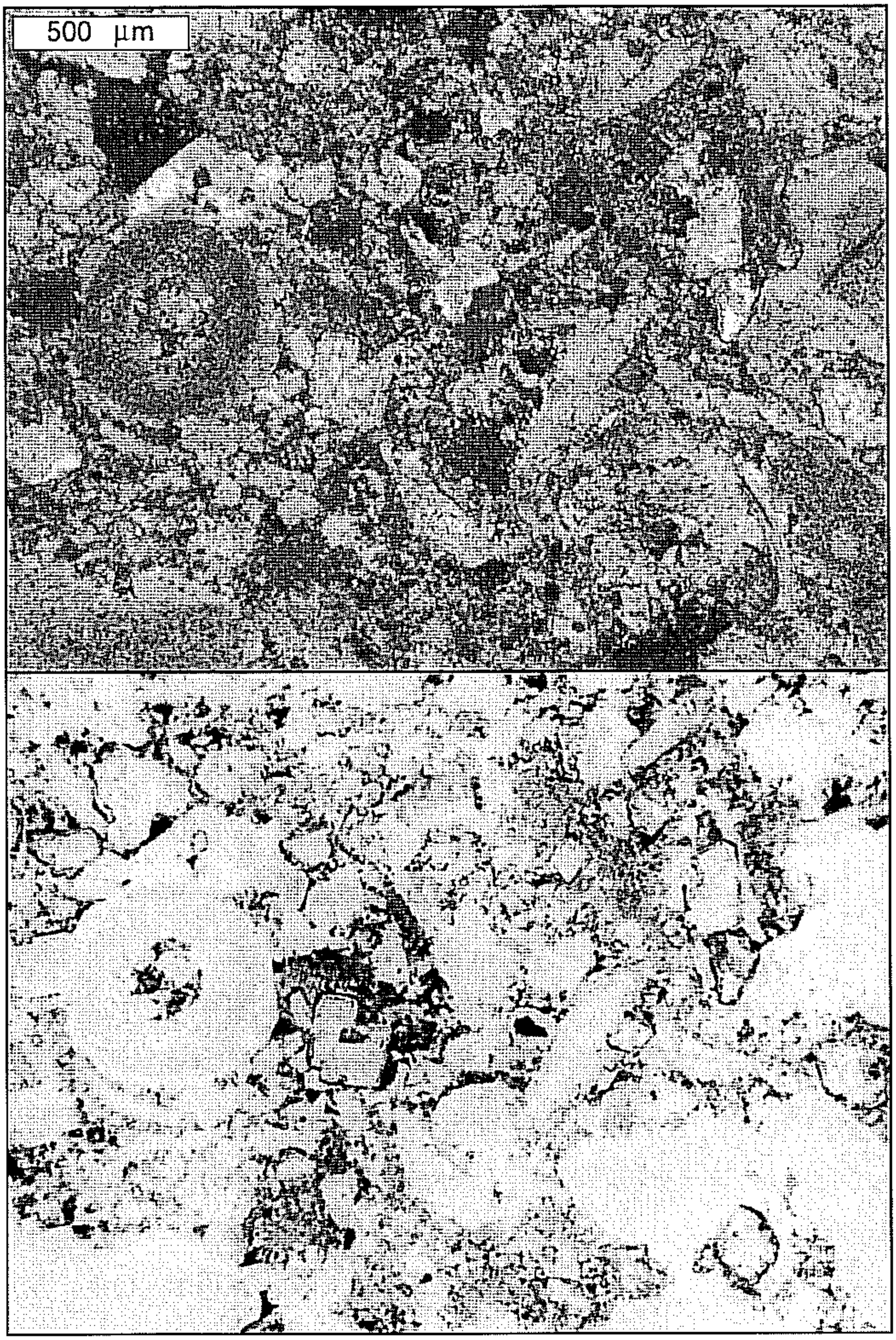

Figure A.3 Thin section of Presque Isle limestone (71-047).

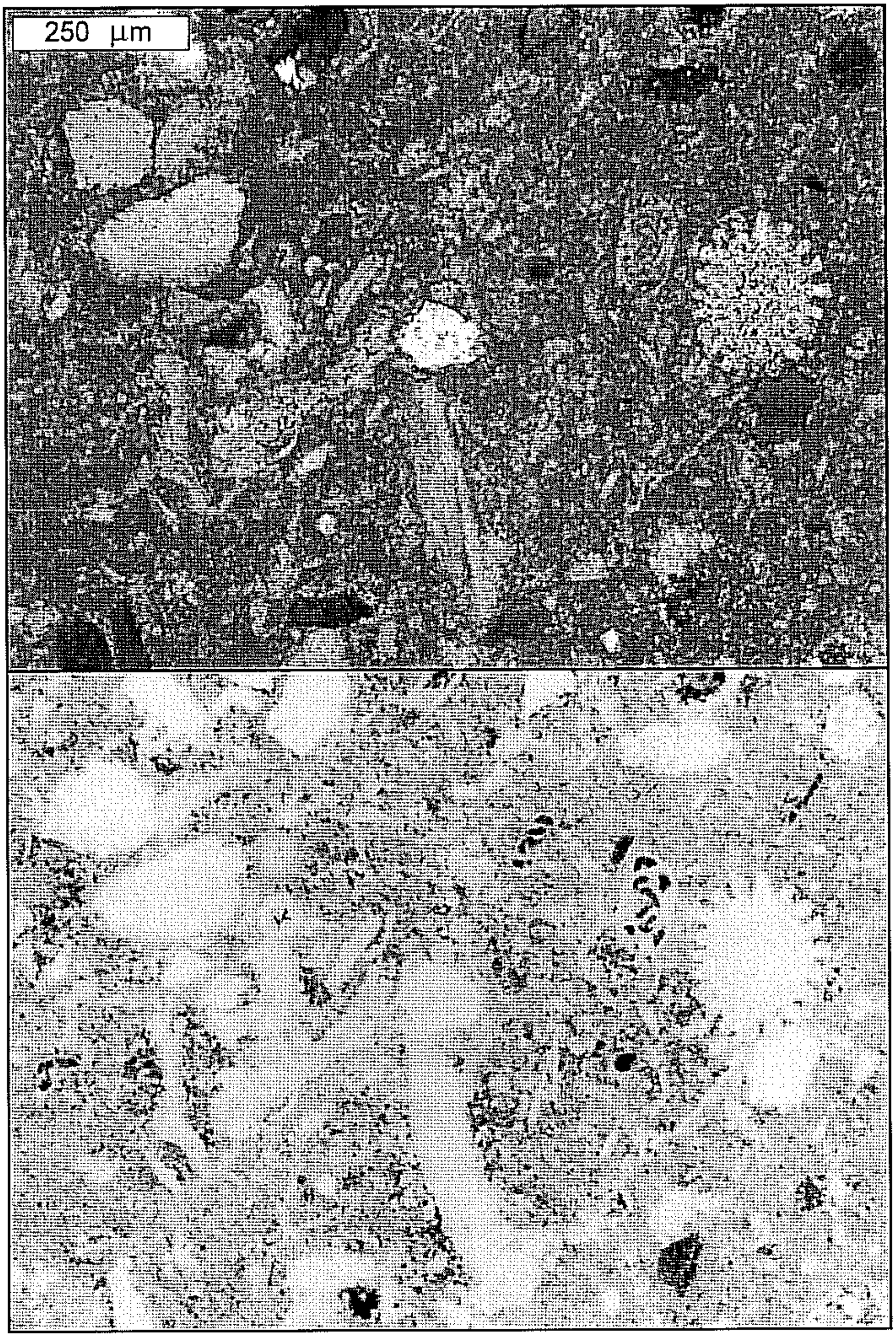

Figure A.4 Thin section of Bay County limestone (06-008).

Figure A.5 Thin section of Port Inland limestone (75-005).

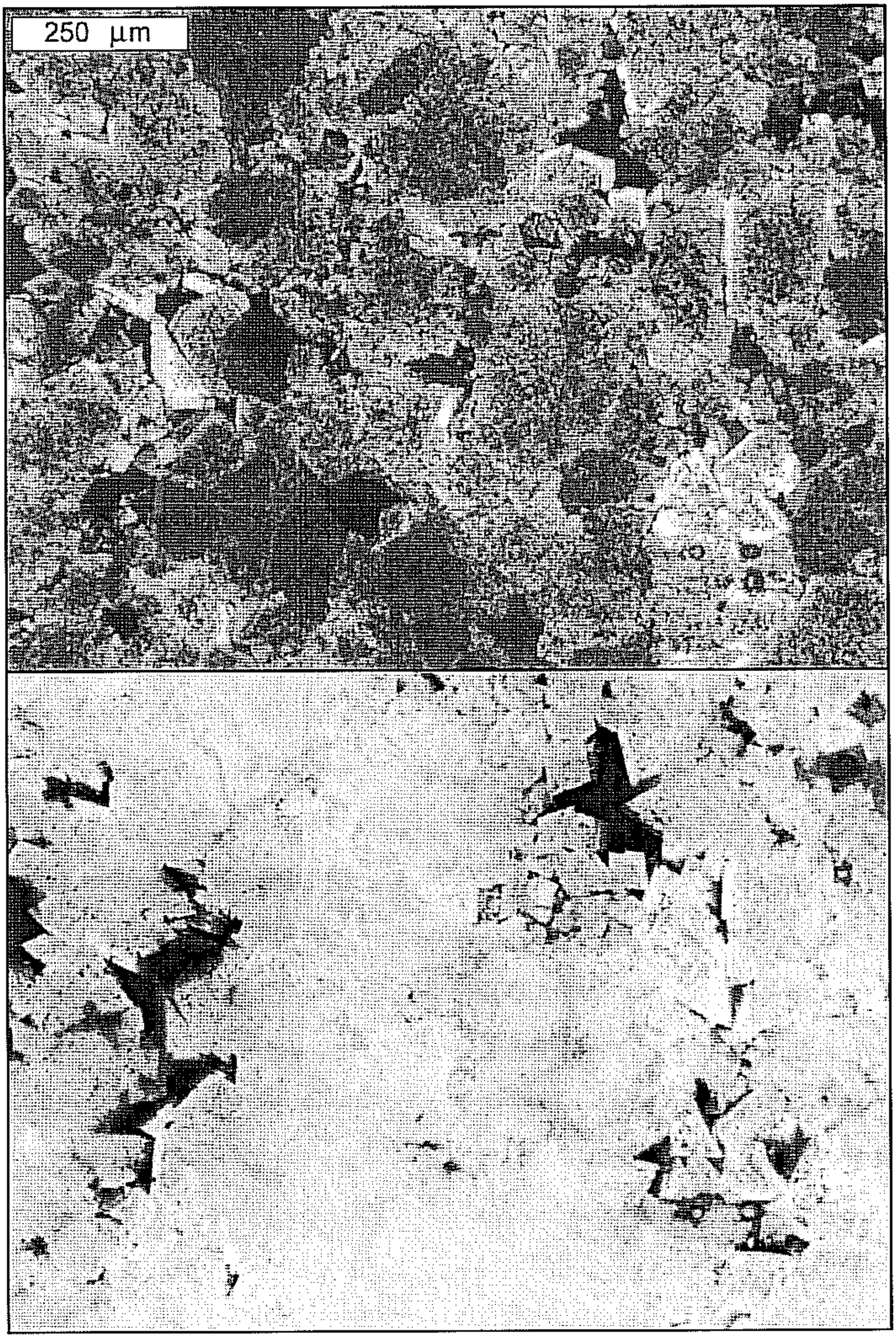

Figure A.6 Thin section of Cedarville dolomite (49-065).

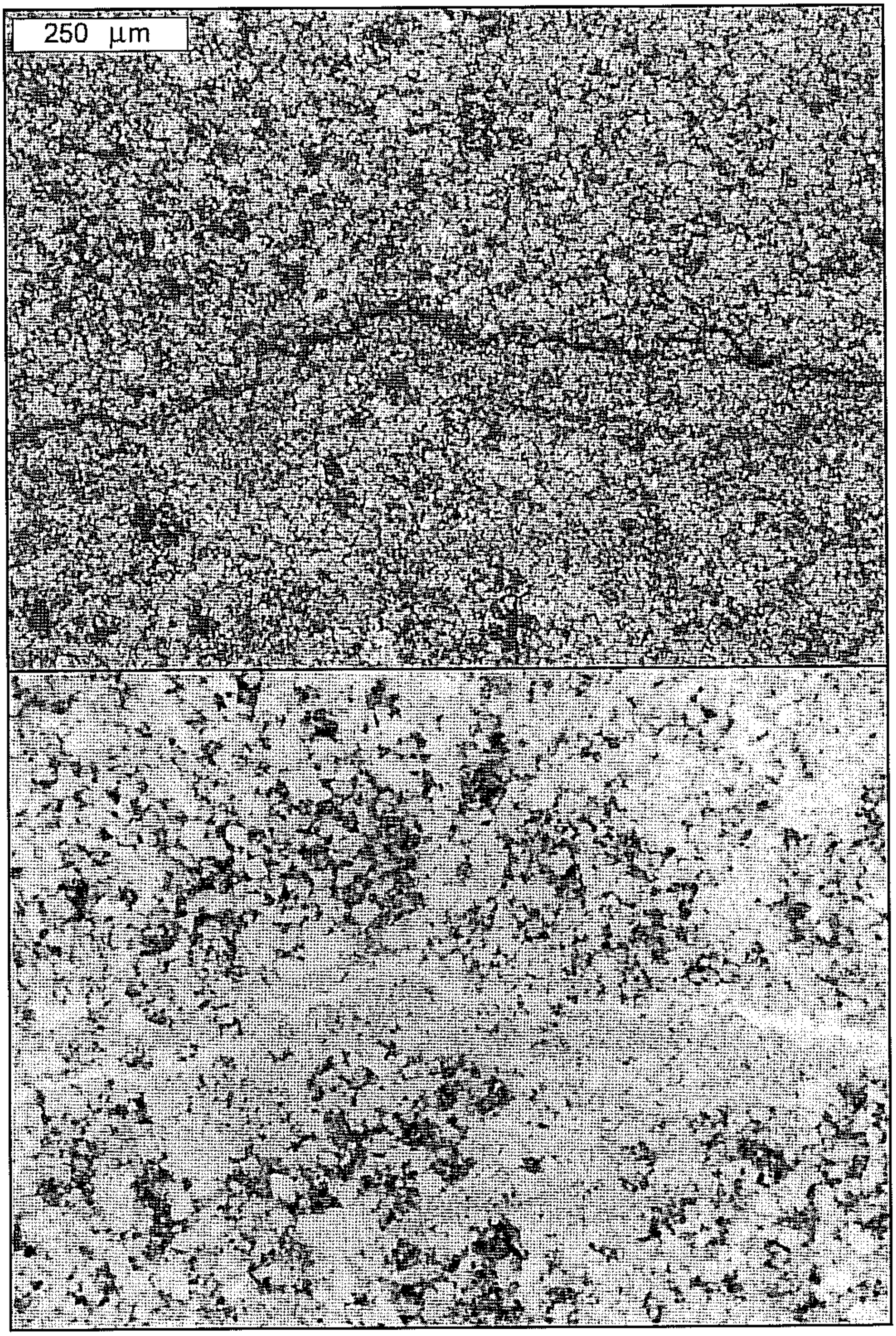

Figure A.7 Thin section of Dennison Farms dolomite (58-009).

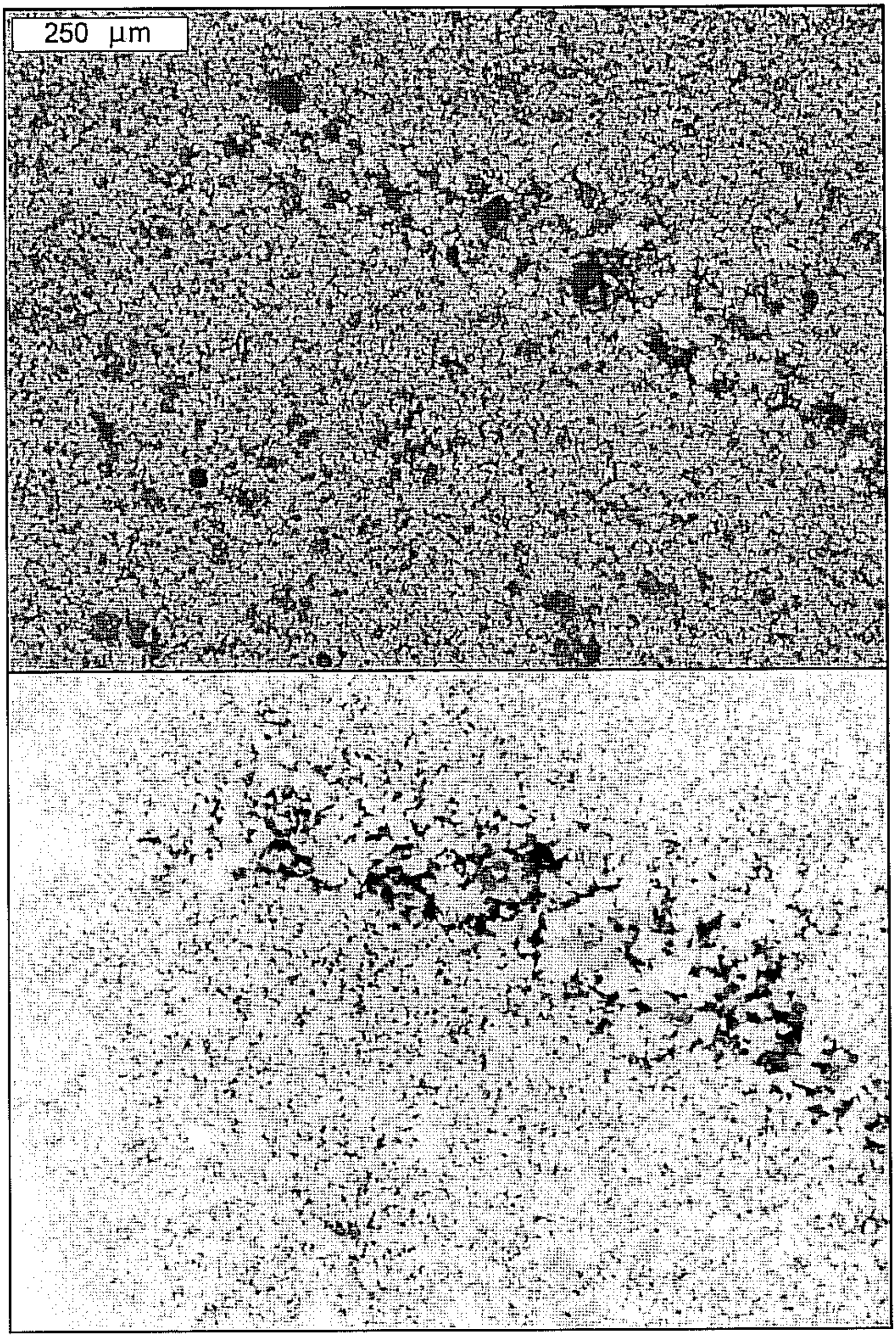

Figure A.8 Thin section of Rockwood dolomite (58-008).

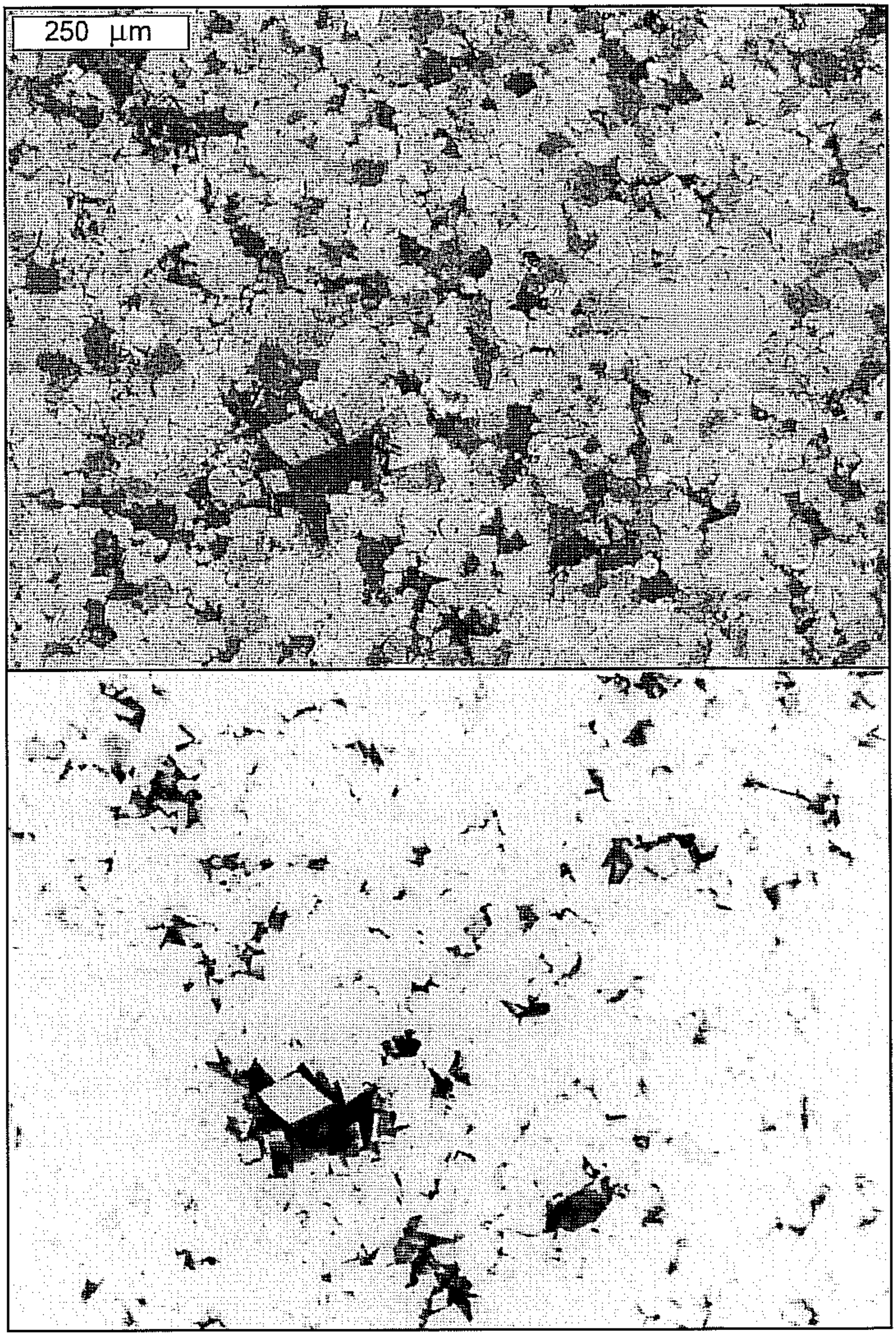

Figure A.9 Thin section of France Stone dolomite (93-003).

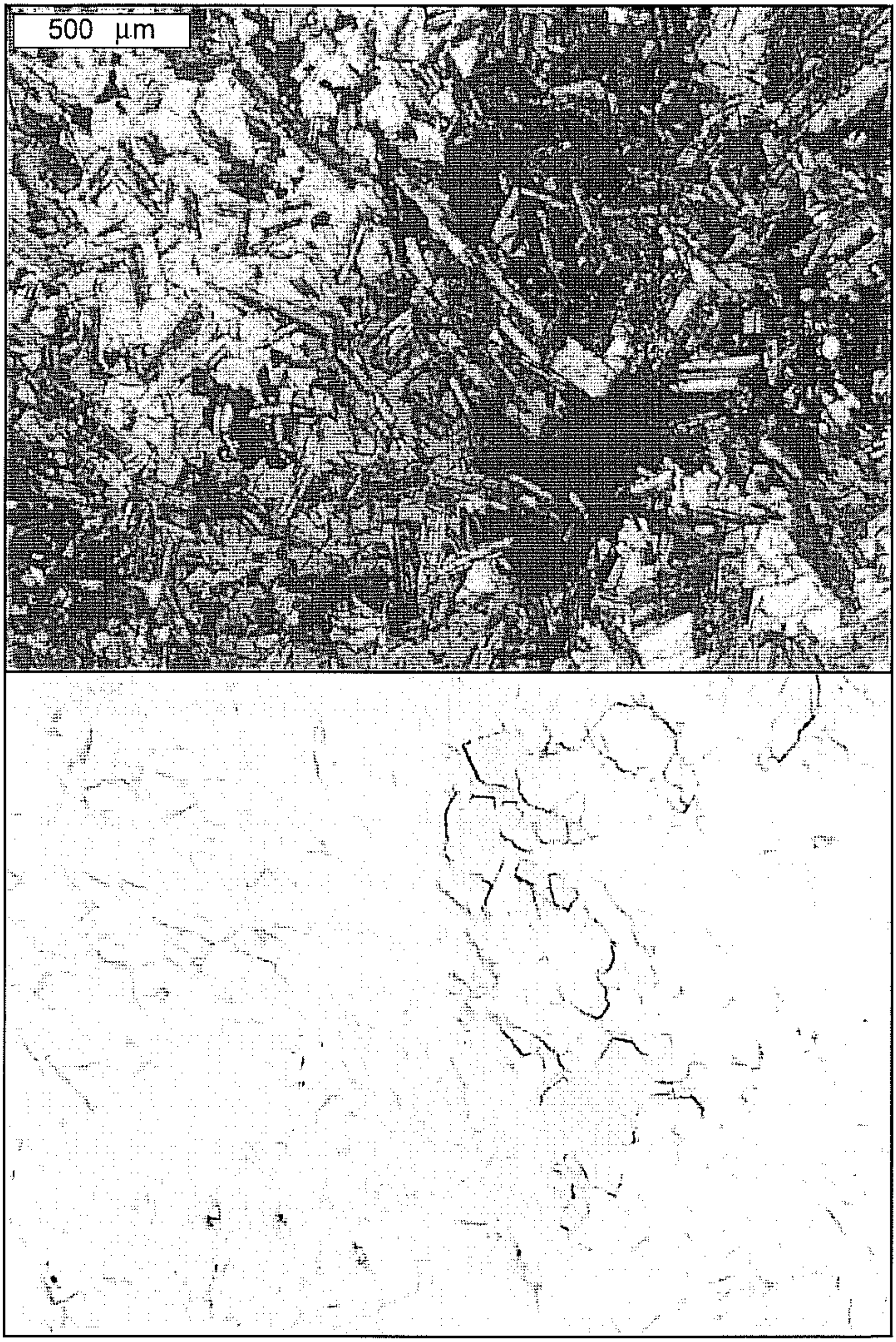

Figure A.10 Thin section of Moyle basalt (31-076).

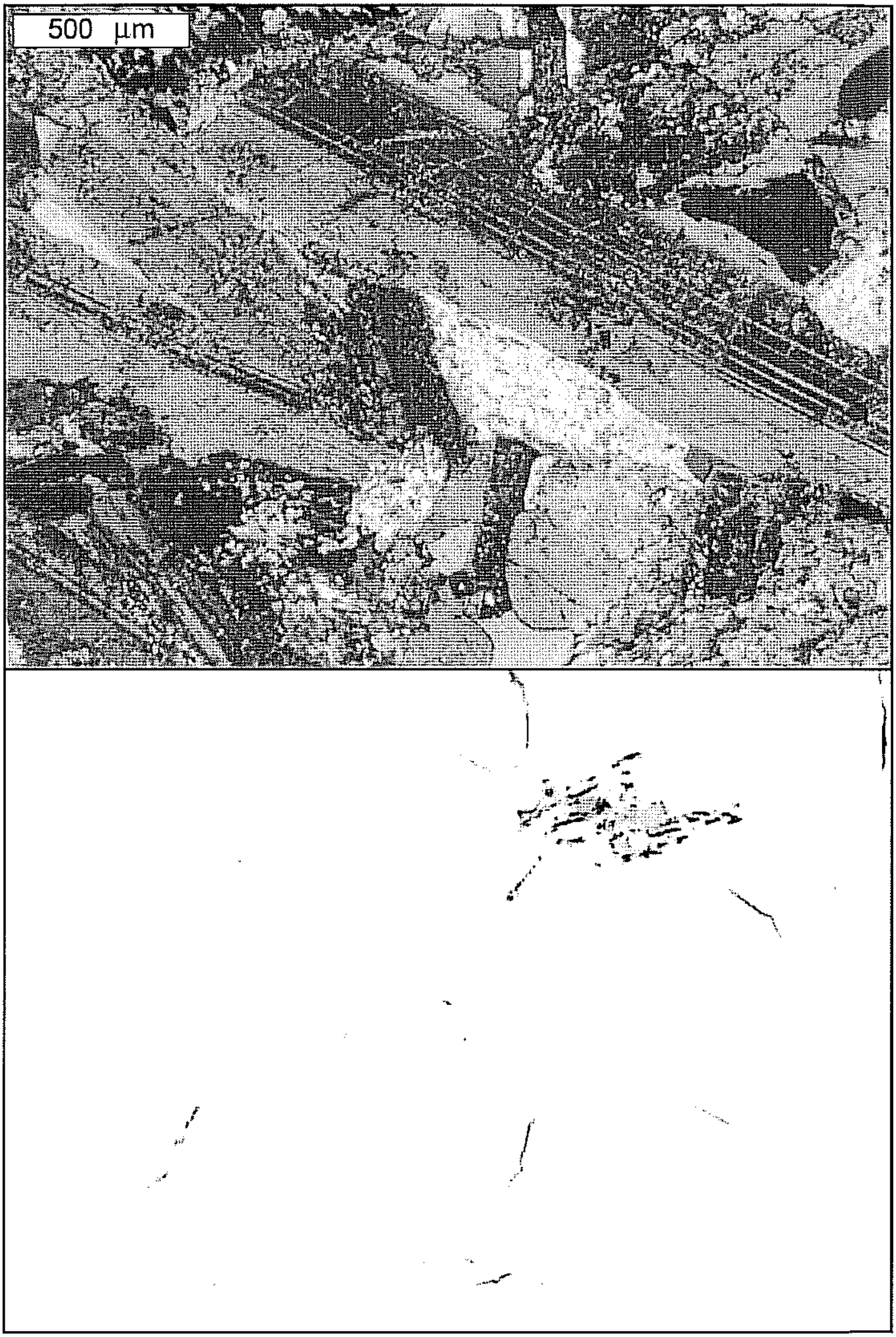

Figure A.11 Thin section of Ontario Trap Rock Diabase (95-010).

APPENDIX 3B

AGGREGATE DQI CORE

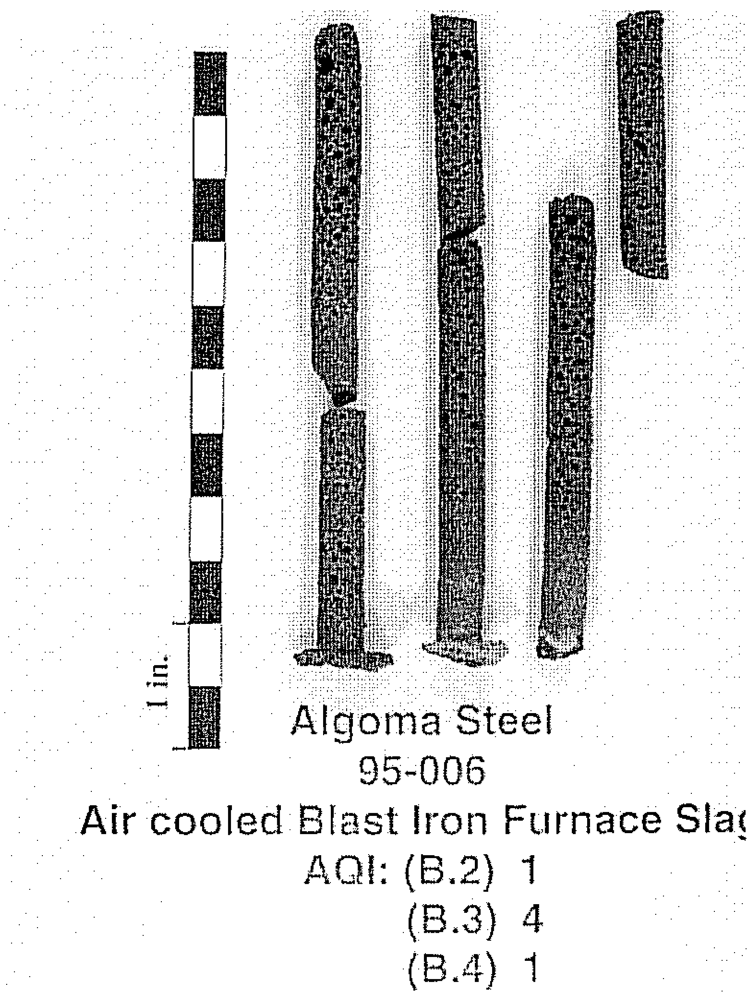

Figure B.1 Algoma air cooled Slag drill core.

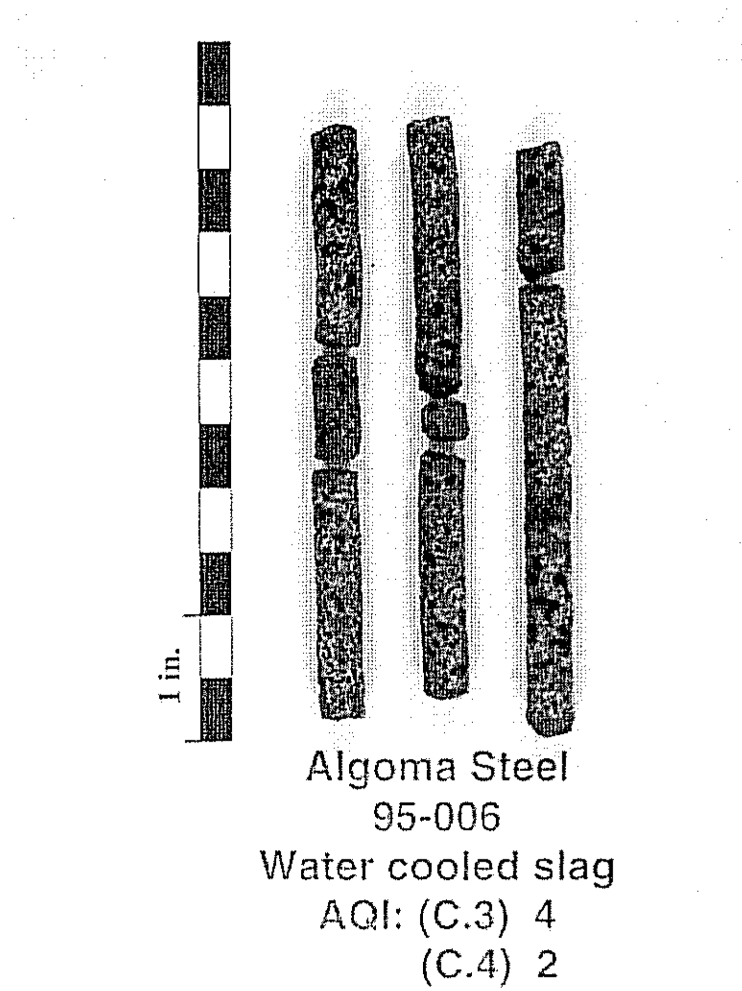

Figure B.2 Algoma slag water cooled drill core

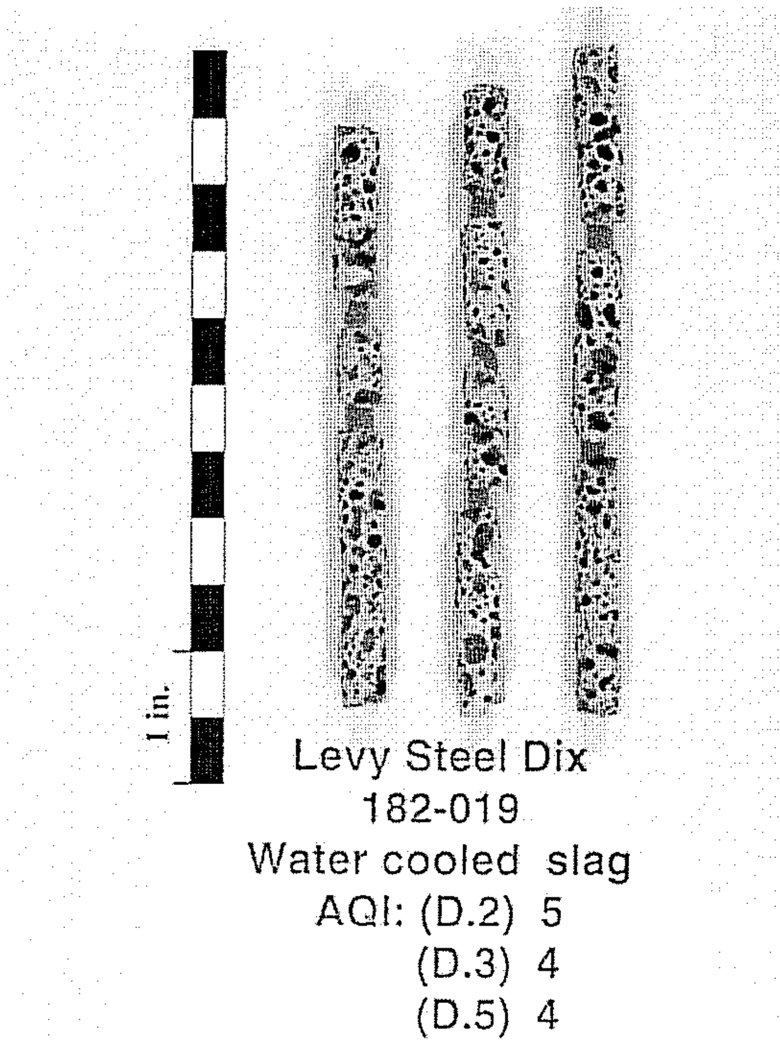

Figure B.3 Levy water cooled Slag drill core.

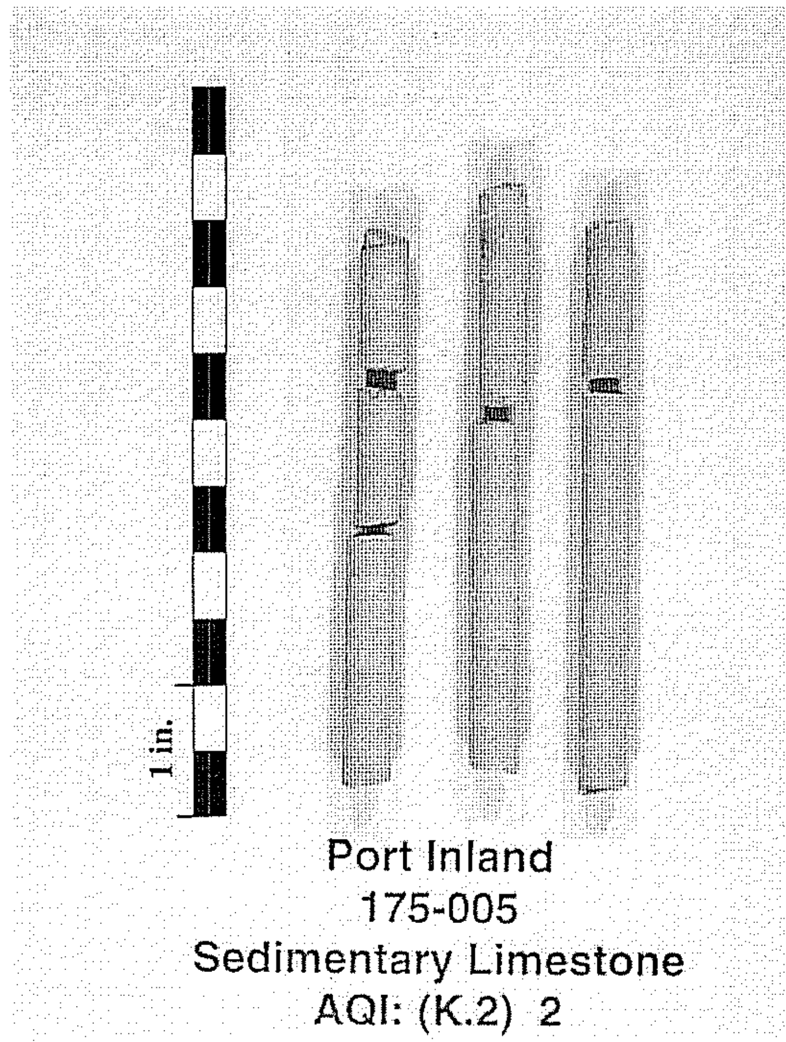

Figure B.4 Port Inland drill core.

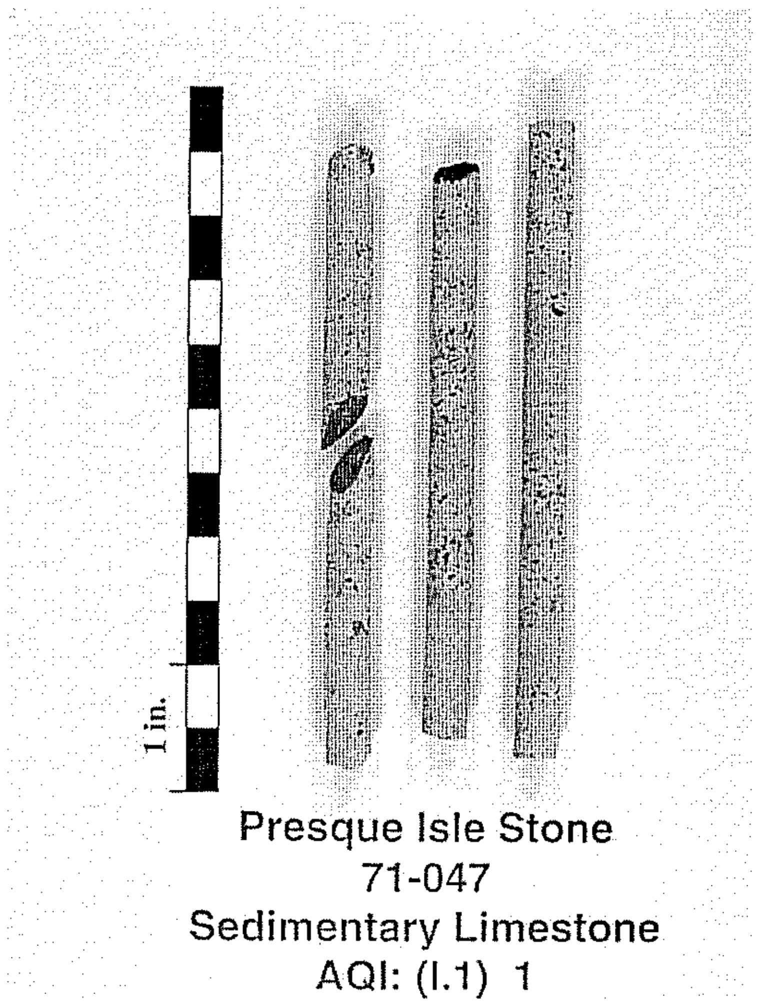

Figure B.5 Presque Isle drill core.

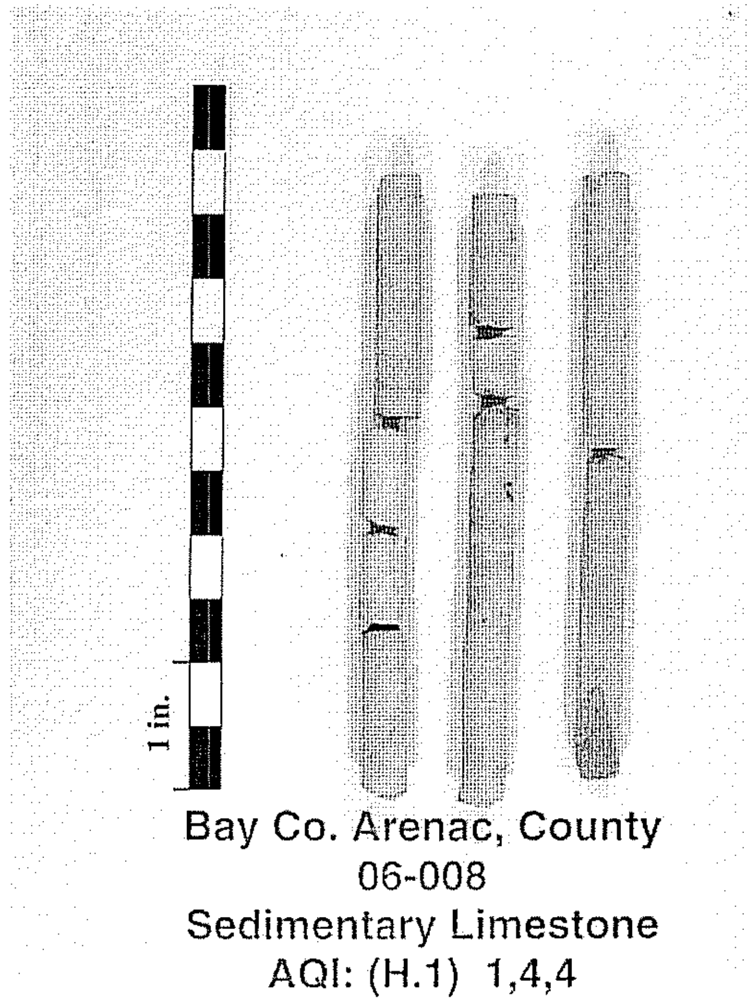

Figure B.6 Bay County drill core.

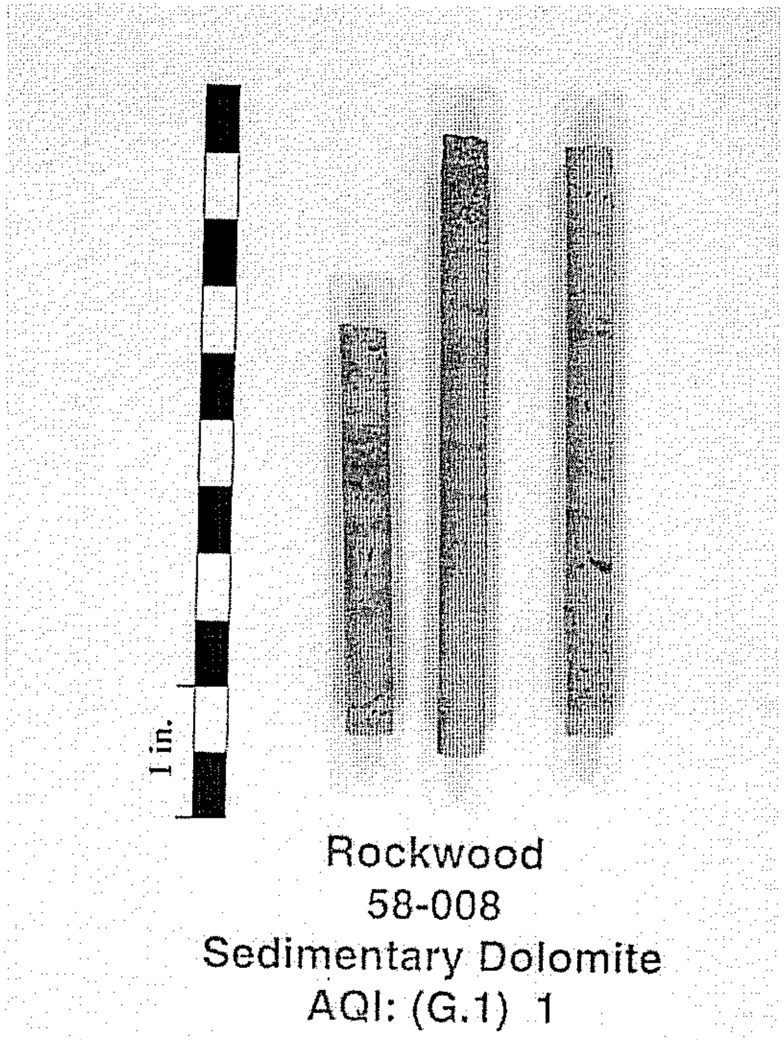

Figure B.7 Rockwood drill core.

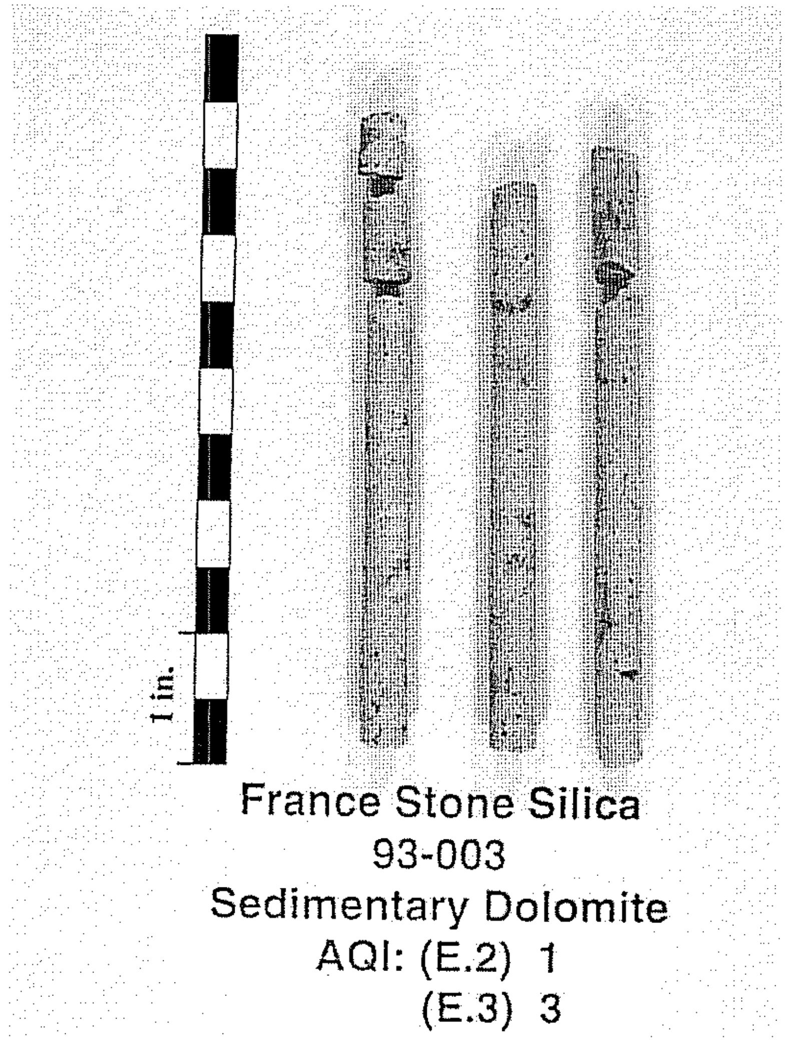

Figure B.8 France Stone drill core.

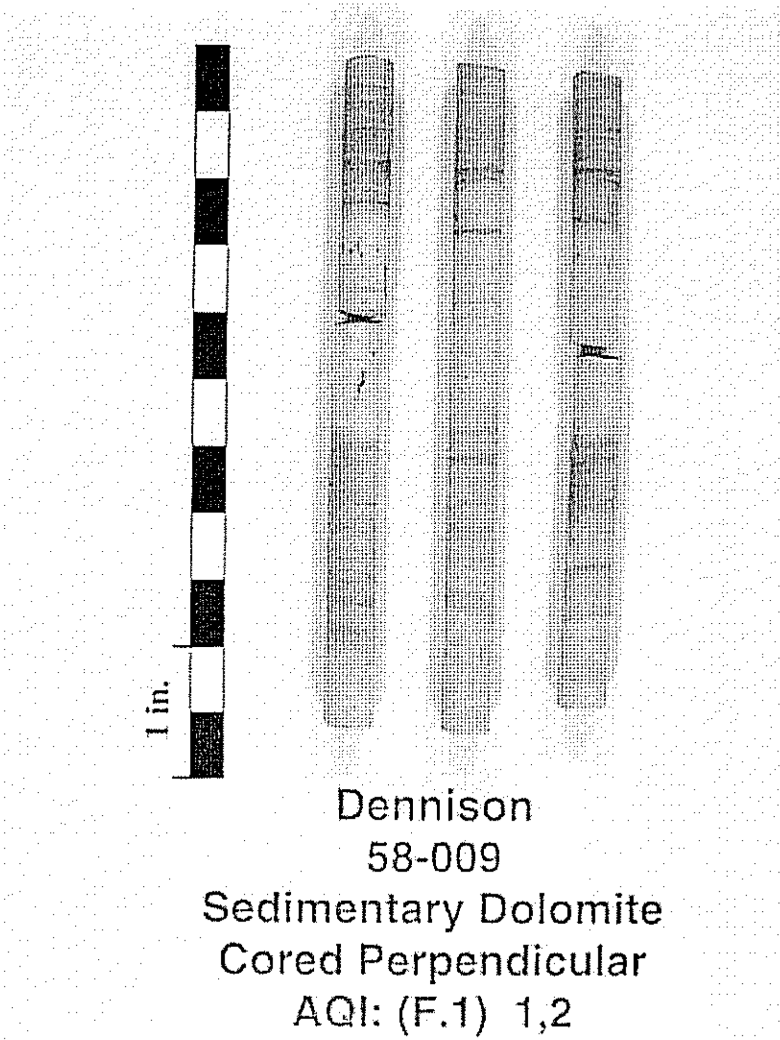

Figure B.9 Denniston Farms drill core.

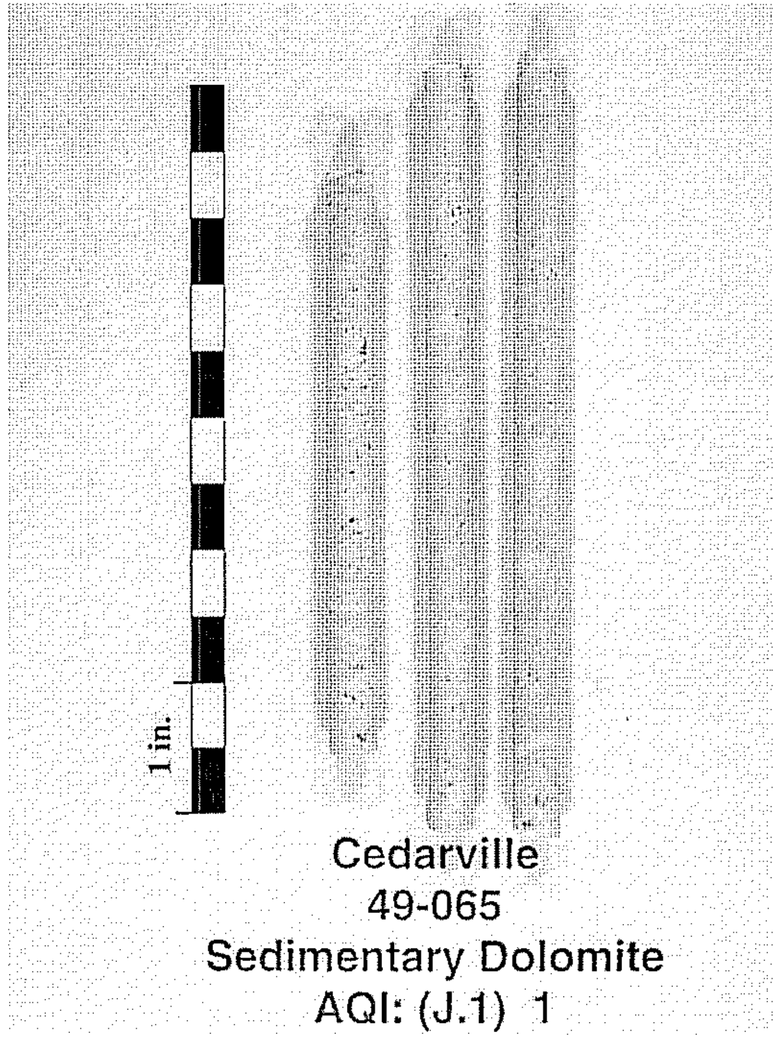

Figure B.10 Cedarville drill core.

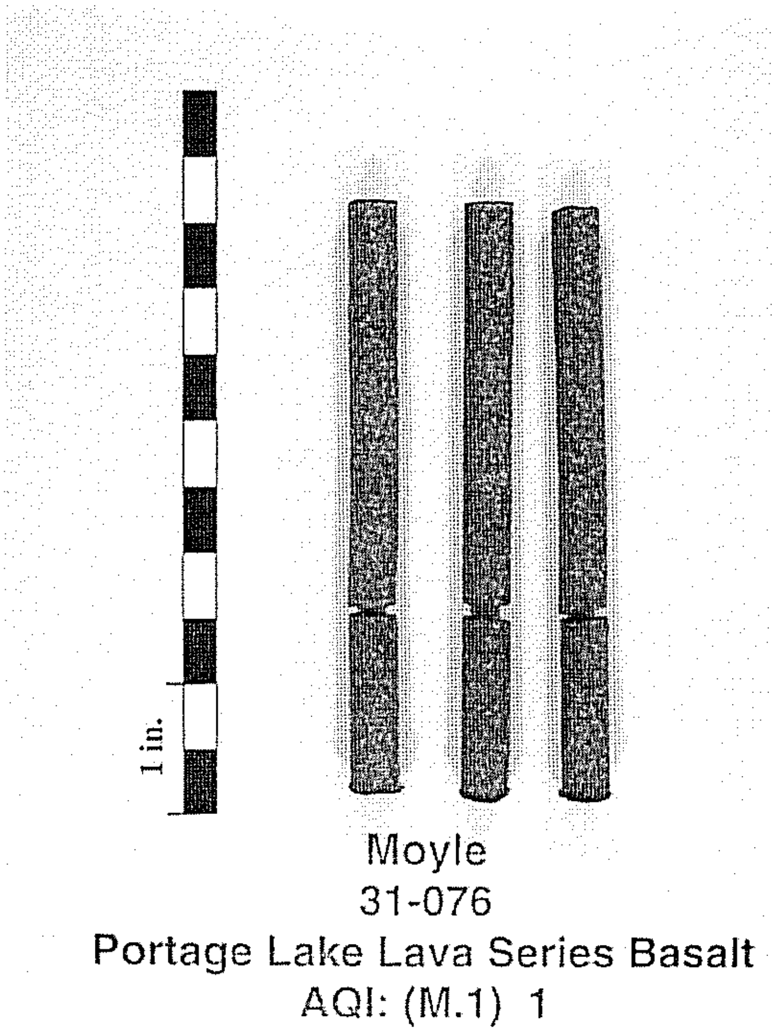

Figure B.11 Moyle drill core.

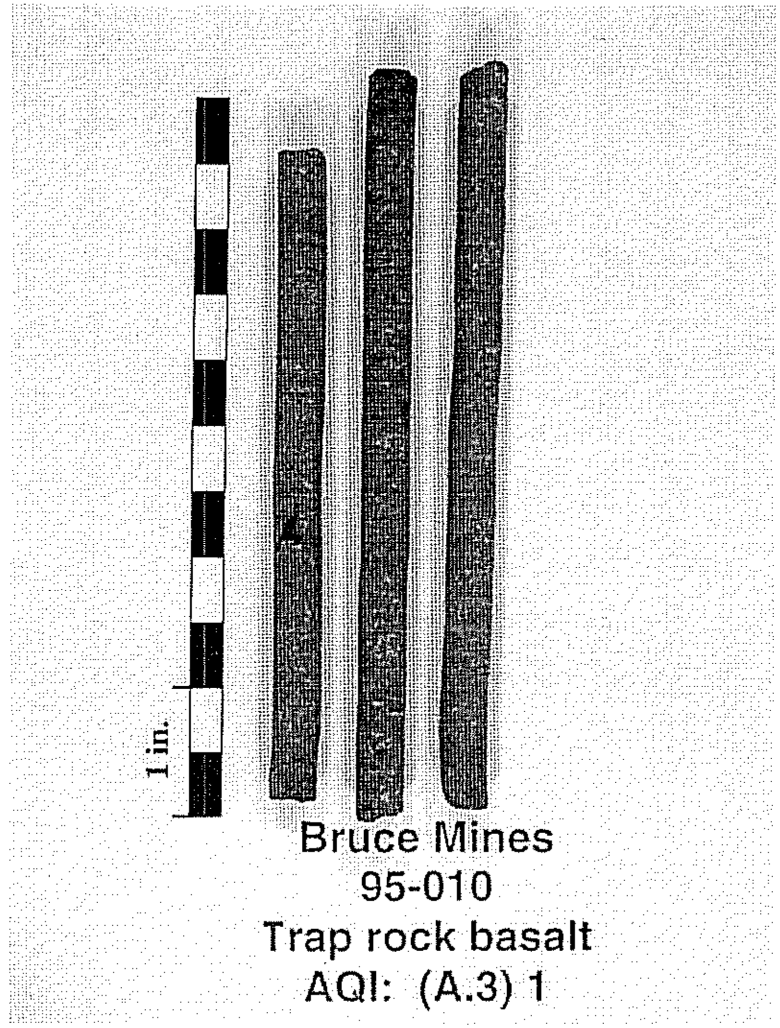

Figure B.12 Bruce Mines drill core.

REFERENCES

American Society for Testing and Materials, (1998), *Annual Book of ASTM Standards*, Vol. 04.02, Concrete and Aggregates:

ASTM C 39-96, Standard Test Method for Compressive Strength of Cylindrical Concrete Specimens.

Cohee, G.V. (1965), "Geologic History of the Michigan Basin," Washington Academy of Science Jurnal, Vol. 55, pp.211-223.

Deere, D.U. and Deere, D.W., (1988) The Rock Quality Designation (RQD) Index in Practice, Rock Classification Systems for Engineering Purposes, (ed. L.Kirkaldie), ASTM Special Publication 984, 91-101 Philadelphia: Am. Soc. Test. Mat.

Dorr, J.A. and Eschman, D. R., (1970) *Geology of Michigan*, University of Michigan Press, Ann Arbor, Mich., 476 p.

LaBerge, G.L. (1994) "*Geology of the Lake Superior Region*," Geoscience Press, Inc., Tucson, AR, 313 p.

MDOT, (1997) "Aggregate Source Inventory" Materials Testing Section, Materials and Testing Division, Lansing, MI, February

Smolczyk, H.G. (1980) "Slag Structure and Identification of Slags. *Inter. Congress on the Chemistr of Cement*, 7th ed., Paris a editions Septima, Pages 3-17.

Vitton, S.J. and Subhash, G.(1999) "Dynamic and Static Strength of Aggregates: An Estimate of Rate Sensitivity of Geologic Materials," Proceedings, Institute of Lake Superior Geology, 45th Annual Meeting, Marquette, MI, Vol. 45, part 1, pp 54-56.

Vitton, S.J., Lehman, M.A., and Van Dam, T.J., (1998) "Automated Soil Particle Specific Gravity Analysis Using Bulk Flow and Helium Pycnometry," *Nondstructive and Automated Testing for Soil and Rock Properties, ASTM STP 1350,* W.A. Marr and C.E. Fairhurst, Eds., American Society for Testing and Materials, pp. 3-13.

SECTION 4

Concrete Preparation and Initial Static Uniaxial Compression and Split Tensile Strength Testing

An initial step in this research was to first develop proper procedures for preparing consistent concrete for strength testing. To accomplish this the concrete was mixed and cured according to the MDOT modified mortar void method using a P1 mix design. This required that a procedure using the Michigan Tech lab equipment be established and used throughout this research. To establish this procedure as well as develop proficiency in the mixing process, a program was initiated to test concrete using three different coarse aggregate types. The program helped establish the concrete mixing. The second step was to investigate how different coarse aggregates, with a range of strengths, affect the compressive and tensile strength of the 28-day P1 concrete.

This section of the report presents the following results:

(1) A description of the MDOT modified mortar voids method used in this research,
(2) How the procedure was adapted at the Michigan Tech concrete laboratory and used to make concrete,
(3) The procedures used for handling and conditioning the coarse and fine aggregate,
(4) An analysis of three aggregate types to investigate how the MDOT mortar voids method varies with coarse aggregate types in uniaxial compression and split tensile testing, and
(5) A discussion concerning the results followed by conclusions and recommendations.

The research reported in this section was conducted by Bruce Hopkins at Michigan Tech and reported in a master's report titled "The Effect of Coarse Aggregate on Concrete Compressive and Tensile Strength." However, the thesis has been modified to a limited extent to conform to the overall report.

1 Introduction and Background

Traditionally, the coarse aggregate fraction of concrete has been made with natural aggregates such as gravels, carbonates, basalts and granites. Due to diminishing supplies of these aggregates, as well as the need to utilize by-product materials, a need exists to understand how the various material properties of the coarse aggregate affect the mechanical behavior of concrete. In general, the main performance criterion used in judging concrete quality is the 28-day uniaxial compressive strength test. To study how the compressive strength and split tensile strength of concrete varies with coarse aggregate, three aggregate types were compared. The coarse aggregates included in this study were basalt, natural gravel, and blast furnace slag. The selection of these material types was based primarily on the strength and shape of the three aggregates. The basalt was selected because it has the highest compressive strength and the most angular shape. The gravel has a relatively high compressive strength but a more rounded shape. Blast furnace slag is weaker in compression, but has a relatively rough surface (Vitton, 1998 b).

1.1 Background

A key portion (about 40 percent by volume) of concrete is the coarse aggregate, which is material larger than 4.75 mm (No. 4 sieve). In general, the material used as coarse aggregate varies from region to region, but typically must meet certain criteria for wear, absorption, and freeze-thaw durability. In this study crushed basalt, glacial gravel, and blast furnace slag were used to investigate how varying coarse aggregate properties may or may not affect concrete strength.

The basalt used in the study was obtained from an underground copper mining operation known as the Isle Royal Mines located near Houghton, Michigan. This mining operation ceased production in the 1930's. During the development of these mines, the basalt rock produced in the drilling and blasting for mine adits and drifts became known as "poor rock" due to the low concentrations of copper. These were considered as waste and were left stockpiled on the surface, termed as poor rock piles. Recently, these poor rock piles were purchased by local aggregate suppliers and crushed into various aggregate sizes.

Geologically, the basalt is of Precambrian age. It was formed as a flood basalt in association with the mid-continental rift zone. Due to the relatively quick cooling of the basalt as it flowed onto the surface of the earth; many gas bubbles were trapped as the lava cooled. Consequently, this basalt is known as amygdaloidal basalt, in which "amygdaloidal" is the term used for trapped gas bubbles. The flood basalts vary in thickness from a meter to ten meters. While the flood basalt was relatively uniform in composition, upon cooling, differentiation of minerals occurs with lighter minerals moving toward the top of the flow and denser minerals settling to the bottom of the flow. Therefore, obvious mineralogical differences occur in the basalt and subsequently in the crushed aggregate.

The glacial sand and gravel was obtained from an aggregate supplier in Hancock, Michigan. This operation mines sand and gravels from a glacial outwash, a deposit that formed during the last glacial episode. As is typical of glacial sand and gravel deposits, there is a very wide range of mineral types ranging from basalts to rhyolites to limestones. In general, rounded basalts and rhyolites dominate, with smaller quantities of limestone, indicative of the dominance of the local geology that consists of interbedded flood basalts and rhyolitic conglomerates. The sand portion, however consist primarily of quartz, with some feldspars present.

Blast furnace slag used in this study was from Detroit, Michigan. Slag is a co-product from the production of pig iron. In this process, iron ore, iron scrap, coke and either limestone or dolomite are added to the blast furnace. The coke combusts to produce carbon monoxide, which combines with the limestone and steel to form pig iron. Blast furnace slag is a nonmetallic byproduct, which contains mostly silicates, aluminosilicates, and calcium-aluminum-silicates.

Depending on the method of cooling, different forms of slag are produced, two of which are air-cooled and water quenched. A slag is formed when molten slag is placed in shallow beds and allowed to cool at ambient conditions in which a more crystalline structure is formed. This slag is typically referred to as air-cooled blast furnace slag (ACBFS). When liquid slag is cooled with the aid of water, it solidifies faster, due to increased thermal cracking of the material, producing a slag, which will be referred to as water quenched slag in this research. Physical properties of slag vary depending on the iron production process. For example higher unit weights are reported when slag contains more metals. This can result when more scrap iron is added to the blast furnace during the production of pig iron. The Federal Highway Administration (FHWA) reported a range of values for specific gravity from 2.0 – 2.5, compacted unit weight from 1120 – 1360 kg/m^3 (70 – 85 lbs/ft^3), and absorption ranging from one to six percent (FHWA, 1998).

ACBFS is used in granular bases, embankment and fills, and hot mix asphalt and Portland Cement Concrete (PCC) applications. While FHWA has user guidelines for these applications, the guideline for PCC only discusses ground granulated blast furnace slag. Currently, the FHWA does not address slag used as a coarse aggregate in PCC.

1.1.1 Previous Research

A study completed in 1933 used slag from two sources and gravel from one source as coarse aggregates for a strength comparison (Michigan State Highway Laboratory, 1933). In this study, the aggregates used were sieved into two uniform gradations and all mix designs were a six-sack mix. A sack is 43 kg (94 lbs) of cement. There were a total of four mixes with three of them containing the same blend of aggregate (one for each type of slag and one for the gravel) and the fourth had a finer blend of slag. This was done to show the effects of aggregate gradation on the strength of concrete. From each of the four mixtures, twenty beams and twenty cylinders were cast.

Axial compressive strength and modulus of rupture (MOR) tests were performed at 7 and 28-day periods on half the specimens made, i.e., ten tests per mix were performed at 7-days and then again at 28-days. In general, the results show slag had lower strengths for MOR and axial compressive strength at both test ages. Based on a 28-day cure, slag possessed an average of 11.6% lower axial compressive strength and a 5.1% less MOR strength than the concrete containing gravel. Also, there was no notable difference in strength when comparing the two slag mixes that contained different gradations. However, water-cement ratios were not consistent between the concrete mixes containing the different types of coarse aggregate possibly accounting for the variations in strength.

1.1.2 Mortar Voids Method

The Michigan Department of Transportation (MDOT) has been using a modified version of the mortar voids method to proportion concrete mix designs since 1928. Talbot and Richart first developed this method at the University of Illinois during the early 1920's (Shehan, 1970). Originally, the basic principal behind the mortar void theory was to seek minimum voids (air + water) in the concrete. Because coarse aggregate is assumed, for the most part, to consist of solid particles, the volume of voids in the concrete is said to be equal to the volume of voids in the mortar (sand, cement, air and water) for that concrete mix. The ratio between volume of voids and volume of cement is directly related to the strength of the concrete, if and only if the void spaces between the coarse aggregate particles are filled with mortar. It is known that the densest concrete mixture gives the highest strength concrete, but it is not necessarily the most durable. MDOT has specified air entrainment for all exposed concrete since 1942, which was done to improve durability. The recommended amount of entrained air specified is 6.5% with a tolerance of $\pm 1.5\%$ (MDOT, 1996). Due to the importance of void space for durability, the mortar void theory was altered to determine the minimum volume of water at the constant entrained air content.

The use of coarse aggregate in concrete is two fold, the first is to reduce volume change (reduce shrinkage) and the second is economy, since coarse aggregate is generally less expensive than cement. In addition, a concrete mixture should contain as much coarse aggregate as possible, while producing a workable mix. The limitation is that there must be enough mortar (sand, cement, air and water) to fill all the voids between the coarse aggregate particles.

The strength of hardened concrete depends upon the strength of the coarse aggregate as well as the strength of the mortar filling the void space between coarse aggregate particles. Two failure mechanisms are believed to be responsible when properly cured concrete fractures under an applied load. The first mechanism can be described as the break (or fracture mechanism), which is through or across the particles of coarse aggregate but not around them indicating that the coarse aggregate is weaker than the surrounding mortar (Shehan, 1970). The second failure mechanism is that "the break (or fracture) should be through some of the coarse aggregate particles with numerous particles pulled away from the mortar bond (as the fracture goes around the coarse aggregate)" (Grove, 1998). These fracture mechanics statements assume that the factors pertaining to the concrete mix remain constant and that the volume of coarse aggregate is not excessively high.

An MDOT laboratory procedure based on the above assumptions consists of a trial batch study using actual job materials. This laboratory procedure uses the job materials to determine the minimum voids at a constant entrained air content for the mortar. Results from the laboratory procedures determine several mix design parameters. After all laboratory work has been completed, a mix design is computed using the bulk dry specific gravity and absorption for both coarse and fine aggregates, as well as the dry loose unit weight of the coarse aggregate. The grade of concrete is also needed for the mix design. A complete description and detailed procedure of the mortar void method is discussed in the Mortar Voids Method of Proportioning Concrete, as used by the Michigan Department of State Highways (Shehan, 1970).

1.2 Research Objective

The main objective for this portion of the research was to determine the degree that the axial compressive and split tensile strength of concrete vary with coarse aggregate type using the MDOT Mortar Voids Method of Proportioning Concrete (Shehan, 1970). All of the concrete testing was conducted on 28-day concrete. To undertake this, three coarse aggregates were used representing a diverse selection of aggregate. The three aggregate types were basalt, glacial gravel, and blast furnace slag. An important issue in the research was to maintain a constant mix design with only the coarse aggregate as the variable (see Section 1.3). Consequently, MDOT guidelines and laboratory procedures were rigorously followed in this research program. This included a complete mixing procedure, as well as the testing methods for freshly mixed concrete.

1.3 Research Scope

Three types of coarse aggregate and one source of fine aggregate were considered in this research. Using a P1 mix design (MDOT, 1996, Section 601), three separate mix "recipes" were determined for the three different coarse aggregates because of the varying properties of each aggregate. This section provides the results for 28-day axial compressive and split tensile strength tests for the concrete made with each of the three types of coarse aggregates. Along with the testing results, the method for mixing the concrete used in this research, which was in accordance with MDOT specifications, is presented.

2 Materials and Casting Methods

The concrete tested in this project consisted of the following materials: cement, coarse and fine aggregates, air entrainer and water. There were no other admixtures used in any of the mix designs. Water used for all concrete was Houghton City water, which came directly from the tap located in the concrete mixing laboratory (B006) of Dillman Hall at Michigan Technological University (MTU). A measured quantity of water was placed in sealed five-gallon containers one day prior to casting a batch of concrete. This was done so the water would be at room temperature by the time a batch was mixed. Each of the remaining constituents is described in the following sections. ASTM procedures were followed with exceptions, where noted.

2.1 Cement

Lafarge (Alpena) Type I cement, which conformed to ASTM C 150-97, was used throughout the entire study. The manufacturer specified specific gravity used for all design calculations was 3.15. Cement was packaged in 43 kg (94 lbs) sacks. In order to eliminate as many variables as possible, care was taken in handling of cement. The cement was measured out to the exact amount needed to produce one batch of concrete (6 ft^3), then placed in moisture proof buckets with tight sealing lids and stored in the concrete mixing laboratory in Dillman Hall. An Ohaus electronic scale with a capacity of 100 kg (220 lb.) and a readability of 0.01 kg was used to weigh the cement.

2.2 Aggregates

As mentioned three types of coarse aggregate and one type of fine aggregate were used for this study. The coarse aggregates chosen included a basalt mine rock, glacial gravel and an iron blast furnace slag. The fine aggregate was natural silica sand. All aggregates were sampled at their sources and brought back to MTU for storage. MDOT source numbers, aggregate types and the reference name used in this report are listed in Table 2.1. A description of each type of aggregate follows herein.

Table 2.1 Aggregate Source Numbers and Reference Names

Reference Name	MDOT Source No.	Agg. Type	% crushed
CA-B	31 - 076	Moyle basalt	100
CA-G	31 - 045	Glacial gravel	50
CA-S	82 - 019	Levy blast furnace slag	100
FA-Y	31 - 045	Natural silica sand	-

In Table 2.1 the reference name listed, e.g., CA-B, will be used throughout this chapter to refer to the concrete made with each of the coarse aggregates. The "CA" stands for coarse aggregate, while the "B" stands for basalt and therefore CA-B would be concrete made with basalt as the coarse aggregate.

Two of the coarse aggregates used for this study were locally available from the Houghton/Hancock area of Michigan. A 100% crushed (highly angular) basaltic mine rock (Moyle, 31-076) was one of the chosen aggregates. This aggregate varied in color from a dark gray to a medium green and contains amygdaloidal inclusions or gas bubbles. In general, the mineralogy consists of pyroxenes and quartz. A 50% crushed glacial gravel (form the Superior Sand and Gravel company, 31-045) was the second coarse aggregate used for the study. The glacial gravel was non-uniform in color and contained a number of different minerals but was mostly composed of quartz and feldspars. These two aggregate types were chosen based on their characteristics, availability and location.

As mentioned, slag is a manufactured aggregate produced as a by-product in the production of pig iron and contains mainly silicates and calcium. The material floats to the top of the blast furnace and is released from the base of the blast furnace after the heavier pig iron has been removed. When the slag is poured into the yard it is generally water quenched but in the past has been air-cooled. Once the slag is cooled, it is broken up and brought to the aggregate pit where it was crushed down and sieved to the proper gradation for stockpiling. As discussed in Chapter 3 water-quenched slag was used in this project. The slag was also 100% crushed.

Sieve analysis was performed on both fine and coarse aggregates using the ASTM C 136-96a procedure. The coarse aggregates were mechanically sieved into four size fractions (1) 25.0 – 19.0 mm (1 – 3/4 in.), (2) 19.0 – 12.5 mm (3/4 – 1/2 in.), (3) 12.5 – 9.5 mm (1/2 – 3/8 in.) and (4) 9.5 – 4.75 mm (3/8 in. – No.4). Immediately after sieving, the aggregate was placed in plastic containers (one container for each size fraction), and covered with tight sealing lids to avoid contamination. A test blend was later created with 25% by weight of each size fraction. This test blend was chosen to produce a uniform gradation, which would pass the MDOT 6AA gradation limits. A standardized test blend also helped to eliminate any effect that various gradations might have on the results, i.e., the same test blend was used throughout the project. For example, specific gravity experiments used 5000 g (11.0 lb.) sample sizes, and the test blend would contain 1250 g (2.8 lb.) of each size fraction.

The fine aggregate was locally available natural silica sand from the Superior Sand and Gravel Company (31-045) in Hancock, Michigan. This fine aggregate was used throughout this study for the primary purpose of eliminating any effect that the use of several types may have had on the research results. Due to storage limitations, however, sand had to be obtained from the source three times. Grain size distribution charts with MDOT specified gradation limits for 6AA coarse and 2NS fine aggregates are provided in Figures 2.1 and 2.2, respectively (MDOT, 1996, Section 902). The grain size distribution curve for fine aggregate was an average of several sieve analyses performed. At least one sieve analysis was performed whenever new aggregate was obtained. The fine aggregate fell within the limits specified for a 2NS aggregate. The fine aggregate had an average fineness modulus of 2.67. To avoid contamination the sand was stored in large plastic containers with tight fitting lids.

Each aggregate in this study was tested to determine apparent specific gravity (G_S), bulk dry specific gravity ($G_{B(DRY)}$), bulk saturated surface dry specific gravity ($G_{B(SSD)}$), percent absorption, and unit weight. Samples of all coarse and fine aggregates were sent to MDOT, where specific gravity and absorption tests were conducted following ASTM C127 for coarse aggregate and C128 for fine aggregate. Companion tests were performed at MTU where specific gravities and absorption values for coarse aggregate were determined according to ASTM C127-88, while ASTM C 128-93, for measuring the specific gravity and absorption of the fine aggregate, respectively. In addition, the same properties were measured at MTU using automated methods (Vitton et al., 1998 a). Dry loose unit weights were also measured at MTU according to the shoveling procedure stated in ASTM C 29-97. Results from these tests are listed in Table 2.2.

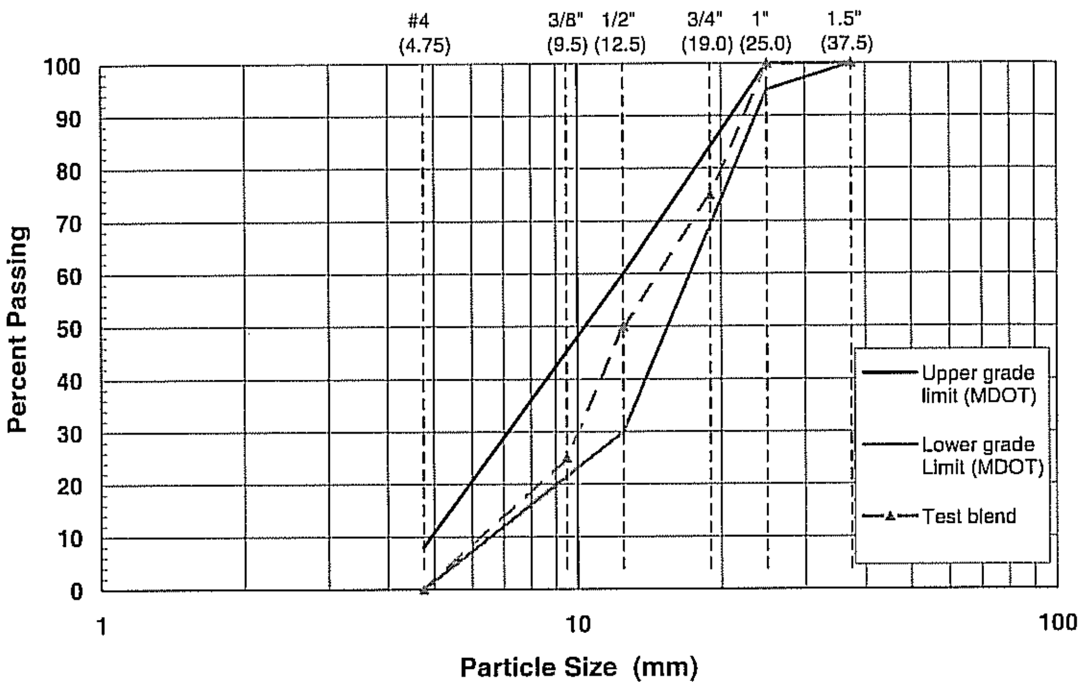

Figure 2.1. Grain Size Distribution for Test Blend 6AA Coarse Aggregate and MDOT Specified Grade Limits.

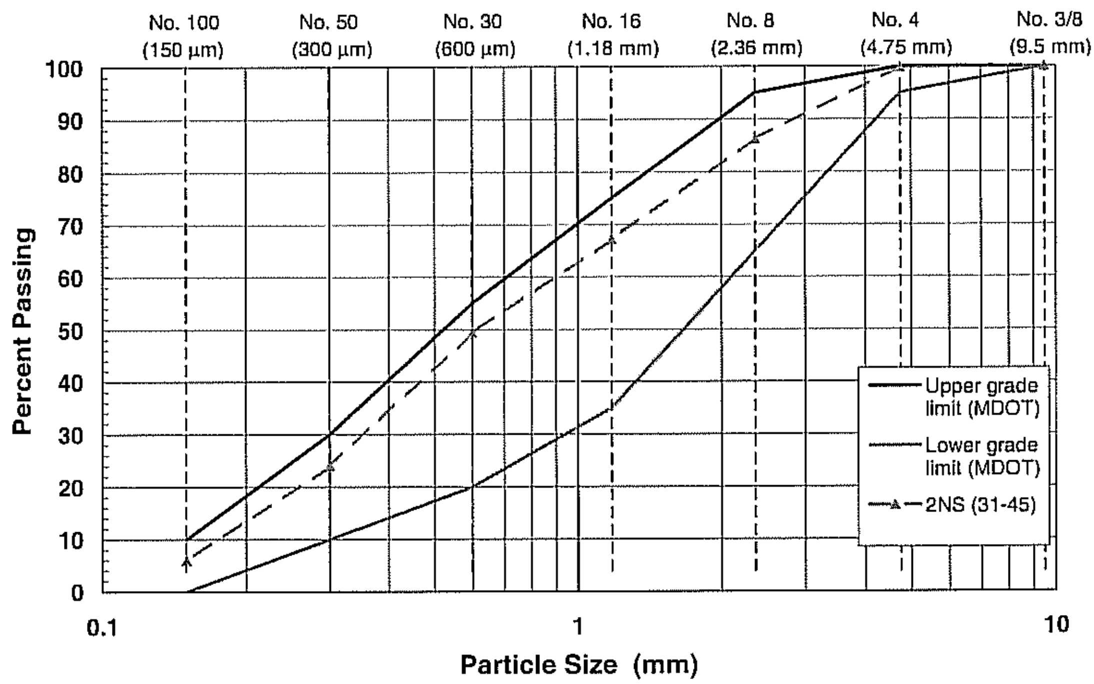

Figure 2.2. Grain Size Distribution for 2NS Fine Aggregate and MDOT Specified Grade Limits.

Table 2.2 Summary of Aggregate Properties

Aggregate Type	Tested by	Apparent Specific Gravity G_S	Bulk SSD Specific Gravity $G_{B(SSD)}$	Bulk Dry Specific Gravity $G_{B(DRY)}$	Absorption %	Unit Weight kg/m^3 (lb/ft^3)
CA-B (basalt)	MDOT	2.91	2.83	2.79†	1.45†	-
6AA Coarse Aggregate	MTU	2.91	2.82	2.78	1.54	1510 (94)†
Source # 31 – 76	Automated	2.89	2.82	2.78	1.44	-
CA-G (glacial gravel)	MDOT	2.83	2.76	2.73†	1.35†	-
6AA Coarse Aggregate.	MTU	2.83	2.76	2.72	1.48	1556 (97)†
Source # 31 – 45	Automated	2.79	2.72	2.69	1.46	-
CA-S (slag)	MDOT	2.47	2.35	2.27†	3.55†	-
6AA Coarse Aggregate.	MTU T1‡	2.68	2.56	2.49	2.74	1212 (76)†
Source # 82 – 19	MTU T2‡	2.71	2.44	2.29	6.76	
	Automated	2.85	2.49	2.29	8.49	-
FA-Y (silica sand)	MDOT	2.73	2.68	2.67†	.87†	-
2NS Fine Aggregate.	MTU	2.75	2.69	2.65	1.30	1728 (108)
Source # 31 – 45	Automated	2.72	-	-	-	-

† Used for mix designs.
‡ MTU Trials 1 and 2, respectively.

Worksheets for computing the specific gravity of the coarse and fine aggregates as tested by MTU are included in Appendix IV-A. For each aggregate, a minimum of three tests were performed to determine average values for G_S, $G_{B(SSD)}$, $G_{B(DRY)}$, and percent absorption. G_S is defined as the oven dry weight of coarse aggregate divided by the apparent volume (no permeable voids included in the volume). $G_{B(SSD)}$ is the saturated surface dry weight of the coarse aggregate divided by the envelope volume (permeable voids included). The oven dry weight of the coarse aggregate divided by the envelope volume is equal to $G_{B(DRY)}$. Each worksheet includes the raw data and the formulae used for computations as well as a summary of average values. These average values were listed in Table 2.2 under the heading MTU. For the case of CA-S, two trials were performed according to the optional procedures allowed by ASTM C127-88. The first trial used a gentle stream of moving air to bring the aggregate to the saturated surface dry condition. The procedure for trial two was to roll the aggregate on towels until the saturated surface dry condition was obtained. Results of each trial are tabulated in Table 2.2 and included in Appendix IV-A.

The three test methods (MDOT, MTU, and Automated) used to determine G_S, $G_{B(SSD)}$, $G_{B(DRY)}$, and absorption were in good agreement for both CA-B and CA-G. Test methods used to determine specific gravity and absorption values for slag did not compare well with one another even though an additional trial was performed by MTU. Because MDOT has more experience working with slag than does the author, and the three methods compared well for CA-B and CA-G, it was decided to use the MDOT values for specific gravities and absorption for both fine and coarse aggregates in the mix designs used in this study.

2.3 Mix Designs

The mortar voids method (Shehan, 1970) for proportioning concrete mixtures was used to determine all mix designs. A standard six-sack grade P1 Portland Cement Concrete (PCC) pavement mix (MDOT, 1996, Section 601) was used in this project. Quantities for each mix design constituent were calculated by MDOT (MDOT Form 1830, File 300, 1998 and included in Appendices B through D of this report). This method of mix design used bulk dry specific gravity for both coarse and fine aggregates. A workability factor (b/b_o) of 0.72, defined as the volume of dry loose coarse aggregate per unit volume of concrete was also used as a mix design parameter. A target slump of 51 - 76 mm (2 – 3 in.) and an air content of 5% ± 1.5% was considered an acceptable batch. The three mix designs, one for each type of coarse aggregate, are listed in Table 2.3.

Table 2.3 Mix Design Proportions, per m^3

	Coarse aggregate type		
	CA-B	CA-G	CA-S
Cement	335	335	335
Coarse agg. (dry)	1087	1120	873
Fine agg. (dry)	791	743	803
Water	165	162	181

Note: All quantities in kg/m^3 (1 kg/m^3 = 1.69 lbs/yd^3).

"Mixing Proportion" worksheets used for computing the proper amount of each constituent per batch of concrete are included as the first page in Appendices IV-B, IV-C, and IV-D corresponding to the three mix designs, CA-B, CA-G, and CA-S, respectively. There is one mix proportion worksheet for each type of coarse aggregate used in this project. MDOT provided values for each material used to make 1 m^3 of concrete (Table 2.3) are shown on each worksheet (MDOT Form 1830, File 300 and included in Appendices IV-B through IV-D of this report). These worksheets were developed to compute quantities for each constituent used to make a 0.078 m^3 (2.75 ft^3) batch of concrete as well as the total amount of absorbed water per m^3. Batch computation worksheets that follow the mix proportion worksheets in each of these appendices are discussed in Section 2.4.

2.4 Aggregate Preparation

A two-step preparation process was used for all coarse aggregate. First, forty-eight hours before mixing concrete, a specified amount of coarse aggregate was oven dried for 24 hours. Each size fraction was kept separate. A tare weight of pails used for soaking aggregate was measured and recorded on the batch computation worksheet. Because of batch size, two containers were used for soaking the coarse aggregate with two of the four size fractions in each container. Each individual size fraction of coarse aggregate was then measured in the dry condition and placed in a container. Finer material was placed at the bottom of the container and the coarser material on top, i.e., materials retained on the 4.75 mm (No. 4) and the 19 mm (3/4 in.) sieves were placed in the first pail with the 4.75 mm aggregate at the bottom of the container. This was done to help hold the finer material in place during the later decanting process of the coarse aggregate.

Second, the aggregate was soaked in water for 24 hours before it was used to make a batch of concrete, which is referred to as moisture conditioning. All aggregates were weighed using an Ohaus electronic scale with a capacity of 100 kg (220 lbs) with 0.01kg (0.01lbs) readability.

Third, the fine aggregate was moisture conditioned for 24 hours before it was used to make a batch of concrete. A fixed drum refractory mortar mixer (10 cubic foot capacity, 10 HP (220 volt), Anchor Manufacturing Co., Chicago, IL) was used for the conditioning. The fine aggregate was first placed in the mixer. While the mixer was running, water was added until the aggregate was moistened slightly above the saturated surface dry condition. A simple test was performed to determine if enough water had been added to the sand. This was accomplished by taking a handful of sand and squeezing it together then letting go. If enough water has been added the sand should just start to clump in the hand. After the sand was moisture conditioned, the mixer was covered with plastic bags and a tarp to help minimize evaporation of water from the sand.

All of the batch computations worksheets for the mixes used in this research are provided in Appendices IV-B, IV-C, and IV-D. Consequently, there is one worksheet for every batch of concrete made. Two batches are included for both CA-B (basalt) and CA-G (glacial gravel), while four batches are presented for CA-S (slag). Included in the coarse aggregate data block on each sheet are pail tare weights and the quantities of coarse aggregate per size fraction. The fine aggregate data block has values for moisture content and the total amount of sand per batch. First the moisture content was calculated then multiplied by the design quantity of fine aggregate to obtain the moisture (amount of water) in the fine aggregate. The moisture was then added to the design weight of fine aggregate. Design weight equals the total amount of aggregate needed to make a batch of concrete.

2.5 Air Entraining Admixture

The air-entraining admixture used for the project was Master Builders Neutralized Vinsol Resin Solution (MB VR) conforming to ASTM C 260-86, which was supplied by MDOT. MB VR admixture has no standard dosage rate, but the manufacturer recommends a dosage rate of 16 to 260 mL/100 kg (1/4 to 4-fl oz/100 lbs) of cement should be used for a trial mix to achieve the desired air content. There are many factors that affect the dosage rate of MB VR including cement type, slump, percent of fine materials, sand gradation, temperature, batch size and type of mixer. Due to the number of factors involved in proportioning air entrainment, a trial and error method was used for determining the proper amount of admixture for each mix design. A range between 19 to 28 ml was found to give the best results to achieve the target value for air content. Proper storage of MB VR was important because exposure to air will decrease its effectiveness. A one-gallon glass container with an airtight lid was used for storing air entrainer. Air entrainer was then measured immediately prior to batching using a plastic graduated cylinder with a least readable division of 1mL. The actual quantity used in each batch of concrete is included on the batch computation sheets in Appendices IV-B, IV-C, and IV-D for each of the three respective mixes.

2.6 Mixing and Casting

All concrete was made and cured at MTU in the concrete laboratory (B006) of Dillman Hall. A three-blade rotating drum mixer powered by a one horsepower (115 volt) electric motor with a six cubic foot capacity was used to make all concrete. A batch size of $0.078m^3$ ($2.75\ ft^3$) was used, which was enough concrete to cast eight cylinders and perform the following tests: one unit weight, one air content and one slump test. All concrete used for unit weight, slump, and air content testing was discarded in order to minimize the effects of aggregate segregation in casting the test cylinders.

Standard 152 x 305 mm (6 x 12 in.) plastic cylinder molds were used to form all concrete cylinders. These cylinder molds conformed to ASTM 470-94 with the exception that a hole was drilled in the bottom of all molds and some molds were reused. Prior to reuse, cylinder molds were visually inspected for defects such as rounding of edges and any cracks or scratches. If any defects were found, those molds were discarded. No molds were used more than twice. A small paper disk was placed inside the mold covering the hole at the bottom and a piece of duct tape was applied to the outside bottom over the hole. This was done to ensure no loss of moisture while the specimen was curing. Each mold was oiled at least 30 minutes prior to use with Clean Strip Form Release Oil.

Each batch of concrete was made in a buttered mixer. Buttering was accomplished by mixing a sand cement mixture with enough water added to make it about the same consistency as a batch of concrete. This mixture was then smeared on the inside the mixer coating it evenly. The excess material was scraped out so that no clumps existed on the inside of the mixer. During the three-minute rest period (discussed in Step

11 of Section 2.6.1) the mixer was scraped down to remove any material that had adhered to the sides. This was done to ensure thorough mixing of all constituents.

2.6.1 Mixing Procedure

The following mixing, casting and testing procedures were used. Batch computation worksheets for each batch were previously discussed. Reference to such worksheets is made in general terms.

1) Lay out all tools and equipment needed.
2) Paper, tape and oil cylinder molds.
3) Calculate moisture content of fine aggregate (FA), (ASTM C 566 microwave method). Multiply design weight of FA by the moisture content, to obtain the amount of water (moisture) in the FA. Add this value back to the design weight of FA to compute the total amount of FA needed for the batch. (See batch computations worksheet).
4) Weigh cement and reserve water.
5) Measure air-entraining admixture.
6) Decant water from coarse aggregate (CA). Weigh each container and add back the amount of water needed for the batch minus a known quantity of reserve water, e.g., 3 kg (6.61 lbs). Cover containers so that no moisture is lost. Use only room temperature water. (See water measurement data block on batch computation worksheet).
7) Weigh out FA from step 3. Cover containers as above.
8) Butter the mixer. Use three shovels full of FA and two scoops of cement (not from either the FA or cement already measured out). Add enough water to produce the same consistency as the batch to be made, i.e., a 51 – 76 mm (2-3 in.) slump. Coat the inside of mixer completely; scrap out excess material and discard.
9) Add materials to mixer in the following order.
10) CA with water (from CA containers, not reserve water).
11) Air entraining admixture- rinse graduated cylinder out completely using a portion of the reserve water and pouring this into the mixer as well.
12) Add FA.
13) Start mixer and add cement while starting timer as soon as all the cement is added.
14) Mix for 3 minutes. During the first 2.5 minutes, add enough reserve water to achieve the desired consistency, i.e., 51 – 76 mm (2-3 in.) slump. Add small quantities at a time, being careful to not add too much water. Concrete should fall off the blades and no concrete should be stuck to the sides of mixer. If there is any stuck to the sides, then more water is needed. No water should be added in the last 30 seconds of mixing time.

15) Rest for 3 minutes. Scrap down mixer if needed. Take temperature of concrete in accordance with ASTM C 1064-86(1993). Determine if more water needs to be added (if the mixer had to be scraped then more water is needed). Testing equipment for step 15 should be in the damp condition now.
16) Mix for 2 minutes. Add more water if needed in very small amounts. Again, no water should be added in the last 30 seconds of mixing time.
17) Weigh the remaining reserve water plus container (surplus + tare) and record on batch computations worksheet in reserve water data block.
18) Discharge concrete into a clean damp pan.
19) Perform tests on freshly mixed concrete.
20) Slump (ASTM C143-90a) completed in the first 2.5 minutes from discharge.
21) Unit weight (ASTM C 138-92).
22) Air content (ASTM C 173-94a).
23) Cast concrete cylinder specimens (ASTM C 192-90a). Cover with tight sealing lids and place in curing room.
24) Record all values (air entrainment used, temperature and test results from step 15) on batch computation worksheets as well as the time and date the batch was made.
25) Perform yield data calculations. (See Section 2.7).

2.7 Yield Data and Report of Test

"Yield Data" worksheets are provided in Appendices IV-B, IV-C, and IV-D of this report for the three respective mixes using three different coarse aggregates (basalt, glacial gravel, and iron blast furnace slag). Each worksheet includes yield data for all batches made using a specific aggregate. Yield data includes calculated values for unit weight of concrete, batch volume, cement used for 1 m^3 of concrete, net water used for 1 m^3 of concrete, and water-cement ratio for each batch that was cast. Formulae used for each computation are also included on the worksheets. A "Report of Test" worksheet follows the yield data sheet in each of the same appendices.

"Report of Test" worksheets include unit weight of concrete, actual cement content, slump, air content, and water-to-cement ratio (w/c) for each batch, in addition to an average value for each quantity. These average quantities are summarized in Table 2.4. Average values for both of these items are also included on the worksheet. A summary of coarse aggregate properties is shown there as well. Other test results listed on the "Report of Test" worksheets include compressive strength (discussed in Section 3.1), and split tensile strength (discussed in Section 3.2).

Table 2.4 Summary of Yield Data

	Coarse Aggregate Type		
	CA-B†	CA-G†	CA-S‡
Slump (mm)	67	64	59
Unit weight (kg/m^3)	2391	2377	2249
Actual cement content (kg/m^3)	334	336	342
Water/cement ratio (by weight)	0.47	0.46	0.46
Air content (%)	5.6	4.6	4.3
Compressive strength (MPa)	41.0	41.4	45.0
Split tensile strength (MPa)	3.49	3.54	3.95

(1 kg/m^3 = 1.69 lb./yd^3) (1 mm = 3.94 x 10^{-2} in.) (1 MPa = 145.0 psi)
† Average of two batches.
‡ Average of four batches.

2.8 Curing, Stripping, and Capping

Following cylinder casting (Step 16, Section 2.6.1), cylinders were immediately placed in a 100% humidity curing room. Cylinders were stripped 24 ± 8 hours after casting and labeled, then immediately returned to the curing room. The curing room was constantly maintained to ensure a 100% humid environment so that cylinders had free water on all sides during the 28-day curing period. When cylinders were taken to be capped or strain gagged, wet towels were wrapped around them to keep them moist. Capping took place when the cylinders were 26-days old in accordance with ASTM C 617-94. Forney Hi-Cap High–Strength capping compound was used for capping all cylinders. Cylinder caps were inspected daily for any defects such as debonding caused by shrinkage. If any such defects were found, cylinders were recapped and returned to the curing room until the time of testing.

3 Experimental Procedure and Results

The three mix designs used to make concrete tested for this project were the same with the exception of coarse aggregate type. All concrete was batched and cured in one location as discussed in Chapter 2. Because the curing facilities and testing laboratory were located in two separate buildings at MTU, cylinders were wrapped in wet towels and covered in heavy canvas for transportation and short-term storage. This was done to ensure cylinders were tested in the moist condition. It also helped to reduce surface shrinkage and residual stresses that could have caused premature failure. Experimental procedures and results for axial compression, splitting tensile strength and strain gaging are presented below.

3.1 Compressive Strength

Concrete cylinders were tested for compressive strength in the Rocks Mechanics Laboratory located in the Mining and Materials Building at MTU. A MTS load frame that had a capacity of 4448 kN (1,000,000 lbs) was used for all compression and split cylinder testing. The load frame has a mass of 6,360 kg and is considered a very stiff frame. Figure 3.1 illustrates the general configuration of the uniaxial testing. An Instron 8500 controller connected to a personal computer with Instron Series IX software operated the load frame. The compression machine hydraulically loaded a specimen in either displacement or load control and met the requirements of ASTM C 39-96.

Standard 152 x 305 mm (6 x 12 in.) concrete cylinders tested were at 28 days and followed ASTM C 39-96 procedure except for rate of loading. Actual load rate was 133 kN/min (30,000 lb./min), which was 12% slower than the minimum ASTM specified rate of 151 kN/min (34,000 lb./min). A shunt-cal calibration system was used to calibrate the machine before a precapped cylinder was placed on the bottom platen. The bottom platen, along with the specimen, was then raised until it was about 10 mm (0.4 in.) from the top platen where it was then centered in the machine. A seating load of

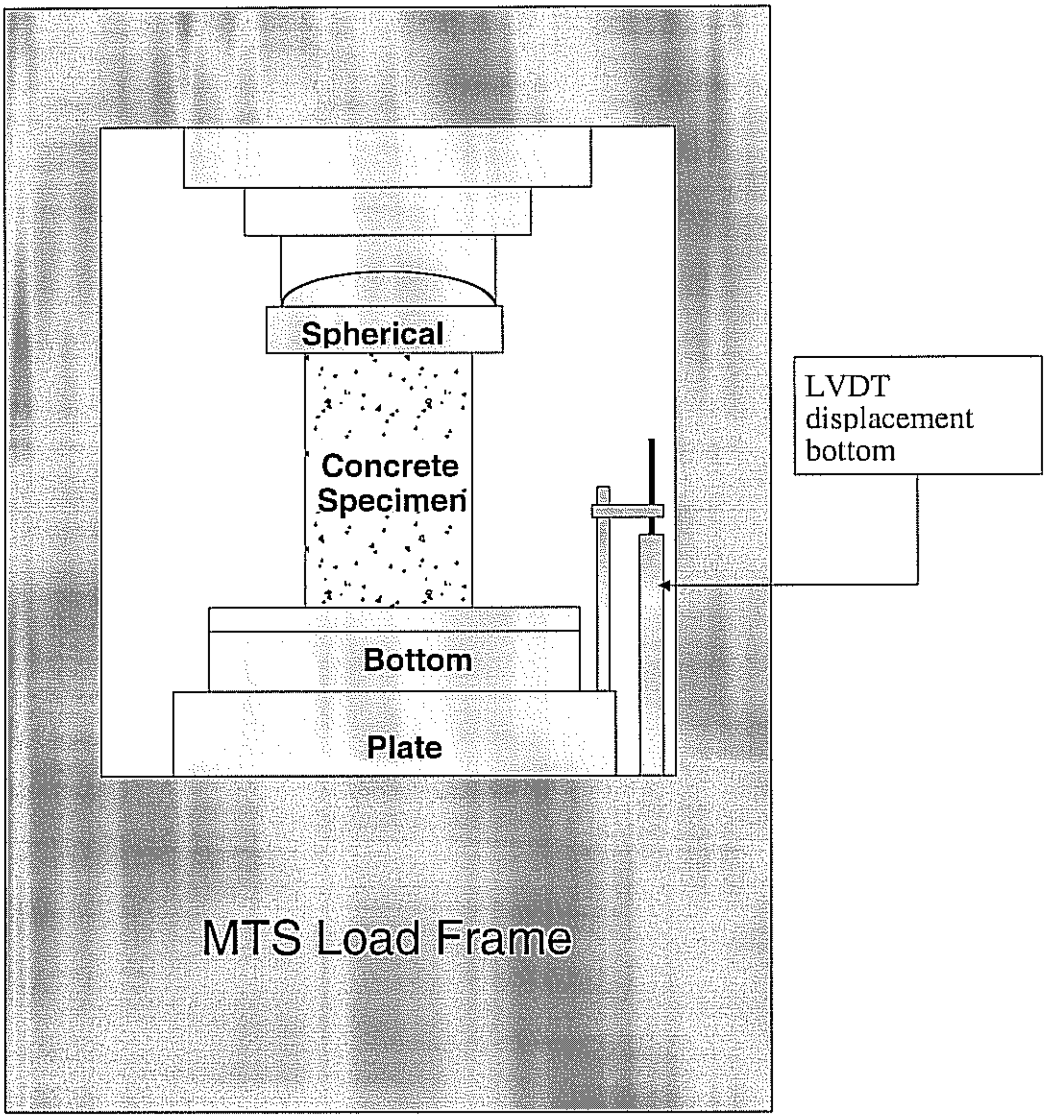

* Not to scale

Figure 3.1 MTS load frame with LVDT.

approximately 4.45 kN (1,000 lb.) was applied to the specimen using displacement control. The Instron Series IX software program automatically switched the machine from displacement control to load control and loaded the specimen until failure. Load and platen displacement were recorded continuously throughout each axial compression cylinder test.

Axial compression test results are shown as load versus crosshead displacement graphs in Figures 3.2 to 3.5. Each figure shows results from two batches of concrete made with the same coarse aggregate, i.e., Figure 3.2 has results from both batches of CA-B (basalt). Because four batches of CA-S (slag) were casted, two figures are included as Figures 3.4 and 3.5, respectively. Each figure contains all cylinders tested for that particular type of coarse aggregate along with the average curve for the group, with the exception of CA-S (slag), which has two figures with half the cylinders tested on each one. Load-displacement curves do not pass through the origin, because of the small seating load applied to each concrete specimen. These curves were not used to calculate modulus of elasticity because a stress-strain curve could not be readily obtained from the data. Instead, apparent stiffness was calculated from the load-displacement curves, and is discussed further in Section 3.1.1. Additionally, an estimated modulus of elasticity discussion is provided in Section 4.1.2.

Tables 3.1-3.3 include values for displacement at failure, apparent stiffness, maximum load, and stress for each cylinder tested. Also included for the same values are the averages and standard deviations per batch. Some cylinders (where noted) did not meet the requirements of ASTM C39-96, thus these cylinders were not included in the averages or standard deviations. Slump and percent air are reported also for ease of comparison. Test results show that the maximum average axial compressive strength for concrete mixes CA-B (41.0 MPa) and CA-G (41.8 MPa) varied by 2%, with CA-G being higher. Mix CA-S (45.0 MPa) showed a 9.8% increase in maximum stress when compared to concrete mix CA-B.

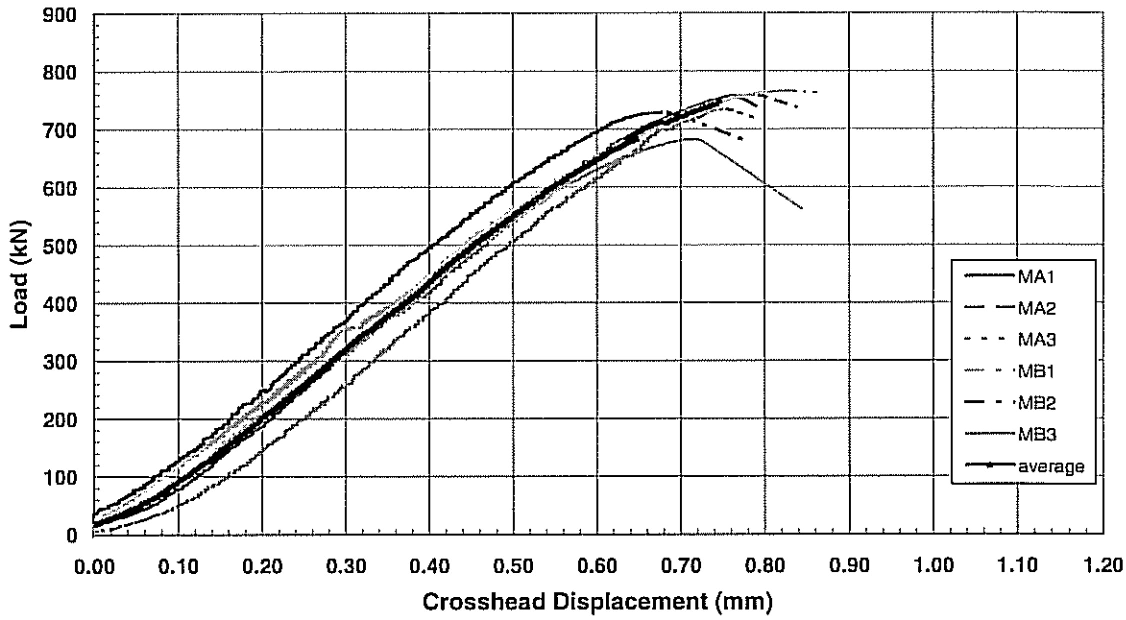

Figure 3.2. Axial Compressive Load versus Crosshead Displacement for Concrete Mix CA-B (basalt).

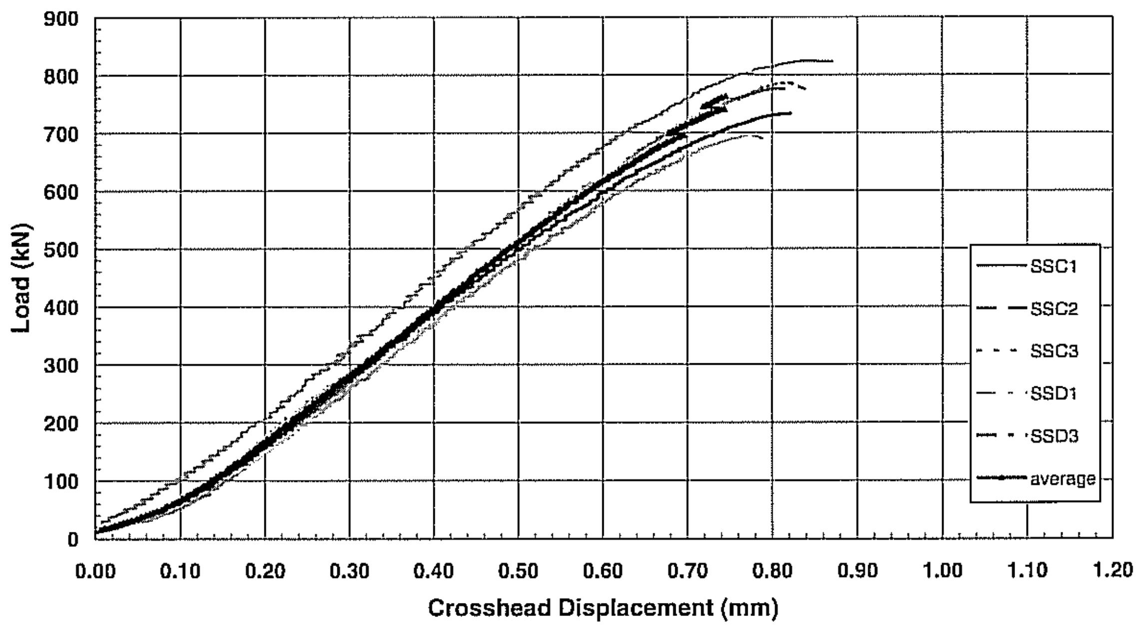

Figure 3.3. Axial Compressive Load versus Crosshead Displacement for Concrete Mix CA-G (glacial gravel).

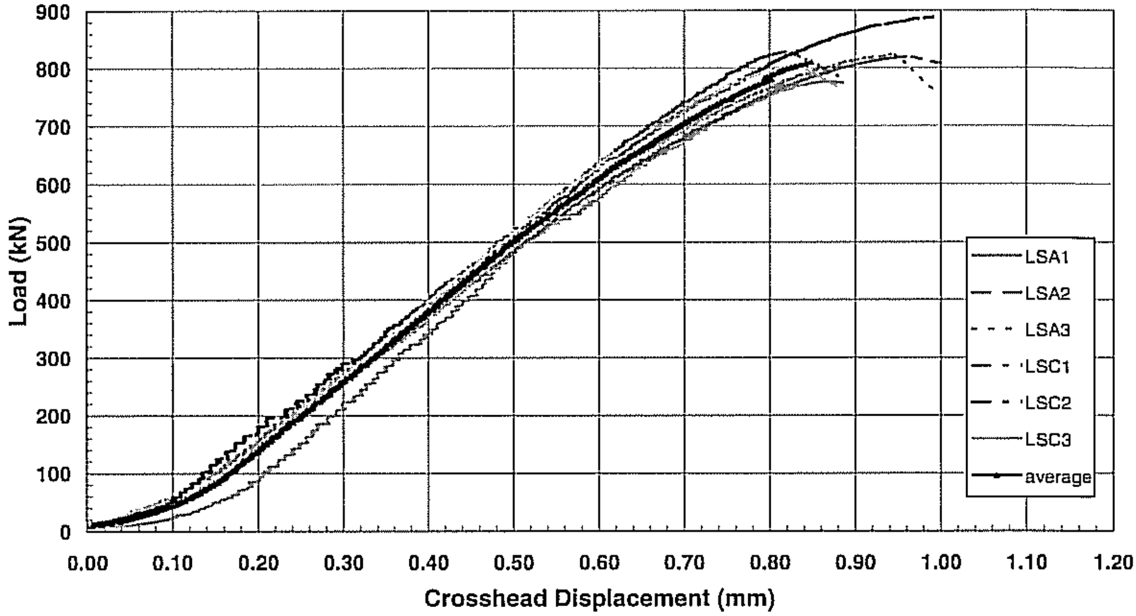

Figure 3.4. Axial Compressive Load versus Crosshead Displacement for Concrete Mix CA-S (slag), Batches LSA and LSC.

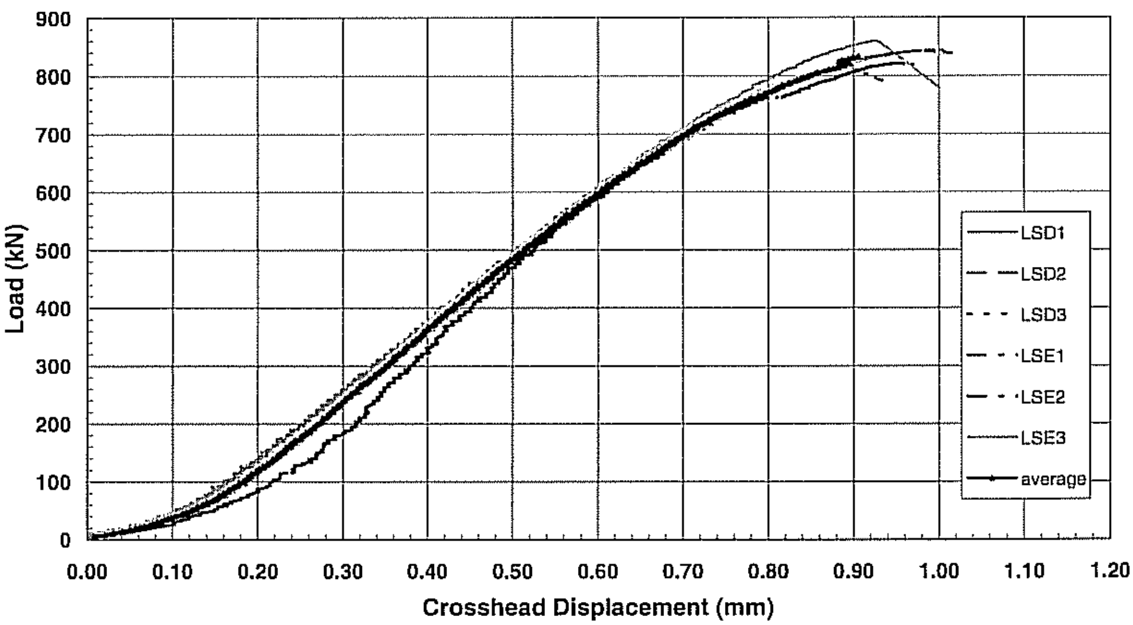

Figure 3.5. Axial Compressive Load versus Crosshead Displacement for Concrete Mix CA-S (slag), Batches LSD and LSE.

Table 3.1 Axial Compression Test Results for Coarse Aggregate CA-B Cylinders

Cylinder Identification	Maximum Load kN	Maximum Stress MPa	Displacement @ Failure mm	Apparent Stiffness kN/mm	Slump mm	Percent Air
Batch A						
MA1	756	41.4	0.756	1189	57.2	5.7 %
MA2	758	41.5	0.794	1130		
MA3	733	40.2	0.747	1142		
Avg.	**749**	**41.0**	**0.766**	**1154**		
STD	**13.7**	**0.8**	**0.02**	**31**		
Batch B						
MB1	765	42.0	0.827	1085	76.2	5.5 %
MB2	728	39.9	0.668	1177		
MB3†	681	37.3	0.712	1141		
Avg.	**747**	**40.9**	**0.747**	**1131**		
STD	**26.7**	**1.5**	**0.11**	**65**		

* 1 kN = 224.8 lb. 1 MPa = 145.0 psi 1 mm = 3.94 x 10^{-2} in.

† Not included in average or standard deviation.

Table 3.2 Axial Compression Test results for Coarse Aggregate CA-G Cylinders

Cylinder Identification	Maximum Load kN	Maximum Stress MPa	Displacement @ Failure mm	Apparent Stiffness kN/mm	Slump mm	Percent Air %
Batch C						
SSC1	824	45.2	0.839	1120	50.8	4.1
SSC2	776	42.6	0.806	1185		
SSC3	786	43.1	0.822	1134		
Avg.	**795**	**43.6**	**0.822**	**1146**		
STD	**25.2**	**1.4**	**0.02**	**34**		
Batch D						
SSD1	695	38.1	0.778	1045	76.2	5.1
SSD2	-	-	-	-		
SSD3	733	40.2	0.824	1115		
Avg.	**714**	**39.2**	**0.801**	**1080**		
STD	**27.0**	**1.5**	**0.03**	**49**		

* 1 kN = 224.8 lb. 1 MPa = 145.0 psi 1 mm = 3.94 x 10^{-2} in.

Table 3.3 Axial Compression Test Results for Coarse Aggregate CA-S Cylinders

Cylinder Identification	Maximum Load kN	Maximum Stress MPa	Displacement @ Failure mm	Apparent Stiffness kN/mm	Slump mm	Percent Air
Batch A						
LSA1	776	42.6	0.866	1287	57.2	4.2 %
LSA2	819	44.9	0.967	1150		
LSA3	821	45.0	0.949	1159		
Avg.	**805**	**44.1**	**0.927**	**1199**		
STD	**25.1**	**1.4**	**0.05**	**77**		
Batch C						
LSC1	827	45.3	0.825	1213	57.2	4.3 %
LSC2†	888	48.6	0.991	1092		
LSC3	803	44.0	0.834	1257		
Avg.	**815**	**44.7**	**0.830**	**1235**		
STD	**16.6**	**0.9**	**0.01**	**31**		
Batch D						
LSD1	857	47.0	0.918	1200	50.8	4.1 %
LSD2	842	46.2	0.985	1165		
LSD3	844	46.2	0.991	1136		
Avg.	**848**	**46.5**	**0.965**	**1167**		
STD	**8.3**	**0.5**	**0.04**	**32**		
Batch E						
LSE1	814	44.6	0.896	1214	69.9	4.5 %
LSE2	820	44.9	0.949	1286		
LSE3	813	44.6	0.890	1206		
Avg.	**816**	**44.7**	**0.912**	**1235**		
STD	**3.8**	**0.2**	**0.03**	**44**		

* 1 kN = 224.8 lb. 1 MPa = 145.0 psi 1 mm = 3.94×10^{-2} in.

† Not included in average or standard deviation.

3.1.1 Apparent Stiffness

Apparent stiffness, *K*, is defined herein as the ratio of the change in load to the change in crosshead displacement. Simply put, *K* is the slope of the load versus crosshead displacement curve. It is not the true stiffness of the specimen nor is it the modulus of elasticity of the concrete. It is the value obtained using the measured crosshead displacement readings and the actual load change. The LVDT mounted on the MTS load frame measured crosshead displacement that included both deformations of the specimen and that of the top platen system. Figure 3.1 is a sketch of the MTS load frame with the LVDT that measured crosshead displacement. Because this measure of total crosshead displacement was larger than the specimen displacement, the slope of each curve was less steep than anticipated causing the apparent stiffness to be smaller in magnitude than the true specimen stiffness. In this setup, the modulus elasticity of the concrete specimen is underestimated because the measured strain (and hence deflection) includes deflections of the loading system and platens.

Apparent stiffness was determined from the slope of the linear portion of the load versus crosshead displacement curve using a linear regression of each cylinder tested axially for ultimate compressive strength. The apparent stiffness of each cylinder is listed in Tables 3.1 to 3.3. The linear portion of the curve was defined between approximately 100 kN (22,480 lb.) to 40% of peak load. Because the stiffness of the top platen system was unknown the modulus of elasticity of the concrete specimens could not be determined directly, only general comparisons between the three types of coarse aggregates can be made from these results. However an attempt was later made to estimate the modulus of elasticity by conducting compliance tests using a steel cylinder. The method used to estimate the modulus of elasticity is discussed further in Chapter 4. In general, the apparent stiffness for concrete mix CA-G was 2.6% lower than CA-B. CA-S exhibited a 5.8% higher apparent stiffness than CA-B.

3.2 Splitting Tensile Strength

Splitting tensile strength was tested according to ASTM C 496-90 with the MTS load frame located in the Mining and Materials Building. On each end of the cylinders tested, diametrical lines were drawn lying in the same plane as the applied load with a jig specifically manufactured for that use. An aligning jig with the horizontally placed specimen was set on the bottom platen of the MTS load frame. The top-bearing block was then set into place and the specimen was aligned using the diametrical drawn lines on the specimen ends. Wood core paneling strips separated the specimen from both the top and bottom bearing blocks. The platen was then raised so that a small seating load was applied to the specimen and bearing blocks before the end plates were removed from the jig. The Instron Series IX program automatically switched the machine to load control and loaded the specimen until failure at a constant rate of 89 kN/min (20,000 lb./min). Load and crosshead (platen) displacement were recorded continuously.

Split cylinder test results are shown as load versus crosshead displacement plots in Figures 3.6 to 3.9. There is one graph for each coarse aggregate CA-B and CA-G with results from two batches included on each figure. Each graph contains all cylinders tested for that particular set of batches along with the average curve for the group. Two figures (Figures 3.8 and 3.9) are included for coarse aggregate CA-S because four batches of concrete were cast from this aggregate. These figures also contain average results from two batches.

Tables 3.4 - 3.6 include values for displacement at failure, apparent stiffness, maximum load, and maximum tensile stress for each cylinder tested in the split tensile test set-up. Also included for the same properties are the averages and standard deviations per batch. Slump and percent air are also reported. Comparing the maximum splitting tensile stress for the three mixes, CA-G is 1.4% higher than CA-B while CA-S showed to be 13.2% higher than CA-B. Slump and percent air as measured on the fresh concrete batches are also tabulated and show consistency independent of coarse aggregate.

3.2.1 Apparent Stiffness

Apparent stiffness is the slope of the linear portion of the load versus the crosshead displacement curve and was calculated using linear regression. The linear portion of the curve was defined between approximately 5 kN (1,124 lb.) and 40% of the peak load. Values for apparent stiffness have the same error associated with them as discussed above for axial compression test. Therefore, only general comparisons between the three types of coarse aggregates can be made from these results. In general, concrete mix CA-G and CA-S showed a 7.0% and a 9.6% decrease in apparent stiffness compared to mix CA-B, respectively.

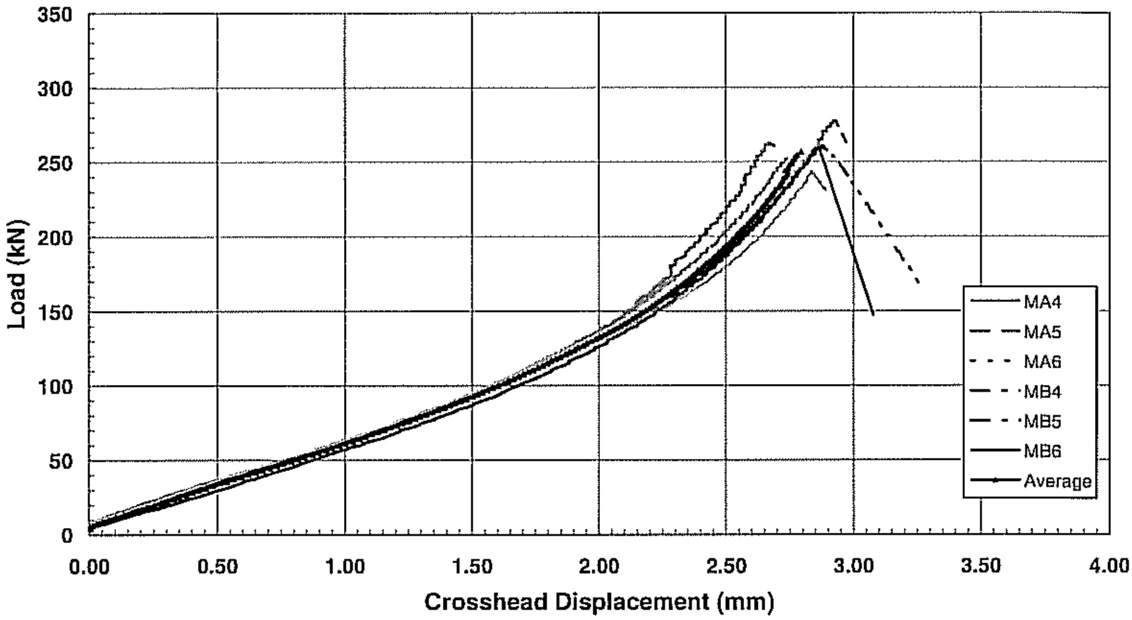

Figure 3.6. Split Tensile Load versus Crosshead Displacement for Concrete Mix CA-B (basalt).

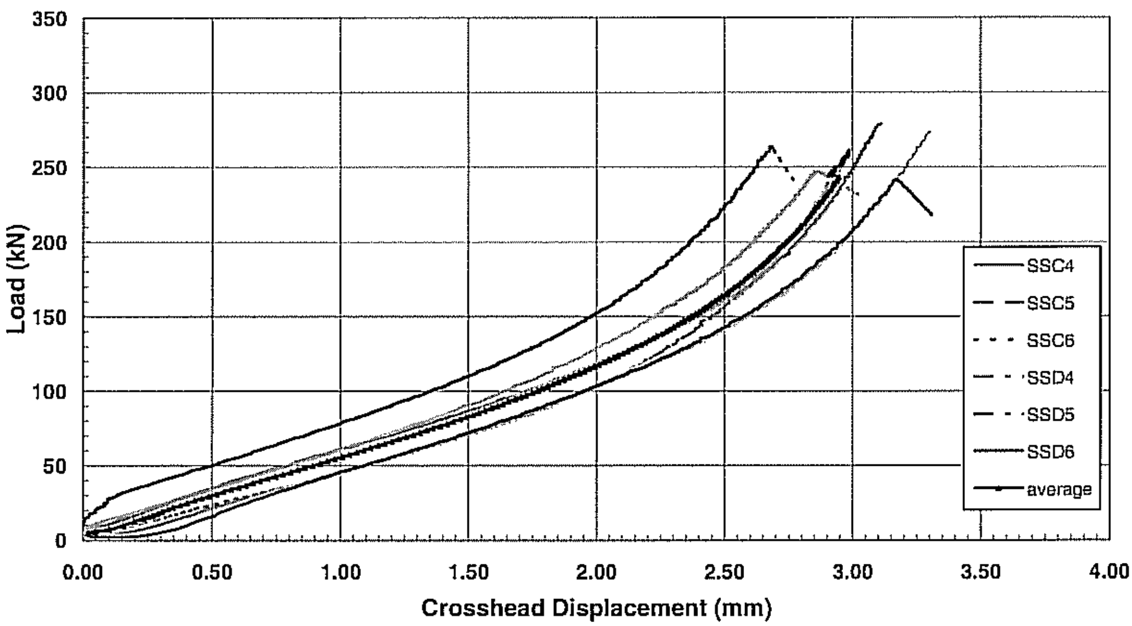

Figure 3.7. Split Tensile Load versus Crosshead Displacement for Concrete Mix CA-G (glacial gravel).

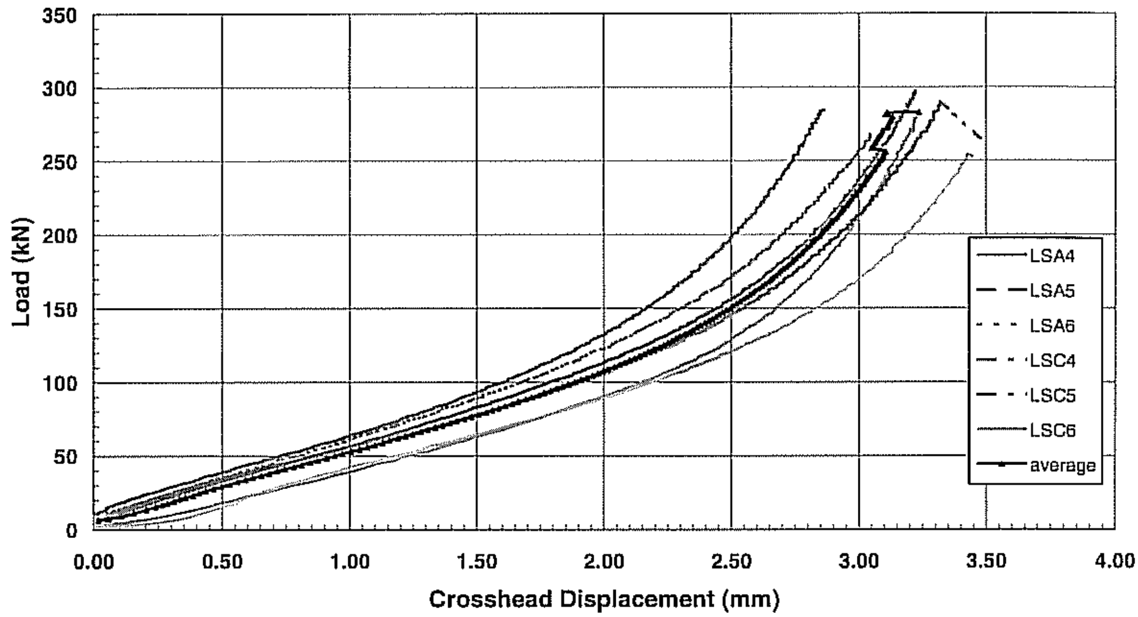

Figure 3.8. Split Tensile Load versus Crosshead Displacement for Concrete Mix CA-S (slag) Batches LSA and LSC.

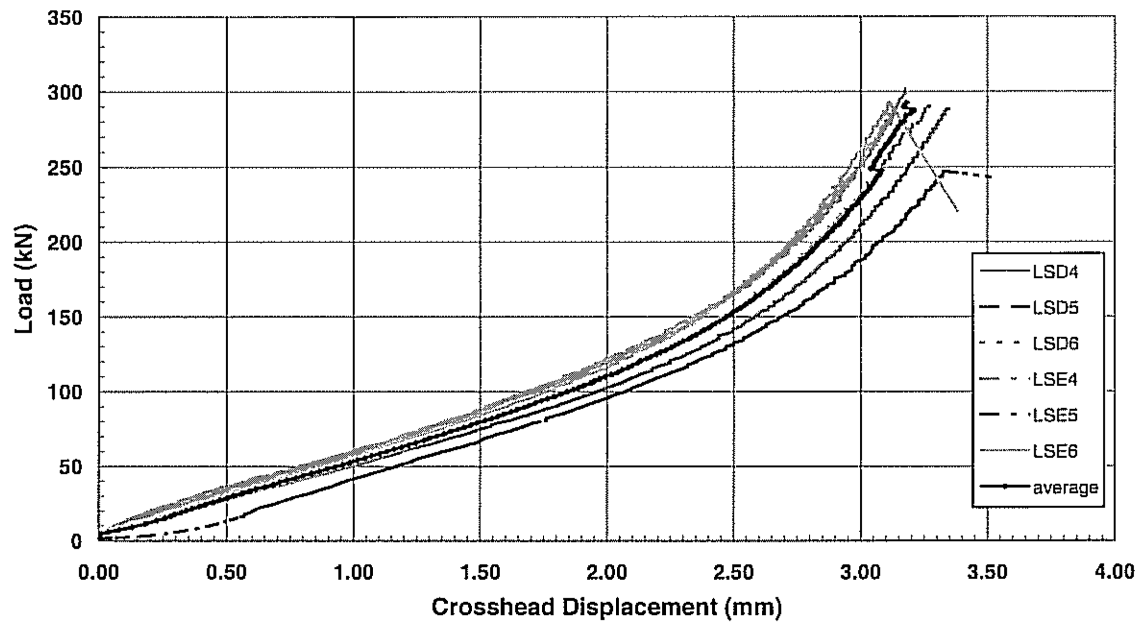

Figure 3.9. Split Tensile Load versus Crosshead Displacement for Concrete Mix CA-S (slag) Batches LSD and LSE.

Table 3.4 Split Tensile Strength Test Results for Coarse Aggregate CA-B Cylinders

Cylinder Identification	Maximum Load kN	Maximum Stress MPa	Displacement @ Failure mm	Apparent Stiffness kN/mm	Slump mm	Percent Air
Batch A						
MA4	243	3.33	2.836	57	57.2	5.7 %
MA5†	277	3.78	2.931	59		
MA6	252	3.47	2.737	59		
Avg.	**248**	**3.40**	**2.787**	**58**		
STD	**6.0**	**0.1**	**0.07**	**1.4**		
Batch B						
MB4	262	3.61	2.670	57	76.2	5.5 %
MB5	260	3.57	2.878	56		
MB6	259	3.54	2.866	58		
Avg.	**261**	**3.57**	**2.805**	**57**		
STD	**1.7**	**0.0**	**0.12**	**1.0**		

* 1 kN = 224.8 lb. 1 MPa = 145.0 psi 1 mm = 3.94×10^{-2} in.

† Not included in average or standard deviation.

Table 3.5 Split Tensile Strength Test Results for Coarse Aggregate CA-G Cylinders

Cylinder Identification	Maximum Load kN	Maximum Stress MPa	Displacement @ Failure mm	Apparent Stiffness kN/mm	Slump mm	Percent Air
Batch C						
SSC4	273	3.75	3.300	52	50.8	4.1 %
SSC5	279	3.82	3.111	54		
SSC6	262	3.61	2.994	50		
Avg.	**271**	**3.72**	**3.135**	**52**		
STD	**8.6**	**0.1**	**0.15**	**2.0**		
Batch D						
SSD4	247	3.36	2.857	55	76.2	5.1 %
SSD5†	263	3.61	2.683	60		
SSD6	241	3.29	3.174	55		
Avg.	**244**	**3.33**	**3.016**	**55**		
STD	**3.6**	**0.0**	**0.22**	**0.0**		

* 1 kN = 224.8 lb. 1 MPa = 145.0 psi 1 mm = 3.94×10^{-2} in.

† Not included in average or standard deviation.

Table 3.6 Split Tensile Strength Test Results for Coarse Aggregate CA-S Cylinders

Cylinder Identification	Maximum Load kN	Maximum Stress MPa	Displacement @ Failure mm	Apparent Stiffness kN/mm	Slump mm	Percent Air
Batch A						
LSA4	279	3.82	3.227	48	57.2	4.2 %
LSA5	284	3.89	2.866	54		
LSA6	267	3.68	3.044	54		
Avg.	**277**	**3.79**	**3.045**	**52**		
STD	**8.8**	**0.1**	**0.18**	**3.5**		
Batch C						
LSC4	297	4.06	3.225	52	57.2	4.3 %
LSC5	289	3.96	3.321	47		
LSC6[†]	254	3.47	3.426	48		
Avg.	**293**	**4.01**	**3.273**	**50**		
STD	**5.4**	**0.1**	**0.07**	**3.5**		
Batch D						
LSD4	302	4.13	3.176	54	50.8	4.1 %
LSD5	288	3.96	3.348	50		
LSD6	291	3.99	3.277	52		
Avg.	**294**	**4.03**	**3.267**	**52**		
STD	**7.0**	**0.1**	**0.09**	**2.0**		
Batch E						
LSE4	284	3.89	3.115	54	69.9	4.5 %
LSE5[†]	247	3.40	3.327	53		
LSE6	293	4.03	3.115	54		
Avg.	**288**	**3.96**	**3.115**	**54**		
STD	**5.8**	**0.1**	**0.00**	**0.0**		

* 1 kN = 224.8 lb. 1 MPa = 145.0 psi 1 mm = 3.94×10^{-2} in.

[†] Not included in average or standard deviation.

3.3 Strain Measurements

Strain gages were mounted on both axial compression and split cylinder specimens one day prior to testing. Two cylinders from each batch, one for axial compression testing and one for split tensile testing, were instrumented with gages. Two types of gages were used: (1) 1000 Ω resistance (WK-06-250BF-10C) strain gages having a gage factor of 2.04 and (2) 350 Ω resistance (WK-06-06ZAP-350) strain gages with a gage factor of 2.02. Each gage had a three-wire connection to compensate for temperature effects and was wired in a quarter bridge arrangement to a wheatstone bridge. An input voltage was supplied (20 and 6 volts for the 1000 Ω and 350 Ω gages, respectively) and the output voltage was recorded with an oscilloscope. The output voltage was then converted to strain with a standard quarter bridge completion equation.

3.3.1 Placement of Strain Gages

Axial compression specimens had a 1000 Ω and a 350 Ω gage mounted in the axial and transverse directions, respectively. Figures 3.10(a) and 3.10(b) show general gage placements for both axial compression and split tensile specimens. These gages were placed approximately in the middle of the cylinder, i.e., six inches from either end of the specimen. Split cylinder specimens had a 1000 Ω gage in the transverse direction while a 350 Ω gage in the axial direction. These gages were mounted on the flat end of the cylinder near the center where maximum tensile strain was expected to occur. In this report, the axial and transverse directions are parallel and perpendicular to the direction of loading, respectively. The specific location of the gages depended upon surface conditions. To eliminate stress concentration effects, strain gages were not mounted on rough surfaces or over holes. In some cases, split cylinder specimens had been lightly wet sanded to produce a desirable surface for mounting a gage. The procedure used for mounting strain gages follows.

Diametrical lines were drawn on the flat ends of each specimen using the jig described in Section 3.2. These lines were used for aligning the gages. A selected area was first dried locally with a hot air drier then cleaned with ethanol. An activator was sprayed on the surface of the cylinder, and then a small amount of adhesive (Loctite 330) was applied to the area. The gage was then aligned and pressed firmly into place, holding it down for approximately one minute. Because the adhesive needed at least two hours to cure, a piece of plastic was taped over the gages and the cylinders were returned to the curing room until they were tested.

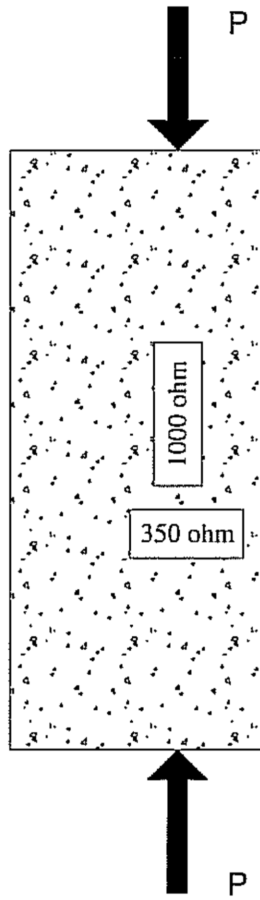

Figure 3.10(a). Axial Compression Test Specimen with Strain Gages.

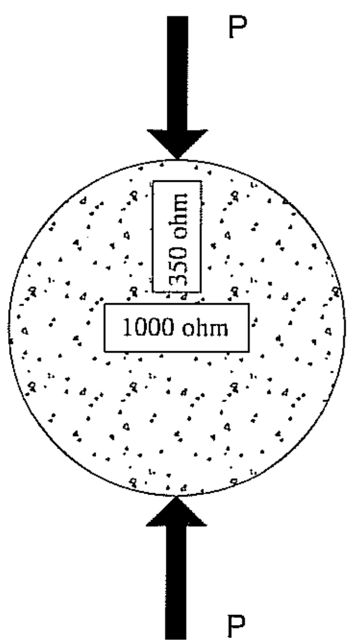

Figure 3.10(b). Split Tensile Specimen with Strain Gages.

3.3.2 Strain Measurement Results

Many factors affected the results for strain gaging, with the major contributor being the gage placement. Strain is not uniform through the specimen because concrete is not a homogenous material. If a gage was mounted over a large piece of aggregate just beneath the surface or away from the failure zone, not much if any strain was felt by the gage. Gages placed near the failure plane gave the best results.

In light of this, strain gage results proved to be unreliable; therefore the results are not presented and were not used in any analysis. One conclusion can be made from the results; strain is not uniform through the specimen, which is why strain gaging concrete specimens produces poor results. For future reference in regards to strain, a better method might be the use of circumferential strain.

4 Discussion and Conclusions

This phase of the research investigated the effects of three different types of coarse aggregate on several fresh and hardened concrete properties, such as unit weight, slump, air content, strength, modulus of elasticity, and fracture characteristics. Included in this chapter will be a discussion on the yield data. As stated in Chapter 2, there was one basic mix design with the types of coarse aggregate being the only intended variable.

4.1 Effects of Coarse Aggregate on Strength

The average strength results for the axial compression and split tensile tests are presented in Figures 4.1 and 4.2, respectively. In these figures load is plotted against crosshead displacement with an average curve for all cylinders tested per type of coarse aggregate, i.e., one curve per coarse aggregate type. Concrete mixes CA-B (basalt) and CA-G (glacial gravel) are the averages of two batches while mix CA-S (slag) is an average of four batches. From these figures it can be seen that concrete mix CA-S has an increase in both axial compression and split tensile strength over mixes CA-B and CA-G. These figures not only show that CA-S has a higher strength but also a higher average displacement at failure of the specimens tested in both axial compression and splitting tensile tests. In general, the shape of the curves is consistent for all mixes. This indicates that the curve's general shape appears to be independent of the coarse aggregate used.

Maximum axial compressive and split tensile strength, f'_c and f_{ct}, respectively are summarized in Table 4.1. All percent differences are based on concrete mix CA-B. Note that CA-S exhibits a 9.8% and a 12.6% increase in f'_c and f_{ct} over CA-B, respectively. Table 4.2 is a summary of crosshead displacements at failure of the specimens. It can be seen that mix CA-S has the largest axial displacement at failure over mixes CA-G or CA-B. Mixes CA-G and CA-S show more than a 10% increase in displacement at failure in split tensile tests when compared to CA-B.

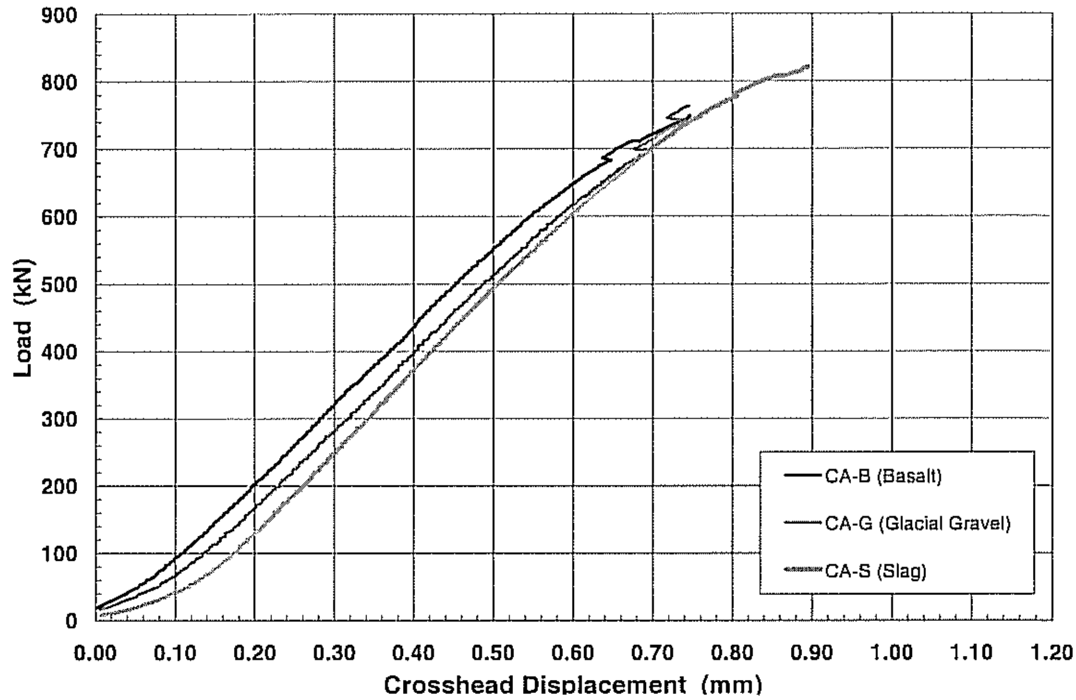

Figure 4.1. Average Axial Load versus Crosshead Displacement for All Concrete Mixes.

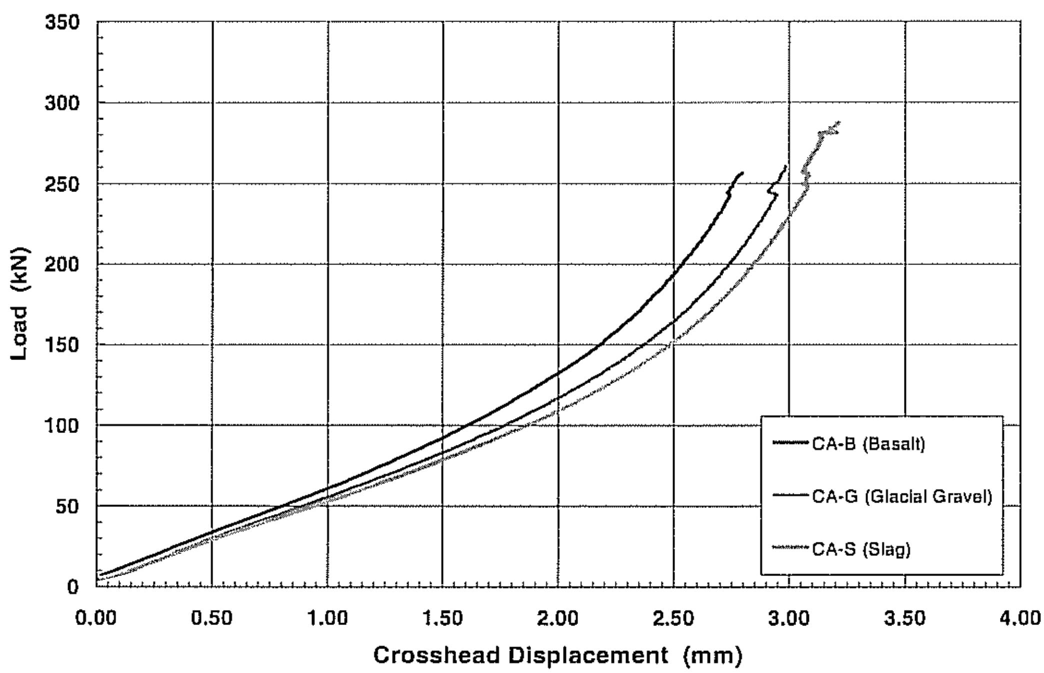

Figure 4.2 Average Axial Load versus Crosshead Displacement for All Concrete Mixes.

Table 4.1 Summary of Axial Compressive Strength and Split Tensile Strength

Aggregate Type	f'_c MPa (psi)	Percent Difference	f_{ct} MPa (psi)	Percent Difference
CA-B	41.0 (5948)	-	3.50 (508)	-
CA-G	41.8 (6066)	2.0	3.56 (518)	1.7
CA-S	45.0 (6523)	9.8	3.94 (572)	12.6

Table 4.2 Summary of Axial and Split Cylinder Displacements at Failure

Aggregate Type	Axial Displacement mm (in.)	Percent Difference	Split Cylinder Displacement mm (in.)	Percent Difference
CA-B	0.758 (0.030)	-	2.797 (0.110)	-
CA-G	0.812 (0.032)	7.1	3.087 (0.121)	10.4
CA-S	0.915 (0.036)	20.7	3.171 (0.125)	13.4

Figures 4.3 and 4.4 summarize the ultimate axial compressive and split tensile strengths per batch of concrete. In terms of each batch, concrete mixes CA-B and CA-S give fairly consistent results for both axial compression and split tensile strength, while CA-G has more variability. CA-B has the most consistent results with respect to axial compressive strength. Concrete mix CA-S consistently shows higher axial compressive and split tensile strengths than either of the other two concrete mixes.

In an attempt to understand strength variations between the concrete mixes made with different coarse aggregates, the yield data was reviewed. Yield data provides unit weight, actual cement content, and water-cement ratio for the freshly mixed concrete. In reviewing the unit weight data, the lowest unit weight was the CA-S (slag) at 2250 kg/m^3 (140 pcf) followed by CA-G (gravel) at 2277 kg/m^3 (148 pcf) and CS-B (basalt) at 2390 kg/m^3 (149 pcf). While this trend would be expected based on the lower bulk density of the slag, it is not clear as to whether or not unit weight affected the strength or stiffness of the concrete. However, a better correlation of strength variation in concrete is the water-cement ratio. The average water-cement ratio for all concrete batches was 0.46, and only varied from 0.45 to 0.47 for individual concrete cylinders tested regardless of coarse aggregate type. This is a fairly tight range making it difficult to draw conclusions concerning strength variations based on water-cement ratio. All of the unit weight data and water-cement ratios for each batch are presented in Appendices IV-B through IV-D.

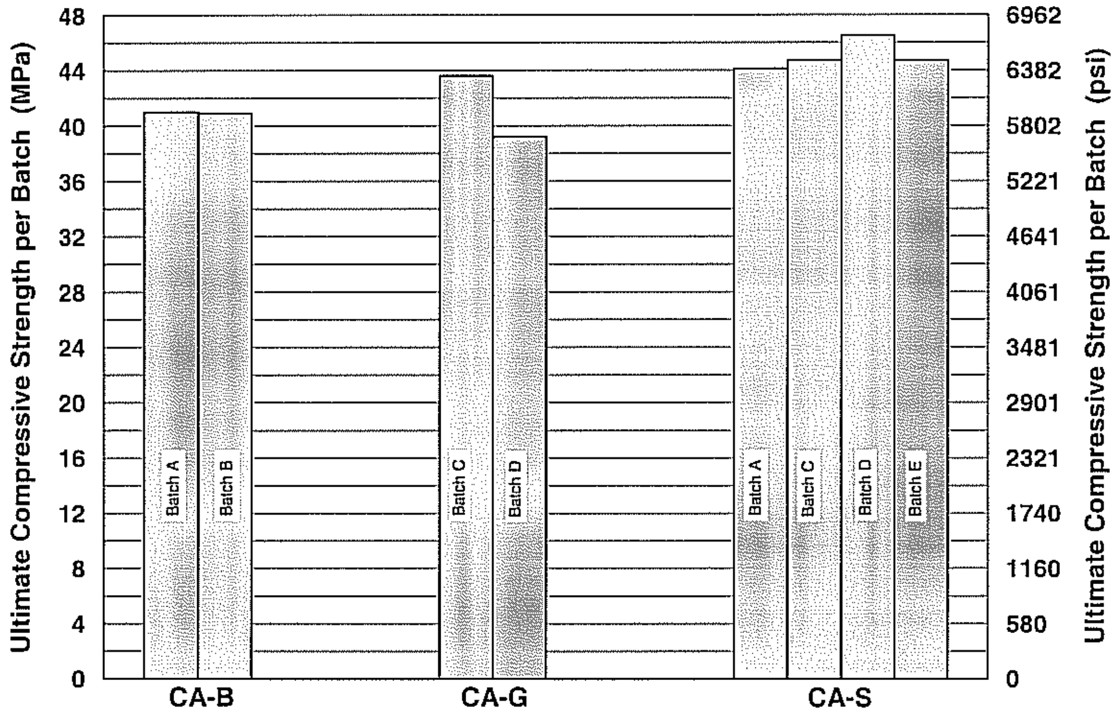

Figure 4.3. Summary of Axial Compressive Strength per Batch of Concrete.

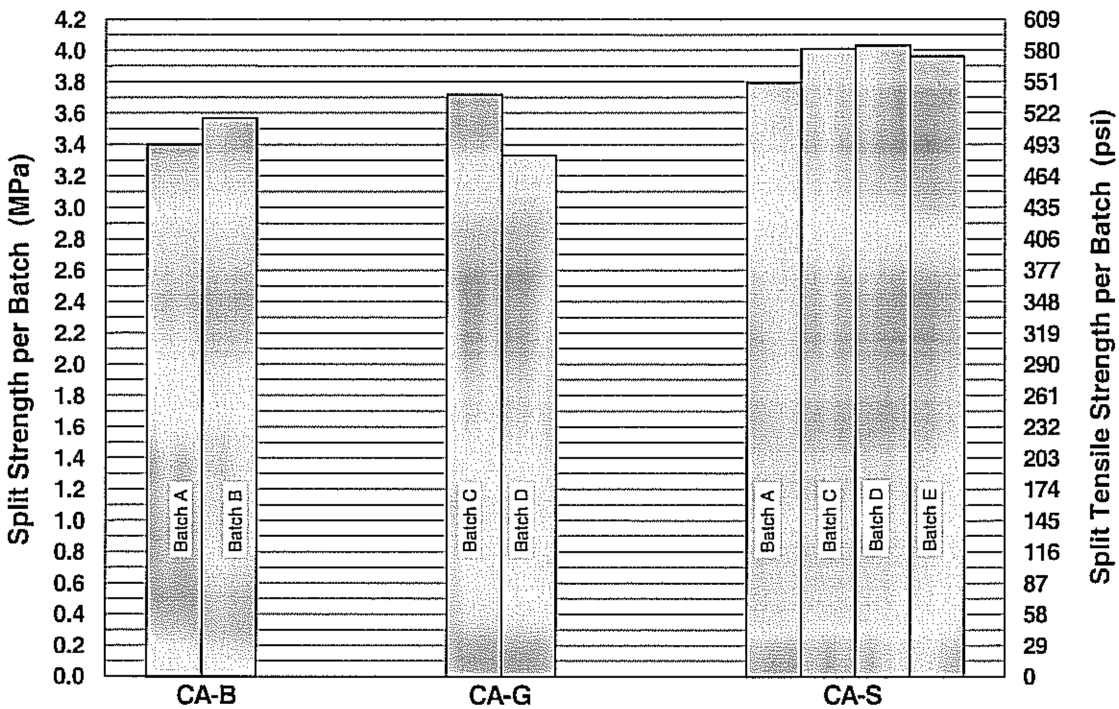

Figure 4.4. Summary of Ultimate Split Tensile Strength per Batch of Concrete.

Apparent cement content for each batch was computed and provided on the "Yield Data" worksheet provided in Appendices IV-B, IV-C and IV-D for the three respective mixes, CA-B, CA-G and CA-S. The design cement content was 335 kg/m^3, i.e., the equivalent of 335 kg of cement was used to produce a cubic meter of concrete. The average measured cement content for CA-B was 334 kg/m^3, CA-G was 336 kg/m^3, and CA-S was 342 kg/m^3. Figure 4.5 shows the actual measured cement content per batch of concrete used in this study. It is observed that each batch of concrete mix CA-S has a higher cement content than the remaining batches for mixes CA-B or CA-G. The actual measured cement content is plotted with compressive strength in Figure 4.6, and Figure 4.7 compares it for the average split tensile strength. From these figures it is shown that concrete mix CA-G, Batch C yields greater strength in terms of both axial compressive and split tensile than does Batch D. Batch C also has higher cement content than batch D. However, a closer review of the yield data also indicates that the measured batch volumes of concrete mix CA-S did not compare with the design volume. Table 4.3 is a summary of measured batch volumes, actual cement content, and axial compressive and split tensile strengths. In addition, the design values for batch volume, cement content and compressive strength are included. It can be seen from Table 4.3 that the batch volumes for CA-B (basalt) and CA-G (gravel) were relatively close to the design volume of 0.0780 m^3. However, the average batch volume for CA-S (slag) was 0.0764 m^3, which was 2.1% less than the nominal design volume. This volume reduction is the main reason for the apparent increase in the "actual cement content" reported in the yield data for CA-S. Because the nominal design quantity of 335 kg/m^3 of cement was used in each batch, there is no reason to believe that the cement content of the mortar varied between mixes (independent of aggregate type). Consequently, the increase in strength with "actual cement content" shown in Figures 4.6 and 4.7 is most likely due to the volume reduction and not necessarily a result of variation in cement content.

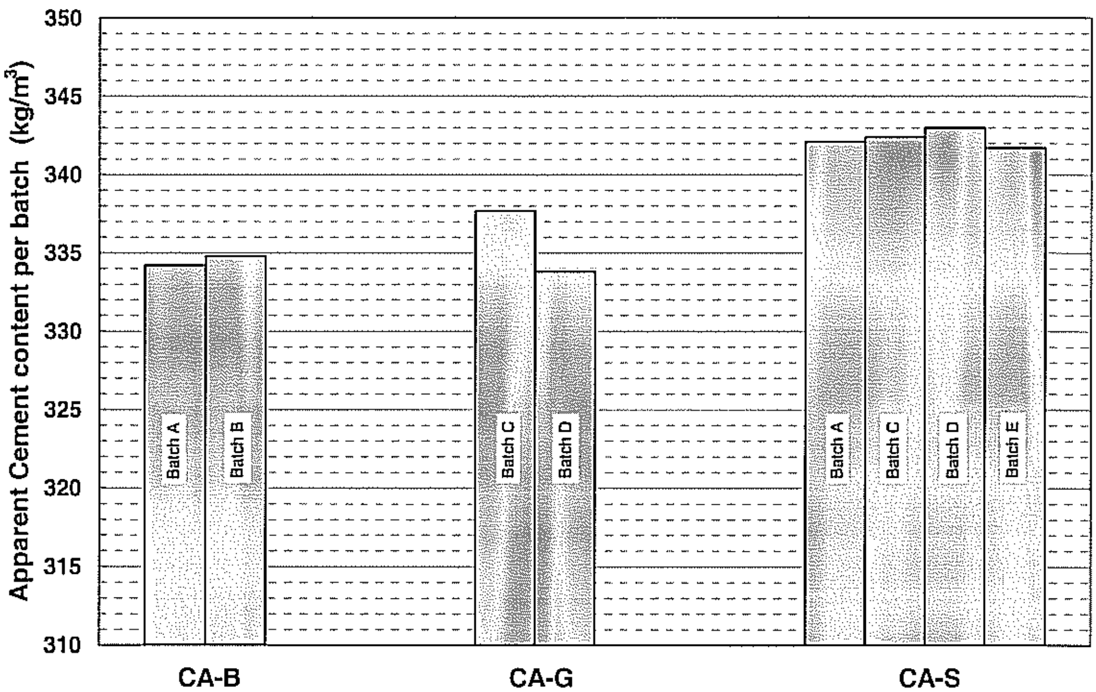

Figure 4.5. Apparent Cement Content per Batch of Concrete as Calculated in Yield Data.

Table 4.3 Summary of Batch Volumes, Apparent Cement Content per Batch, f'_c and f_{ct}.

Coarse Aggregate	Batch Name	Batch Volume m^3	Cement Content kg/m^3	f'_c MPa (psi)	f_{ct} MPa (psi)
CA-B	MA	0.0782	334.2	41.0 (5957)	3.40 (493)
	MB	0.0780	334.8	40.9 (5935)	3.57 (518)
CA-G	SSC	0.0772	337.7	43.6 (6323)	3.72 (540)
	SSD	0.0783	333.8	39.2 (5680)	3.33 (485)
CA-S	LSA	0.0764	342.1	44.1 (6403)	3.79 (550)
	LSC	0.0763	342.4	44.7 (6480)	4.01 (583)
	LSD	0.0762	343.0	46.5 (6740)	4.03 (585)
	LSE	0.0765	341.7	44.7 (6483)	3.96 (537)
Design values		**0.0780**	**335.0**	**24.1 (3500)**	-

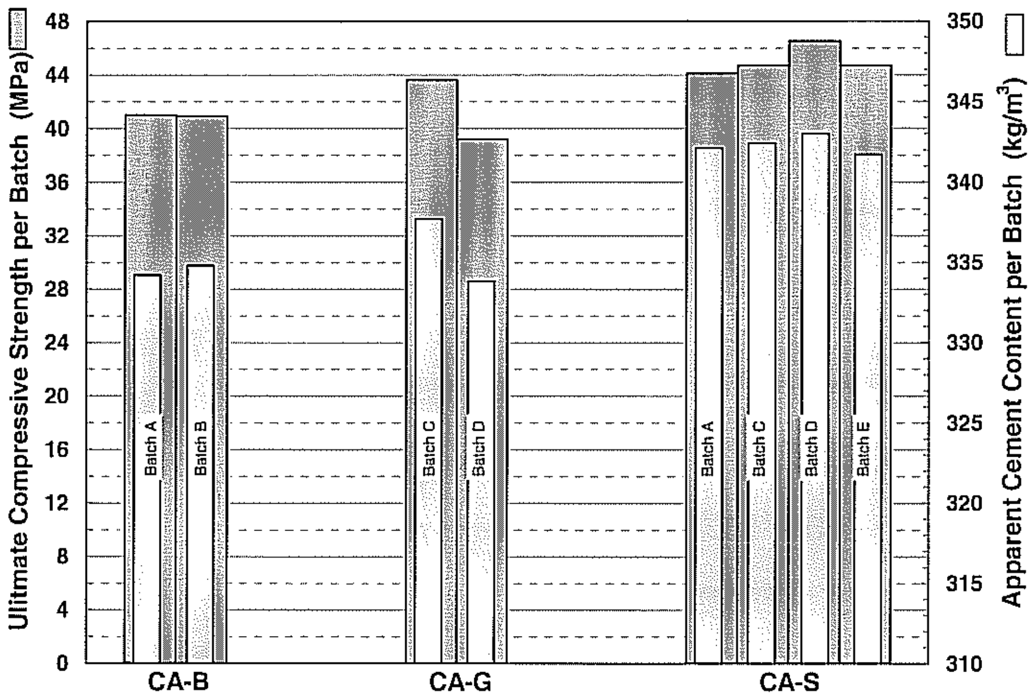

Figure 4.6. Axial Compressive Strength with Apparent Cement Content per Batch of Concrete.

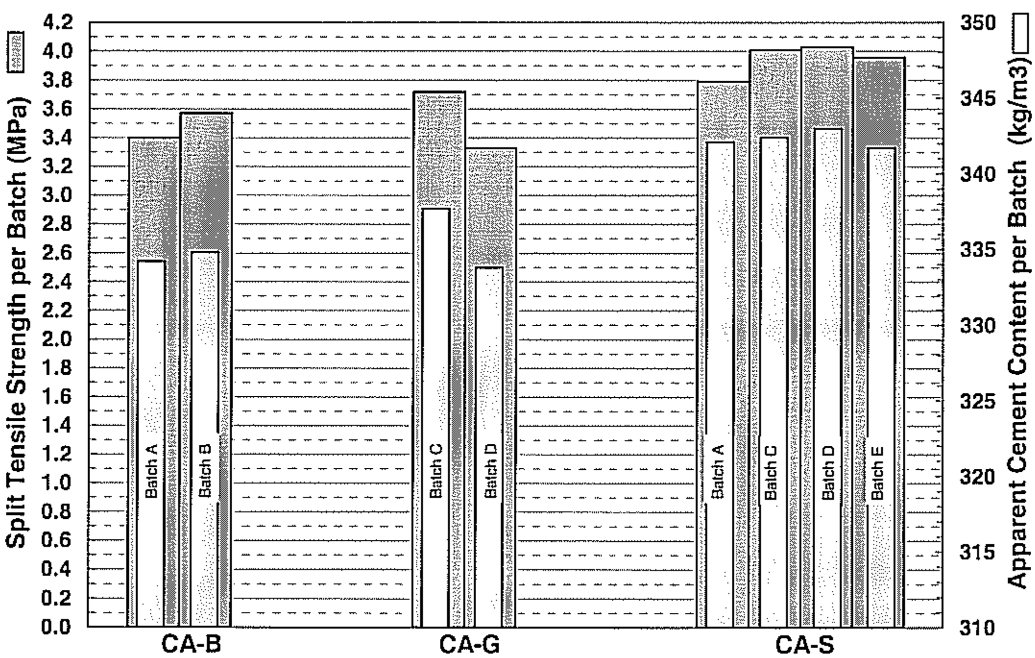

Figure 4.7. Split Tensile Strength with Apparent Cement Content per Batch of Concrete.

The volume reduction observed in mix CA-S (Table 4.3) can be explained by the physical properties of the coarse aggregate. Slag (mix CA-S) has a higher porosity (as noted indirectly by the higher percent absorption in Table 2.2) as well as larger surface pores than either the basalt (mix CA-B) or glacial gravel (mix CA-G). The increased porosity enables the mortar to penetrate the slag particles more readily. Therefore, it takes more mortar to fill the void space, including not only void spaces between coarse aggregate pieces, but also within the aggregate itself. This "higher mortar demand" phenomenon for concrete made with slag aggregate is believed to have an effect on strength and the type of failure observed with CA-S. This is also believed to be the reason why CA-S not only consistently "yields" low (in terms of volume) but also shows a slight increase in strength over both CA-B and CA-G. However, additional research will be required to confirm this possibility.

An additional observation was made concerning the fracture surface of the concrete. In general, the fracture surface of the CA-G (gravel) was the roughest, followed by CA-B (basalt) while CA-S (slag) was the smoothest. This indicated that the failure surface was a function of the coarse aggregate type. However, the roughest fracture surface did not correlate with the highest strength. In fact, the highest strength concrete CA-S had the smoothest fracture surface. A possible explanation for the higher strength CA-S is that the mortar penetrated into the surface pores of the slag, in effect reinforcing (strengthening) the slag aggregate. Because the slag has more surface area than the basalt and glacial gravel aggregate of the same diameter, the contact area between the aggregate and the mortar increases thereby increasing the load to cause failure. CA-S appeared to have no failures along the paste-to-aggregate interface in either the axial compression or split tensile specimens, whereas both CA-B and CA-G had approximately 20 to 30% bond failure present. A consequence of the greater reinforcement would be to force the fracture through the coarse aggregate increasing overall concrete strength.

Another interesting observation is in comparing the measured air content (ASTM C 173 Volumetric Method), presented in the "Report of Test" pages in Appendices IV-B, IV-C, and IV-D, and the back-calculated air content (ASTM C 138 Gravimetric Method) of the concrete for the three respective mixes. While an air content of 6.5% is generally required in design for durability, this study used a 5 ±1% target value. The measured air content percent using the Volumetric Method is presented with ultimate compressive and tensile strengths in Figures 4.8 and 4.9, respectively. In general, this method shows that an increase in air content results in a strength decrease.

The target value for air content was met based on the Volumetric Method (rollometer) as summarized in Table 4.4. Based on the Gravimetric Method, the back-calculated values for air content are considerably below the target value. However, the Gravimetric Method is based on bulk saturated surface dry specific gravity ($G_{B(SSD)}$) values. It can be questioned in this research whether the $G_{B(SSD)}$ values used to determine theoretical unit weights (air free basis) were correct. From Table 2.2, there was considerable variability in the measured $G_{B(SSD)}$ for the slag aggregate while the results for basalt and glacial gravel were relatively consistent between testing laboratories. Consequently, it is believed that the volumetric measurement is more representative of the actual air content because it is independent of coarse aggregate property measurements. It is interesting to note, however, the difference in the results between the two methods, which indirectly correlates with the absorption of the coarse aggregate. The absorption values used in the mix design were 3.55% for the slag, 1.45% for the basalt and 1.35% for the glacial gravel. This compares with an average difference of 3.2% for slag, 2.2% for basalt, and 1.2% for glacial gravel as seen in Table 4.4. It is not known why this difference occurs but it is speculated that a possible reason for the difference is due to the difficulty in measuring the correct specific gravity and absorption values of the coarse aggregate.

Table 4.4 Measured and Calculated Air Content

Coarse Aggregate	Batch Name	Measured Air Volumetric Method (%)	Calculated Air Gravimetric Method (%)	Direct Difference (Vol. – Grav.)
CA-B	MA	5.7	3.6	2.1
	MB	5.5	3.3	2.2
CA-G	SSC	4.1	2.9	1.2
	SSD	5.1	3.8	1.3
CA-S	LSA	4.2	1.0	3.2
	LSC	4.3	1.4	2.9
	LSD	4.1	1.0	3.1
	LSE	4.5	1.0	3.5
Nominal Design		5 ± 1%		

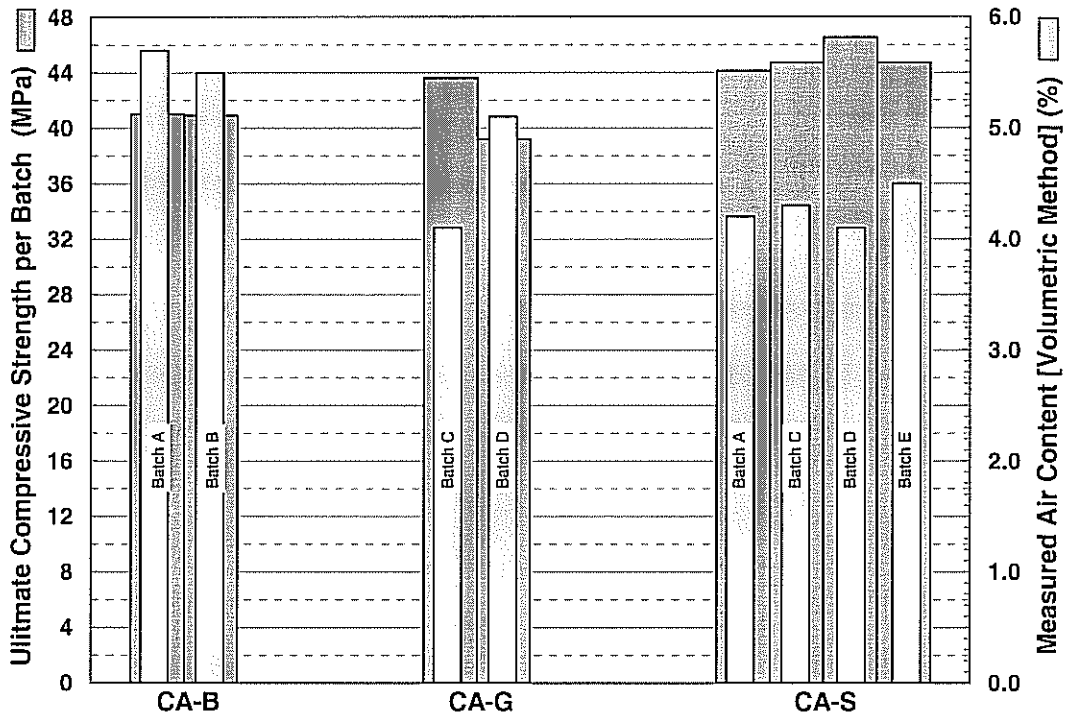

Figure 4.8. Axial Compressive Strength with Measured Air Content per Batch of Concrete.

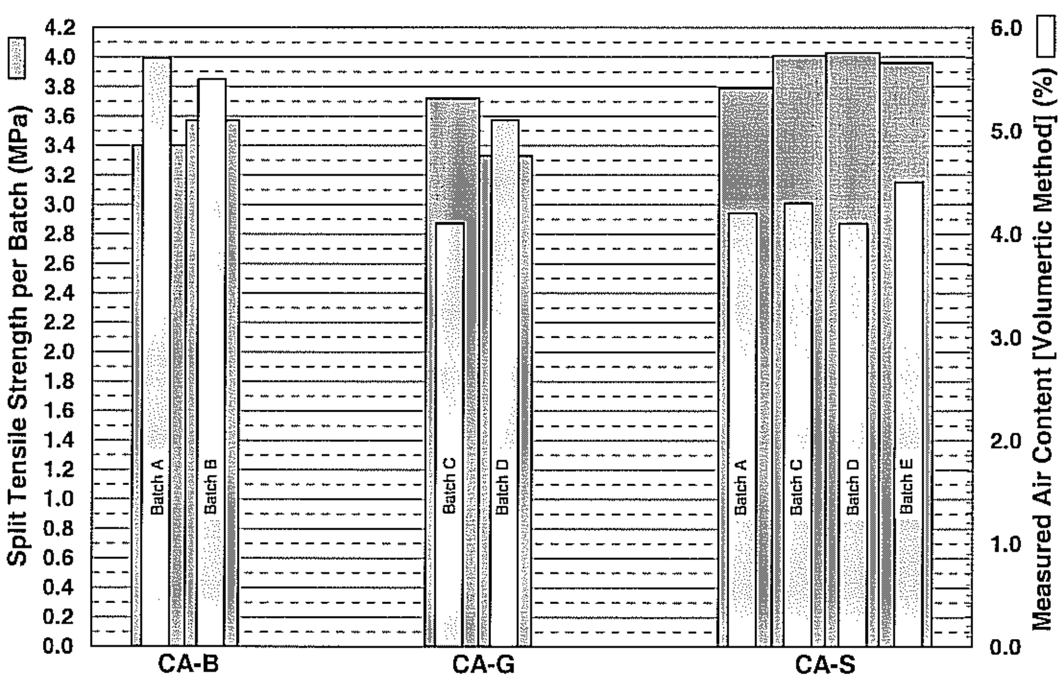

Figure 4.9. Split Tensile Strength with Measured Air Content per Batch of Concrete

Another reason why CA-S developed higher strength may be related to the absorption (water) characteristics of the slag. As discussed in Section 2.1, absorption measurements for the slag aggregate did not compare well between testing laboratories. The range for absorption was found to be approximately 2.5 to 8.5% (Table 2.2). If the actual absorption was larger than the 3.55% used in the initial mix design, then more water would be absorbed into the coarse aggregate. Less free water would be available to react with the cement, resulting in a lower water-cement ratio and thereby leading to higher strength. This would not be apparent in the calculation for water-cement ratio because the amount of absorbed water is a constant based on the absorption value of the coarse aggregate selected for the mix design.

4.1.1 Split Tensile Comparison

Split tensile strength data obtained from this study was compared to predictions from the ACI Concrete Building Code, ACI 318-95. The following ACI 318-95 relationship is for normal weight concrete.

$$f_{ct} = 0.56 \times \sqrt{f'_c} \quad \text{(SI)} \qquad f_{ct} = 6.7 \times \sqrt{f'_c} \quad \text{(USC)} \qquad 4.1$$

where

f_{ct} = split tensile strength of concrete (MPa, psi),
f'_c = axial compressive strength of concrete (MPa, psi).

Taking the split tensile strength obtained from test data and dividing it by the square root of the measured compressive strength gives a measured constant for comparing to the ACI factor 0.56 (SI units) or 6.7 (USC). Table 4.5 compares the factor calculated from the data to the empirical factor stated in ACI 318-95. The results are in good agreement as indicated in Table 4.5. Although CA-S has the largest percent difference, this was expected because CA-S has the largest relative difference between axial compressive and split tensile strengths (Table 4.3).

Table 4.5 Factor for Split Tensile Strength Data compared to ACI 318-95

Aggregate Type	f_{ct} Factor Calculated from Data SI (USC)	f_{ct} Factor from ACI 318-95 SI (USC)	Percent Difference from ACI 318-95 %
CA-B	0.547 (6.59)	0.56 (6.7)	-2.4
CA-G	0.551 (6.65)		-1.6
CA-S	0.587 (7.08)		4.8

4.1.2 Modulus of Elasticity

The modulus of elasticity, E, was calculated using a stiffness method because of a discrepancy associated with the true displacement of the specimen, as discussed in Section 3.1.1. The following stiffness method is used to develop a "calibration" type relationship to eliminate effects of the displacement discrepancy and to obtain E for each cylinder tested. Figure 3.1 illustrated the load frame used in this study. A system of two springs in series was used to model the specimen and the load frame including the bottom and top platens. From this model it was possible to isolate the stiffness of the specimen. As a result E was calculated using the relationship relating the specimen stiffness to E. The procedure and the assumptions used are described in the following paragraphs.

To obtain the overall system stiffness, a steel cylinder that was approximately the same size as a concrete cylinder was placed into the MTS load frame along with a digital dial gage with a readability of 0.0025 mm (0.0001 in.). The dial gage was placed between the top and bottom platen along side of the steel cylinder. In this configuration the dial gage gives the true displacement of the steel cylinder. The steel cylinder was then loaded and unloaded in axial compression several times to a maximum load of 1334 kN (300 kip), or approximately 23% of the ultimate steel strength. Load and crosshead displacement were recorded continuously throughout each of the tests using a personal computer. The crosshead displacement was measured using the LVDT as discussed in Chapter 3. The specimen displacement was manually recorded from the dial gage every 89 kN (20 kip) until a load of 623 kN (140 kip) was reached, and thereafter every 44.5 kN (10 kip) up to the maximum load. Figure 4.10 is a load versus displacement curve for the data obtained from the axial compressive loading of the steel cylinder. Included in

Figure 4.10 is curves obtained from the dial gage and LVDT displacement readings as well as the theoretical and corrected curves for the steel cylinder. The following discussion explains how the corrected and theoretical curves were obtained.

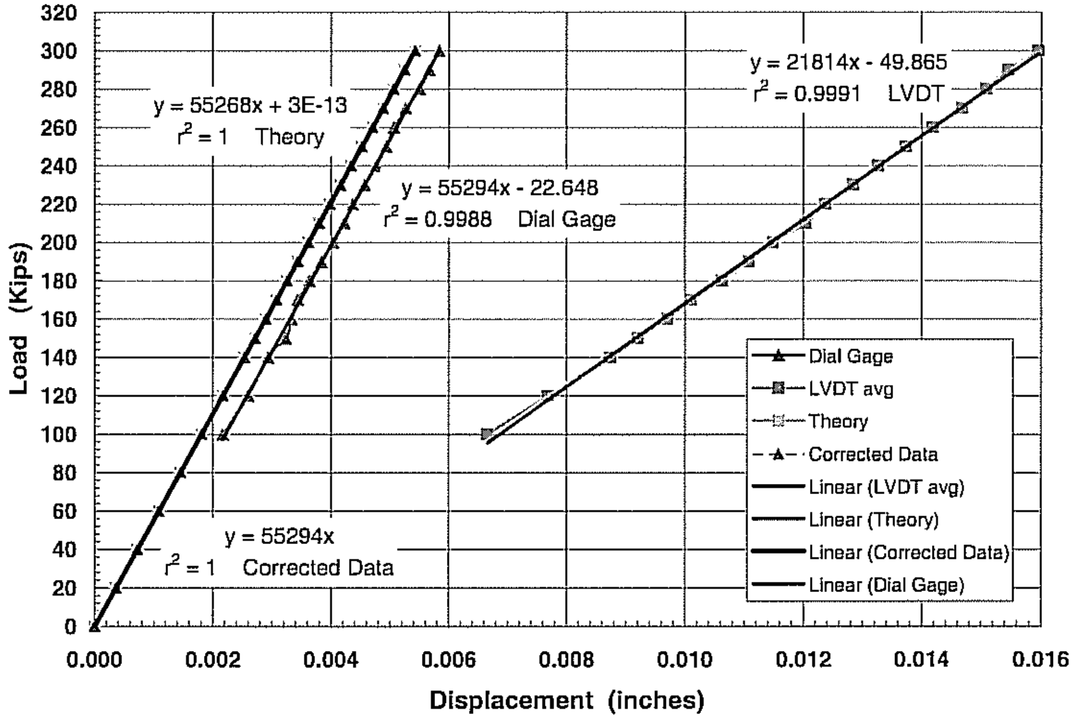

Figure 4.10. Axial Compressive Load versus Displacement for the Steel Cylinder Used for Compliance Testing.

A corrected load-displacement curve can be obtained from a combination of LVDT and dial gage data from the steel cylinder. The correction can later be applied to approximate the modulus of elasticity of the concrete cylinders tested. The slope of LVDT curve is the equivalent stiffness of the system when the steel cylinder was tested. The slope of the dial gage curve is the stiffness of the steel specimen. Using the relationship for springs in series, the stiffness of the top platen can be calculated from Equation 2,

$$\frac{1}{K_{syss}} = \frac{1}{K_{steel}} + \frac{1}{K_{TP}} \qquad 4.2$$

where

K_{syss} = system stiffness with the steel cylinder in place (measured by the LVDT),
K_{steel} = stiffness of steel specimen (measured by the dial gage),
K_{TP} = stiffness of the top platen.

The stiffness of the top platen can also be written as the load divided by the deflection such that

$$K_{TP} = \frac{P}{\Delta_{TP}} \tag{4.3}$$

where

P = applied load,
Δ_{TP} = displacement of top platen.

The top platen displacement, Δ_{TP}, is solved for at known load steps using measured LVDT and dial gage data in Equation 2 and substituting into Equation 3. Subtracting Δ_{TP} from Δ_{syss} (the LVDT measurement) gives the true displacement of the steel cylinder, Δ_s. The plot of load versus Δ_s is the "corrected" curve shown in Figure 4.10.

Assuming the modulus of elasticity of the steel cylinder, E_s, is 200 GPa (29,000 ksi), the theoretical cylinder stiffness, K_s, can be obtained directly from

$$K_s = \frac{P}{\Delta} = \frac{A \times E_s}{L} \tag{4.4}$$

where

K_s = steel specimen stiffness,
E_s = modulus of elasticity of steel cylinder,
A = cross sectional area of steel specimen,
L = length of steel specimen.

Plotting the theoretical stiffness (load versus displacement) yields the theoretical curve shown in Figure 4.10. The theoretical and corrected curves overlap each other indicating that they are in perfect agreement. This also indicates that the MTS testing machine is properly recording the load measurements.

The same principles were applied to the concrete specimens with the exception that E_c was calculated directly from the measured concrete stiffness, K_{con}. The following methodology was used to obtain the stiffness of the concrete specimen.

$$\frac{1}{K_{sysc}} = \frac{1}{K_{con}} + \frac{1}{K_{TP}} \tag{4.5}$$

where

K_{sysc} = system stiffness with concrete specimen in place (measured by LVDT),
K_{con} = stiffness of concrete cylinder (desired quantity),
K_{TP} = stiffness of top platen (from Eqn. 2).

The displacement of the top platen is assumed to be only a function of the applied load, and is therefore independent of the composition of the test specimen. Thus the stiffness of the top platen is not affected by the stiffness of the specimen. Equation 6 can then be written by solving Equations 2 and 5 for $1/K_{TP}$ and setting the results equal to one another.

$$\frac{1}{K_{syss}} - \frac{1}{K_{steel}} = \frac{1}{K_{sysc}} - \frac{1}{K_{con}} \qquad 4.6$$

Solving Equation 6 for $1/K_{con}$ results in

$$\frac{1}{K_{con}} = \frac{1}{K_{sysc}} + \frac{1}{K_{steel}} - \frac{1}{K_{syss}} \qquad 4.7$$

Now that the stiffness of the concrete specimen, K_{con}, is solved, E_c is related to the stiffness of the concrete specimen in the following manner. Solving Equation 4 and substituting concrete for steel gives the following expression for E_c.

$$E_c = \frac{K_{con} \times L}{A} \qquad 4.8$$

where

E_c = modulus of elasticity of concrete,
K_{con} = concrete specimen stiffness from Eqn. 7,
L = length of concrete specimen (12 in.),
A = cross sectional area of concrete specimen.

Modulus of elasticity was estimated for comparison using the relationships for normal weight concrete from the ACI Concrete Building Code 318-95.

$$E_c = 0.043 \times w^{1.5} \times \sqrt{f'c} \quad \text{SI} \qquad E_c = 33 \times w^{1.5} \times \sqrt{f'c}\ \text{USC} \qquad 4.9$$

where

E_c = modulus of elasticity of concrete specimen (MPa, psi),
w = unit weight of concrete (kg/m^3, lb./ft^3).

Table 4.6 is a summary of the modulus of elasticity for each of the three coarse aggregates used in this study and the percent difference from CA-B as well as from ACI 318-95. Moduli of elasticity shown are averages for all axial compression cylinders tested for that particularly type of coarse aggregate. Test data results did not compare well with ACI 318-95 predictions.

Table 4.6 Summary of Modulus of Elasticity Results

Aggregate Type	E_c Calculated from Data MPa (ksi)	Percent Difference from CA-B	E_c Estimated from ACI 318-95 MPa (ksi)	Percent Difference from ACI 318-95
CA-B	23,400 (3,387)	-	32,200 (4,640)	-27.4
CA-G	22,750 (3,299)	-2.6	32,250 (4,647)	-29.4
CA-S	24,950 (3,616)	6.7	30,800 (4,439)	-19.0

Caution needs to be taken when examination of modulus of elasticity is considered. Results presented were not obtained using the standard ASTM procedure. End effects may exist due to not only the barreling the specimen experiences during loading, but also the effect of end capping. Capping provides greater surface area in contact with the platens that translates to larger frictional forces holding the ends of the cylinder together.

4.2 Conclusions

The objective of this phase of the research was two-fold. The first objective was to become proficient in the preparation of concrete using the MDOT Mortar Voids method. The second objective was to determine if axial compressive and split tensile strength of concrete vary with coarse aggregate type based on a 28-day cure using the MDOT P1 mix design. Based on this research the following conclusions and observations are presented:

(1) Automated methods were used to determine the apparent specific gravity, bulk dry specific gravity and absorption. The results showed excellent agreement with standard ASTM methods for the basalt and glacial gravel aggregates. However, there was significant variation for the blast furnace slag aggregate.

(2) Based on the results of the strength testing and yield data results it is believed that consistent concrete was prepared using the MDOT Mortar Voids method.

(3) It was found that all concrete mixes gave superior strength results independent of coarse aggregate type (basalt, sand and gravel, or blast furnace slag) when compared to the design strength of 24 MPa (3500 psi) for a P1 mix design.

(4) There were, however, strength variations based on the coarse aggregate type. The slag concrete had a ten percent increase in axial compressive strength over the basaltic concrete. Similar results were found for split tensile strength with the slag concrete having a 12 percent increase over the basaltic concrete. The sand and gravel concrete was in between the slag and basalt concrete.

(5) From the yield data it was observed that the slag concrete had an overall volume reduction per concrete batch (and hence an apparent increase in cement content per cubic meter), which was believed to be due to the increased penetration of the mortar into the surface pores of the slag. It is believed that by increasing the contact area between the slag and the mortar provided increased strength in both compression and tension.

(6) It was observed that the concrete's facture surface, in relation to coarse aggregate fracture versus pullout, was dependent on the coarse aggregate type. The slag

coarse aggregate exhibited the very high surface fractures of approximately 80 to 100% of the coarse aggregate particles, while the bond failure for the basaltic concrete and sand and gravel concrete was estimated to be approximately 20 to 30 percent of the total. It was speculated that the higher mortar to aggregate interface caused the fracture surface to be forced through the slag as opposed at the interface.

(7) The air content of the slag concrete was much lower than the basaltic concrete or the sand and gravel concrete using both the Volumetric and Gravimetric Methods. The variability between the two methods was the greatest for the slag concrete because of difficulty in accurately measuring coarse aggregate properties (specific gravity and absorption) of the slag.

(8) The split tensile test results compared well with the ACI Concrete Building Code (ACI 318-95) predictions. However, the modulus of elasticity results did not compare well with ACI 318-95 predictions.

4.3 Recommendations for Future Work

(1) The automated specific gravity devices show excellent promise in quickly and accurately determining an aggregate's apparent specific gravity, bulk dry specific gravity and in estimating the maximum absorption. However, there was significant scatter estimating these properties for the slag aggregate. It is recommended that additional testing be considered to determine if the variation is due to the ASTM test method, which uses water to penetrate the aggregate, or with the helium pycnometer, which uses helium gas to penetrate the aggregate.

(2) It is apparent that the surface characteristics and shape of the coarse aggregate affect the overall strength of the concrete to a limited degree. While this level of strength increase may not be significant given the total strength of a concrete mix, it does provide an understanding of the fracture process, which can be important in studying the long-term durability of concrete. Therefore, it is recommended that additional research be conducted to better understand the effect of surface texture and shape.

Appendix 4A

Coarse Aggregate Specific Gravity and Absorption

Coarse Aggregate :	**CA-B (Basalt)**
Source Number :	**31 - 76**
Specification :	**6AA**
Test date:	**4/17/98**
Test laboratory:	**MTU, B004 Dillman**

Test number	M1	M2	M3	
Bucket Identification	X	Y	Z	
Pan Identification	X_1	Y_2	Z_3	
A. SSD Agg. + Bucket	7228.9	7267.5	7014.6	
B. Weight of Bucket	2181.6	2225.8	1974.2	
C. Weight of SSD Agg. (A - B)	5047.3	5041.7	5040.4	
D. Weight of SSD Agg. + Bucket in H_2O	4640.4	4659.4	4518.1	
E. Weight of Bucket in H_2O	1377.7	1405.6	1261.4	
F. Weight of SSD Agg. In H_2O (D - E)	3262.7	3253.8	3256.7	
G. Pan Weight + Oven Dry Agg.	5515.5	5264.9	6393.7	
H. Pan Weight	543.4	299.4	1431.1	
J. Weight of Oven Dry Agg. (G - H)	4972.1	4965.5	4962.6	
C - F (SSD Volume)	1784.6	1787.9	1783.7	
J - F (Dry Agg. - Dry Weight)	1709.4	1711.7	1705.9	
C - J (SSD - Dry Weight)	75.2	76.2	77.8	**Average**
Bulk Dry S.G. = J/(C -F)	2.79	2.78	2.78	**2.78**
Bulk SSD S.G. = C/(C - F)	2.83	2.82	2.83	**2.82**
Apparent S.G. = J/(J - F)	2.91	2.90	2.91	**2.91**
Absorption, % = [(C - J)/J]*100	1.51	1.53	1.57	**1.54**

Notes: All weights in grams

Coarse Aggregate Specific Gravity and Absorption

Coarse Aggregate :	**CA-G (Glacial Gravel)**
Source Number :	**31 - 45**
Specification :	**6AA**
Test date:	**4/15/98**
Test laboratory:	**MTU, B004 Dillman**

Test number	SSG1	SSG4	SSG5	
Bucket Identification	Y	Y	Z	
Pan Identification	Y_1	Y_4	Z_5	
A. SSD Agg. + Bucket	7270.2	7269.8	7011.4	
B. Weight of Bucket	2225.9	2225.8	1974.2	
C. Weight of SSD Agg. (A - B)	5044.3	5044.0	5037.2	
D. Weight of SSD Agg. + Bucket in H_2O	4622.7	4620.3	4468.9	
E. Weight of Bucket in H_2O	1405.6	1405.6	1261.4	
F. Weight of SSD Agg. In H_2O (D - E)	3217.1	3214.7	3207.5	
G. Pan Weight + Oven Dry Agg.	6354.0	5510.5	5504.8	
H. Pan Weight	1384.8	539.2	539.8	
J. Weight of Oven Dry Agg. (G - H)	4969.2	4971.3	4965.0	
C - F (SSD Volume)	1827.2	1829.3	1829.7	
J - F (Dry Agg. - Dry Weight)	1752.1	1756.6	1757.5	
C - J (SSD - Dry Weight)	75.1	72.7	72.2	Average
Bulk Dry S.G. = J/(C -F)	2.72	2.72	2.71	**2.72**
Bulk SSD S.G. = C/(C - F)	2.76	2.76	2.75	**2.76**
Apparent S.G. = J/(J - F)	2.84	2.83	2.83	**2.83**
Absorption, % = [(C - J)/J]*100	1.51	1.46	1.45	**1.48**

Notes: All weights in grams

Coarse Aggregate Specific Gravity and Absorption

Coarse Aggregate :	CA-S(1) (Slag)
Source Number :	82 - 19
Specification :	**6AA**
Test date:	**4/18/98 Trial 1**
Test laboratory:	**MTU, B004 Dillman**

Test number	LS1	LS2	LS3	
Bucket Identification	Z & Y	X & Y	X & Y	
Pan Identification	Z_1 & Y_1	X_2 & Y_2	X_3 & Y_3	
A. SSD Agg. + Bucket	9325.8	9471.2	9490.9	
B. Weight of Bucket	4200.0	4407.4	4407.4	
C. Weight of SSD Agg. (A - B)	5125.8	5063.8	5083.5	
D. Weight of SSD Agg. + Bucket in H_2O	5753.6	5906.8	5881.9	
E. Weight of Bucket in H_2O	2667.0	2783.3	2783.3	
F. Weight of SSD Agg. In H_2O (D - E)	3086.6	3123.5	3098.6	
G. Pan Weight + Oven Dry Agg.	6044.2	6041.9	6037.5	
H. Pan Weight	1090.9	1083.1	1083.4	
J. Weight of Oven Dry Agg. (G - H)	4953.3	4958.8	4954.1	
C - F (SSD Volume)	2039.2	1940.3	1984.9	
J - F (Dry Agg. - Dry Weight)	1866.7	1835.3	1855.5	
C - J (SSD - Dry Weight)	172.5	105.0	129.4	**Average**
Bulk Dry S.G. = J/(C -F)	2.43	2.56	2.50	**2.49**
Bulk SSD S.G. = C/(C - F)	2.51	2.61	2.56	**2.56**
Apparent S.G. = J/(J - F)	2.65	2.70	2.67	**2.68**
Absorption, % = [(C - J)/J]*100	3.48	2.12	2.61	**2.74**

Notes: All weights in grams

Coarse Aggregate Specific Gravity and Absorption

Coarse Aggregate :	CA-S(2) (Slag)
Source Number :	82 - 19
Specification :	6AA
Test date:	7/7/98 Trial 2
Test laboratory:	MTU, B004 Dillman

Test number	LS4	LS5	LS6	
Bucket Identification	X	Y	Z	
Pan Identification	X_4	Y_5	Z_6	
A. SSD Agg. + Bucket	4831.3	4885.4	4828.7	
B. Weight of Bucket	2178.9	2225.5	2178.9	
C. Weight of SSD Agg. (A - B)	2652.4	2659.9	2649.8	
D. Weight of SSD Agg. + Bucket in H_2O	2941.2	2973.8	2947.0	
E. Weight of Bucket in H_2O	1376.2	1405.1	1376.2	
F. Weight of SSD Agg. In H_2O (D - E)	1565.0	1568.7	1570.8	
G. Pan Weight + Oven Dry Agg.	3030.9	2883.8	2882.4	
H. Pan Weight	545.4	395.8	397.7	
J. Weight of Oven Dry Agg. (G - H)	2485.5	2488.0	2484.7	
C - F (SSD Volume)	1087.4	1091.2	1079.0	
J - F (Dry Agg. - Dry Weight)	920.5	919.3	913.9	
C - J (SSD - Dry Weight)	166.9	171.9	165.1	**Average**
Bulk Dry S.G. = J/(C -F)	2.29	2.28	2.30	**2.29**
Bulk SSD S.G. = C/(C - F)	2.44	2.44	2.46	**2.44**
Apparent S.G. = J/(J - F)	2.70	2.71	2.72	**2.71**
Absorption, % = [(C - J)/J]*100	6.71	6.91	6.64	**6.76**

Notes: All weights in grams

Fine Aggregate Specific Gravity and Absorption

Coarse Aggregate :	**FA-Y (Sand)**
Source Number :	**31 - 45**
Specification :	**2NS**
Test date:	**7/7/98**
Test laboratory:	**MTU, B004 Dillman**

Test number	1	2	4	
Flask Number	M	N	N	
Pan Identification	M_1	N_2	N_4	
A. SSD Agg. + Flask	695.4	688.5	679.3	
B. Weight of Flask	180.7	171.2	171.2	
C. Weight of SSD Agg. (A - B)	514.7	517.3	508.1	
D. Weight of SSD Agg. + Flask + H_2O	1001.9	993.9	988.3	
E. Weight of Flask + H_2O	678.8	669.2	669.2	
F. Weight of SSD Agg. In H_2O (D - E)	323.1	324.7	319.1	
G. Pan Weight + Oven Dry Agg.	1005.0	1027.4	1040.3	
H. Pan Weight	496.7	516.5	539.1	
J. Weight of Oven Dry Agg. (G - H)	508.3	510.9	501.2	
C - F (SSD Volume)	191.6	192.6	189.0	
J - F (Dry Agg. - Dry Weight)	185.2	186.2	182.1	
C - J (SSD - Dry Weight)	6.4	6.4	6.9	**Average**
Bulk Dry S.G. = J/(C -F)	2.65	2.65	2.65	**2.65**
Bulk SSD S.G. = C/(C - F)	2.69	2.69	2.69	**2.69**
Apparent S.G. = J/(J - F)	2.74	2.74	2.75	**2.75**
Absorption, % = [(C - J)/J]*100	1.26	1.25	1.38	**1.30**

Notes: All weights in grams

Coarse Aggregate Unit Weight (Dry Loose)

CA-B (Basalt) Source No. 31-76		English		SI	
		Test 1	Test 2	Test 1	Test 2
A. Bucket weight	lbs,kg	17.95	17.95	8.14	8.14
B. Bucket + Agg.	lbs,kg	63.80	63.75	28.94	28.92
C. Weight of Agg. (B - A)	lbs,kg	45.85	45.80	20.80	20.78
D. Bucket Volume	ft^3,m^3	0.4863	0.4863	0.0138	0.0138
E. Bulk Density {dry loose} (C/D)	ft^3,m^3	94.29	94.18	1510.63	1509.18
F. Average		94.2 lbs/ft^3		1509.9 kg/m^3	

CA-G (Glacial Gravel) Source No. 31-45		English		SI	
		Test 1	Test 2	Test 1	Test 2
A. Bucket weight	lbs,kg	17.95	17.95	8.14	8.14
B. Bucket + Agg.	lbs,kg	64.90	65.45	29.44	29.68
C. Weight of Agg. (B - A)	lbs,kg	46.95	47.50	21.30	21.54
D. Bucket Volume	ft^3,m^3	0.4863	0.4863	0.0138	0.0138
E. Bulk Density {dry loose} (C/D)	ft^3,m^3	96.55	97.68	1546.95	1564.38
F. Average		97.1 lbs/ft^3		1555.7 kg/m^3	

CA-S (Slag) Source No. 82-19		English		SI	
		Test 1	Test 2	Test 1	Test 2
A. Bucket weight	lbs,kg	17.95	17.95	8.14	8.14
B. Bucket + Agg.	lbs,kg	54.90	54.60	24.90	24.75
C. Weight of Agg. (B - A)	lbs,kg	36.95	36.65	16.76	16.61
D. Bucket Volume	ft^3,m^3	0.4863	0.4863	0.0138	0.0138
E. Bulk Density {dry loose} (C/D)	ft^3,m^3	75.98	75.37	1217.22	1206.33
F. Average		75.7 lbs/ft^3		1211.8 kg/m^3	

Fine Aggregate Unit Weight (Dry Loose)

FA-Y (Sand) Source No. 31-45		English		SI	
		Test 1	Test 2	Test 1	Test 2
A. Bucket weight	lbs,kg	17.95	17.95	8.14	8.14
B. Bucket + Agg.	lbs,kg	70.35	70.45	31.92	31.95
C. Weight of Agg. (B - A)	lbs,kg	52.40	52.50	23.78	23.81
D. Bucket Volume	ft^3,m^3	0.4863	0.4863	0.0138	0.0138
E. Bulk Density {dry loose} (C/D)	ft^3,m^3	107.76	107.96	1727.06	1729.24
F. Average		107.9 lbs/ft^3		1728.2 kg/m^3	

Appendix 4B

CA-B Mix Design Worksheets

Basalt

MICHIGAN DEPARTMENT OF TRANSPORTATION

FORM 1830 CONCRETE PROPORTIONING DATA FILE 300

CONTROL SECTION ID: GENERAL
JOB NUMBER: MTU
LAB NUMBER:
GRADE OF CONCRETE: P1
INTENDED USE OF CONCRETE: Pavement (Conv. Form)

MDOT mix design for CA-B

DATE: 4/27/1998
SPECIFICATION: 1996 STD SPECS
MIX DESIGN NUMBER:

CONCRETE MATERIALS

MATERIAL	SOURCE	PIT NUMBER	CLASS	SPECIFIC GRAVITY	ABSORPTION PERCENT
CEMENT	(SEE REMARKS)		I/IA	3.15	
FINE AGG.	SUPERIOR SAND & GRAVEL	31-45	2NS	2.67	0.87
COARSE AGG.	MOYLE	31-76	6AA	2.79	1.45
FLY ASH					

CEMENT CONTENT, kg/m^3 335
AIR CONTENT (DESIGN): 6.5% (SPECIFIED): 6.5%
R.W.C: 1.15
FLY ASH CONTENT, kg/m^3: 0

B/Bo : 0.72
SPECIFICATION TOLERANCE (±): 1.5%
THEORETICAL YIELD: 100.00%

WEIGHT OF COARSE AGG. (DRY/LOOSE) kg/m^3	AGGREGATE AND WATER PROPORTIONS QUANTITIES, kg/m^3 OF CONCRETE		
	FINE AGG (OVEN DRY)	COARSE AGG (OVEN DRY)	TOTAL WATER
1460	821	1051	167
1470	815	1058	167
1480	809	1066	166
1490	803	1073	166
1500	797	1080	166
1510	791	1087	165
1520	785	1094	165
1530	779	1102	165
1540	773	1109	165
1550	767	1116	164
1560	761	1123	164

REMARKS:
THIS CHART FOR USE WITH CEMENTS OF THE CLASS SHOWN FROM APPROVED SOURCES.

TYPICAL UNIT WEIGHT (DRY, LOOSE) OF COARSE AGGREGATE AS DESCRIBED ABOVE IS 1510 kg/m^3

SPECIAL MESSAGES:

CC:
MTU

JOHN F. STATON
MATERIALS RESEARCH ENGINEER

MIX PROPORTIONS WORKSHEET

	Laboratory No	Bulk Dry Specific Gravity	% Absorption
Cement: Lafarge (Alpena) Type 1		3.15	–
Coarse Aggregate: CA-B (Basalt) Source No. 31-76 Specification 6AA	MTU	2.79 ★	1.45 ★
Fine Aggregate: FA-Y Source No. 31-45 Specification 2NS		2.67 ★	0.87 ★

Material	Weight, kg/m³	Batch Proportions kg (batch size 0.0779779 m³)	
Cement	335 ★	26.12	**Total cement** (C)
Coarse Aggregate (DRY)	1087 ★	84.76	**Total Coarse Agg.** (a)
Fine Aggregate (DRY)	791 ★	61.68	**Total Fine Agg.** (b)
Total Water	165 ★	12.87	**Total Water per Batch** (d)
Absorbed Water		22.64	**Absorbed water kg/m³** (W)

Coarse aggregate gradation:

		Pass	Ret	%
21.190	21.19	25.0mm	19.0mm	25
21.190	21.19	19.0mm	12.5mm	25
21.190	21.19	12.5mm	9.5mm	25
21.190	21.19	9.5mm	4.75mm	25
	84.76			

Absorbed water:

	agg	*absorption =	absorbed $h_2 0$
Coarse Agg	1087	0.0145	15.76
Fine Agg	791	0.0087	6.88
			22.64

Total Aggregate Contains 42.1 % Fine Aggregate

Note: ★ Provided by MDOT (Form 1830, File 300) and listed in Table 2.3

BATCH COMPUTATIONS WORKSHEET

WEIGHT IN kg

Coarse Aggregate

84.76 Coarse Agg (a)

Pail tare	1.65	1.64	3.29 + pails
			88.05 = total
25.0 - 19.0mm	21.19	0.00	
19.0 - 12.5mm	0.00	21.19	
12.5 - 9.5mm	0.00	21.19	
9.5 - 4.75mm	21.19	0.00	
Sub total	44.03	44.02	88.05 Total

Fine Aggregate

61.68 Fine Agg (b)

Moisture content

wet	dry
335.38	323.37
0.0371	MC

0.0371 MC

2.29 Moisture

Dry weight 61.68

\+

Moisture 2.29

Total 63.97

Cement

26.12 Cement (C)

Pail ID K, L

Tare weight 0.83 — 1.66 tare

Tare weight 0.83 — 27.78 Pail + cement

Total tare 1.66

Air Entraining Admixture

28 ml

Batch Summary

(a)	Coarse Aggregate as Designed	84.76 kg
(b)	Fine Aggregate as Designed	61.68 kg
(C)	Cement as Designed	26.12 kg
(D)	Total Water of Batch	14.12 kg
(e)	**Total Weight of Batch**	**186.68** kg

BATCH NO. MA

COARSE AGG CA-B (Basalt)

DATE: 6/3/98

Batch Made WED @ 9:30am

WATER MEASUREMENT

Coarse Agg +pail	44.03		
Coarse Agg +pail	44.02		
Total	88.05		
+ Total Batch Water	12.87	(d)	12.87
- Reserve Water	3.00		3.00
= Pails, Agg&Water	**97.92**	H_20	9.87

RESERVE WATER

Res water	3.00	1.33 surplus & Tare
+ Tare	0.29	0.29 - tare
= Total	3.29	1.04 = surplus

Reserve Water	3.00		
- Surplus Water	1.04		
=	1.96	H_2O +	9.87
Subtotal of water in batch		=	11.83
+ Moisture in Fine Aggregate		+	2.29
Total Water in Batch		**(D) =**	**14.12**

UNIT WEIGHT

Weight of Concrete & Bucket	41.03	
- Weight of Bucket	8.14	
= Weight of Concrete in Bucket	32.89	(f)

SLUMP = 2.25 " — 57.2 mm

AIR CONTENT

- Factor of Aggregate Porosity

= Percent Air 5.7

CONCRETE TEMPERATURE, C 19

Note: a,b,C,d come from mix proportions worksheet

BATCH COMPUTATIONS WORKSHEET **WEIGHT IN kg**

Coarse Aggregate

84.76 Coarse Agg (a)

Pall tare	1.65	1.65	3.30	+ pails
			88.06	= total
25.0 - 19.0mm	21.19	0.00		
19.0 - 12.5mm	0.00	21.19		
12.5 - 9.5mm	0.00	21.19		
9.5 - 4.75mm	21.19	0.00		
Sub total	44.03	44.03	88.06	Total

BATCH NO.	MB
COARSE AGG	CA-B (Basalt)
DATE:	6/3/98
Batch Made	WED @ 11:30am

WATER MEASUREMENT

Coarse Agg +pail	44.03		
Coarse Agg +pail	44.03		
Total	88.06		
+ Total Batch Water	12.87	(d)	12.87
- Reserve Water	3.00		3.00
= Pails, Agg&Water	97.93	H_2O	9.87

Fine Aggregate

61.68 Fine Agg (b)

Moisture content

wet	dry
335.38	323.37
0.0371	MC

0.0371 MC

2.29 Moisture

Dry weight	61.68
+ Moisture	2.29
Total	63.97

RESERVE WATER

Res water	3.00	1.29	surplus & Tare
+ Tare	0.29	0.29	- tare
= Total	3.29	1.00	= surplus

Reserve Water	3.00		
- Surplus Water	1.00		
=	2.00	H_2O +	9.87
Subtotal of water in batch		=	11.87
+ Moisture in Fine Aggregate		+	2.29
Total Water in Batch		**(D) =**	**14.16**

Cement

26.12 Cement (C)

Pail ID	M , N		
Tare weight	1.16	2.37	tare
Tare weight	1.21	28.49	Pail + cement
Total tare	2.37		

UNIT WEIGHT

Weight of Concrete & Bucket	41.09	
- Weight of Bucket	8.14	
= Weight of Concrete in Bucket	32.95	(f)

Air Entraining Admixture 28 ml

SLUMP = 3.00 " 76.2 mm

Batch Summary

(a)	Coarse Aggregate as Designed	84.76 kg
(b)	Fine Aggregate as Designed	61.68 kg
(C)	Cement as Designed	26.12 kg
(D)	Total Water of Batch	14.16 kg
(e)	**Total Weight of Batch**	186.72 kg

AIR CONTENT

AIR CONTENT	
- Factor of Aggregate Porosity	
= Percent Air	5.5

CONCRETE TEMPERATURE, C 19

Note: a,b,C,d come from mix proportions worksheet

YIELD DATA

Coarse Aggregate :	CA-B (Basalt)
Source Number :	31-76
Specification :	6AA

	Formulae for Computation	Batch Identification MA	Batch Identification MB	Yield Data MA	Yield Data MB	Units
g	Unit Weight of Concrete f / Volume of unit weight bucket	32.89 / 0.01377	32.95 / 0.01377	2388.5	2392.9	kg/m³
h	Batch Volume of Concrete e / g	186.68 / 2388.5	186.72 / 2392.9	0.07816	0.07803	m³ batch
i	Cement used for one m³ of concrete C / h	26.12 / 0.07816	26.12 / 0.07803	334.2	334.8	kg/m³
j	Net water used for one m³ of concrete D / h - Absorbed Water (W)	14.12 / 0.07816 minus 22.64	14.16 / 0.07803 minus 22.64	157.98	158.78	kg/m³
k	Water / Cement Ratio j / i	157.98 / 334.23	158.78 / 334.77	0.47	0.47	w/c

Note: C,D,e,f,W come from batch computations worksheet

REPORT OF TEST

Coarse Aggregate :	CA-B (Basalt)
Source Number :	31-76
Specification :	6AA

Properties of Coarse Aggregate

Bulk Specific Gravity (dry basis)	2.79
Absorption % (24 hour soak)	1.45
Unit weight (dry loose) kg/m^3	1510

Concrete Mixture Data

	Batch Identification				
	MA	MB			Average
Date of Batch	6/3/98	6/3/98			
Slump (mm)	57	76			**67**
Unit weight of Concrete (kg/m^3)	2389	2393			**2391**
Apparent Cement Content (kg/m^3)	334	335			**334**
Water/Cement Ratio (by weight)	0.47	0.47			**0.47**
Air Content (%)	5.7	5.5			**5.6**

Compressive Strength (MPa)

28 Days	41.1	40.9			**41.0**

Split Tensile Strength (MPa)

28 Days	3.40	3.57			**3.49**

Appendix 4C
CA-G Mix Design Worksheets
Glacial Gravel

MICHIGAN DEPARTMENT OF TRANSPORTATION

FORM 1830 CONCRETE PROPORTIONING DATA FILE 300

CONTROL SECTION ID: GENERAL
JOB NUMBER: MTU
LAB NUMBER:
GRADE OF CONCRETE: P1
INTENDED USE OF CONCRETE: Pavement (Conv. Form)

MDOT mix design for CA-G

DATE: 4/27/1998
SPECIFICATION: 1996 STD SPECS
MIX DESIGN NUMBER:

CONCRETE MATERIALS

MATERIAL	SOURCE	PIT NUMBER	CLASS	SPECIFIC GRAVITY	ABSORPTION PERCENT
CEMENT	(SEE REMARKS)		1/IA	3.15	
FINE AGG.	SUPERIOR SAND & GRAVEL	31-45	2NS	2.67	0.87
COARSE AGG.	SUPERIOR SAND & GRAVEL	31-45	6AA	2.73	1.35
FLY ASH					

CEMENT CONTENT, kg/m^3 335
AIR CONTENT (DESIGN): 6.5% (SPECIFIED): 6.5%
R.W.C: 1.15
FLY ASH CONTENT, kg/m^3: 0

B/Bo : 0.72
SPECIFICATION TOLERANCE (±): 1.5%
THEORETICAL YIELD: 100.00%

WEIGHT OF COARSE AGG. (DRY/LOOSE) kg/m^3	AGGREGATE AND WATER PROPORTIONS QUANTITIES, kg/m^3 OF CONCRETE		
	FINE AGG (OVEN DRY)	COARSE AGG (OVEN DRY)	TOTAL WATER
1506	773	1084	163
1516	767	1092	163
1526	761	1099	163
1536	755	1106	162
1546	749	1113	162
1556	743	1120	162
1566	737	1128	161
1576	731	1135	161
1586	724	1142	161
1596	718	1149	160
1606	712	1156	160

REMARKS:
THIS CHART FOR USE WITH CEMENTS OF THE CLASS SHOWN FROM APPROVED SOURCES.

TYPICAL UNIT WEIGHT (DRY, LOOSE) OF COARSE AGGREGATE AS DESCRIBED ABOVE IS 1556 kg/m^3

SPECIAL MESSAGES:

CC:
MTU

JOHN F. STATON
MATERIALS RESEARCH ENGINEER

MIX PROPORTIONS WORKSHEET

	Laboratory No	Bulk Dry Specific Gravity	% Absorption
Cement: Lafarge (Alpena) Type 1		3.15	-
Coarse Aggregate: CA-G (Glacial Gravel) Source No. 31-45 Specification 6AA	MTU	★ 2.73	★ 1.35
Fine Aggregate: FA-Y Source No. 31-45 Specification 2NS		★ 2.67	★ 0.87

batch size 0.0779779 m^3

Material	Weight, kg/m^3	Batch Proportions kg	
Cement	335 ★	26.12	**Total cement (C)**
Coarse Aggregate (DRY)	1120 ★	87.34	**Total Coarse Agg. (a)**
Fine Aggregate (DRY)	743 ★	57.94	**Total Fine Agg. (b)**
Total Water	162 ★	12.63	**Total Water per Batch (d)**
Absorbed Water		21.58	**Absorbed water (W) kg/m^3**

Coarse aggregate batch breakdown:

		Pass	Ret	%
21.834	21.84	25.0mm	19.0mm	25
21.834	21.83	19.0mm	12.5mm	25
21.834	21.84	12.5mm	9.5mm	25
21.834	21.83	9.5mm	4.75mm	25
	87.34			

Absorbed water:

	agg	*absorption	= absorbed h_2O
Coarse Agg	1120	0.0135	15.12
Fine Agg	743	0.0087	6.46
			21.58

Total Aggregate Contains 39.9 % Fine Aggregate

Note: ★ Provided by MDOT (Form 1830, File 300) and listed in Table 2.3

BATCH COMPUTATIONS WORKSHEET

WEIGHT IN kg

Coarse Aggregate

87.34 Coarse Agg (a)

Pail tare	1.64	1.65	3.29 + pails
			90.63 = total
25.0 - 19.0mm	21.84	0.00	
19.0 - 12.5mm	0.00	21.83	
12.5 - 9.5mm	0.00	21.84	
9.5 - 4.75mm	21.83	0.00	
Sub total	45.31	45.32	90.63 Total

BATCH NO. SSC

COARSE AGG CA-G (Glacial Gravel)

DATE: 6/4/98

Batch Made Thur @ 9:30am

Fine Aggregate

57.94 Fine Agg (b)

Moisture content

wet	dry
344.74	332.36
0.0372	MC

0.0372 MC

2.16 Moisture

Dry weight 57.94
+
Moisture 2.16
Total 60.10

WATER MEASUREMENT

Coarse Agg +pail 45.31
Coarse Agg +pail 45.32

Total 90.63
+ Total Batch Water 12.63 (d) 12.63
- Reserve Water 3.00 3.00
= Pails, Agg&Water **100.26** H_2O 9.63

Cement

26.12 Cement (C)

Pail ID O , P

Tare weight 1.19 — 2.48 tare
Tare weight 1.29 — 28.60 Pail + cement
Total tare 2.48

RESERVE WATER

Res water	3.00	1.53 surplus & Tare
+ Tare	0.29	0.29 - tare
= Total	3.29	1.24 = surplus

Reserve Water 3.00
- Surplus Water 1.24
= 1.76 — H_2O + 9.63
Subtotal of water in batch = 11.39
+ Moisture in Fine Aggregate + 2.16
Total Water in Batch (D) = 13.55

Air Entraining Admixture 28 ml

UNIT WEIGHT

Weight of Concrete & Bucket 41.06
- Weight of Bucket 8.14
= Weight of Concrete in Bucket **32.92** (f)

Batch Summary

(a)	Coarse Aggregate as Designed	87.34 kg
(b)	Fine Aggregate as Designed	57.94 kg
(c)	Cement as Designed	26.12 kg
(D)	Total Water of Batch	13.55 kg
(e)	**Total Weight of Batch**	**184.95** kg

SLUMP = 2.00 " **50.8** mm

AIR CONTENT

- Factor of Aggregate Porosity
= Percent Air **4.1**

CONCRETE TEMPERATURE, C 19

Note: a,b,C,d come from mix proportions worksheet

BATCH COMPUTATIONS WORKSHEET

WEIGHT IN kg

Coarse Aggregate

87.34 Coarse Agg (a)

Pail tare	1.65	1.65	3.30 + pails
			90.64 = total
25.0 - 19.0mm	21.84	0.00	
19.0 - 12.5mm	0.00	21.83	
12.5 - 9.5mm	0.00	21.84	
9.5 - 4.75mm	21.83	0.00	
Sub total	45.32	45.32	90.64 Total

BATCH NO. SSD

COARSE AGG CA-G (Glacial Gravel)

DATE: 6/4/98

Batch Made Thur @ 11:30am

Fine Aggregate

57.94 Fine Agg (b)

Moisture content

wet	dry
344.74	332.36
0.0372	MC

0.0372 MC

2.16 Moisture

Dry weight 57.94

\+

Moisture 2.16

Total 60.10

Cement

26.12 Cement (C)

Pail ID Q , R

Tare weight 1.31

Tare weight 1.19

Total tare 2.50

2.50 tare

28.62 Pail + cement

Air Entraining Admixture

28 ml

Batch Summary

(a)	Coarse Aggregate as Designed	87.34 kg
(b)	Fine Aggregate as Designed	57.94 kg
(c)	Cement as Designed	26.12 kg
(D)	Total Water of Batch	13.59 kg
(e)	**Total Weight of Batch**	**184.99** kg

WATER MEASUREMENT

Coarse Agg +pail	45.32		
Coarse Agg +pail	45.32		
Total	90.64		
+ Total Batch Water	12.63	(d)	12.63
- Reserve Water	3.00		3.00
= Pails, Agg&Water	**100.27**	H_2O	9.63

RESERVE WATER

Res water 3.00	1.49	surplus & Tare
+ Tare 0.29	0.29	- tare
= Total 3.29	1.20	= surplus

Reserve Water	3.00		
- Surplus Water	1.20		
=	1.80	H_2O +	9.63
Subtotal of water in batch		=	11.43
+ Moisture in Fine Aggregate		+	2.16
Total Water in Batch		**(D) =**	**13.59**

UNIT WEIGHT

Weight of Concrete & Bucket	40.69	
- Weight of Bucket	8.14	
= Weight of Concrete in Bucket	**32.55**	**(f)**

SLUMP = 3.00 " **76.2** mm

AIR CONTENT

- Factor of Aggregate Porosity
= Percent Air **5.1**

CONCRETE TEMPERATURE, C 19

Note: a,b,C,d come from mix proportions worksheet

YIELD DATA

Coarse Aggregate :	CA-G (Glacial Gravel)
Source Number :	31-45
Specification :	6AA

Formulae for Computation		Batch Identification		Yield Data		Units
		SSC	SSD	SSC	SSD	
g	**Unit Weight of Concrete** f / Volume of unit weight bucket	32.92 / 0.01377	32.55 / 0.01377	2390.7	2363.8	kg/m^3
h	**Batch Volume of Concrete** e / g	184.95 / 2390.7	184.99 / 2363.8	0.07736	0.07826	m^3 batch
i	**Cement used for one m^3 of concrete** C / h	26.12 / 0.07736	26.12 / 0.07826	337.7	333.8	kg/m^3
j	**Net water used for one m^3 of concrete** D / h - Absorbed Water (W)	13.55 / 0.07736 minus 21.58	13.59 / 0.07826 minus 21.58	153.58	152.08	kg/m^3
k	**Water / Cement Ratio** j / i	153.58 / 337.67	152.08 / 333.81	0.45	0.46	w/c

Note: C,D,e,f,W come from batch computations worksheet

REPORT OF TEST

Coarse Aggregate :	CA-G (Glacial Gravel)
Source Number :	31-45
Specification :	6AA

Properties of Coarse Aggregate

Bulk Specific Gravity	(dry basis)	2.73
Absorption %	(24 hour soak)	1.35
Unit weight	(dry loose) kg/m^3	1556

Concrete Mixture Data

	Batch Identification				
	SSC	SSD			Average
Date of Batch	6/4/98	6/4/98			
Slump (mm)	51	76			**64**
Unit weight of Concrete (kg/m^3)	2391	2364			**2377**
Apparent Cement Content (kg/m^3)	338	334			**336**
Water/Cement Ratio (by weight)	0.45	0.46			**0.46**
Air Content (%)	4.1	5.1			**4.6**

Compressive Strength (Mpa)

28 Days	43.6	39.2			**41.4**

Split Tensile Strength (Mpa)

28 Days	3.72	3.33			**3.53**

Appendix 4D
CA-S Mix Design Worksheets
Slag

MICHIGAN DEPARTMENT OF TRANSPORTATION

FORM 1830 CONCRETE PROPORTIONING DATA FILE 300

CONTROL SECTION ID: GENERAL
JOB NUMBER: MTU
LAB NUMBER:
GRADE OF CONCRETE: P1
INTENDED USE OF CONCRETE: Pavement (Conv. Form)

MDOT mix design for CA-S

DATE: 4/27/1998
SPECIFICATION: 1996 STD SPECS
MIX DESIGN NUMBER:

CONCRETE MATERIALS

MATERIAL	SOURCE	PIT NUMBER	CLASS	SPECIFIC GRAVITY	ABSORPTION PERCENT
CEMENT	(SEE REMARKS)		I/IA	3.15	
FINE AGG.	SUPERIOR SAND & GRAVEL	31-45	2NS	2.67	0.87
COARSE AGG.	LEVY SLAG	82-19	6AA	2.27	3.55
FLY ASH					

CEMENT CONTENT, kg/m^3 335
AIR CONTENT (DESIGN): 6.5% (SPECIFIED): 6.5%
R.W.C: 1.15
FLY ASH CONTENT, kg/m^3: 0

B/Bo : 0.72
SPECIFICATION TOLERANCE (±): 1.5%
THEORETICAL YIELD: 100.00%

WEIGHT OF COARSE AGG. (DRY/LOOSE) kg/m^3	AGGREGATE AND WATER PROPORTIONS QUANTITIES, kg/m^3 OF CONCRETE		
	FINE AGG (OVEN DRY)	COARSE AGG (OVEN DRY)	TOTAL WATER
1162	840	837	183
1172	832	844	182
1182	825	851	182
1192	818	858	182
1202	810	865	182
1212	803	873	181
1222	796	880	181
1232	788	887	181
1242	781	894	181
1252	774	901	181
1262	766	909	180

REMARKS:
THIS CHART FOR USE WITH CEMENTS OF THE CLASS SHOWN FROM APPROVED SOURCES.

TYPICAL UNIT WEIGHT (DRY, LOOSE) OF COARSE AGGREGATE AS DESCRIBED ABOVE IS 1212 kg/m^3

SPECIAL MESSAGES:

CC:
MTU

JOHN F. STATON
MATERIALS RESEARCH ENGINEER

MIX PROPORTIONS WORKSHEET

	Laboratory No	Bulk Dry Specific Gravity	% Absorption
Cement: Lafarge (Alpena) Type 1		3.15	-
Coarse Aggregate: CA-S (Slag) Source No. 82-19 Specification 6AA	MTU	2.27 ★	3.55 ★
Fine Aggregate: FA-Y Source No. 31-45 Specification 2NS		2.67 ★	0.87 ★

Batch size 0.0779779 m^3

Material	Weight, kg/m^3	Batch Proportions kg					
Cement	335 ★	26.12	**Total cement**				**(C)**
Coarse Aggregate (DRY)	873 ★			Pass	Ret	%	
		17.019	17.01	25.0mm	19.0mm	25	
		17.019	17.02	19.0mm	12.5mm	25	
		17.019	17.02	12.5mm	9.5mm	25	
		17.019	17.02	9.5mm	4.75mm	25	
			68.07				
		68.07	**Total Coarse Agg.**				**(a)**
Fine Aggregate (DRY)	803 ★	62.62	**Total Fine Agg.**				**(b)**
Total Water	181 ★	14.11	**Total Water per batch**				**(d)**

Absorbed Water	agg*absorption =		absorbed h_2O			
Coarse Agg	873	0.0355	30.99	37.98	**Absorbed water kg/m^3**	**(W)**
Fine Agg	803	0.0087	6.99			
			37.98			

Total Aggregate Contains 47.9 % Fine Aggregate

Note: ★ Provided by MDOT (Form 1830, File 300) and listed in Table 2.3

BATCH COMPUTATIONS WORKSHEET **WEIGHT IN kg**

Coarse Aggregate

68.07 Coarse Agg (a)

Pail tare	1.65	1.65	3.30 + pails
			71.37 = total
25.0 - 19.0mm	17.01	0.00	
19.0 - 12.5mm	0.00	17.02	
12.5 - 9.5mm	0.00	17.02	
9.5 - 4.75mm	17.02	0.00	
Sub total	35.68	35.69	71.37 Total

Fine Aggregate

62.62 Fine Agg (b)

Moisture content

wet	dry
329.69	317.54
0.0383	MC

0.0383 MC

2.40 Moisture

Dry weight 62.62

\+

Moisture 2.40

Total 65.01

Cement

26.12 Cement (C)

Pail ID A', B'

Tare weight 0.85 — 1.70 tare

Tare weight 0.85 — 27.82 Pail + cement

Total tare 1.70

Air Entraining Admixture

19 ml

Batch Summary

(a)	Coarse Aggregate as Designed	68.07 kg
(b)	Fine Aggregate as Designed	62.62 kg
(c)	Cement as Designed	26.12 kg
(D)	Total Water of Batch	15.00 kg
(e)	**Total Weight of Batch**	**171.81** kg

BATCH NO. LSA

COARSE AGG CA-S (Slag)

DATE: 6/5/98

Batch Made Fri @ 9:30am

WATER MEASUREMENT

Coarse Agg +pail	35.68		
Coarse Agg +pail	35.69		
Total	71.37		
+ Total Batch Water	14.11	(d)	14.11
- Reserve Water	3.00		3.00
= Pails, Agg&Water	82.48	H_2O	11.11

RESERVE WATER

Res water	3.00	1.80	surplus & Tare
+ Tare	0.29	0.29	- tare
= Total	3.29	1.51	= surplus

Reserve Water	3.00		
- Surplus Water	1.51		
=	1.49	H_2O +	11.11
Subtotal of water in batch		=	12.60
+ Moisture in Fine Aggregate		+	2.40
Total Water in Batch		**(D) =**	**15.00**

UNIT WEIGHT

Weight of Concrete & Bucket	39.12	
- Weight of Bucket	8.14	
= Weight of Concrete in Bucket	**30.98**	**(f)**

SLUMP = 2.25 " **57.2** mm

AIR CONTENT

- Factor of Aggregate Porosity
= Percent Air **4.2**

CONCRETE TEMPERATURE, C 20

Note: a,b,C,d come from mix proportions worksheet

BATCH COMPUTATIONS WORKSHEET **WEIGHT IN kg**

Coarse Aggregate 68.07 Coarse Agg (a)

Pail tare	1.64	1.65	3.29 + pails
			71.36 = total
25.0 - 19.0mm	17.01	0.00	
19.0 - 12.5mm	0.00	17.02	
12.5 - 9.5mm	0.00	17.02	
9.5 - 4.75mm	17.02	0.00	
Sub total	35.67	35.69	71.36 Total

BATCH NO. LSC

COARSE AGG CA-S (Slag)

DATE: 6/8/98

Batch Made Monday@10:30am

Fine Aggregate 62.62 Fine Agg (b)

Moisture content

wet	dry
313.09	301.21
0.0394	MC

0.0394 MC

2.47 Moisture

Dry weight 62.62
\+
Moisture 2.47
Total 65.09

WATER MEASUREMENT

Coarse Agg +pail 35.67
Coarse Agg +pail 35.69

Total 71.36
\+ Total Batch Water 14.11 (d) 14.11
\- Reserve Water 3.00 3.00
= Pails, Agg&Water 82.47 H_20 11.11

RESERVE WATER

Res water 3.00	2.26	surplus & Tare
+ Tare 0.29	0.29	- tare
= Total 3.29	1.97	= surplus

Reserve Water 3.00
\- Surplus Water 1.97
= 1.03 H_2O + 11.11
Subtotal of water in batch = 12.14
\+ Moisture in Fine Aggregate + 2.47
Total Water in Batch (D) = 14.61

Cement 26.12 Cement (C)

Pail ID K, G'

Tare weight 0.83 1.68 tare

Tare weight 0.85 27.80 Pail + cement

Total tare 1.68

UNIT WEIGHT

Weight of Concrete & Bucket 39.08
\- Weight of Bucket 8.14
= Weight of Concrete in Bucket **30.94** (f)

Air Entraining Admixture 20 ml

SLUMP = 2.25 " **57.2** mm

Batch Summary

(a)	Coarse Aggregate as Designed	68.07 kg
(b)	Fine Aggregate as Designed	62.62 kg
(c)	Cement as Designed	26.12 kg
(D)	Total Water of Batch	14.61 kg
(e)	**Total Weight of Batch**	**171.43** kg

AIR CONTENT

\- Factor of Aggregate Porosity
= Percent Air **4.3**

CONCRETE TEMPERATURE, C 21

Note: a,b,C,d come from mix proportions worksheet

BATCH COMPUTATIONS WORKSHEET **WEIGHT IN kg**

Coarse Aggregate

			68.07	Coarse Agg (a)
Pail tare	1.65	1.65	3.30	+ pails
			71.37	= total
25.0 - 19.0mm	17.01	0.00		
19.0 - 12.5mm	0.00	17.02		
12.5 - 9.5mm	0.00	17.02		
9.5 - 4.75mm	17.02	0.00		
Sub total	35.68	35.69	71.37	Total

Fine Aggregate

		62.62	Fine Agg (b)
Moisture content			
wet	dry		
313.09	301.21	0.0394	MC
0.0394	MC	2.47	Moisture
Dry weight	62.62		
+			
Moisture	2.47		
Total	65.09		

Cement

		26.12	Cement (C)
Pail ID	A" , B"		
Tare weight	0.85	1.70	tare
Tare weight	0.85	27.82	Pail + cement
Total tare	1.70		

Air Entraining Admixture 21 ml

Batch Summary

(a)	Coarse Aggregate as Designed	68.07 kg
(b)	Fine Aggregate as Designed	62.62 kg
(c)	Cement as Designed	26.12 kg
(D)	Total Water of Batch	14.73 kg
(e)	**Total Weight of Batch**	**171.55** kg

BATCH NO.	LSD
COARSE AGG	CA-S (Slag)
DATE:	6/8/98
Batch Made	Monday@11:00am

WATER MEASUREMENT

Coarse Agg +pail	35.68		
Coarse Agg +pail	35.69		
Total	71.37		
+ Total Batch Water	14.11	(d)	14.11
- Reserve Water	3.00		3.00
= Pails, Agg&Water	82.48	H_20	11.11

RESERVE WATER

Res water	3.00	2.14	surplus & Tare
+ Tare	0.29	0.29	- tare
= Total	3.29	1.85	= surplus

Reserve Water	3.00		
- Surplus Water	1.85		
=	1.15	H_2O +	11.11
Subtotal of water in batch		=	12.26
+ Moisture in Fine Aggregate		+	2.47
Total Water in Batch		**(D) =**	**14.73**

UNIT WEIGHT

Weight of Concrete & Bucket	39.16	
- Weight of Bucket	8.14	
= Weight of Concrete in Bucket	31.02	(f)

SLUMP = 2.00 " 50.8 mm

AIR CONTENT

AIR CONTENT	
- Factor of Aggregate Porosity	
= Percent Air	4.1

CONCRETE TEMPERATURE, C 21

Note: a,b,C,d come from mix proportions worksheet

BATCH COMPUTATIONS WORKSHEET

WEIGHT IN kg

Coarse Aggregate

68.07 Coarse Agg (a)

Pail tare	1.64	1.65	3.29 + pails
			71.36 = total
25.0 - 19.0mm	17.01	0.00	
19.0 - 12.5mm	0.00	17.02	
12.5 - 9.5mm	0.00	17.02	
9.5 - 4.75mm	17.02	0.00	
Sub total	35.67	35.69	71.36 Total

BATCH NO.	LSE
COARSE AGG	CA-S (Slag)
DATE:	6/8/98
Batch Made	Monday@12:00am

Fine Aggregate

62.62 Fine Agg (b)

Moisture content

wet	dry
313.09	301.21
0.0394	MC

0.0394 MC

2.47 Moisture

Dry weight 62.62

\+

Moisture 2.47

Total 65.09

WATER MEASUREMENT

Coarse Agg +pail	35.67		
Coarse Agg +pail	35.69		
Total	71.36		
+ Total Batch Water	14.11	(d)	14.11
- Reserve Water	3.00		3.00
= Pails, Agg&Water	82.47	H_2O	11.11

RESERVE WATER

Res water	3.00	1.80	surplus & Tare
+ Tare	0.29	0.29	- tare
= Total	3.29	1.51	= surplus

Reserve Water	3.00		
- Surplus Water	1.51		
=	1.49	H_2O +	11.11
Subtotal of water in batch		=	12.60
+ Moisture in Fine Aggregate		+	2.47
Total Water in Batch		**(D) =**	**15.07**

Cement

26.12 Cement (C)

Pail ID D", E"

Tare weight	0.84	1.69	tare
Tare weight	0.85	27.81	Pail + cement
Total tare	1.69		

UNIT WEIGHT

Weight of Concrete & Bucket	39.10	
- Weight of Bucket	8.14	
= Weight of Concrete in Bucket	30.96	(f)

Air Entraining Admixture 21 ml

Batch Summary

(a)	Coarse Aggregate as Designed	68.07 kg
(b)	Fine Aggregate as Designed	62.62 kg
(c)	Cement as Designed	26.12 kg
(D)	Total Water of Batch	15.07 kg
(e)	**Total Weight of Batch**	**171.89** kg

SLUMP = 2.75 " 69.9 mm

AIR CONTENT

- Factor of Aggregate Porosity

= Percent Air 4.5

CONCRETE TEMPERATURE, C 21

Note: a,b,C,d come from mix proportions worksheet

YIELD DATA

Coarse Aggregate :	CA-S (Slag)
Source Number :	82-19
Specification :	6AA

	Formulae for Computation	Batch Identification				Yield Data				Units
		LSA	LSC	LSD	LSE	LSA	LSC	LSD	LSE	
g	Unit Weight of Concrete f / Volume of unit weight bucket	30.98 / 0.01377	30.94 / 0.01377	31.02 / 0.01377	30.96 / 0.01377	2249.8	2246.9	2252.7	2248.4	kg/m^3
h	Batch Volume of Concrete e / g	171.81 / 2249.8	171.43 / 2246.9	171.55 / 2252.7	171.89 / 2248.4	0.07637	0.07629	0.07615	0.07645	m^3 batch
i	Cement used for one m^3 of concrete C / h	26.12 / 0.07637	26.12 / 0.07629	26.12 / 0.07615	26.12 / 0.07645	342.1	342.4	343.0	341.7	kg/m^3
j	Net water used for one m^3 of concrete D / h - Absorbed Water (W)	15.00 / 0.07637 minus 37.98	14.61 / 0.07629 minus 37.98	14.73 / 0.07615 minus 37.98	15.07 / 0.07645 minus 37.98	158.44	153.56	155.50	159.19	kg/m^3
k	Water / Cement Ratio j / i	158.44 / 342.06	153.56 / 342.39	155.50 / 343.04	159.19 / 341.70	0.46	0.45	0.45	0.47	w/c

Note: C,D,e,f,W come from batch computations worksheet

REPORT OF TEST

Coarse Aggregate :	CA-S (Slag)
Source Number :	82-19
Specification :	6AA

Properties of Coarse Aggregate

Bulk Specific Gravity (dry basis)	2.27
Absorption % (24 hour soak)	3.55
Unit weight (dry loose) kg/m^3	1212

Concrete Mixture Data

	Batch Identification				
	LSA	LSC	LSD	LSE	Average
Date of Batch	6/5/98	6/8/98	6/8/98	6/8/98	
Slump (mm)	57	57	51	70	**59**
Unit weight of Concrete (kg/m^3)	2250	2247	2253	2248	**2249**
Apparent Cement Content (kg/m^3)	342	342	343	342	**342**
Water/Cement Ratio (by weight)	0.46	0.45	0.45	0.47	**0.46**
Air Content (%)	4.2	4.3	4.1	4.5	**4.3**

Compressive Strength (Mpa)

28 Days	44.1	44.7	46.5	44.7	**45.0**

Split Tensile Strength (Mpa)

28 Days	3.79	4.01	4.03	3.96	**3.95**

References

ACI Committee 318. "Building Code Requirements for Reinforced Concrete and Commentary." ACI 318-95, American Concrete Institute (ACI), Detroit, Michigan. (1995).

American Society for Testing and Materials. *Annual Book of ASTM Standards.* Vol. 04.01, Cement; Lime; Gypsum. (1998).

ASTM C 150-97a, Standard Specification for Portland Cement

American Society for Testing and Materials. *Annual Book of ASTM Standards.* Vol. 04.02, Concrete and Aggregates. (1998).

ASTM C 29/C 29M-97, Standard Test Method for Bulk Density (Unit Weight) and Voids in Aggregates

ASTM C 39-96, Standard Test Method for Compressive Strength of Cylindrical Concrete Specimens

ASTM C 127-88 (Reapproved 1993), Standard Test Method for Specific Gravity and Absorption of Coarse Aggregate

ASTM C 128-97, Standard Test Method for Specific Gravity and Absorption of Fine Aggregate

ASTM C 136-96a, Standard Test Method for Sieve Analysis of Fine and Coarse Aggregate

ASTM C 138-92, Standard Test Method for Unit Weight, Yield, and Air Content (Gravimetric) of Concrete

ASTM C 143/C 143M-97, Standard Test Method for Slump of Hydraulic-Cement Concrete

ASTM C 173-94a, Standard Test Method for Air Content of Freshly Mixed Concrete by the Volumetric Method

ASTM C 192/C 192M-95, Standard Practice for Making and Curing Concrete Test Specimens in the Laboratory

ASTM C 260-97, Standard Specification for Air-Entraining Admixtures for Concrete

ASTM C 470-94, Standard Specification for Molds for Forming Concrete Test Cylinders Vertically

ASTM C 496-96, Standard Test Method for Splitting Tensile Strength of Cylindrical Specimens

ASTM C 566-97, Standard Test Method for Total Evaporable Moisture Content of Aggregate by Drying

ASTM C 617-94, Standard Practice for Capping Cylindrical Specimens

ASTM C 1064-86 (Reapproved 1993), Standard Test Method for Temperature of Freshly Mixed Portland Cement

Grove, Gail H., *Concrete Mix Design Process Manual*, Final Report Prepared for Michigan Department of Transportation, Department of Civil and Environmental Engineering, University of Michigan, Ann Arbor, Michigan. (August, 1998).

Michigan Department of Transportation (MDOT), *1996 Standard Specifications for Construction*, Sections 601 and 902. MDOT Engineering Print Office, Lansing, Michigan. (May, 1996).

Michigan State Highway Laboratory, *Report of Investigation I 205-2.* Comparative Strength Tests of Pavement Concrete Using Slag and Gravel Coarse Aggregates, Ann Arbor, Michigan. (September, 1933).

Shehan, E.L., "The Mortar Voids Method of Proportioning Concrete as Used by the Michigan Department of State Highways", MDOT. (September, 1970).

U.S. Department of Transportation, "User Guidelines for Waste and By-Product Materials in Pavement Construction", Publication No. FHWA-RD-97-148, pp 3-1, 3-9 (Blast Furnace Slag: Material Description). (April 1998).

Vitton, S.J., Lehman, M.A., and Van Dam, T.J., (1998) "Automated Soil Particle Specific Gravity Analysis Using Bulk Flow and Helium Pycnometry," *Nondstructive and Automated Testing for Soil and Rock Properties, ASTM STP 1350,* W.A. Marr and C.E. Fairhurst, Eds., American Society for Testing and Materials, pp. 3-13.

Vitton, S.J., Personal Communication, Michigan Technological University, Department of Civil and Environmental Engineering, Houghton, Michigan. (August 1998 b).

SECTION 5

Dynamic and Quasi-Static Strength Testing

1 Introduction and Background

1.1 Introduction

The focus of this section is the strength evaluation of aggregate, cement matrix (mortar) and PCC under static and dynamic loading conditions. Typically, the duration of pavement loading is in the order of 50 to 60 milliseconds and in some cases faster depending on the condition of the joint. For example, joints that are faulted may experience shock loading due to the vertical weight of the vehicles crossing the joint. Hence the proposed approach views the loading process as a dynamic event to capture the strain rate dependent response of aggregate, mortar and concrete. It is well established in high strain rate literature that when bodies/structures are subjected to rapidly changing loads, their response differs significantly from those under static or quasi-static conditions. Generally, brittle materials fail by means of crack nucleation and growth, with limited plastic flow. Under compressive loading, failure consists of the eventual coalescence of multitude microcracks. It has been shown that compressively loaded brittle materials actually fail in tension at a multiplicity of sites where the overall compressive stress field is distributed into highly localized tensile regions (Lee and William, 1997).

The failure and fracture characteristics of many quasi-brittle and brittle materials have been found to be strongly rate dependent (e.g., Lankford 1983, Ravichandran and Subhash 1995). In considering the rate dependency of materials, the following three technical factors are important:

1. *Dependence of fracture strength and toughness on strain rate:* Compressive failure strength of brittle materials (ceramics and rocks) increases dramatically at strain rates greater than 10^2/sec (e.g., Lankford 1981, 1983, Grady and Lipkin 1980). This rate sensitivity is generally attributed to the inertia dominated dynamic crack growth from

pre-existing flaws (Lankford, 1983) and can be seen in the increase in compressive strength with an increasing strain rate as illustrated in Fig. 1.1 for limestone. Moreover, Suresh, et al. (1990) and Yang and Kobayashi (1990) have observed an increase in fracture toughness of ceramics with strain rate. However, not all brittle materials demonstrate an increase in compressive strength with increased strain rate. Figure 1.2 illustrates four materials in which one of the materials shows a flat or slightly decreasing compressive strength with increased strain rate (Lankford, 1983). It is speculated by Lankford that the reason for this occurring is a possible change in the failure mode through a grain boundary phase transformation induced by high stresses. Lankford further speculates that the brittleness of the transformed grain boundary could alter the failure process to the extent that the strength is lowered. This may also apply to aggregates since there are significant variations in grain and crystalline structure of aggregates.

2. *Variation of Fragment Size with Strain Rate:* Investigations under dynamic loading conditions of brittle materials have revealed that fragmentation size is inversely proportional to strain rate (Kipp and Grady 1985). That is, as the strain rate increases the fragment size at failure decreases. This effect is shown in Fig. 1.3 (Lankford and Blanchard, 1991). Smaller fragment size and narrow distribution imply nucleation and rapid coalescence of numerous micro-cracks at high strain rates. Such a phenomenon may have profound implications on rock blasting and fragmentation studies as well as for natural and man-made materials used as aggregate.

3. *At higher strain rates, the damage tends to be more local:* This is seen for example, when a large structure is slowly loaded the influence of the load is felt simultaneously at distances far away from the region where the load is applied. However, when a load is applied rapidly to the same structure damage concentrates around a very localized region of the structure. Consequently, the fracture strength may increase with strain rate (as illustrated in Figure 1.1), but the concentration of the stresses under dynamic loading may initiate damage and influence crack propagation and load transfer characteristics in a more localized area.

The study of material rate dependency has been investigated using a split Hopkinson pressure bar (also called Kolsky bar) technique, which has been widely used at high strain rates in the range of 10^2-10^4 s^{-1}. The split Hopkinson Pressure bar (SHPB) consists of a striker bar, an incident bar and a transmission bar, as shown schematically in Fig.1.4. The specimen to be characterized is placed between the incident and transmission bars. The free end of the incident bar is impacted by the striker bar, which is launched from a gas gun at a predetermined velocity. The impact generates a compression loading pulse in the incident bar which travels towards the specimen, subjecting it to the required compressive loading. A part of this pulse is transmitted into the transmission bar and the rest is reflected back into the incident bar as a tensile pulse. Strain gages are mounted at the center of each bar to measure the magnitude and duration of the strain pulses as they pass by. Based on one-dimensional calculations (Meyers, 1994; Follansbee, 1985), it can be shown that the magnitude of the transmitted pulse gives a measure of stress to which the specimen is subjected and the magnitude of the reflected wave gives a measure of strain rate within the specimen. Integrating the strain rate with respect to time yields the strain in the specimen. Thus, the stress-strain response of a material can also be obtained at high strain rates. The equations for calculating stress, strain rate and strain within the specimen are given by

$$\sigma_s(t) = \frac{A_b E_b \varepsilon_T(t)}{A_S} \qquad 1.1$$

$$\dot{\varepsilon}_S = -\left(\frac{2c_o \varepsilon_R(t)}{l}\right) \qquad 1.2$$

$$\varepsilon_S(t) = \int_0^t \dot{\varepsilon}_S(\tau)d\tau \qquad 1.3$$

where, A, E, σ, ε and $\dot{\varepsilon}$ refer to area, Young's modulus, stress, strain and strain rate respectively, and the subscripts b, s, T, and R refer to the bar, specimen, transmitted pulse and reflected pulse, respectively. The length of the specimen is l; c_0 is the longitudinal bar wave velocity and t is time.

There are, however, some drawbacks to the traditional SHPB for testing brittle materials when studying the way in which fracture develops in brittle materials. The main problem is that a reflected tensile pulse (generated from the specimen) travels back through the incident bar reaching the striker-end and then is reflected back as a compression pulse reloading the specimen. This process is repeated several times causing multiple loading on the specimen and subsequent additional damage to the specimen. While the stress-strain response and fracture strength can be obtained from the first transmitted load pulse, the multiple loading further damages the specimen making it very difficult to investigate the fracture process. Therefore, correlations between the actual energy input and the microstructural changes (such as crack density, energy absorbed, etc.) are difficult to obtain. Therefore, when investigating the fracture characteristics of a material the specimen must only receive a single compression pulse. This is achieved by designing a momentum trap (MT) at the impact end of the incident bar. The MT is designed in such a way that when the reflected tensile pulse reaches the striker-end of the incident bar, it absorbs the tensile wave energy and does not allow subsequent compression pulses to travel towards the specimen. Thus, the specimen is subjected to a single compression loading. A SHPB with a momentum trap is referred to as a Modified Split Hopkinson Pressure Bar (MSHPB) and is shown schematically in the Fig. 1.5.

The amplitude of the input stress pulse depends on the impact velocity of the striker bar as it contacts the incident bar while the length of the striker bar governs the pulse's duration. Choosing suitable lengths of the striker bar can generate compressive stress pulses with durations between 100-400 μs. Longer compressive stress pulses with duration of up to 0.5 ms are possible with a larger SHPB system using longer striker bars. A strain gage, mounted on the incident bar measures the complete history of the input loading pulse. A unique aspect of this technique is that a well-defined and controlled loading of a specimen can be achieved by controlling the amplitude and the duration of the input loading pulse. This is similar to a "quick-stop" technique so that a controlled amount of damage can be induced for further microstructural characterization. Moreover, the loading and unloading rates of the input pulse can be customized through insertion of a work hardening material e.g., Cu or Al, between the striker and the incident bar (Nemat-Nasser et al 1991, Subhash and Nemat-Nasser 1993). Such customization capabilities facilitate initiation and propagation of microcracks to desired stages, while preventing their coalescence and subsequent macro-scale failure. This then allows the specimen to be investigated for further microstructural observations of induced crack morphology.

By properly adjusting the incident wave amplitude, one can induce controlled amount of damage and then study, after the impact, the amount of damage and the damage initiation and propagation characteristics. The damage also can be quantified by using ultrasonic measurements techniques. The input amplitude can also be adjusted to cause complete fracture of the specimen to obtain fracture strength at a specific strain rate. Since the specimen is subjected to a single pulse in MSHPB, the signals not only reveal the fracture strength of the specimen, but also allow for comparison of fracture characteristics to the energy absorbed in the fracture process. The above technique can also be used to conduct indirect tension tests (split tensile) on short cylindrical specimens. By conducting tests at a range of strain rates, one can also obtain the variation of failure strengths with strain rate, which will be used for damage quantification as a function of rate. An additional possibility is that specimens may also be tested in various environmental conditions, e.g., moisture, temperature or in triaxial confinement.

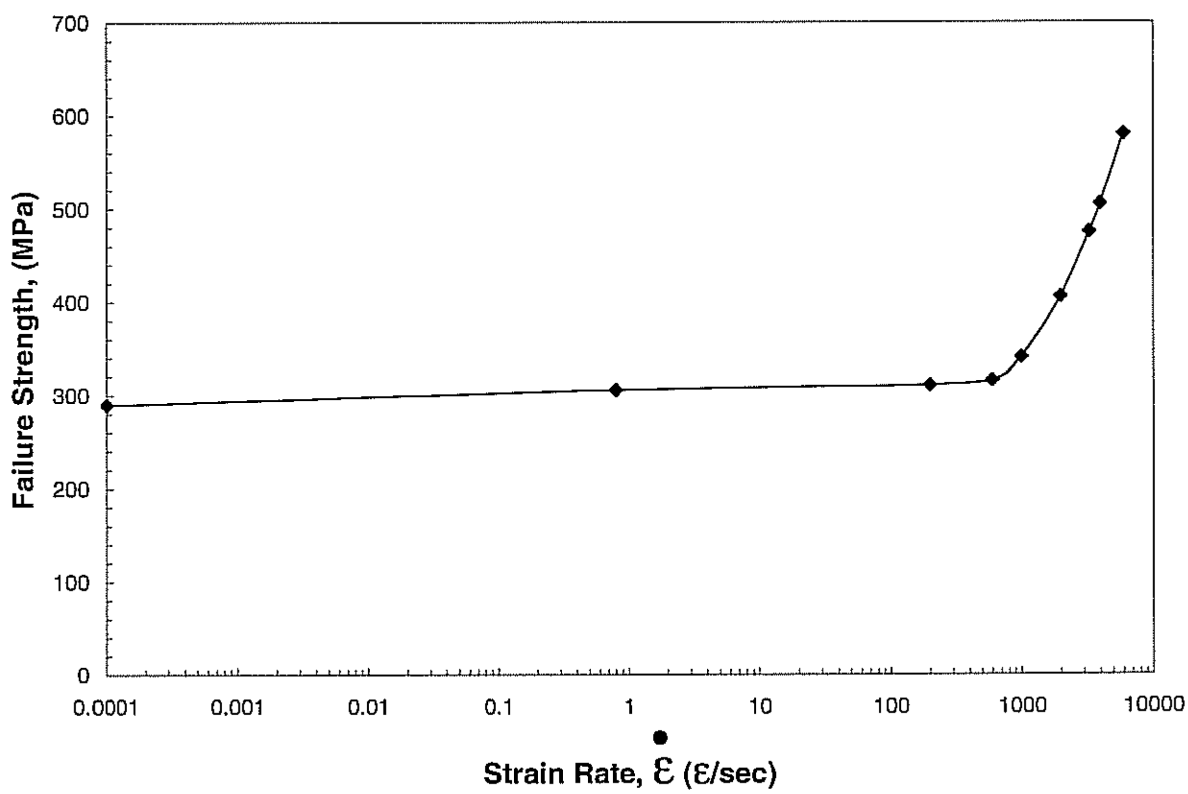

Figure 1.1 Compressive strength versus strain rate for limestone (after Lankford, 1983).

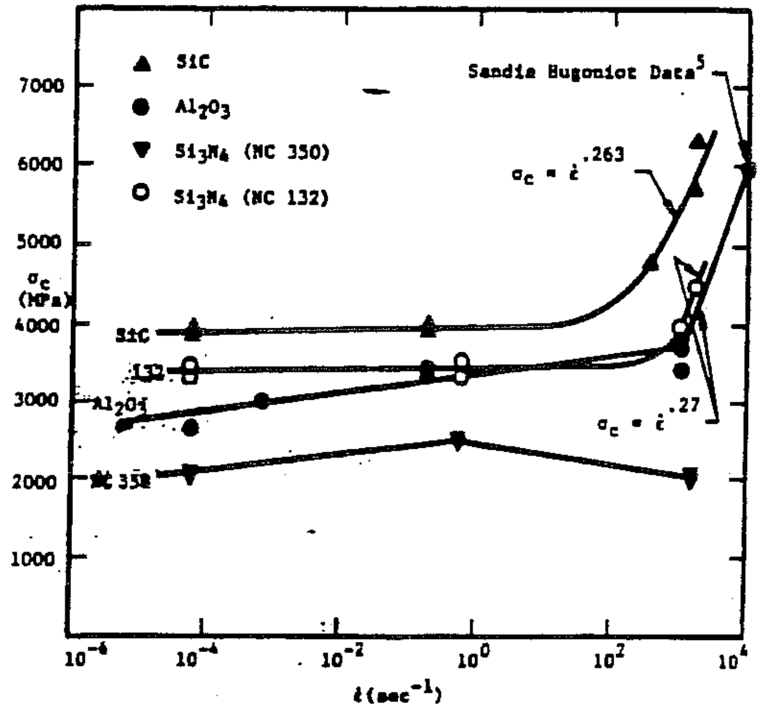

Figure 1.2 Compressive strength of various ceramic materials versus strain rate (from Lankford, 1983).

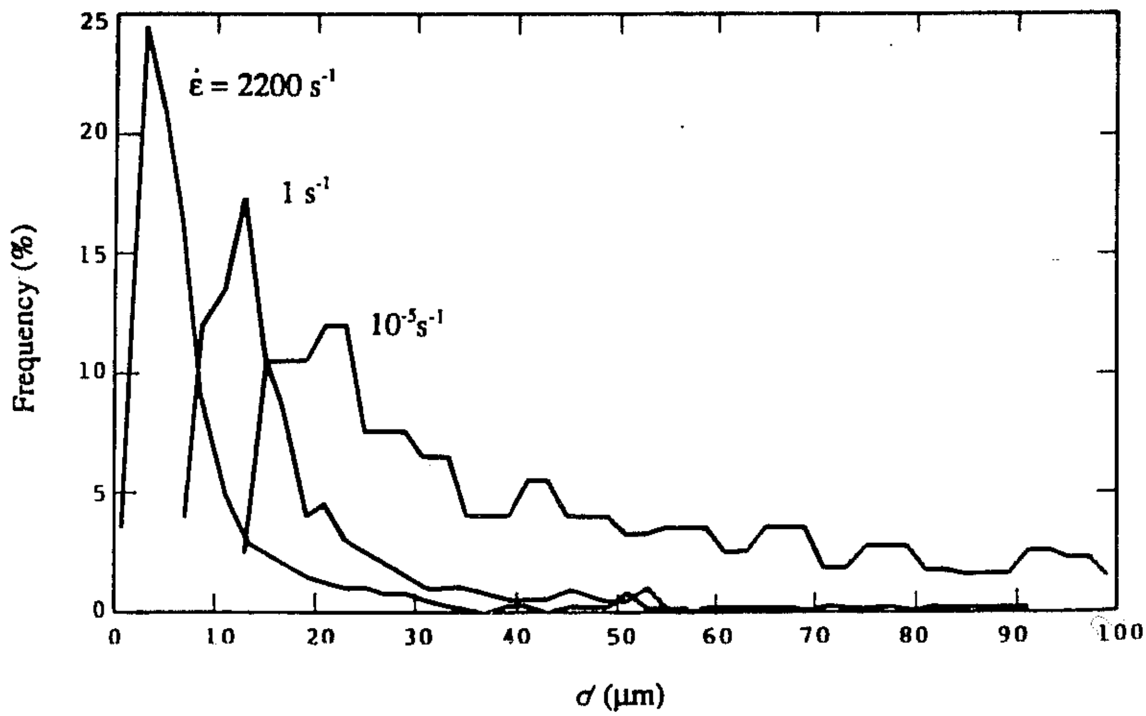

Figure 1.3. Affect of fragment size versus strain rate (From Lankford and Blanchard, 1991)

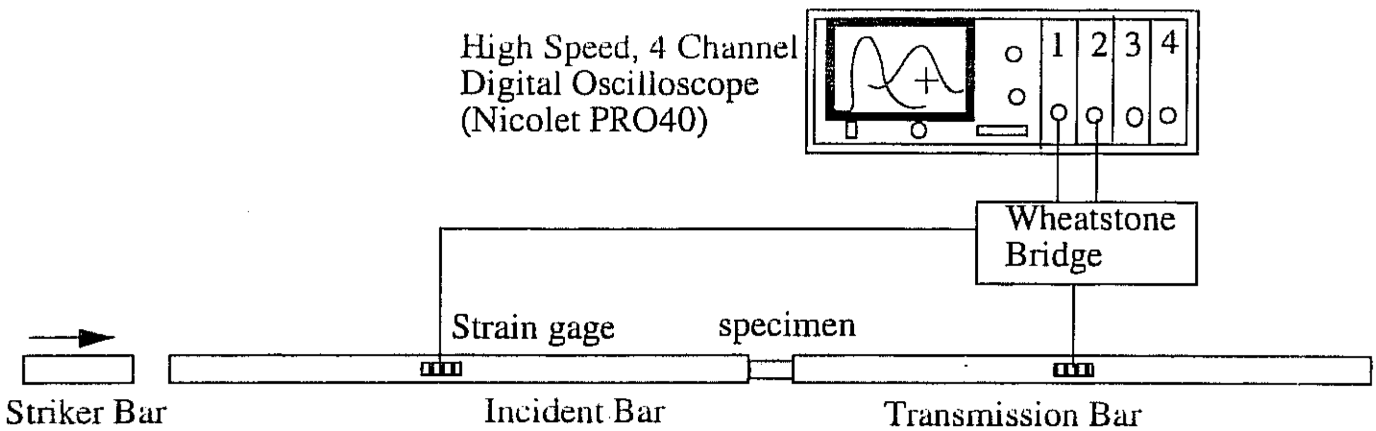

Figure 1.4 Split Hopkinson pressure bar.

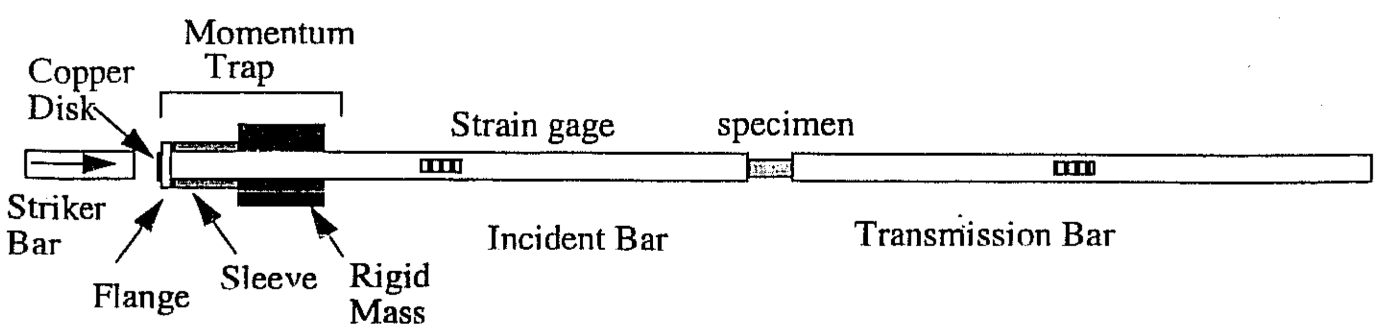

Figure 1.5 Modified Split Hopkinson pressure bar with momentum trap.

1.2 Background

1.2.1 Geological Materials

While the study of rate effects in ductile metals occurred in the late 1940s' and 1950s', the study of rate effects in geologic materials was not investigated until the 1960s' when Kumar (1968) studied the effects of both strain rate and temperature on the strength of basalt and granite. It was found that increased strain (and stress) rates increased the strength and stiffness of rock, as did decreasing temperature. Mellor (1971) conducted an extensive study into the effects of temperature on the strength and deformability on a wide range of igneous and sedimentary rocks and found that decreasing temperature caused an increase in both strength and stiffness of the rocks tested. Although the rate of increase varied for different rock types, all of the research indicates a marked increase in strength and deformation characteristics with decreasing temperature and increasing strain rate of loading.

The effects of temperature on the strength and fracture characteristics of rock were also investigated in the 1970s' as a result of a dramatic decrease in the grinding efficiency at iron ore mines located in northern climates during winter months by Vitton (1977) and later by Kawatra and Eisele (1989). Vitton investigated the effects of cold temperatures on the strength of various iron ore types as well as granite, sandstone and shale in both dry and saturated conditions. He found that cold temperatures increased the strength of the sandstone and granite tested, but not for all of the iron ore types tested or for the saturated shale samples. Vitton attributed the lack of increase in strength of some of the iron ore types to the lack of pore structure or the lack of softer mineral inclusion that can blunt the propagation of microcracks. In the case of saturated shale, he cited the inability of the pore water to freeze, which was due to the shale's small pore size, thus preventing a strength increase. Dutta and Kim (1993) investigated the effect of both temperature and strain rate on rocks and found that tensile strength and deformability of rock was significantly more sensitive to increasing loading rate than to decreasing temperature.

In the 1970s' and 1980s', with the introduction of the Split Hopkinson Pressure Bar for testing brittle materials, significant research was conducted at high strain rates for both rock and ceramic materials by Janach (1976), Grady (1982), Grady and Kipp (1980), Lankford (1981) and others.

1.2.2 Concrete

The U.S. Corps of Engineers conducted research on concrete for military applications, which included the effect of strain rate on concrete from impact loading (Mellinger and Birkimer, 1966). Later, Oh (1987), as well as others, investigated the strain rate effect on concrete using a SHPB. The most extensive study on the rate effect on concrete, however, was conducted under a research program sponsored by the U.S. Air Force and reported in a series of four papers (Ross et al., 1989, Ross et al., 1995, Ross, et al., 1996, and Malvar and Ross, 1998). In this research the dynamic strength data results are presented as a ratio of dynamic strength to static strength and plotted as a function of strain rate. The strain rate in the quasi-static range (standard compression testing range) was 10^{-7} to 10^{-5}/sec, while the dynamic strain rates went as high as 1000/sec (10^{3}/sec). Since the strain rate is plotted on a log (10) basis in these results, the abscissa (x-axis) values for 10^{-7}/sec for example would be plotted as a –7 and 10^{3}/sec would be plotted as a 3. As a comparison the strain rate loading used in this research testing was approximately 10^{-5}/sec for static loading and 10 to 100/sec (10^{1} to 10^{2}/sec) for the dynamic loading, which would be plotted on the abscissa as –5 and 1 to 2, respectively.

Ross et al. (1989) investigated the dynamic and quasi-static strength of mortar and concrete using a two-inch diameter SHPB. A series of tests were conducted on mortar and concrete in compression, direct tension and split tensile (indirect tension) testing. In the SHPB the indirect tension test is conducted by placing the cylindrical side of the mortar or concrete specimen directly between the loading bars, thus placing a line load diametrically opposed to each other. As a load is applied the specimen is forced to split apart in tension. While this test is an indirect measure of a materials tensile strength, it has become the standard test for tension in both concrete and rock testing at least for static testing conditions. The results of the tensile testing on mortar are shown in Figure 1.6. Ross et al. found that the dynamic tensile strength of mortar, at strain rates of 1/sec to 100/sec, is approximately 1.5 to 3 times that of the tensile strength at quasi-static strain rates. In addition, they found that there is close agreement in the test results between the direct and the indirect tension testing of mortar, which can be seen in Figure 1.6. Since indirect tension testing is significantly easier to conduct than direct tension, this is an important finding. In effect, since the indirect tension testing uses cylindrical specimen both tensile and compressive strength can be determined from cylindrical specimens, which can more easily be prepared in a laboratory. Interestingly, Ross et al. only presented the uniaxial compression results for mortar (in Figure 11 in Ross et al., 1989) but did not provide any discussion or evaluation of the results. However, from Figure 11 the unaixial compression tests for mortar show a dynamic/static ratio of 1.1 to 2.0 in the strain rate range of 1 to 300/sec.

Ross et al., (1995) conducting tests on the dynamic tensile and compressive strength of concrete (tested at similar strain rates) found that concrete is significantly more rate sensitive in tension than in compression. This can be seen in Figure 1.7 (from Ross et al., 1995) where, above a strain rate of 1/sec, the increase in dynamic strength over the static strength increases dramatically in tension, but not as much for compression. For example, at a strain rate of 100/sec (2 on Figure 1.7) the ratio of dynamic to static strength ratio is 8 for tension, but approximately only 1.2 to 1.8 for compression. However, it should be noted that the majority of the test results presented by Ross et al., are below a ratio of 4 and only a few data points, which were taken from other researchers, have higher ratio values (6 to 8) in the strain rate range of 10 to 100/sec.

Ross et al., (1996) also studied the effect of moisture and strain rate on concrete strength, i.e., they studied at what critical strain rate the strength and stiffness of concrete start increasing as the strain rate is increased. The main finding of this investigation was that for concrete the critical strain rate occurs at a lower strain rate for tension than for compression. This can be seen in Figure 1.8 for tension and Figure 1.9 for compression. It can also be seen in Figures 1.8 and 1.9 that the ratio of dynamic to static strength is significantly higher in tension than compression. The critical strain rate range for concrete begins between 1 and 10/sec and 60/sec for tension and at a higher strain rate of 60 to 80/sec for compression. The effect of moisture was also investigated in this study where they found that moisture increases the rate sensitivity of concrete. However, no percent of increase was provided.

Malvar and Ross (1998) conducted a literature review to characterize the available stain rate data that exists for concrete in tension and compression. The data was presented as a dynamic increase factor (DIF) versus strain rate, where DIF is the ratio of dynamic strength to static strength. From this data it was observed that the strain rate data fits more of a bilinear model than a gradual increase model. This indicates, unlike the initial research, that there is a gradual increase in the DIF for strain rates up to a point and then more of a rapid increase. The data also indicates that there is no increase in strain rate below 10^{-6}/sec.

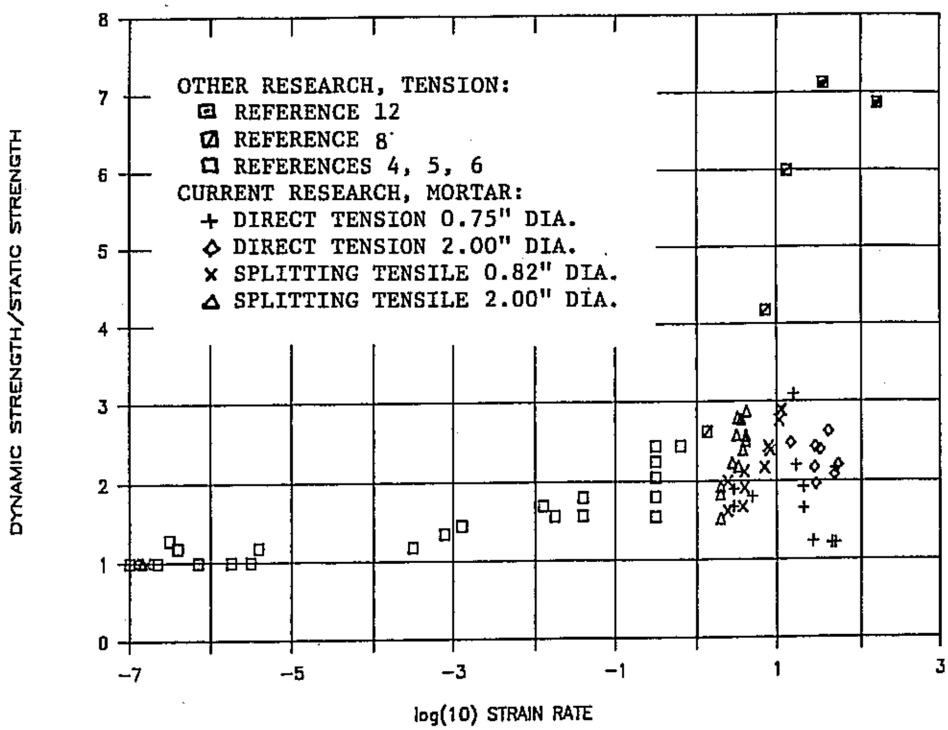

Figure 1.6. Tensile strength ratios of mortar versus $\log_{10}$ (from Ross et al., 1989).

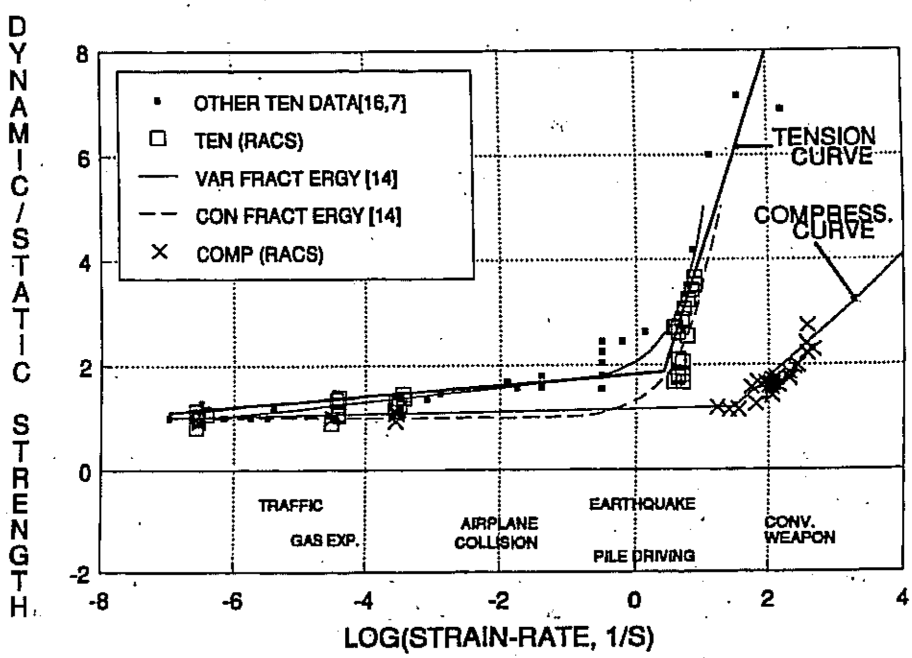

Figure 1.7 Ratio of concrete dynamic to static strength as a function of strain rate, based on a log 10, (from Ross et al., 1995).

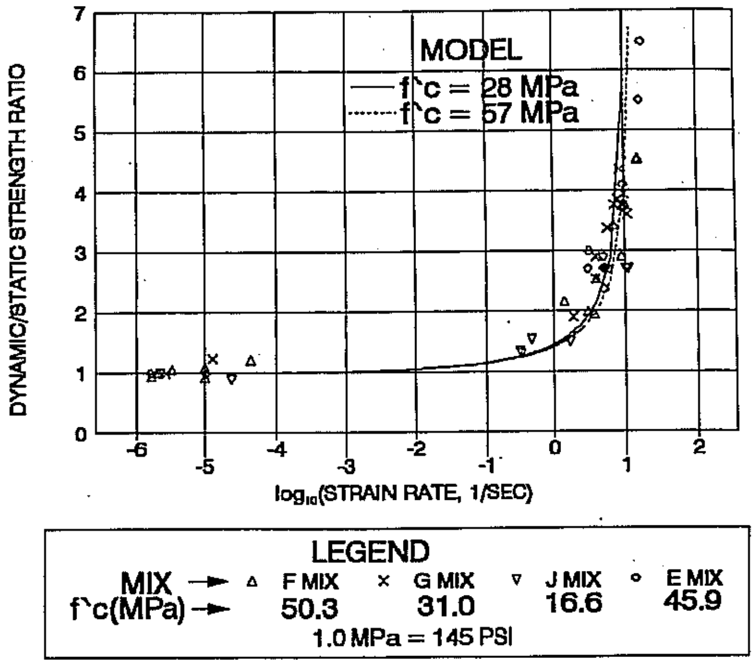

Figure 1.8 Ratio of dry concrete tensile strength to static strength as a function of strain rate log 10 (from Ross et al., 1996)

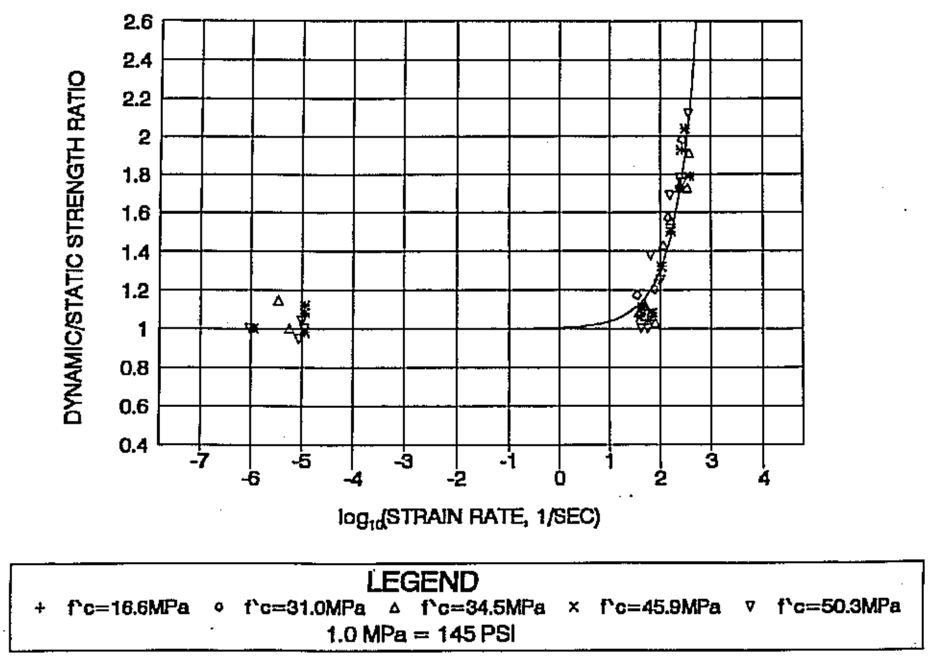

Figure 1.9 Ratio of dry concrete compressive strength to static strength as a function of strain rate log 10 (from Ross et al., 1996)

2 Specimen Preparation

2.1 Aggregate

All of the natural aggregate speciemens were obtained from active quarries, while the blast furnace slag specimens were obtained directly from steel production plants. A number of blocks were obtained from each source weighting between 20 to 100 pounds. The blocks were cored with a SE2025 Solberga direct drive drill and a 3/8 inch ID diamond tip core bit using water as coolant. Initially some basalt specimens were cored with a lightweight (#10) cutting oil as a coolant. The 3/8 inch diameter core was selected, since this dimension falls within the range of coarse aggregate used in PCC as well as the size of the half-inch dynamic uniaxial compression testing equipment, which has a maximum testing size of 0.5 inches. After coring, the specimens were cut to a 2:1 length to diameter ratio using a ISOMET 1000 precision saw. Samples were tested for end parallelism, which must be within 0.001 inch according to ASTM's procedures for compression testing. For aggregates that showed distinct bedding planes, specimens were cored both parallel and perpendicular to the bedding in order to investigate the strength variations that might result from the texture present in the rocks. Specimens were also extracted from a range of blocks and locations to represent the statistical variations typically present in geological materials. A minimum ten specimens were prepared for each test condition, e.g., dynamic, static, dry and saturated.

2.2 Mortar

In addition to the dynamic and static testing of aggregate, mortar was also prepared and tested. Two batches of mortar were mixed and formed into beams using fabricated metal forms. The beams were extracted from the metal forms and placed in the MTU curing room for moisture control. The initial mortar mix was prepared at an air content of 5%. However, discussions with MDOT personnel indicated that this air content was too low giving the mortar an unrealistically high strength. Consequently, an additional batch of mortar was mixed into beams with a target air content of 9 to 10%. The mix proportioning worksheet, batch computations and yield data for the mortar are provided in Appendix A of this section.

The mortar was also cored using the SE2025 Solberga direct drive drill with a 3/8 inch ID diamond tip core bit using water as coolant. Approximately ten specimens were tested each week for 18 weeks. All of the specimens were cored from the two mortar beams prior to the first week of testing. After coring, the samples were cut to a 2:1 length to diameter ratio using the ISOMET 1000 precision saw. Samples were tested for end parallelism, which had to be within 0.001 inches, using a digital micrometer. Also, there was some concern as to the possibility of unequal curing of the mortar beam, i.e., the surfaces of the mortar beam may have cured differently than in the center of the beam. To avoid possible variations in the mortar properties, all of the cored samples were placed in a container and randomly mixed prior to being separated and placed into plastic bags. It was hoped that this would provide a more statistical representation of the entire mortar beam. Water was added to the plastic bags to assist in the curing process.

2.3 Portland Cement Concrete (PCC)

2.3.1 Indirect Tension and Uniaxial Compressive Strength PCC Specimens

Two batches of PCC were prepared for a given coarse aggregate type. The first set was prepared for the static and dynamic indirect tension and compressive strength testing while the second set was prepared for the aggregate interlock testing. For the compressive strength testing the following five coarse aggregate types were selected:

Bruce Mines Diabase	95-010
Port Inland #1, Limestone	75-005
Presque Isle Stone, Limestone	71-047
Superior Sand & Gravel	31-045
Levy Steel Dix #1, Slag	82-019

An important aspect of the PCC was that it be consistent between batches and that the only variable be the coarse aggregate type. The mixing procedures used to produce the PCC for the strength testing followed the procedures outlined in Section Four. The fine aggregate used in the PCC was from Superior Sand and Gravel of Hancock, MI, the same fine aggregate that was used in Section Four. In addition, the same cement and air entrainer was used as in Section Four.

The specimen test size for the static and dynamic strength testing was three-inch diameter by six-inch long specimens. In addition, three six-inch by twelve-inch cylinders from each batch were also cast for 28-day strength testing. While plastic forms were available for casting the three-inch by six-inch specimens, it was thought that the coarse aggregate arrangement within the PCC could be affected by the side constraint of the plastic molds and that variations in the test results may result. Consequently, it was decided to cast the PCC into beams and to core the beams with a diamond core bit, creating the three-inch by six-inch specimens. Special metal forms were, therefore, fabricated for casting the PCC beams. The metal forms were designed such that ten specimens could be cored from each PCC beam. The depth of the beam was seven inches so that a six-inch length specimen could be cut from the cored sample. Each PCC batch produced two PCC beams. The beams were cored using a portable electric Milwaukee heavy-duty Model 4004 Dymodrill drill with a three-inch diamond core barrel. The cored specimens were cut on a diamond cut-off saw to a six-inch length for a 2:1 length-to-diameter ratio for compression testing and 1:1 for indirect tension testing. Water was used as the coolant during the coring and cutting operations. After cutting, the specimen's ends were surface ground to a parallelism of 0.001 inch, which is required under ASTM for uniaxial testing, using a Reid Model 618 PF surface grinder shown in Figure 2.1. A dilute water solution with water solvable oil was used to cool the specimens during the grinding operation. A special jig was design and machined to hold the concrete specimens during the grinding process. In general, the grinding operation took approximately ten to fifteen minutes per specimen, with each side of the specimen being surfaced. The grinding wheel was periodically dressed to ensure proper grinding efficiency. Overall, the grinding operation went well, with the exception of a couple of the blast furnace slag PCC specimens in which the specimens failed in shear failure during grinding.

In addition to the three-inch diameter PCC specimens prepared, compression testing was also conducted on two existing PCC pavements, which have been referred to as "aged concrete." One aged pavement had been made with natural sand and gravel coarse aggregate while a second pavement consisted of a blast furnace slag coarse aggregate. These pavements were obtained from MDOT in six-inch diameter cores. Due to the size of the core as well as observable microcracking, only two-inch diameter specimens could be cored. Consequently, a two-inch diameter high precision diamond core barrel was obtained and used to extract the two-inch cores from the six-inch cores.

Tests were conducted in both a moist condition and a dry condition. The moist condition were essentially the moisture condition of the PCC at 30 day, i.e., the moisture added during concrete mixing and the humidity from the curing room, while the dry conditions were obtained by drying the PCC in an oven until there was no moisture loss, i.e., moisture content was zero. A drying temperature of 110° C was used to dry the PCC. In general, the drying time took approximately three days and was determined by periodically taking representative PCC specimens out of the oven and weighting them to determine when moisture loss was complete.

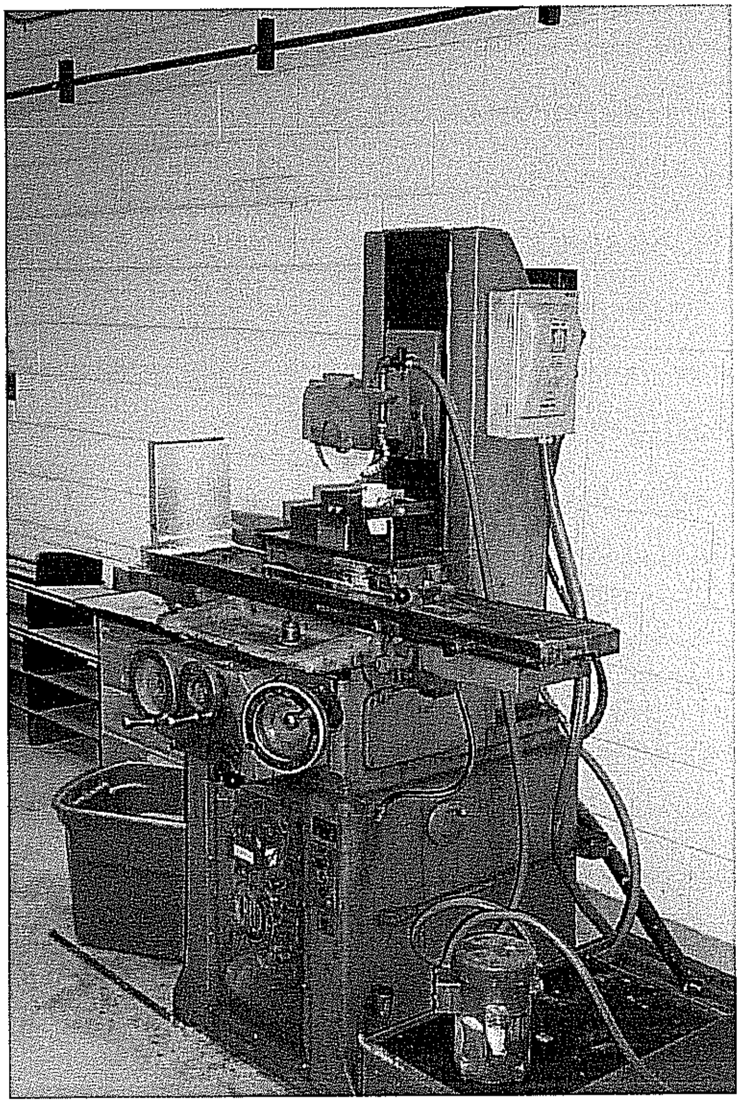

Figure 2.1 Reid surface grinder used for paralleling PCC test specimens.

3 Experimental Procedures

3.1 Aggregate and Mortar

The aggregate specimens were tested in both dry and water saturated conditions. The dry specimens were maintained at room temperature and humidity prior to testing and were not dried in an oven. It was assumed that the moisture content of the specimens would be relatively low and were considered as being "dry." The saturated specimens were submerged in water for approximately 30 days prior to testing. No vacuum saturation was used to saturate any of the test specimens. Although the specimens were described as saturated, it is unlikely that they were at 100% saturation, but were believed to be a relatively close to being saturated.

Approximately one-half of the test specimens were tested at a quasi-static strain rate, while the other half was tested at a high strain rate. The quasi-static tests were conducted on a 5 kip MTS system with a TestStar II digital controller. The 5-kip testing system has a 22 kip rated frame and a three-gallon per minute hydraulic pump supply. The system is located in the Soil Dynamics Laboratory in the Civil & Environmental Engineering Department at Michigan Tech. The system is configured to conduct resilient modulus test with the hydraulic actuator positioned on the top of the system applying vertical loaded downward. The tests were conducted in displacement control and conducted according to ASTM standards for uniaxial compression testing of rock.

The high strain rate tests were conducted using a half-inch diameter modified split Hopkinson pressure bar (MSHPB) located in the Engineering Mechanics and Mechanical Engineering Department at Michigan Tech. A schematic of the half-inch modified Split Hopkinson Pressure Bar and measurement system is shown in Figure 1.12. A Nicolet digital oscilloscope was used to collect and store the dynamic fracture information. To start the testing, the striker bar is placed in the gas gun and pressurized to approximately 30 psi. The specimen is then placed between the incident bar and the transmission with the two bars being butted up against the specimen to hold it in place. After the specimen is in place, a piece of thin copper plate is placed at the end of the incident bar for the striker bar to hit. The purpose of the copper plate is to alter the loading pulse from a square wave to more of a triangular wave. The triangular loading pulse has been found to produce better results on brittle material than the traditional square wave pulse (Subhash and Nemat-Masser, 1993). Once the specimen and copper plate are in place, the trigger system of the oscilloscope is set and the system fired. The initial load pulse travels through the incident bar where it triggers the oscilloscope to start collecting data. The loading pulse then contacts the specimen where energy is released in the fracture process. Part of the energy will travel back into the incident bar, where it is recorded by the strain gages on the bar and part of the energy will travel into the transmission bar where it is also recorded by strain gages. The data are recorded and stored for later analysis. The testing and data reduction and analysis procedures are more fully described in Ravichandran and Subash (1995).

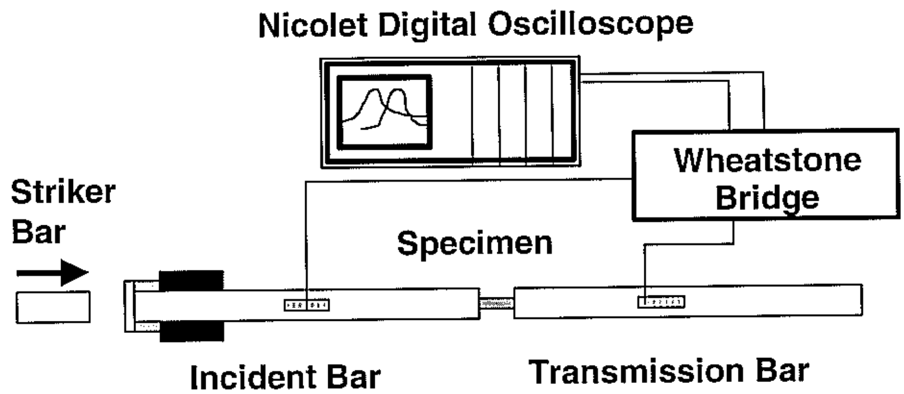

Figure 3.1 Half-inch diameter Split Hopkinson Pressure Bar schematic.

3.2 Portland Cement Concrete

The PCC specimens were tested in both quasi-static and at high strain rates and consisted of both uniaxial compression and indirect tension testing. In addition, PCC specimens were tested in both moist and dry conditions at 30 days instead of 28 to be more consistent with the research conducted at Eglin Air Force Base (Ross et al., 1985, 1995, 1996, and 1998) on the dynamic fracture of concrete. The quasi-static tests were conducted on a 55 kip MTS system with a TestStar II digital controller. The 55-kip testing system has a 55 kip rated frame and a six-gallon per minute hydraulic pump supply. The hydraulic actuator in this system is located on the bottom of the testing system in the traditional configuration with the load being applied upward. The system is located in the Structural Testing Laboratory in the Civil & Environmental Engineering Department at Michigan Tech. Approximately half of the PCC specimens were tested in quasi-static conditions and half at a high strain rate.

The high strain rate tests were conducted using a three-inch diameter Split Hopkinson Pressure Bar (SHPB) located in the Concrete Testing Laboratory at Michigan Tech. The system functions in basically the same way as the half-inch diameter system but has not been modified for single load testing, which is not required for measuring the dynamic strength of materials. A modified system would be needed when investigating the microfracture of brittle materials. A Nicolet digital oscilloscope is used to collect the data during testing in the same fashion as in the half-inch MSHPB. The SHPB system is shown in Figure 3.2 and the instrumentation in Figure 3.3. The uniaxial compression tests were conducted using the same procedures as with the half-inch MSHPB. However, the indirection tension tests used fabricated platens to apply the line load to the specimen. Figure 3.4 illustrates the set up of the indirect tension platens.

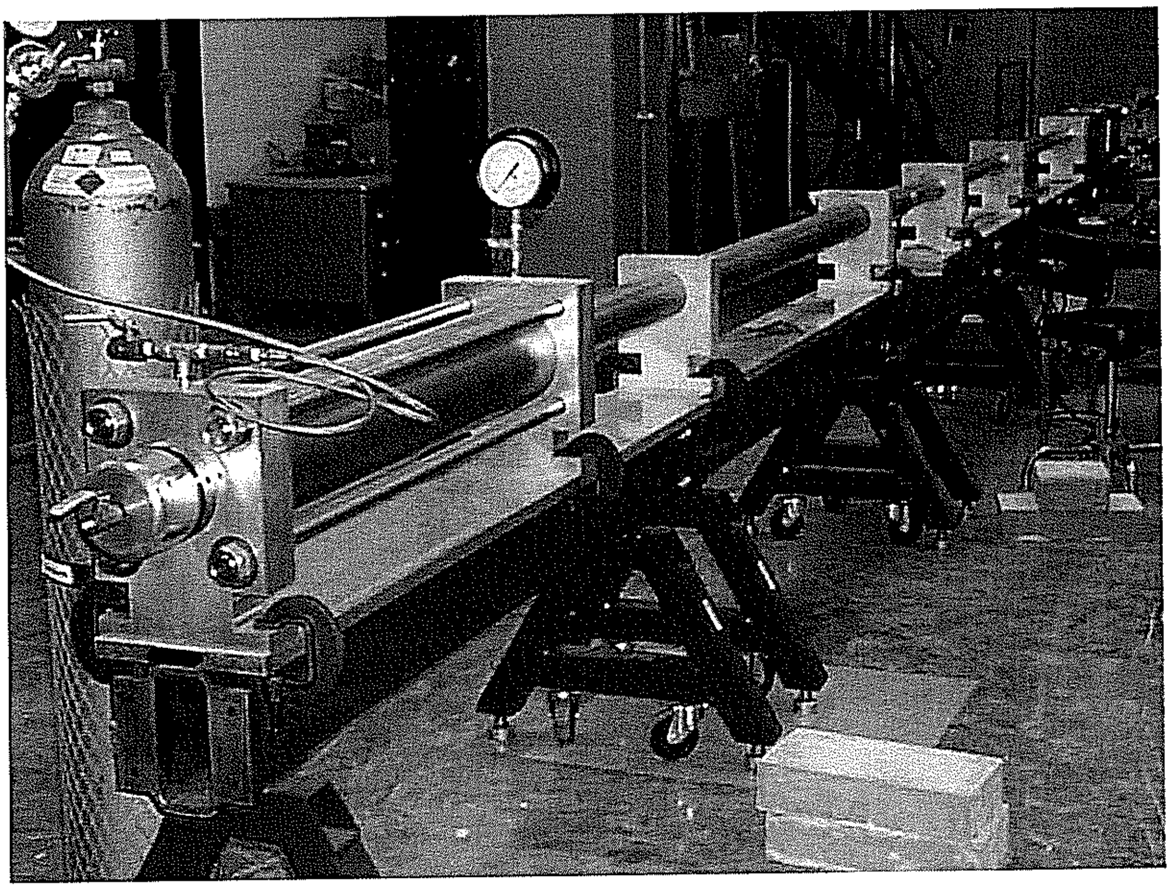

Figure 3.2 Three inch Split Hopkinson Pressure Bar.

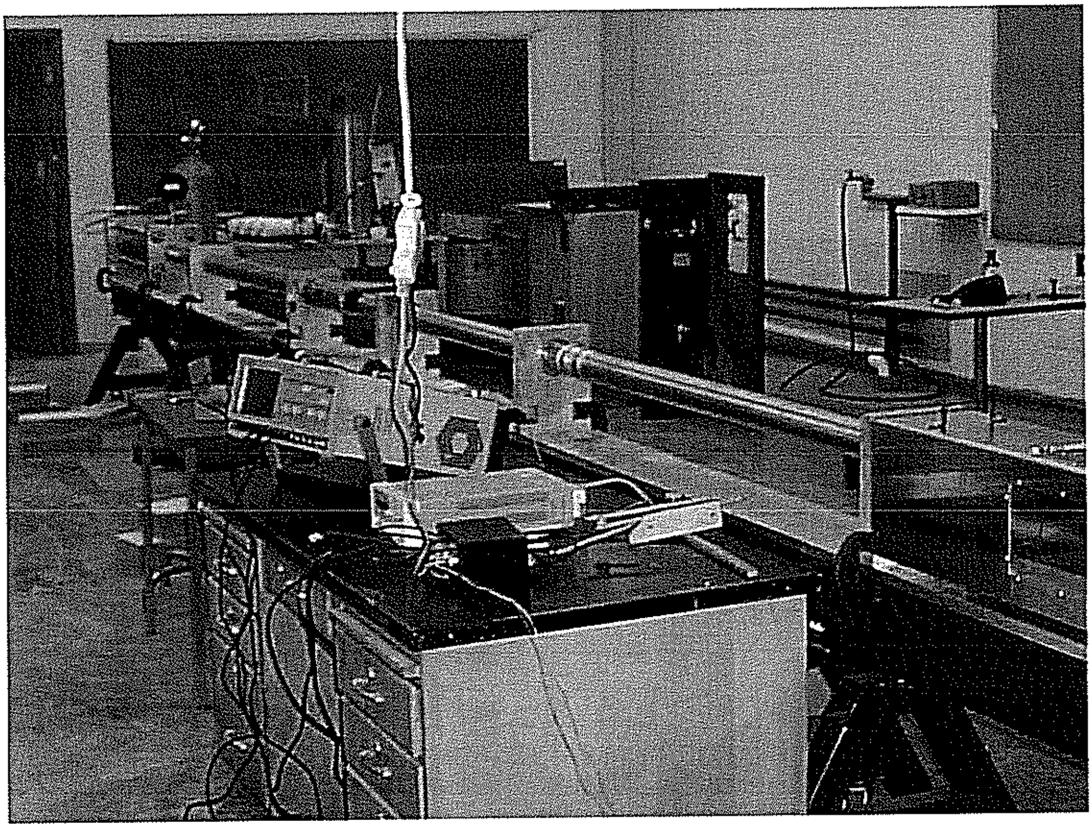

Figure 3.3 SHPB measurement equipment.

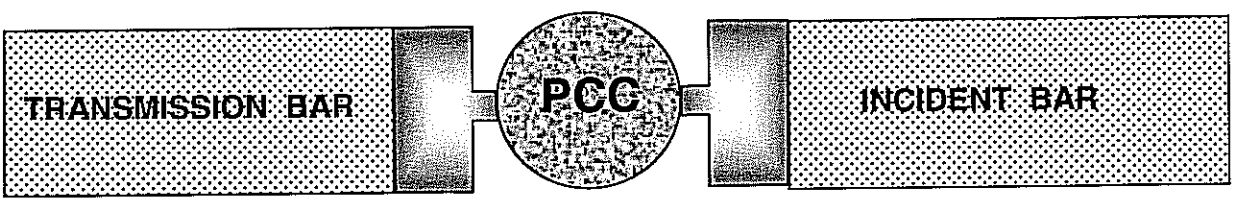

Figure 3.4 Indirect test platens for the SHPB.

4 Experimental Results

4.1 Aggregates

Uniaxial compression tests were conducted at both a quasi-static strain rate of approximately 10^{-6}/sec (following ASTM standards) and at a high strain rate near 10^{2}/sec for each aggregate type. Approximately eight to ten specimens were tested for each test condition, i.e., quasi-static, dynamic, dry, and saturated. Table 4.1 summarizes the compressive strength data for all the aggregates in dry and saturated conditions. The raw data for the static and dynamic uniaxial fracture strength in dry and saturated conditions, respectively, is presented in Figures 4.1(a) and 4.1(b). However, for ease of comprehension, the same data are presented in terms of mean and standard deviation in Figs. 4.2(a) and 4.2(b). It is clear from the plots that the dynamic fracture strength of aggregates is consistently greater than the static strength in both dry and saturated conditions. In general, the slag aggregates exhibited the lowest compressive strength, followed by the carbonates (limestone and dolomite families) with an intermediate strength. The mafic igneous aggregates (Bruce Mines and Moyle) exhibited the highest compressive fracture strength. The air-cooled slag consists of two distinct structures: one extremely porous region and the other a dense structure with considerably lower porosity. The denser structure (slag specimen 1.2) exhibited strength comparable to that of carbonates. It is interesting to note that there is no significant difference in the uniaxial compression strength of limestones and dolomites when the specimens were cored either parallel or perpendicular to the bedding (see specimen nos. 5, 8 and 10). The minor differences may be due to the limited number of specimens tested, since the data also falls within the statistical variations of the carbonate.

The above data is replotted in Figures 4.3(a) and 4.3(b), so as to compare the static and dynamic strengths separately in dry and saturated conditions, respectively. The plots clearly reveal that no significant strength variations occur under saturated conditions compared to the dry conditions. However, in the case of the mafic igneous aggregates, slightly higher compressive strength was noticed in dry condition than in the saturated condition in static loading. A plot of aggregate density versus the mean uniaxial compressive strength is shown in

Figures 4.4(a) and 4.4(b) for dry and saturated aggregates, respectively. In these plots, the data for specimens cored parallel and perpendicular to the bedding are combined since there is no significant variation in uniaxial strength as discussed before. Both static and dynamic values are plotted on the same graph. Although there is considerable scatter in the experimental data, it can be seen that, in general, the compressive strength increases with density and the dynamic strength data shows a steeper slope compared to the static data.

Figures 4.5(a) and 4.5(b) illustrate the axial stress-strain curves obtained from the strain gage measurements under static and dynamic loads for all the aggregates except slag. Almost all the rocks exhibit initially a linear elastic response followed by a non-linear response just before failure. The inelastic response is more pronounced in stiffer (higher strength) rocks under dynamic loads than static loads. The inelastic strain is a representation of the strain associated with the onset of microcracks, their growth and coalescence leading to eventual failure of the specimen. From these experiments, one can more accurately estimate the strain rate during a test, which will be discussed later in Chapter Five of this section.

4.2 Cement Matrix

Ten mortar specimens were tested approximately each week for 18 weeks at seven-day intervals, i.e., the first set of tests were conducted seven days after PCC mixing. The dynamic strength tests were conducted on the half-inch MSHPB while the static tests were conducted on the 5 kip closed loop servo-hydraulic MTS system. All of the static tests were conducted in displacement control. As reported previously the mortar air content was approximately 9%. The results of the combined mortar testing are shown in Figure 4.6 in a raw date from while the statistical analysis showing the mean and standard deviation of the data is shown in Figure 4.7.

4.3 Portland Cement Concrete

Approximately forty PCC specimens were prepared from each aggregate type PCC while twenty were prepared for the aged concrete. Ten specimens were tested under indirect tension and uniaxial compression loading in each condition, i.e., static, dynamic, moist and dry. The raw data indirect tension results are shown in Figure 4.8 for the 30 day concrete while the statistical analysis of the data providing the mean and standard deviation are presented in Figure 4.9. Figure 4.10 provided the raw data for uniaxial compression results for the 30-day PCC, while Figure 4.11 presents the mean and standard deviation for the test data. In addition, aged concrete was also tested in uniaxial compression from cores extracted from highway pavement. The highway pavements consisted of two different coarse aggregates, a natural aggregate PCC and a blast furnace slag PCC. The aged concrete cores were only tested in a dry condition. The mean and standard deviation of the test data are plotted in reference to the 30-day PCC results in Figure 4.12.

Table 4.1 Compressive strength data for all the aggregates in dry and saturated conditions.

ID No. Pit ID	Aggregate/ (Quarry)	Orientation and Batch	Compressive Fracture Strength (MPa) Static Dry	Static Saturated	Dynamic Dry	Dynamic Saturated
1	AC Slag	Batch 1	12.1 ± 4.1	16.3 ± 5.0	33.2 ± 10.1	39.5 ± 5.3
95-006	(Algoma)	Batch 1.2	97.6 ± 34.1		163.1 ± 32.8	
2	WC Slag	Batch 2.0	22.8 ± 6.7	19.1 ± 8.6	43.4 ± 26.4	52.6 ± 11.1
95-006	(Algoma)	Batch 2.1		10.0 ± 3.9		34.9 ± 33.6
3	WC Slag	Random	21.1 ± 8.4	33.5 ± 11.3	30.0 ± 10.2	68.7 ± 19.6
82-019	(Levy)					
4	Limestone	Random	77.7 ± 17.1	43.9 ± 17.0	147.5 ± 37.5	117.0 ± 38.9
71-047	(Presque Is.)					
5	Limestone	Normal	91.6 ± 37.3	94.1 ± 31.8	186.8 ± 24.2	177.3 ± 40.2
06-008	(Bay Co.)	Parallel	65.4 ± 21.5	73.4 ± 24.3	165.9 ± 37.3	168.5 ± 33.7
6	Limestone	Random	103.6 ± 31.8	107.9 ± 16.2	282.2 ± 43.2	221.3 ± 4.2
75-005	(Port In.)					
7	Dolomite	Random	85.2 ± 43.9	86.8 ± 34.6	157.1 ± 27.8	186.8 ± 22.5
49-065	(Cedarville)					
8	Dolomite	Normal	92.8 ± 29.2	90.0 ± 59.8	154.2 ± 22.2	139.2 ± 57.0
58-009	(Denniston)	Parallel	76.6 ± 29.1	75.0 ± 27.6	149.1 ± 22.3	153.5 ± 82.4
9	Dolomite	Normal	124.4 ± 22.1	99.9 ± 33.3	156.0 ± 37.9	181.5 ± 31.9
58-008	(Rockwood)	Parallel		74.6 ± 39.6		150.3 ± 33.1
10	Dolomite	Normal	131.2 ± 27.8		206.8 ± 46.5	
93-003	(France St.)	Parallel	134.9 ± 30.5	148.3 ± 43.2	212.9 ± 25.2	211.1 ± 69.8
11	Basalt	Random	183.6 ± 23.6	121.3 ± 34.7	371.9 ± 35.5	352.8 ± 53.1
31-076	(Moyle)					
12	Diabase	Water Cut	270.5 ± 59.1	203.9 ± 106.8	489.5 ± 57.9	445.3 ± 99.5
95-010	(Ontario Traprock)	Oil Cut	226.8 ± 46.2		342.8 ± 65.9	

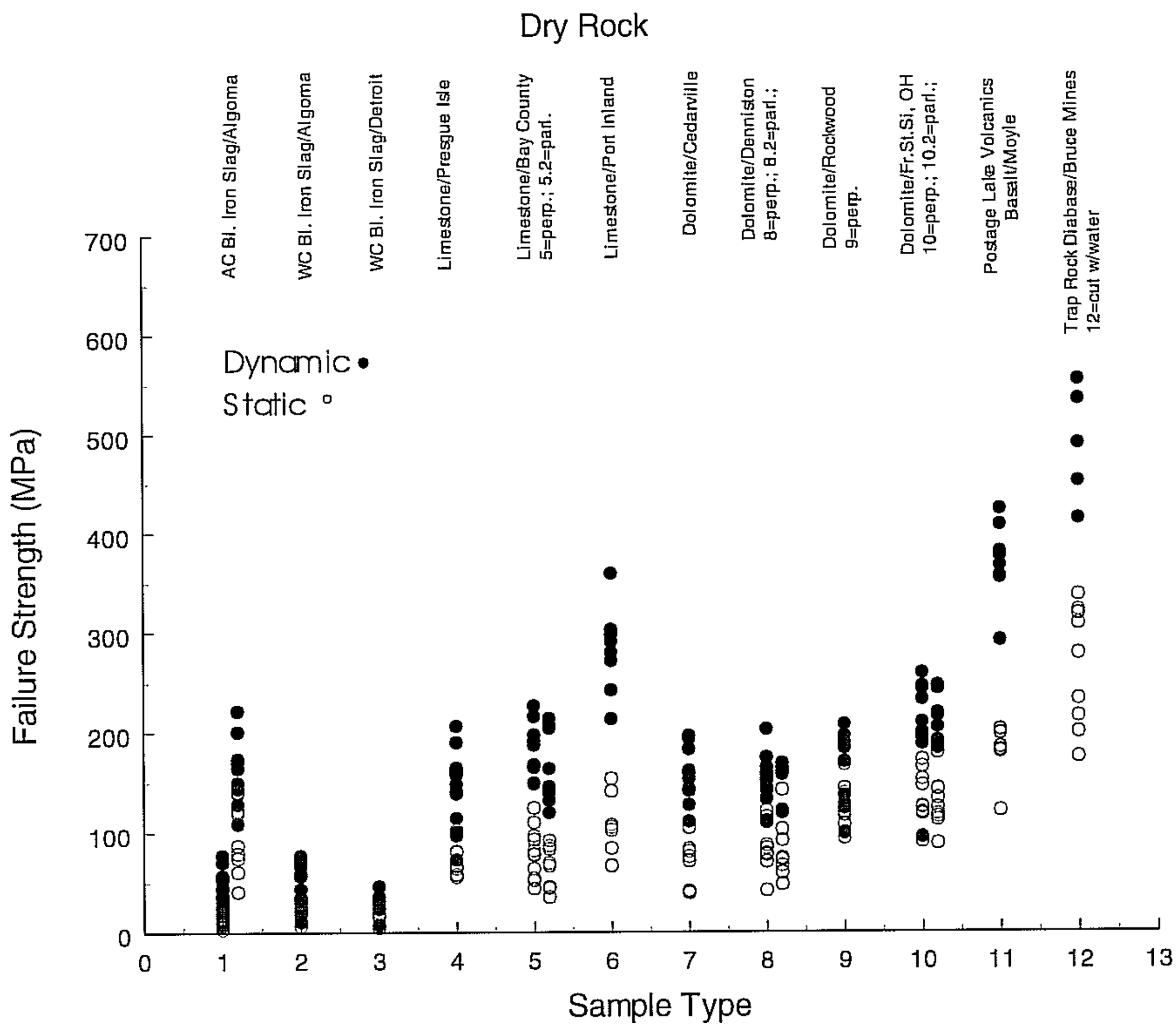

Figure 4.1(a) Raw data for static and dynamic compressive strengths for dry aggregate results.

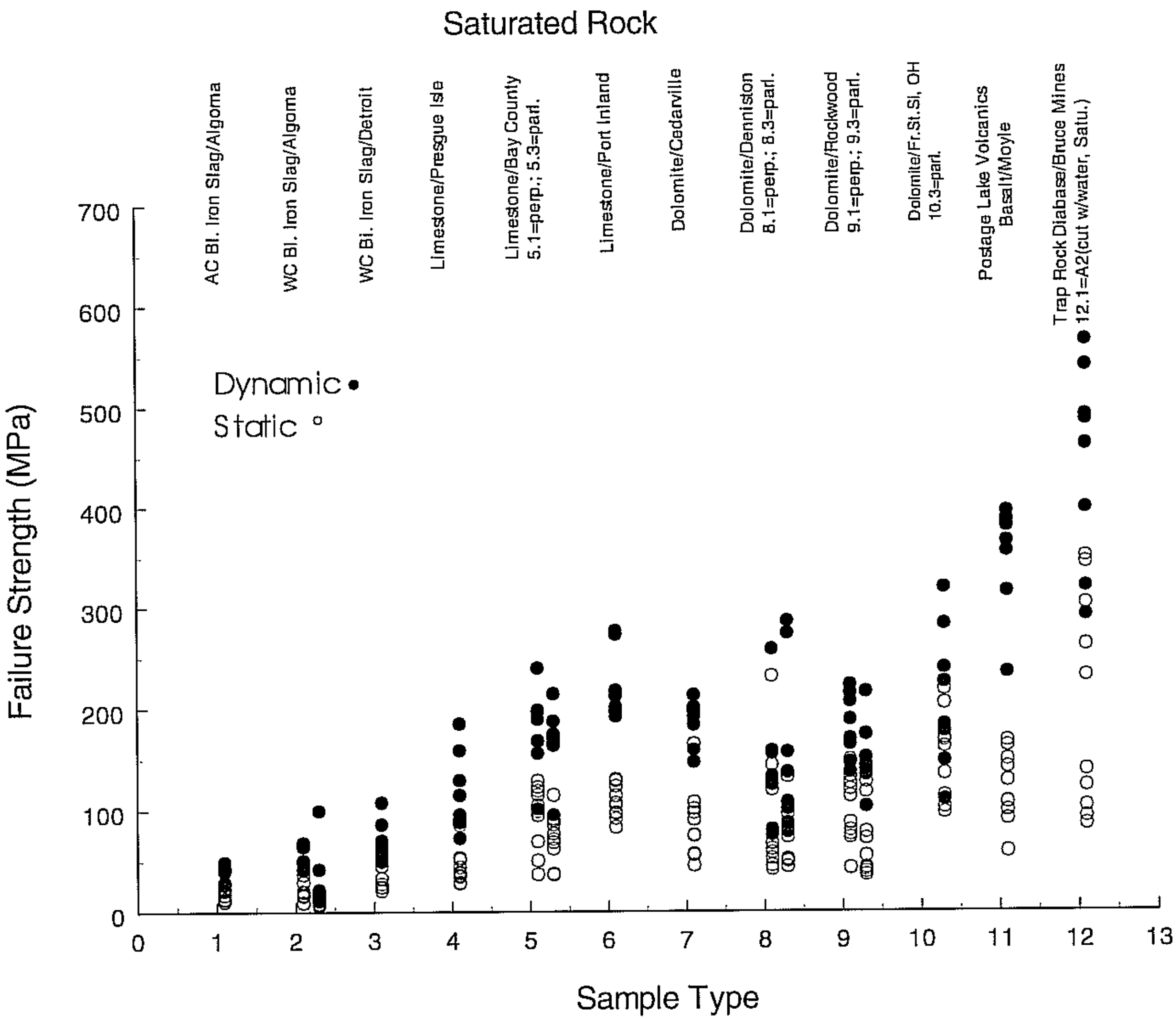

Figure 4.1(b) Raw data for static and dynamic compressive strengths for saturated aggregate results.

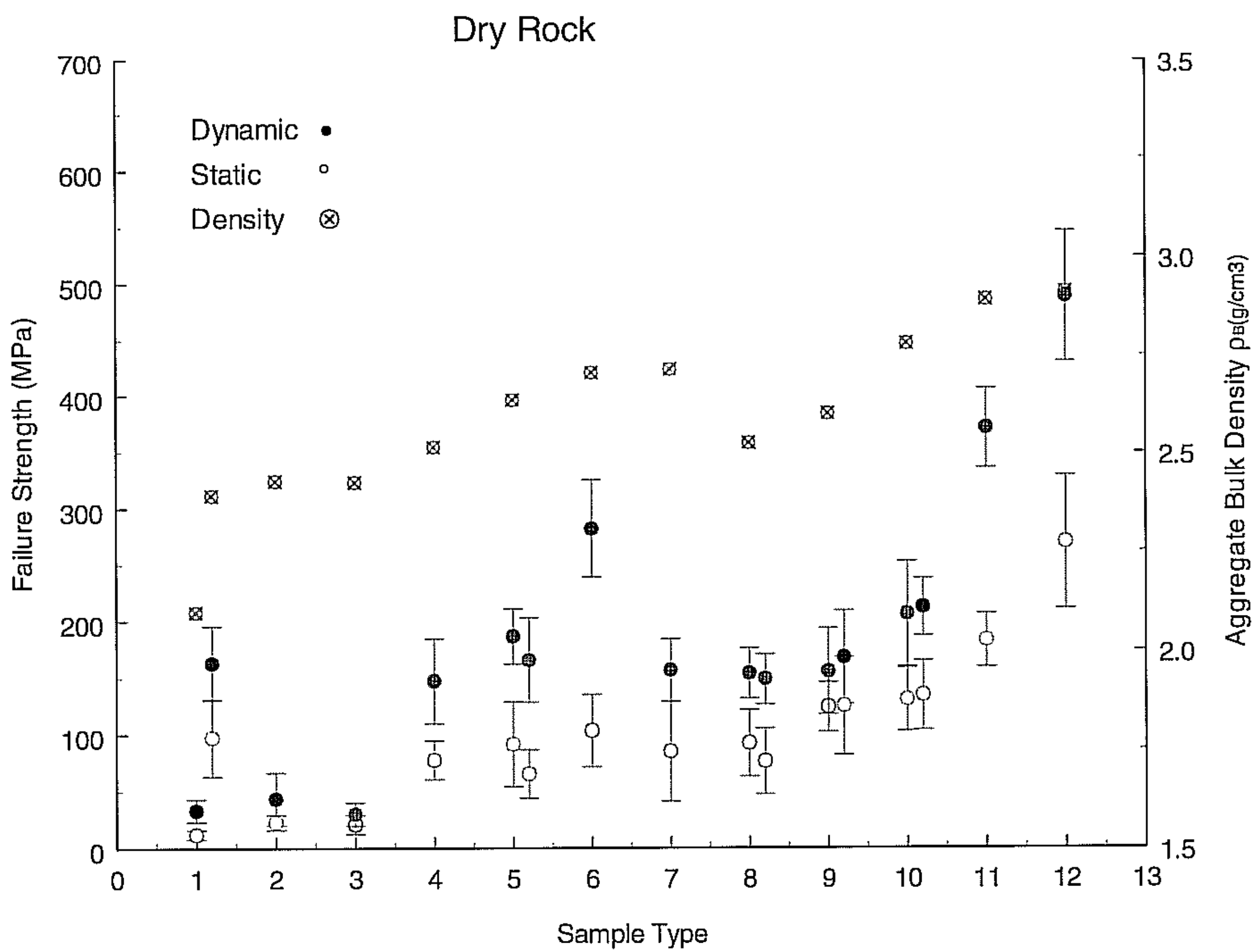

Figure 4.2(a) Statistical analysis showing mean and standard deviation of static and dynamic compressive strength of dry aggregate including aggregate dry bulk density.

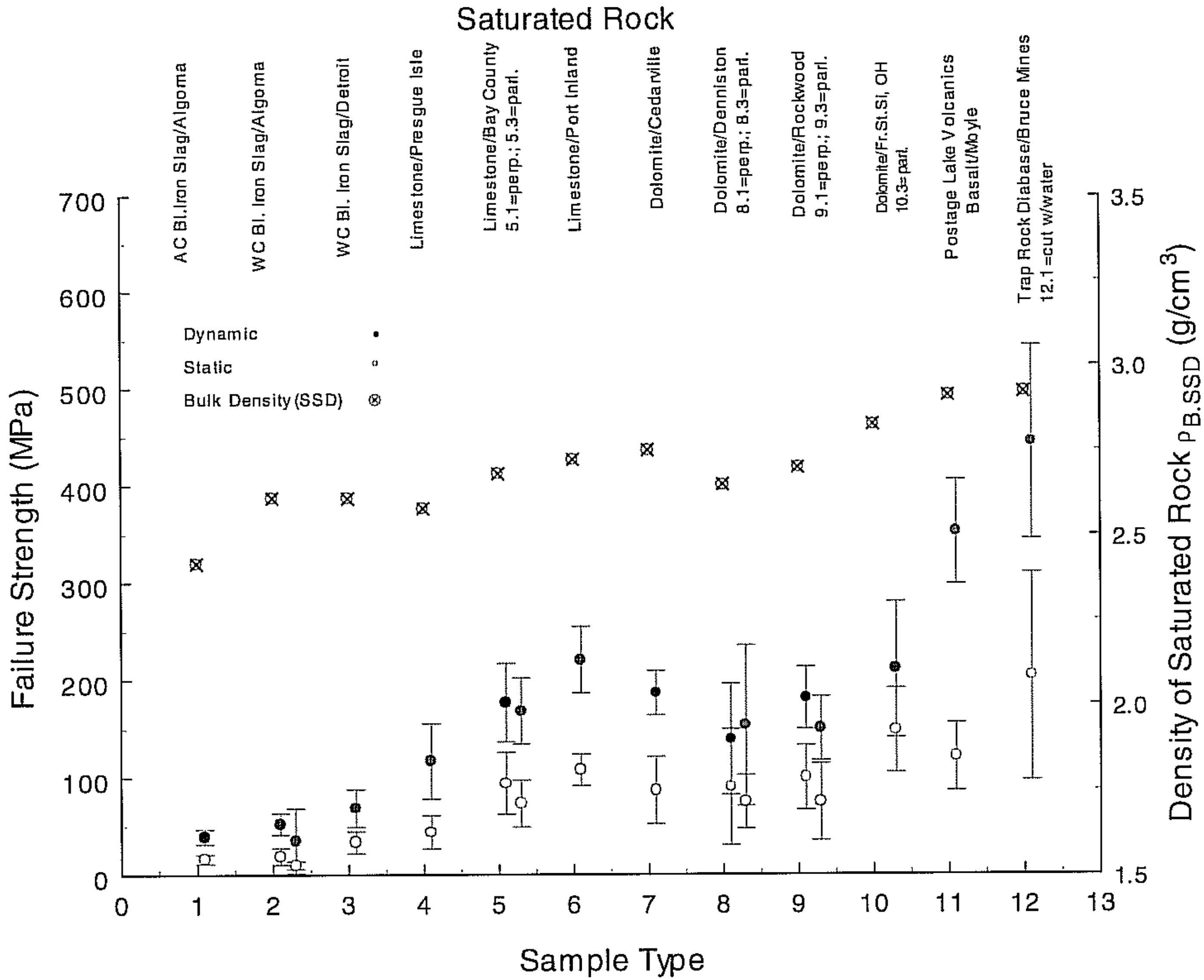

Figure 4.2(b) Statistical analysis showing mean and standard deviation of static and dynamic compressive strength of saturated aggregate including aggregate bulk dry density.

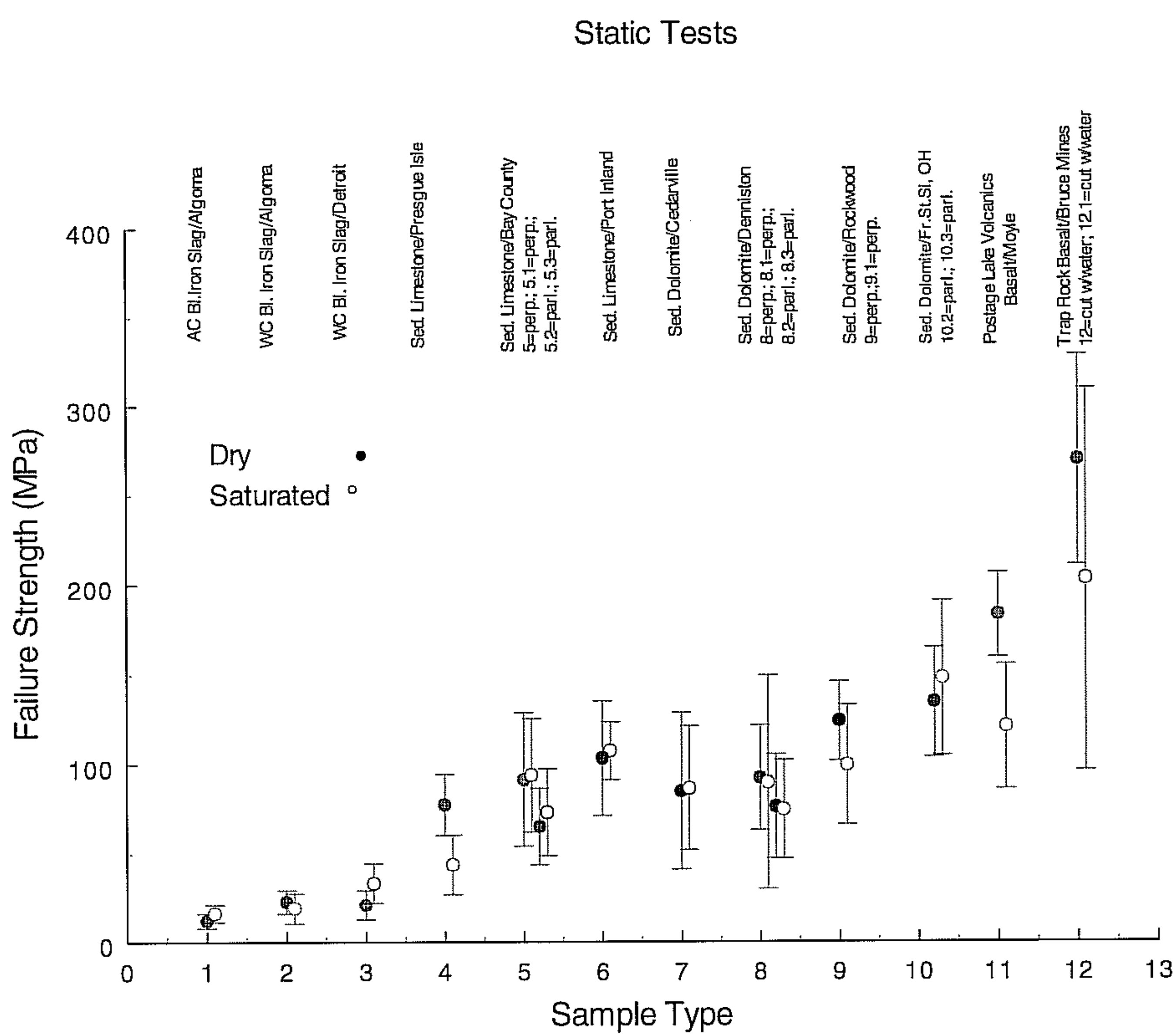

Figure 4.3(a) Comparison of dry and saturated strength results for static test results.

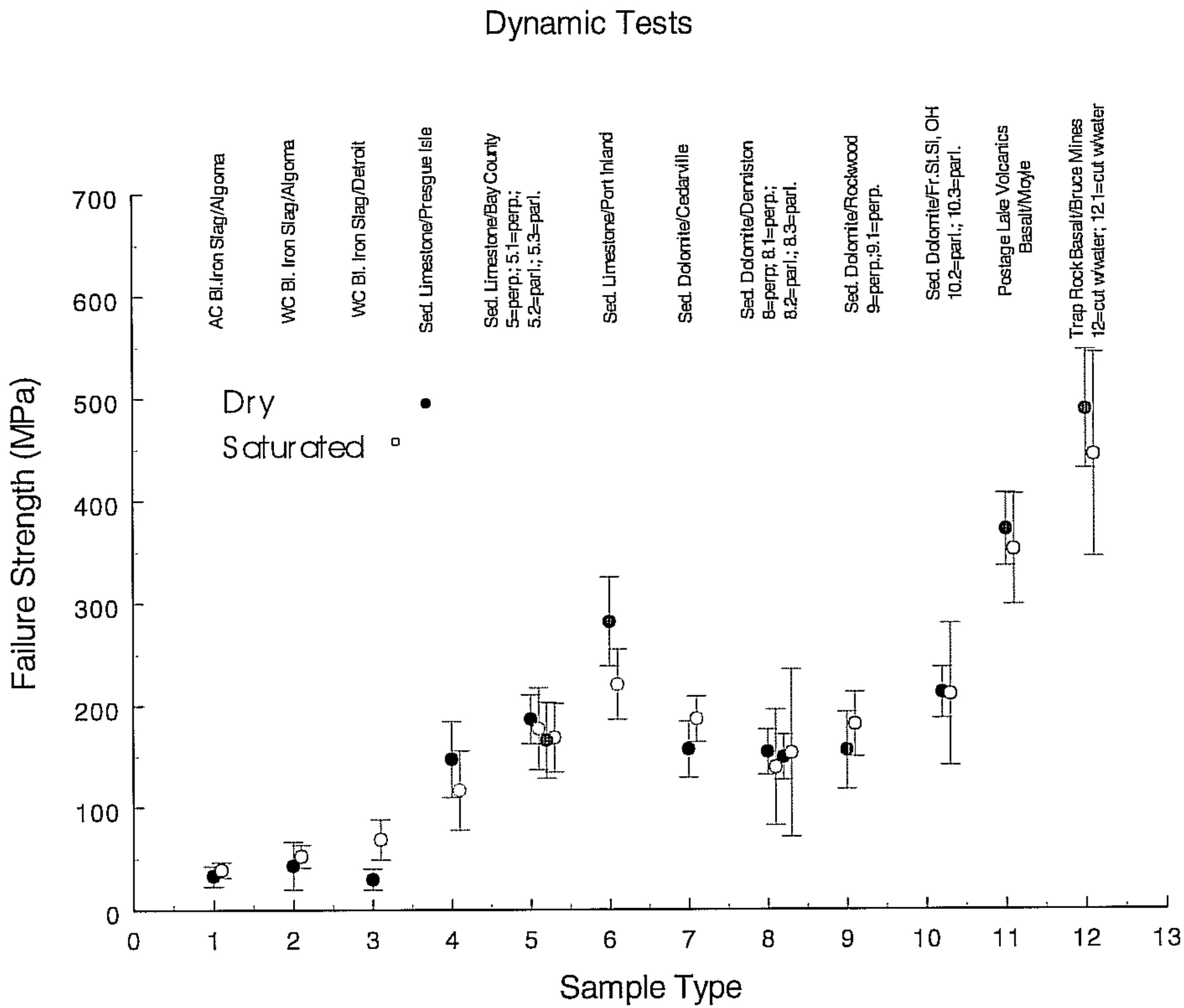

Figure 4.3(b) Comparison of dry and saturated strength results for dynamic test results.

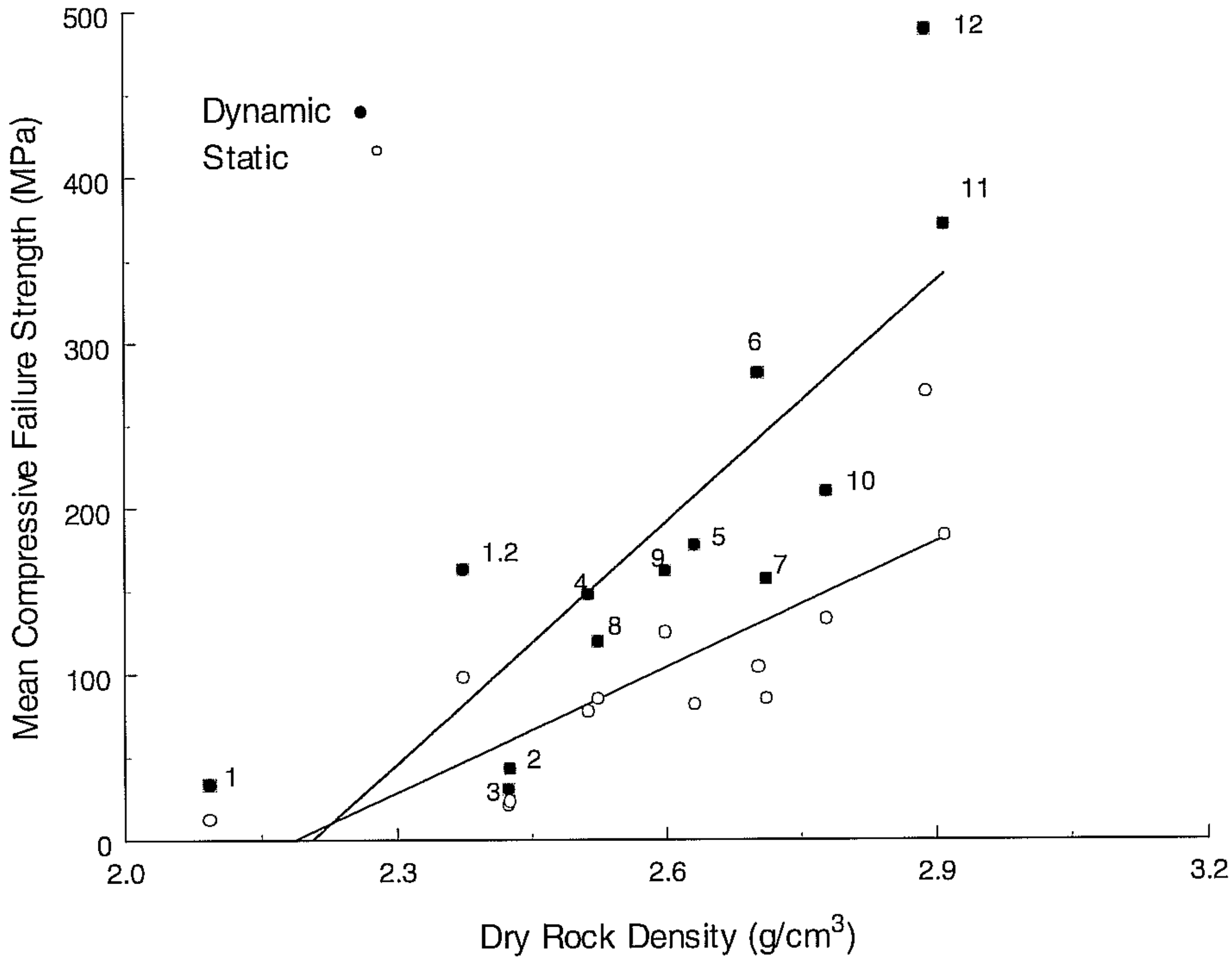

Figure 4.4 (a) Comparison of static and dynamic failure strength with dry bulk density.

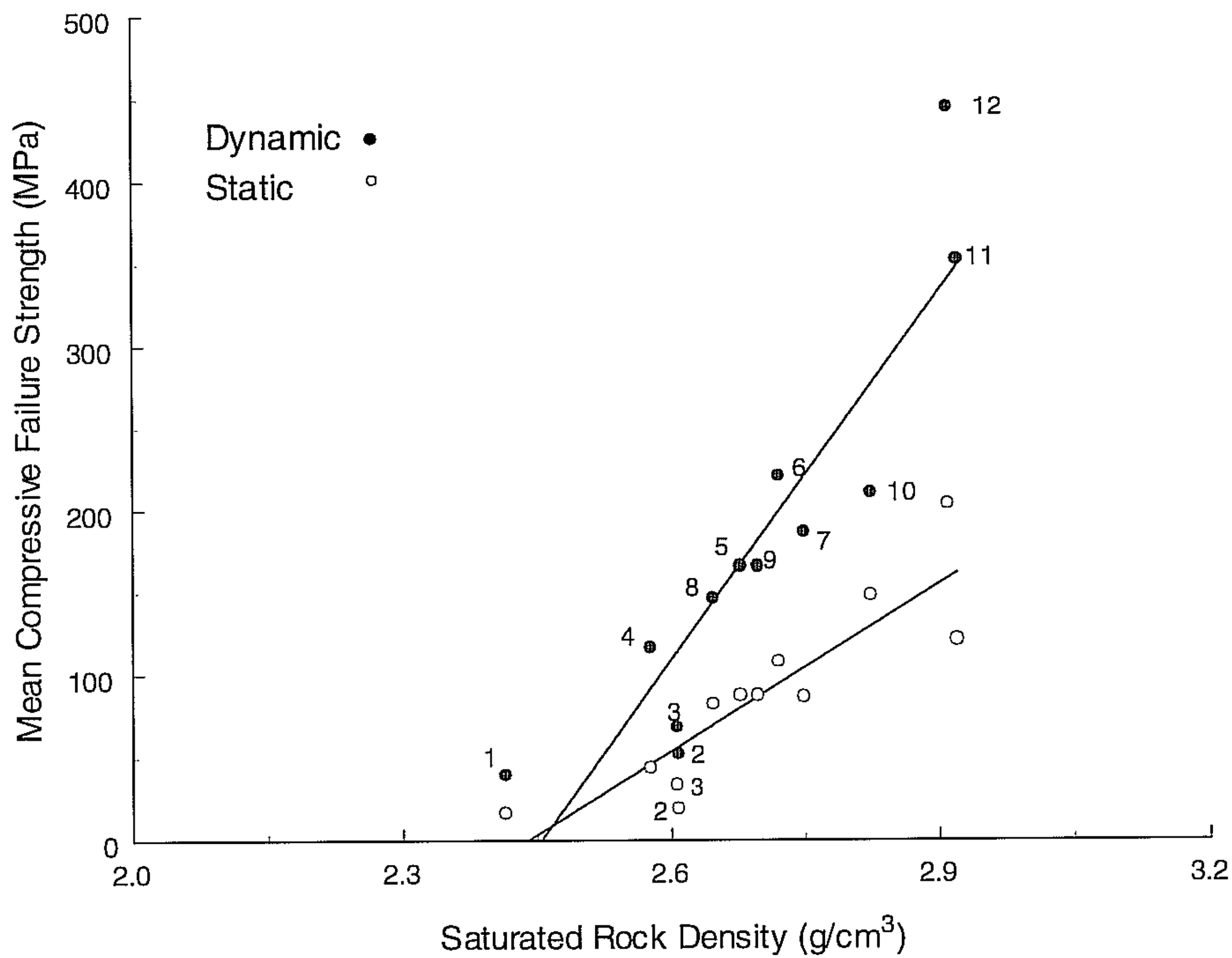

Figure 4.4 (b) Comparison of static and dynamic failure strength with saturated bulk density.

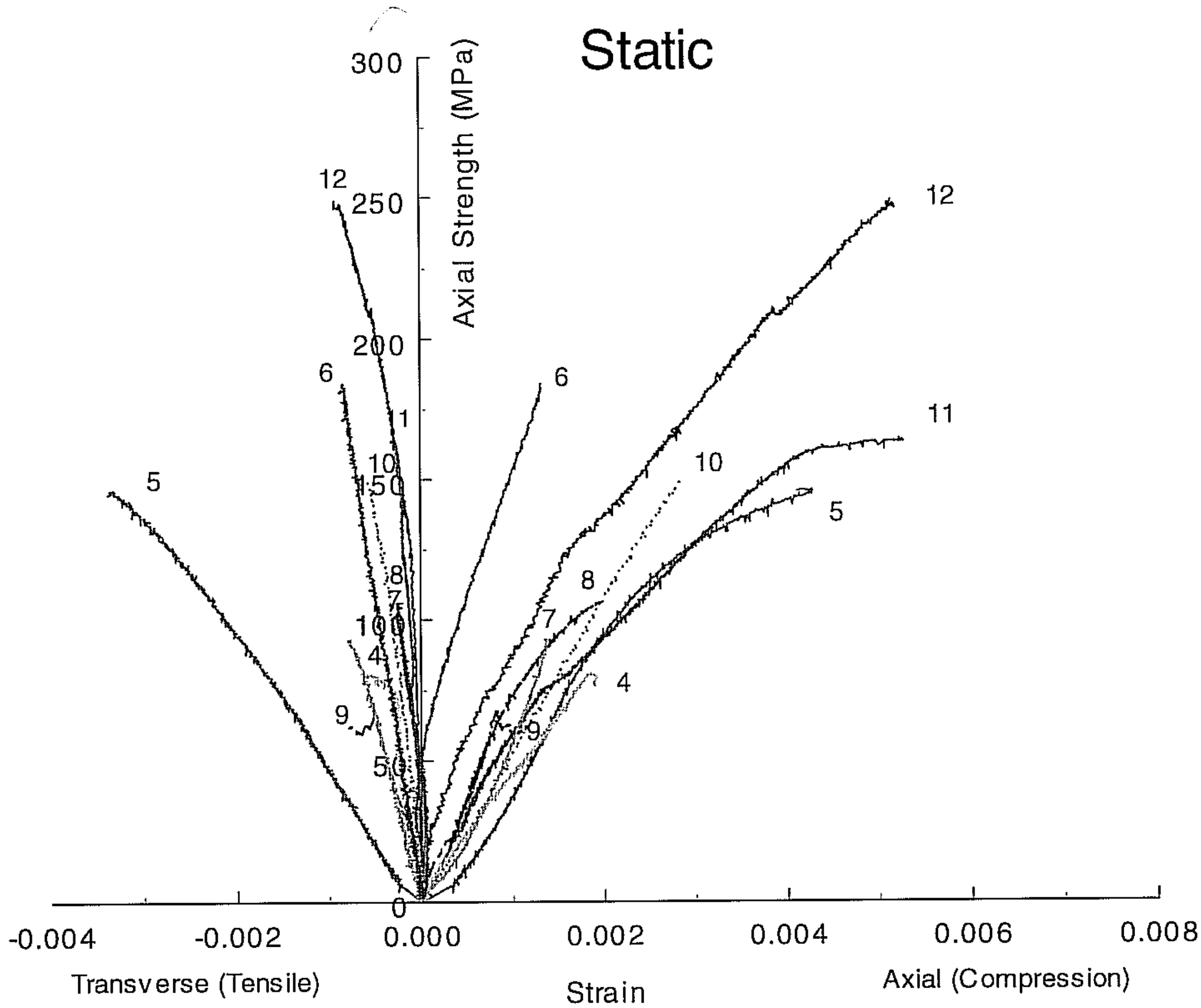

Figure 4.5(a) Axial stress-strain curves for static compressive strength test results.

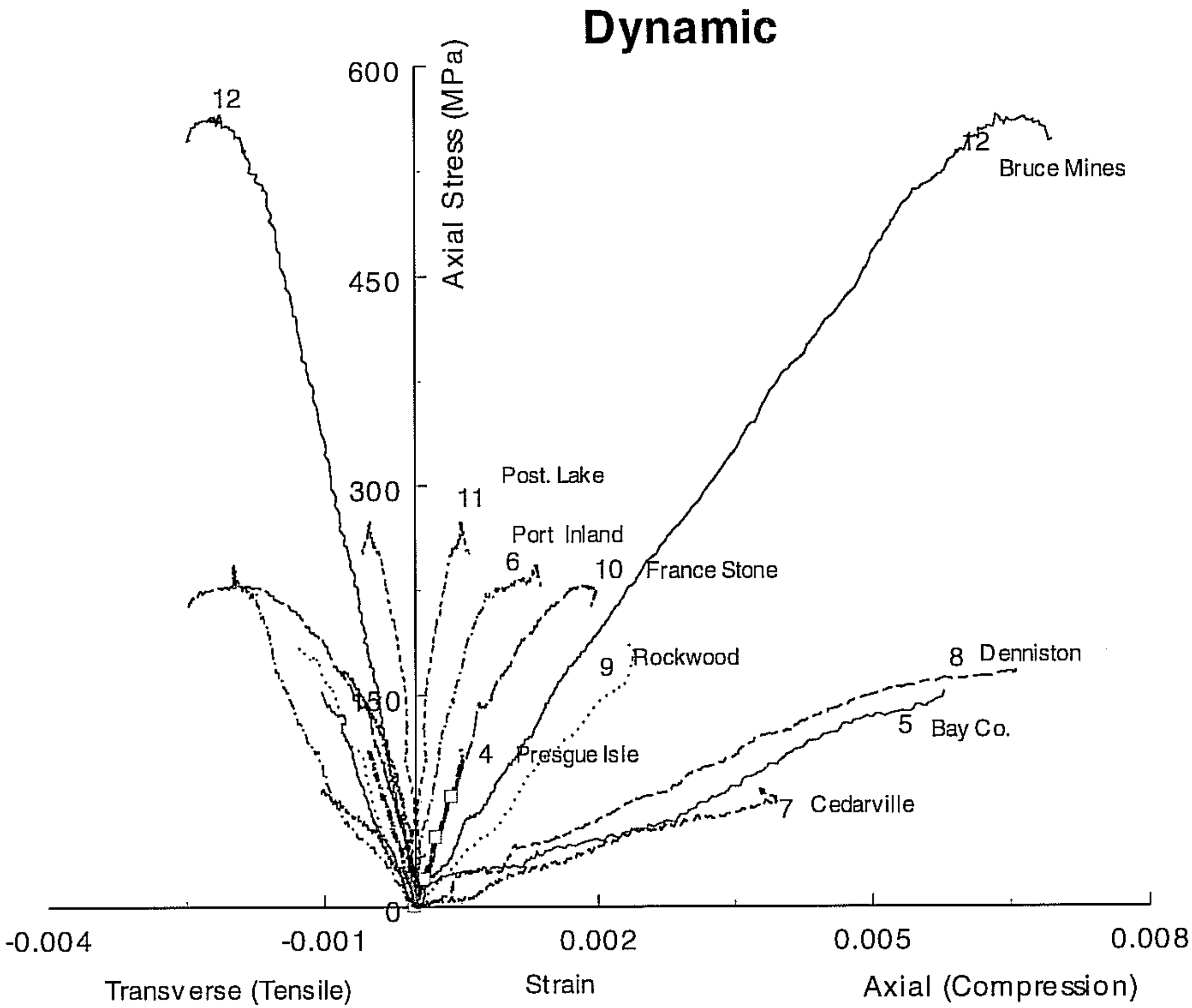

Figure 4.5(b) Axial stress-strain curves for dynamic compressive strength test results.

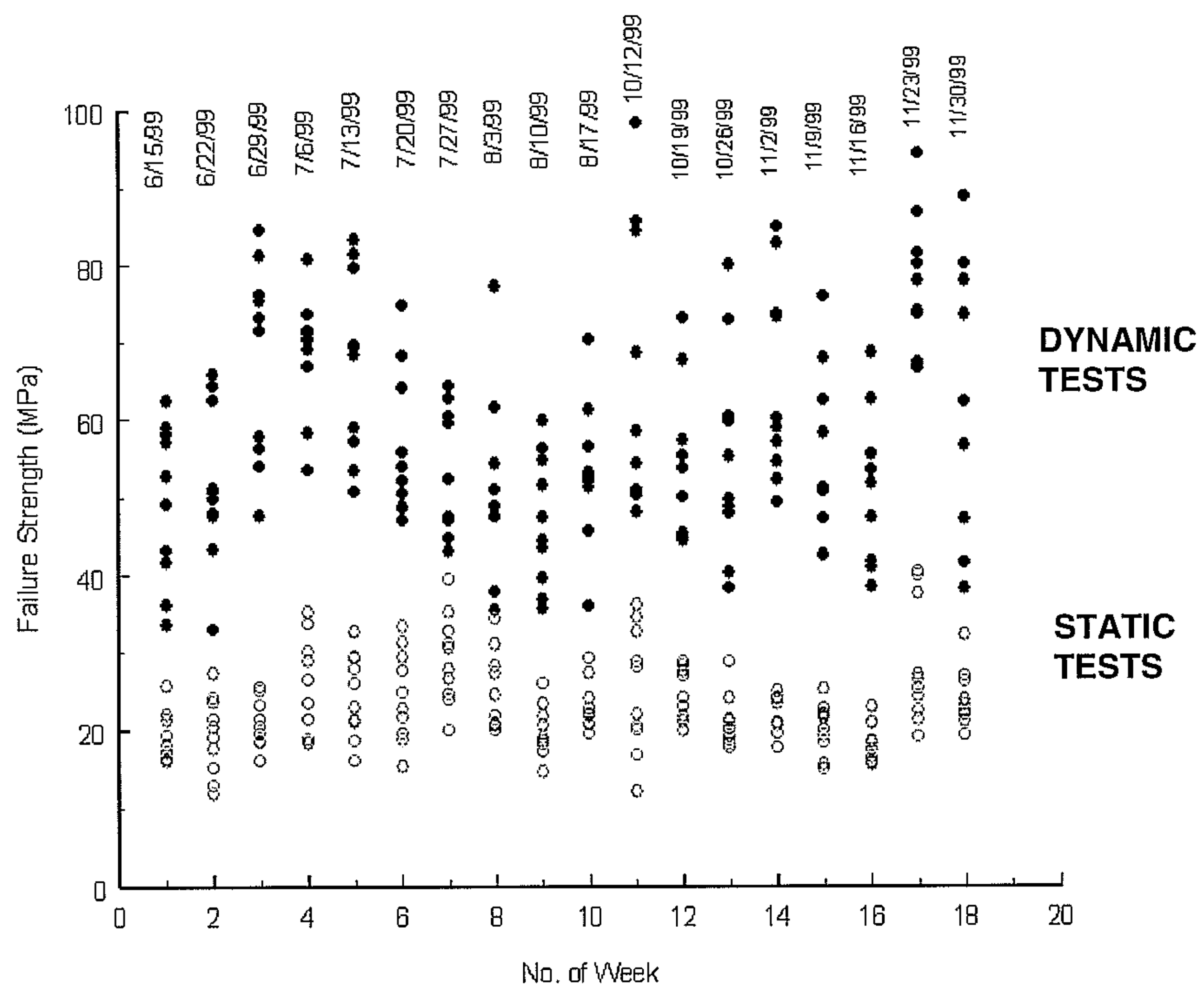

Figure 4.6 Raw data for static and dynamic mortar testing.

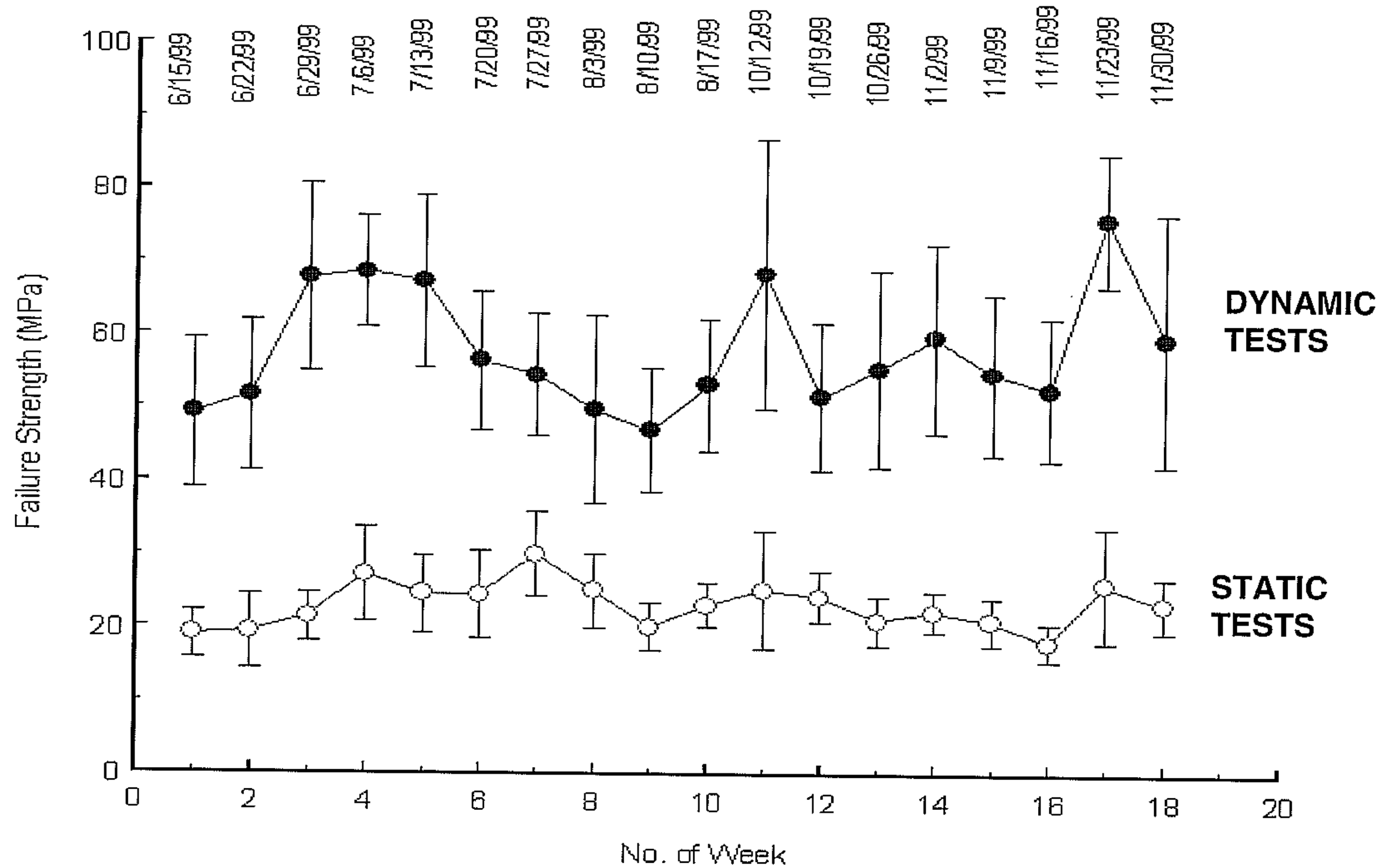

Figure 4.7 Results of mortar static and dynamic uniaxial compression testing.

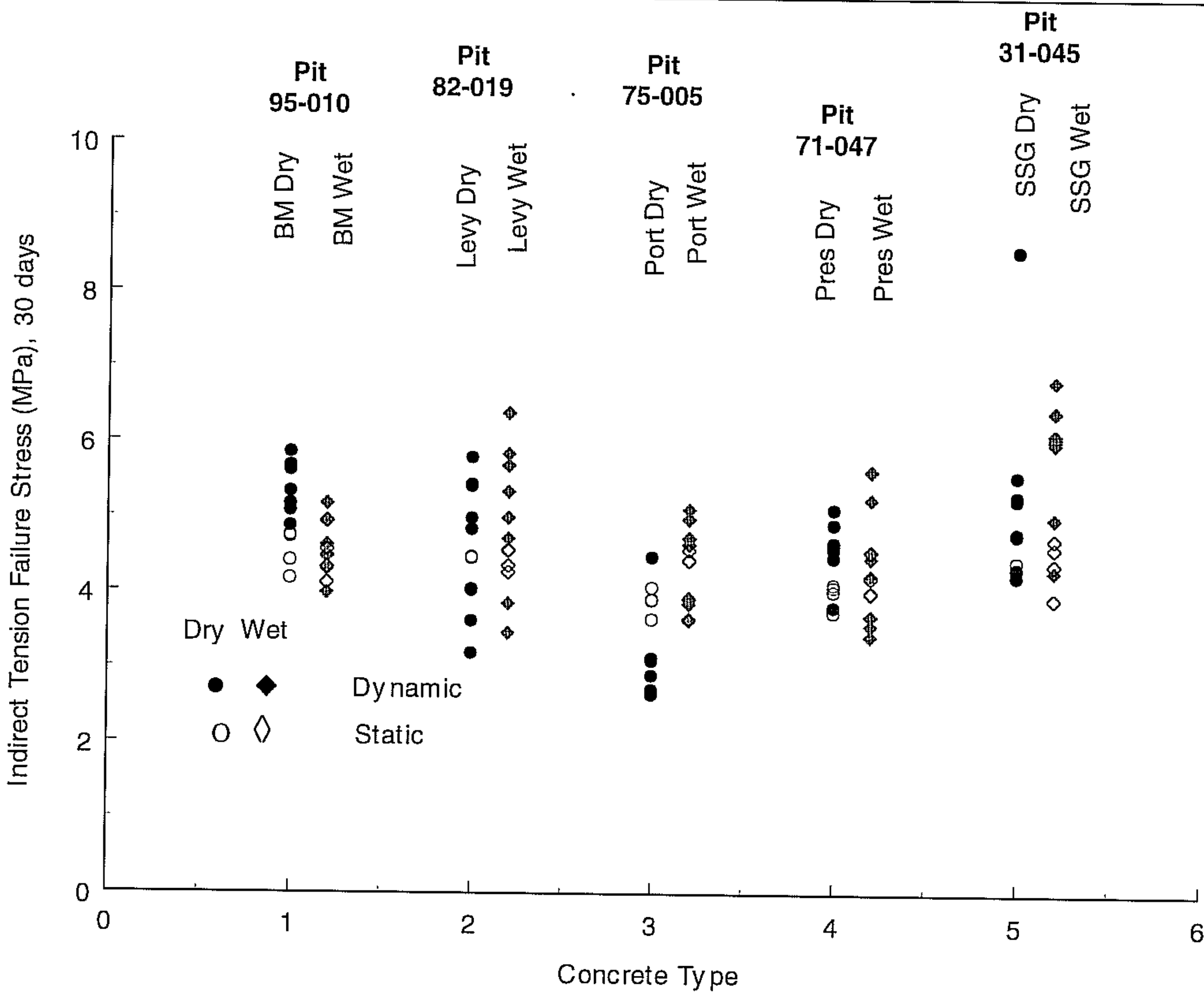

Figure 4.8 Raw data from static and dynamic indirect tensile testing of concrete with different coarse aggregate types.

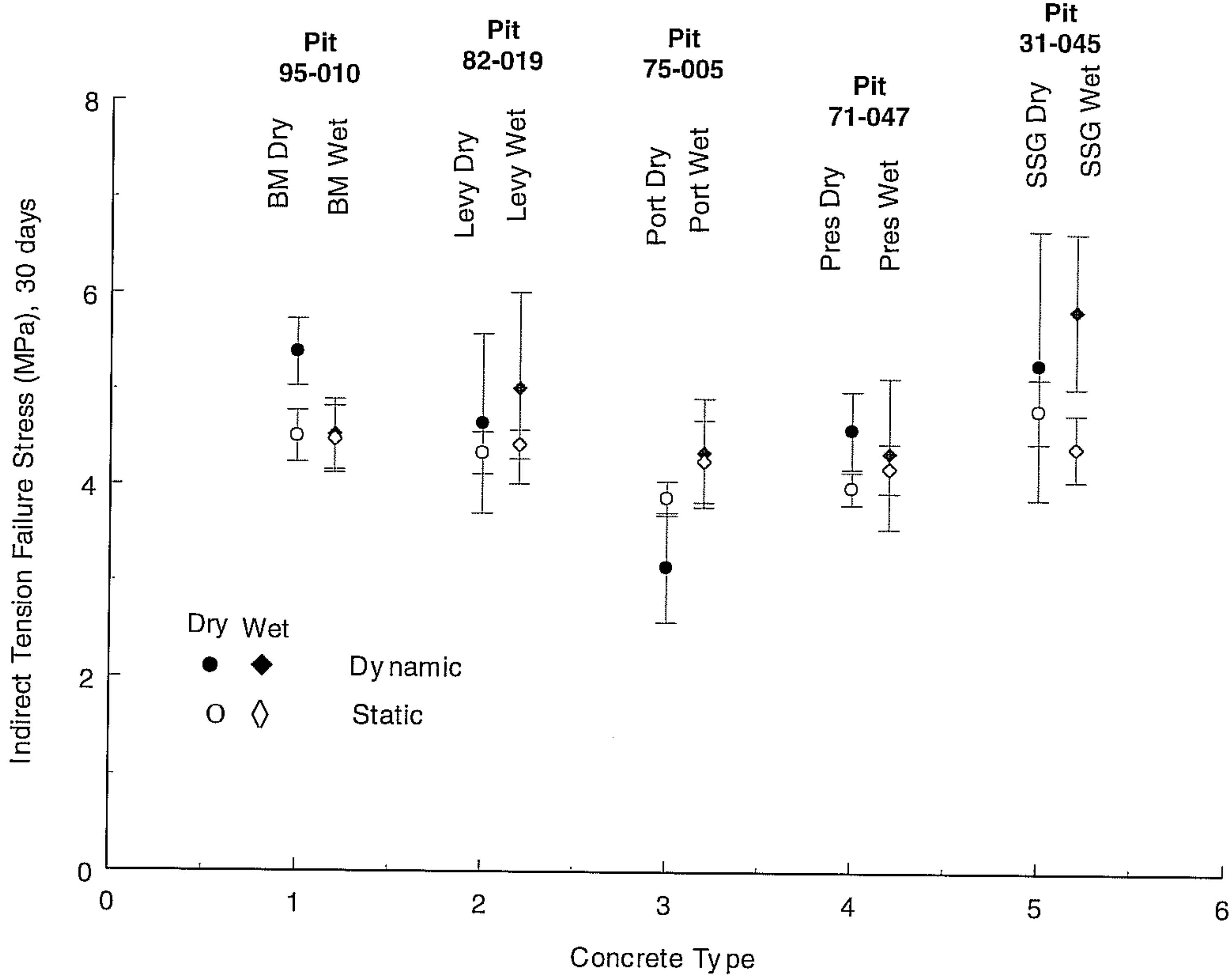

Figure 4.9 Statistical analysis showing mean and standard deviation of the static and dynamic tensile testing of concrete with different coarse aggregate types.

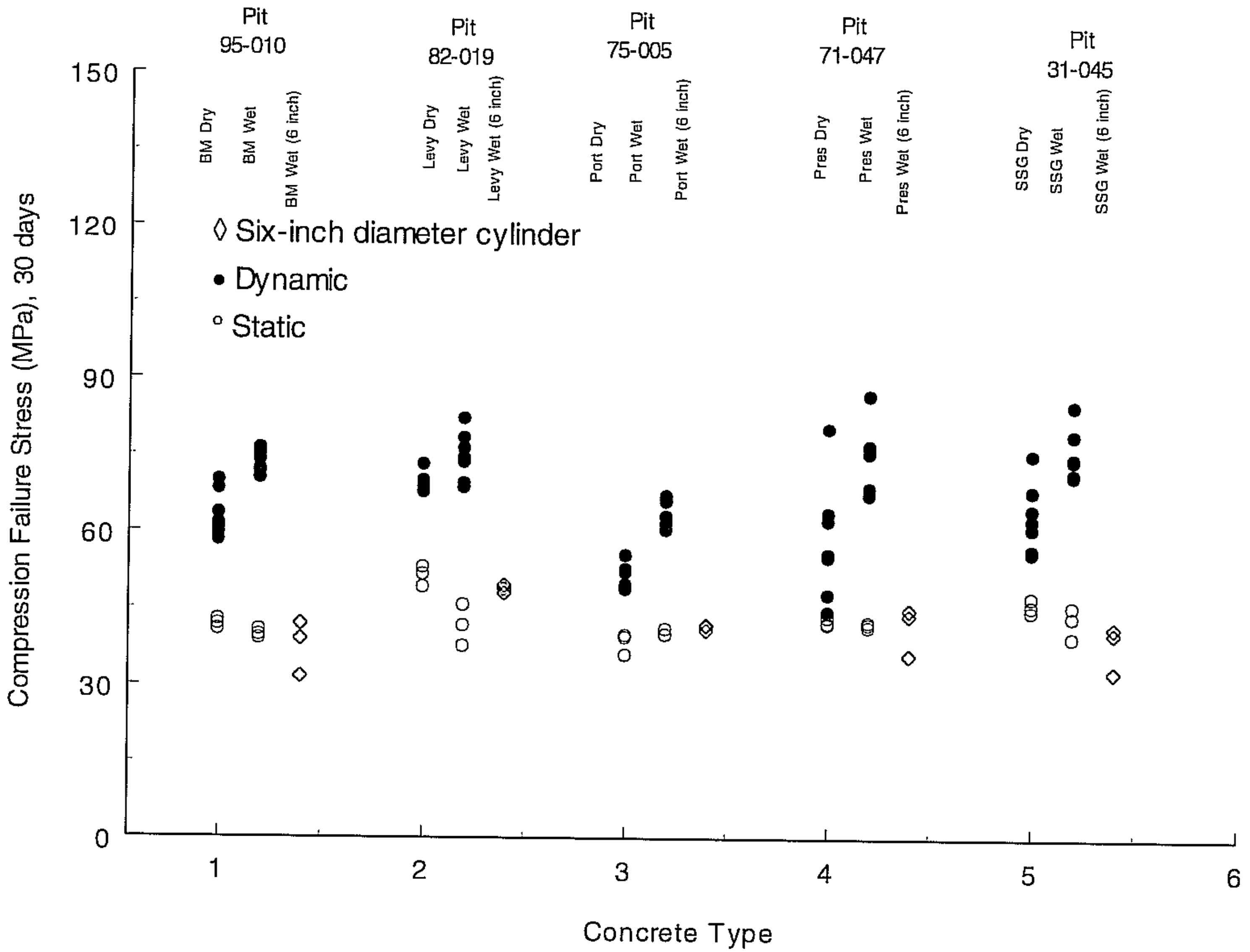

Figure 4.10 Raw data from static and dynamic uniaxial compression testing of concrete with different coarse aggregate types.

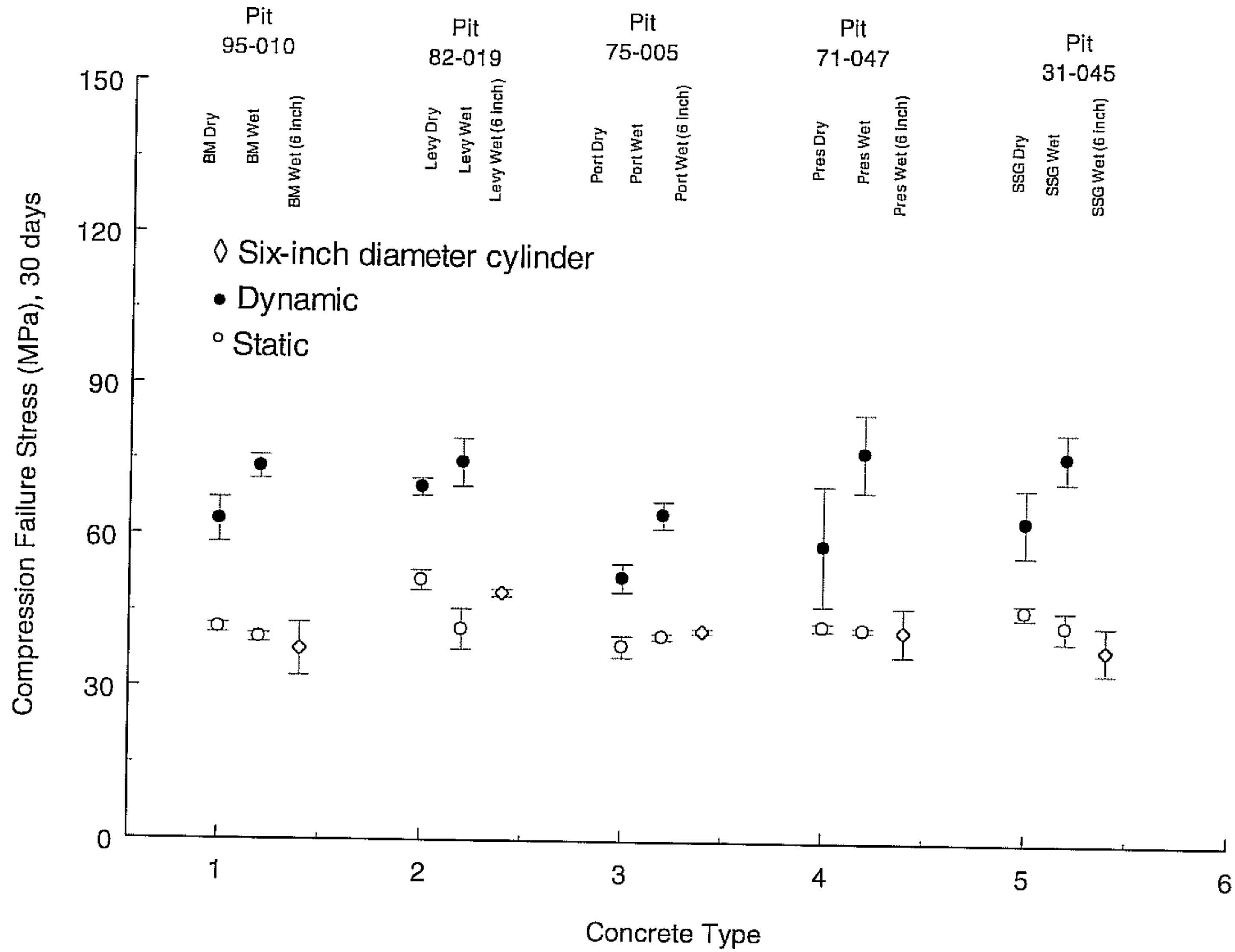

Figure 4.11 Statistical analysis showing mean and standard deviation of the static and dynamic uniaxial compression testing of concrete with different coarse aggregate types

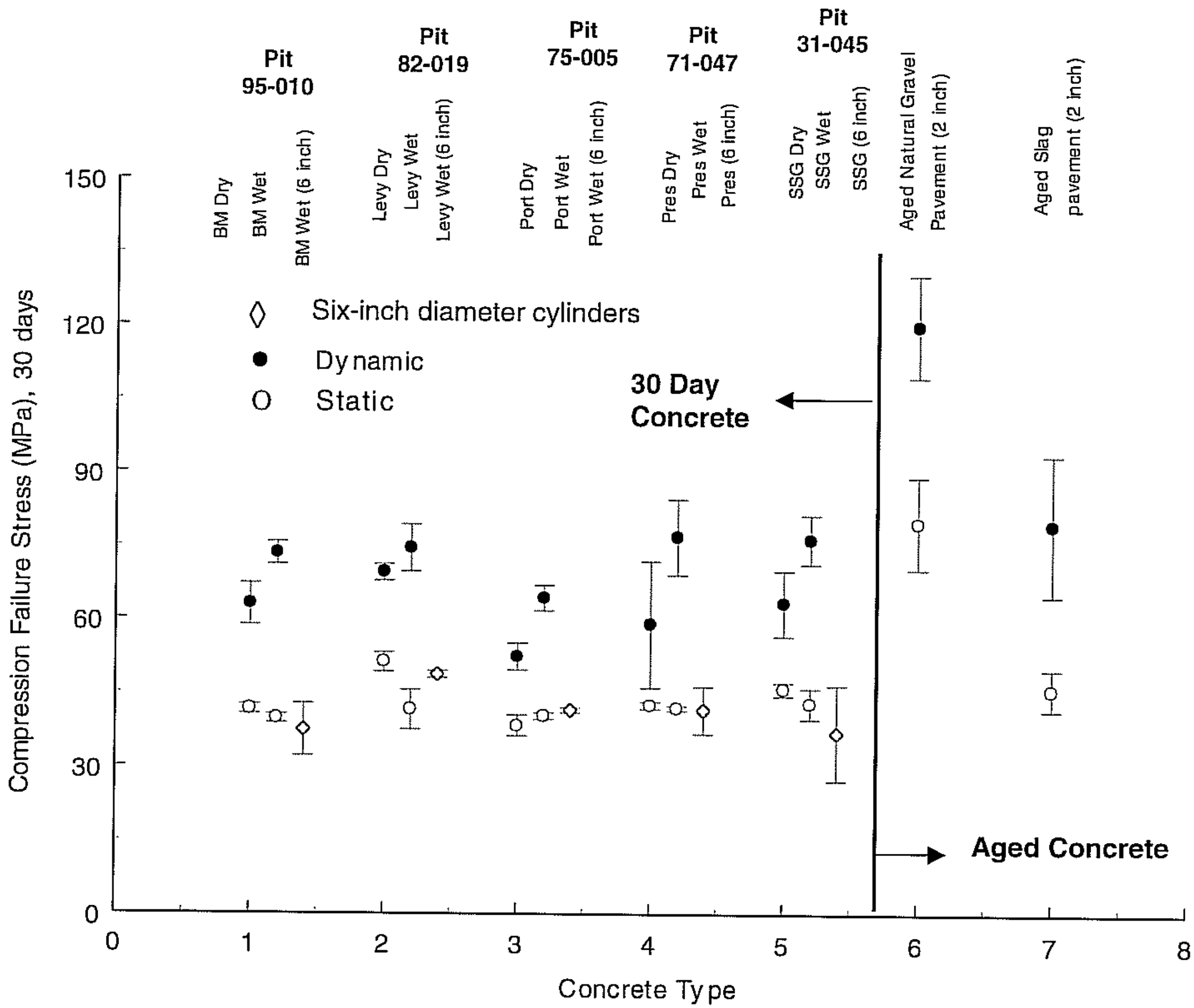

Figure 4.12 Statistical data for the dry and moist PCC static and dynamic compression testing including aged concrete data.

5 Discussion

5.1 Aggregates

5.1.1 Static and Dynamic Strength

Deere and Miller (1966) produced an engineering classification for intact rock based on uniaxial compressive strength that has gained wide acceptance in engineering practice. This classification categorizes rocks from very high strength (Category A) through very low strength (Category E) using a geometric progression of uniaxial static compressive strength values. Accordingly, the Deere and Miller classification (from Jumikis, 1983) has been applied to the uniaxial compression results obtained in this research for the dry testing conditions given in Figure 4.2(a). The correlation of uniaxial failure strength between this research and the Deer and Miller classification is presented in Figure 5.1, along with the aggregate's bulk density.

Starting with the slag specimens 1 through 3, it can be seen that the static test results of three out of the four slag specimens lie in the very low strength category **E**, while the higher density air-cooled slag specimen 1.2 lies in the medium strength category **C**. However, in both cases the dynamic results move into the next higher strength category, low strength **D** and high strength **B**, respectively. The increase in the dynamic strength over the static strength can also be seen in the results of static testing of limestone and dolomite specimens 4 through 8, which lie in the medium strength category **C**, and aggregates 9 and 10, which just lie in the high strength category **B**. Again, the dynamic test results lie in the next higher strength category; high strength **B** for aggregates 4 through 8, except 6, which moves two categories higher into category **A** "very high strength." However, the results for aggregates 9 and 10 stay in the same strength category of the static strength category **B** but are at the lower and upper boundaries of this category. Following this general pattern, aggregate 11 (basalt) moves from high strength category **B** to very high strength category **A**. Moreover, the static strength of aggregate 12 (diabase) is already in the highest strength category **A** (very high strength) while the dynamic strength is considerably higher. Continuing the geometric progression sequence of uniaxial compressive strength 440 MPa would be the start of the next category. The dynamic strength of aggregate 12

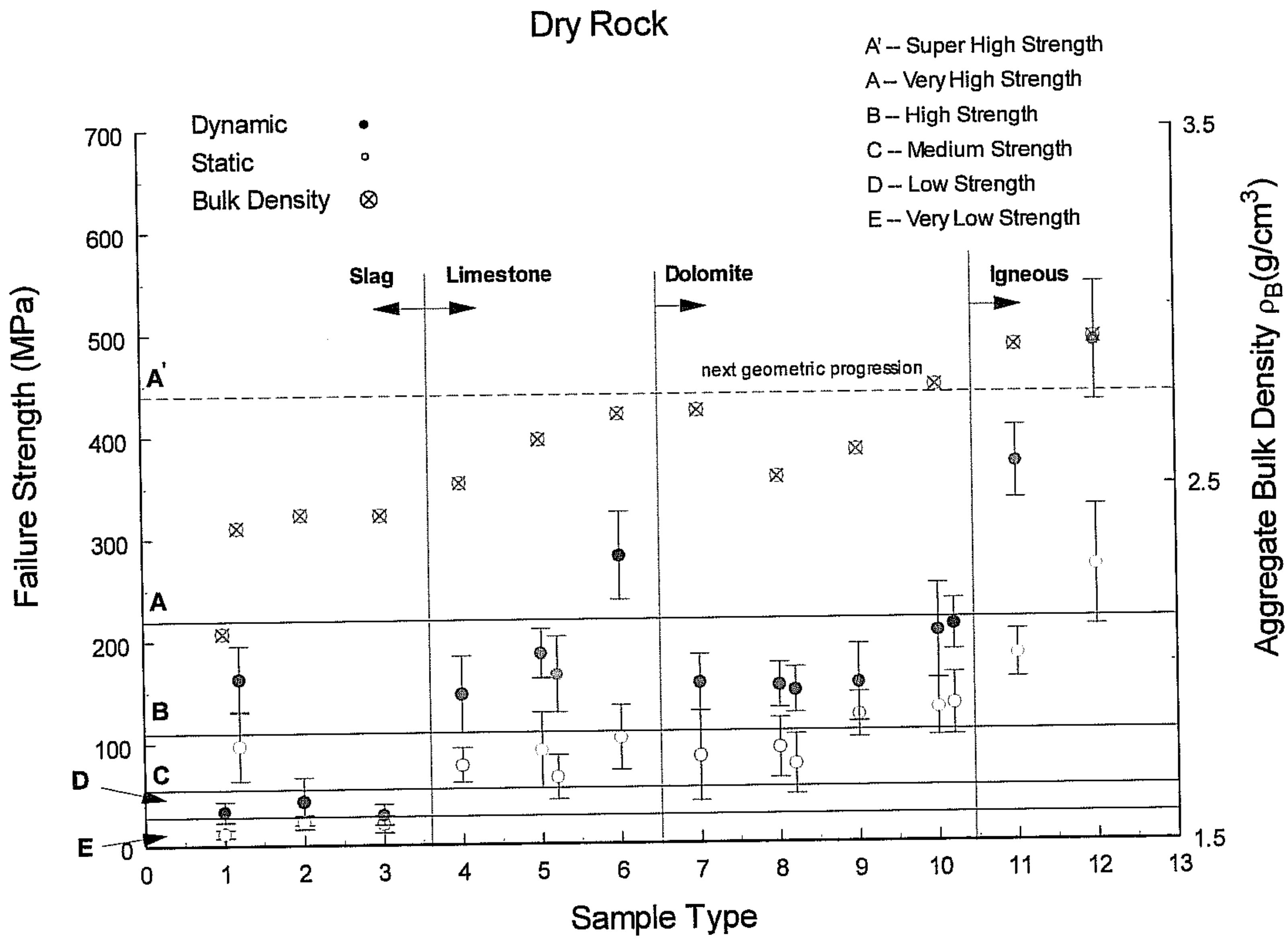

Figure 5.1 Uniaxial compression strength classification system for static and dynamic tests.

at 490 MPa would place this aggregate above the 440 MPa boundary into a new category that has been labeled **A'** and identified as "super high strength."

Comparing all of the aggregates, the blast furnace slag specimens have the lowest overall strength, which originates from a combination of factors including extensive porosity and compositional and the microstructural variations. Since slag is produced during the metallurgical treatment of iron ore, it consists of gangue and the secondary constituents from iron ores including, coke residue and limestone with a chemical composition consisting primarily of CaO, SiO_2, $A1_2O_3$ and MgO and trace amounts of sulfur and some alkalis (Lea, 1971). The final structure of the slag depends on available chemical constituents and the cooling conditions of the molten slag. Since slag melt has a high thermal energy of about 1700 kJ/kg, slow cooling conditions facilitate full dissipation of this energy and results in a stable dense crystalline structure with high density and mechanical properties close to that of natural aggregates (Lea, 1971). When the molten slag is quickly air-cooled or water-quenched with limited amounts of water, it traps steam in the mass and produces a relatively porous, glassy material with poorer mechanical properties. In this research both air-cooled (specimen 1) and water-quenched slag (specimen 2 and 3) were tested. The Algoma air-cooled slag (specimen 1), however, consisted of two distinct regions, a porous lighter colored region (listed as specimen 1.0) and a darker colored denser region (listed as specimen 1.2). While the air-cooled slag specimen 1.0 had approximately the same strength as the water-quenched specimens 2 (also from the Algoma Steel mill) and 3 (from the Levy Company) at approximately 20 MPa, specimen 1.2 had significantly higher strength at 98 MPa, which was in the range of the carbonates aggregates. Three possible explanations can be given for the higher strength for the denser air-cooled specimen 1.2. First, and most likely is that the denser slag had less porosity then specimen 1.0, 17 versus 30%. However, the bulk density of specimen 1.2 is approximately the same as the water-quenched slag specimens 2 and 3 at approximately 2.4 g/cm^3 and has basically the same porosity at 17% versus an average of 18% for specimen's 2 and 3. Interestingly, the air-cooled slag specimen 1.0, which only had a bulk density of 2.09 g/cm^3 and a significantly higher porosity at 30%, has about the same strength as the water-quenched slag specimen's 2 and 3. A second reason as mentioned previously is that the air-cooled slag may have had more time to cool since water was not used to increase the cooling rate of the slag by inducing thermal cracking in the slag mass. A longer cooling time would allow a denser crystalline structure to form resulting in higher strength.

However, the climatic conditions between an air-cooled site and a water-quenched site may not differ substantially and therefore the cooling rate may be approximately the same whether water quenching is used or not. A more significant factor, though, may be the subsequent breaking and crushing of the slag soon after placement in the cooling trench, which is conducted typically within 48-hours. Breaking up and crushing the slag reduces the thermal mass and greatly increases thermal cooling since the surface area of the slag exposed to the atmosphere is significantly increased. Air-cooled slag on the other hand, is deposited in a disposal area and left for a longer period of time prior to breakage and crushing and in some cases such as with the Algoma slag many years. A third possible reason, which was speculated in Section Three, is that the air-cooled slag due to its transportation and deposition may have been better mixed allowing improved chemical association and nucleation sites for crystal development. In general, the molten air-cooled slag was placed in large metal crucibles and transported to the disposal area by heavy equipment. The slag was then dumped down a slope providing additional mixing and onto other slag that would act as an insulator allowing slower cooling and better crystal development. A difference in crystalline structure between the air-cooled slag and the water-quenched slag can also be seen in Figure's A.1 and A.2 in Section Three of this report. The air-cooled slag, while also having numerous pores, appears the have a more developed crystalline structure as opposed to the water-quenched slag, which has a more glassy structure. It is probable that the more developed crystalline structure of the air-cooled slag, even at a porosity of 30% and a bulk density of 2.09 g/cm^3, gives the air-cooled slag an equivalent strength to the water-quenched slags, which has a higher bulk density at 2.40 g/cm^3 and a lower porosity of approximately 17%. Moreover, the higher density air-cooled slag specimen 1.2 with approximately an equivalent bulk density and porosity of the water-quenched slag has strength similar to that of carbonates. One likely reason for a denser region in the air-cooled slag is the higher density minerals will settle in the molten slag while the gas bubbles and lighter minerals will rise in the molten slag, thus forming the two regions in the slag. This is also seen in the water-quenched slags, where a lighter region forms at the top of the slag and a darker region towards the base of the slag. However, there was no discernable difference in bulk density and strength in the specimens cored and tested from either region. Based on these observations, it is recommended that additional research be conducted to better understand the factors that affect the development of slag's mechanical strength.

Inspecting the limestone and dolomite test results in Figure 5.1 a number of observations can be made. First, Jumikis (1983) indicates that dolomites are typically stronger than limestones in static strength, although not by a large margin. This relationship is confirmed in this research with the average dry static strength of limestones (aggregates 4, 5, and 6) equal to 84.6 MPa and the dolomites (aggregate types 7 through 10) equal to 107.5 MPa. However, the reverse occurs in the dynamic test results, where the average dynamic dry strength of the limestones are equal to 195.6 MPa while the dolomites are equal to 170.4 MPa. Second, while the static strengths of the three limestones tested (specimens 4, 5 and 6) are relatively close in value, the dynamic strength shows a strong increase that correlates well with the aggregate's bulk density. The dolomites also show an increase in dynamic strength with bulk density, however, this increase is also seen in the static strength results with the exception of specimen 7 (Cedarville dolomite). The Cedarville dolomite has a lower static and dynamic strength but has a relatively high bulk density. Consequently, by excluding the Cedarville dolomite it can be seen that there is a good correlation in dynamic strengths with bulk density for the carbonate aggregates. Inspecting the microstructure of the four dolomite aggregates from the thin sections shown in Figures A.6 through A.9 (Section Three), it can be observed that specimen 7 (Cedarville) and specimens 10 (France Stone) have relatively large grain structures, compared to specimens 8 (Denniston) and 9 (Rockwood), which have relatively fine grain structures. Although only four dolomites were investigated, the larger gain size appears to correlate with higher bulk density and conversely the finer grained dolomites with lower bulk density. What appears noticeably different, however, between the Cedarville and France Stone dolomite is that while the Cedarville dolomite has a larger grain size, it also has a more random and non-uniform grain size distribution. It is not clear as to how this microstructure controls the mechanical properties of the Cedarville dolomite; however, it possible that the more irregular nature of the crystalline grain structure may cause some of the deviations in the static and dynamic test results.

Finally, the igneous aggregates had the highest strength as expected. It is also interesting to note that although only two igneous aggregates were tested, their strengths to a smaller degree also correlated with bulk density. From this data it appears that in general dynamic strength correlates well with bulk density for the aggregate tested with the exception of the Cedarville Dolomite. In addition, it is also apparent that microstructural variations within aggregate types, e.g., carbonates, will influence this relationship.

5.1.2 Rate Sensitivity

A material's rate sensitivity is an important parameter that quantifies the ability of the material to resist higher dynamic versus static loads and is observed by an increase in compressive strength at higher applied strain rates. Many researchers provide the rate sensitivity for a material as a ratio of the dynamic to static strength (D/S). A material with a D/S of one would not be rate sensitive while a D/S greater than one would be rate sensitive. The D/S ratios for all of the aggregate tested in this research are presented in Table 5.1.

Table 5.1 Dynamic/Static strength (D/S) ratio data for dry and saturated aggregates.

			Compressive Fracture Strength Dynamic/Static Strength (D/S) Ratio			
ID No. Pit ID	**Aggregate/ (Quarry)**	**Orientation and Batch**	**Dry**	**Aggregate Average**	**Saturated**	**Aggregate Average**
1 95-006	AC Slag (Algoma)	Batch 1 Batch 1.2	2.74 1.67	**Slag**	2.42	**Slag**
2 95-006	WC Slag (Algoma)	Batch 2.0 Batch 2.1	1.90	1.93	2.75 3.49	2.68
3 82-019	WC Slag (Levy)	Random	1.42		2.05	
4 71-047	Limestone (Presque Isle)	Random	1.90	**Limestone**	2.67	**Limestone**
5 06-008	Limestone (Bay Co.)	Normal Parallel	2.04 2.54	2.30	1.88 2.30	2.23
6 75-005	Limestone (Port Inland)	Random	2.72		2.05	
7 49-065	Dolomite (Cedarville)	Random	1.84	**Dolomite**	2.15	**Dolomite**
8 58-009	Dolomite (Denniston)	Normal Parallel	1.66 1.95	1.64	1.55 2.05	1.83
9 58-008	Dolomite (Rockwood)	Normal Parallel	1.25		1.82	
10 93-003	Dolomite (France St.)	Normal Parallel	1.58 1.58		1.42	
11 31-076	Basalt (Moyle)	Random	2.03	**Igneous**	2.91	**Igneous**
12 95-010	Diabase (Ontario)	Water Cut Oil Cut	1.81 1.51	1.78	2.18	2.55

In reviewing the D/S results in Table 5.1, it can be seen that the aggregates all have a D/S greater than one, and consequently are considered to be rate sensitive. However, the amount of increase varied between aggregate types, ranging from 1.33 to 2.68. There was a noticeable increase in D/S between saturated and dry conditions for the blast furnace slag and the igneous aggregates with an average of 1.86 and 2.62 respectively. On the other hand, there was essentially no difference between saturated and dry conditions for the carbonate aggregates with limestones at a D/S of 2.30 and 2.23 respectively and the dolomites an average D/S of 1.64 and 1.83 respectively. However, there is a noticeable difference in the D/S between limestones and dolomites with the limestones having an average D/S of 2.26 and the dolomites an average of 1.73. The difference between the average D/S for limestone is relatively significant considering that the D/S ranged from 1.33 to 2.68, thus representing a variation of approximately 40% of the total range. It is also interesting to note that the high strength igneous and the very low strength blast furnace slag had similar D/S ratios of 1.93 and 1.78 for dry conditions and 2.68 and 2.55 for saturated conditions, respectively. The comparable D/S ratios may be an indication of the similarity of the microstructure of these materials since both made of igneous materials.

Another parameter that is used to assist in evaluating the applicability (or the effectiveness) of a specific aggregate to resist dynamic loads, e.g., impact or blasting, is the strain rate sensitivity (of fracture strength) parameter 'λ'. This parameter is also used in the development of rate dependent constitutive models for aggregates. From the strain gage data provided in Fig. 4.5(a) and (b) the strain rate ($\dot{\varepsilon}$) can be estimated during a test based on the measured strain (ε) and the time to fracture (t), i.e., $\dot{\varepsilon} = \varepsilon/t$. The strain rate for quasi-static tests was determined to be approximately in the range of 10^{-5}/s and for dynamic tests it was measured to be in the range of 10^{2}/s. The strain rate sensitivity parameter 'λ' is defined as follows:

$$\lambda = \frac{d\sigma_f}{d\left(\log\dot{\varepsilon}\right)} = \frac{\sigma_d - \sigma_s}{\log\left(\dfrac{\dot{\varepsilon}_d}{\dot{\varepsilon}_s}\right)} \qquad \textbf{5.1}$$

where, σ_d and σ_s refer to dynamic and static fracture strengths, $\dot{\varepsilon}_d$ and $\dot{\varepsilon}_s$ refer to corresponding dynamic and static strain rates, respectively. The numerator can be calculated from the average static and dynamic fracture strengths of the aggregates provided in Table 4.1. Since all the tests were performed either at a constant static strain rate 10^{-5}/s or a constant dynamic strain rate 10^{2}/s, the denominator is approximately 7. The strain rate sensitivity λ values are tabulated in Table 5.2. In this table it can be seen that the low strength slag aggregates also have the lowest rate sensitivity (λ<l0), ranging from 1.17 to 3.00 but 9.29 for the dense portion of the air-cooled slag (specimen 1.2). The high strength basalts have the highest rate sensitivity (λ>25), ranging from 26.90 to 31.30, while the carbonates have the intermediate values ranging from 4.52 to 25.52.

Table 5.2 Strain rate sensitivity λ values.

ID Number	Strain Rate Sensitivity, λ Aggregate	λ	λ Average
1.0	Algoma air cooled blast furnace slag – porous section	3.00	
1.2	Algoma air-cooled blast furnace slag – dense section	9.81	
2	Algoma water-quenched blast furnace slag	2.93	4.2
3	Levy water-quenched blast furnace slag	1.27	
4	Limestone, Presque Isle	9.97	
5	Limestone, Bay County	13.59	16.4
6	Limestone, Port Inland	25.52	
7	Dolomite, Cedarville	10.27	
8	Dolomite, Denniston	8.77	
9	Dolomite, Rockwood	4.52	8.6
10	Dolomite, France Stone	10.81	
11	Basalt, Portage Lake Lava Series, Moyle	26.90	
12	Diabase, Ontario Traprock	31.30	29.1

In crystalline brittle solids, such as ceramics, the rate sensitivity has been found to originate from microstructural inhomogenieties such as pores, cracks and impurities that exist along the grain boundaries (Lankford, 1981; Grady and Lipkin, 1980; Lankford and Blanchard, 1991; Ravichandran and Subhash, 1995). Typically these inhomogenieties form a small fraction of the overall material volume. Although it is known that inhomogenieties control the fracture characteristics of brittle materials, an important aspect of brittle failure is that resistance to crack growth from these inhomogenieties varies with strain rate. At low strain rates (traditional static testing rates), the rate sensitivity has been found to originate from the thermally activated stable sub-critical crack growth from these pores, cracks, and geologic discontinuities. But beyond a critical strain rate of 10^2/s, the compressive fracture strength increases dramatically with strain rate, which is attributed mainly to inertia dominated crack growth, i.e., as the loading rate increases, the time available for crack to initiate and grow reduces. The inertia associated with the crack growth acceleration will inhibit early fracture while the applied stress continues to rise rapidly, thus elevating the compressive failure strength under dynamic loads. Similar situation can be envisioned for the aggregates tested in this investigation. All the aggregates consist of highly inhomogeneous microstructure with small amounts of porosity (with the exception of slag) and impurities, which are potential sites for crack nucleation and growth under applied loads. Therefore, at higher loading rates, the stress level rises rapidly before the crack growth is initiated thus resulting in a higher compressive strength and rate sensitivity. In the case of slag aggregates, which are highly porous, it is believed that this porosity and lack of a well-defined crystalline structure (rather than impurities and inhomogeneities) dominate the deformation process and therefore, the failure strength is relatively low at both static and dynamic loading rates as seen in this research. However, a significant increase in strain rate sensitivity was seen in the dense air-cooled slag specimen 1.2, with a $\lambda = 9.81$ for the dense air-cooled compared to a $\lambda = 2.10$ for the water-quenched slag specimen 1.0. The primary reason for the increase in strength and rate sensitivity is believed to be due to the better developed crystalline structure of the air-cooled slag versus the water quenched slag. This can be seen in Figures A.1 and A.2, which show the difference in microstructure between the two slags. It is also interesting to compare the strain rate parameter λ results with the D/S results for both slags and igneous aggregates. Basically, the D/S results are similar for slag and the igneous aggregates, while the strain rate parameter results are significantly different for the two aggregate types. This indicates that while the strain rate parameter λ provides a measure of strength (and potentially a classification method), the normalization of the static and dynamic strength results, i.e., D/S, may possibly provide an indication of an aggregate's microstructural characteristics, e.g., igneous versus sedimentary or within a specific geologic category such as limestones.

Another significant feature of the strain rate sensitivity parameter λ is that it summarizes the results of both the static and dynamic testing results into one parameter. One correlation already discussed is strength (both static and dynamic) with bulk density. A plot of bulk density versus strain rate sensitivity parameter λ for all the aggregates is plotted in Figure 5.2. From this figure it can be seen that there is a general increase in λ with respect to bulk density with a linear correlation coefficient (trendline) of 0.61. Also, it is interesting to note in Figure 5.2 that some of the aggregates tend to group together. For example, the air-cooled slag lie on one side of the

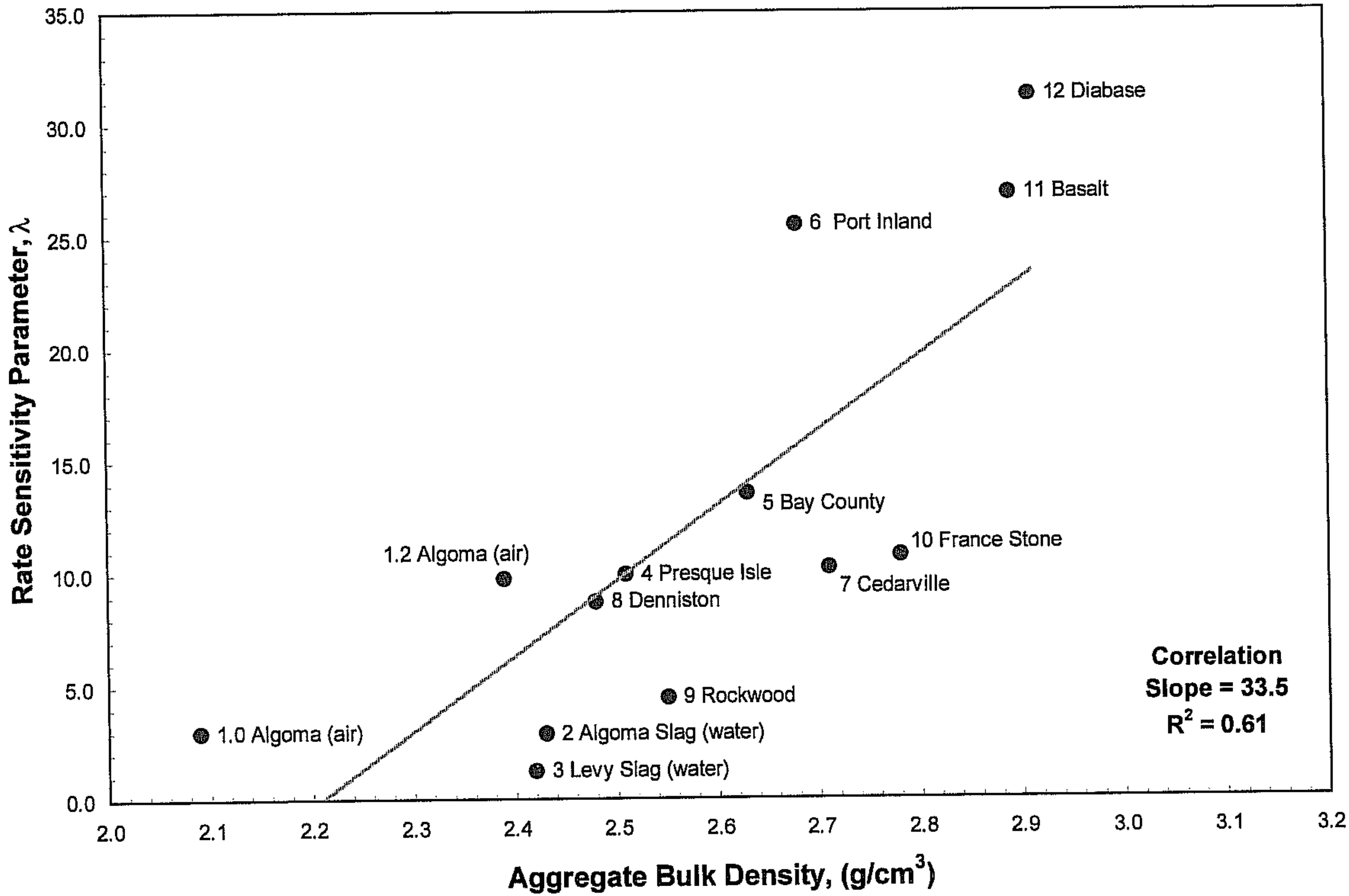

Figure 5.2 Strain rate versus aggregate bulk density for compression testing.

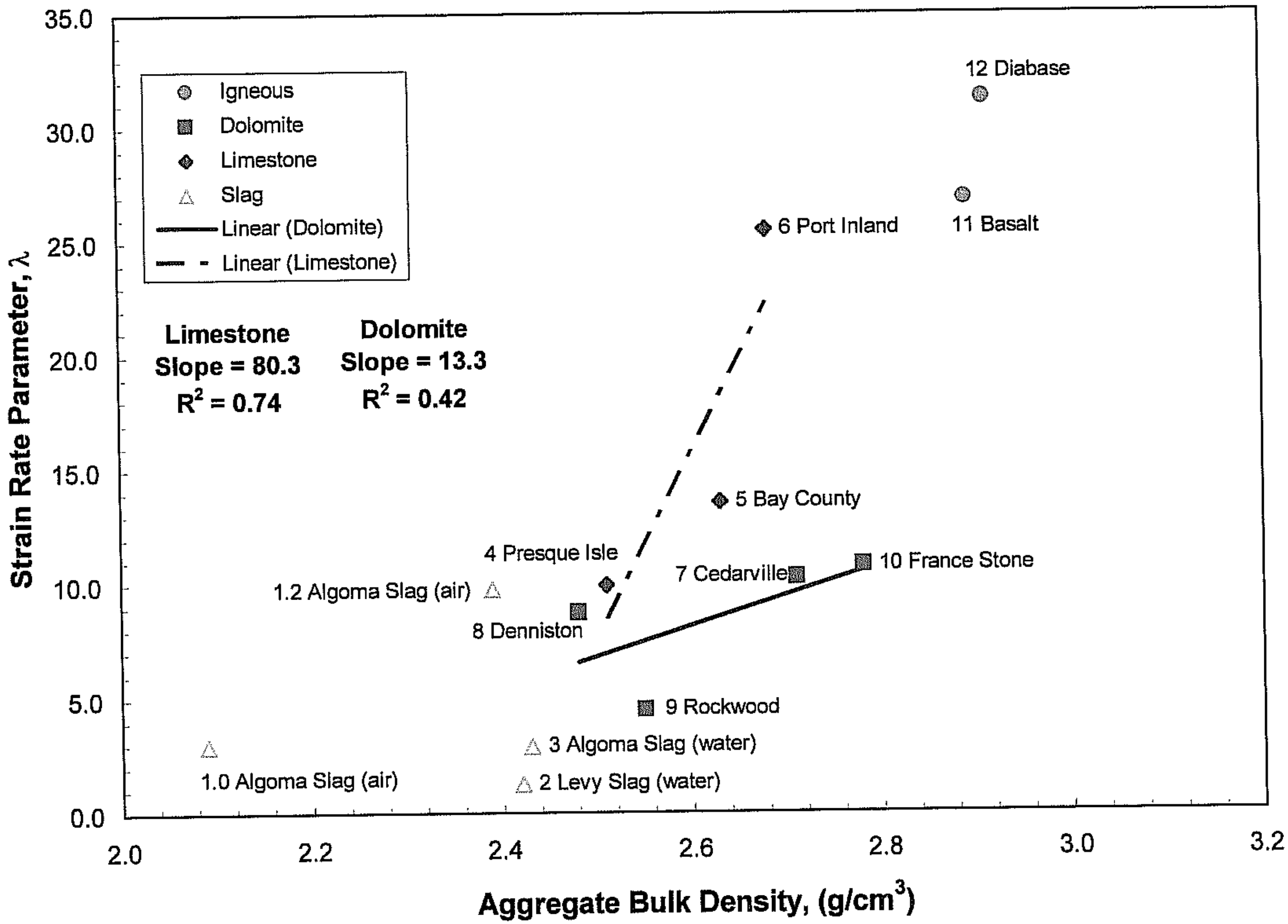

Figure 5.3 Rate sensitivity versus aggregate bulk density grouped by aggregate type.

trendline while the water-quenched slag are grouped on the other side. Further grouping based on geologic types is presented in Figure 5.3. From this figure it can be seen that there are more or less linear increases in strain rate sensitivity for both the limestone and dolomite aggregates. Therefore, trendlines were also added for the limestone and dolomites carbonates. The dolomite had the lowest linear correlation of 0.42 while the limestones had a linear correlation of 0.74. No correlation is provided for the igneous aggregate since only two aggregates types were tested. Also, no correlation was provided for the slag since there is such a large difference between the dense air-cooled specimen 1.2 and the other lower strength slags. However, excluding specimen 1.2 it can be seen that the general trend would be approximately level suggesting that there is limited to no increase in the rate sensitivity with bulk density for the slag aggregates.

Inspecting the strain rate sensitivity of the carbonate aggregates, the limestones range from 9.97 to 25.52 with an average of 16.4, while the dolomites on the other hand range from a low of 4.52 to a high of 10.81, with an average of 8.6. Thus, the limestones have average rate sensitivity almost twice that of dolomites. The limestone aggregates not only have higher strain rate sensitivity but also have a greater increase in strain rate sensitivity with bulk density. This same trend can be seen in the D/S results with the limestones having a higher D/S than the dolomites (2.30 versus 1.64). These results suggest that there may be a greater difference in microstructure between the limestone and dolomite aggregates than may have been previously considered given the similarity in static compressive strengths.

Inspecting the carbonate's microstructure shown in the thin-sections provided in Figures A.3 through A.9 (Section Three) a couple of generalization can be made concerning the testing results and the aggregate's microstructure[1]. In considering the limestone aggregates, it appears based on the size and uniformity of the grain size that the limestones are composed primarily of micrite or microcrystalline calcite and fossils. According to Blatt et al., (1972), micrite is by far the most common constituent in carbonate rocks with the individual crystals in ancient rocks usually less than 5 um in diameter. Micrite in turn commonly converts to calcite grains. From the thin-sections it can be seen that the Presque Isle limestone has the largest and most disorganized grain structure along with skeletal remains. The Bay County limestone has a smaller and somewhat more uniform grain size as well as skeletal fragments compared to the

[1] The following discussion provides only provide possibilities, since not enough information is available to make conclusive statements.

Presque Isle limestone. The Port Inland limestone has the smallest and most uniform grain size of the three limestones in addition to skeletal remains. Comparing the grain size of the limestones to its bulk density and rate sensitivity λ, it can be seen that as the grain size decreases both the bulk density and rate sensitivity parameter λ increase. In addition, the D/S values also increase from 1.90 for Presque Isle, to 2.3 for Bay County and finally to 2.7 for Port Inland limestone, which also corresponds to increasing dynamic strength. Interestingly, in ceramic engineering, it has been shown that for a given material the smaller the grain size and uniformity of the grain size the harder and higher dynamic strength of the material. This appears to fit with the general trend in the limestones, with the smaller grain size limestones having the higher strength. The benefit of the smaller grain size in increasing the strength of the material is that the failure cracks must fracture along a greater number of grains boundaries. As noted above, the strength (and rate sensitivity) of a material is a function of the microstructural inhomogenieties such as pores, cracks and impurities that exist along the grain boundaries. However, if the strength of the grain boundary is low due to significant inhomogenieties and other defects, the overall strength of the material will likely also be low regardless of grain size.

While there is wide agreement on the formation of limestone carbonates, there has been significant controversy over the formation of dolomitic rocks. The controversy centers on whether the dolomite develops as a primary mineral, i.e., that form naturally in bodies of water or whether the dolomites form as a secondary replacement product of limestone carbonates. That is, where limestones ($Ca\text{-}CO_3$) forms and then later transition into dolomite ($Mg\text{-}CO_3\text{-}Ca\text{-}CO_3$) due to migrating groundwater or changes in ocean chemistry. In general, the evidence suggests that dolomite forms as a replacement product of limestone. This is seen in thin sections of ancient dolomites where the individual dolomite crystals or clusters of crystals penetrate the original calcite carbonate particles. It has also been observed in the field where layered carbonate rocks abruptly change from limestone to dolomite with the change cutting across the carbonate bedding indicating that the dolomite is secondary. Another issue involving the formation of dolomites is that the dolomite crystals depart significantly from ideal conditions as opposed to calcite crystal formation. According to Blatt et al. (1972), dolomite is not stoichiometric but ranges in composition from approximately 56 mole % calcium and 44 moles % magnesium instead of an ideal value of 50%. A secondary problem in the formation of dolomite crystals during replacement of calcite crystals is the isomorphus substitution of other divalent ions such as magnesium, iron and aluminum ions for calcium in the structure. Typically, the most common and abundant substitute for calcium other than magnesium is ferrous iron, e.g., $Ca(Mg, Fe)(CO_3)_2$. This is the primary reason that dolomites have a higher absolute density than limestones due to the inclusion of the heavier magnesium and iron ions.

The above discussion on limestone and dolomite suggests two possibilities related to the results of this research. First, Blatt et al. (1972) points out that due to the depositional and environmental formation of carbonates, they tend to be relatively uniformed in composition and structure as opposed to other sedimentary rock types. This is primarily due to carbonates forming in basins as opposed to being transported as in the case of sand and other clastic sediments. This can be seen to some degree in the results from Table 1.2 (Section Three) for the absolute density (G_{ab}) values for the carbonate aggregates. The absolute density measurements were made using a Micromeritics 1330 helium pycnometer, which can provide accurately a material density to four significant digits due to the use of helium gas to penetrate the internal structure of the material. The results from Table 1.2 are as follows:

		G_{ab}		
Limestones:	Presque Isle	2.687	Average:	2.691
	Bay County	2.697	Standard deviation:	± 0.005
	Port Inland	2.690		
Dolomites:	Cedarville	2.770	Average:	2.813
	Denniston	2.828	Standard Deviation:	± 0.296
	Rockwood	2.836		
	France Stone	2.818		

Clearly, the limestone aggregates have a very constant density value with relatively little variation. This is somewhat surprising since the geological age of the limestone ranges from Silurian (France Stone) to Mississippian (Bay County) as well as in geographic location. The dolomites, on the other hand, show a larger variation in absolute density with the Cedarville aggregate lying between the limestone and dolomite carbonates although the remaining three dolomites are reasonably close in value. While certainly not conclusive, the variation may also suggest the secondary nature of the dolomite and may also help explain why there appears to be more variability in the dolomites results as opposed to the limestone results. It may also help explain the variation in the Cedarville dolomite in relation to the other dolomites. Although speculative, it is possible that the lower absolute density of the Cedarville dolomite may indicate that the replacement process was significantly different than for the other dolomites. That is, less magnesium and ferric iron ions were involved since the higher absolute densities of the dolomites is due to the replacement of calcium with heavier magnesium and iron ions. It is also interesting to note that there is an inverse relationship between the absolute density and the bulk density for the Rockwood, Denniston and France Stone dolomites. That is, as the absolute density increased the overall bulk density decreased. However, an important aspect of bulk density is the size and distribution of the pores and fractures within the aggregate, which can dramatically affect an aggregate's performance in a number of areas such as strength and freeze-thaw durability.

A second possibility is that the mechanism of dolomitic replacement would obviously affect the development of new grain boundaries and pore spaces during and after transition of limestone to dolomite. Cleary, if migrating ground waters or ocean waters are resulting in the growth of new minerals within the existing structure of the limestone, grain boundaries and pore spaces will change. Again, while speculative it is possible that a net result in the replacement process is an overall decrease in the stability and strength of the grain boundaries, especially if the crystal development is to result in larger crystal or clusters of crystals. Inspecting Figures A.6 through A.9, it can be seen that the structure of the four dolomites are generally different than the limestones. In particular, it is interesting to examine the Cedarville dolomite, which has very large grains and a somewhat irregular and disorganized structure as compared to the France Stone dolomite, which has a somewhat smaller grain size but is also much more uniform. The grain size of the Denniston and Rockwood dolomites, however, are even smaller and equally uniform, with Rockwood somewhat smaller than the Denniston dolomite. In reviewing the rate sensitivity parameters for the dolomites, i.e., France Stone λ=10.81, Cedarville, λ=10.27, Denniston λ=8.77 and Rockwood λ=4.52, the apparent trend is for the larger grain size dolomites to have higher rate sensitivity. This trend is opposite to what was observed with the limestones in which the strain rate parameter increased with smaller grain size. As noted above, the rate sensitivity of a material is a function of the microstructural inhomogenieties such as pores, cracks and impurities that exist along the grain boundaries. Clearly, due to the secondary nature of dolomite as a replacement product it is possible that there could be a change in the microstructure of the dolomite after transition from a limestone with the development and growth of new crystals. As a consequence, there may also be a marked difference in the dynamic response between limestones and dolomites. This is seen in the D/S results where the average D/S = 2.30 for limestones and D/S = 1.64 for the dolomites. While it is speculative that the variations in dynamic test results are a result of the replacement process of limestones into dolomites, it does suggest that the dynamic testing may provide a means of characterizing some aspects of the microstructural features of carbonates and in turn providing a means of better classifying carbonate aggregates.

The igneous aggregates tested, while both mafic in composition, also represent two very different formational environments. The basalt (specimen 11) is from the Portage Lake Lava Series and is known as a flood basalt. That is, the molten rock (magma) flowed out onto the earth's surface as lava, thus being exposed to the earth's atmosphere. Consequently, the cooling of the basalt was relatively rapid as compared to magmas that are trapped within the earth. This is seen by a large number of gas bubbles trapped in the rock as well as a differentiation of the lighter and heavier minerals due to gravity. The diabase, on the other hand, (Specimen 12) while primarily composed of the same chemical composition as the basalt, formed as a traprock (the reason for the quarries name Ontario Traprock). A traprock is a magma that is trapped below the surface of the earth where it crystallized under higher pressures and temperatures than the temperature and pressure at the earth's surface. Consequently, the crystal size of the diabase is considerably larger than the basalt. The difference in microstructure between the basalt and the diabase can be seen in Figures A.10 and A.11 (Section Three). As would be expected the diabase, with a slower cooling environment, forms a more stable crystalline structure. Although the grain structure is larger, it is likely that the strength of the grain boundaries is also higher with less inhomogenieties and defects due to the more stable cooling environment. This is seen in both higher strength and in higher rate sensitivity for the diabase with λ=31.30 versus λ=26.90 for the basalt. It is also interesting to compare the structure of the Algoma air-cooled slag with that of the basalt in that both have a similar splinter-like crystalline structure. The diabase, on the hand, has very well developed crystals. Although only two igneous aggregates in addition to the slag aggregate were tested, the dynamic testing results tend to indicate variations in microstructure. However, as note above additional research will be required to fully explore this relationship.

5.1.3 Aggregate Index Correlations

The primary aggregate index correlations used to classify aggregates used in PCC are the dilation and durability index values, which are used to assess freeze/thaw susceptibility and the LA abrasion index. These index values were obtained from the Michigan Department of Transportation (MDOT, 1997) and are presented in Table 5.3. These index values were than compared to the static and dynamic compressive strength results from this research. It should be noted, however, that while the index values are generally representative of the aggregate from each quarry, there might be some variation in these index values when applying them to the aggregates investigated in this research. This is due in part to the MDOT index values being derived from quarry samples taken at a specific point in time but where natural variations can occur as mining progresses over a longer period of time. Consequently, additional deviations are associated with comparing the MDOT index data with the results from this research. In general, the index values were compared to the static and dynamic strength, the D/S ratio, and the rate sensitivity parameter λ of the aggregates tested. Overall, the rate sensitivity parameter λ had a better correlation with the index values than the other research results. However, there also were some variances within the index values themselves. For example, the Bay County limestone (5) has very poor dilation, durability, and LA abrasion values. Moreover, its index values differ significantly from the other two limestones, the Presque Isle (4) and Port Inland (6) limestone, which were investigated in this research. However, the strength, bulk density and porosity values as well as the microstructure observed in the Bay County limestone thin section compared very well with the other two other limestone aggregates investigated. [2]

The first correlation investigated was between the dilation and durability index values and the strain rate parameter λ. This correlation is plotted in Figure 5.4 where it can be seen that there is considerable scatter when all of the data is plotted together. However, as with previous data sets there are data that group together. In particular, data with rate sensitivity parameters less than 15 and those greater than 25, which are also identified on Figure 5.4. Inspecting the

[2] It should be noted, though, that when initially coring the test samples of the Bay County limestone with an oil-based coolant, it was observed that unlike the other aggregates the Bay County limestone absorbed the coolant into its pores. It is speculated that the absorption was due, in part, to the fossils incorporated in to the limestone and not necessarily from the limestone matrix itself.

index values based on geologic origin it can be seen that if the carbonate data for rate sensitivity less than 15 are plotted together while excluding the Port Inland limestone, which has a high rate sensitivity and the Bay County limestone, which appears to have erratic index values, there is an excellent correlation between both dilation and durability with the strain rate parameter λ. This plot is presented in Figure 5.5 along with the linear correlation lines plotted on the figure and having a linear regression coefficient of 0.98 for the dilation data and a linear regression coefficient of 0.99 for the durability data[3]. The data includes all four dolomites and the Presque Isle limestone. This is particularly interesting result, since the dilation and durability index tests are performed on concrete specimens.

Table 5.3 Relevant aggregate index properties from MDOT.

Aggregate	Dilation	Durability	LA Abrasion		
			Max	Min	Last
1 AC Algoma Slag	---	----	41	28	32
3 WQ Levy Slag	0.001	99	43	36	40
4 Limestone, Presque Isle	0.005	88	31	25	24
5 Limestone, Bay County	0.131	6	44	23	44
6 Limestone, Port Inland	0.004	86	28	26	26
7 Dolomite, Cedarville	0.002	95	38	28	31
8 Dolomite, Denniston	0.008	80	35	30	30
9 Dolomite, Rockwood	0.035	41	38	21	21
10 Dolomite, France Stone	0.002	96	42	26	26
11 Basalt, Moyle	0.008	80	16	15	15
12 Diabase, Ontario Trap.	0.000	100	14	12	13

In regards to the LA abrasion index values, a relatively linear inverse relationship (dashed lines) exists between the maximum LA abrasion index values and the unconfined compressive strength (both static and dynamic) as shown in Figure 5.6. While both the static and dynamic compressive strength data exhibit an inverse relationship with LA abrasion index, the dynamic strength data gives a much broader slope and is able to separate the aggregates (or spread the

[3] The two correlations are basically equal in value since the durability index is calculated from the dilation results.

data) for better correlation. For example, the static data for all the carbonates is clustered and provides only limited information for comparison of one aggregate against the other based on this property. However, the dynamic data provides a broader range allowing for separation of the data, which may better assist in ranking of these materials based on this property. It can also be noted that the dynamic values should in some way correlate with the LA abrasion since the abrasion process (or material fracture) during the test occurs typically in milliseconds and hence one can argue that the use of dynamic strength data as a more realistic representation of the process. Therefore, the relationship between the strain rate sensitivity parameter, λ, and the maximum LA abrasion values for the aggregates are plotted in Figure 5.7. Again a relatively linear relationship is also observed in this figure illustrated by the gray trend line, although the correlation coefficient is only 0.74. However, the carbonates taken collectively clearly do not fit a linear relationship and in fact appear to have a reverse relationship if the Port Inland limestone (λ=25) is excluded. This relationship is presented in Figure 5.8 where the linear correlation coefficient is only 0.23 and where the relationship indicates that the LA abrasion values increase with increasing strain rate parameter.

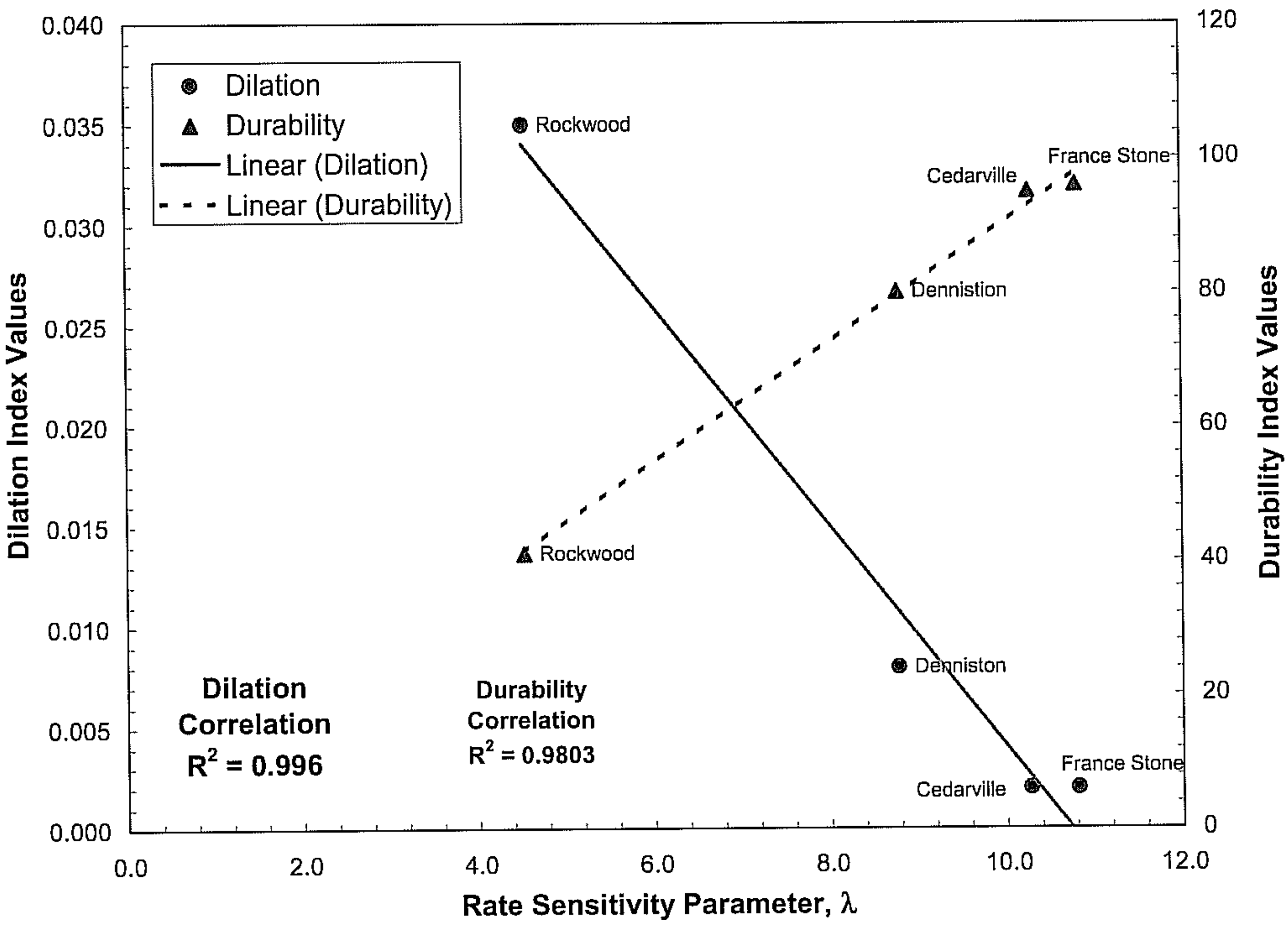

Figure 5.5 Dilation and durability index values for carbonate aggregates versus strain rate parameter λ.

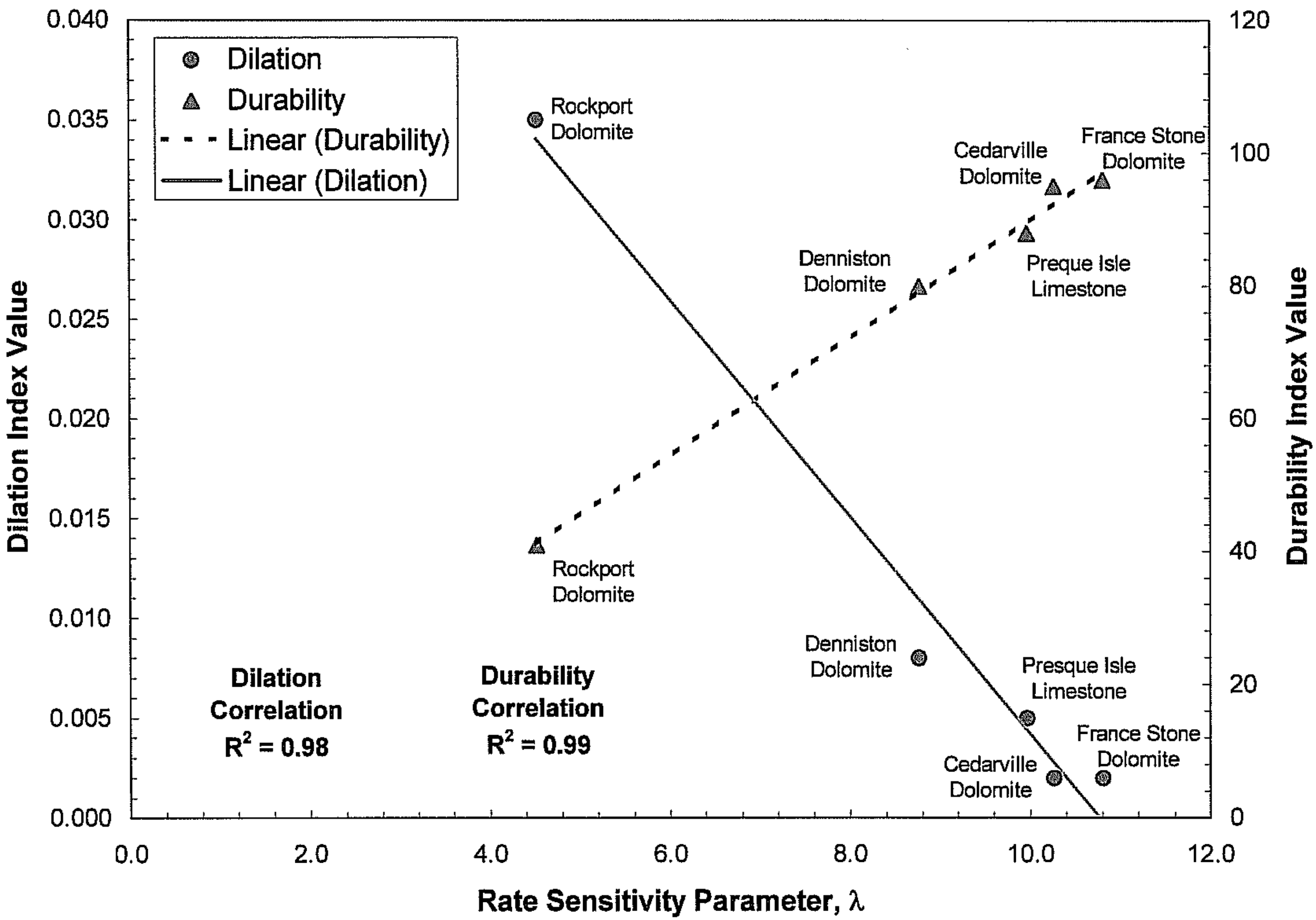

Figure 5.5 Dilation and durability index values for carbonate aggregates versus strain rate parameter λ.

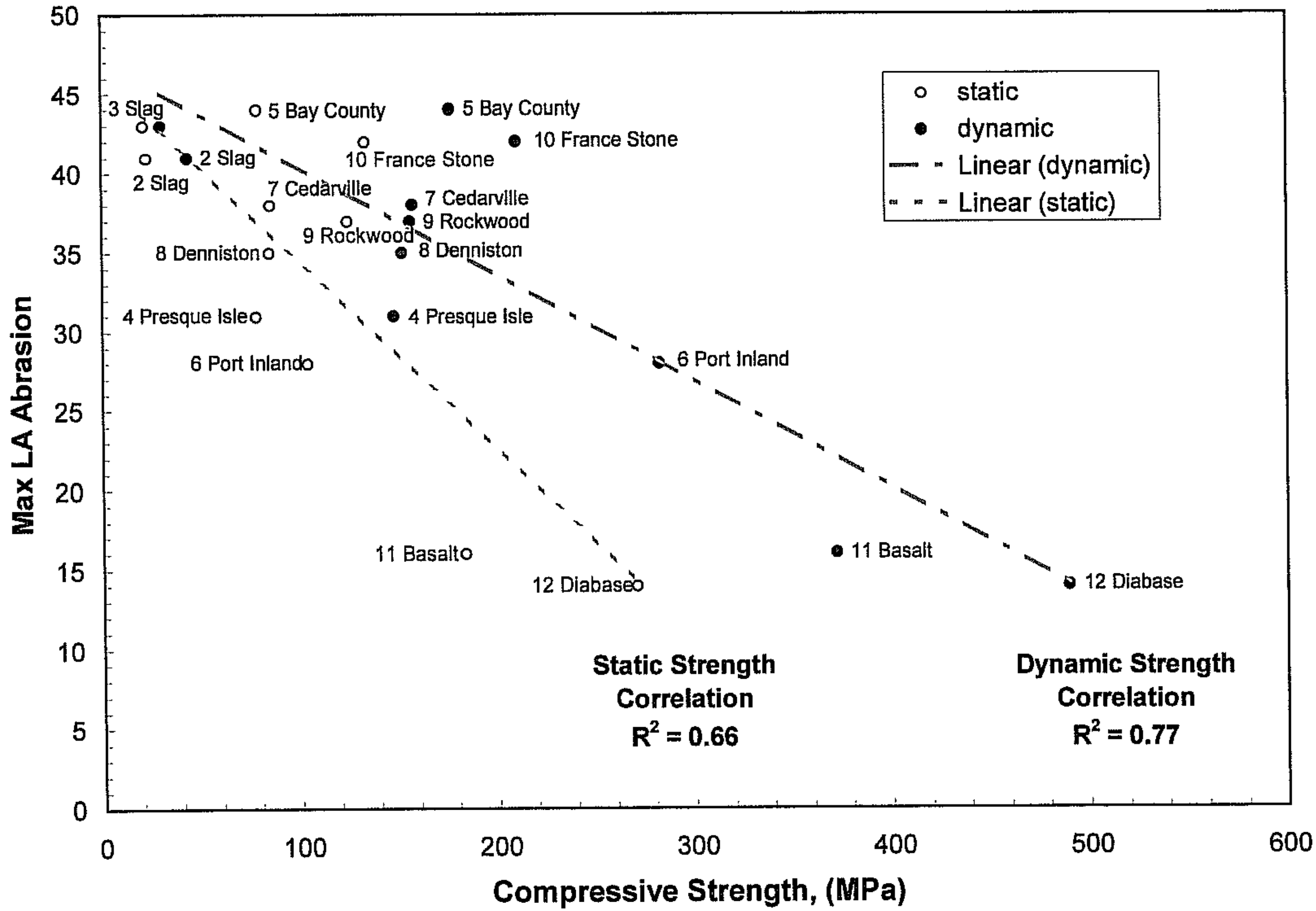

Figure 5.6 Maximum LA Abrasion values versus compressive strength.

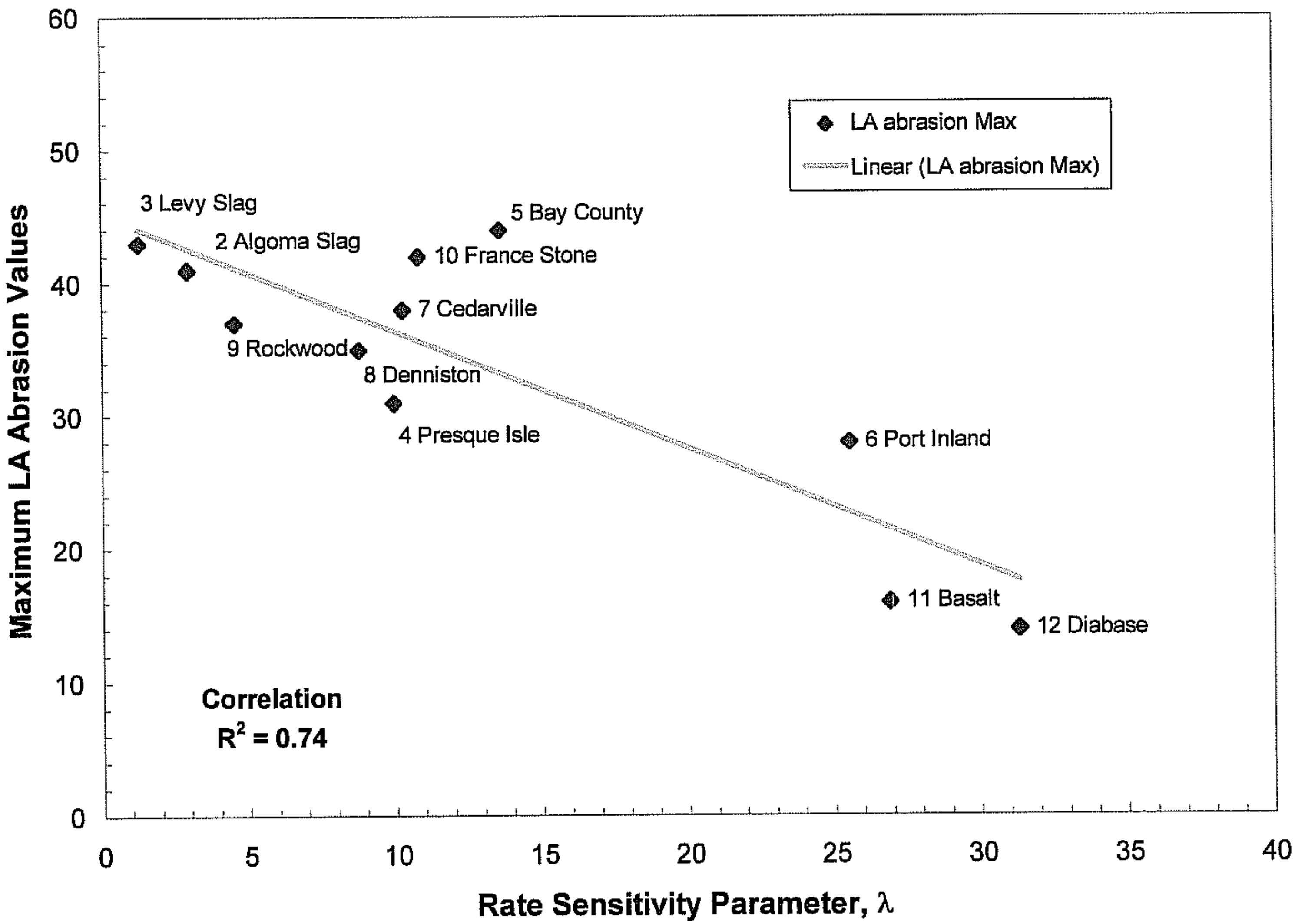

Figure 5.7 Maximum LA abrasion values versus the rate sensitivity parameter.

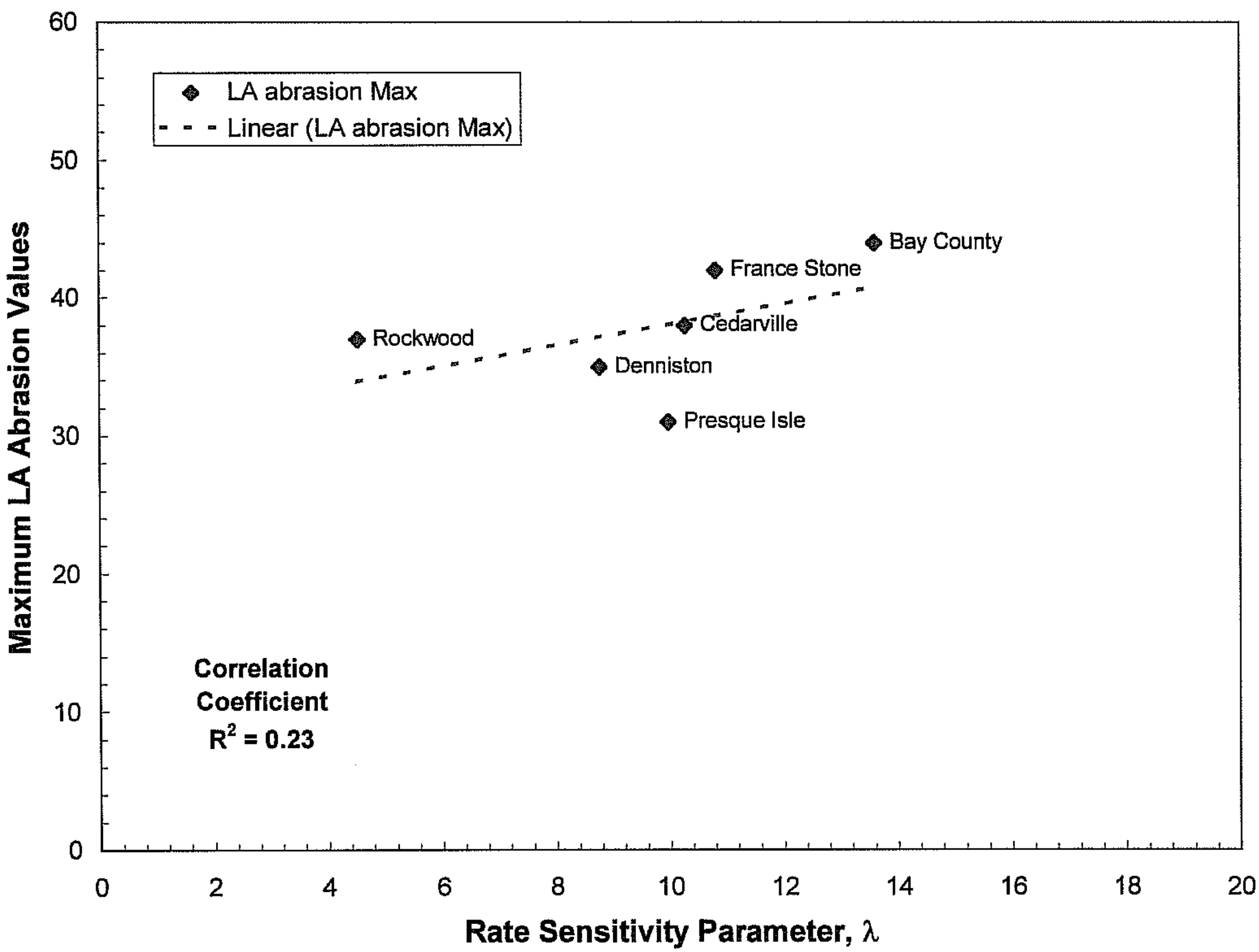

Figure 5.8 Maximum LA abrasion values for the carbonate aggregate versus the rate sensitivity parameter.

5.2 Cement Matrix

The uniaxial compression test results, shown in Figure 4.7, indicates that the cement matrix (mortar) is also rate sensitive. In general, the results show a dynamic strength to static strength (D/S) ratio of 1.5 to 3.5 in uniaxial compression. This compares well with the research by Ross et al., (1985) who also reported a 1.5 to 3 increase for mortar. However, the details concerning the mixing method and curing of the mortar tested in Ross's et al. research were not provided. As mentioned in Chapter Three of this section, the mortar's air content is critical to correctly representing the actual mortar in PCC. The mortar was mixed following the MDOT mortar voids method discussed in Section 4 at a 5% air. However, this produced a stronger mix than exists in PCC. A second batch was then prepared at 9% air, which was believed to be more representative of the mortar in PCC. In general, the average static strength of the mortar (over the testing period) was 24 MPa while the dynamic strength was approximately 58 MPa. It is interesting to compare the mortar's static and dynamic strengths versus the aggregate strengths, which is provided in Table 5.4 and grouped by geologic categories. From these data it can be seen that the mortar and slag are relatively close in compressive strength with the mortar's dynamic strength higher than the dynamic strength of the slag. Otherwise, all of the aggregate types tested are (at a minimum) four times stronger than the mortar in both static and dynamic strength. As discussed in Section Four, since the 28-day strength of PCC is primarily a function of the mortar strength; the strength of the coarse aggregate does not play as important a role in overall strength. However, it is unclear what the effects (if any) to PCC are when the coarse aggregate strength is approximately or somewhat lower than the mortar strength.

Table 5.4 Average static and dynamic compressive strengths of mortar and aggregates.

Material Type	Static[4] Strength Mpa	Dynamic[4] Strength MPa
Mortar	24	58
Slag	22 (20)	37 (52)
Limestone	85 (80)	195 (170)
Dolomite	107 (106)	173 (162)
Igneous	226 (162)	430 (398)

[4] Compressive strengths are from dry testing conditions while the compressive strengths for saturated test conditions are in parenthesis. No saturated mortar samples were tested.

Another interesting aspect of the mortar testing presented in Figure 4.7 is the variations in strength over the 18-week testing period with both increases and decreases in static and dynamic strengths. The static strengths increase during the first four weeks and then decrease slightly in weeks five and six and then increase again to about a maximum in week seven to approximately 30 MPa. However, after seven weeks the static strength levels off to about 20 MPa (±5 MPa).

The dynamic strength results mirror to some degree the static results in general overall increases and decreases. The fact that both the static and dynamic tests have similar variations is important since it verifies that the variations are occurring in the mortar instead of due to experimental errors since the static and dynamic tests were independent tests. The most obvious dynamic strength increase occurs after the first two weeks where the mortar, at around 50 MPa, reaches a maximum dynamic strength of approximately 70 MPa and maintains this strength over three weeks. This three-week period of time is also when the standard 28-day PCC tests, i.e., fourth week, are conducted. After the fifth week the strength drops dramatically off to a low of 50 MPa at week nine. Interestingly, this is also accompanied by a decrease in the static strength to the minimum strength reached in the static test of 20 MPa. At this point the D/S ratio has dropped from a high of 3 at 28-days to a low of 1.5 at week nine. This occurs two more times throughout the testing at 11 and 15 weeks where the mortar reaches a maximum dynamic strength of 70 MPa followed by a decrease. It is unclear as to the reasons for these variations in both static and dynamic strength during curing, which was conducted in the same manner as the concrete specimens tested in this research. One possibility for the variations is that the mortar specimens, which were cored from two larger mortar blocks, may have been taken at different locations within the blocks that were at different points of curing. For example, core specimens taken near the edge of the blocks may be at a different point of curing than specimens taken in the middle of the mortar blocks. However, during testing all of the cores were mixed together in an attempt to minimize this problem. A second possibility is that during cement hydration some micro cracking may be occurring, thus indicating that the developing microstructure of the mortar is altering during the curing time. It was speculated in the aggregate section that the D/S ratio might be a function of a material's microstructure. If this is the case, the D/S changing from a low of 1.5 to a high of 3.5 (week 11) may indicate that microstructural changes are occurring; resulting in both increases and decreases in strength. However, additional testing along with petrographic analysis would be required to confirm this hypothesis.

5.3 Portland Cement Concrete

Concrete specimens with the coarse aggregate as the only variable were tested in indirect tension and uniaxial compression at both static and dynamic loading rates. In addition, the tests were performed under both moist and dry conditions while being tested at 30 days[5]. The following materials were used as coarse aggregates in the PCC: Bruce Mines diabase (BM) 95-101, Levy Slag 82-019, Presque Isle limestone 71-047, Port Inland limestone 75-005 and Superior Sand and Gravel (SSG) 31-045. As discussed in Chapter Four of this section, the dry test conditions were achieved by oven drying the specimens at a temperature of 110° C for approximately three days. In addition, PCC from two older concrete pavements (aged PCC), which had been test cored, were also tested in uniaxial compression. One of the PCC pavements had a natural coarse aggregate while the other pavement had a slag coarse aggregate. However, the aged concrete, which was originally cored from six-inch diameter cylinders in the field, was later cored to two-inch diameter cores in the lab. This is a smaller diameter than the three-inch diameter specimens, which were prepared for testing the PCC with different coarse aggregates and tested after a 30-day cure. Consequently, in analyzing the test results the diameter of the specimens should be kept in mind since smaller diameter specimens tend to result in higher strengths. Also, the size of the maximum aggregate in the PCC compared to the diameter is also a factor in the strength of the PCC when testing smaller size cores.

5.3.1 Indirect Tension Testing

The indirect tension testing results were presented in Figures 4.8 and 4.9, in which Figure 4.8 provided the raw results and Figure 4.9 provided statistically processed data. From these figures the following observations were made. First, the indirect tensile strength results ranged from a low of 3 MPa to a high of 6 MPa. The static tensile strengths vary from 3.9 MPa to 4.9 MPa, a difference of only 1 MPa, while the dynamic tensile strength results ranged from 3 MPa to 6 MPa, a difference of 3 MPa. Therefore, the difference in the static and dynamic strength indicated that the concrete was rate sensitive in tension but not by a wide margin. The exception was the Port Inland PCC, which had a negative result with the dynamic strength being

[5] The 30-day cure time was selected to be consistent with the research by Ross et al. (1985, 1995 and 1996).

less than the static strength for dry conditions but essentially the same for moist conditions. It is believed that the Port Inland PCC was incorrectly prepared (as will be discussed in the uniaxial compression test discussion section) since the Port Inland PCC data had a rate sensitivity increase in uniaxial compression but none in tension. It is highly unlikely that the PCC would have no rate sensitivity in tension but have rate sensitivity in compression. Third, the results varied between dry and moist conditions for the PCC aggregate types. The Bruce Mines PCC and Presque Isle PCC had higher rate sensitivity in the dry condition then in the moist condition, whereas, the Levy slag and Superior Sand & Gravel PCC had higher rate sensitivity in the moist condition than in the dry condition. Finally, there was no statistical correlation between PCC strength and coarse aggregate strength with either the static or dynamic strengths.

While the results of the indirect tension tests were variable, the dynamic to static strength ratio (D/S) ranged from 1.0 to 1.35 at a strain rate of 80/sec. These results, however, do not compare with the D/S ratios by Ross et al., (1989, 1996) who found a D/S ratio between 6 to 8 for PCC in indirect tension; clearly a significant difference in D/S ratios. The results of the Ross et al. (1996) research were previously presented in Figure 1.9. It is unclear as to the reason for this lower rate sensitivity or the variations in the dry and moist conditions in this research, since both the dry and moist specimens were tested at the same time, which eliminated (to some degree) variations between testing the dry and moist PCC specimens. However, European researchers (Comité Euro-International du Béton, 1990) also investigated the rate sensitivity of concrete in tension. In this research they developed a model known as the CEB model to predict the D/S factors for concrete in tension based on the concrete's static compressive strength. According to the CEB model, the D/S at a strain rate of 80/sec is 1.8 (for a concrete with a static compressive strength of 70 MPa) and 2.4 (for a concrete at a static compressive strength of 30 MPa). The average static compressive strength of the PCC used in this research was approximately 45 MPa, which by interpolating the CEB model between a D/S of 1.8 and 2.4 would predict a D/S ratio of 2.2, which is considerably closer to the indirect tension results in this research, i.e., between 1.0 and 1.35 versus the results from Ross et al., at between 6 and 8. The CEB model showing the predicted dynamic to static ratio (termed a dynamic increase factor) along with the model developed by Malvar and Ross (1998) is shown in Figure 5.9. Malvar and Ross, however, in analyzing the CEB model stated that the strain rate at which rate sensitivity begins to increase was too high and that a lower strain rate should be used. By readjusting the

CEB model to a lower starting strain rate value Malvar and Ross were able to raise the predicted rate sensitivity of concrete in tension to a D/S of 6 to 8, which would be comparable to the results of Ross et al. and other researchers. In effect, they simply moved the CEB curves to the left to match their model curves. However, the CEB model, regardless of the model readjustment by Malvar and Ross was based on experimental results. As noted above, the CEB model also varied based on concrete uniaxial compressive strength, e.g., 30 MPa and 70 MPa, which show that the D/S ratios increase for lower compressive strength concrete at a given strain rate than for higher strength concrete.

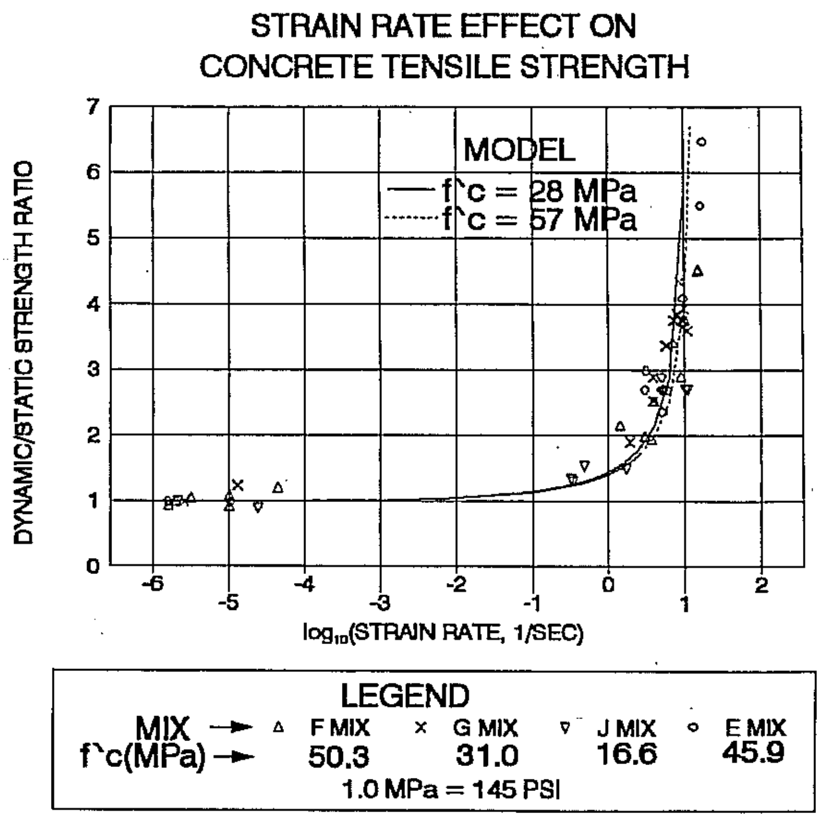

Figure 5.9 CEB and Ross et al. models for the rate sensitivity of concrete in tension, (From Malvar and Ross (1998).

It appears, however, that even discounting Malvar and Ross readjustment of the CEB model that the rate sensitivity of concrete found in this research was still lower than that predicted by the CEB model. In addition, according to Ross et al., (1996) the moist tensile strength of concrete is greater than the dry strength at high strain rates. This was seen in the Levy slag and Superior Sand & Gravel PCC but not the remaining PCC specimens tested. Ross et al. attributes the increase in dynamic tensile strength due to moisture to a tendency of the moisture to amplify the inertia effects (resistance to cracking) of the concrete. Again, the results of this research were not consistent in regard to moisture. However, the indirect tension tests procedures used in this research were based on those provided in Ross et al. (1996). For example, the same specimen length to diameter ratio of one was used, i.e., three-inch diameter by three-inch length. In addition, platens were machined in the same configuration as the platens used by Ross et al. Finally, a strain rate of 80/sec was used in this research while Ross et al. conducted the indirect tension tests in the strain rate range of 1 to 100/sec. The primary difference in the testing procedures was that Ross et al. used two-inch diameter specimens while this research used three-inch diameter specimens. This introduces a "size effect" between the two tests results with the smaller diameter two-inch specimens more likely stronger and stiffer than the larger three-inch specimens. However, as will be discussed in the following section on the PCC compression results, the difference between two and three-inch specimens should not be that large, although the difference may be larger in tension than in compression due to the lower tensile strength of PCC. Consequently, it is unclear as to what caused the lower D/S ratios and variations in moisture conditions in this research. One possible explanation, however, may be how the platens, which were used to apply a line load to the sample, were kept in alignment with respect to the test specimen. While in the static indirect tension testing the specimen can be carefully aligned as the loading platens make vertical contact with the specimen. In effect, the static test is self-aligning. However, in the dynamic testing it was harder to maintain the alignment since the specimen had to be held horizontally between the platens through friction (see Figure 3.4) from the SHPB bars. In this situation it was possible to misalign the specimen and therefore care had to be taken to align each specimen. If any misalignment did occur than the line load would not be applied diametrically across the specimen and lower failure strength would result since a smaller area across the specimen would fail in tension. However, there was no mention by Ross et al. (1996) concerning using an alignment fixture. If the dynamic indirect tension testing is continued it is highly recommended that a self-aligning fixture mechanism to hold the sample correctly in place be designed, tested, and used in future research.

In considering the results of the Ross et al. (1996) research, it is also unclear as to why the PCC is more rate sensitive in tension than in compression in regards to concrete failure. It is possible that the significantly lower tensile strength of concrete (both static and dynamic strength) compared to the compressive strength may account for this increase rate sensitivity. That is, lower strengths would be more affected by the rate of loading than higher strength materials. This is in fact seen in the CEB model where the lower strength concrete, as determined by the concrete's static compressive strength, had higher rate sensitivity than the higher strength concrete. In considering tensile testing, the main difference between the indirect tension test and the uniaxial compression test is that in tension, failure is forced to occur along a predefined surface, i.e., diametrically through the center of the concrete disk. In the uniaxial compression test, failure occurs along many surfaces (resulting in significantly higher material strength), which may mask higher rate sensitivity since each surface has a greater potential to find a surface of lower fracture strength. It should also be noted that the length of the failure surface in uniaxial compression is typically twice as long as in the indirect tension test, since failure takes place along the length of the sample in compression but only has to travel through the diameter of the sample in tension. Taking into account the higher rate sensitivity of concrete in tension and that failure is forced through a predefined surface, coarse aggregate strength may in fact have an influence on rate sensitivity, although this was not observed in the testing in this report. It was observed, however, that failure occurred through both pop outs and coarse aggregate fracture, but that the majority of failures appeared to be through aggregate fracture, possibly due to forcing the failure surface through the diameter of the specimen. While Ross et al. (1996) tested concrete of different strengths; it appears that they used the same coarse aggregate in all of their mixes so no variation in strength would have been observed due to coarse aggregate strength. It is suggested that additional dynamic indirect tension testing may be warranted considering the large variation in coarse aggregate strength.

Lastly, it should be noted that the conclusion given in Ross et al. (1996) that the rate sensitivity of PCC in tension is independent of the PCC compressive strength appears to be incorrect. This conclusion is based on the results presented in Figure 1.9 where four different concrete mixes were tested in tension. After plotting the results for these mixes, the data is curve-fitted by two equations, one for PCC with a compressive strength of 28 MPa and one for PCC at 57 MPa. As seen in Figure 1.9 the two curve-fitted equation essentially overlap. However, the CEB model, which was discussed above and will be further discussed in the following section, as well as in a paper by Malvar and Ross (1998) clearly show that the rate sensitivity of concrete in tension is in fact a function of the PCC compressive strength.

5.3.2 Uniaxial Concrete Compression Testing

The results of uniaxial concrete compression testing were presented in Figure 4.10 through 4.12 for the following concrete test specimens: six-inch diameter cylinders (required ASTM cylinders for strength testing), 30-day (fresh) three-inch diameter specimens, which were cored from freshly cast PCC blocks, and the two-inch diameter PCC cored from the six-inch concrete pavement cores and referred to as "aged" concrete in this report. The three-inch diameter fresh PCC specimens were also tested in both dry and moist (curing room) conditions, while the aged PCC specimens were only tested in dry conditions.

Overall, the static compressive strength results for the fresh PCC ranged from 40 to 50 MPa (5,800 to 7,250 psi), while the dynamic compressive strength results ranged from 50 to 75 MPa (7,250 to 10,875 psi). Consequently, all of the fresh PCC tested are rate sensitive in compression. Remarkably, the aged natural aggregate (sand and gravel) PCC had a static strength of 80 MPa (11,600 psi) and was higher then all of the dynamic compressive strength results for the fresh PCC. Moreover, its dynamic compressive strength was even significantly higher at 120 MPa (17,400 psi). The aged highway slag PCC had a static compressive strength approximately equal to the average static strength of the fresh PCC while its dynamic strength was higher than the dynamic compressive strength of the fresh PCC. The high strength of the aged natural aggregate PCC, however, was somewhat surprising given the environmental factors and vehicle loading that the concrete experienced over its history. It would be expected that these factors would have reduced the concrete strength due to micro-cracking and other possible distresses. Still, both the aged natural aggregate and slag aggregate concrete were also rate sensitive with the dynamic strength greater than their static strength.

In comparing test cylinders of different diameters the size effect must also be considered. In the case of the aged highway PCC, the specimens were cored at a two-inch diameter while the 30-day PCC specimens were cored at a three-inch diameter. According to Sender (1997), smaller diameter specimens may be stronger and stiffer than larger diameter specimens given geometrical similar specimens, i.e., the same diameter to length ratio. Sender investigated the strength difference between 37.5 mm (1.5 in.), 75 mm (3 in.) and 150 mm (6 in.) diameter concrete specimens and found that there was at most a 20% between the 37.5 mm (1.5 in.) and 150 mm (6 in.) specimens. The difference between the 1.5-inch and three inch diameter specimens, however, was significantly lower at only 4%. This suggests that the size effect is not significant in comparing the two and three inch diameter specimens in this research. The size effect in compressive strength between the three-inch and six-inch diameter specimens in this research resulted in a 6% difference for the Bruce Mines PCC, 2% for the Presque Isle PCC, 2% for the Port Inland PCC, 15% for the Levy Slag PCC and 14% for the Superior Sand & Gravel PCC. On average, the Bruce Mines, Presque Isle, and Superior Sand and Gravel PCC six-inch diameter specimens had lower strength then the three-inch diameter specimens, while Levy Slag and Port Inland PCC the reverse occurred, with the larger specimens sizes having a higher strength. However, in all cases, the values were within 15%, which is lower then the variation cited by Sender (1997) of 20%. It is unclear as to why the Levy slag and Superior Sand and Gravel PCC had a higher strength for the larger six-inch specimens than the three-inch specimens.

An important part of this research was to investigate the degree that coarse aggregate strength plays in concrete's overall static and dynamic strength. In comparing the coarse aggregate strength (both static and dynamic) to the strength of the concrete it was found that there was no statistical correlation between either the static and dynamic strength of the coarse aggregate and the static and dynamic strength of the fresh PCC (after a 30 day cure) in either dry or moist conditions. While there was some concern about the quality of the mixing operations for the Port Inland PCC, the results confirm the generally held belief that the strength of fresh PCC is not strongly dependent on coarse aggregate strength. This supports the research results presented in Section Four that indicated that the concrete mixes gave adequate strength independent of coarse aggregate type, although there was up to a 10% variation is strength with the slag PCC being somewhat higher in strength than the basalt PCC followed by the natural aggregate PCC. For the strength results in this section, however, there was no clear order to the strength increases or decreases in either the dynamic or static results or in the dry and moist conditions with respect to coarse aggregate type. Taken as a whole, the average static compressive strength of the PCC in Section Four was 48.1 MPa (6,975 psi) while in this section it was 45 MPa (6,525 psi). There were, however, larger variations in strength between the PCC specimens tested in this section than in the PCC tested in Section Four. Again, it is unclear for the increase in variation between the PPC tested in this section and Section Four, since the same mixing procedures were used.

A very consistent trend in the uniaxial compressive strength results, however, was the difference in dynamic strength between moist and dry conditions. Essentially, all of the fresh PCC specimens[6] had greater dynamic strength in moist conditions than in dry conditions. In contrast, the fresh PCC static strength had both increases and decreases between moist and dry conditions, with the difference between the two conditions relatively small. Again, this agrees well with the findings of Ross et al. (1996) where a significant difference in the dynamic strength in moist and dry conditions was also observed. Moreover, Ross et al., found that the strain rate at which concrete becomes rate sensitive, i.e., the strain rate at which the dynamic strength starts to increase over the static strength, was at a lower strain rate for moist conditions than for dry conditions. This clearly indicates that water in the concrete's pore structure plays an important function during dynamic fracture and failure. Ross et al. attributes the increase in strength from moisture to inertial effects, i.e., the more mass in a specimen the more resistance to failure. Since moisture increases the concrete's overall mass, it therefore increases the concrete's resistance to failure at higher strain rates. While this is reasonable, another significant factor that must be considered is the water's state of stress in the concrete's pore space. When concrete's saturation is less than 100% and in an unsaturated state, the free water is in tension (also referred to as suction or capillary stress). The tension stress of water places an effective tension stress on the concrete specimen that in effect pulls the concrete pores together thus increasing the concrete's overall strength. This is the same concept as in soil and rock mechanics where capillary stresses act to increase the soil or rock's overall strength. Moreover, when dynamically loaded, the pores in the concrete will slightly compress reducing further the pore volume and resulting in even higher tension stresses (capillary stress). The net effect is to increase the concrete strength. However, if the concrete (or soil) become fully saturated the capillary stress is lost along with the increased strength component. The same situation will occur in soil when it becomes 100% saturated. As the dynamic stress moves through a fully saturated soil, the soil structure will attempt to compress the pore space within the soil. But since the water will not be able to escape due to the speed of the loading as well as the low permeability of the soil, the net

[6] The moisture condition of the PCC at 30-day during testing was the moisture content of the PCC immediately after curing. It was based on the water added to the concrete during mixing plus the moisture that migrated into the concrete during the 30-day curing process. The plastic molds were removed after 24 hours and the specimens exposed to 100% humidity in the curing room for 30 days. However, the concrete would still not be at 100% saturation but at a somewhat lower saturation.

effect is to increase the pore water pressure. Increasing the pore water pressure in turn causes a decrease in the soil's effective stress resulting in a decrease in soil strength, since the pore water pressure is now positive and pushing the soil grains apart. It is speculated that this same phenomenon may occur in concrete. That is, while there is an increase in dynamic strength with moisture in unsaturated conditions, the reverse may occur at 100% saturation where a strength decrease can result. This may be very important in concrete pavement performance during the springtime of the year or when concrete pavements become saturated. However, a more useful role for the dynamic testing of concrete in moist conditions is the possibility that it may provide a better means of quantifying a concrete's pore structure such as pore size, distribution and connectivity. Essentially, a majority of a concrete's pore system is in the mortar with a smaller amount (in general) in the coarse aggregate. Therefore, by changing a concrete's air content and subsequently the size and distribution of the air voids, its response to dynamic loading in unsaturated and fully saturated conditions may be different indicating important aspects of the air-void system. In addition, since the dynamic loading tests the entire concrete specimen, it may better quantify the properties of the concrete than can be done with testing smaller parts of the concrete such as for example with thin-sections. However, additional research will have to be conducted to verify this hypothesis. If Ross's hypothesis is correct, then fully saturated concrete should have the highest dynamic strength and then decreasing with decreasing moisture content. However, if the hypothesis presented in this research is correct then the dynamic strength should increase to just near full saturation but then decrease when fully saturation is reached due to a loss of capillary stress. Again, if the hypothesis presented above is correct it may also provide significant information concerning the size, distribution and connectivity of the concrete's pore structure.

As discussed above, all of the PCC specimens tested in uniaxial compression were rate sensitive, i.e., the dynamic to static strength ratios were greater than one. The dynamic to static strength ratios (D/S) for the compressive test results varied from an average 1.4 to 1.9 at a strain rate of 25/sec and compare extremely well to the results from Ross (1989, 1995 and 1996). As noted above, moisture affects the rate sensitivity of concrete, with moisture increasing the concrete's rate sensitivity. Accordingly, Table 5.5 provides the D/S of the PCC for dry and moist conditions. Table 5.5 clearly shows the difference between dry and moist conditions with the average D/S for dry conditions 1.41 and for moist conditions 1.79. While the results for dry condition are relatively consistent, the main deviation in the moist D/S results is the Port Inland PCC. However, as noted above it is believed that there were possible problems in the preparation of this concrete. While it had adequate static strength, although somewhat low, its failure mode during static compression was also different than the other PCC tested. The primary difference in failure was that it did not exhibit a brittle failure such as in a double cone or planar failure. Instead, the PCC failed in a plastic crushing manner with very limited failure surfaces developing. The concrete is also suspect when reviewing the yield work sheets in Appendix A. While the PCC mixing procedures developed and used in Section Four resulted in very consistent concrete performance, the same procedures were also followed in preparing the PCC for concrete preparation in this section. During concrete preparation, all of the data concerning the individual components were recorded. However, the only data sheet lacking complete information was the Port Inland PCC, where the surplus water was not recorded and consequently the total water in the batch could not be determined to complete the records. Although this data was missing, the unit weight (145 pcf), percent air (4.5%) and slump (2 inches) for the Port Inland PCC were all within range of the other PCC prepared and tested. Since all of this data was within the range of the other PCC, it was believed that the PCC was acceptable for testing. However, the results from the indirect tension testing also show that the Port Inland PCC was problematic in that the dynamic strength results were lower than the static strength results. If in fact there was a problem with the preparation of the Port Inland PCC, it is interesting that the difference did not show up in the dry D/S, but only in the moist conditions D/S ratio data. As discussed in the aggregate D/S results, the D/S appears to be strongly a function of the material's microstructure. For example, the basalt and slag aggregates had similar D/S ratios suggesting a similar microstructure. Freshly prepared concrete therefore should also have a similar microstructure or pore structure if prepared in similar proportions and manner. In fact, this is seen in the relative consistency of the dry and moist D/S results. The obvious contradiction to this trend is the Port Inland PCC, which appears to have been improperly made. However, if the D/S ratio is sensitive to the microstructure of the mortar and it is assumed that the Port Inland PCC had some form of variation in its microstructure due to the improper mixing, than the moist D/S results would have provided an indication of this problem. That is, the D/S ratio would indicate a deviation in the performance of the PCC, while the unit weight, percent air and slump all indicated acceptable PCC.

Table 5.5 Ratio of dynamic to static strength tests for uniaxial compression test in dry and moist conditions.

PCC Type		Dry Dynamic/Static	Moist Dynamic/Static
Bruce Mines	(95-101)	1.50	1.86
Levy Slag	(82-019)	1.38	1.80
Port Inland	(75-005)	1.38	1.59
Presque Isle	(71-047)	1.40	1.84
Superior Sand & Gravel	(31-045)	1.40	1.79
Natural Aggregate:	Aged PCC	1.50	Not Tested
Slag Aggregate:	Aged PCC	1.73	Not Tested

In reviewing the D/S results of the aged PCC, the natural aggregate PCC had a D/S ratio of 1.50 in the range of the fresh PCC dry conditions, while the slag PCC a 1.73 ratio in the range of the fresh PCC moist conditions. It was assumed prior to testing that the aged PCC would most likely have decreased in strength due to environmental and loading factors. However, the aged natural aggregate PCC had the highest strength of any of the PCC tested. While this may be due to difference in mix design, preparation, placement and curing, the D/S ratio was still in the range of the fresh PCC again suggesting that the microstructure of the fresh PCC and aged PCC were similar. Interestingly, the slag coarse aggregate PCC has a higher D/S, which may again be the result of a different PCC mix design, PCC preparation, placement and curing. But another possibility may be that there was a difference in the microstructure between the natural aggregate and the slag aggregate PCC, resulting in a different D/S ratio between the two.

The above discussion suggests (but does not prove) that the rate sensitivity of concrete in compression, as defined by the D/S ratio, is relatively independent of the concrete's static or dynamic compressive strength and more a function of the concrete's microstructure. Ross et al., (1996) also presented data strongly showing that the D/S ratio is independent of concrete strength. This data is presented in Figure 5.10 and has also been annotated with the uniaxial compression results from this research for both dry and moist test conditions. The data presented in Figure 5.10 represents uniaxial compression results concrete at five different strengths: 16.6, 31.0, 34.5, 45.9 and 50.3 MPa and tested over a strain rate range of 10^{-6} to 300/sec. Although not clearly stated in the Ross et al. research, it is assumed that the same coarse and fine aggregates as well as cement type were used to create the different mixes with the only variation in the water-to-cement ratio. It can be observed in Figure 5.10 that regardless of the concrete's static strength, the D/S ratio appears to increase at the same rate for the different strength concrete with increasing strain rate. In addition, since the results of this research are relatively close to Ross et al. results, it suggests that the D/S is basically independent of overall concrete strength. In support of this, Ross et al. also provides the following statement:

> "In all of the strain work by the authors (Ross et al., 1989, 1995 and 1996) all data is usually normalized with respect to data obtained at low strain rate (static test) using the same kind of specimens. This results in the use of the dynamic increase factor, defined as the ratio of dynamic strength to static strength. Hopefully, by using this one may eliminate problems such as different maturates relative to each cure time and different mix strengths. Also, it is believed that the effects of scale due to specimen size and aggregate may also be minimized by the use of the dynamic increase factor."

In regards to the issue of maturity and specimen size it is interesting to note that in the results presented in Table 5.5 show that the aged natural slag PCC had approximately the same D/S ratio as the fresh PCC indicating that maturities and specimen size may not be a factor. However, it should also be noted that moisture affects the D/S of concrete, which has been shown in both the results in this research as well as in the results of Ross et al.

As discussed previously, in crystalline brittle material the rate sensitivity originates from the microstructural inhomogenieties such as pores, cracks, and impurities that exists along grain boundaries. Although these inhomogenieties only form a small fraction of the overall volume of material, it is known that the resistance to crack growth from these inhomogenieties is a function of strain rate. In regards to concrete, previous research as well as the results in this research indicates that for concrete the mortar's microstructure and its bonding characteristics with the coarse aggregate primary control the strength of concrete. Consequently, it is the formation of the mortar's microstructure, which includes the pore structure and bonding of the coarse aggregate, that controls its dynamic failure characteristics. This also helps explain, at least in part, the significant influence moisture has on the D/S ratio, since water in the pore space affects the state of stress during dynamic failure as was discussed previously. It was also shown that the D/S results were very consistent with a D/S ratio of 1.4 (±0.05) for dry conditions and 1.8 (±0.11) for moist conditions. However, the D/S ratio for the mortar uniaxial compression results presented in Figure 4.7 showed that the D/S ratio varied between 1.5 and 3 over the 18 weeks after mixing. One possible reason for the variations in the mortar D/S results may be due to the curing procedure used. After mixing, the mortar blocks were placed in the curing room and cored after one week of curing. The mortar test specimens were then placed in a plastic bag with water. In contrast, the PCC blocks while also placed in a curing room were cored throughout the 30-day curing period. After coring the PCC specimens were placed back into the curing room until they were tested at 30 days. Consequently, the mortar specimens may have had better access to water. It was suggested that the variation in D/S ratios over the 18-week period might have also been from microstructural changes due to cement hydration, which also may have been affected by the availability to water during the curing process. However, additional research will be needed to determine if in fact the D/S ratio is changing during the curing of the mortar and how this affects the D/S ratio of PCC.

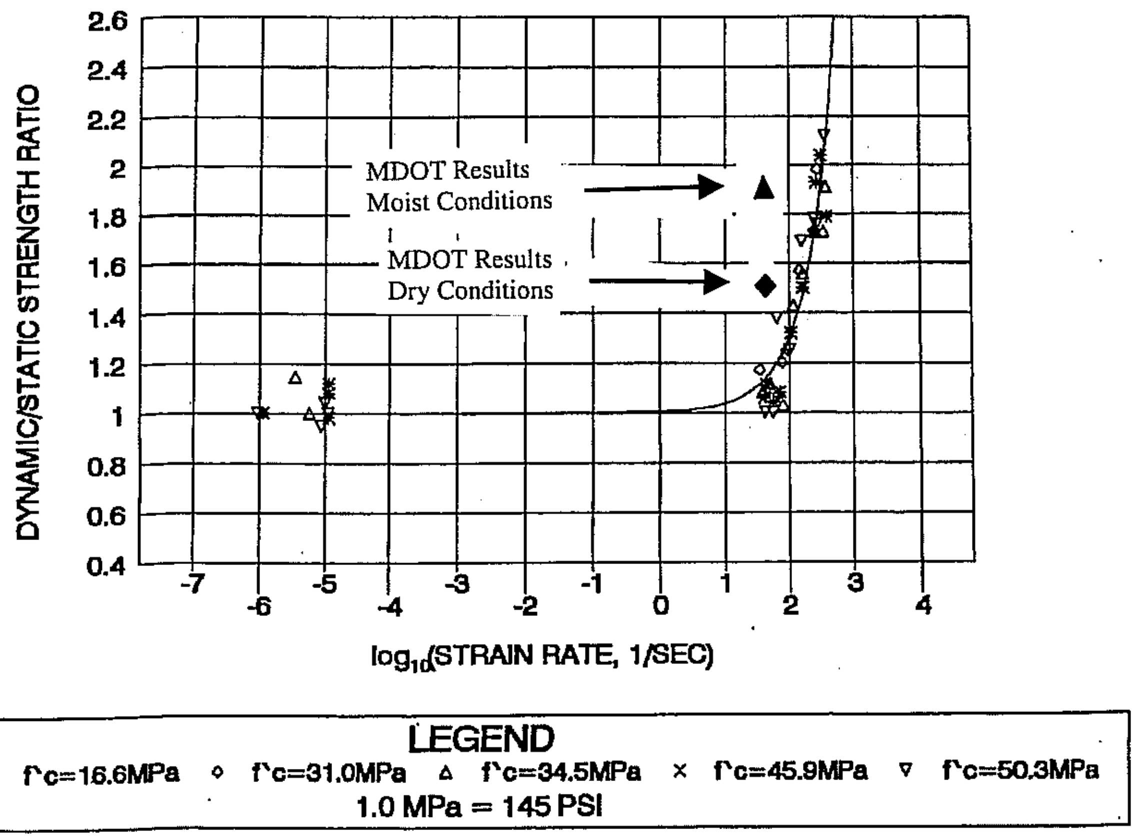

Figure 5.10 Dynamic to static compressive strength ratio for concrete compressive strength from Ross et al. (1996) and annotated with the results from this research.

Another interesting observation discussed previously is that Ross et al. (1996) states that the D/S ratio for concrete in *tension* is independent of the concrete's original static strength. However, in a later paper by Malvar and Ross (1998) it is basically shown that tension is in fact a function of the concrete's static strength. Although this point is not explicitly stated in the paper, they cite the CEB model (Comité Euro-International du Béton, 1990), which is considered the most comprehensive model for strain for the strain rate enhancement of concrete, to compare dynamic strain rate data from their research as well as others. According to the CEB model, the D/S ratio in *tension* at high strain rates is *not* independent of the static compressive strength of concrete, which was also discussed in indirect tension results. This is shown mathematically (for the CEB model) for strain rates above 30/sec as follows:

$$\frac{D}{S} = \beta\left(\frac{\dot{\varepsilon}}{\dot{\varepsilon}_s}\right)^{1/3} \qquad \textbf{5.2}$$

where:

where:	D	=	dynamic strength
	S	=	static strength
	$\text{Log}\,\beta$	=	$7.11\delta - 2.33$
	δ	=	$1/(10 + 6f'_c/f'_{co})$
	f'_c	=	Concrete static compressive strength
	f'_{co}	=	10 MPa
	ε	=	dynamic strain rate
	ε_s	=	dynamic strain rate

Equation 5.2 from the CEB model shows that the tensile D/S ratio for concrete is directly a function of concrete's static compressive strength, since the δ variable is a function of the concrete's static compressive strength. Since this data was based on experimental test results, it can be assumed that tensile D/S ratio does vary with the concrete's compressive strength. This then suggests that static and dynamic tension testing of concrete may provide more information concerning the characteristics of the concrete then compression testing does. For example, it has been pointed out by a number of researchers that compression testing is in fact a series of tensile failures as the concrete barrels and splits apart. This may also explain why there is a greater range in tension D/S ratios with respect to strain rate than for compression D/S ratios, i.e., in tension there is only generally one failure surface while in compression there are many making the failure more complex and stochastic in nature. Consequently, direct or indirect tensile testing

of concrete may better describe the overall concrete strength and possibly durability and may provide a better indication of the significance of the characteristics of the coarse aggregate in the concrete.

An estimate of the rate sensitivity parameter λ for the PCC in compression is given in Table 5.6[7]. As in the D/S ratio results, the effect of moisture can clearly be seen in these results with the moist condition at an average strain rate parameter value of 5.3 (excluding the Port Inland PCC) and the dry condition at an average value of 2.7. However, the Port Inland PCC had a similar λ value in the dry condition, as the does the other PCC specimens, but the λ value is noticeably lower in the moist condition. Again, it is in the moist test conditions that give an indication that the Port Inland PCC was different than the other concrete. It can also be seen that the dried condition λ for the aged PCC is almost double the fresh PCC results. It is also interesting to compare the strain rate parameters from Table 5.5 with the strain rate results for aggregate presented in Table 5.2. Essentially, the strain rate parameters for dry and moist condition PCC (2.3 to 5.4) are within the range of strain rate parameters for water-quenched slag aggregate while the carbonate and igneous aggregates are considerably above. However, due to the relatively consistent values in the two testing conditions, it appears that the strain rate parameter for the PCC again indicates that the mortar controls the strength of the PCC. It appears that both the D/S ratio and the strain rate parameter λ provide additional information regarding the characteristics of concrete. However, additional research will be required to better understand if and how they relate ultimately to concrete field performance.

Table 5.6 Rate sensitivity parameter λ for dry and moist conditions.

PCC Type		Dry Dynamic/Static	Moist Dynamic/Static
Bruce Mines	(95-101)	3.3	5.3
Levy Slag	(82-019)	2.8	5.2
Port Inland	(75-005)	2.3	3.6
Presque Isle	(71-047)	2.4	5.4
Superior Sand & Gravel	(31-045)	2.7	5.1
Natural Aggregate:	Aged PCC	6.2	Not Tested
Slag Aggregate:	Aged PCC	5.1	Not Tested

[7] Strain gages were not placed on the PCC specimens to measure exact strain rates. Instead, the strain rates were based on the strain readings measured from the strain gages placed on the bars of the Split Hopkinson Pressure Bar.

6 Conclusions and Recommendations for Future Research

The research focus in this section was to investigate the static and dynamic strength of coarse aggregate, mortar and concrete with a primary emphasis on the relationship between coarse aggregate strength and concrete performance. In particular, the research was focused on the development of an improved aggregate classification system that would relate the properties of coarse aggregate with concrete performance. The conclusions reached in this research are presented in the following sections followed by recommendations for future research.

6.1 Strength Conclusions

6.1.1 Aggregates

1) The static uniaxial compression test results for the igneous and carbonates had excellent agreement with the commonly used Deere & Miller rock strength classification system, verifying the static uniaxial compression testing procedures used in this research.

2) The mafic igneous aggregates had the highest uniaxial compressive strength under static loading conditions and are rated as "high strength" (Category A) according to the Deere and Miller Rock Classification System. The carbonate aggregates had average strength and are rated as "medium strength" (Category C), although three of the dolomites carbonates are in the next higher category "high strength" (Category B). The blast furnaces slag had the lowest strength of all the aggregate tested and are rated as "very low strength" (Category E). However, the dense portion of the air-cooled slag (specimen 1.2) had significantly higher strength and is rated as "medium strength" (Category C). This strength was just below the "high strength" boundary and was close to the strength of dolomites.

3) The dynamic strength for most of the aggregates increased by one strength category on the Deere & Miller Rock Strength Classification System over the aggregate's static strength. Since the static strength of the Bruce Mines aggregate was already in the "high

strength category," an additional strength category needed to be added to the Deer & Miller classification system. This was accomplished by creating the next higher strength category following the geometric progression used to generate the existing categories. The new category is termed "super high strength" (Category A') and is the category where the dynamic strength of the Bruce Mine aggregate (95-010) lies. The static strengths of the limestones are "medium strength," while the dynamic strength of the Presque Isle (71-047) and Bay County (06-008) limestones are rated as "high strength." However, the Port Inland aggregate (75-005) increased two categories to the "very high strength" category. The static strength of the Cedarville (49-065) and Denniston (58-009) dolomites are "medium strength" while their dynamic strengths increased to "high strength". However, both the static and dynamic strength of the Rockwood (58-008) and France Stone (93-003) dolomite are in the same category "high strength."

4) Both the Algoma (95-006) and Levy (82-019) water-quenched slag had the lowest aggregate strength tested and is rated as "Very Low Strength." The Algoma air-cooled slag is also rated as "Very Low Strength." However, the dense portion of the Algoma air-cooled slag (specimen 1.2) is significantly stronger and is two strength categories higher at "Medium Strength" and is approximately equivalent to the carbonate strength. It was also observed that even at very low bulk density of 2.09 g/cm^3 the porous air-cooled slag had strength equal to the water-quenched slag, which had a significantly higher bulk density of 2.40 g/cm^3. It is speculated that the early crushing of the water-quenched slag may result in a more rapid cooling of the slag reducing the mechanical properties of the slag.

5) While the static dry strength of the dolomite aggregates are higher than the limestone aggregate, the opposite occurs for the dynamic strength with the limestone having a higher strength than dolomites.

6) There is a very good correlation with dynamic strength and bulk density for the limestone aggregate and similarly for the dolomites with the exception of the Cedarville dolomite. It appears that the random and non-uniform grain size distribution of the Cedarville

dolomite, which is believed due to the secondary replacement nature of dolomite, may account for this discrepancy.

7) Rate sensitivity is defined as the increase in dynamic strength of a material over its static strength. All of the aggregate types tested are rate sensitive, although the amount of increase varied between aggregate types. The dynamic to static strengths ratios (D/S) ranged between 1.33 and 2.68 for all of the aggregates tested. There was a noticeable increase in the average D/S value between saturated and dry conditions for the blast furnace slag and the mafic igneous aggregate with an average of 1.86 and 2.62 respectively. However, there was no noticeable difference in the carbonate aggregates between saturated and dry conditions. There was, though, a significant difference in the D/S between limestones and dolomites at 2.27 and 1.74, respectively. This represents a 40% difference in the total range in the D/S of the aggregates tested.

8) A strain rate sensitivity parameter λ was defined, which takes into account the difference in static and dynamic strength and normalizes it to the difference in strain rate between the static and dynamic loading rates. The low strength slag aggregates have the lowest rate sensitivity, ranging from 1.17 to 3.00 for the water quenched slag and 9.29 for the dense air-cooled slag (specimen 1.2) for an overall average of 4.2. The carbonates have the intermediate values ranging from 4.52 to 25.52, with an average of 11.9. The high strength igneous aggregates have the highest rate sensitivity, ranging from 26.90 to 31.30, with an average of 29.1. Based on the rate sensitivity parameter, the trend in highest to lowest rate sensitivity was as follows: diabase > basalt > limestone > dolomite > slag. Clearly there was significant differentiation between aggregate types and even within aggregate types to be used as a potential classification system.

9) The first correlation investigated was between the rate sensitivity parameter λ and bulk density. There is a general increase in the strain rate parameter λ and bulk density for all the aggregates tested, with the exception of the slag specimens, having a correlation coefficient of 0.61. Grouping the limestone aggregates increased the correlation coefficient to 0.74 but decreased the correlation coefficient for dolomite to 0.42. By

excluding the higher density slag specimen (1.2) it appears that there is no increase in rate sensitivity with increasing bulk density for the slag aggregates.

10) There was a significant difference in the average strain rate sensitivity parameter λ between the dense air-cool slag (specimen 1.2) at 9.8 and the remaining slag at 2.4, which is over a four-fold difference. The rate sensitivity of the air-cooled slag was even higher than the average rate sensitivity of the dolomite aggregates at 8.6.

11) The results of the dynamic testing as represented by the D/S and rate sensitivity parameter λ results, indicated a significant difference between limestones and dolomites. In general, dolomites were stronger in static strength than limestones. However, the situation is reversed with the limestones having a higher dynamic strength than the dolomites. In addition, the limestone had a D/S of 2.30 and the dolomites had a D/S of 1.64 while the average rate sensitivity parameter λ for limestone was 16.4 and 8.6 for dolomite. Inspecting the microstructure of the carbonates indicates that for the limestone the rate sensitivity increases (both in D/S and λ) for decreasing grain size while the opposite occurred for the dolomite where the D/S and λ decreased with decreasing grain size. It is hypothesized that the formational history of the limestone and dolomite may explain this observation. Basically, limestone forms as a primary rock while dolomite forms by chemically altering the structure of the limestone. This includes recrystallizing and replacing calcium with heavier magnesium and iron ions. It is speculated that this replacement results in a weakening of the grain boundaries of the dolomite and thus results in lower dynamic strength. However, it also likely that the higher *static* strength of the dolomites versus the limestones may results from a healing of some of the larger defects due to the replacement process. The larger defects such as bedding planes and fractures generally control the static strength of an aggregate. It was also noted that the D/S ratios for the igneous and slag aggregates were approximately equal indicating similar microstructures but had significantly different strain rate parameter values (4.2 versus 29.1) indicating that the grain boundary strength was significantly different between the igneous and slag aggregate. It was again speculated that the D/S ratio might provide an indication of microstructure type while the rate sensitivity parameter strength.

12) The rate sensitivity parameter λ was compared to the freeze/thaw susceptibility dilation and durability index values for all the aggregates tested. While there was considerable scatter in the data, the aggregates could be separated into two groups; those with rate sensitivity parameters greater than 25 and those less than 15. In addition, when correlating the carbonate aggregates with rate sensitivity parameters less than 15 and excluding the Bay County limestone, which is believed to have erratic values, there was an excellent agreement between rate sensitivity and the frost susceptibility index values dilation and durability with a linear correlation coefficient of 0.98.

13) There was a general linear inverse relationship between the LA abrasion index values and the static and dynamic compressive strength results. However, the dynamic strength results had a somewhat better correlation with a linear correlation coefficient of 0.77 versus 0.66 for the static strength results. In addition, the slope of the dynamic strength versus LA abrasion results was steeper providing a broader separation of dynamic strength and LA abrasion data.

14) There was also a linear inverse relationship between the strain rate sensitivity parameter and LA abrasion data, with a linear correlation coefficient of 0.74. However, this relationship does not necessarily hold for the carbonate aggregate, which already excludes the Port Inland limestone due to its high rate sensitivity value greater than 25. For the carbonates, it appears that the relationship is reversed with the LA abrasion values increasing with increasing rate sensitivity, which does not appear to be realistic.

6.1.2 Mortar Strength

1) The mortar was found to be rate sensitive with the dynamic to static strength ratio (D/S) ratio range between 1.5 and 3.5 over the 18-week testing period.

2) Both the static and dynamic strength of mortar varied over an 18-week period with both increases and decreases over the 18-week period. Interestingly, a high strength period

where the D/S was approximately 3 occurred at the 28-day testing period followed by a decrease to a D/S of 1.5 in week nine.

3) The D/S changes may indicate that the development of the mortar microstructure during the curing process may not be constant. However, it is possible that testing procedures may have also played a role in the increase and decrease in strength over the 18-week period, although the testing procedure attempted to minimize possible variations by pre-coring and mixing the test specimens prior to testing.

6.1.3 Concrete Strength

6.1.3.1 Indirect Tension Test Results

1) The PCC was found to be only slightly rate sensitive in tension. The dynamic to static strength ratio (D/S) ranged between 1 and 1.3. In addition, there was no statistical correlation between PCC strength and coarse aggregate type in either the static or dynamic indirect tension testing.

2) The results of the indirect tension did not correlate with the results of Ross et al., (1989) who found a 6 to 8 D/S ratio. However, similar research in Europe where a model known as the CEB model predicted that the rate sensitivity of the concrete tested in this research should have a D/S ratio of approximately 2.2, significantly closer to the results in this research.

3) It is believed, however, that the results of the indirect tension testing may not have been properly conducted although the reasons for this remain unclear since the same procedures that were used in this research were based on the research of Ross et al. (1989). It is suspected that one reason for the lower results may be attributed to not having proper alignment of the specimen in the split Hopkinson pressure bar device.

6.1.3.2 Uniaxial Compression Test Results

1) All of the 30-day cured PCC tested in uniaxial compression were rate sensitive. In general the PCC had an average static compressive strength of 45 MPa, while the dynamic compressive strength was approximately 67 MPa. The Dynamic to Static strength ratio (D/S) ranged between 1.4 and 1.9, which agrees extremely well with the results from Ross et al. (1989, 1995, and 1996).

2) The aged concrete was also found to be rate sensitive. Interestingly, the natural aggregate PCC had a static compressive strength at 80 MPa, which was higher than any of the 30-day cured PCC tested, while its dynamic strength was significantly higher at 120 MPa. On the other hand, the aged slag coarse aggregate PCC had a static compressive strength of 45 MPa, which was also close to the average strength of the 30-day cured PCC, while its dynamic strength was 78 MPa, which was approximately the same strength as the static strength of the aged PCC but higher than the dynamic strength of the 30-day cured PCC. The excellent strength of the aged PCC, especially the natural aggregate PCC, was surprising since it had been obtained from existing pavement and had been exposed to both loading and environmental stresses.

3) There was generally good agreement between the six-inch specimens and the three-inch specimens tested in static loading conditions with a 6% difference for the Bruce Mines PCC, 2% for the Presque Isle PCC, and 2% for the Port Inland PCC. However, the Levy slag and Superior Sand & Gravel PCC had a 15% and 14% difference respectively.

4) There was no statistical correlation found between either the static and dynamic strength of the coarse aggregate in the PCC and the static or dynamic strength of the concrete.

5) The dynamic strength of the concrete increased with moisture, which agrees with the research by Ross et al. The increase in dynamic strength was attributed to inertial effects where an increase in moisture increases the mass of the concrete and therefore increases its resistance to failure. However, it was also noted that the moisture's state of stress must also

be considered since in unsaturated concrete the moisture is in a state of tension, which increases the overall strength of a material. Dynamic loading would cause a volume decrease, which would further increase the tension stress in the concrete. It was speculated that a fully saturated concrete would act in the opposite manner, i.e., a decease in pore volume due to dynamic loading would decrease the strength of the concrete by increasing the pore's fluid pressure.

6) The dynamic to static strength ratio (D/S) for the fresh PCC was very consistent for the dry PCC at an average ratio of 1.41 while the moist conditions were at 1.79, excluding the Port Inland PCC, which is believed to have been mixed improperly. While the D/S ratio for dry Port Inland PCC was consistent with the other PCC tested, its moist D/S was 1.59, below the other moist D/S values. Since a material's rate sensitivity, as defined by the D/S ratio, has been found to originate from microstructural inhomogenieties such as pores, cracks and impurities that exist along the grain boundaries, the PCC D/S ratio results are a function of the concrete's microstructure. In addition, it has been shown that the presence of water in the pore space (Conclusion 5) also affects the rate sensitivity of concrete. Consequently, the D/S values for concrete are an indication or a possible quantification of the concrete's microstructure. The combined D/S results for aggregate, mortar and concrete *suggests* (but does not prove) that D/S value is primarily influenced by the microstructure of the mortar followed by the microstructure of the mortar-coarse aggregate bond and lastly by the structural characteristics of the coarse aggregate.

7) The compression testing of concrete indicates that the rate sensitivity (as defined as the D/S ratio) is relatively independent of the concrete's static or dynamic compressive strength. However, indirect tension testing of concrete clearly shows that the concrete's rate sensitivity *is* a function of the concrete's strength, which is more consistent with a stronger mortar and therefore a change in the mortar's microstructure. That is, if the concrete has a higher compressive strength than the mortar strength and consequently its microstructure characteristics must also be stronger, which should result in a different rate sensitivity value, e.g., D/S ratio. This conclusion suggests that indirect tension testing may provide a better estimate of a concrete's performance than the traditional uniaxial compression testing. In

addition, since a single fracture surface generally develops in tension failure, it may also provide a better indication of the significance of mortar-coarse aggregate bond as well as the coarse aggregate strength in concrete.

8) The results of the rate sensitivity parameter λ for concrete were similar to the D/S ratio results in that it shows a significant change in value between the dry and saturated conditions. In addition, it also indicated that there was a problem with the Port Inland PCC, which had a significantly lower λ value than the other PCC tested. However, a significant difference between the D/S ratio and the λ values was between the fresh (30-day cured) and the aged concrete in dry conditions. The average λ value for aged concrete was 5.6 and 2.7 for the fresh concrete, which was over a two-fold difference. This suggest that the λ is sensitive to the concrete's maturity while the D/S ratio appears to be more a function of the concrete's microstructure. However, it is unclear at this point the relationship between the D/S ratio and the λ and why the λ is sensitive to the maturity of a concrete, while the D/S ratio is not. It appears, though, that both the D/S ratio and λ may provide significant information to better predict the performance of concrete. However, additional research will be required to better understand this relationship.

6.2 Recommendation for Future Research

The primary objective of this research was essentially two-fold. The first objective was to develop a coarse aggregate classification system while the second objective was to relate this classification system to the performance of concrete. The first objective was met with the development of the strain rate parameter λ. This parameter, which is function of the static and dynamic strength of the aggregate, provides a very broad range for differentiating aggregates. However, the research also showed that there is no statistical relationship between the strength of the aggregate and the strength of concrete, although it appears that the surface characteristics between the coarse aggregate do influence the compressive strength of the concrete to some degree. In effect, the compressive strength of concrete, as is generally assumed, is primarily a function of the mortar. The second objective was not completely successful. However, the research did show very interesting results for the rate sensitivity of concrete and in particular its' relationship to the microstructure of the mortar, as seen in the dynamic response between saturated and unsaturated conditions. In addition, the research indicates that the strain rate parameter λ for the coarse aggregate may provide performance information in regards to issues such as freeze-thaw and long-term durability. To investigate these issues the following three research areas are suggested: (1) continued investigation on the strain rate parameter λ and dynamic to static (D/S) strength ratios, (2) investigation into the microstructural characteristics of mortar using the strain rate parameter λ and dynamic to static (D/S) strength ratios, and (3) investigation of tensile testing versus compression testing as a performance test for concrete. The specific recommendations for each area are provided below.

6.2.1 Aggregate Research Recommendations

a) The strain rate parameter λ provided a means to better differentiate coarse aggregates. This was particularly important for the carbonate aggregates, where a very wide range of values were obtained with some carbonates close in value to slag and one Port Inland in the range of igneous aggregate. However, this broad range was not observed in the traditional static compression test. In addition, the dynamic to static ratios (D/S) values clearly indicated the difference in formation of the limestones and dolomites and in turn the difference in microstructure, which can relate to durability issues in concrete, e.g., freeze-thaw durability. Consequently, it is recommended a broader range of carbonate aggregates be investigated to form a larger database for carbonate, which can then be related to concrete performance tests.

b) The research results also indicated that blast furnace slags have very low strain rate parameter values. While the research shows that this low strain rate parameter values do not affect concrete's uniaxial compressive strength, the strength of the aggregate may be important in functions such as aggregate interlock. The research indicated, however, the process by which the slag forms (air-cooled versus water-quenched) may dramatically affects its overall strength. Essentially, the air-cooled slag showed greater crystallinity then the water-quenched slag with its low-density portion having equal strength with the water-quenched slag while its dense portion had strength compatible with carbonates.

To improve the strength characteristics of slag it is recommended that research be conducted into the mechanism by which the air-cooled dense portion of the slag gained its strength. Knowing the limits of this strengthening process may provide information by which slag may still be processed by water quenching and crushing, but by altering the process to some degree may provide a stronger slag product.

6.2.2 Concrete Research Recommendations

a) As discussed in this chapter dynamic testing is used to study the fracture characteristics of brittle materials. This research has shown that in crystalline brittle solids, such as ceramics, the rate sensitivity has been found to originate due to the microstructural inhomogenieties such as pores, cracks and impurities that exist along the grain boundaries. In effect, dynamic testing provides a method to study the microstructural characteristics of these materials. The results of this research suggest that dynamic testing can also be used to study the microstructural characteristics of concrete. Both the rate parameters λ and dynamic to static ratio (D/S) indicated significant properties of concrete independent of the traditional testing methods. For example, the D/S results suggest that the D/S ratio is independent of concrete strength but a function of the microstructural framework or type, while the strain rate parameter appears to provide the strength of the microstructure of the mortar and secondarily to the mortar-coarse aggregate interface bond. In addition, both parameters are affected by the presence of water in the pore space. This may be a very important finding and one that could lead to a relatively straightforward test method in quantifying differing pore size and distribution within the mortar. It is also suggested that this may lead to a more definitive tests for the long-term durability of concrete in both strength and in freeze-thaw conditions. Based upon these findings the following research projects are suggested:

(i) Conduct static and dynamic tests on representative samples of concrete prepared by MDOT over a period of six months to obtain a database of strain rate parameter λ values and dynamic to static strength ratios. In addition, the coarse aggregate used in the PCC should also be tested for λ and D/S values as suggested in the recommendation on aggregates and compared to the results of the concrete testing.

(ii) Concrete that shows variation in λ or the D/S values should be investigated for microstructural characteristics using scanning electron microscopic techniques to determine the primary reason for the variation and to validate the dynamic testing results.

(iii) Concrete specimen subjected to freeze-thaw testing should be tested dynamically to determine whether there are changes in the λ or D/S values before and after freeze-thaw testing. This may indicate whether the freeze/thaw process affected the microstructure of the mortar and subsequently may be used as a test criteria for the effects of freeze/thaw on PCC.

(iv) The research suggested that there should be significant variations between partially saturated concrete, i.e., 28-day concrete, and fully saturated concrete. It is recommended that a series of tests be conducted on concrete consisting of three different coarse aggregate types, basalt, carbonate and a blast furnace slag. The saturated specimens can be saturated using standard pressure saturation techniques used to saturate low permeability soils. The primary emphasis of the saturation is to fully saturate the mortar. The significance of this testing may provide a means to differentiate the connectivity and pore size distribution of the mortar, which may provide a better estimate of a concrete's durability such as in its susceptibility to freeze-thaw conditions.

6.2.3 Compression, indirect tension and direct shear testing of concrete research recommendations

While the dynamic and static compression tests were successful, it was questioned whether the indirect tension tests were valid. Research by Ross et al and others indicate that indirect tension testing may be important in the analysis of concrete. The following recommendations are provided concerning this testing:

a) The indirect tension testing procedure used in this research should be improved and addition indirect tests conducted to provide a better estimate of the rate sensitivity of the

PCC tested in this research in tension. The research by Ross et al. (1985, 1995 and 1996), indicates that the rate sensitivity of concrete as described by the D/S ratio is independent of the concrete's compressive strength. However, research by Malvar and Ross (1998) and the European researchers show that the rate sensitivity of concrete (D/S) in *tension* is a function of the concrete's compressive strength. This dependency suggests that indirect tension testing of concrete may be more sensitive to variations in concrete composition and structure than is compression testing. It has been noted that compression failure is a combination of multiple tensile fractures as the specimen splits apart.

b) However, for higher strength concrete shear failure is also important. Consequently, direct shear tests should also be conducted on the concrete. While direct shear testing of concrete has not been established as a standard test for concrete, it is believed this testing may provide a more definitive test regarding the role of coarse aggregate in concrete. In addition, defining the dynamic rate sensitivity of concrete in direct shear may also be an important parameter in the analysis of aggregate interlock.

APPENDIX A

Concrete and Mortar Mix Sheets

BATCH COMPUTATIONS WORKSHEET — WEIGHT IN kg

Coarse Aggregate

Coarse Agg (a)

Pail tare			+ pails
			= total
25.0 - 19.0mm	0.00	0.00	
19.0 - 12.5mm	0.00	0.00	
12.5 - 9.5mm	0.00	0.00	
9.5 - 4.75mm	0.00	0.00	
Sub total			Total

BATCH NO. Motar1

COARSE AGG None

DATE: 6/8/99

Batch Made Tuesday @ 3:00

Fine Aggregate

23.71 Fine Agg (b)

Moisture content

wet	dry
173.3	165.7

0.0459 MC

0.0459 moisture content — 1.09 Moisture

Dry weight 23.71
\+
Moisture 1.09
Total 24.80

WATER MEASUREMENT

Coarse Agg +pail ____
Coarse Agg +pail ____

Total ____

\+ Total Design Water 0.00 (d) 0.00
\- Reserve Water 4.00 — 4.00
= Pails, Agg&Water — H_2O 0.00

RESERVE WATER

Res water	4.00	0.29 surplus & Tare
+ Tare	0.29	0.29 - tare
= Total	4.29	0.00 = surplus

Reserve Water 4.00
\- Surplus Water 0.00
= 4.00 — H_2O + 0.00

Subtotal of water in batch = 4.00
\+ Moisture in Fine Aggregate + 1.09
Total Water in Batch (D) = 5.09

Cement

10.20 Cement (C)

Pail ID L'

Tare weight 0.85 — 1.68 tare

Tare weight 0.83 — 11.88 Pail + cement

Total tare 1.68

UNIT WEIGHT

Weight of Concrete & Bucket ____
\- Weight of Bucket 8.14
= Weight of Concrete in Bucket ____ (f)

Air Entraining Admixture

10 ml

Batch Summary

(a)	Coarse Aggregate as Designed	0.00 kg
(b)	Fine Aggregate as Designed	23.71 kg
(c)	Cement as Designed	10.20 kg
(D)	Total Water of Batch	5.09 kg
(e)	**Total Weight of Batch**	**39.00 kg**

SLUMP = ____ " ____ mm

AIR CONTENT

AIR CONTENT ____
\- Factor of Aggregate Porosity ____
= Percent Air 9

CONCRETE TEMPERATURE, C 21

Note: a,b,c,d come from mix proportions worksheet

BATCH COMPUTATIONS WORKSHEET — **WEIGHT IN kg**

Coarse Aggregate — Coarse Agg (a)

Pail tare			+ pails
			= total
25.0 - 19.0mm	0.00	0.00	
19.0 - 12.5mm	0.00	0.00	
12.5 - 9.5mm	0.00	0.00	
9.5 - 4.75mm	0.00	0.00	
Sub total			Total

Fine Aggregate — 23.71 Fine Agg (b)

Moisture content

wet	dry		
173.3	165.7	0.0459	MC
0.0459	moisture content	1.09	Moisture

Dry weight 23.71
\+
Moisture 1.09
Total 24.80

Cement — 10.20 Cement (C)

Pail ID	L', H'		
Tare weight	0.85	1.68	tare
Tare weight	0.83	11.88	Pail + cement
Total tare	1.68		

Air Entraining Admixture 11 ml

Batch Summary

(a)	Coarse Aggregate as Designed	0.00	kg
(b)	Fine Aggregate as Designed	23.71	kg
(c)	Cement as Designed	10.20	kg
(D)	Total Water of Batch	5.09	kg
(e)	**Total Weight of Batch**	**39.00**	kg

BATCH NO. Motar 2

COARSE AGG None

DATE: 6/8/99

Batch Made Tuesday @ 5:30

WATER MEASUREMENT

Coarse Agg +pail			
Coarse Agg +pail			
Total			
+ Total Design Water		(d)	
- Reserve Water	4.00		4.00
= Pails, Agg&Water		H_2O	0.00

RESERVE WATER

Res water	4.00	0.29	surplus & Tare
+ Tare	0.29	0.29	- tare
= Total	4.29	0.00	= surplus

Reserve Water	4.00		
- Surplus Water	0.00		
=	4.00	H_2O +	0.00
Subtotal of water in batch		=	4.00
+ Moisture in Fine Aggregate		+	1.09
Total Water in Batch		**(D) =**	**5.09**

UNIT WEIGHT

Weight of Concrete & Bucket		
- Weight of Bucket	8.14	
= Weight of Concrete in Bucket		(f)

SLUMP = " mm

AIR CONTENT

- Factor of Aggregate Porosity	
= Percent Air	9.8

CONCRETE TEMPERATURE, C 21

Note: a,b,c,d come from mix proportions worksheet

YIELD DATA

Coarse Aggregate:	Source Number:	Specification:
Bruce Mines	95-10	6AA
Presque Isle	71-47	6AA
Port Inland	75-5	6AA
Superior Sand & Gravel	31-45	6AA
Levy Slag	82-19	6AA

	Formulae for Computation	Batch Identification					Yield Data					Units
		BM	Pr.Is.	Po.In.	SSG	LS	BM	Pr.Is.	Po.In.	SSG	LS	
g	Unit Weight of Concrete f / Volume of unit weight bucket	33.65 / 0.01377	32.00 / 0.01377	32.35 / 0.01377	32.39 / 0.01377	31.07 / 0.01377	2443.7	2323.9	2349.3	2352.2	2256.4	kg/m^3
h	Batch Volume of Concrete e / g	187.00 / 2443.7	178.77 / 2323.9	#VALUE! / 2349.3	185.11 / 2352.2	172.05 / 2256.4	0.07652	0.07693	-	0.07870	0.07625	m^3 batch
i	Cement used for one m^3 of concrete C / h	26.12 / 0.07652	26.12 / 0.07693	26.12 / -	26.12 / 0.07870	26.12 / 0.07625	341.4	339.6	-	331.9	342.6	kg/m^3
j	Net water used for one m^3 of concrete D / h - Absorbed Water (W)	12.56 / 0.07652 minus 13.23	13.77 / 0.07693 minus 22.39	#VALUE! / - minus 14.67	13.71 / 0.07870 minus 23.59	15.23 / 0.07625 minus 40.15	150.91	156.59	-	150.67	159.63	kg/m^3
k	Water / Cement Ratio j / i	150.91 / 341.38	156.59 / 339.58	- / -	150.67 / 331.94	159.63 / 342.59	0.44	0.46	-	0.45	0.47	w/c

Note: C,D,e,f,W come from batch computations worksheet

BATCH COMPUTATIONS WORKSHEET

WEIGHT IN kg

Coarse Aggregate

		84.53	Coarse Agg (a)
Pail tare	1.75	1.75	3.50 + pails
		88.03 = total	
25.0 - 19.0mm	21.13	0.00	
19.0 - 12.5mm	0.00	21.14	
12.5 - 9.5mm	0.00	21.13	
9.5 - 4.75mm	21.13	0.00	
Sub total	44.01	44.02	88.03 Total

BATCH NO. BM

COARSE AGG CA-B (Bruce M.)

DATE: 12/2/99

Batch Made Thurs @ 4:30

Fine Aggregate

63.79 Fine Agg (b)

Moisture content

wet	dry
128.69	125.83
0.0227	MC

0.0227 MC

1.45 Moisture

Dry weight 63.79

\+

Moisture 1.45

Total 65.24

WATER MEASUREMENT

Coarse Agg +pail 44.01

Coarse Agg +pail 44.02

Total	88.03		
+ Total Batch Water	12.32	(d)	12.32
- Reserve Water	3.00		3.00
= Pails, Agg&Water	97.35	H_2O	9.32

RESERVE WATER

-1.012449

Res water	3.00	1.50	surplus & Tare
+ Tare	0.29	0.29	- tare
= Total	3.29	1.21	= surplus

Reserve Water	3.00		
- Surplus Water	1.21		
=	1.79	H_2O +	9.32
Subtotal of water in batch		=	11.11
+ Moisture in Fine Aggregate		+	1.45
Total Water in Batch		**(D) =**	**12.56**

Cement

26.12 Cement (C)

Pail ID A', B'

Tare weight 0.85

1.70 tare

Tare weight 0.85

27.82 Pail + cement

Total tare 1.70

UNIT WEIGHT

Weight of Concrete & Bucket	41.80	
- Weight of Bucket	8.15	
= Weight of Concrete in Bucket	33.65	(f)

Air Entraining Admixture

29 ml

Batch Summary

(a)	Coarse Aggregate as Designed	84.53 kg
(b)	Fine Aggregate as Designed	63.79 kg
(c)	Cement as Designed	26.12 kg
(D)	Total Water of Batch	12.56 kg
(e)	**Total Weight of Batch**	**187.00 kg**

SLUMP = 1.75 " 44.5 mm

AIR CONTENT

- Factor of Aggregate Porosity

= Percent Air 4.5

CONCRETE TEMPERATURE, C 20

Note: a,b,C,d come from mix proportions worksheet

BATCH COMPUTATIONS WORKSHEET

WEIGHT IN kg

BATCH NO. Pr.Is.

COARSE AGG CA-I (Pres. Isle)

DATE: 12/6/99

Batch Made Mon. @ 11:30

Coarse Aggregate

77.35 Coarse Agg (a)

Pail tare	1.75	1.75	3.50 + pails
			80.85 = total
25.0 - 19.0mm	19.34	0.00	
19.0 - 12.5mm	0.00	19.33	
12.5 - 9.5mm	0.00	19.34	
9.5 - 4.75mm	19.34	0.00	
Sub total	40.43	40.42	80.85 Total

Fine Aggregate

61.52 Fine Agg (b)

Moisture content

wet	dry
89.44	86.95
0.0286	MC

0.0286 MC

1.76 Moisture

Dry weight 61.52

\+

Moisture 1.76

Total 63.29

Cement

26.12 Cement (C)

Pail ID A', B'

Tare weight 0.85

Tare weight 0.85

Total tare 1.70

1.70 tare

27.82 Pail + cement

Air Entraining Admixture

20 ml

Batch Summary

(a)	Coarse Aggregate as Designed	77.35 kg
(b)	Fine Aggregate as Designed	61.52 kg
(c)	Cement as Designed	26.12 kg
(D)	Total Water of Batch	13.77 kg
(e)	**Total Weight of Batch**	**178.77** kg

WATER MEASUREMENT

Coarse Agg +pail	40.43		
Coarse Agg +pail	40.42		
Total	80.85		
+ Total Batch Water	12.87	(d)	12.87
- Reserve Water	3.00		3.00
= Pails, Agg&Water	90.72	H_20	9.87

RESERVE WATER

Res water	3.00	1.15 surplus & Tare
+ Tare	0.29	0.29 - tare
= Total	3.29	0.86 = surplus

Reserve Water	3.00		
- Surplus Water	0.86		
=	2.14	H_2O +	9.87
Subtotal of water in batch		=	12.01
+ Moisture in Fine Aggregate		+	1.76
Total Water in Batch		**(D) =**	**13.77**

UNIT WEIGHT

Weight of Concrete & Bucket	40.15	
- Weight of Bucket	8.15	
= Weight of Concrete in Bucket	32.00	(f)

SLUMP = 2.5 " 63.5 mm

AIR CONTENT

- Factor of Aggregate Porosity

= Percent Air 4.25

CONCRETE TEMPERATURE, C 19

Note: a,b,C,d come from mix proportions worksheet

BATCH COMPUTATIONS WORKSHEET

WEIGHT IN kg

Coarse Aggregate

83.67 Coarse Agg (a)

Pail tare	1.75	1.75	3.50 + pails
			87.17 = total
25.0 - 19.0mm	20.92	0.00	
19.0 - 12.5mm	0.00	20.91	
12.5 - 9.5mm	0.00	20.92	
9.5 - 4.75mm	20.92	0.00	
Sub total	43.59	43.58	87.17 Total

Fine Aggregate

59.26 Fine Agg (b)

Moisture content

wet	dry
126.47	122.71
0.0306	MC

0.0306 MC

1.82 Moisture

Dry weight 59.26

\+

Moisture 1.82

9.16

Total **61.08**

Cement

26.12 Cement (C)

Pail ID A' , B'

Tare weight 0.85

1.70 tare

Tare weight 0.85

27.82 Pail + cement

Total tare 1.70

Air Entraining Admixture

25 ml

Batch Summary

(a)	Coarse Aggregate as Designed	83.67 kg
(b)	Fine Aggregate as Designed	59.26 kg
(c)	Cement as Designed	26.12 kg
(D)	Total Water of Batch	#VALUE! kg
(e)	**Total Weight of Batch**	###### kg

BATCH NO.	Po.In.
COARSE AGG	CA-P (Port In.)
DATE:	12/8/99
Batch Made	Wed. @ 11:30

WATER MEASUREMENT

Coarse Agg +pail	43.59		
Coarse Agg +pail	43.58		
Total	87.17		
+ Total Batch Water	12.16	(d)	12.16
- Reserve Water	3.00		3.00
= Pails, Agg&Water	96.33	H_2O	9.16

RESERVE WATER

Res water	3.00	-	surplus & Tare
+ Tare	0.29	0.29	- tare
= Total	3.29	#VALUE!	= surplus

Reserve Water	3.00		
- Surplus Water	#VALUE!		
=	#VALUE!	H_2O +	9.16
Subtotal of water in batch		=	######
+ Moisture in Fine Aggregate		+	1.82
Total Water in Batch		**(D) =**	**#####**

UNIT WEIGHT

Weight of Concrete & Bucket	40.50	
- Weight of Bucket	8.15	
= Weight of Concrete in Bucket	32.35	(f)

SLUMP = 2 " 50.8 mm

AIR CONTENT

- Factor of Aggregate Porosity
= Percent Air 4.5

CONCRETE TEMPERATURE, C 18

Note: a,b,C,d come from mix proportions worksheet

BATCH COMPUTATIONS WORKSHEET

WEIGHT IN kg

Coarse Aggregate

87.34 Coarse Agg (a)

Pail tare	1.71	1.73	3.44 + pails
			90.78 = total
25.0 - 19.0mm	21.84	0.00	
19.0 - 12.5mm	0.00	21.83	
12.5 - 9.5mm	0.00	21.84	
9.5 - 4.75mm	21.83	0.00	
Sub total	45.38	45.40	90.78 Total

BATCH NO. SSG

COARSE AGG CA-G (Glacial Gravel)

DATE: 12/13/99

Batch Made Mon. @ 4:00

Fine Aggregate

57.94 Fine Agg (b)

Moisture content

wet	dry
321.5	312.8
0.0278	MC

0.0278 **MC**

1.61 **Moisture**

Dry weight 57.94

\+

Moisture 1.61

Total 59.55

WATER MEASUREMENT

Coarse Agg +pail 45.38

Coarse Agg +pail 45.40

Total 90.78

\+ Total Batch Water 12.63 **(d)** 12.63

\- Reserve Water 3.00 — 3.00

= Pails, Agg&Water 100.41 — H_20 9.63

RESERVE WATER

Res water	3.00	0.82	surplus & Tare
+ Tare	0.29	0.29	- tare
= Total	3.29	0.53	= surplus

Reserve Water 3.00

\- Surplus Water 0.53

= 2.47 — H_2O + 9.63

Subtotal of water in batch = 12.10

\+ Moisture in Fine Aggregate + 1.61

Total Water in Batch (D) = 13.71

Cement

26.12 Cement (C)

Pail ID G , H

Tare weight 0.85 — 1.68 tare

Tare weight 0.83 — 27.80 Pail + cement

Total tare 1.68

UNIT WEIGHT

Weight of Concrete & Bucket 40.54

\- Weight of Bucket 8.15

= Weight of Concrete in Bucket **32.39** **(f)**

Air Entraining Admixture

29 ml

Batch Summary

(a)	Coarse Aggregate as Designed	87.34	kg
(b)	Fine Aggregate as Designed	57.94	kg
(c)	Cement as Designed	26.12	kg
(D)	Total Water of Batch	13.71	kg
(e)	**Total Weight of Batch**	**185.11**	kg

SLUMP = 2.75 " — **69.9** mm

AIR CONTENT

\- Factor of Aggregate Porosity

= Percent Air **5.25**

CONCRETE TEMPERATURE, C 19

Note: a,b,C,d come from mix proportions worksheet

BATCH COMPUTATIONS WORKSHEET

WEIGHT IN kg

Coarse Aggregate

68.07 Coarse Agg (a)

Pail tare	1.74	1.74	3.48 + pails
			71.55 = total
25.0 - 19.0mm	17.01	0.00	
19.0 - 12.5mm	0.00	17.02	
12.5 - 9.5mm	0.00	17.02	
9.5 - 4.75mm	17.02	0.00	
Sub total	35.77	35.78	71.55 Total

Fine Aggregate

62.62 Fine Agg (b)

Moisture content

wet	dry
143.6	138.9
0.0338	MC

0.0338 MC

2.12 Moisture

Dry weight 62.62

\+

Moisture 2.12

Total 64.74

Cement

26.12 Cement (C)

Pail ID A', B'

Tare weight 0.85

Tare weight 0.85

Total tare 1.70

1.70 tare

27.82 Pail + cement

Air Entraining Admixture

22 ml

Batch Summary

(a)	Coarse Aggregate as Designed	68.07 kg
(b)	Fine Aggregate as Designed	62.62 kg
(c)	Cement as Designed	26.12 kg
(D)	Total Water of Batch	15.23 kg
(e)	**Total Weight of Batch**	**172.05** kg

BATCH NO. LS

COARSE AGG CA-S (Slag)

DATE: 12/15/99

Batch Made Wed. @ 4:00

WATER MEASUREMENT

Coarse Agg +pail 35.77

Coarse Agg +pail 35.78

Total 71.55

\+ Total Batch Water 14.11 (d) 14.11

\- Reserve Water 3.00 3.00

= Pails, Agg&Water 82.66 H_2O 11.11

RESERVE WATER

Res water	3.00	1.29 surplus & Tare
+ Tare	0.29	0.29 - tare
= Total	3.29	1.00 = surplus

Reserve Water 3.00

\- Surplus Water 1.00

= 2.00 H_2O + 11.11

Subtotal of water in batch = 13.11

\+ Moisture in Fine Aggregate + 2.12

Total Water in Batch (D) = 15.23

UNIT WEIGHT

Weight of Concrete & Bucket 39.22

\- Weight of Bucket 8.15

= Weight of Concrete in Bucket 31.07 (f)

SLUMP = 1.5 " 38.1 mm

AIR CONTENT

\- Factor of Aggregate Porosity

= Percent Air 4.5

CONCRETE TEMPERATURE, C 18

Note: a,b,C,d come from mix proportions worksheet

References

Abdel-Maksoud, M.G., N. Hawkins, and Barenberg (1997): E. Behavior of Concrete Joints under Cyclic Shear. *Proceedings,* ASCE, Aircraft Pavement Technology: In the Mist of Change, pp. 190-204.

Anton, R.J. and Subhash, G. (1999): Dynamic Vickers Indentation of Brittle Materials. *Wear* (in Print).

Blatt, H., Middleton, G. and R. Murray: (1972), *Origins of Sedimentary Rocks*, Prentice-Hall, Inc., Englewood Cliifs, New Jersey, p. 634.

Cargill, J. S. and Shakoor, A. (1990): Evaluation of empirical methods for measuring the uniaxial compressive strength of rock. *Int. J. Rock Mech. Min. Sci. & Geomech. Abstr.*, 27, 495-503.

Cohee, G. V. (1965): Geologic History of the Michigan Basin, Washington Academy of Science Journal, Vol. 55, pp. 211-223.

Deere, D. U., and R. P. Miller (1966): Engineering Classification and Index Properties for Intact Rock. Technical Report No. AFWLTR-65 116, Air Force Weapons Laboratory, Kirkland Air Force Base, New Mexico.

Dutta, K. and Kim, K. (1993): High-Strain-Rate Tensile Behavior of Sedimentary and Igneous Rocks at Low Temperatures, U.S Army Corps of Engineers, CRREL Report 93-16, pp. 11.

Fairbanks, C. J. , Polvani,R. S. , Wiederhorn, S. M. , Hockey B. J., and Lawn, B. R. (1982): *J. Material Sci. Letts.,* 1982, 1, pp. 391-393.

Follansbee, P.S. (1985): The Hopkinson Bar, *Materials Testing, Metals Handbook,* 9th Edition, American Society of Metals, Metals Park, OH, Vol. 8, pp. 198-203.

Grady, D. E., and Lipkin, J. (1980): Criteria for Impulsive Rock Fracture. *Geophys. Res. Lett.,* 7, pp. 255-258.

ICE, (1976): Manual of Applied Geology for Engineers, Institution of Civil Engineers, London, p. 378.

Jumikis, A. R., (1983): Rock Mechanics, Second edition, Trans Tech Publications, Zellerfield, Germany, pp. 62-63.

Kawatra and Eisele (1989): Effect of temperature on the performance of an autogenous grinding circuit. Advances in Autogenous and Semiautogenous Grinding Technology (A. L. Mular and G. F. Agar, Eds.) Dept. of Mining and Mineral Process Engineering, University of British Columbia, Canada, pp. 485-499.

Koeppel, B. J. and Subhash,G. (1999): Characteristics of Residual Plastic Zone Under Static and Dynamic Indentations, *Wear* 224, pp. 56-67.

Lankford, J. (1981): Mechanisms Responsible for Strain-Rate Dependent Compressive Strength in Ceramic Materials, *J. Am. Cer. Soc.,* 64, c-33- c-35.

Lankford, J. and Blanchard, C. R. (1991): Fragmentation of Brittle Materials at High rates of Loading, *J. Material. Sci,* 26, pp. 3067- 3072.

Lankford, J.(1998): Predebon, W.W., Staehler, J.M. , Subhash,G. , Pletka, B. J. and Anderson, C.E. The Role of Plasticity as Limiting Factor in the Compressive Failure of High Strength Ceramics. *Mech. of Material* 29, pp. 205-218.

Lea, F. M. (1971): The Chemistry of Cement and Concrete, Third edition, Chemical Publishing Company, pp. 455-562.

Lee, Y. H. and Williams, K. (1997): Mechanical Properties of Concrete in Uniaxial Compression, ACI Materials Journal, V. 94, No. 6, pp. 457-471.

MDOT (1997): Aggregate Source Inventory, Materials Testing Section, Materials and Testing Division, Lansing, MI, February.

Malvar, L. J. and Ross, C. A. (1998): Review of Strain Rate Effects for Concrete in Tension, ACI Materials Journal, November/December, pp. 735-739.

Meyers, M. A. (1994): *Dynamic Behavior of Materials*, John Wiley & Sons, Inc., New York. Nemat-Nasser, S., Issacs, J. B., and Starrett, J. E. (1991): Hopkinson Techniques for Dynamic Recovery Experiments, *Proceedings of the Royal Society of London, A,* 435, 37 pp. 1-385.

Okubo S., Nishimatsu Y. and He C. (1990): Loading Rate Dependent of Class II Rock Behavior in Uniaxial and Triaxial Compression Tests-An Application of a Proposed New Control Method," *Int. J. Rock Mech. Min. Sci & Geomech. Abstr.* 27, pp. 559-562.

Ravichandran, G. and Subhash, G. (1994): Critical Appraisal of Limiting Strain Rates for Compression Testing of Ceramics in a Split Hopkinson Pressure Bar, *J. of the Am. Ceram. Soc.* 77, pp. 263-267.

Ravichandran, G. and Subhash, G. (1995): A Micromechanical Model for High Strain Rate Behavior of Ceramics, *Int. J. of Solids and Structures.* 32, pp. 2627-2646.

Ross, C.A., Thompson, P. Y. and J. W. Tedesco, (1985): Split-Hopkinson Pressure-Bar Tests on Concrete and Mortar in Tension and Compression, ACI Materials Journal, September/October, pp. 475-481.

Ross, C.A., Tedesco, J. W. and S. T. Kuennen, (1995): Effects of Strain Rate on Concrete Strength, ACI Materials Journal, January-February, pp. 37-47.

Ross, C.A., Jerome, D. M., Tedesco, J. W. and M. L. Hughes, (1996): Moisture and Strain Rate Effects on Concrete Strength, ACI Materials Journal, May-June, pp. 293-300.

Sender, S. (1997): Size Effect Tests of High Strength Concrete," Journal of Materials in Civil Engineering, ASCE, Vol. 9, No. 1, pp. 46-48.

Subhash, G. and Nemat-Nasser, 5. (1993): Dynamic Stress-Induced Transformation and Texture Formation in Uniaxial Compression of Zirconia Ceramics, *J. of the Am. Ceram. Soc., 76,* pp. 153-65.

Subhash G. and Ravichandran, G. (1998): Mechanical Behavior of Hot Pressed Aluminum Nitride Under Uniaxial Compression. *J. Material Sci.,* **33,** pp. 1933-1939.

Suresh, S., Nakamura, T., Yeshurun, Y., Yang, K.-H., and Duffy, J. (1990): Tensile Fracture Toughness of Ceramic Materials: Effects of Dynamic Loading and Elevated Temperatures," J. Am. Ceram. Soc., 73, pp. 2457-2466.

Vitton, S. J. and Subhash, G. (1999): Dynamic and Static Strength of Aggregates: An Estimate of Rate Sensitivity of Geologic Materials, Proceedings, Institute of Lake Superior Geology, 45th Annual Meeting, Marquette, MI, Vol. 45, part 1, pp. 54-56.

Wawersik W. R. and Fairhurst C. A.(1970): A study of brittle rock fracture in laboratory compression experiments, *Int. J. Rock Mech. Min. Sci.,* 7, pp. 56 1-575.

SECTION 6

Aggregate Interlock Test System Development

An important mechanism in the performance of PCC pavements is the ability to effectively transfer shear loading across joint systems. In general, this mechanism is accomplished through dowel and aggregate interlock action. In addition to joint performance, aggregate interlock is also very important in the transfer of shear stress across cracks that form in the in the PCC due to shrinkage, durability problems or excessive vehicle loading. An important parameter in the effectiveness of aggregate interlock, especially at larger cracks, is the strength and durability of the aggregate itself. Recent research at the University of Illinois has shown that aggregate interlock is directly related to aggregate strength. Section Five presented the results of the both the static and dynamic strength testing of the aggregate, cement matrix and PCC, where the rate sensitivity of each of these materials was determined. To compare these results with aggregate interlock in PCC, an aggregate interlock test system was designed and constructed for this research. In addition, initial testing was conducted to evaluate the performance of the system.

There were a number of design criteria for the aggregate interlock test system and the PCC tested. First, the system had to be designed such that a test could be set up and conducted in a minimum amount of time. Second, the system had to simulate as close as possible the behavior of a joint and in particular maintaining the crack at a constant crack width during shear loading. Third, the data acquisition and control system needed to be able to control the test and collect the load level and displacements to verify the performance of the testing. Fourth, the PCC had to be as consistent as possible with the only variable being the coarse aggregate.

The research reported in this section is taken from a master's thesis conducted by Richard Ver Strate at Michigan Tech and advised by Dr. Stan Vitton.

1 Introduction and Background

1.1 Introduction

An important aspect of rigid pavement design (concrete pavements) is the design and installation of construction joints, which are used to accommodate initial shrinkage and later expansion and contraction of the pavement due to changes in temperature. Historically, two types of joints have been used in concrete pavements: contraction joints and expansion joints. Contraction joints are placed at regular intervals soon after the concrete has been placed by cutting a partial depth groove in the fresh pavement. As the concrete begins to shrink due to moisture loss, shrinkage cracks will develop at the groove location thus controlling the placement of the cracks at regular intervals. Expansion joints are placed at less frequent intervals in the pavement to handle thermal expansion as the pavement experiences daily and seasonal temperature changes. However, expansion joints are now used less frequently since field experience has indicated that the contraction joints appear sufficient to handle thermal changes. In addition, it has been noted that a possible negative affect of expansion joints is that they may allow the contraction joints, which are located between the expansion joints, to open up resulting in less efficiency in transferring wheel loads across the joint.

The ability of the joint to transfer wheel loads from one slab to the next is an important factor in maintaining the integrity of the roadway. There are at least three important mechanisms involved in the functioning of joints: (1) aggregate interlock, (2) dowel reinforcement, and (3) base support. When the ability of the joint to transfer wheel loads decreases, faulting at that joint occurs resulting in an uneven roadway. When the faulting at the joint becomes excessive the joint must be removed or the entire roadway reconstructed. Consequently, it is important that the design of the joint be considered in pavement design.

The emphasis of this report will be on the development and evaluation of a test system to study aggregate interlock as the mechanism for transferring shear stress at joints in Portland Cement Concrete (PCC) pavements. Aggregate interlock is the interlocking action of the aggregate particles at the joint surfaces, as illustrated in Figure 1.1. Even though most joints are reinforced with dowels to aid in shear transfer, it has been shown by Reinhardt and Walraven (1982) that aggregate interlock still plays a major role in shear transfer. This is especially true for smaller crack widths in which aggregate interlock plays a dominant role. The effectiveness of aggregate interlock is dependent on the composition and surface characteristics of the crack interface. The surface characteristics or roughness of the crack interface may be different for each type of aggregate used in concrete. The greater the roughness, the more protrusions of aggregates, the greater ability a joint within pavements has to withstand the loading of vehicle traffic. It has been found that for similar aggregates of the same hardness, the effectiveness is increased with an increase in particle angularity as well (Colley and Mumphrey, 1967). In the past, research has concentrated on understanding the mechanism of shear transfer across joints in pavements by varying crack width, aggregate size (whether reinforced or not reinforced) and type of loading. However, to better understand how to make a long-lasting pavement, a better understanding of the materials is still needed.

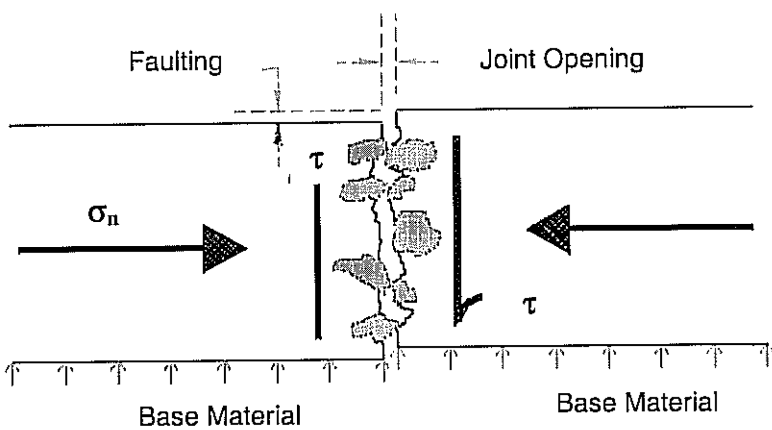

Figure 1.1. Shear transfer mechanism through aggregate interlock.

1.2 Background

In addition to vehicle loading, concrete pavements develop stresses from temperature change, shrinkage, warping, and freeze-thaw conditions. All of these stresses can result in cracks developing in concrete pavements. Once the cracks develop, however, then the performance of the concrete pavement will depend to a large extent on the interaction of the crack surfaces. Common forms of cracks in concrete pavements are transverse cracks, which generally form due to shrinkage (tensile stress) of concrete during curing. As discussed previously, contraction joints are placed in the pavement to relieve the tensile stresses that develop in the concrete. However, cracks will continue to develop throughout the life of the pavement at mid-panel locations due to a combination of wheel loading, temperature changes, and warping and will also affect the performance of the pavement. In both the contraction joints as well as the transverse cracks, aggregate interlock becomes an important factor in the service life of the pavement. For pavements with high traffic levels and traffic loads over time both the contraction joints and transverse cracks will undergo faulting. Faulting of the joint is the break down of the shear mechanisms resulting in relative vertical displacement of pavement sections as illustrated in Figure 1.1.

1.2.1 Previous Research

Due to the importance of aggregate interlock in concrete pavements, research has been conducted to understand the mechanisms involved. The Bureau of Public Roads (now the Federal Highway Administration), Portland Cement Association (PCA), Delft University, and more recently the University of Illinois are some of the institutions that have conducted research in aggregate interlock.

1.2.1.1 Large-scaled research

One of the first organizations to conduct a field study on aggregate interlock was the Bureau of Public Roads during the 1940's and early 1950's (Sutherland, 1956). This field study characterized contraction and expansion joint geometry and performance. Since the publication of this report, researchers have used this information as a basis for the design of aggregate interlock experiments. In the 1960's the Portland Cement Association conducted a large scale laboratory experiment that studied five variables that were considered significant in the performance of joints: (a) joint opening, (b) depth of concrete slab, (c) vehicle loading, (d) base support, and (e) shape of aggregate. Some of the important conclusions reached in this study were as follows (Colley and Humphrey, 1967):

1) as the joint opening increases, the effectiveness of the joint decreases,
2) usually 90% of the joint efficiency was lost during the first 500,000 cycles when the joint opening, test load, slab depth and base material were held constant,
3) joint effectiveness increased with increasing base support,
4) for a given joint design, effectiveness is not influenced by loads less than a critical value,
5) For a given aggregate of the same hardness, effectiveness increases with increase in angularity.

Nowlen (1968) reported that aggregate interlock also improved with increasing aggregate hardness. Additionally, Nowlen reported that early fracture of the joint, which resulted in aggregate pullouts as opposed to aggregate fracture, increased joint efficiency under repeated loads.

1.2.1.2 Small-scaled research

Due to of the complexities of completing a large-scale experiment in the laboratory, research has been conducted on smaller size samples, which were then correlated to field conditions. Delft University and University of Illinois are a few of the institutions that have concentrated their work on the smaller size samples. With a smaller scaled experiment, a larger number of tests can be completed in the lab in addition to effectively controlling test variables.

The study at Delft University used a direct shear test set up to investigate aggregate interlock during shearing (Reinhardt and Walraven, 1982). As shearing develops at the interface the resulting dilation forces the blocks outward. To restrain this motion steel bars were used, resulting in a normal force developing at the interface. Their sample used in the testing was similar to that used by Mattock (1980), who also studied aggregate interlock. The sample size was roughly 60 x 40 x 12 cm, with a shear area of 360 cm^2. The samples were cast in the horizontal position. Two days later the molds were stripped and the samples were placed back in a curing room for the remainder of the time. Before the samples were tested a crack was initiated along the shear plane by splitting forces (knife-edges) at grooves, which were formed on the front and rear faces. The crack width was measured as the sample was being split to control its desired width. Portions of the samples were tested with external restraining bars so that the normal stress could be controlled. The bars were used to vary the external stiffness between different tests, thus controlling the normal stress. The other portion had reinforced bars cast in the samples, which were varied in diameter to study different reinforcement ratios. The samples were loaded with a specified shear displacement rate (monotonic loading) in which loading was applied until a displacement value of 2 mm was achieved. The crack width, shear load, and shear displacement were measured throughout each test.

Walraven (1982) has also done analytical modeling work in studying the shear mechanism of aggregate interlock. The fundamental aspect of this model is that the concrete is represented by a two-phase system, a matrix, which is the hardened cement paste, and the coarse aggregate particles. According to Walraven, the weakest link of the system is the contact area between both the mortar and the coarse aggregate. Therefore, during the curing stages it is at the interface, which fails during shrinkage. An important assumption in this work is that the paste is weaker than the coarse aggregate and breaks down during shearing action. This is illustrated in Figure 1.2, where one surface moves with respect to the other and where the paste that is in direct contact with the aggregate is being crushed and worn down, which allows for the faulting of the joint. In addition, Walraven states that the micro-roughness of the crack, caused by the aggregate particles projecting from the crack plane, dominates the macro-roughness, due to overall undulations of the crack faces.

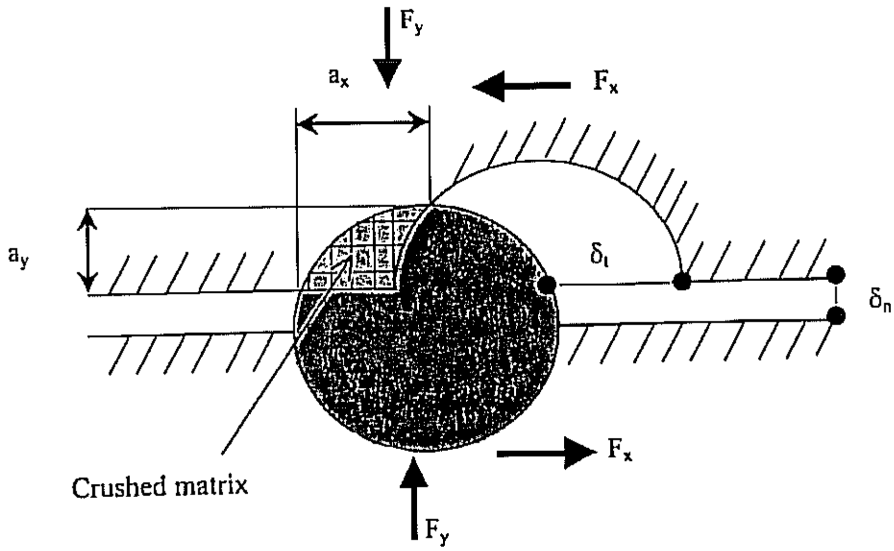

Figure 1.2. Contact stresses on aggregate particle and matrix.

A study at the University of Illinois (Abdel-maksoud, 1997), is one of the latest projects that has been conducted on aggregate interlock. The sample size used in the study was roughly 30.5 x 30.5 x 61 cm, with a shear area of 645 cm^2. The sample is fractured in tension to create the crack interface representing a joint in the field. To produce the crack a groove is made in the sample during casting using 25.4 mm steel strips. The strips are placed at the center of the mold, leaving a reduced area concentrated at midpoint of the sample. The mold has a set of four threaded bars placed at both ends, which were cast in the concrete sample. These threaded bars were used to grip the sample to fracture the sample in tension. At eight hours of cure the sample was then prepared for fracturing. After the eight hours the end plates of the mold were loosened and shims placed between them and the side plates of the mold. During casting the threaded bars were held in place by two nuts on either side of the end plates. The nuts on the outside of the mold were then tightened to place a tension stress in the sample. By tightening one nut at a time, the sample was slowly pulled apart. It was found that when both sides of the mold were tightened at the same time a higher quality fractured surface was obtained as shown in Figure 1.3. The sample was then set aside for the remainder of it's curing time. After the sample has cured for a designated time it was placed in a device that utilized a 100 kip MTS actuator to apply the shear loading. The sample is oriented so that the crack plane is horizontal making it easier for actuator placement. The actuator was then attached to the top half of the sample while the bottom half was securely fixed in place. Using different sized rollers, which are set between the two sample halves, controlled the crack width. Four load cells were attached to the top half of the sample to monitor the normal loads being generated by the shear force. Two types of shear loading were used including fully reversed cyclic shear and monotonic shear loading. The data measured was shear load, normal load, shear displacement, and change in crack width during testing. With the work completed thus far, an important conclusion made was that the aggregate interlock is dependent on the joint opening, joint tortuosity and surface roughness. With large joint openings the resistance is mobilized by dilatancy rather than small joint openings where the resistance is mobilized by trying to shear through the roughness by friction. Therefore, the roughness of the crack interface is dependent upon aggregate type and size.

a) Pulling from one side b) Pulling from both sides

Figure 1.3. Shape of crack from two methods.

1.3 Research Objective

An important area of research at the Michigan Department of Transportation is the study of aggregate interlock, and in particular the effect that coarse aggregate type has on aggregate interlock. To study aggregate interlock it was proposed that a small-scaled (or bench type) test system be constructed to evaluate the fracture characteristics of different coarse aggregate types under an applied shear stress. The focus of the project is to closely simulate shrinkage cracks in PCC pavements subjected to vehicle loading, investigating coarse aggregate type as the main variable in its behavior. The focus of this research report was to construct and evaluate an aggregate interlock test system for testing concrete samples under a shear load.

The detailed objectives of this study are as follows:

1) Design and construct a structural testing frame that will handle the envisioned loading with its orientation of test sample.
2) Develop and construct a system to restrain the bench type sample used for testing so that it replicates pavement movement in the field.
3) Design and construct a device that would create a shrinkage crack within a concrete sample in the lab.
4) Develop the data acquisition and control system for monitoring and controlling the sample movement during the test.
5) Mix and prepare samples that will be used for running and evaluating the test system.
6) Develop test procedures for operating the test system.
7) Evaluate the test system performance.

2 Experimental Design

2.1 General Design

During the design phase of this research a number of factors had to be considered. One of the major considerations was simulating field conditions in the experimental design. In general the movement of the concrete pavement, after the contraction joints have formed, is due to environmental factors, such as warping from moisture changes, and expansion/contraction and shrinkage conditions from temperature changes. In undoweled pavements, vehicle loading is transferred from one panel to the next across the contraction joint by aggregate interlock, where the opposing joint surface is considered fixed with the exception of movement in the vertical direction. Therefore, in an experimental situation the longitudinal and transverse directions need to remain fixed. These directions are shown in Figure 2.1. In the transverse direction the pavement would see very minimal movement due to temperature changes, which would have little effect on aggregate interlock. Walraven (1982) claims that in this direction all forces are cancelled out due to shear loading, resulting in no transverse movement. Based on this information, the transverse direction was not restrained in this research study, although this motion was monitored. Due to temperature changes, though, there will be movement in the longitudinal direction, which will be greatest between summer and winter. However, for testing purposes it was assumed that relatively little movement occurs during the testing period, thus resulting in a constant crack width during the test. Consequently, the longitudinal direction had to be held constant.

Two 55 kip MTS actuators were available to provide the required loading. One actuator was used to apply the shear force while the other actuator was used to maintain a constant crack width by reacting against any normal force generated from the shearing action of the interface. Unlike the research at the University of Illinois, which had the crack plane placed in the horizontal direction, the interface was placed in the vertical plane so that any debris created from the shearing force could fall downward and be collected. In the Illinois research, the sheared particles remained at the interface.

Vertically orienting the joint better simulates the crack orientation in the field, thus if material worked loose from the shearing action it would work its way through the crack and potentially fall out. To utilize the two actuators in this orientation, one actuator was placed in the vertical direction and the remaining actuator in the horizontal direction. To accomplish this a large structural frame was required to hold both the actuators and concrete sample.

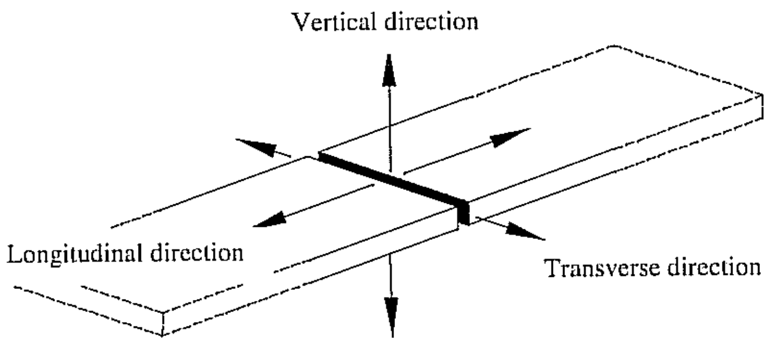

Figure 2.1. Referred pavement directions within text.

2.1.1 Structural Frame

As mentioned previously, the structural frame had to accommodate two MTS hydraulic actuators each with a 55 kip loading capacity. Therefore, the frame design ultimately had to withstand full loading of a single 55 kip actuator in either direction. In addition, the frame had to be designed for other research applications, thus requiring the design to be as versatile as possible. Due to limited funds, it was decided to design the frame so that only a portion had to initially be built, but when additional funds became available, the remaining portions could be constructed. The design of the frame was entirely based on the LRFD steel codes. An overview of the designed frame is illustrated in Figure 2.2.

The frame was designed so that it could be fabricated elsewhere then moved and assembled using bolted connections, which made it ideal for future modifications. With the bolted connections, some parts were also designed with the capability of being adjustable. One of which was a crossbeam on a vertical tower, consisting of two columns, which enabled a single actuator to be placed vertically, as can be seen in Figure 2.2b. It was given roughly a 15-ft travel so that whatever position might be needed in the future additional drilling would not be required. Another consideration was to pre-drill two floor beams, to which the single tower was connected, to handle three additional towers. These two floor beams are connected by three cross beams placed at quarter points. The addition of more towers would then develop a structural cage that could be utilized for many applications in the future. One unique feature of the frame design was that it is self-reacting, meaning that it does not rely on the building floor to supply load reactions, but only the self-weight of the frame. By making it self-reacting, an additional beam was placed along the center points of the three crossbeams, which also aided in mounting the second actuator. This allowed any force that would be generated from the hanging actuator to be transferred into the frame and not against the floor. The second actuator was placed in the horizontal direction to control the crack width of the sample during testing, as illustrated in Figure 2.2a. Two thrust boxes were designed for the horizontal loading, which one thrust box held the horizontal actuator while the second held the fixed-end holder. Discussion on the fixed-end holder is provided in the following section. The structural frame's final length is 30 ft. and the height is 20 ft. The completed structural frame can be seen in Figure 2.3. The dimensions of the frame were designed so that it would fit in the limited space contained in the structural bay area in Dillman Hall at Michigan Tech.

A time consuming task for the project was the drawing and detailing of the frame and sample holders, which were sent to Yalmer Mattila Contracting Inc., of Houghton Michigan, for fabrication and construction. During the final detailing of the drawings, the contractor reviewed the plans and estimated the time and cost of construction. With some exceptions, the frame materials were ordered, cut and welded within four weeks. Installation of the frame took approximately two days. After erection of the frame, it was found that a misalignment occurred on the drilled holes of the two floor beams used for placement of the diagonal bracing to the tower. However, this was easily fixed by re-drilling onsite. As-built drawings for the frame are provided in Appendix 6-A.

2.1.2 Sample Holders

An important design element for the test system was the fixtures or holders for the concrete blocks. The holders needed to be designed so that loading and unloading of the samples was easy and required a minimum amount of installation time. The holders also needed to be designed to restrict movement of the concrete blocks within the holders with respect to the acting force. For simplification of the test, one side of the sample was fixed to the frame in the fixed-end holder while the other side received the shear loading. What allowed the fixed-end holder to be fixed to the frame and still allow the capabilities of monitoring and controlling the normal stress, which is developed from the shear force, the horizontal actuator was to attached to the same side of the sample as the vertical actuator. Consequently, one actuator was attached to the top of the holder providing the shear load and the other actuator was attached to the end of the same holder, which would then react against any normal loading that is developed due to dilation of the interface. By allowing the actuators to pivot at their ends it would eliminate the need for an elaborate roller system to restrain the movement of the sample, but yet maintain an average crack width throughout the testing.

The resulting design of the holders was two steel boxes that had removable lids for the loading and unloading of the concrete samples. The lids acted as a clamping mechanism to restrain the sample, thus preventing sample movement during a test. A projected face on each end of the two holders would give them the ability to bolt up to the actuators and frame. The design was simplified so that each holder was the mirror image of the other, which assisted in fabrication as well. However, the lids had to be designed differently. The fixed-end holder required only a steel plate that is bolted to the top for restraining the sample. The load-bearing holder on the other and had to be designed to

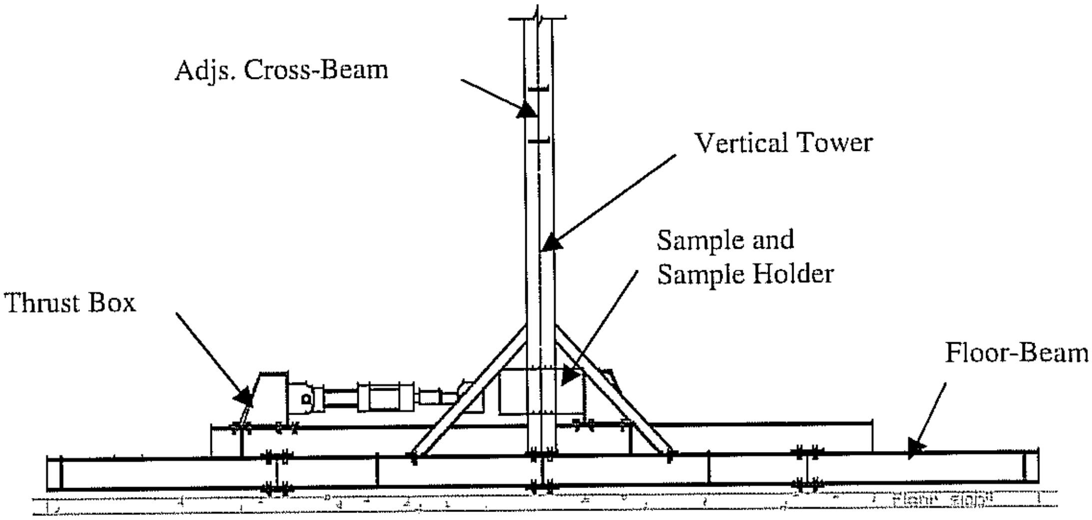

Figure 2.2a. Side view of structural frame.

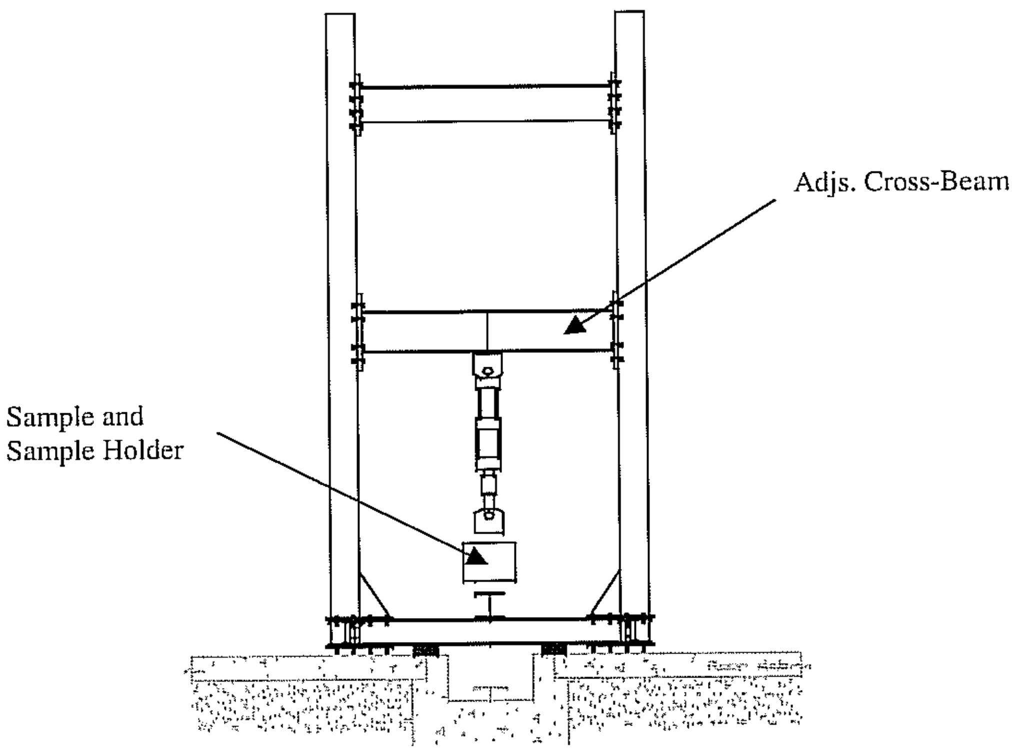

Figure 2.2b. Front view of structural frame.

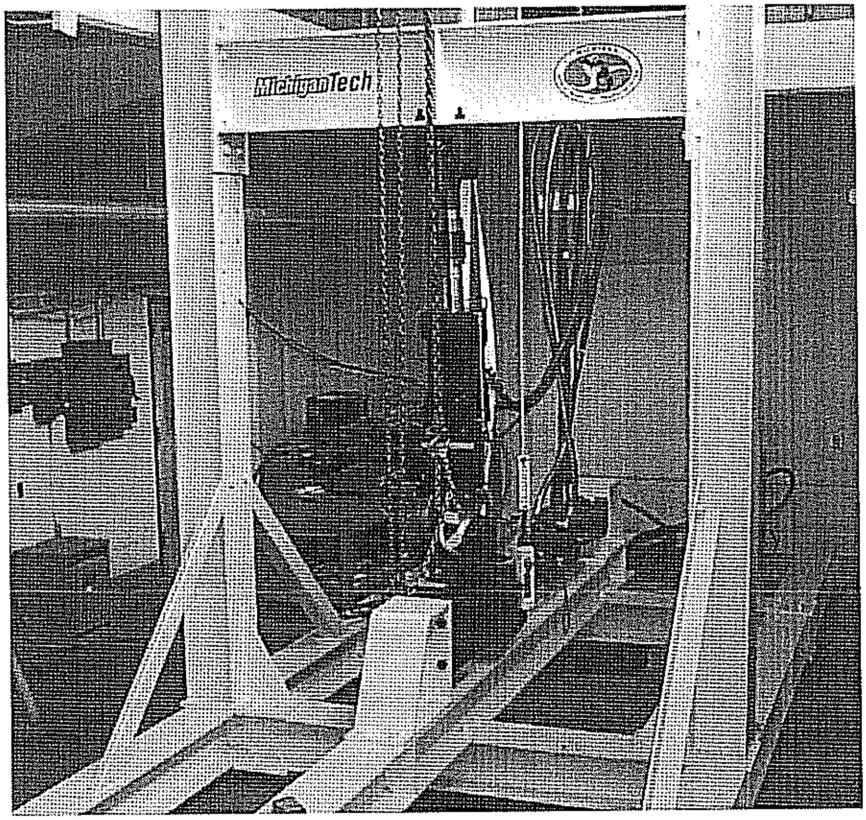

Figure 2.3. Structural testing frame after construction.

apply the shear loading. By looking at the forces on the sample the logical position of the acting force should be placed right along the crack plane. This created a problem in attaching the actuator to the moveable half, which will be referred to as the load-bearing holder, so that it would not get in the way of the fixed half, or the fixed-end holder. Therefore, the actuator needed to be offset from the load-bearing holder so that its line of action would coincide with the plane of the crack. The result was a flanged box connection, which was permanently mounted on the vertical actuator as shown in Figure 2.4a and 2.4b. The flanged box was designed to provide a maximum shear displacement of one inch. Since most pavements have been considered to fail before this point, no need of a greater displacement is foreseen.

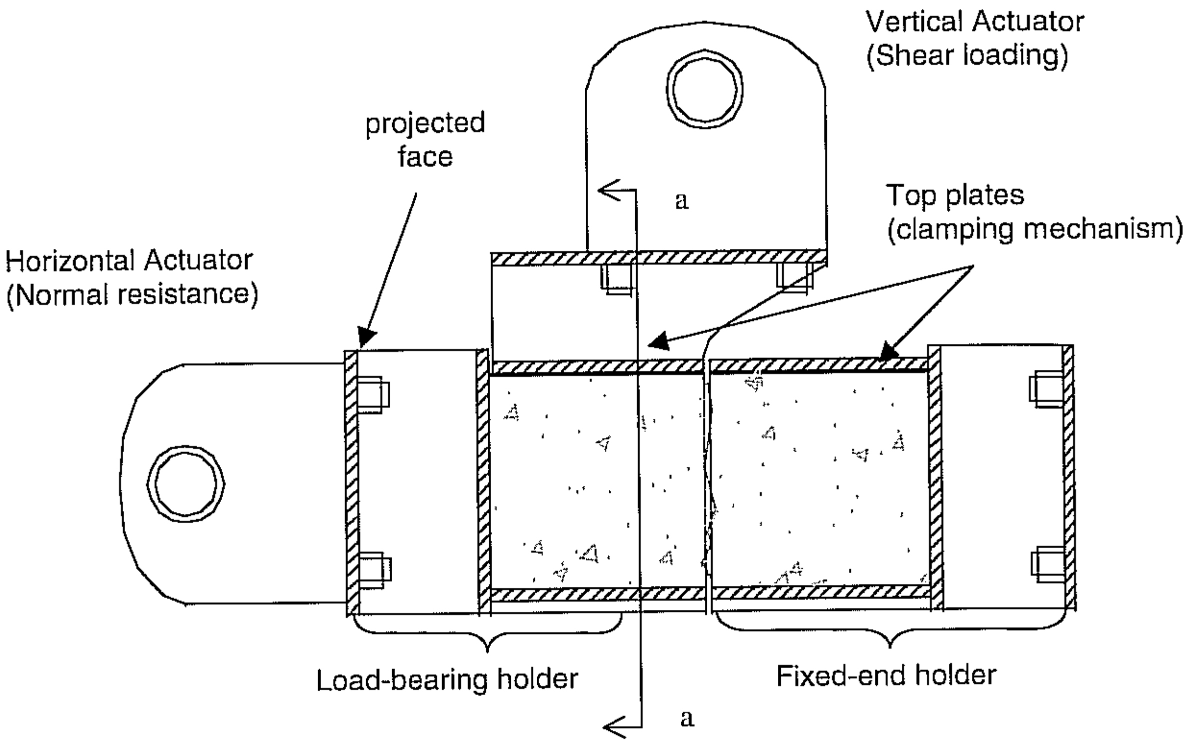

Figure 2.4a. Cross-section view of sample holder.

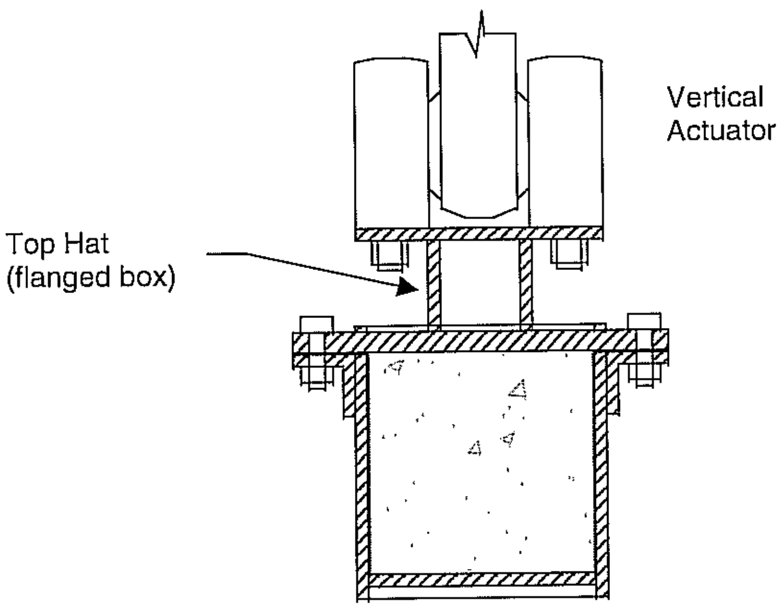

Figure 2.4b. Cross-section view of sample holder (section a-a).

There were some minor problems with the fabrication of the sample holders however. As designed, the two halves were supposed to be identical except for the lids. Due to some recalculations the plate involving the attachment of the sample holder to the thrust box was found to be inadequate for the specified factored loads. The fabricator, Royal Fabrication, Kearsarge, Michigan, was then contacted and notified of the change in dimensioning. Once in place in the lab it was also noticed that alignment of the frame and sample holders were off ¾ of an inch. This was due to the absence of adequate dimensioning on the drawings as well as some incorrect assumptions made on behalf of the fabricator. The offset put the fixed sample ¾ of an inch too far under the vertical actuator thus would create both a x and y force applied to the sample if used as fabricated instead of a pure shear force. The fixed sample holder was then taken back to the fabricator for the end plate to be moved, which made the one discrepancy in the two sample halve-holders. As-built drawings are provided in Appendix 6-A.

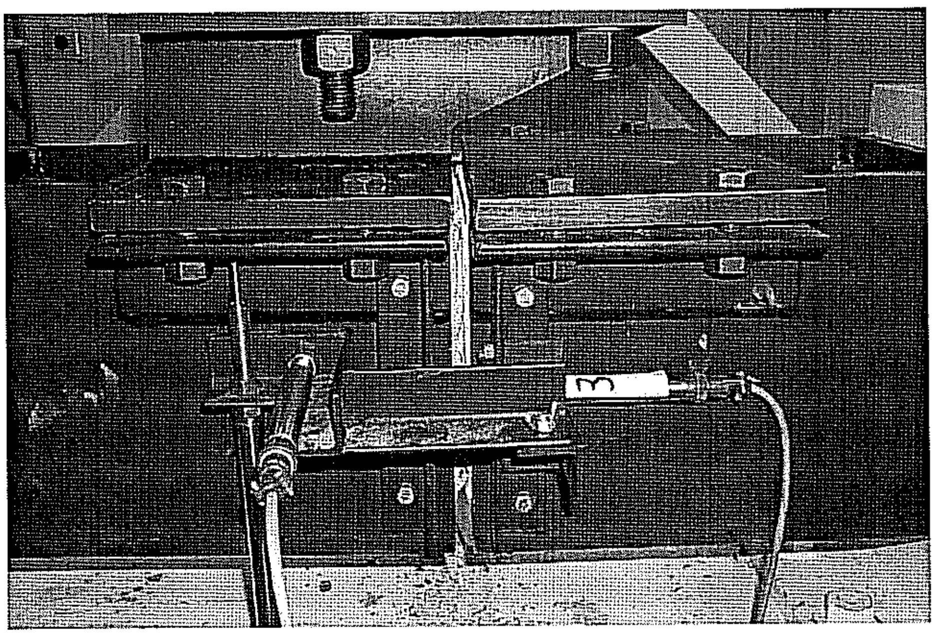

Figure 2.5. Sample holders after construction.

2.1.2.1 Platform

Aligning the two concrete surfaces together was an important consideration in the design of the test system. In addition, the design required that space be available below the sample holders so that a pan could be placed underneath the sample during a test to capture the debris created from the shearing action. To accommodate these requirements, a movable platform was constructed to support the horizontal actuator and the load-bearing sample holder prior to attaching the vertical actuator. This would also ease loading of the sample as well. Since both actuators were attached to the load-bearing holder it relied on both of them to position the sample with respect to the fixed half. The platform was used to align the sample both in the vertical and transverse directions (directions parallel to crack plane). Two guide rails were placed on the platform to keep the movable half inline with the fixed half so that the concrete sample could be positioned back together for testing. The platform was also designed so that it could be moved out of the way during a test to leave room for placement of the debris pan. The platform consisted of a steel frame mounted to a couple of screw type jacks with a piece of ¾ inch plywood fixed to the top. The platform used the weight of the actuator and the reaction of the fixed half to help position it with the two jacks at the center point as seen in Figure 2.6.

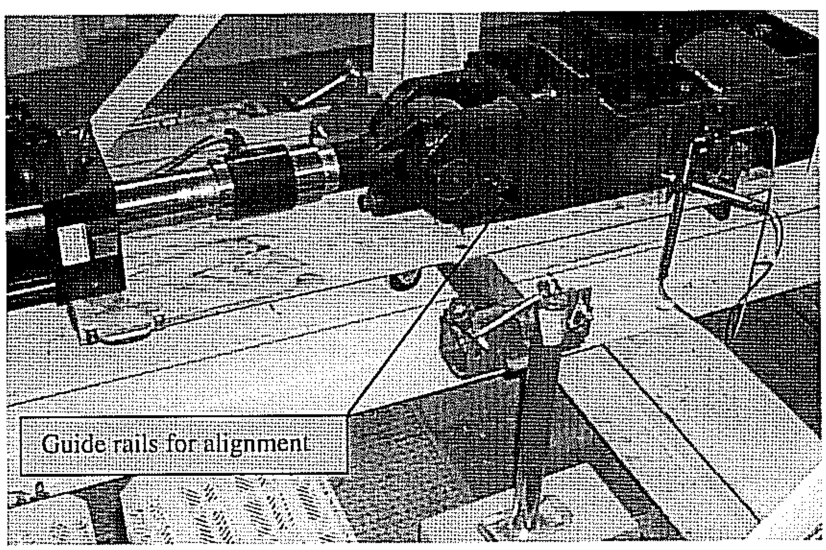

Figure 2.6. Platform for leveling and loading sample.

2.1.3 Sample Molds

The size of the concrete sample was based on three criteria. First, the sample weight had to be small enough so that it could be easily handled. Second, the cross-sectional area of the sample had to be a particular size to accommodate the maximum loading capacity of the actuator. Third, the sample size was required to be large enough so that results could be related to field conditions. Based on these criteria, the cross-sectional dimensions are 9 x 9 inches (22.9 x 22.9 cm), with a length of 18.25 in. (46.4 cm) for the sample were selected. While the cross-sectional area was based on the last two criteria, the length was based on the requirement to fracture the sample into two pieces of equal length. An obvious consideration was that it had to be cubic so that the sample could be securely fastened in the sample holders.

The mold for casting the concrete sample was made of steel so that it would last throughout the life of the project. The design of the molds was based on the standard MOR beam mold, but with the modified dimensions. The mold consisted of a base plate with two C-channels for the sides and two stock plates for the ends. The sample mold is shown in Figure 2.7.

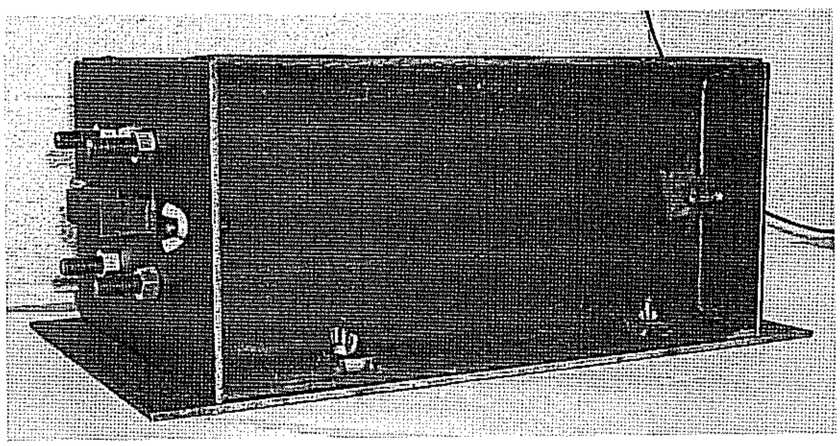

Figure 2.7. Molds for casting test sample.

In addition to the different size, the mold had to be constructed to allow the placement of eight threaded rods, which were to be cast into the sample ends to assist in pulling the sample apart. Therefore, the end plates had four holes drilled to allow for rod placement as shown in Figure 2.8. Four threaded rods were used on each end of the sample. The threaded rods were all cut to an equal length and placed so that six inches are embedded in the concrete sample after casting, having a total length of eight inches. A single nut is placed on each rod, three inches from the mold end plate to help resist in pullout. Two molds were constructed for this study.

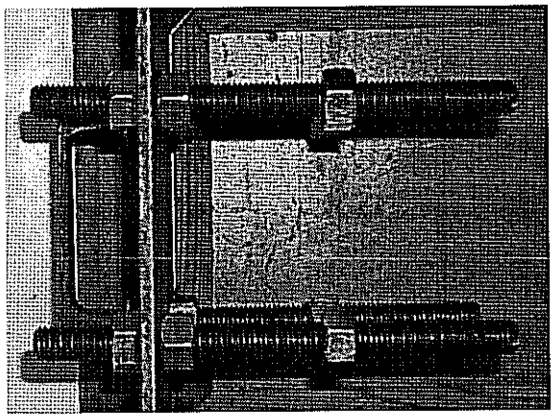

Figure 2.8. Threaded rod location on mold end plate.

An additional modification to the mold was made so that the concrete sample could fit into the sample holders. This was due to the size of the welds needed on the sample holders. To accommodate these welds, the concrete sample had to have beveled edges. To accomplish this, triangular pine strips were used in the corners of the mold as shown in Figure 2.9.

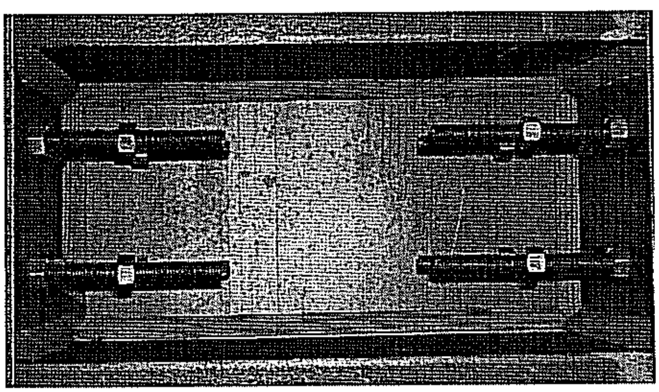

Figure 2.9. Pine stripping placement in molds.

2.1.4 Sample-Fracturing Device

To simulate field conditions as closely as possible it was decided to fracture the concrete sample in tension. In past studies the crack interface of a concrete sample was developed by three point bending or with knife-edges. In this study a fracture by a method that utilizes more of a direct tension was used since the research findings at Illinois on the crack interface indicate that this method produces a more representative crack, and that a pure tension force would better replicate the stresses out in the field. It was found at Illinois that if the sample could be pulled at both ends with equal pressure then the best available surface could be obtained. When both sides of the concrete sample were pulled apart, the crack surface tended to be more planer rather than concave. It is believed that this would better replicate the cracked surface that forms in the concrete slabs in the field during the shrinkage period.

To initiate the crack, a groove was cut around the sample center, reducing its cross-sectional area allowing the crack to be controlled and initiate at the groove. Unlike the method used by Illinois where the groove was created by the placement of steel strips laid into the concrete while it was cast, the method chosen is to cut a groove after the concrete has been allowed to cure. This would allow the coarse aggregate placement within the mix to not be controlled by the steel strips.

A hydraulic powered device was constructed to fracture the sample. In this device two hydraulic cylinders were used to apply a tension load at each end of the sample. The gripping capabilities of the threaded rods within sample made this possible. By connecting the hydraulic lines from the two cylinders together, resulting in equal pressure in each line, both sides could be pulled at the same time. Two ENERPAC cylinders, each with a 10-ton loading capacity, were set to act opposite of each other to apply the tension load. To develop the reaction to the hydraulic cylinders, two plates were welded to the face of a 9" C-channel, spaced so that a sample could be placed between them and some additional length for the threaded rods within the sample. The sample would then rest on this channel during the splitting action. The two plates were drilled with oversized holes to allow threaded rod extensions, that would attach to the sample threaded rods, to pass through and be attached to a plate that bore against the cylinder ends. This device can be viewed in Figure 2.10. A ball bearing was attached to the end of the cylinders to allow the plate to rotate and aid in equalizing pressure among the threaded rods. When hydraulic pressure was applied to the cylinders they pushed against the bearing plates, which in turn pulled on the threaded rods attached to the sample. With adequate curing time the sample could then be fractured into two blocks creating the cracked surface to be tested. Since the sample is to rest on the C-channel during fracture, friction between the concrete surface on the steel platform was of concern. To solve this, pieces of Teflon stripping were placed between the sample and the channel to reduce friction.

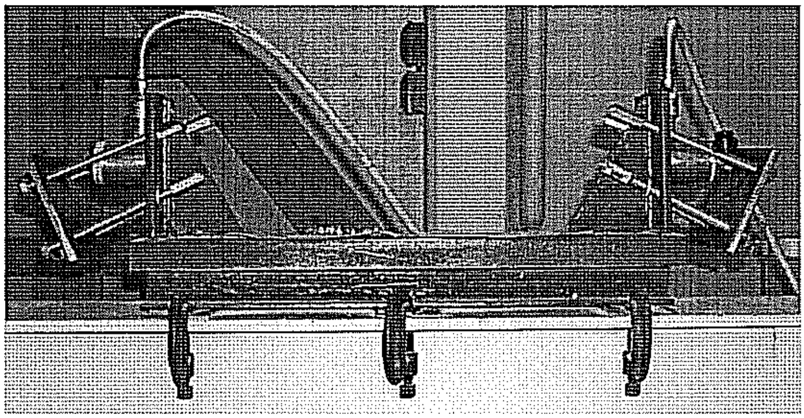

Figure 2.10. Sample-fracturing device after construction.

2.1.5 Control Systems

An important control function of the test was having the vertical actuator operate in load control, while the horizontal actuator operated in displacement control. Thus, the vertical actuator simulated vehicle wheel loading while the horizontal actuator maintained a constant crack width during the vertical loading. As the vertical load is applied to the interface, dilation occurs with a tendency to separate the surfaces outward. Since a concrete pavement remains rigid, with virtually no movement, the dilation develops a normal force at the interface. To simulate this situation the horizontal actuator must generate a normal reaction to the dilation effect of the interface in maintaining a constant crack width.

Due to the nature of this experimental design, both accurate control and high-speed data acquisition and processing was required. The loading of the concrete was accomplished using two MTS 55 kip hydraulic actuators, with each actuator controlled by a MTS 407 digital controller. A control signal was fed into the controllers from a data acquisition and control system interfaced into a PC computer.

The networking of the MTS 407 controllers and data acquisition was accomplished using the software package DASYLab version 5.0. DASYLab has 16 data acquisition channels with two channels of control. The vertical actuator was controlled by the 407 controller by a control signal produced by DASYLab, while the horizontal actuator was maintained in displacement control also by a 407 controller. Thus, the horizontal actuator was controlled in displacement control to maintain a constant crack width, while the vertical actuator was controlled in load control. The convenience of having two actuators gives the capability of controlling the crack width with greater ease, which also supplies the necessary normal loads it takes to control that crack width. Limit levels were set in each controller according to test failure criteria. A failure criterion is discussed in detail in Chapter V. The specific settings of the controllers during the preparation period of a test will also be discussed further in Chapter IV.

Each actuator was equipped with an internal LVDT (Linear Variable Differential Transformer) and a load cell. Additional displacement measurements were made using external LVDTs, which were placed on the sample to capture the sample movement. The LVDTs were rigidly attached to the fixed half of the sample holder to measure the relative displacement between the two sample holders. The external LVDTs were spring-loaded DC sensors (model GHSD), manufactured by Macro Sensors (Pennsauken, NJ). They were placed in all three directions to measure movement during testing, with two half-inch sensors measuring vertical (shearing) displacement, two quarter-inch sensors measuring crack width displacement, and two quarter-inch sensors measuring traverse movement of the sample as shown in Figure 2.11. A Tektronic dual power supply was used to supply a ±15 volts (30 volt) DC excitation source to the LVDTs. The DASYLab

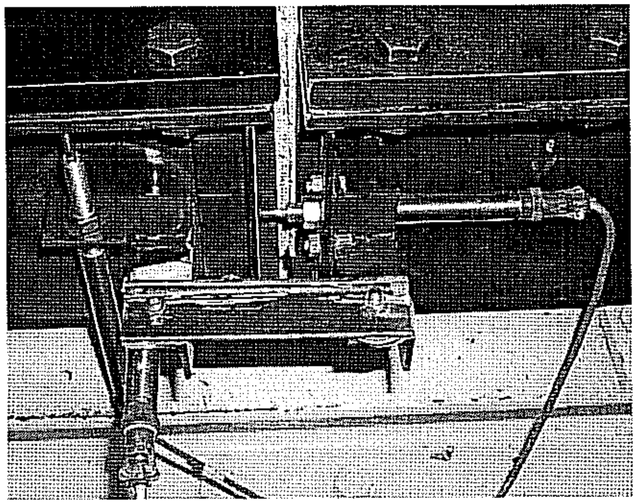

Figure 2.11. LVDT placement on one side of sample holder.

software program was used to collect data from the LVDTs accessing a high-speed 16-bit data acquisition and control board made by Mircostar Laboratories (Bellevue, WA). The Microstar board is a DAP1216a/b board with an onboard Intel 80c186XL processor. The onboard processor is used to both control and collect data independent of the main computers CPU. The DASYLab software and Microstar board were installed on a 100 MHz Pentium lunchbox style computer.

The DASYLab software is programmed to produce a loading signal for controlling the vertical actuator. The load function is a 10 Hz haversine waveform as shown in Figure 2.12. This waveform was sent to the 407 controller as an analog signal via external hook-up of the controller. The loading sequence was conducted at 1 Hz, with nine-tenths of a second at zero loading and the last tenth of a second ramping up similar to the first 180 degrees of a sine wave. The max loading or peak of the load signal is set near nine kips, while a small 100 pound load was maintained on the actuator to simulate zero loading condition to retain the stability of the actuator in load control. This loading waveform was selected to replicate field conditions when a vehicle crosses a joint.

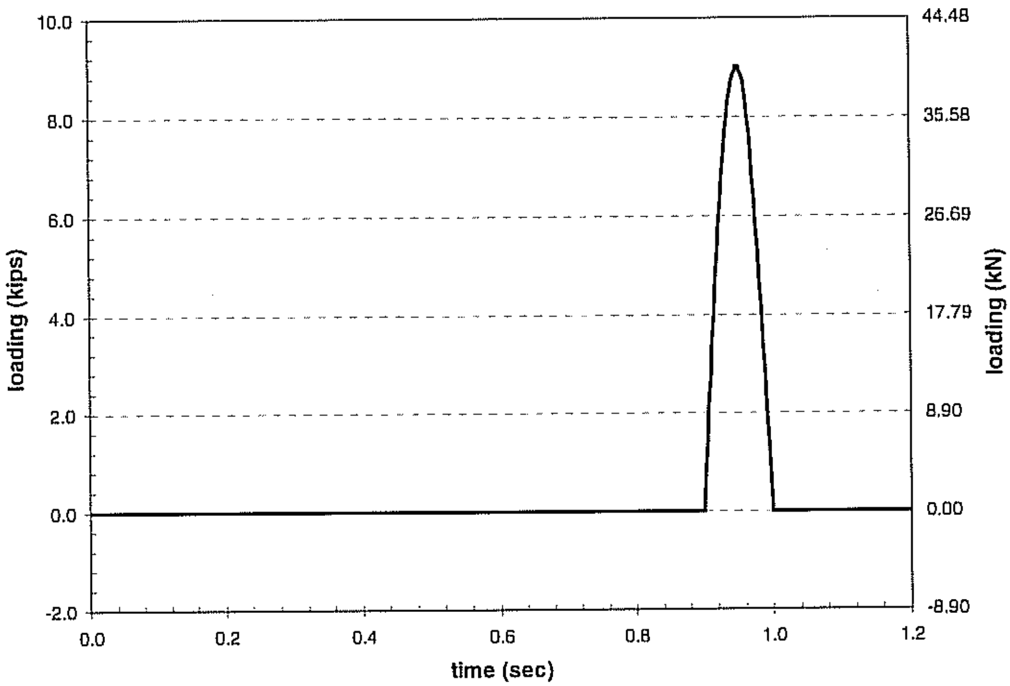

Figure 2.12. Loading control wave for vertical actuator (one cycle).

A total of ten channels of data are collected during testing. Six of these channels were the external LVDTs, while the remaining four are the internal load and displacement readings from each actuator. All ten channels are collected as analog voltage signals by the Microstar board, digitized and inputted to DASYLab. DASYLab then performs a number of functions on the data. First, the LVDT data is scaled into engineering units, from volts to inches. Second, the data is sent to a digital meter module so that the data can be observed during testing. The data acquisition rate is set at 2000 samples per second. However, data is then extracted from this data stream at two time periods. Third, one data set is collected using a maximum function module, which selects the maximum shear load for each cycle (time period 1). When the module determines that a maximum shear load has been obtained, the data is collected from all sensors and saved to a file. Therefore, if the frequency is set at 1 Hz, one set of data is taken each second. Fourth, in addition to this maximum data, every half-hour the data from a complete cycle is saved (time period 2). That is, one second of data, representing 2000 data points, is collected and stored to a file every half-hour the test is running. The full

DASYLab data acquisition worksheet is illustrated in Figure 2.13. All data is collected and stored as ASCII text. However, these two data collection methods create fairly large files, which are manipulated in a spreadsheet program. Consequently, a data-reducing program was developed to reduce these files further. This procedure will be discussed in more detail in Chapter 5.

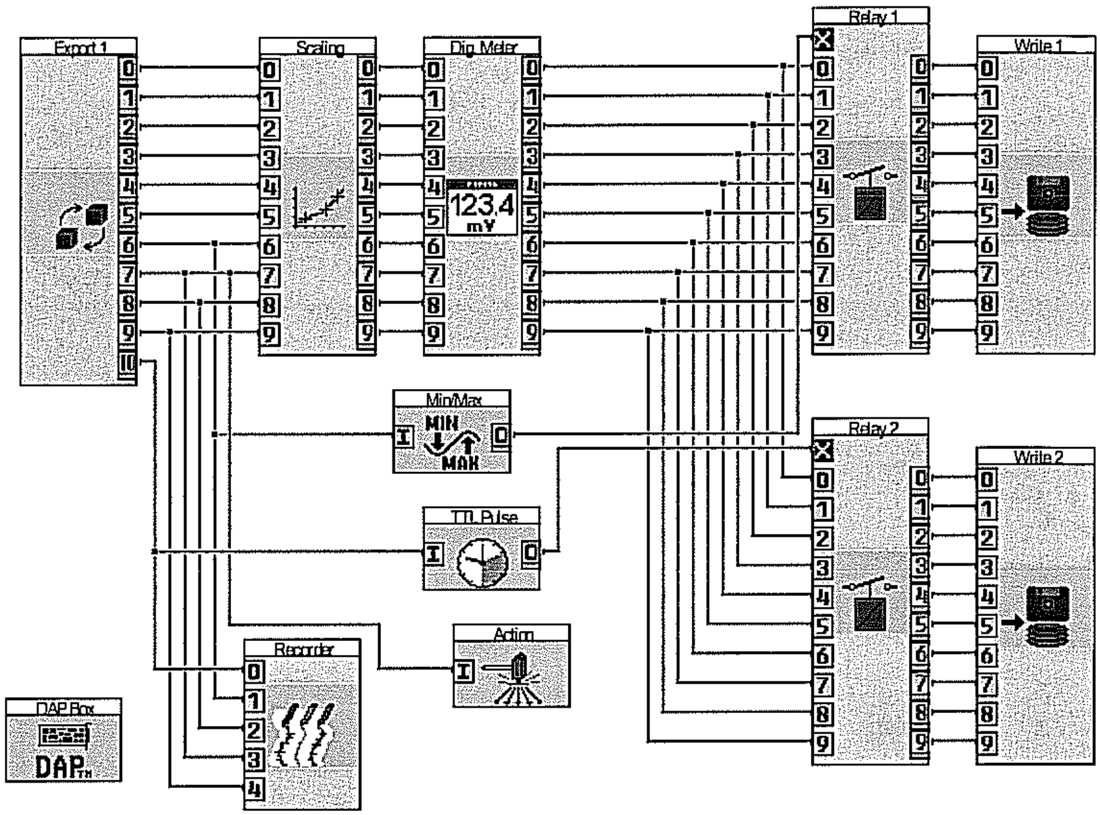

Action – Stops program when displacement reaches 0.5 in.
DAP Box – Toggle window from the Data Acquisition Processor to DASYLab
Digital Meter – Digital Meter to display displacement readings
Export 1 – Export window to import data from DAP
Min/Max – Reading maximum value from load wave to switch relay for time period 1

Recorder – Displays ongoing measurements in graphic form
Relay 1 – Switches data for time period 1
Relay 2 – Switches data for time period 2
Scaling – Scales displacement data from volts to inches
TTL Pulse – Opens relay at specific time intervals for time period 2
Write 1 – Saves data from time period 1 as an ASCII file
Write 2 – Saves data from time period 2 as an ASCII file

Channel listing

External LVDTs
0 – West side vertical displacement
1 – West side transverse displacement
2 – West side crack width displacement
3 – East side vertical displacement
4 – East side transverse displacement
5 – East side crack width displacement

Internal readings from actuator
6 – Shear load
7 – Shear displacement
8 – Normal load
9 – Crack width displacement

Figure 2.13. DASYLab program (“cyclemax”).

3 Materials and Casting Methods

3.1 General

This aggregate interlock research used the same materials and concrete mixing procedures were used as in the previous dynamic fracture research where five different coarse aggregates were investigated. Since this phase of the aggregate interlock deals with the development of the aggregate interlock testing system only two of the five coarse aggregate types were used while also maintaining the fine aggregate constant. The concrete mix design was based on MDOT's Mortar Voids Method. The details of this procedure are described in Section 4 of this report (Hopkinson, 1998). All aggregate preparation, concrete mixing, and casting conformed to ASTM standards with exceptions noted.

3.1.1 Materials

The aggregate types used in the dynamic fracture research were crushed basalt, glacial gravel, two crushed limestones, and blast furnace slag. Of these aggregates the basalt and limestone were used in this study. The limestone was obtained from the Presque Isle quarry while the igneous basalt aggregate was obtained from Bruce Mines, Ontario.

3.1.2 Casting Methods

All concrete was mixed and cured in the concrete lab in the Civil Engineering Department at Michigan Tech. Two beam samples and three cylinders were cast per batch, with a batch size of 2.75 ft^3 (0.078 m^3). In addition, unit weight testing, slump, and air content were conducted.

The beam size was 9 x 9 x 18.25 in. (22.9 x 22.9 x 46.4 cm) for casting of the concrete samples. Standard sized 6 x 12 in. (15.2 x 30.5 cm) plastic cylinder molds were used to form the concrete cylinders. All molds were oiled prior to casting.

Before the beam molds are oiled the threaded rods were placed in the predrilled holes of the mold end plates, as shown in Figure 2.7. The rods were held in place by two nuts on either side of the end plates. Precaution was taken so as to keep oil from being applied to the threaded rods when preparing the molds.

3.1.3 Curing and Stripping

All samples were placed on a cart at the time of casting and then moved into the curing room, which was at 100 % humidity. Cylinders were stripped at 24 hrs of the time of casting. All cylinders were capped prior to testing for 28-day strength. The two beam molds were removed from the curing room prior to fracturing into two blocks. This time ranged from 8 to 12 hours.

4 Experimental Procedures

4.1 General Procedure

An important consideration in this project was the consistency and repeatability of the tests. A significant amount of effort, therefore, was expended in developing the experimental procedures used in this study. These procedures include (1) fracturing the concrete sample to create the crack interface, (2) placing the concrete blocks within the sample holders and repositioning the blocks for correct alignment, (3) initiation of the computer program, data acquisition and zeroing of LVDTs, (4) sample tear down after completion of testing, and (5) reducing the data for analysis.

4.1.1 Concrete Fracturing

After the concrete has been cast and cured for 12 hrs the sample was removed from the curing room and prepared to be fractured. After stripping the molds from the samples, the surfaces of the samples were allowed to dry for a short time for handling purposes. A groove was cut around the center of the sample using a skillsaw equipped with a masonry blade. After one side of the sample was cut the sample was rolled to the adjacent side to make another cut and so on until all four sides were grooved. The depth of the groove was 0.5 inches, which then left a reduced cross-sectional area of 8 x 8 in. at midsection of the sample. A L-shaped straight edge was constructed to produce a straight line and allow the four cuts to match up. Once the sample was cut, it was placed in the sample-fracturing device to produce the crack interface. To eliminate friction between the concrete sample and the steel base of the fracturing device, Teflon strips were placed between them. To attach the sample to the device, the "coupled end extensions" of the device are attached to the threaded rods of the sample as shown in Figure 4.1. The nuts located at the end plates were used to make final adjustments. By hand tightening the nuts at the ends, equal pressure was applied to each of the threaded rods. After insuring that all rods have equal stress on both sides of the sample, the sample was then ready to be tensioned (fractured). Using a hand hydraulic pump, pressure was increased at a constant rate until fracture occurred. The two blocks were then removed and placed back into the curing room to allow further curing until shear testing began. A fractured sample, now referred to as blocks, can be seen in Figure 4.1.

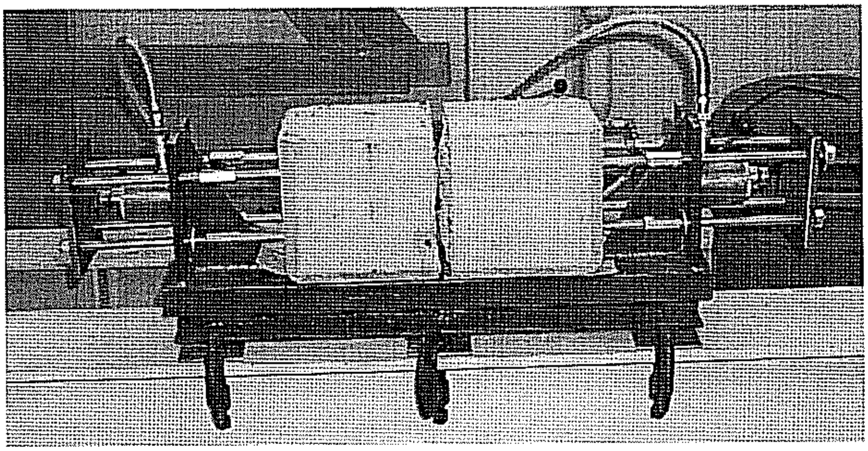

Figure 4.1. Sample after fracture creating two halves.

4.1.2 Test Preparation Methods

4.1.2.1 Installation of concrete blocks

Once the blocks were cured to a designated time, they were ready for testing. Prior to testing, the blocks were removed from the curing room early enough to allow for the sample to dry so that they would be tested in a dry condition. For trial testing the samples were set out a week before testing commenced. When preparing the blocks for testing caution was taken at all times to not disturb the fractured surface. Between the time of fracturing and testing the blocks are kept apart and are not placed back together until the time of testing.

When the blocks were ready for testing the following general steps were performed. First, the moveable platform was placed under the sample holders and horizontal actuator as shown in Figure 2.6. This allows the vertical actuator to be disconnected from the moveable half and tied off to the side for placement of the blocks. Second, each block is then placed in a holder and pushed together by hand, seating the fractured surfaces together in an attempt to minimize the damage to the interface. Third, once the fracture surfaces are together, pressure is applied by the horizontal actuator to close the remaining gap between the two surfaces. To do this an initial load of approximately 500 pounds is applied to the interface. A rubber mallet is then used to vibrate the holders allowing better seating of the interface. As the vibration causes the two surfaces to move closer together the applied load is lost since the actuator is in displacement control. A higher load is then applied in addition to vibrating the holders with the mallet. Again, if additional seating occurs load will be lost. This procedure is repeated until the interface can maintain a 1.5 kip loading without load loss due to vibration. Fourth, the vertical actuator and top plates are then connected to the sample holders. Fifth, nuts are placed on the threaded rods, which were cast into the sample ends, to secure the blocks against the sample holders. Sixth, once this is completed the platform is removed out from under the sample holders. At this point the control and data acquisition system is ready to be set up. Table 4.1 presents a detailed procedure for experimental set up of the concrete blocks.

4.1.2.2 Preparation of control and acquisition systems

After the concrete blocks have been properly installed, aligned and seated, the measurement instruments, computer control, and data acquisition are set up to control and monitor the test. Each LVDT is placed in position and adjusted to zero readings using an adjusting program in DASYLab. Two vertical displacement and transverse displacement sensors are positioned and adjusted so that a positive reading will be achieved throughout the test. At this time the vertical actuator, which applies the shear load, is then switched from displacement control to load control. This is a crucial step in the procedure, since a mistake can damage the sample before it is tested. The next crucial step is setting the crack width, which is done by controlling the horizontal actuator. After this, the crack width displacement sensors are adjusted to obtain positive readings throughout the test. At this point all readings are recorded to establish initial values, which will be used to adjust the data collected to actual displacement readings (adjusting initial value to zero). The main control and testing worksheet is then opened and initialized for testing. A pan is placed under the sample holder to retain any debris that falls during the test. Finally, the test is ready to begin. In Table 4.2 is the detailed procedure for setting up the data receiving equipment

Table 4.1. Sample placement and alignment.

1) Place the moveable platform under the horizontal actuator and adjust to bring actuator in leveled position
2) Pull the vertical actuator away from its hanging position to provide clearance for placement of concrete blocks into holders (SetPnt to -5.0 in.)[B].
3) Retract the horizontal actuator (SetPnt to -5.0 in.)[A].
4) Place blocks in sample holders.
5) Move horizontal actuator forward (SetPnt to -0.30 in.)[A].
6) Align blocks by hand to ensure a closed gap.
7) Change the scale on the horizontal controller to one inch (SETUP #2)[A].
8) Move horizontal actuator forward (SetPnt to 0.5 kips)[A].
9) Tap holders with mallet, then readjust controller (SetPnt to 0.5 kips)[A].
10) Continue seating after tapping sample until a steady 1.5 kips is obtained.
11) Release vertical actuator and reset (SetPnt to -0.2 in.)[B].
12) Insert 5/8-inch bolts to ensure alignment of top hat.
13) Adjust the vertical actuator so that the top hat is sitting directly on the concrete sample. Make sure that only a small load is applied to the sample (SetPnt w/in 1.5 kips)[B].
14) Turn nuts on bolts and tighten down by alternating sides.
15) Place the top plate on other half of sample and tighten bolts in similar manner.
16) Bolt up sample ends with washers.
17) Remove platform from below sample holders.

[A] refers to controller for horizontal actuator
[B] refers to controller for vertical actuator

Table 4.2. Preparing data acquisition and LVDTs to start testing.

1) Open up the program file 'alignment' from DASYLab and start experiment.
2) Set the vertical and side LVDT's to correct positions.
   - 2 Vertical LVDT's – metered reading roughly to 0.0 in.
   - 2 Side LVDT's – metered reading roughly to 0.125 in.
3) Record displacement from vertical actuator (SetPnt @ startvalue)[B]
4) Switch vertical controller from displacement control to load control.
   - Adjust loading before applying pressure (SetPnt to -0.60 kips)[B].
5) Adjust pressure on horizontal actuator (SetPnt to 0.0 kips)[A].
6) Set desired crack width (SetPnt to XX in.)[A].
7) Set the crack width LVDT's to correct positions.
   - 2 Crack LVDT's – metered reading roughly to 0.125 in.
8) Stop program and take initial readings of all channels.
9) Open up the program file 'cyclemax' from DASYLab.
10) Place pan under sample to retain debris.
11) Make sure everything is clear to run test safely.
12) Make sure that the 'write module' is saving the data under the correct file names.
13) Begin testing by starting DASYLab program.

[A] refers to controller for horizontal actuator
[B] refers to controller for vertical actuator

4.1.2.3 Shut down of control and acquisition systems and removal of blocks

Once the test was complete, the vertical and transverse displacement sensors were removed by swinging the bracket arm away. The bracket arm can be seen in Figure 2.11. The debris from the test was then saved for future analysis. The vertical actuator was then switched back to displacement control so that the sample can be pulled apart without additional damage. The debris that develops within the crack during the test is then collected and saved. The vertical actuator was then set to the beginning displacement value from the start of the test so the platform can be placed back under the sample holders. The vertical actuator and top plates are disconnected and removed. After the nuts on the threaded rods are taken off the sample can be removed. The concrete blocks are removed as carefully as possible minimizing damage to the interface. The fracture surfaces are inspected to observe the nature of degradation, whether it was mostly the pulverizing of the paste or the fracturing of the aggregates. Table 4.3 is a detailed procedure for removing the sample from the test frame.

Table 4.3. Test clean-up.

1) After the test has reached its failure point, which will be defined in the following section, both the actuators and DASYLab should be in a paused mode.
2) Remove LVDT's by swinging arm away.
3) Place debris from pan into labeled bag.
4) Record displacement of vertical actuator (SetPnt @ endvalue)[B].
5) Switch vertical actuator from load control to displacement control
   - Reset controller at proper position before applying pressure (SetPnt to endvalue)[A].
6) Retract horizontal actuator after placing debris pan back under sample (SetPnt to –1.0 in.)[A]
7) Change the scale on the horizontal actuator to full scale (SETUP #1)[A].
8) Brush loose debris off of sample crack interface and place in labeled bag.
9) Extract horizontal actuator to close gap (SetPnt to 0.3 in.)[A].
10) Retract vertical actuator back to start value (SetPnt to startvalue)[B].
11) Place platform back underneath actuator and sample holders.
12) The vertical actuator is shut down so that the top hat can be disconnected. The top plate can also be disconnected at this time.
13) Once the top hat is disconnected turn the vertical actuator back on and retract (SetPnt to -5.0 in.)[B].
14) Strap actuator off to side to clear for unloading.
15) Retract horizontal actuator (SetPnt to -5.0 in.)[A].
16) Unbolt sample ends and remove sample.

[A] refers to controller for horizontal actuator
[B] refers to controller for vertical actuator

If a second sample is ready to be tested, start on step #4 of Table 4.1. If a sample is not ready then the vertical actuator can be released and hydraulic pumps shut down. Note that it is necessary that the platform be left in place under the horizontal actuator when the pumps are not on.

4.1.3 Data Reduction

The data collected for the test was taken at two different time periods. The first time period is triggering the data for collection from all ten channels at every maximum shear load. Since the test is running at a frequency of 1 Hz, a data set is collected every second. The second time period is triggering the data to be collected continually for one second at a specific time duration throughout the test. Due to the large amount of data being collected, the data is reduced for analysis. Using the same software that runs the test (DASYLab 5.0) the data can be sent through a module called "Separate" that will select specific data that is desired and discards the rest. It was selected for the initial trials that the data would simply be reduced by a factor of 10, taking every tenth value while letting nine pass. Both sets of data (full and reduced) are saved on zip disks for future reference. In Table 4.4 is the procedure used in reducing the data using the DASYLab software.

Table 4.4. Data reduction.

1) Once the test has stopped, open program file 'datareduce' from DASYLab.
2) Determine that the 'read modules' are opening the correct files and that the 'write modules' are saving the data under the correct file name.
3) When the data has been completely reduced, the read modules will both indicate EOF (end of file).
4) The DASYLab program can then be stopped and data transferred to a zip disk for analysis.

5 System Performance Evaluation

The system performance evaluation consisted of three main elements. First, failure criteria had to be established such that the test could be conducted in a reasonable amount of time, but yet allow adequate evaluation of the system. Second, actual aggregate interlock tests needed to be conducted and analyzed. Finally, the overall system performance, including the test frame, sample holders, control and data acquisition, and the sample-fracturing device had to be assessed in relation to the test results. The following sections discuss these main evaluation elements.

5.1 Failure Criteria

The general failure criterion for roadway faulting across transverse joints varies from state to state, although a commonly accepted value is 0.5 inches. In this study a failure criteria was also set such that sufficient loading cycles were applied to evaluate the efficiency of the aggregate interlock. Therefore, the test needed the capability of running unattended for a relatively long period of time. One consideration was that no equipment damage would occur if the shear displacement were allowed to increase continually without set boundaries. A second consideration was the time it would take to bring a sample to reach the failure criteria. For the first criteria, a 0.5 inch max shear displacement, was set due to the restrictions of the LVDTs (as well as 0.5 inch being a generally accepted maximum displacement for faulting). The 0.5 inch criterion was programmed into the DASYLab program and the MTS 407 controllers so that the test would automatically stop if the 0.5 inch displacement was reached. Not knowing how long this would take, it was decided to run the tests for a time period of 24 hours to observe how the displacements progressed. In addition, the testing had to be within a time period that allowed for the two samples from a batch to be tested without the influence of additional curing time of the second sample. After running the first sample for 24 hours it was realized that only limited shear displacements resulted and that it would take an exceptionally long time to reach 0.5 inches. Therefore, it was decided to limit the testing to 24 hours, which represented approximately 80,000 cycles, and then to compare the shear displacement at 24 hours of the samples tested.

5.2 Aggregate Interlock Results

To evaluate the aggregate interlock tests, concrete samples were made using the two coarse aggregate types previously described (Bruce Mines and Presque Isle). After casting the samples they were later fractured in tension and cured further until testing. After being placed in the holders and seated, a crack width opening was set. This is an extremely important parameter in the testing. A small joint opening has been determined to be very effective in transferring shear and load through aggregate interlock. However, as the crack opening increases, the aggregate interlock reduces its effectiveness thus resulting in faulting.

Information from the Federal Highway Administration (1989) noted that aggregate interlock is "ineffective at crack widths greater than 0.035 inch." Furthermore, FHWA added, "a smaller crack width, generally 0.025 inch, is considered necessary for satisfactory long-term performance of undoweled pavements." Below is a table from the WSDOT Pavement Guide of seasonal joint openings (1995). To evaluate the system the joint opening or crack width was based on the measure seasonal joint opening for the state of Michigan value as reported in the WSDOT report and shown in Table 5.1. However, in reviewing the technical data from Sutherland (1956), where this information was obtained it should be noted that the 0.024 inch was a minimum value measured in contraction joints. From Table 14 in Sutherland's report the average contraction joint opening varied from 0.024 inch to 0.252 inches for a variety of joints e.g., doweled and non-doweled. These openings are also consistent with calculated joint openings using the WSDOT formulas, which can be up to 0.1 inches. In light of the range of joint openings, it was decided to conduct all the tests at 0.024 to fully evaluate the performance of the system, since this should provide good aggregate interlock efficiency. For example, if the results of the test and evaluation confirmed the effectiveness of the interface at 0.024 inch, then the performance of the test system can be better evaluated.

Table 5.1. Measured seasonal joint openings

State	Contraction Joint Spacing, ft (m)	Expansion Joint Spacing, ft (m)	Measured Seasonal Joint Opening, in. (mm)
• Oregon	15 (4.6)	5280 (1609)	0.034 (0.86)
• Michigan	10 (3.0)	2700 (823)	0.024 (0.61)
• California	15 (4.6)	5280 (1609)	0.025 (0.64)
• Minnesota	15 (4.6)	5260 (1603)	0.043 (1.09)

Three complete tests were conducted in evaluating the performance of the system. These three tests consisted of two concrete samples made from Bruce Mines coarse aggregate and one concrete sample made with Presque Isle coarse aggregate. The reason for only one Presque Isle test is due to the difficulty in producing the crack interface, which is discussed in more detail at the end of this chapter.

General Analysis

In general, all three aggregate interlock tests produced very similar results. As expected none of the tests failed completely due to shear displacement within the 24-hour period at the set crack opening of 0.024 inch. Two samples were allowed to run for 96 hours with only limited shear displacement. Analyzing the shear displacement curve (Figure 5.1), shear failure would not occur until 2.0×10^6 cycles had elapsed to reach a displacement of 0.5 inch, which would take approximately 23 days of testing. However, it is not known whether by continuing the test the displacement would have developed at the same rate, or would possibly at some time increase its rate to reach the half-inch displacement sooner.

As mentioned previously the results of the three tests were all relatively similar. Therefore, only the results from one of the tests, the Presque Isle aggregate concrete, are discussed in detail. However, the Bruce Mine aggregate concrete results are provided in

Appendix C. The results from the Presque Isle aggregate tests are shown in Figures 5.1 to 5.6. In general, it appears that the shear and transverse displacement have three stages. The first stage appears to be a seating period. The second stage develops as the interface stiffness increases. Finally, the third stage appears to develop as the interface stiffness becomes relatively constant. The different stages are believed to result from the initial seating of the two concrete surfaces under shear load, as well as loose material in the crack interface breaking down initially to allow for shear displacement. During this period the sample appeared to slightly twist as the interface attempts to find the path of least resistance, which is seen mostly in the transverse displacement curves. The movement appears to be more three-dimensional rather than the single one-dimensional movement in the vertical direction, which is generally assumed. As the loose material wears down and the stiffness of the system begins to increase the shear displacement becomes relatively constant but does continue to increase slightly as the concrete interface starts to break down and aggregate interlock becomes less effective. In light of this initial three-dimensional movement the results suggest that the test performed closely to what was expected, i.e., an increase in shear displacement with increase in number of cycles at a constant shear load. In addition, normal stress develops at the interface due to dilation of the interface and the restraint of the horizontal actuator maintaining a constant crack width, i.e., the interface is restrained from movement thus generating normal stresses. However, at the initiation of the shear loading this vertical load is resisted by both shear and vertical normal resistance of the concrete surfaces. As shear loading continues the interface breaks down, thus reducing the vertical normal resistance. This then results in an increase in the horizontal normal stress, which is monitored by the load cell.

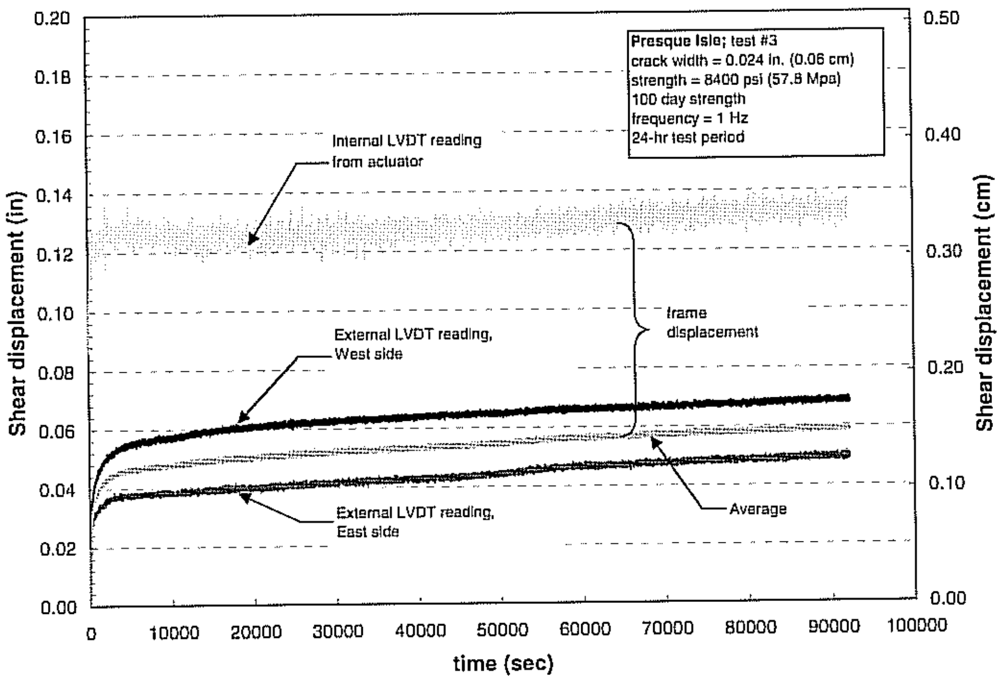

Figure 5.1. Shear displacement from aggregate interlock test (test #3).

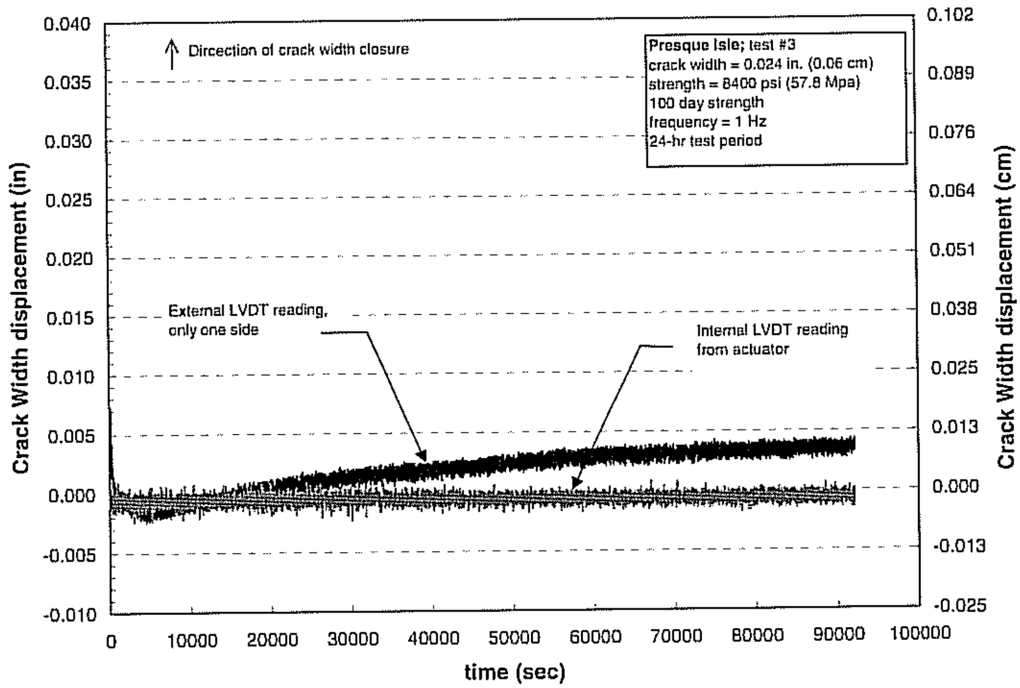

Figure 5.2. Crack width displacement from aggregate interlock test (test #3).

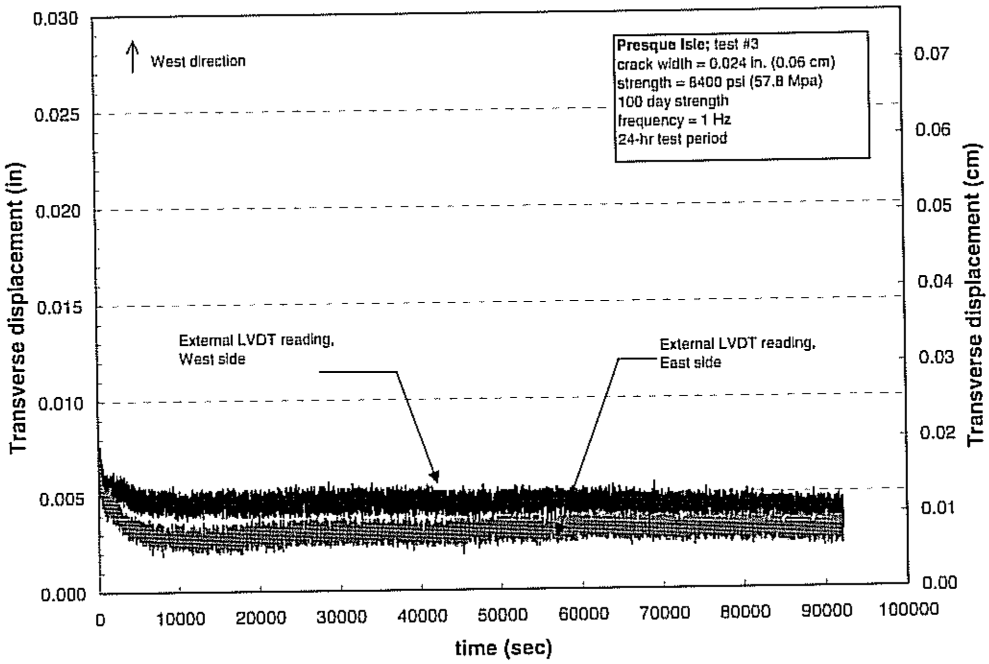

Figure 5.3. Transverse displacement from aggregate interlock test (test #3).

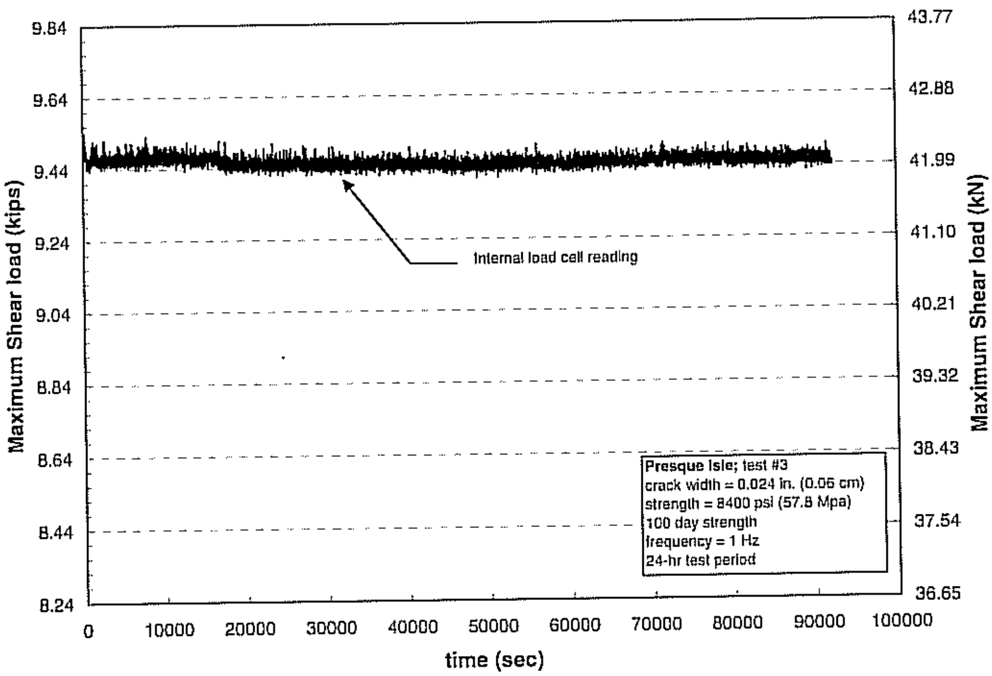

Figure 5.4. Maximum shear load from aggregate interlock test (test #3).

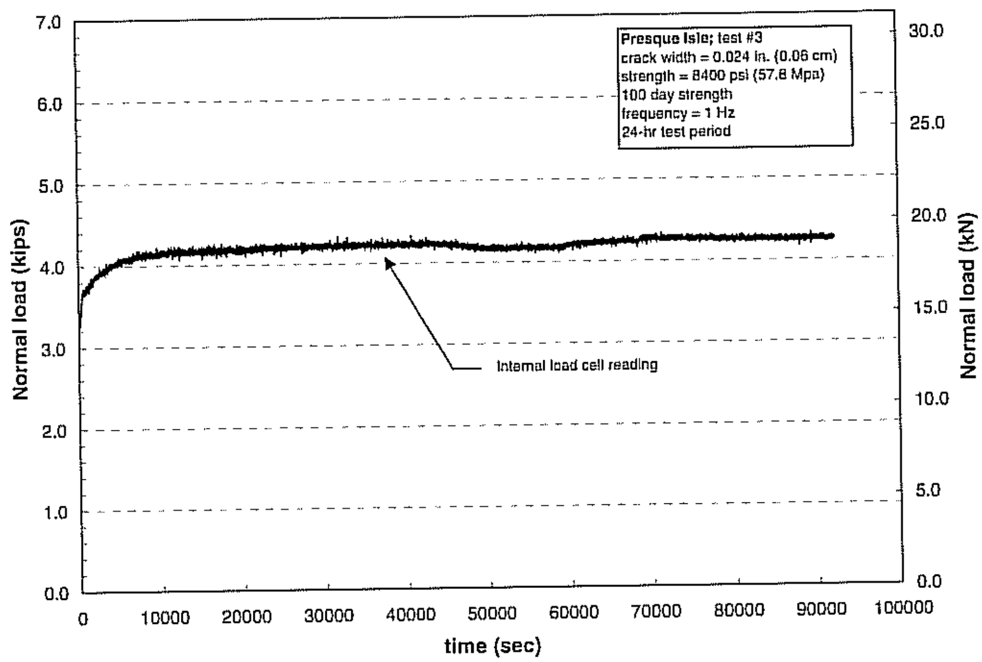

Figure 5.5. Normal load from aggregate interlock test (test #3).

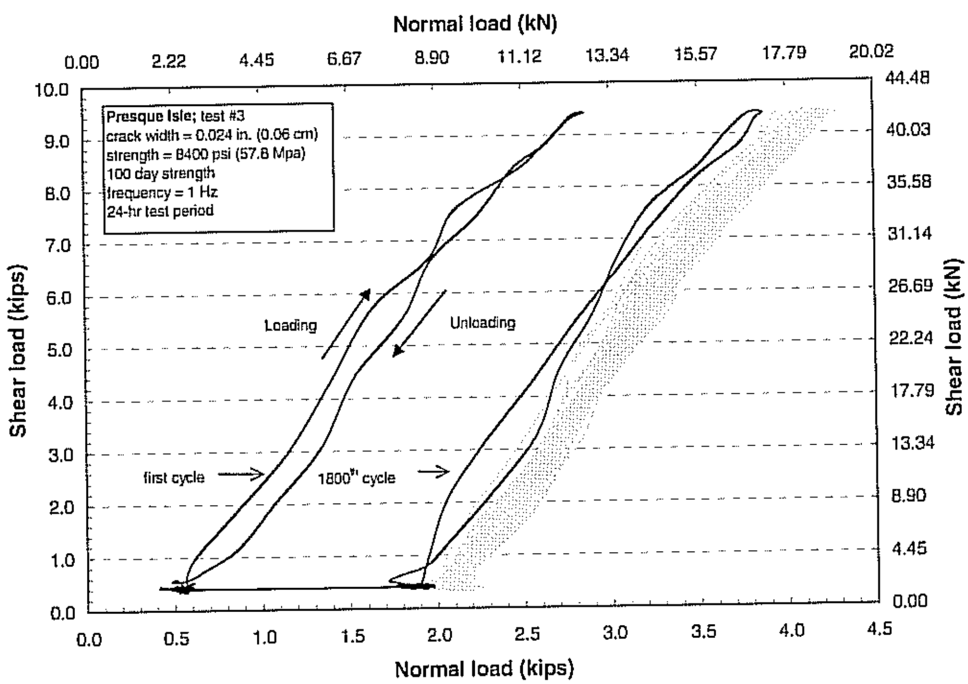

Figure 5.6. Shear vs. normal load for aggregate interlock test (test #3).

5.2.2 Detailed Analysis

The data collected from each test included vertical loading, shear displacement, crack width displacement (longitudinal), transverse displacement, and normal load. As mentioned, the results for the Presque Isle are presented in Figures 5.1 through 5.6. A detailed discussion on each of these figures is provided below.

The shear displacements, i.e. relative vertical movement between concrete blocks, were monitored during the test with two external LVDTs and the internal LVDT from the vertical actuator. All three of these readings have been plotted and are presented in Figure 5.1. The difference between the external and internal readings is due to the deflection of the frame. A big part of this deflection is due to the cantilevered position of the fixed sample holder as shown in Figure 5.7. Observation of the displacement of the fixed-end sample holder during the tests drew concern as to whether this holder should be stiffened, thus preventing vertical displacement during testing. A more detailed discussion concerning this matter is provided later in the next section. The difference between the two external LVDT readings was found to be the fault of a slight malfunction of the braces that mounted the sensors to the fixed half of the sample holder. This was later solved and was not a problem in additional testing. For this discussion, the two external LVDT readings have been averaged for comparisons.

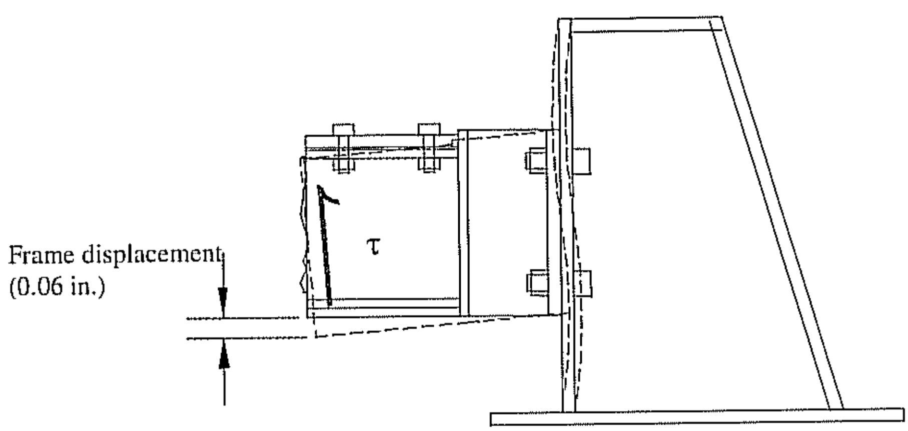

Figure 5.7. Movement of fixed-end holder.

The crack width displacement or joint movement during the test was monitored with a single external LVDT and the internal LVDT from the horizontal actuator. These readings are provided in Figure 5.2. It was planned to use two external LVDTs, but at the time of testing the second LVDT was malfunctioning and had to be sent back to the manufacture. In Figure 5.2 the crack width setting of 0.024 in. represents the origin. Also, note the indicated direction of crack closure on the figure. While the external reading shows that the sample had a rapid change in crack width during the first few cycles, followed by a slight change throughout the test, the internal reading suggests that it stayed constant. An explanation of this effect is due to the sample twisting slightly at the beginning of the test, but with the movement averaging out throughout the area of the crack interface as shown by the internal reading. That is, while on one side the crack width is opening on the other side is closing and the two together average to no movement. The actuators are equipped with swivels heads to allow rotation. While the vertical actuator swivel head is tightened at the end of the sample holder to restrict the motion, the top end is free to move, as are both ends of the horizontal actuator. This allows the sample to twist, but still maintain an average constant crack width. For future testing, four LVDTs will be used to monitor the movement at each corner, thus better describing the movement of the crack width.

Figure 5.3 plots the transverse displacement of the load-bearing block during testing. As discussed above the transverse movement of a sample under a shearing force should not occur due to the cancellation of forces in this direction. The transverse displacement for the tests were monitored with two external LVDTs as illustrated in Fig. 2.11. According to the readings the sample did move in one direction approximately 13 percent of the initial setting of the crack width opening of 0.024 inches. This would seem reasonable because there is no restraint in the transverse direction and the sample was seating itself under the initial 9,000 lb. load. Therefore, the two concrete surfaces moved until they made contact, in which the movement could be in both the vertical and transverse directions. However, it should be noted that the total transverse movement was approximately 0.003 inches while the vertical displacement was approximately 0.06 inches and therefore only represented 5% of the vertical movement. At the point when contact was made the transverse displacement remained constant, proving the validity of that the transverse shear forces cancel out.

The shear load was monitored with the load cell within the vertical actuator. A plot of this data can be found in Fig. 5.4. As noted the maximum shear load for the Presque Isle sample was close to 9.5 kips. The control signal was designed for a maximum load of 9.0 kips, however a calibration offset increased it an additional 400 lb. To be consistent, the other tests were all kept with the same control signal, although the actual load reading varied from 9.2 to 9.4 kips between all tests. As can be observed in Figure 5.4 the loading remained constant throughout the remainder of the test. However, the remaining two tests, which can be viewed in the appendix, appeared to develop some irregularity at the beginning of the test. This irregularity was believed to be due to the PID control settings of the MTS controllers not matching the initial stiffness of the interface. Although, soon after the initial cycles the loading became constant when the stiffness of the interface better matched the set PID control parameters. It should be noted that the control of a closed loop system is dependent on the PID control setting, which is set based on the stiffness of the material being tested. For example, at the beginning of a test when the shearing action is breaking down the loose material the stiffness of the system is changing dramatically. Once the stiffness increases the controllers can then adjust and keep up with the changes. For all three tests the shear load did remain constant after the first 5000 cycles.

The normal load was monitored by the load cell within the horizontal actuator and is shown in Figure 5.5. The data shows that the normal load increases with the initial cycles, indicating that in the early shear cycles the crack interface is breaking down and wearing the surfaces of the concrete so that dilation begins to increase which results in an increase in horizontal normal loading. The normal load did increase slightly over the duration of testing, again similar to what was expected.

All of the data presented in Figures 5.1 to 5.5 represents the peak values from each loading cycle. A plot of the shear vs. normal load data for the complete cycles is shown in Fig. 5.6, where every 1800th cycle is presented starting with cycle one. For the first Bruce Mines and Presque Isle samples the increment was set at 30 min, i.e., DASYLab collected a full cycle of data every 30 minutes or 1800 seconds (or 1800th

cycle). The second Bruce Mines sample had a time increment of 1 hour. The first two cycles, which were recorded (cycle 1 and cycle 1800), are indicated by a darker shade in Figure 5.6 than the following cycles. This graph shows the normal load stabilizing through this time period of testing for a given shear load, which would be indicative of an efficient interface. That is, one that transfers the shear load without inducing an increase in dilation. Again, this would be consistent with a crack width of 0.024 inches, which was determined to be an effective crack width for aggregate interlock regardless of coarse aggregate type.

5.3 Overall System Performance

The overall functionality of the structural frame and holders appeared to work well. Structurally the frame was found to be sound. Both actuators were loaded to 2/3 of the maximum load (55 kips) with no signs of distress or noticeable deformations. One of the major design features of the test system was in utilization and ease of operation. The system for placing the concrete blocks into the holders worked well, even though the concrete blocks were lifted into place by hand, the design was such that they could be put into place and secured within a reasonable amount of time. However, an exception is that the operator had to have the capability of lifting and inserting the concrete block into the holders, which weighed approximately 65 pounds.

The most important part in successfully operating the system is the operator's working knowledge of the MTS 407 controllers and DASYLab program. The procedures that have been included in chapter four rely on the ability of the operator to understand those two systems. The estimated time spent on testing a sample was an overall design criterion from the beginning. The time required for testing a sample is divided into a number of steps and presented in Table 5.2. Overall the time to prepare and test a sample based on a 24-hour test period is 32 hours, while testing took on average 8.25 hours.

Table 5.2. Time commitment for testing a single sample

	time commitment
aggregate preparation	4.00 hr.
mixing	1.00 hr.
stripping and block splitting	1.25 hr.
test set-up	1.50 hr.
duration of test	24.00 hr.
test clean-up	0.50 hr.
Total	32.25 hr.

While the structural integrity of the frame and holders functioned well, it was noticed that the fixed-end holder had noticeable deflections during testing, as discussed in the previous section. This deformation had a maximum vertical displacement of approximately 0.06 inches. In addition to the maximum displacement during the loading cycle there also appeared to be a vibrational response of the system. The effects of this response can be seen in the normal load measured by the horizontal actuator during testing and is shown in Figure 5.8. These responses, the 0.06 inch displacement of the fixed-end holder and the vibrational response immediately following the loading cycle, present concerns regarding system performance. An additional concern can be observed in Figure 5.6 and 5.8 in which the normal load does not return to zero during the 0.9 second no load period of the loading cycle. Although, a 100-pound load is maintained on the vertical actuator (to maintain stability in load control), the corresponding normal should be similar or less than 100 lb. However, from Figure 5.6 and 5.8 it can be seen that at the minimum shear load the normal load is approximately 2,000 lb.

In investigating these concerns it became apparent that the main reason for this occurrence was that the two concrete blocks were coming into contact with each other, as opposed to contact being initiated by aggregate interlock. This became obvious when calculating the geometry of the interface at maximum deflection. From Figure 5.7 it can be seen that the fixed-end holder rotates during testing to a maximum displacement of 0.06 inches. In addition the load-bearing end holder also rotates but at a greater radius of curvature due to the length of the horizontal actuator. Consequently, there will be closure of the crack width at the top of the concrete blocks while the bottom will open up, thus not maintaining parallel surfaces. While it was recognized that there would be some minor rotation of the load-bearing holder, the rotation of the fixed-end holder was not considered and assumed to be stiff enough to prevent substantial deformation. A conservative estimate of the amount of closing and opening can be made assuming the following criteria: 1) a maximum deflection of the fixed-end holder of 0.06 inches, 2) a crack width of 0.024 inches, 3) a rotational arm of the fix-end holder of 15 inches, 4) a rotational arm of the load-bearing holder of 84 inches and 5) that the rotation is along the centerline of the test system. Given these assumptions it was calculated that the fixed-end holder will rotate a maximum 0.03 inches, while the load-bearing holder will rotate a maximum of 0.006 inches due to its longer rotation arm. At maximum deflection the bottom crack width will be at an opening of 0.07 inches while the top is closed at -0.012 inches indicating that the concrete is in contact.

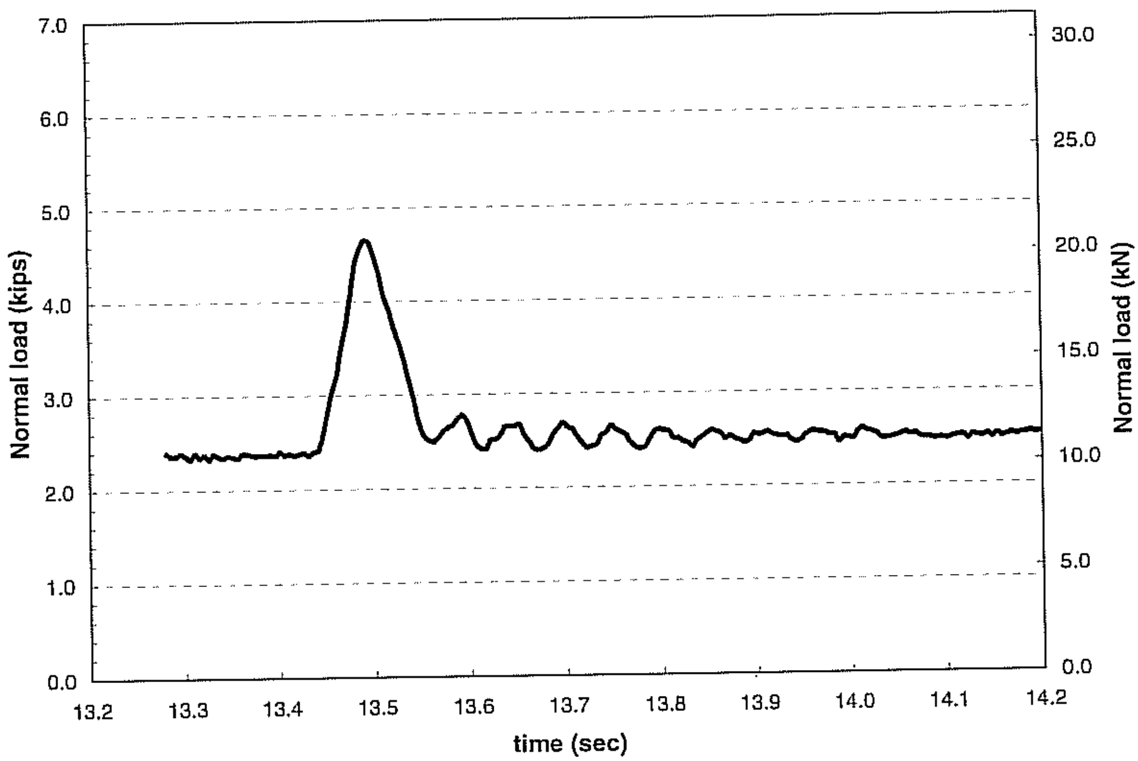

Figure 5.8. Typical cycle of normal load.

Two possible explanations for the normal load not reducing to zero are as follows: 1) a wedging effect of the concrete in contact and 2) the actual seating condition from the initial cycles relatively closes the gap. Although, it is not known exactly why the wedging effect continues after the shear load has reduced to zero within the cycle, but it may be due to conducting the loading in load control as well as the stiffness of the interface, e.g., it doesn't take much of a displacement to relieve the 9 kip vertical load, thus keeping the interface in a weighed condition. Therefore, being in a wedge condition with the vertical actuator in load control allows for the normal load (approx. 2,000 lb) to be maintained at the interface in addition to transferring the vibrational response as shown in Figure 5.8 of the fixed-end holder. However, this may be somewhat realistic for field conditions especially with narrow crack widths such as 0.024 inches. For example, Huang (1993) illustrates a field distress in Figure 5.9, where deflection of the pavement indicates the same situation. It is unknown at this point how this situation may or may not relate to our test situation. Obviously, both the rigidity of the pavement and stiffness of the base material play an important role in the development of this situation.

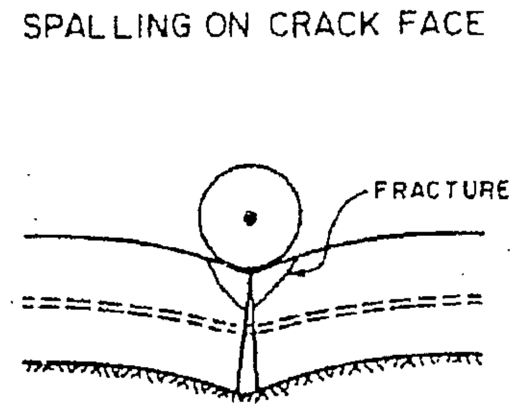

Figure 5.9. Deflections of pavement under vehicle loading

The second possibility is that the shear loading simply places the two surfaces in contact. Once in contact the vertical shearing load generates a normal load across the interface. However, upon releasing the shearing load, which is in load control and requires only an insignificant amount of displacement to release, a portion of the normal is maintained at the interface due to friction. In turn, the surfaces remain in contact.

5.4 Sample-Fracturing Performance

An essential aspect of studying aggregate interlock is producing fracture surfaces in test samples similar to those in field contraction joints, which required the development of the sample-fracturing device described in chapter two. The main task of this device was to fracture the concrete in tension, simulating shrinkage conditions. As discussed in chapter two a major consideration was the time at which to fracture the freshly cast concrete. According to personnel at the University of Illinois, they fractured their concrete at eight hours due primarily to the load limitations of their device. Following this example, eight hours was selected to fracture the initial test sample in this study. The first sample tested in the device was a gravel aggregate PCC, but it did not fracture along the inscribed groove. Instead, failure occurred at one end of the sample as shown in Figure 5.10. The next sand and gravel sample was then tested at ten hours, which did fracture at the correct position. In fracturing the two Bruce Mines concrete samples at the ten-hour period, both had fractured at the inscribed groove. However, this was not the case for the first Presque Isle sample, which fractured in the same manner as shown in Figure 5.10. To avoid this occurring with the second sample, it was fractured at 12 hours, at which it fractured correctly. Two possibilities were reviewed to account for this incorrect fracture. One possibility is that the concrete cross-sectional area at the intended fracture surface is larger than the concrete cross-sectional area at the nut location. The second possibility is that the hydraulic cylinders were not seated against the bearing plates correctly causing additional forces to react on the sample other than tension. The first possibility is ruled out with some simple calculations, proving that the concrete cross-sectional area at the groove was less than the cross-sectional area at the location of the nuts. To eliminate the second possibility, the holes on the bearing plates that allow the extended rods to pass through and attach to the concrete sample were enlarged so that the system can be better adjusted and aligned with the cylinders. If at all possible, the fracture tests should be conducted at the same time. The later the fracture tests are conducted the stronger the mortar becomes. This then may cause more fracture through the aggregate as opposed to pullout failure around the aggregate particles. An additional consideration is that it is likely that the later the fracture test, the less irregular the fracture surface will become. That is, later fracture tests may be straighter, resulting in less aggregate interlock.

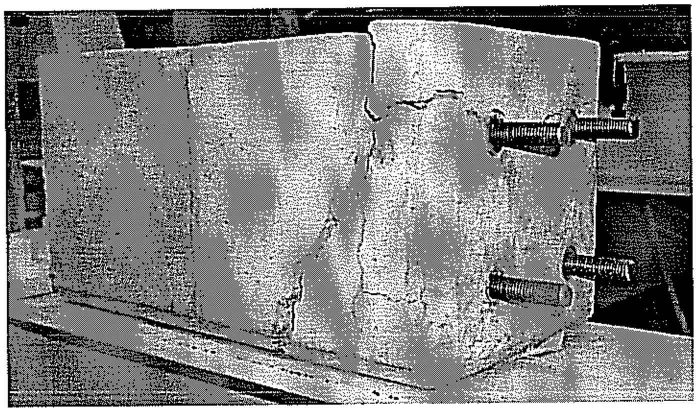

Figure 5.10. Incorrect fracture of sample.

6 Conclusions and Recommendations

The objective of this study was the design, construction, and evaluation of a test system for investigating the mechanics of aggregate interlock,. concentrating on the effect of different types of coarse aggregate. The result of this work was a functional test system. In addition, during the evaluation of the test system a number of learning experiences have occurred that will be used to modify the test system for future research. This chapter provides the conclusions developed in this work along with recommendations for future studies.

6.1 Conclusions

Based on the research conducted in this study, the following conclusions have been reached:

1) The design, fabrication and construction of the structural frame and sample holders functioned well for their intended purpose, providing a frame that was structurally sound and adaptable for other research requirements. In addition, the sample holders performed very well securely restraining the concrete blocks in place during testing. It was also found that the utilization of the holders, such as inserting the concrete blocks and alignment could be accomplished in an efficient manner.

2) The concrete fracturing device performed moderately well in developing the fractured surfaces used in this study. It is believed that the method of fracturing replicates field conditions better than by other methods used by other researchers.

3) The control and data acquisition system performed well together. The control signal was easily transferred to the 407 controller and proved to be an adequate control system.

4) Procedures that were developed allowed for minimal differences to occur between the testing of multiple samples. For example, each sample that is tested would undergo the same methods of handling from the beginning, where the concrete is cast in the mold, to the end, where the sample is removed from the sample holders at the end of testing.

5) The operation of the entire system required minimal operator time although this required a working knowledge of DASYLab and the MTS controllers.

6) It is believed that the test system appears to closely replicate aggregate interlock at contraction joints. However, some concern exists concerning the stiffness of the fixed-end holder, which may generate too much deflection and may need to be stiffened. In addition the twisting of the vertical actuator unit is of some concern as whether the surfaces remain parallel throughout the time of testing.

6.2 Recommendations for Future Work

A number of improvement areas have been mentioned in this paper. In the continuation of the work certain areas will have to be modified. A few of the most important recommendations will be discussed in this section.

An important need in this research is to better understand when contraction joint cracks are formed in the field, i.e., at what time do the stresses in the pavements overcome the concrete strength capacity? Once this is known, a better way of producing the sample in the lab can be achieved. For example, if the stress is continually gaining throughout the life of the concrete in the field then maybe the sample should be set up so that a scaled increase in stress is replicated in the lab until the crack forms. It's believed that both the strength and level of stresses generated in a pavement are increasing during the first few days of curing, but at some point the stresses generated are higher than the bonding force that keeps the concrete panels together and a crack is formed. Instead of a quick break to form the crack in the sample, a slower, more controlled break may be needed. Another benefit would be to replace the hand pump used in the splitting of the sample with an automated pump to achieve a constant loading rate.

It is important in the future work to stay focused on developing better ways in testing the samples. The direction of which the research takes is very critical in the usefulness of the data obtained. The following is the suggested direction that might want to be considered:

1. **Accelerated test conditions:** For a larger testing range and possibly the ability capture how a sample fails, an accelerated test should be considered. Increasing the frequency of loading or increase the amplitude of the applied loading can accomplish this. Both would result in obtaining a greater life history of the sample being tested by staying with the set 24-hour period. The time duration of the test could be altered as well, but

is suggest to stay within a time period so that testing of the second sample within a single batch is not introduced to additional curing time to effect the comparison of the two.

2. **Multiple tests at various constant crack widths:** For a better understanding of the mechanism of shear transfer, various crack width settings should be tested. With the current setting at 0.024 inches the rates of degradation between the tests seems to be constant. Changing the number of contact points by increasing the crack width opening might trigger different characteristics of the aggregate within the concrete to become more visible in the reaction of restraining the applied loading. Testing samples at different crack widths would provide a measure of efficiency of aggregate interlock for each type of coarse aggregate tested.

3. **Changing crack width during test:** A specific joint in the pavement does not sustain a constant crack width throughout it's life. During the course of a year the pavement goes through expansion and shrinkage cycles due to temperature change. Therefore there are times that the pavement joint opening is at 0.024 in. and other times, most likely in the winter months, that the crack width is much larger. The life span of a joint in a pavement depends on this cyclic movement. With the capabilities of the dual actuators in the system a scaled version of this cycle could be replicated. While the vertical actuator is administering the shear loading the horizontal actuator could in fact be cycling at the same time. For instance, if the frequency of the shear loading was kept at 1 Hz then the crack width could open and close with a range of 0.024-0.06 in. within a time period of 12 hours. This would better replicate the conditions in the field.

Appendix A

Detailed sketches for construction

Self Reaction Frame

design based on 50 ksi on rolled steel, 36 ksi on plates

Column and Beam Schedule

Description	Drawing Detail	Size	Length (in)	no.	bolt holes drilled (/each)	Remark
Column	C7	W10 x 49	240	2	54	
Long. Beams	C5	W10 x 60	360	2	62	
Sample Beam	C6	W10 x 60	240	1	28	
Cross Beams	C4	W10 x 60	94	3	26	
Mid. Cross Beam	C8	W16 x 67	84.5	1	12	
Top Cross Beam	C9	W12 x 26	84.5	1		
Diagonal Brace	C10	L4 x 4 x 3/8	67	4	1	

Plate Steel Schedule

Description	Drawing Detail	Size (in)	no.	bolt holes drilled (/each)	Remark
Col. end plates	C3	12 x 22 x 0.75	2	8	
Cross beam plates	C1	12 x 22 x 0.75	10	8	
Mid. Beam end plates	C2	11.5 x 30 x 0.75	2	8	
Top Beam end plates	C2	9.5 x 24.5 x 0.75	2	8	
Diagonal brace end plates	C10	7 x 5 x 0.5	4	1	
Bulk Head			*2*		*Total*
Act. plate	C11	17.25 x 10 x 0.75	2	4	
End plate	C11	25 x 10 x 0.75	2	8	
Web plate	C11	16.5 x 16 x 0.75	2		See sketch, Top is cut down to 9"
Top plate	C11	10 x 10 x 0.75	2		See sketch, length is approx.
Back plate	C11	18.75 X 10 x 0.75	2		See sketch, length is approx.
Stiffeners					
Col. end plate stiffeners	C3	18 x 10 x 0.75	2		Rt. Triangle
Long. Beam stiffeners	C5	8.86* x 4 x 0.5	28	3	* through depth of web on W10 x 60
Mid. Beam stiffener	C8	15* x 4.5 x 0.5	2		* through depth of web on W16 x 67
Sample Beam stiffeners	C6	8.86* x 4 x 0.5	4		* through depth of web on W10 x 60

Total number of holes in all pieces		548
Total number of bolts (A490 7/8" dia. - various length)		182
	lengths (in)	
	2.0	22
	2.25	48
	2.5	112
	Total	182

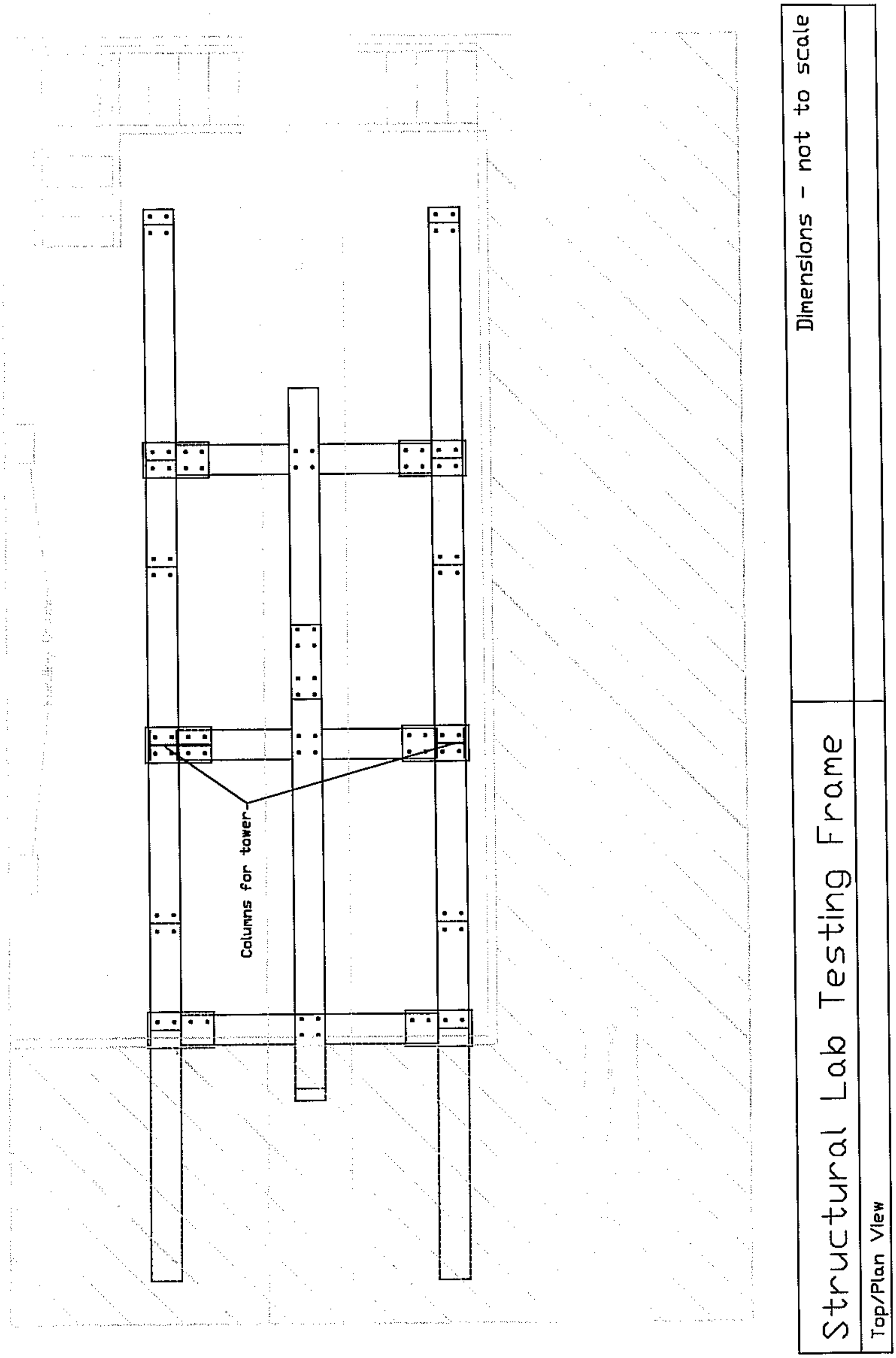
Columns for tower
Dimensions - not to scale
Structural Lab Testing Frame
Top/Plan View

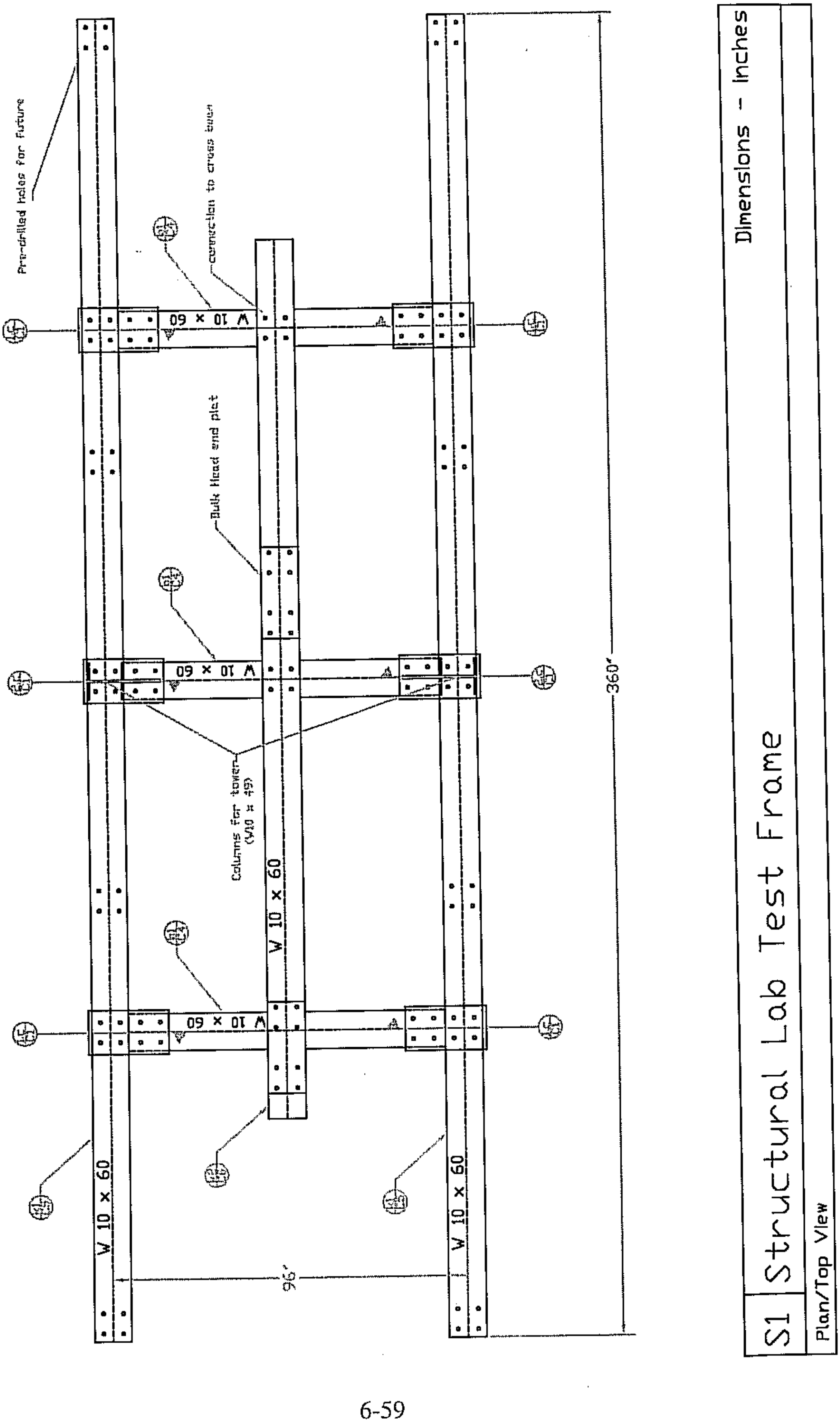
Pre-drilled holes for future
connection to cross beam
Bulk Head end plat
Columns for tower
(W10 x 49)
W 10 x 60
W 10 x 60
W 10 x 60
W 10 x 60
W 10 x 60
W 10 x 60
W 10 x 60
360"
96"
Dimensions - Inches
S1 Structural Lab Test Frame
Plan/Top View

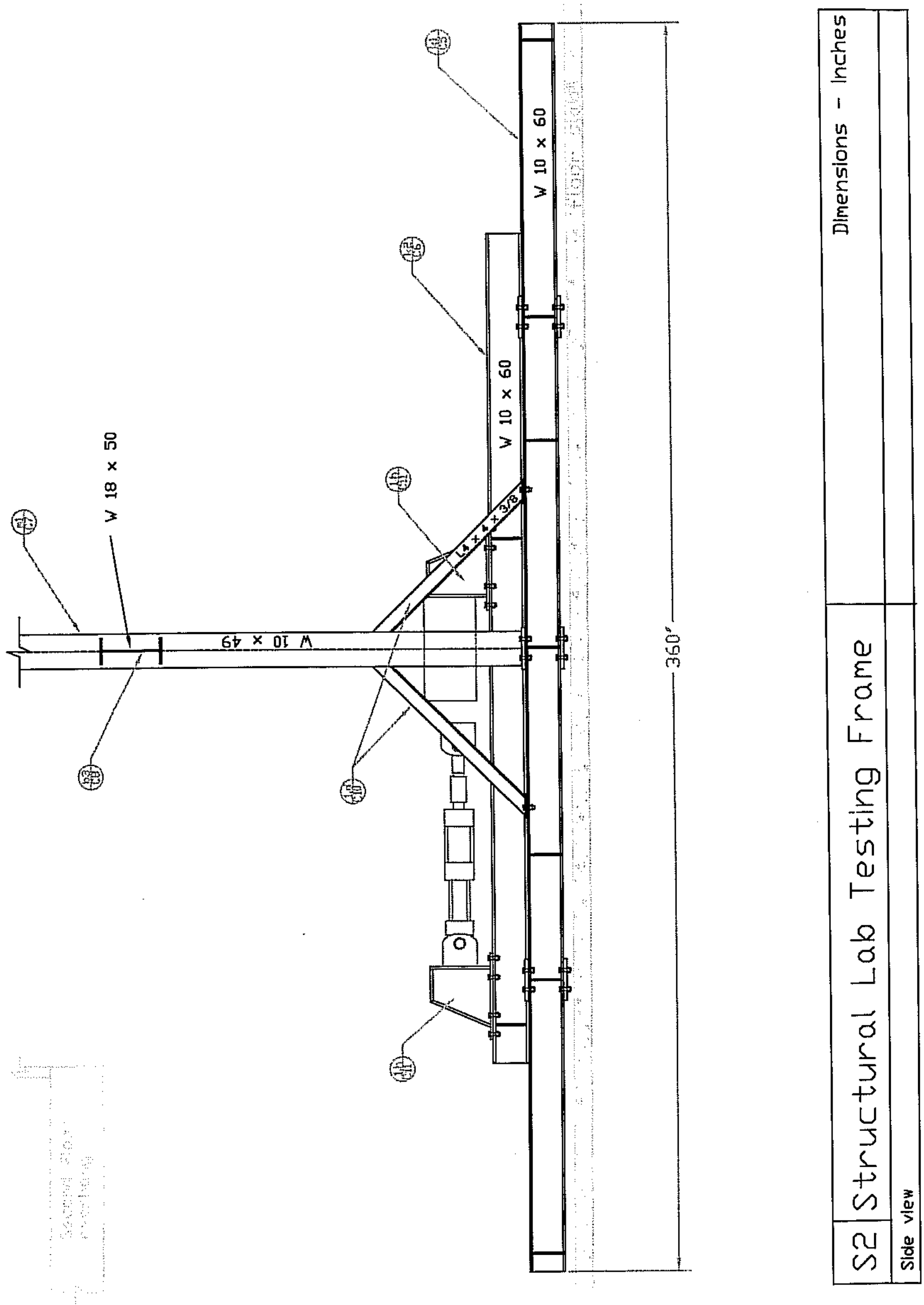
W 18 x 50
W 10 x 49
W 10 x 60
W 10 x 60
L4 x 4 x 3/8
360"
S2 Structural Lab Testing Frame
Side view
Dimensions - Inches

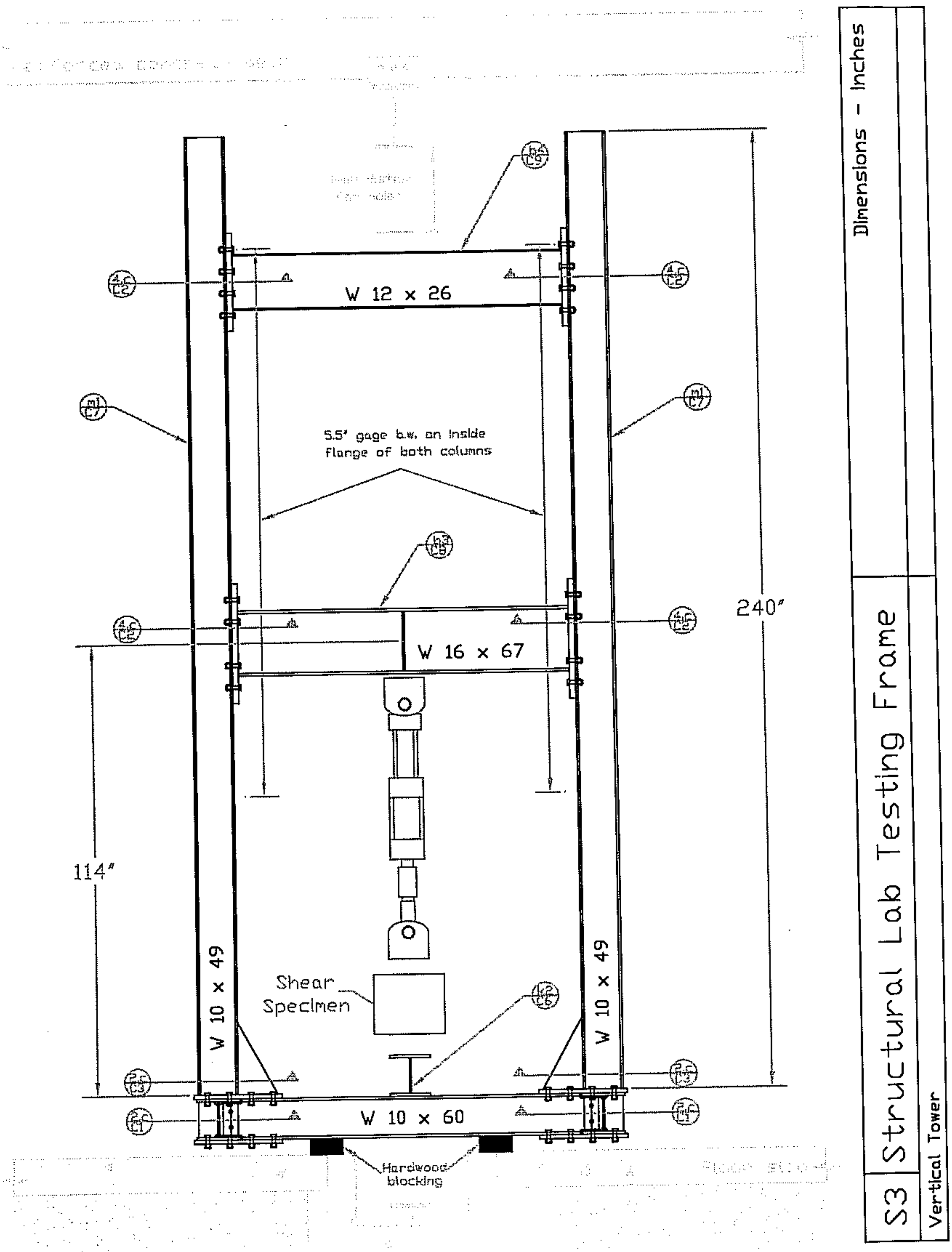
W 12 x 26
5.5" gage b.w. on inside flange of both columns
W 16 x 67
240"
114"
W 10 x 49
W 10 x 49
Shear Specimen
W 10 x 60
Hardwood blocking
Dimensions - Inches
S3 Structural Lab Testing Frame
Vertical Tower

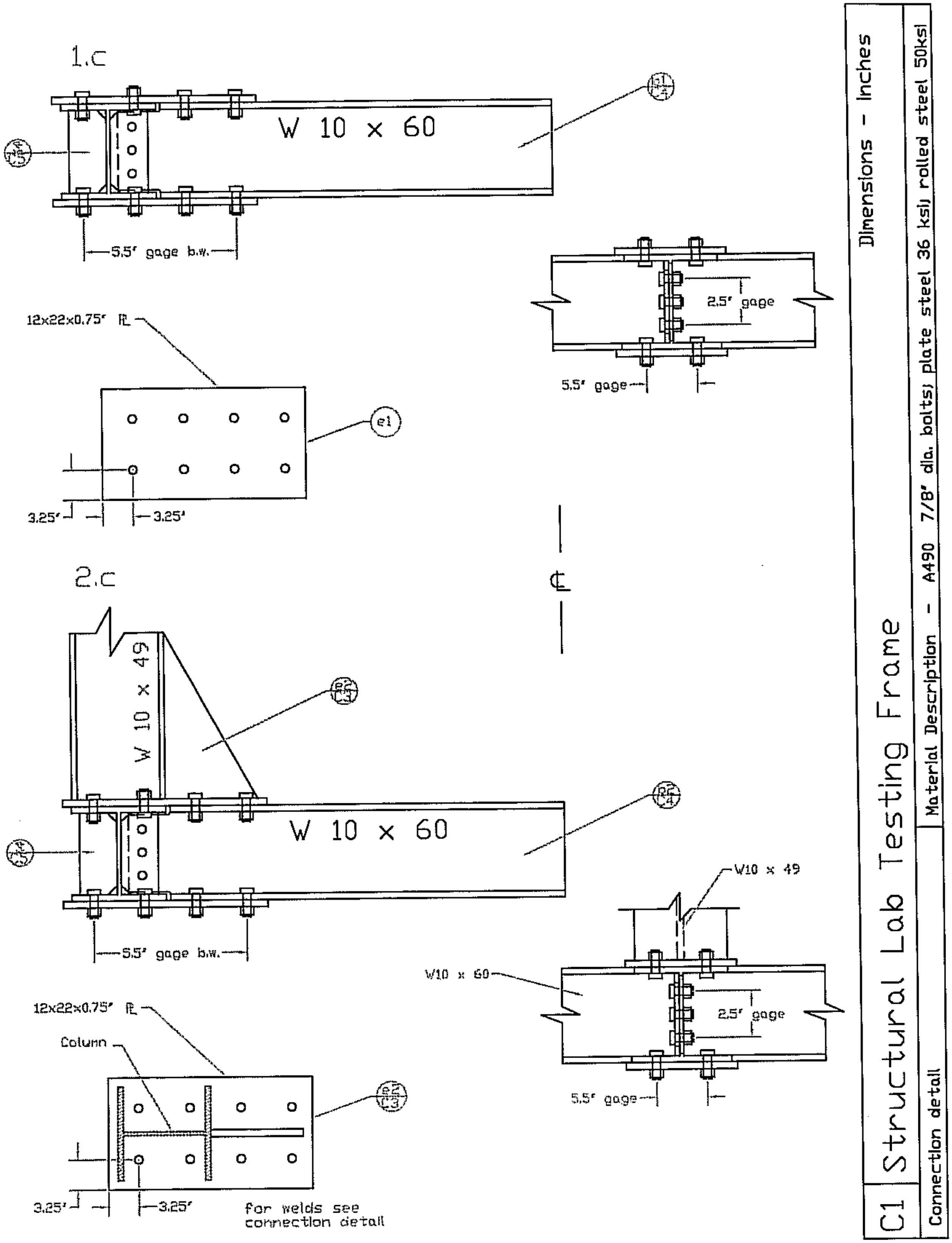
1.c
W 10 x 60
5.5" gage b.w.
12x22x0.75" PL
2.5" gage
5.5" gage
3.25"
3.25"
2.c
W 10 x 49
W 10 x 60
5.5" gage b.w.
W10 x 49
W10 x 60
2.5" gage
5.5" gage
12x22x0.75" PL
Column
3.25"
3.25"
For welds see connection detail
Dimensions - Inches
C1 Structural Lab Testing Frame
Material Description - A490 7/8" dia. bolts; plate steel 36 ksi; rolled steel 50ksi
Connection detail

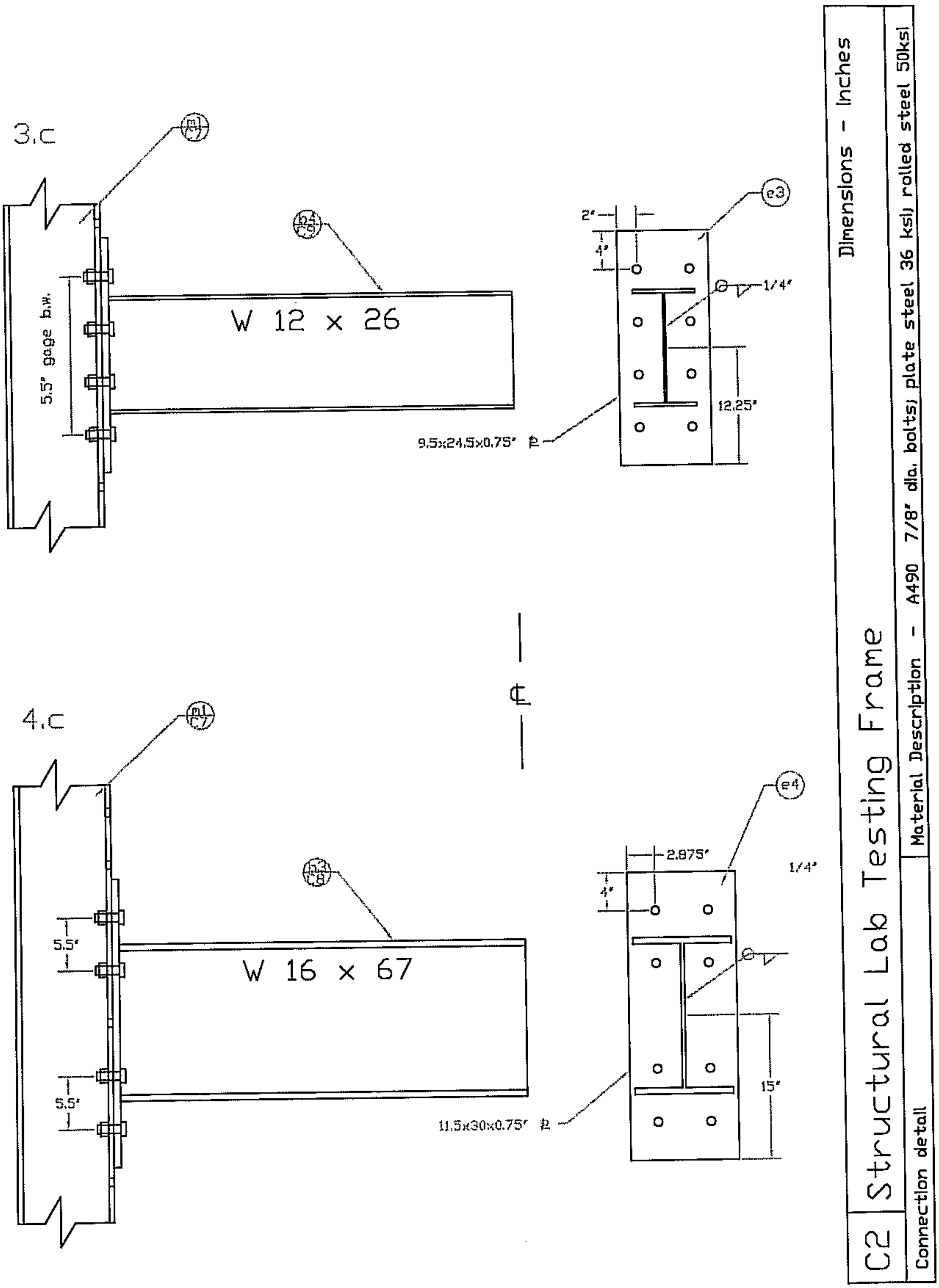
3.c
m1 C7
b4 C5
W 12 x 26
5.5" gage b.w.
e3
2"
4"
1/4"
12.25"
9.5x24.5x0.75" PL
4.c
m1 C7
b3 C8
W 16 x 67
5.5"
5.5"
e4
2.875"
4"
1/4"
15"
11.5x30x0.75" PL
℄
Dimensions - Inches
C2 Structural Lab Testing Frame
Material Description - A490 7/8" dia. bolts; plate steel 36 ksi; rolled steel 50ksi
Connection detail

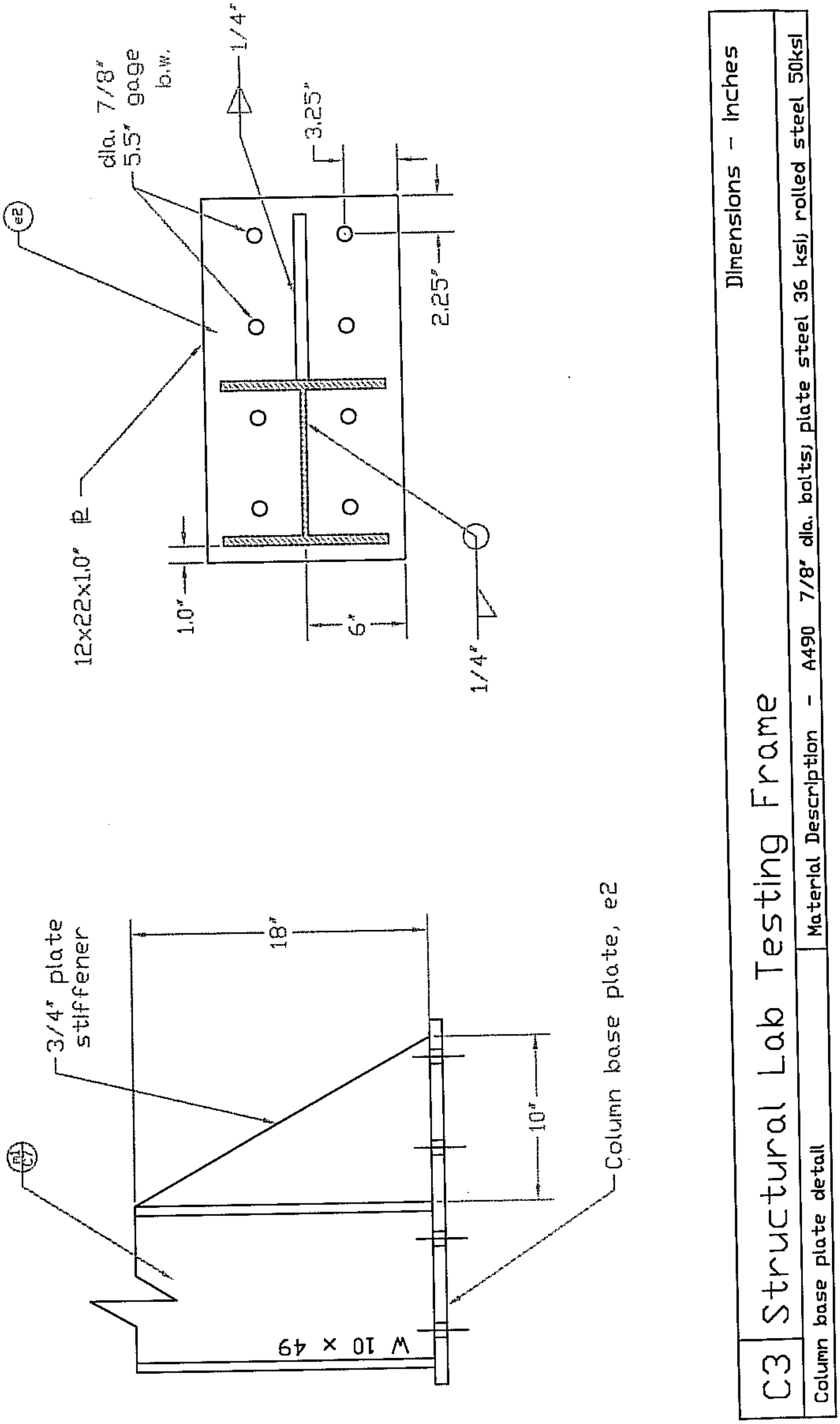
C3 Structural Lab Testing Frame
Dimensions - Inches
Column base plate detail
Material Description - A490 7/8" dia. bolts; plate steel 36 ksi; rolled steel 50ksi
W 10 × 49
3/4" plate stiffener
18"
10"
Column base plate, e2
12x22x1.0" ℙ
dia. 7/8"
5.5" gage
b.w.
1/4"
3.25"
2.25"
1.0"
6"
1/4"

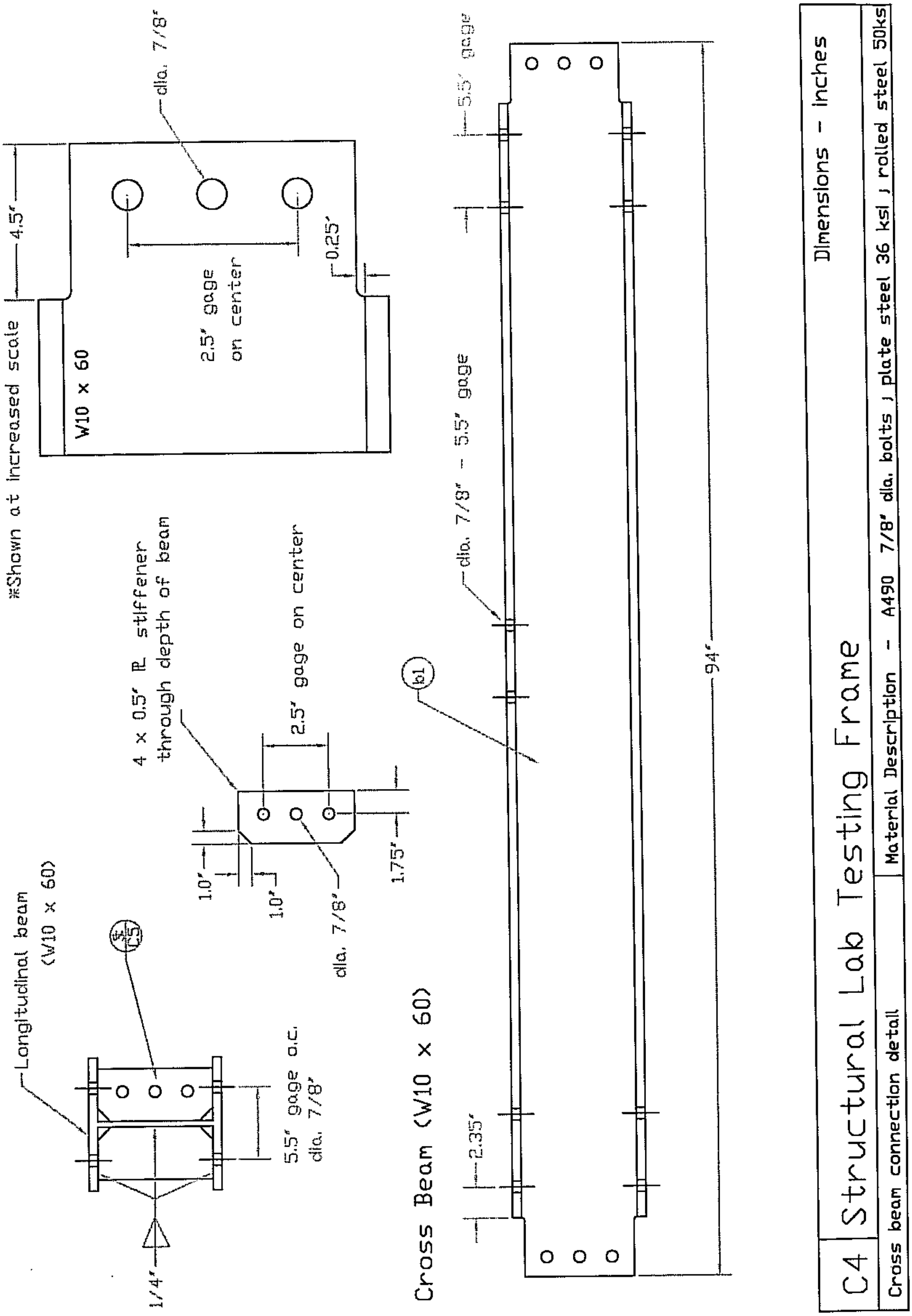
*Shown at increased scale
4.5"
dia. 7/8"
W10 x 60
2.5" gage
on center
0.25"
Longitudinal beam
(W10 x 60)
1/4"
5.5" gage o.c.
dia. 7/8"
4 x 0.5" PL stiffener
through depth of beam
2.5" gage on center
2.5"
1.0"
1.0"
dia. 7/8"
1.75"
Cross Beam (W10 x 60)
b1
dia. 7/8" - 5.5" gage
5.5" gage
2.35"
94"
C4 Structural Lab Testing Frame
Dimensions - inches
Material Description - A490 7/8" dia. bolts ; plate steel 36 ksi ; rolled steel 50ks
Cross beam connection detail

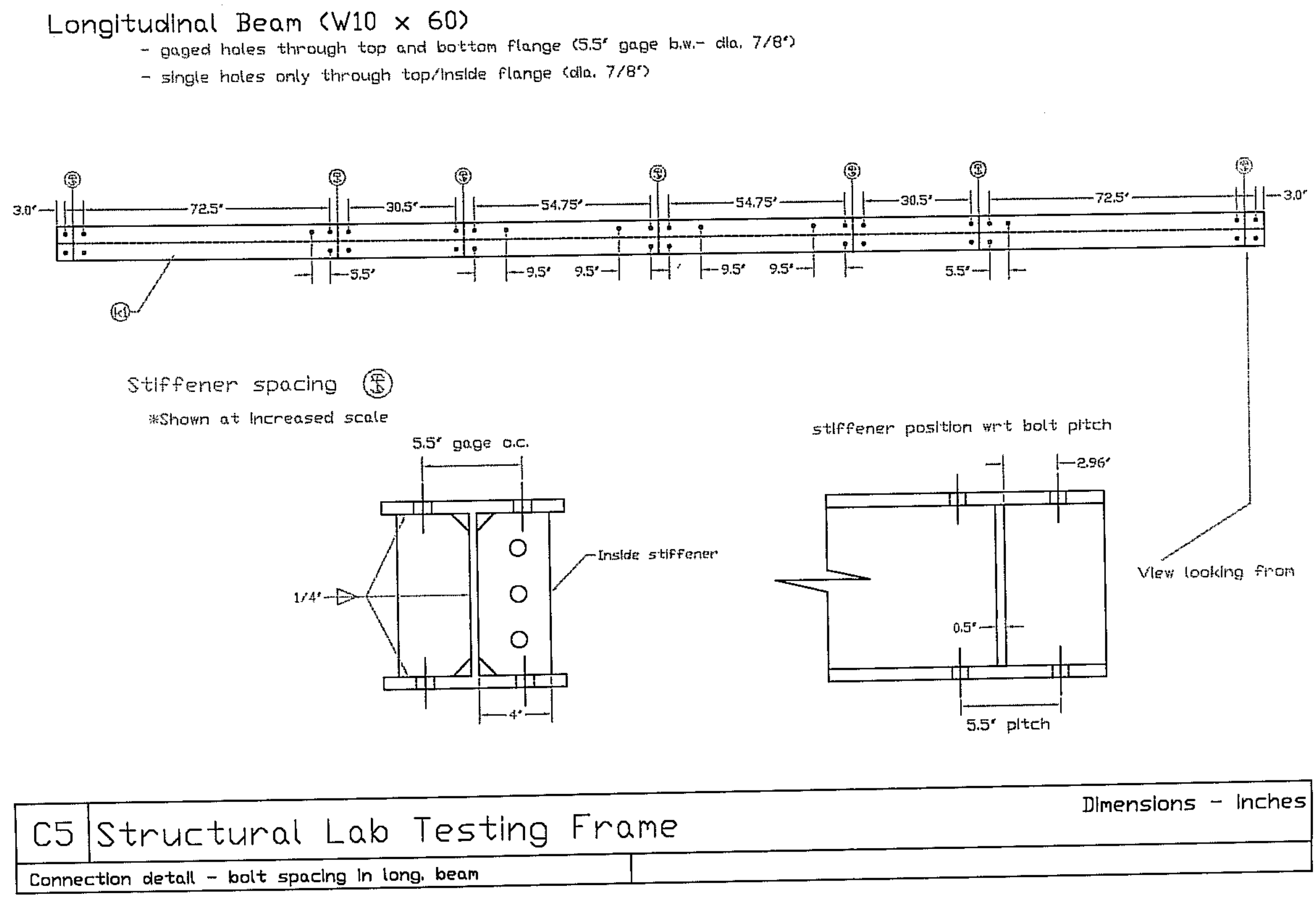

Longitudinal Beam (W10 x 60)
- gaged holes through top and bottom flange (5.5" gage b.w.- dia. 7/8")
- single holes only through top/inside flange (dia. 7/8")
3.0"
72.5"
30.5"
54.75"
54.75"
30.5"
72.5"
3.0"
5.5"
9.5"
9.5"
9.5"
9.5"
5.5"
Stiffener spacing
*Shown at increased scale
5.5" gage o.c.
Inside stiffener
1/4"
4"
stiffener position wrt bolt pitch
2.96"
0.5"
5.5" pitch
View looking from
Dimensions - Inches
C5 Structural Lab Testing Frame
Connection detail - bolt spacing in long. beam

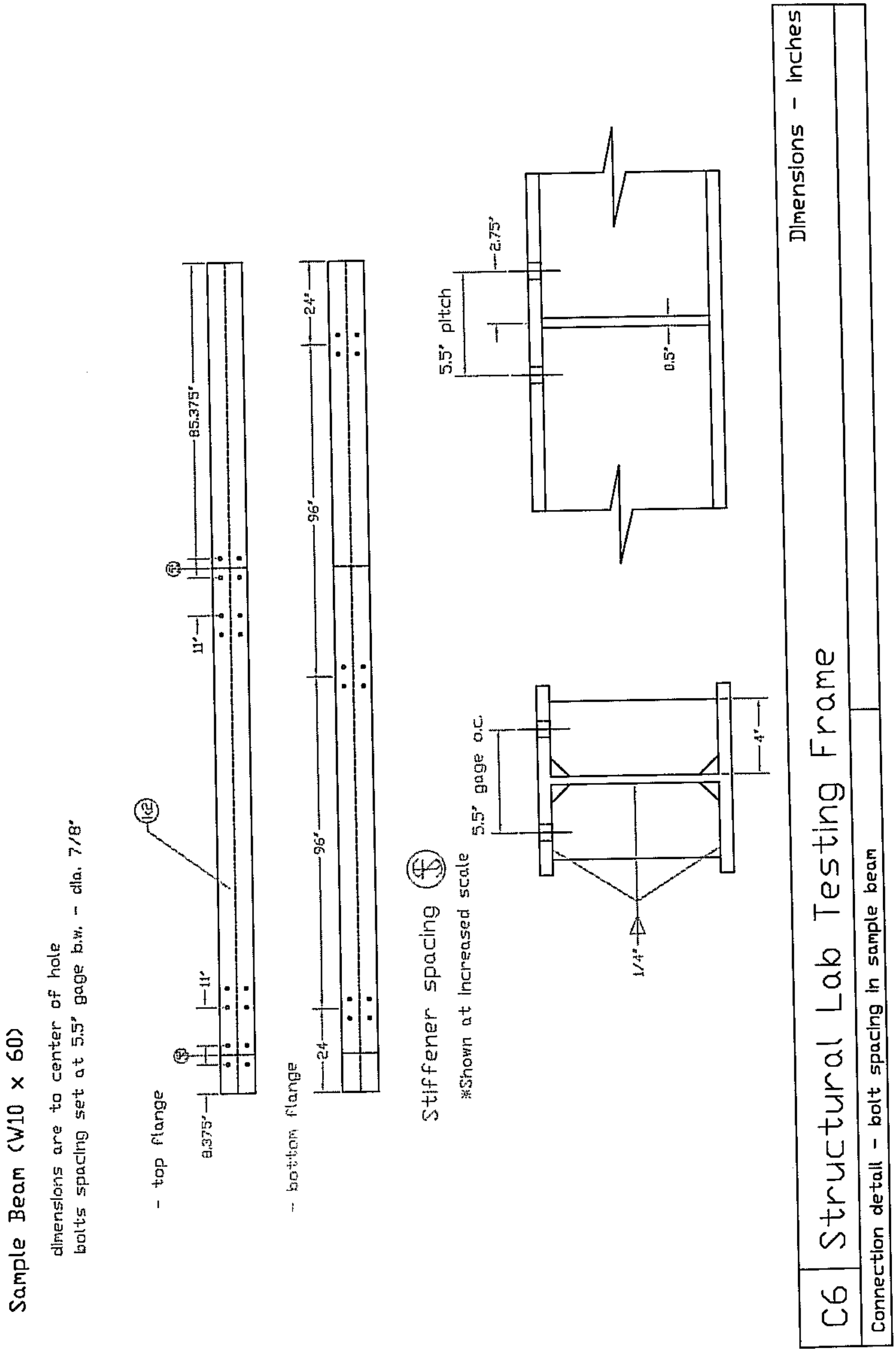
Sample Beam (W10 x 60)
dimensions are to center of hole
bolts spacing set at 5.5" gage b.w. - dia. 7/8"
- top flange
8.375"
11"
11"
85.375"
- bottom flange
24"
96"
96"
24"
Stiffener spacing
*Shown at increased scale
5.5" gage o.c.
4"
1/4"
5.5" pitch
2.75"
0.5"
Dimensions - Inches
C6
Structural Lab Testing Frame
Connection detail - bolt spacing in sample beam

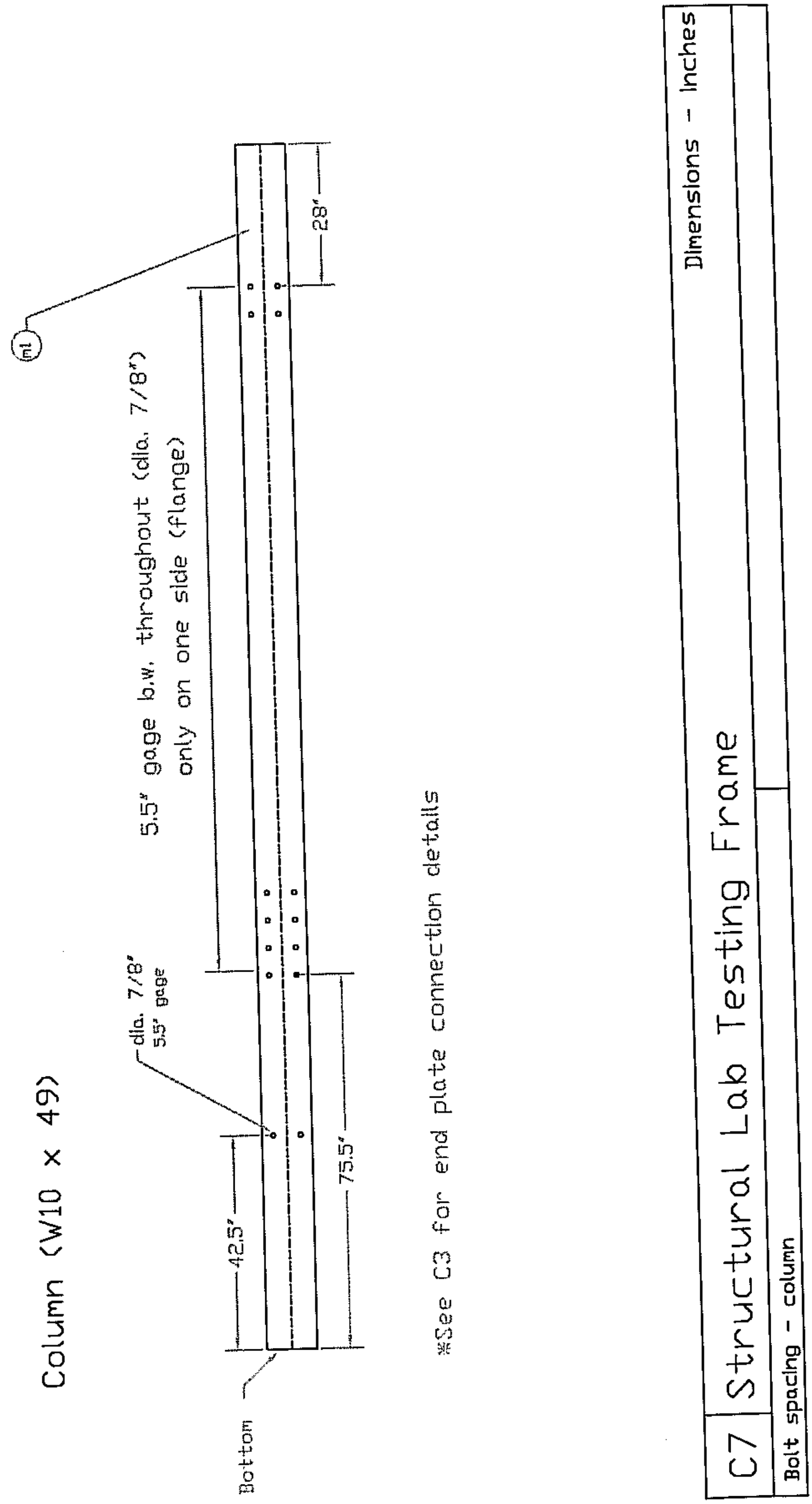
Column (W10 x 49)
m1
28"
5.5" gage b.w. throughout (dia. 7/8")
only on one side (flange)
dia. 7/8"
5.5" gage
42.5"
75.5"
Bottom
*See C3 for end plate connection details
C7
Structural Lab Testing Frame
Dimensions - Inches
Bolt spacing - column

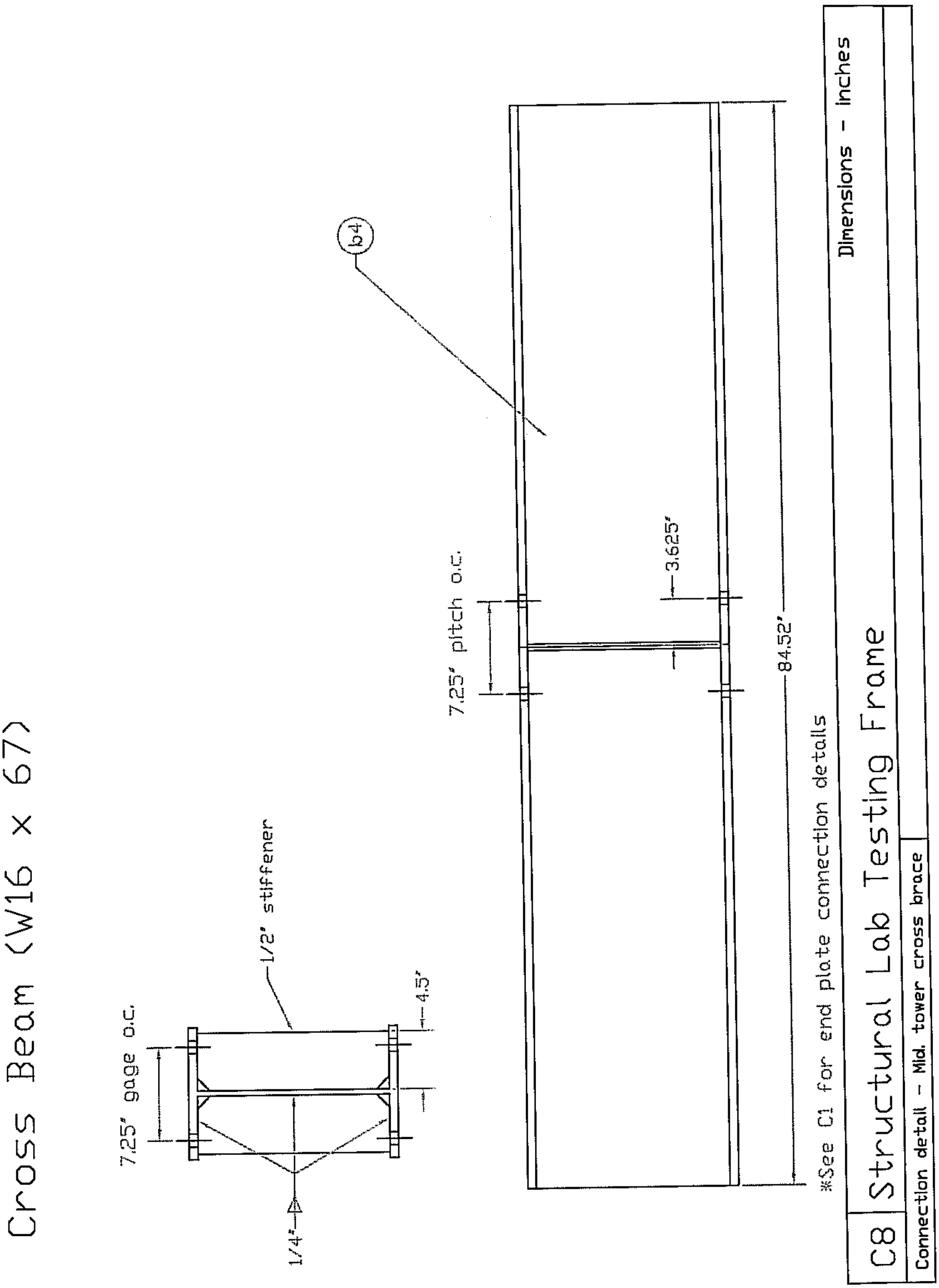
Cross Beam (W16 x 67)
7.25" gage o.c.
1/2" stiffener
4.5"
1/4"
7.25" pitch o.c.
3.625"
84.52"
b4
*See C1 for end plate connection details
C8 Structural Lab Testing Frame
Dimensions - inches
Connection detail - Mid. tower cross brace

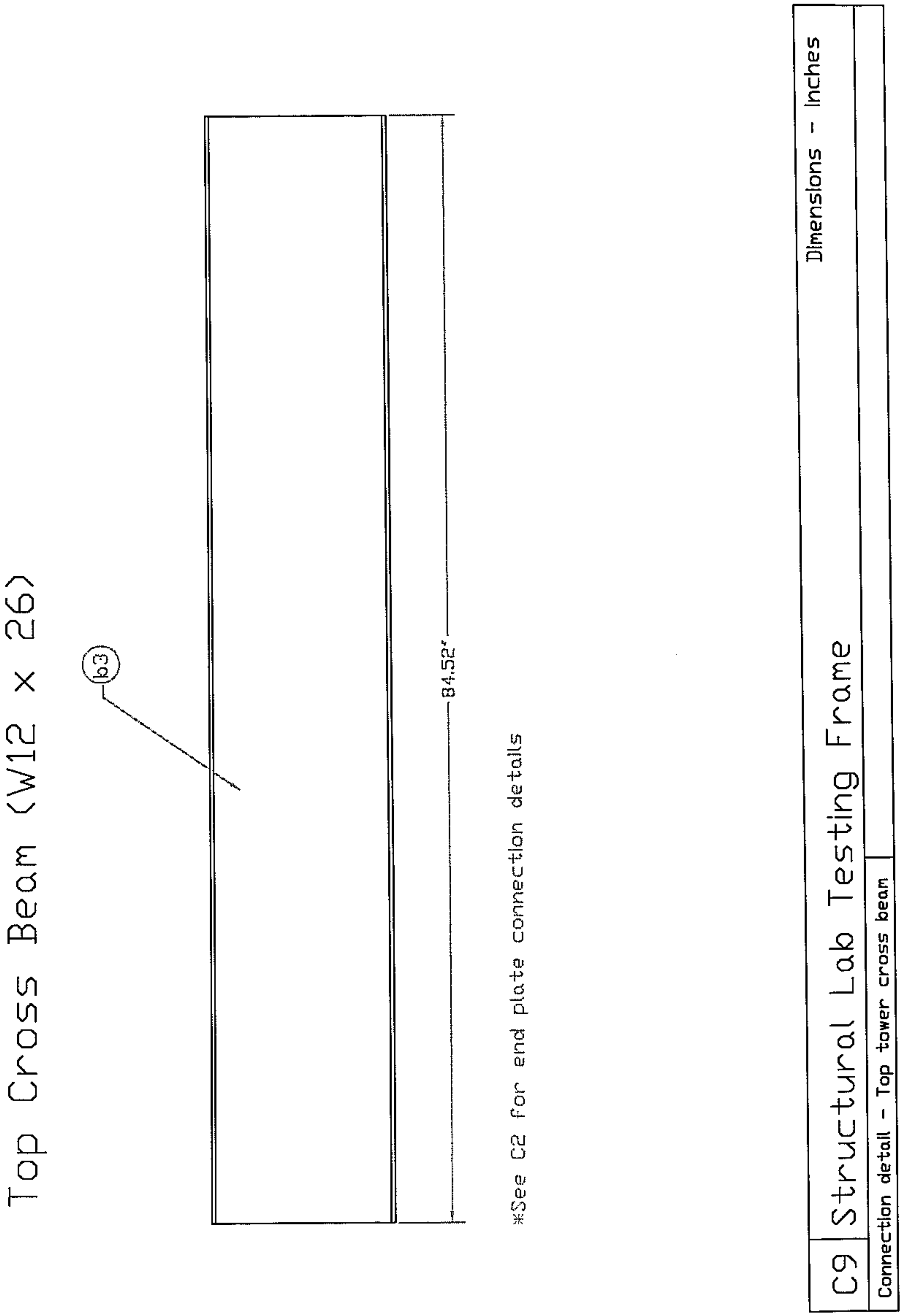
Top Cross Beam (W12 x 26)
b3
84.52"
*See C2 for end plate connection details
Dimensions - Inches
C9
Structural Lab Testing Frame
Connection detail - Top tower cross beam

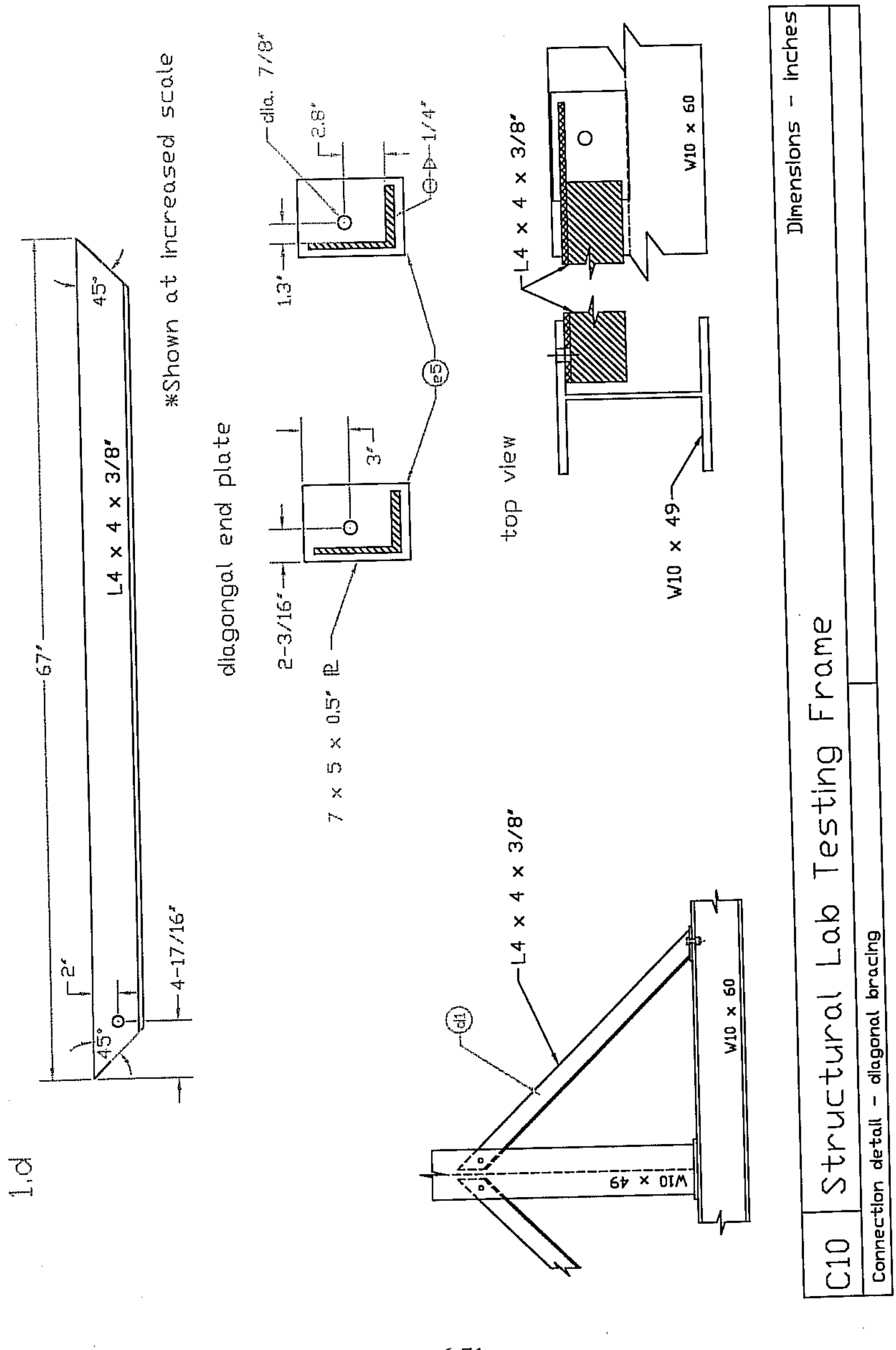
1.d
67"
45°
45°
2"
4-17/16"
L4 x 4 x 3/8"
*Shown at increased scale
diagonal end plate
dia. 7/8"
2.8"
1/4"
1.3"
3"
2-3/16"
7 x 5 x 0.5" PL
e5
top view
L4 x 4 x 3/8"
W10 x 60
W10 x 49
d1
L4 x 4 x 3/8"
W10 x 60
W10 x 49
Dimensions - inches
C10
Structural Lab Testing Frame
Connection detail - diagonal bracing

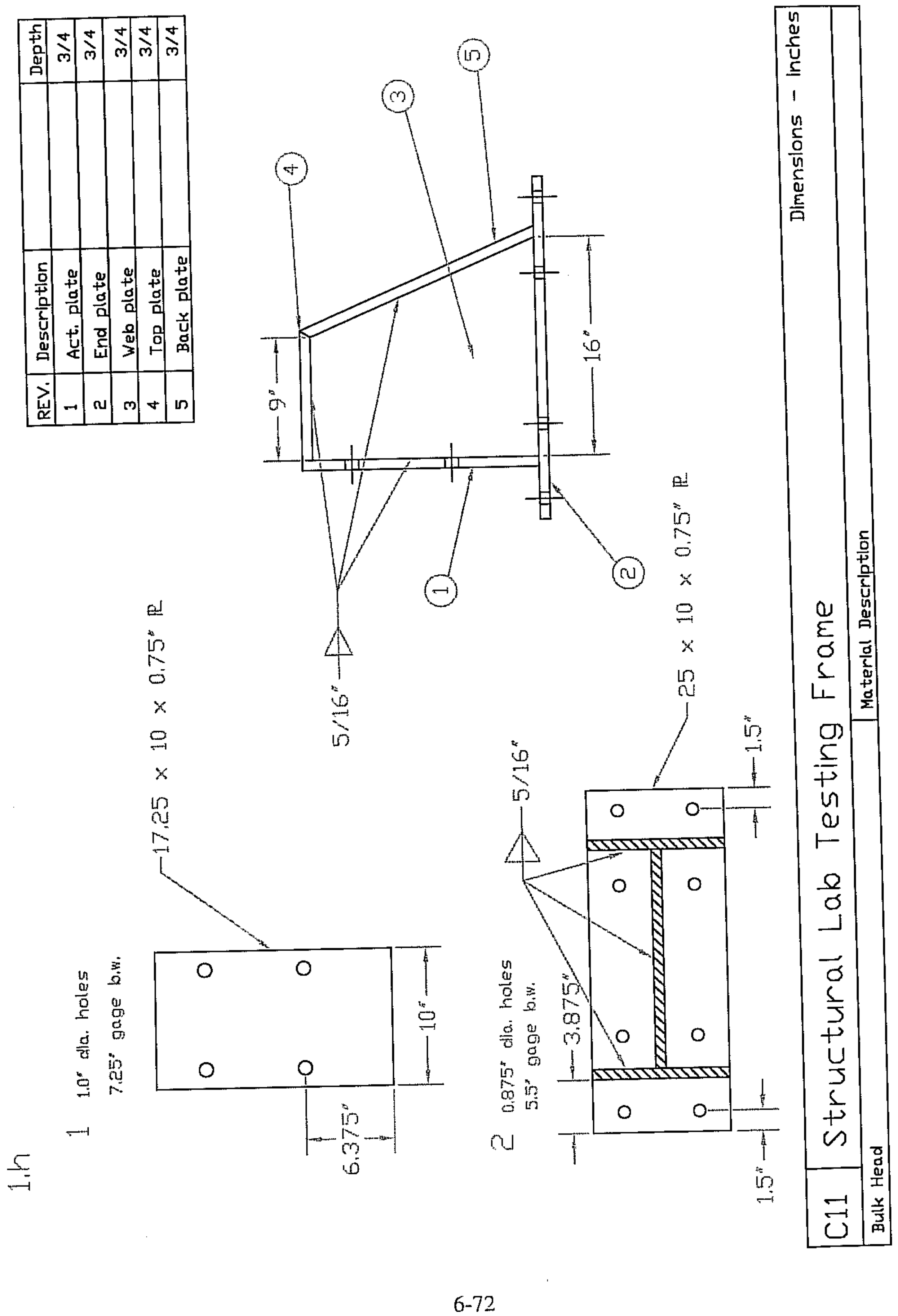

REV.	Description		Depth
1	Act. plate		3/4
2	End plate		3/4
3	Web plate		3/4
4	Top plate		3/4
5	Back plate		3/4

Direct Shear System

design based on 50 ksi yeild strength for all plates

Plate Steel Schedule

Discription	Size (in)	no.	bolt holes drilled (/each)	Remark
Half Specimen Mount		*2*		*Total*
Actuator plate	11 x 10.25 x 0.75	2	4	
Specimen plate	11 x 10.25 x 0.5	2	4	
Side plate	15 x 11* x 0.5	4		*length varies, see sketch
Floor plate	9 x 9.25 x 0.5	2		
Angle	L 2-1/2 x 2-1/2 x 1/2	4	2	
Verticle Hat Mount				
Actuator plate	15 x 10 x 0.5	1	4	
Specimen plate	15.25 x 8.875 x 0.75	1	4	
Side plate	15* x 3.75 x 0.5	2		*length varies, see sketch
Restraint Plate				
Top plate	15.25 x 8.875 x 0.75	1	4	

Total number of holes in all pieces	36
Total number of bolts (5/8" dia. - length=2.25")	8
Total number of bolts (1.0" dia. - ? length)	2

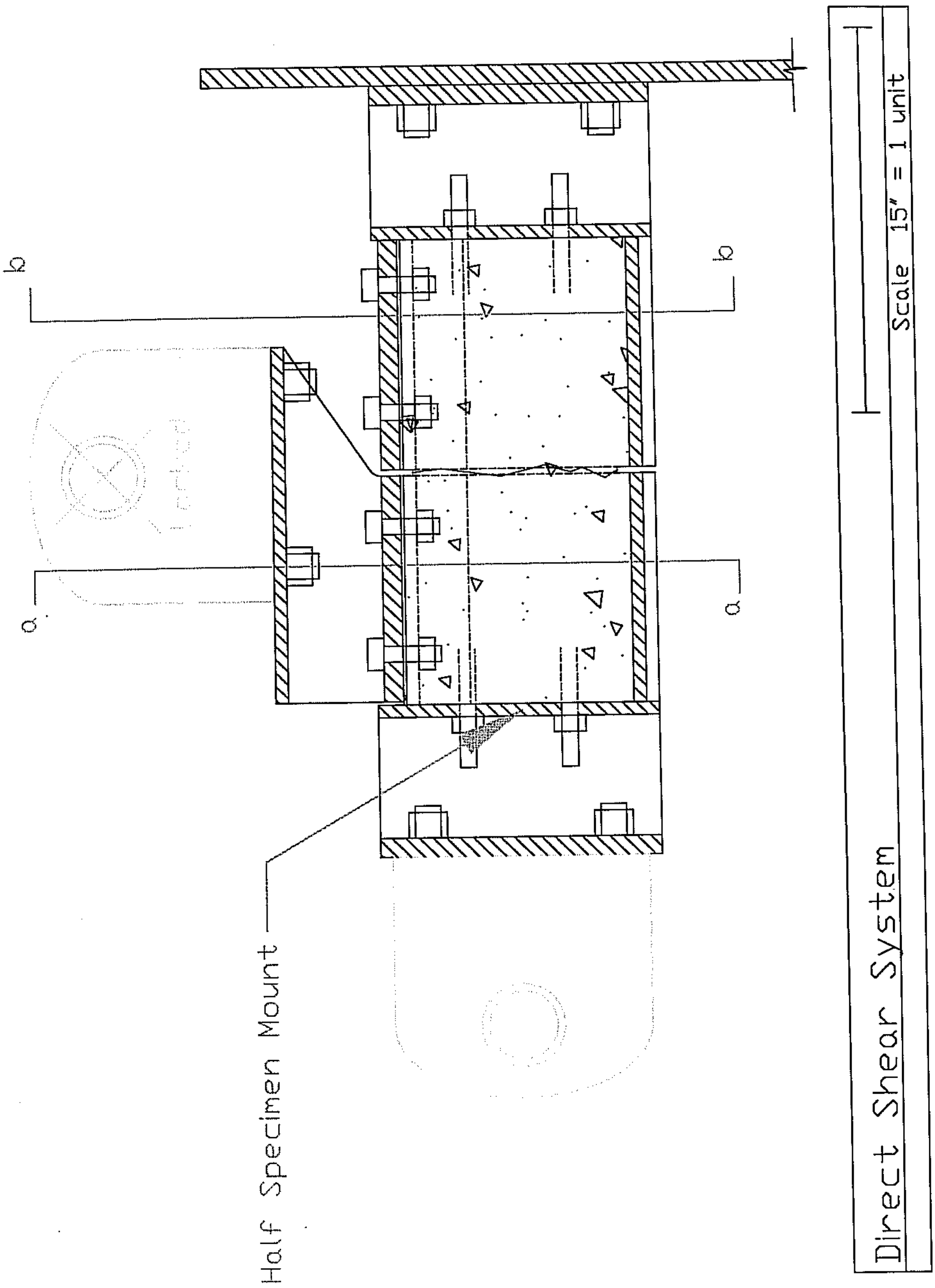
Direct Shear System
Scale 15" = 1 unit
Half Specimen Mount
a
a
b
b

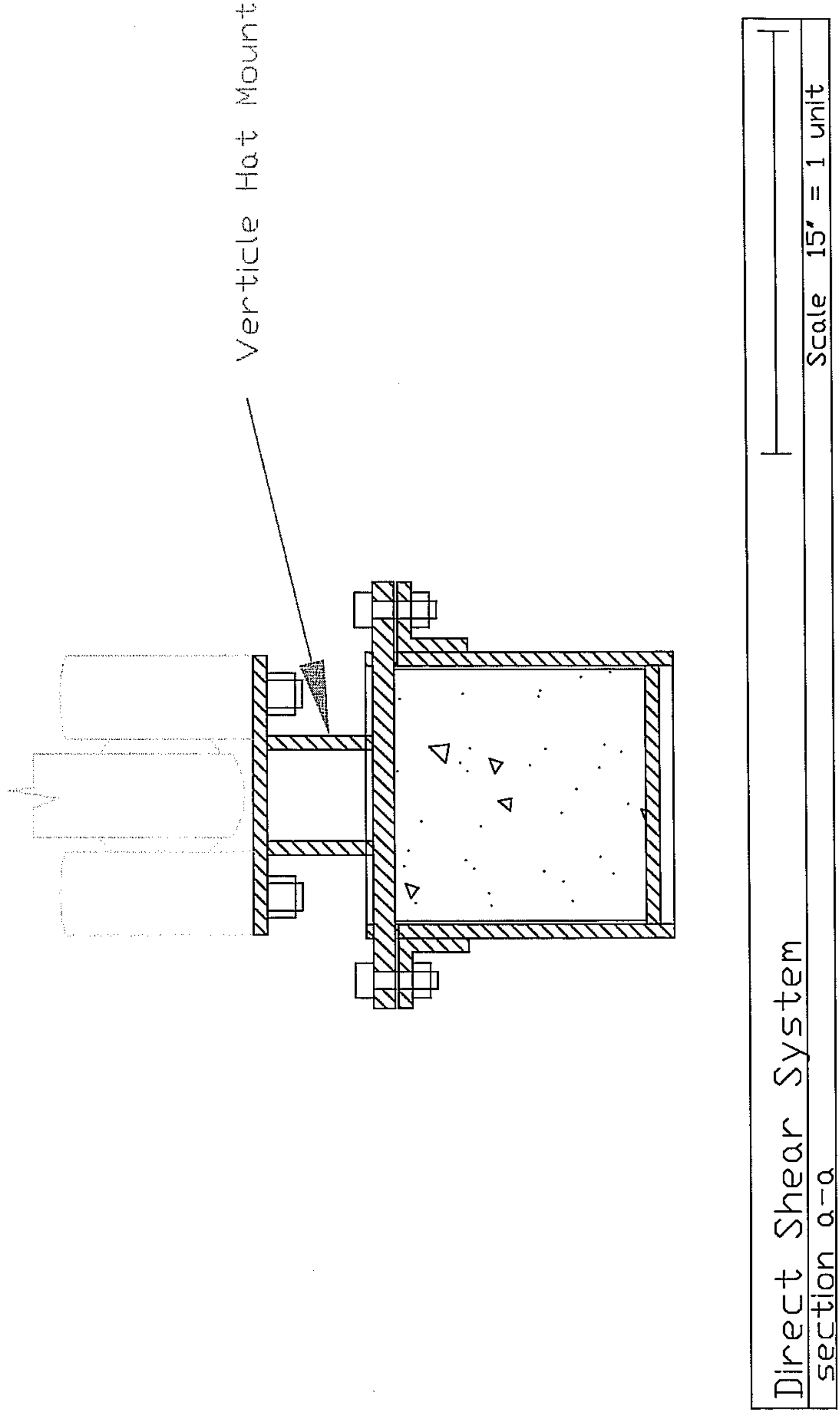
Verticle Hat Mount
Direct Shear System
section a-a
Scale 15' = 1 unit

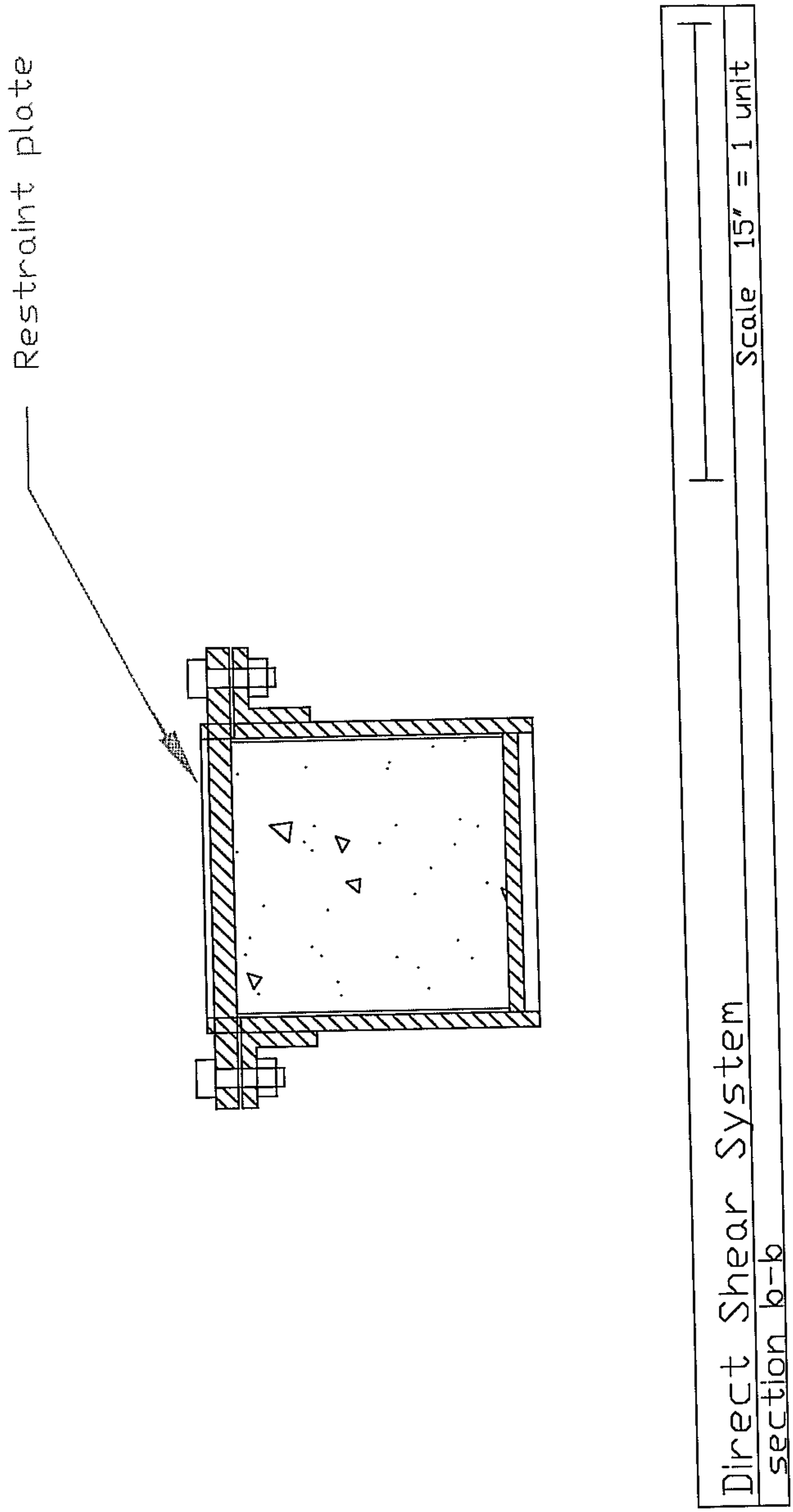
Restraint plate
Direct Shear System
section b-b
Scale 15" = 1 unit

REV.	Description		Depth
1	Act. plate		3/4
2	Spec. plate		1/2
3	Angle	L2-1/2x2-1/2x2-1/2	1/2
4	Side plates		1/2
5	Floor plate	9x9.25	1/2

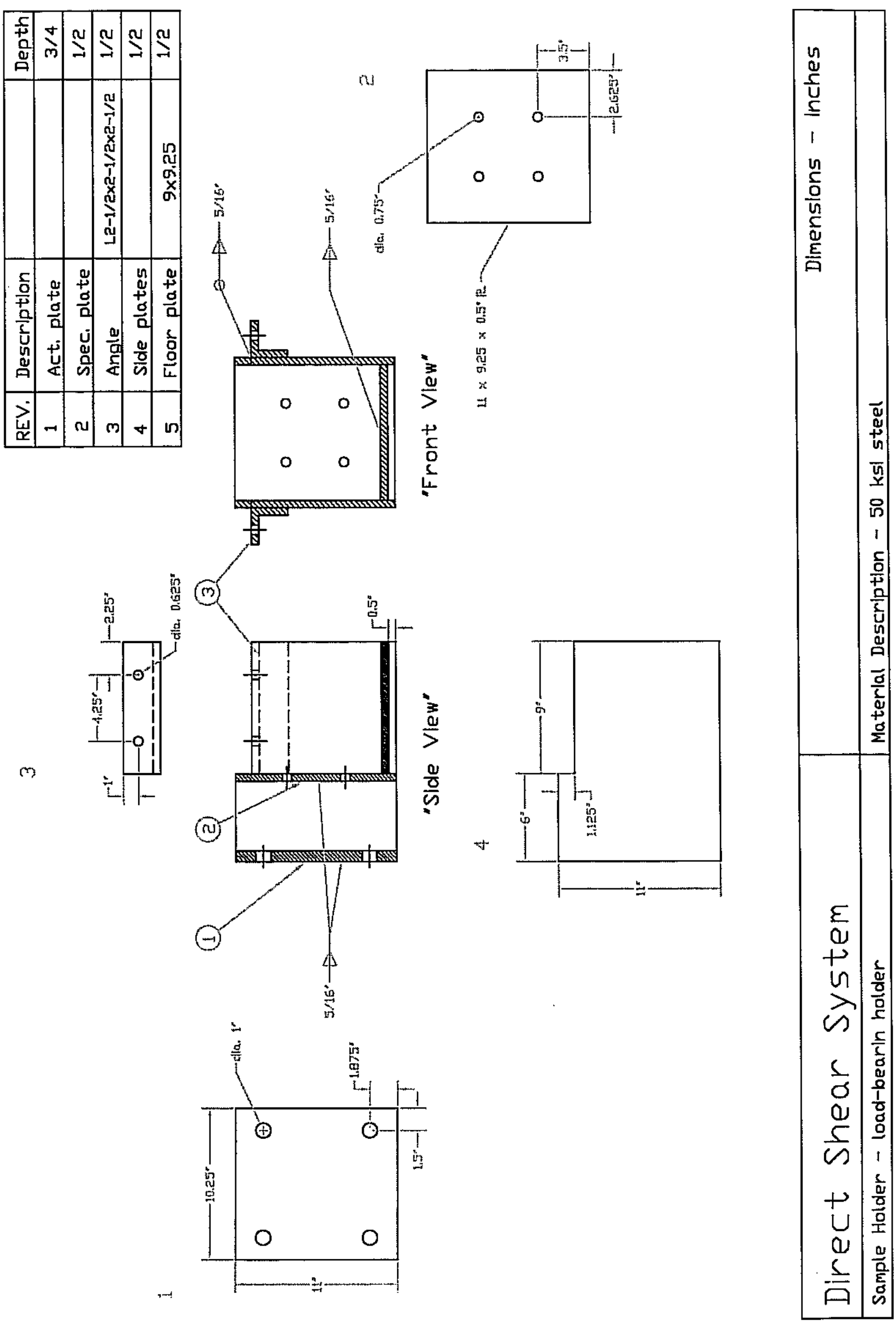

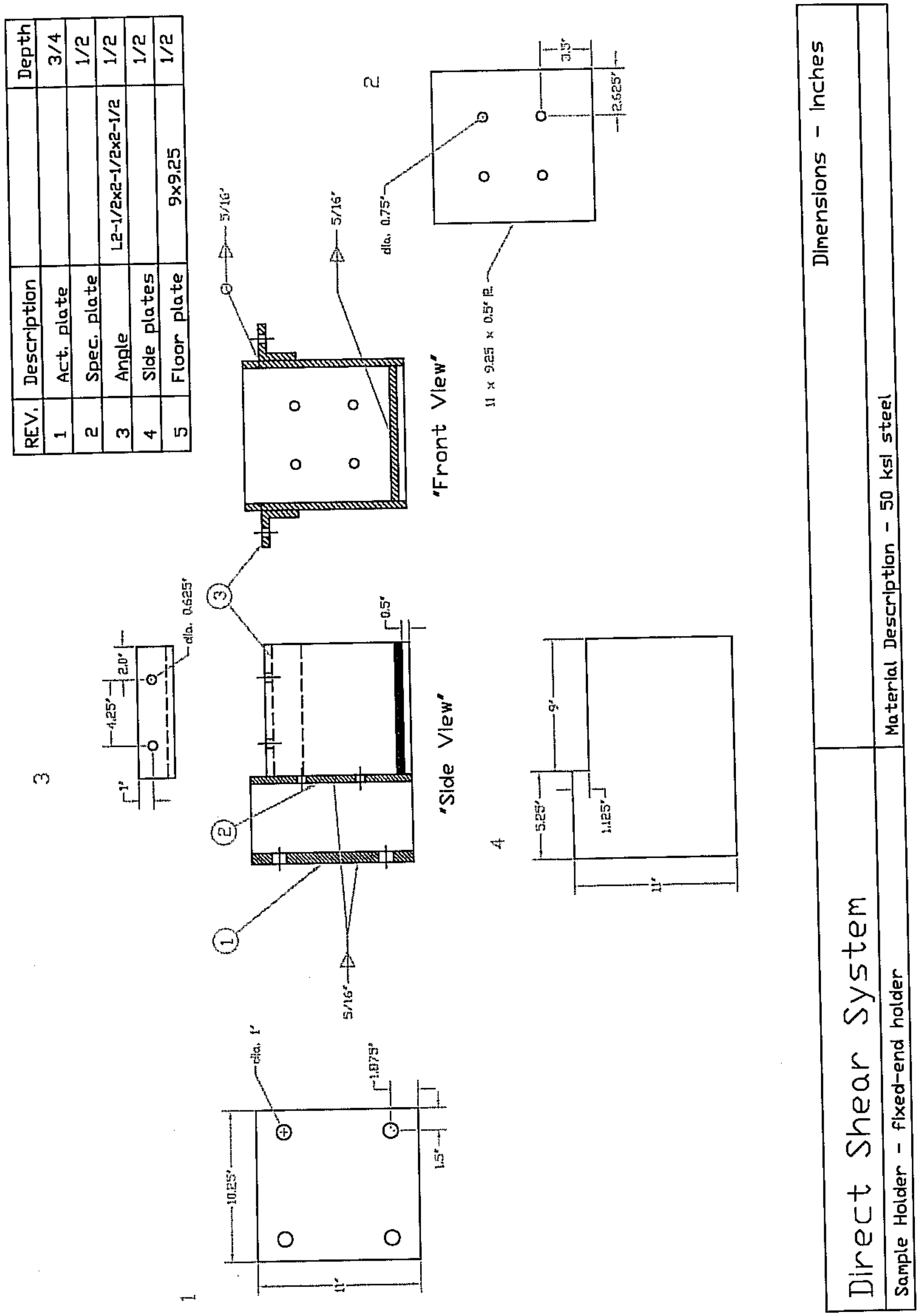

REV.	Description		Depth
1	Act. plate		3/4
2	Spec. plate		1/2
3	Angle	L2-1/2x2-1/2x2-1/2	1/2
4	Side plates		1/2
5	Floor plate	9x9.25	1/2

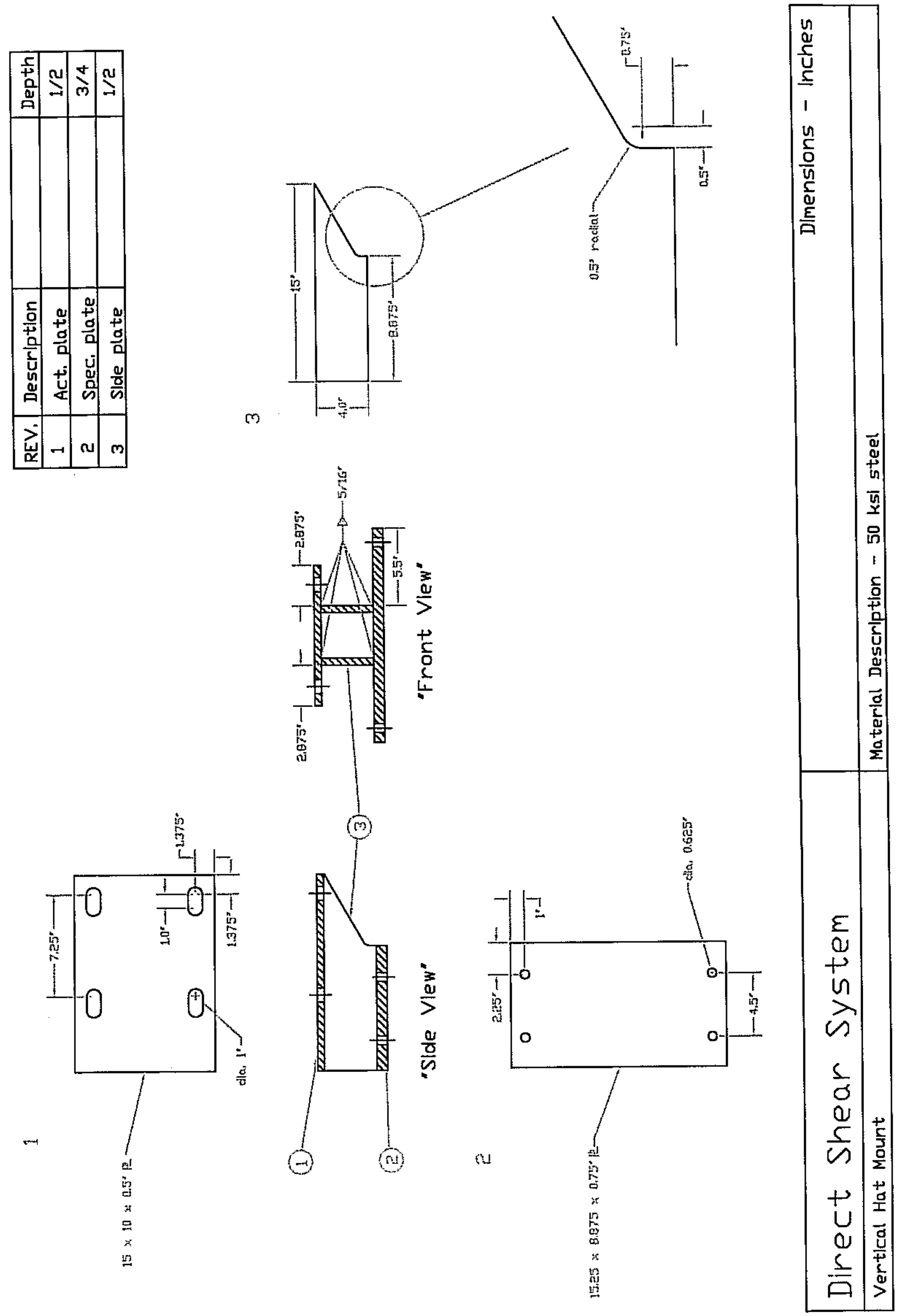
REV.
Description
Depth
1
Act. plate
1/2
2
Spec. plate
3/4
3
Side plate
1/2
Direct Shear System
Vertical Hat Mount
Material Description - 50 ksi steel
Dimensions - Inches
"Side View"
"Front View"
15 x 10 x 0.5' PL
15.25 x 8.875 x 0.75' PL
7.25'
1.375'
1.0'
dia. 1'
2.25'
4.5'
1'
dia. 0.625'
2.875'
5/16'
5.5'
15'
8.875'
4.0'
0.5' radial
0.5'
0.75'

REV.	Description		Depth
1	R. plate		3/4

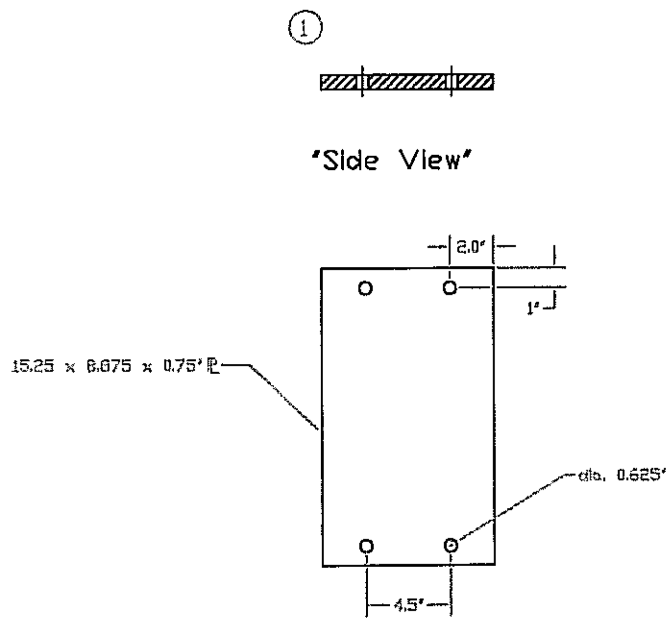

Direct Shear System	Dimensions - Inches
Restraint plate	Material Description - 50 ksi steel

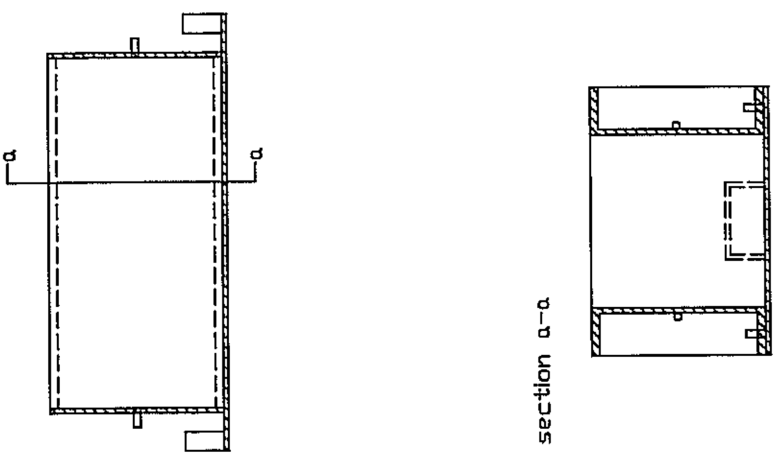

Direct Shear System

Mold for direct shear sample

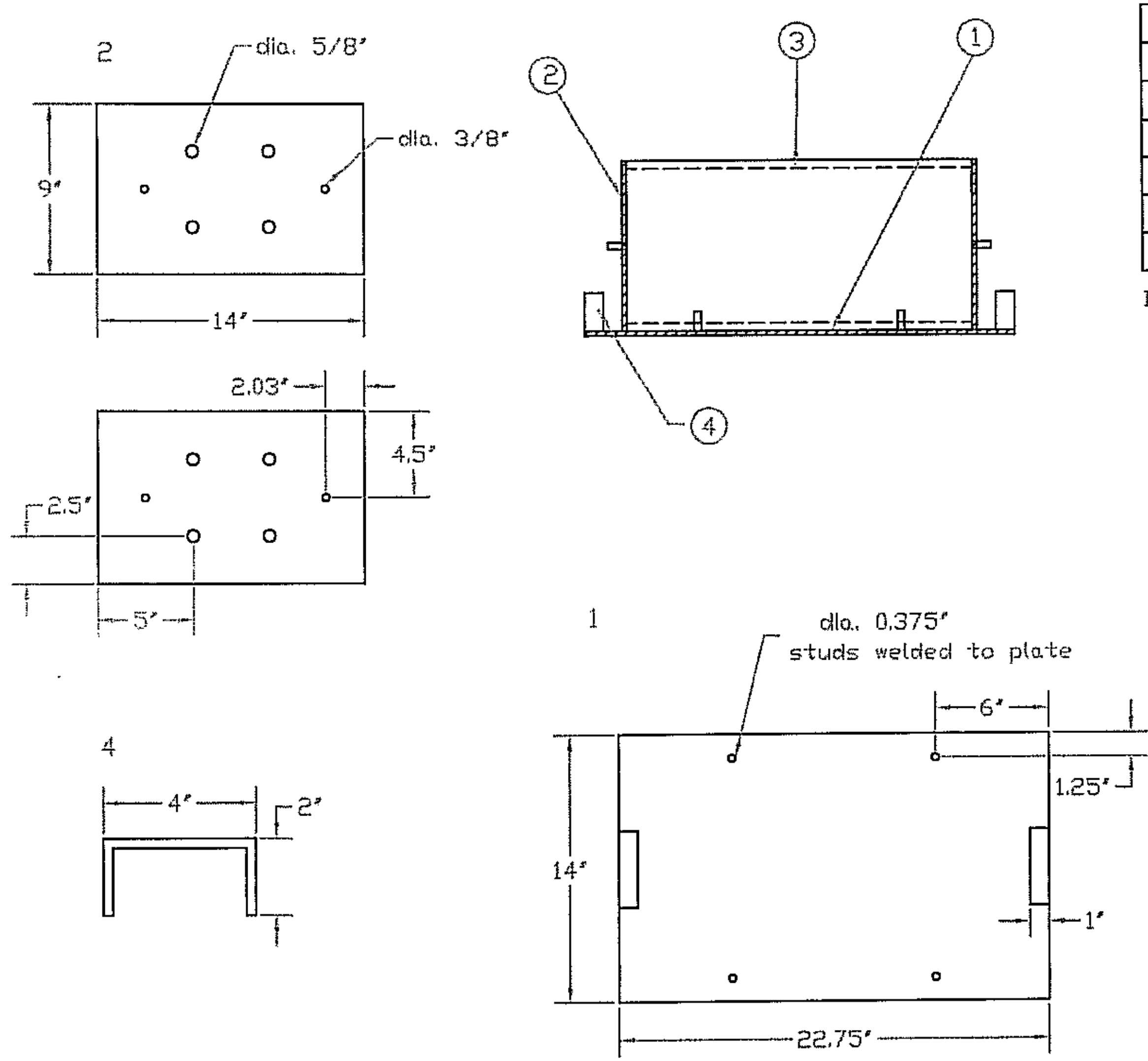

REV.	Description		Depth
1	Base plate		1/4
2	Side plate		1/4
3	C-channels	C9 x 15	
4	Handle		1/4
	Studs	dia. 3/8"	

Interior dimensions need to be: 9 x 9 x 18.25"

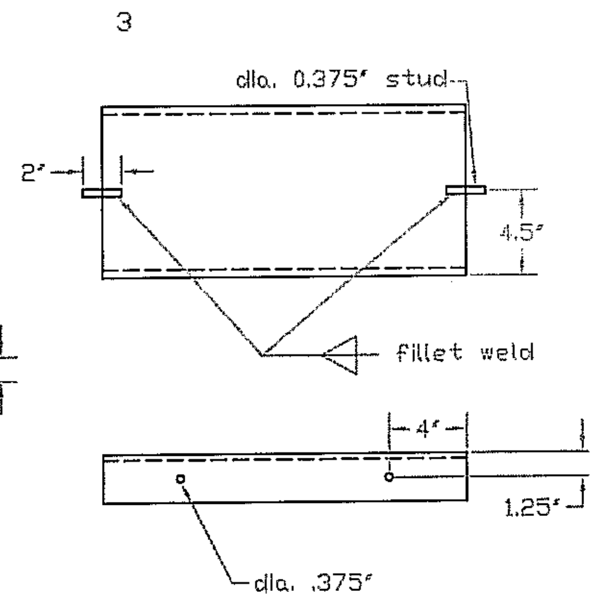

Direct Shear System	Dimensions - Inches
Mold for direct shear sample	Material Description

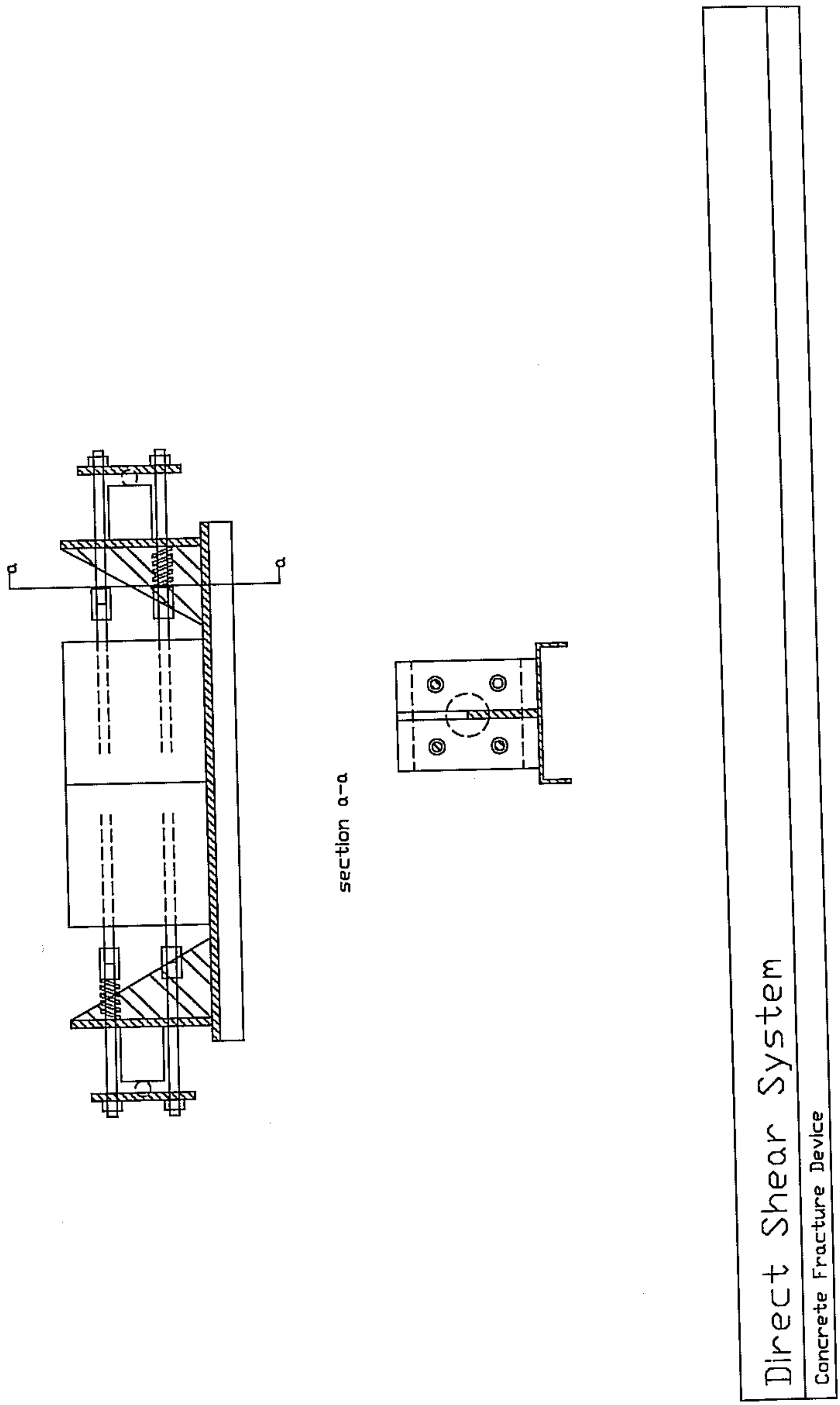
a
a
section a-a
Direct Shear System
Concrete Fracture Device

Appendix B

Mix design worksheets

MICHIGAN DEPARTMENT OF TRANSPORTATION

FORM 1830

CONCRETE PROPORTIONING DATA

FILE 300

CONTROL SECTION ID: RESEARCH
JOB NUMBER: MI. TECH.
LAB NUMBER: 99C-1028
GRADE OF CONCRETE: P1
INTENDED USE OF CONCRETE: Pavement (Conv. Form)

DATE: 7/01/1999
SPECIFICATION: 1996 STD SPECS
MIX DESIGN NUMBER: 99-1038

CONCRETE MATERIALS

MATERIAL	SOURCE	SOURCE NUMBER	CLASS	SPECIFIC GRAVITY	ABSORPTION PERCENT
CEMENT	(SEE REMARKS)		1/1A	3.15	
FINE AGG.	Superior S & G	31-45	2NS	2.66	1.14
COARSE AGG.	Bruce Mines	95-10	6AA	2.88	0.36
FLY ASH					

CEMENT CONTENT, kg/m^3 335
AIR CONTENT (DESIGN): 6.5% (SPECIFIED): 6.5%
R.W.C: 1.15
FLY ASH CONTENT, kg/m^3: 0

B/Bo : 0.72
SPECIFICATION TOLERANCE (±): 1.5%
THEORETICAL YIELD: 100.00%

WEIGHT OF COARSE AGG. (DRY/LOOSE) kg/m^3	AGGREGATE AND WATER PROPORTIONS QUANTITIES, kg/m^3 OF CONCRETE		
	FINE AGG (OVEN DRY)	COARSE AGG (OVEN DRY)	TOTAL WATER
1456	847	1048	160
1466	841	1056	159
1476	836	1063	159
1486	830	1070	158
1496	824	1077	158
1506	818	1084	158
1516	812	1092	157
1526	807	1099	157
1536	801	1106	157
1546	795	1113	156
1556	789	1120	156

REMARKS:
THIS CHART FOR USE WITH CEMENTS OF THE CLASS SHOWN FROM APPROVED SOURCES.

TYPICAL UNIT WEIGHT (DRY, LOOSE) OF COARSE AGGREGATE AS DESCRIBED ABOVE IS 1506 kg/m^3

SPECIAL MESSAGES: Dynamic Fracture Research Project

CC:
S. Vitton-Mi. Tech.
T. Woodhouse-MDOT

JOHN F. STATON
MATERIALS RESEARCH ENGINEER

MIX PROPORTIONS WORKSHEET

	Laboratory No	Bulk Dry Specific Gravity	% Absorption
Cement: Lafarge (Alpena) Type 1		3.15	-
Coarse Aggregate: CA-B (Bruce M.) Source No. 95-10 Specification 6AA	MTU	★ 2.88	★ 0.36
Fine Aggregate: FA-Y Source No. 31-45 Specification 2NS		★ 2.66	★ 1.14

Batch size 0.0779779 m^3

Material	Weight, kg/m^3	Batch Proportions kg					
Cement	335 ★	26.12		**Total cement**			**(C)**
Coarse Aggregate (DRY)	1084 ★			Pass	Ret	%	
		21.132	21.13	25.0mm	19.0mm	25	
		21.132	21.14	19.0mm	12.5mm	25	
		21.132	21.13	12.5mm	9.5mm	25	
		21.132	21.13	9.5mm	4.75mm	25	
			84.53				
		84.53		**Total Coarse Agg.**			**(a)**
Fine Aggregate (DRY)	818 ★	63.79		**Total Fine Agg.**			**(b)**
Total Water	158 ★	12.32		**Total Water per batch**			**(d)**

Absorbed Water	agg*absorption =		absorbed h_20			
Coarse Agg	1084	0.0036	3.90	13.23	**Absorbed water kg/m^3**	**(W)**
Fine Agg	818	0.0114	9.33			
			13.23			

Total Aggregate Contains 43.0 % Fine Aggregate

Note: ★ Provided by MDOT (Form 1830, File 300) and listed in Table 2.3

BATCH COMPUTATIONS WORKSHEET **WEIGHT IN kg**

Coarse Aggregate

84.53 Coarse Agg (a)

Pail tare	1.71	1.73	3.44 + pails
			87.97 = total
25.0 - 19.0mm	21.13	0.00	
19.0 - 12.5mm	0.00	21.14	
12.5 - 9.5mm	0.00	21.13	
9.5 - 4.75mm	21.13	0.00	
Sub total	43.97	44.00	87.97 Total

BATCH NO.	BM-T1
COARSE AGG	CA-B (Bruce M.)
DATE:	12/1/99
Batch Made	Wed. @ 4:30

Fine Aggregate

63.79 Fine Agg (b)

Moisture content

wet	dry
121.15	116.1
0.0435	MC

0.0435 MC

2.77 Moisture

Dry weight 63.79

\+

Moisture 2.77

Total **66.56**

WATER MEASUREMENT

Coarse Agg +pail	43.97		
Coarse Agg +pail	44.00		
Total	87.97		
+ Total Batch Water	11.32	(d)	11.32
- Reserve Water	3.00		3.00
= Pails, Agg&Water	96.29	H_2O	8.32

RESERVE WATER

Res water	3.00	1.45	surplus & Tare
+ Tare	0.29	0.29	- tare
= Total	3.29	1.16	= surplus

Reserve Water	3.00		
- Surplus Water	1.16		
=	1.84	H_2O +	8.32
Subtotal of water in batch		=	10.16
+ Moisture in Fine Aggregate		+	2.77
Total Water in Batch		**(D) =**	**12.93**

Cement

26.12 Cement (C)

Pail ID A', B'

Tare weight	0.85	1.70	tare
Tare weight	0.85	27.82	Pail + cement
Total tare	1.70		

UNIT WEIGHT

Weight of Concrete & Bucket	42.20	
- Weight of Bucket	8.15	
= Weight of Concrete in Bucket	**34.05**	(f)

Air Entraining Admixture

29 ml

SLUMP = 0.5 " **12.7** mm

Batch Summary

(a)	Coarse Aggregate as Designed	84.53 kg
(b)	Fine Aggregate as Designed	63.79 kg
(c)	Cement as Designed	26.12 kg
(D)	Total Water of Batch	12.93 kg
(e)	**Total Weight of Batch**	**187.37** kg

AIR CONTENT

- Factor of Aggregate Porosity

= Percent Air 4

CONCRETE TEMPERATURE, C 19

Note: a,b,C,d come from mix proportions worksheet

MICHIGAN DEPARTMENT OF TRANSPORTATION

FORM 1830 CONCRETE PROPORTIONING DATA FILE 300

CONTROL SECTION ID: RESEARCH
JOB NUMBER: MI. TECH.
LAB NUMBER: 99C-1030
GRADE OF CONCRETE: P1
INTENDED USE OF CONCRETE: Pavement (Conv. Form)

DATE: 7/01/1999
SPECIFICATION: 1996 STD SPECS
MIX DESIGN NUMBER: 99-1040

CONCRETE MATERIALS

MATERIAL	SOURCE	SOURCE NUMBER	CLASS	SPECIFIC GRAVITY	ABSORPTION PERCENT
CEMENT	(SEE REMARKS)		I/IA	3.15	
FINE AGG.	Superior S & G	31-45	2NS	2.66	1.14
COARSE AGG.	Presque Isle Stone	71-47	6AA	2.55	1.35
FLY ASH					

CEMENT CONTENT, kg/m^3 335
AIR CONTENT (DESIGN): 6.5% (SPECIFIED): 6.5%
R.W.C: 1.15
FLY ASH CONTENT, kg/m^3: 0

B/Bo : 0.72
SPECIFICATION TOLERANCE (±): 1.5%
THEORETICAL YIELD: 100.00%

WEIGHT OF COARSE AGG. (DRY/LOOSE) kg/m^3	AGGREGATE AND WATER PROPORTIONS QUANTITIES, kg/m^3 OF CONCRETE		
	FINE AGG (OVEN DRY)	COARSE AGG (OVEN DRY)	TOTAL WATER
1328	822	956	167
1338	815	963	167
1348	809	971	166
1358	802	978	166
1368	796	985	166
1378	789	992	165
1388	783	999	165
1398	776	1007	165
1408	769	1014	164
1418	763	1021	164
1428	756	1028	164

REMARKS:
THIS CHART FOR USE WITH CEMENTS OF THE CLASS SHOWN FROM APPROVED SOURCES.

TYPICAL UNIT WEIGHT (DRY, LOOSE) OF COARSE AGGREGATE AS DESCRIBED ABOVE IS 1378 kg/m^3

SPECIAL MESSAGES: Dynamic Fracture Research Project

CC:
S. Vitton-Mi. Tech.
T. Woodhouse-MDOT

JOHN F. STATON
MATERIALS RESEARCH ENGINEER

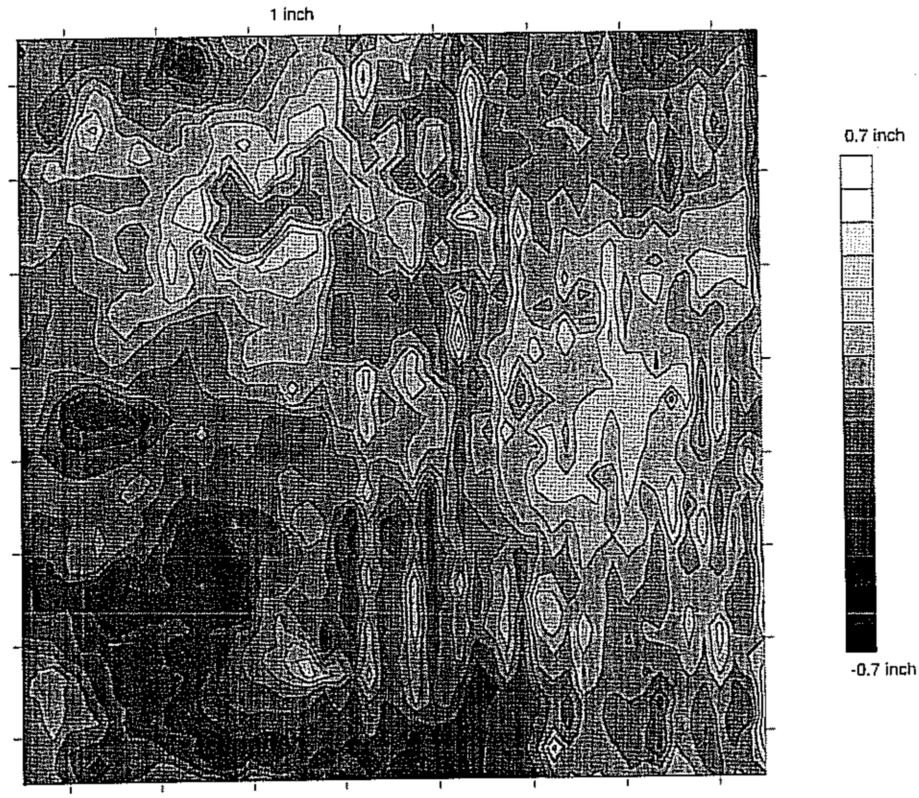

Figure 4.7 (a) Bruce Mines #3 Before testing

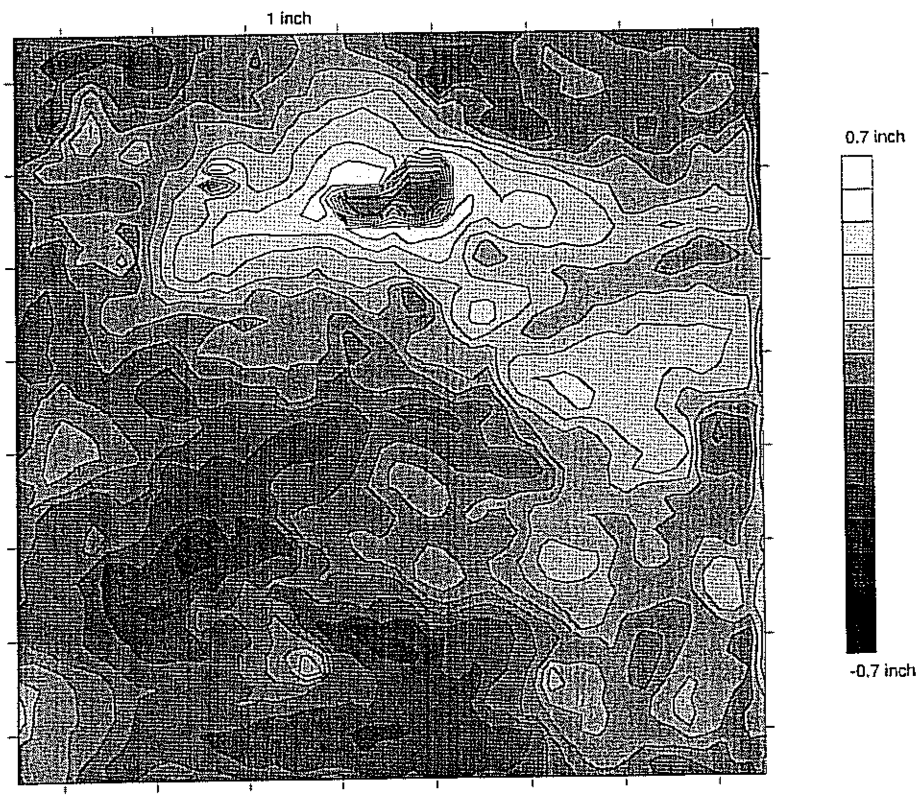

Figure 4.7 (b) Bruce Mines #3 After testing

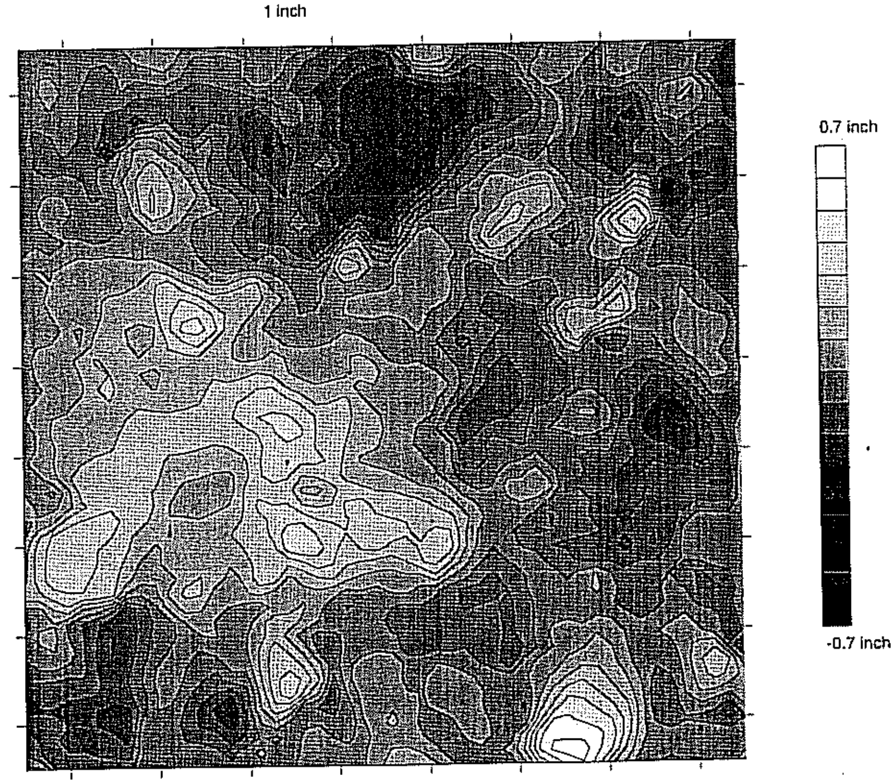

Figure 4.8 (a) Bruce Mines #4 Before testing

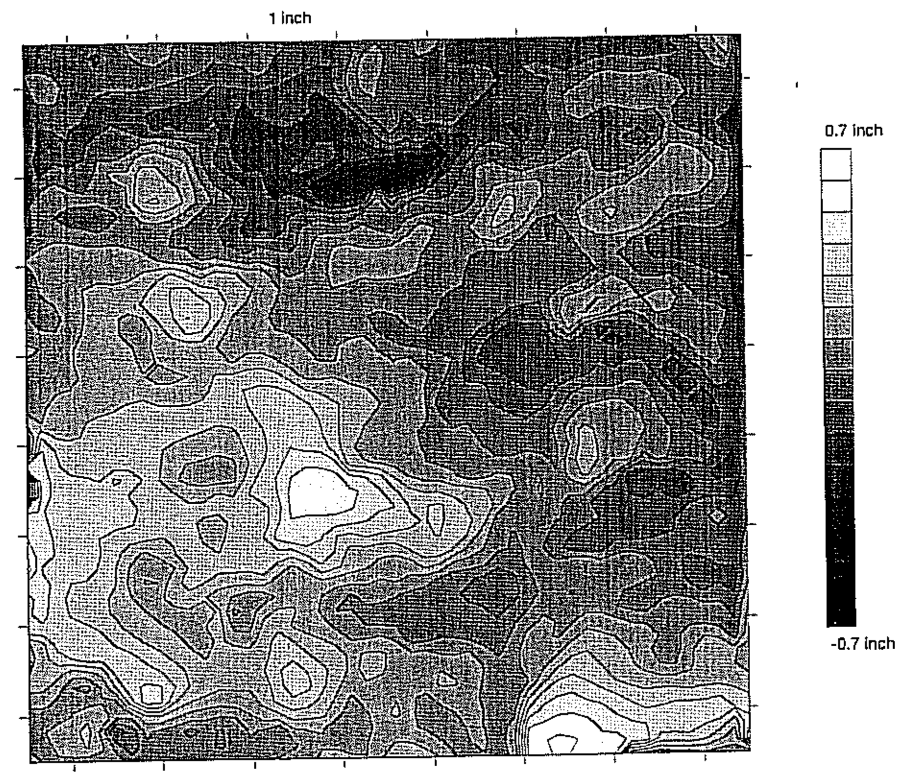

Figure 4.8 (b) Bruce Mines #4 After testing

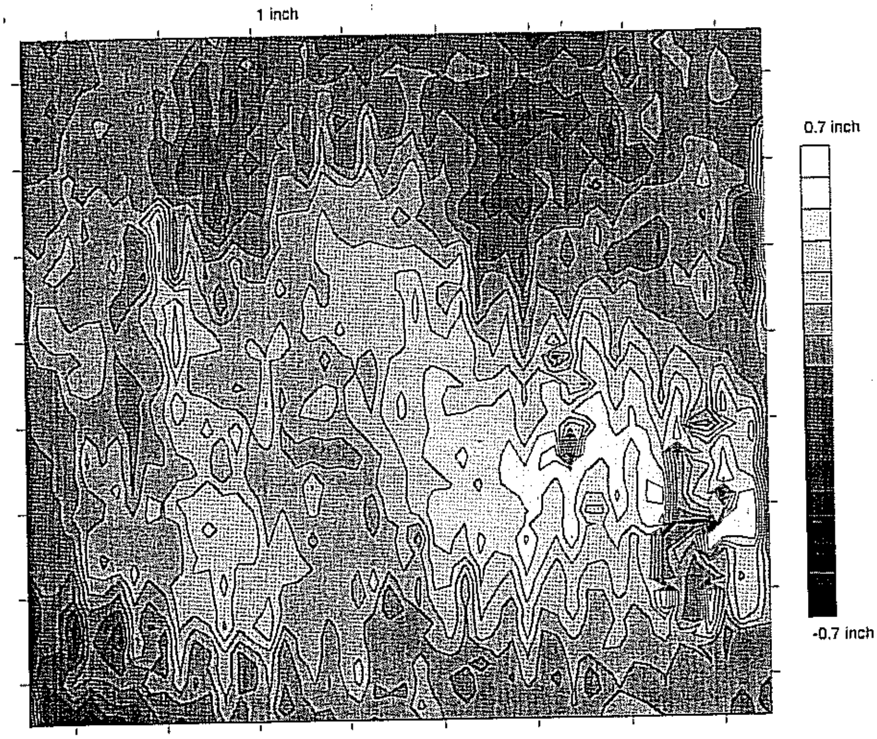

Figure 4.9 (a) Presque Isle #2 Before testing

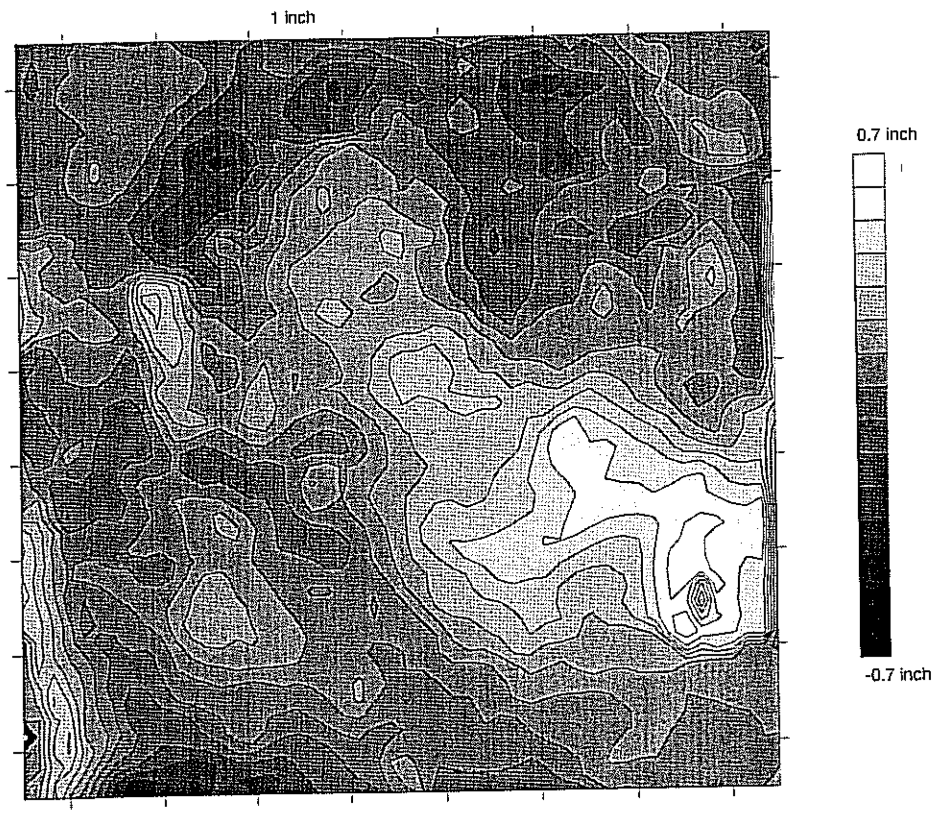

Figure 4.9 (b) Presque Isle #2 After testing

Three observations were made from the topographic results presented in Figures 4.6 through 4.9. First, the black regions on the plots indicate a low region, while the white represent high region on the samples. A general view of the two Bruce Mines, blocks #3 and #4 show a greater black and white contrast than do the Levy #5 and Presque Isle #2. This is confirmed by the data presented in Table 4.2, showing that the maximum distance between the high and low points on the surfaces are greater for the Bruce Mines surfaces than the Levy and Presque Isle concrete surfaces. However, it is recognized that this is not conclusive, but it does suggest that the Bruce Mines surfaces are rougher than the Levy and Presque Isle. A second and somewhat interesting observation, is the linear features that appear in the Levy #5, Bruce Mines #4, and Presque Isle #2 surfaces, prior to aggregate interlock testing, but not present after interlock testing. One possible explanation is that the linear features are due to the effects of rodding during the casting process. Then during aggregate interlock testing, they were eliminated. A second possible explanation is that the linear features are an artifact of the CNC mill measuring system or the software itself, but one would expect the linear feature to be present on all of the surfaces, both before and after.

The third observation is that the topographic plots show a smoothing of the surfaces after interlock testing. This is seen by large areas of more equal elevation. This is also seen in Table 4.2, where the max distances for the before and after results show a reduction in three of the four surfaces, after aggregate interlock testing

While some useful data was obtained from the surface roughness measurements, there were a number of problems with this system. These problems include: (1) the length of time required to record the data (in excess of 4 hours per sample), (2) data acquisition failures (no data recorded mid-stream), and (3) analysis time (from 0.5 to 8 hours per sample).

4.4 Aggregate Interlock Test Results

Sixteen aggregate interlock tests were planned for testing. However, 18 concrete sample blocks were cast since one batch of Levy concrete had low slump (1 batch produced two concrete test samples) an additional batch was made generating two additional Levy samples. Due to system set up and evaluation requirements as well as difficulty with the hydraulic pump system, not all of the 18 samples were successfully tested. While the procedure for setting up the system parameters consumed some of the test samples, the hydraulic pump's problems during sample testing consumed significantly more. The difficulty in the testing, when the hydraulic pump shut down prematurely, was that both the vertical and horizontal loads were lost, making it almost impossible to resume the test where it had stopped. Table 4.3 lists the results of all 18 tests. Of these 18 tests, eight were considered useful tests. Although the number of tests is significantly lower than expected, some useful trends were observed, as well as comparisons with previous aggregate interlock research.

The first test that was considered useful was an initial test that was conducted at a crack width of 0.024 inches and a shear load of 3 kips. This test was conducted on the Levy #1 concrete specimen.

The next two tests that are useable and were tested under the same parameters at a 0.05-inch crack width and a 4.5 kip load are as follows:

Levy specimen #3
Presque Isle specimen #3

The next five useable tests that are directly comparable are the following tests:

Levy specimen #5,
Presque Isle specimen #2
Presque Isle specimen #4,
Bruce Mines specimens #3
Bruce Mines specimen #4

These five tests all had the same crack width of 0.035 inches; a continuous loading cycle at 2 Hz, and amplitude of 3.0 kips. All of the load and displacement versus time plots are provided in Appendix A through D.

The first test conducted was on the Levy #1 specimen, which had a low slump and high compressive strength and was considered expendable, was tested with a 0.0240-inch crack width, 3.0 kip load at 2.5 Hz. The sample lasted for 48 hours without reaching the failure criteria. After 48 hours, it was decided to discontinue the test since it was planned to run the tests so that they would not exceed 48 hours. However, to complete the Levy #1 test, the crack width was increased to 0.050 inches, and the test continued. It failed after 240 cycles or approximately two hours at the 0.050 inches crack width. It was determined, at this point; that the 0.024 inch crack width was too tight (too efficient) to conduct testing in a reasonable time frame, at 3.0 kips.

Following this test, the Presque Isle specimen #3 was placed in the apparatus and tested at a crack width of 0.050 inches and a load of 4.5 kips. This test lasted 41 hours, and reached failure at 147,000 cycles. Following this test, the Levy #3 block was tested under the same conditions as the Presque Isle #3. The results of this test were surprising since the sample failed after 50 minutes, with only 2900 cycles. Based on these test results, it was decided to use a 0.035 inch crack width with a 3.0 kip load at 2 Hz for the remaining test specimens, which now numbered 14. However, as stated previously, trouble with the hydraulic pump system started after these initial tests were completed.

4.4.1 Analysis of Aggregate Interlock Tests

The primary parameter investigated is the amount of degradation that occurred over a given number of cycles for a fully reversing sine wave load. Since the interface degradation results in greater vertical (shear) displacement, which is required to resist the shear load, the aggregate interlock degradation can be given in terms of displacement versus the number of loading cycles.

The first two tests that are comparable are the Levy #3 and Presque Isle #3, which were conducted in the test evaluation phase with a crack width at 0.050 inches and a load of 4.5 kips. The shear displacement versus loading cycles for these tests is shown in Figure 4.10. Note that the loading cycles are plotted on a log scale. In these tests, as noted above, the Levy sample only lasted 2,900 cycles, while the Presque Isle sample lasted 147,000 cycles, or 50 times the cycles to failure for the Levy sample.

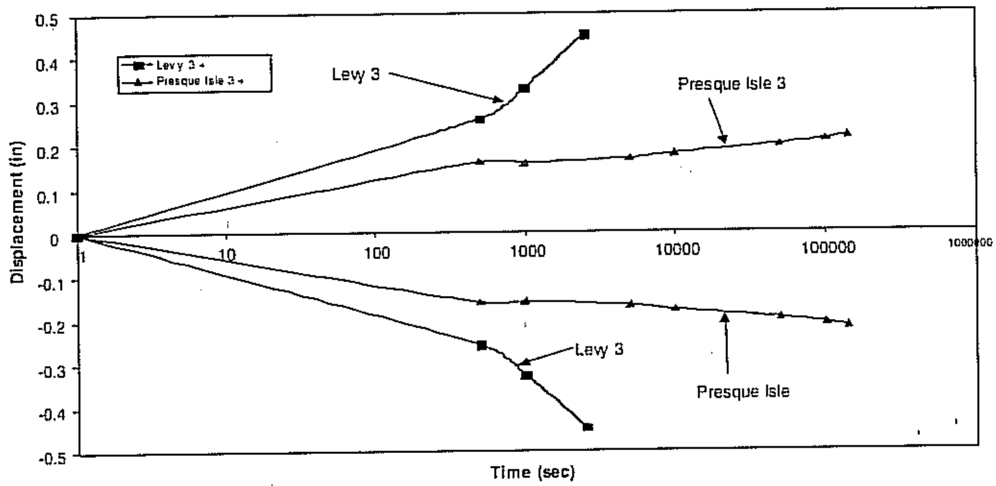

Figure 4.10 Aggregate interlock failure at 0.050 inches, 2.5 Hz, 4.5 kips, 0.4 sec sine wave, 0.6 sec rest, and the load wave produced by DasyLab.

The five tests that are comparable are shown in Figures 4.11 through 4.13, with the Levy #5 test is shown in Figure 4.11, the Presque Isle tests #2 and #4 shown in Figure 4.12 and the Bruce Mines tests #3 and #4 in Figure 4.13. Since two tests were performed for the Presque Isle and Bruce Mines concrete, a dashed line has been placed on the figures to illustrate the average of the two tests. It can be noticed in Figure 4.13, the Bruce Mines concrete specimens, that the two tests are very consistent. The two tests for the Presque Isle specimens in Figure 4.12 are not as close but have the same pattern of interface degradation. Unfortunately, there was only one Levy test for this test parameter so no comparison can be made.

Figure 4.14 presents the combined results of the aggregate interlock test at a crack width of 0.0350 inches and a shear load of 3 kips. Based on previous research it was anticipated that the stronger coarse aggregate concrete would provide better aggregate interlock and degrade slower than the weaker coarse aggregate concrete, as suggested by Colley and Humphrey (1967) and Abdel-maksoud, (2000). However, the opposite happened as seen in Figure 4.15. Under the same loading condition, crack width and failure limit, which was set at 0.5 inches overall; the Bruce Mines concrete reached the failure limit in approximately, 21,000 cycles for block #3 and 43,000 cycles for block #4, an average of 32,000 cycles; the two Presque Isle samples (#2 and #4), reached 345,000 and 350,000 cycles respectively; the one Levy slag concrete sample reached 500,000 cycles and was stopped prior to reaching the failure limit. As stated earlier, these results were opposite of what was expected.

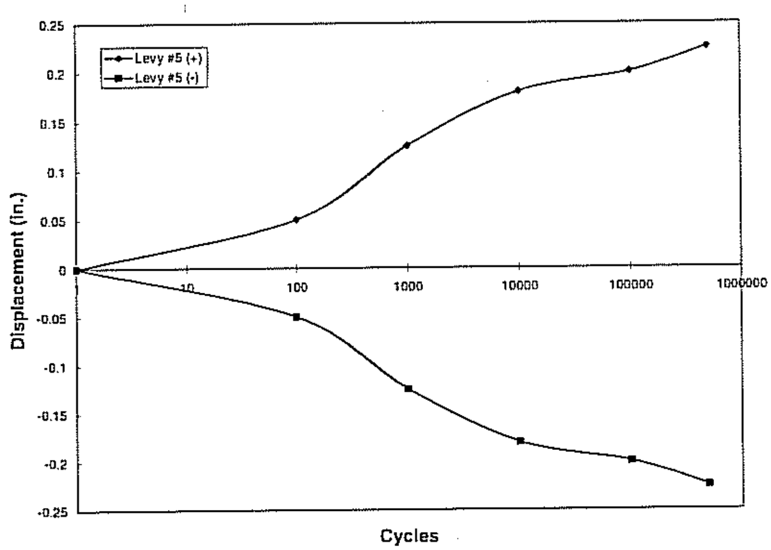

Figure 4.11 Vertical displacement versus loading cycles for the Levy concrete specimen illustrating concrete interface degradation at 0.035 inch crack width.

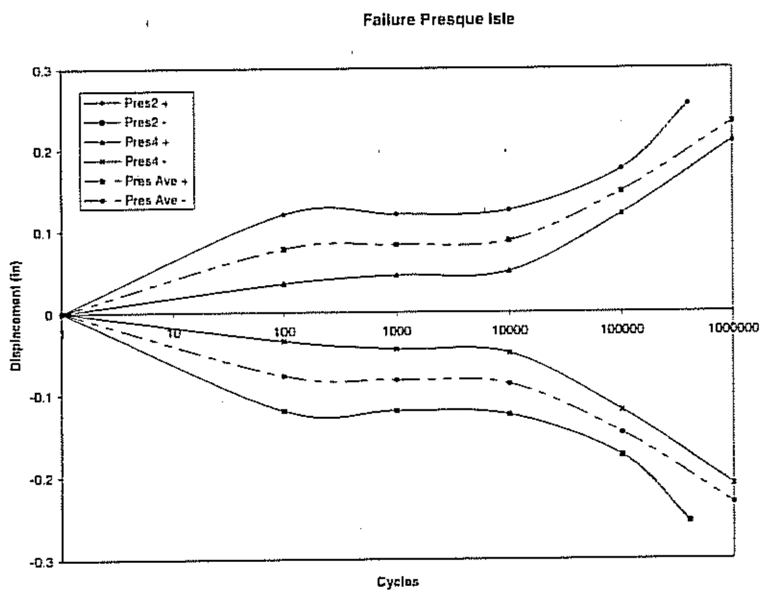

Figure 4.12 Vertical displacement versus loading cycles for the Presque Isle specimens #2 and #4 illustrating concrete interface degradation at a crack width of 0.035 inches.

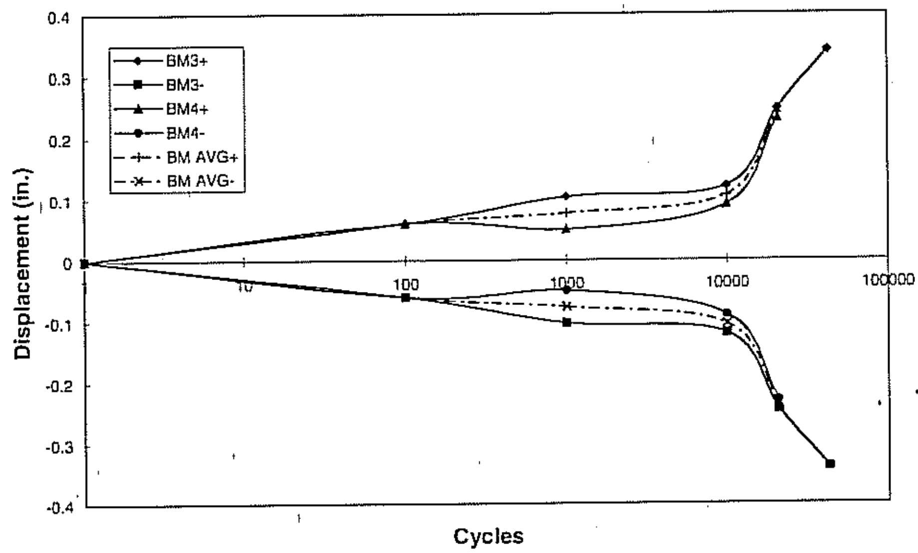

Figure 4.13 Vertical displacement versus loading cycles for Bruce Mines specimens #3 and #4 showing interface degradation at a crack width of 0.035 inches.

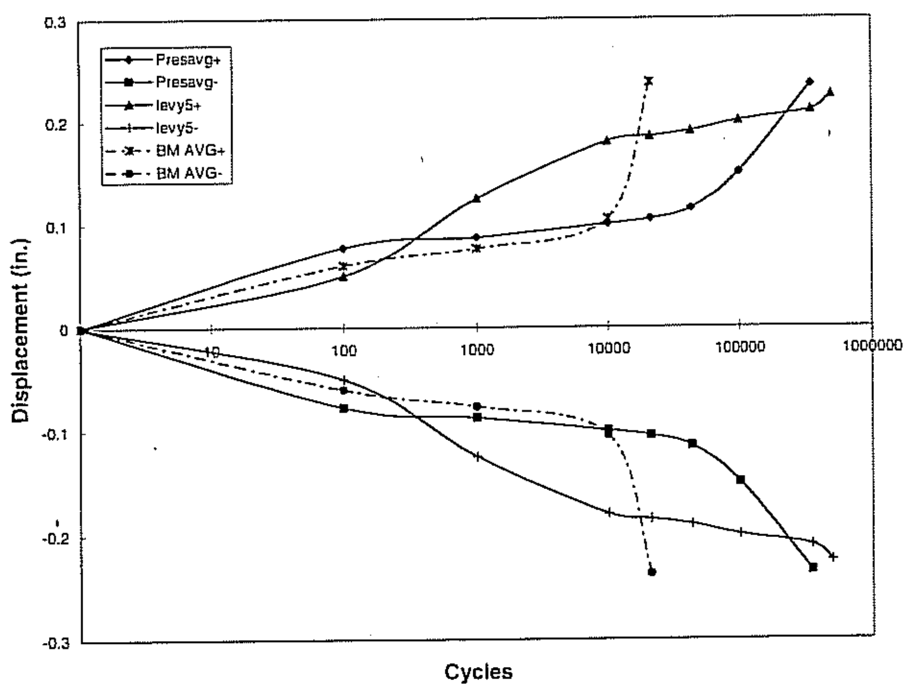

Figure 4.14 Aggregate Interlock sample Failure at 0.0350 inch crack width, 2 Hz, 3.0 kips, continuous sine wave, and load wave produced by MTS 407 controller.

An additional measurement made during the test was to collect the material that was generated below the crack interface. As expected, the majority of this material was well pulverized, with some larger pieces, which fell off the concrete faces when the samples were removed from the sample holders. This material was weighed for each test and the measurements presented in Figure 4.15. From this data, it can be seen that the Bruce Mines samples produced the greatest amount of debris while the Levy samples produced the least amount. This is in light of the Levy concrete being under the same test conditions, with 15 times more loading cycles. Again, it is important to note that these tests were at a crack width of 0.0350 inches.

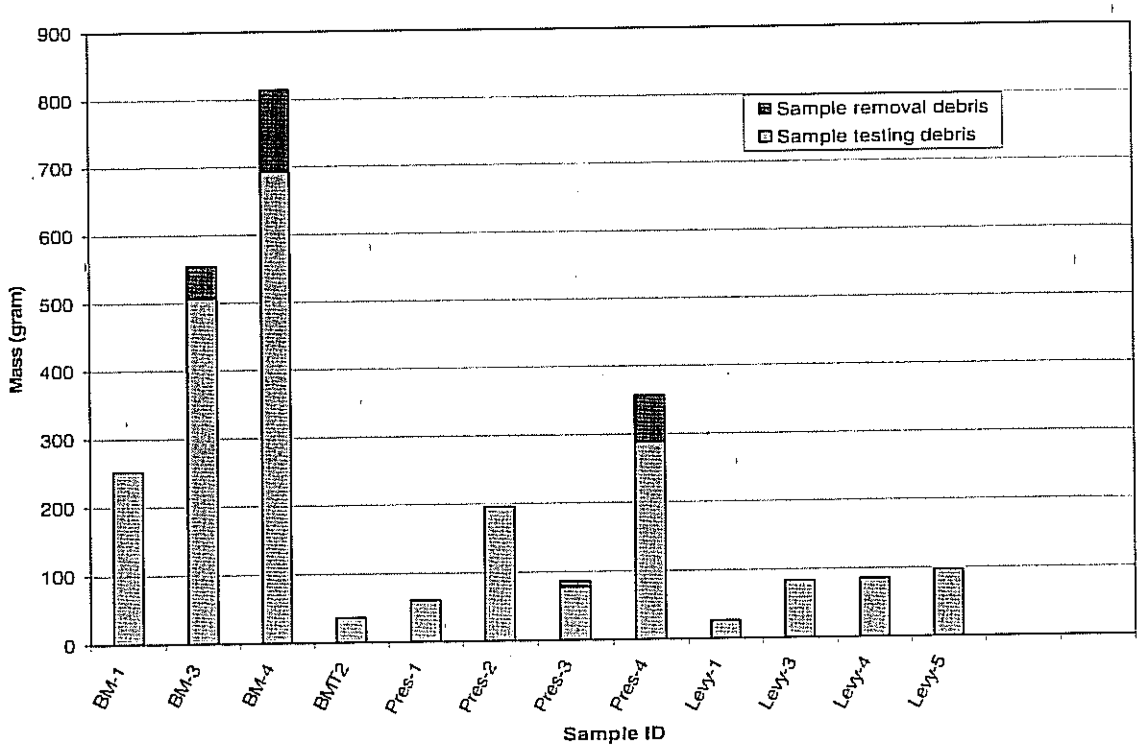

Figure 4.15 Joint interface debris collected after interlock testing.

Table 4.3 Aggregate interlock tests data.

Bold face indicates usable test:

Sample ID	Crack width (in)	Load signal (per sec)	Load Amplitude (kips)	Load Frequency (Hz)	Time test ran	Cycles	Date Tested	Comments
Levy 1	0.024	0.40 sec sine, 0.60 sec rest.	3	2.5	Over 48 hours		8/2/00	Had 2 hrs of operation but failed
Levy 2								Sample had low slump: not used
Levy 3	**0.05**	**0.40 sec sine, 0.60 sec rest.**	**4.5**	**2.5**	**50 minutes**	**2900**	**8/7/00**	Full displacement of 0.5 inches
Levy 4	0.035	continuos	3-5	5	1.5 hours	450	9/20/00	Pump shut down 3 time: Failed
Levy 5	**0.035**	**continuos**	**3**	**2**	**69.5 hours**	**500000**	**10/13/00**	**Good test.**
Levy 6	0.035	continuos	3	2	1 hour	120	10/19/00	Pump shut down 3 time: Failed
Presque 1	0.024	continuos	3	5	3 - 4 hours		9/14/00	Used for system setup.
Presque 2	**0.035**	**continuos**	**3**	**2**	**48 hours**	**345600**	**10/8/00**	**Good test.**
Presque 3	**0.05**	**0.40 sec sine, 0.60 sec rest.**	**4.5**	**2.5**	**41 hours**	**147000**	**8/5/00**	**Good test.**
Presque 4	**0.035**	**continuos**	**3**	**2**	**48.5 hours**	**350000**	**10/16/00**	**Good test.**
Port In 1	**0.024**	**0.1 sec sine, 0.9 sec rest**	**3**	**2**	**5.75 hours**	**20750**	**9/11/00**	**Adjust p-gain after 1 hour Reached 1.5 inches**
Port In 2	0.035	continuos	3-5	5	30 minutes		9/22/00	System failure, bad Accumulator?
Port In 3	0.024	5X0.2 sec sine	8	5	5 minutes	300	9/13/00	Bad data, too high of loads. used for system setup. Failed
Port In 4	0.035	continuos	5-3	5	220 sec	1100	10/8/00	System could not keep up. Failed
Bruce Mines 1	0.024	3X0.1 sec sine, 0.2 sec rest		10	800 sec	2400	9/9/00	New chip, new wave. Failed
Bruce Mines 2	0.024						9/5/00	Failed, new e-prom chip
Bruce Mines 3	**0.035**	**continuos**	**3**	**3, then 2 at 5116**	**2.25 hours**	**21348**	**10/12/00**	**Good test.**
Bruce Mines 4	**0.035**	**continuos**	**3**	**2**	**6 hours**	**43000**	**10/18/00**	**Good test.**

4.5 Aggregate Interlock Results Discussion

Although fewer tests were successful than anticipated, the results are useful. Basically, the aggregate interlock test results at a 3 kip load and a crack width of 0.035 inches showed that the weaker coarse aggregate concrete handled more loading cycles than the stronger coarse aggregate concrete. This result was surprising based on the research results of Colley and Humphrey (1967) and the University of Illinois (2000),. which resulted in the opposite findings. However, in evaluating the test conditions and results as well as examining previous literature, other factors may have contributed to this result. To discuss the results the following six factors will be examined: (1) stress level, (2) crack width, (3) joint surface morphology, initial shear loading degradation, (5) effect of concrete strength, and (6) hydraulic system performance.

4.5.1 Stress Level

The first factor examined concerns the stress level applied to the concrete specimens. The original load applied to the specimens was 9.0 kips, which was based on a wheel load of 9.0 kips and previous research using a 9.0 kip load. After initial testing, this load was found to cause excessive damage to the concrete interface and was subsequently reduced to 4.5 kips and later to 3.0 kips, based on a simplified 2:1 slope stress distribution at mid-depth as discussed previously. This would be consistent with other researchers who also used lower shear stress levels when conducting aggregate interlock testing. Although a relatively simplified analysis, the average shear stress acting on the concrete interface in this research was estimated by dividing the load applied to the interface by the cross-sectional area of the concrete specimen. For a 3.0 kip load[1] the average shear stress was 47 psi at the concrete interface. As a comparison, the University of Illinois's research on studying airport pavements used 72 psi in their original testing, then after experiencing excessive damage to the concrete interface, reduced the loading to 49 psi. The research by Colley and Humphrey (1967) used an average shear stress that ranged from 12 psi to 28 psi. This would suggest that the 47 psi

[1] The cross-sectional area of the concrete specimens was 64 inches.

average shear stress used in this research was high in comparison to the Colley and Humphrey research on road pavements and the Illinois research on airport pavements. For example, an 18 kip single axial load, on a 12-foot wide, 10-inch thick slab, would place an average shear stress of 12.5 psi on the joint interface, assuming of course that the wheel loads were equally distributed across the joint interface.

Interestingly, Colley and Humphrey's research indicated that there appears to be a critical stress level below which the effectiveness of the joint does not appear to degrade. That is, there is a stress level at which, once below this stress level, limited degradation to the interface will occur. On the other hand, Illinois's research suggests that there is both a lower limiting stress at which when exceeded limited joint interface degradation begins and a higher stress level that when exceeded significant interface damage starts. Based on this observation, Illinois suggests that the "allowable stresses (on a joint interface) should be designed in a manner that protects joint interfaces from significant damage rather than designing it as a function of concrete strength." That is, Illinois is suggesting that the joint should be design based on its maximum expected stress level as opposed to specifying a given concrete strength for the PCC pavement.

4.5.2 Crack Width

The second factor is the crack width used during testing. In all of the tests conducted the crack width remained relatively constant during the shear loading as shown in Table 2.1. This indicates that the horizontal hydraulic actuator functioned well.

From field evidence and previous research, the crack width of 0.024 inch is considered an efficient crack width. Consequently, testing at this width for any concrete type, i.e., for different coarse aggregates, should prove effective, as long as excessive loads are not placed on the interface. This was seen in the first slag concrete specimen tested, which ran for 48 hours, with minimal damage and in which the 0.5-inch failure limit was not reached. However, joint openings in Michigan have been measured at 0.060 inches and larger. The Illinois research tested crack width ranging from 0.030 to 0.100 inches. A crack width of 0.060 inches would be considered mid-range, while the joint opening used in this research, 0.0350 inches, would be on the lower end of the

Illinois research. Even at the smaller crack widths, though, the Illinois research indicated that stronger coarse aggregate concrete provides better aggregate interlock than weaker coarse aggregate concrete as seen in Figure 1.5 of this section. Nowland (1968) also suggests that stronger coarse aggregate concrete should provide stronger aggregate interlock. However, the tests conducted at a crack width of 0.0350 inches crack showed that the slag and limestone aggregates, which are weaker aggregates, performed better than the stronger igneous aggregate, as shown in Figure 4.14. That is, the number of cycles to failure was greater for the slag and limestone concrete than for the traprock (basalt) concrete. At a crack width of 0.05 inches for the slag and limestone concrete, however, the stronger limestone performed significantly better than the weaker slag. This finding is consistent with the Illinois research. That is, as the crack width increases the strength of the aggregate becomes more important for aggregate interlock.

A possible explanation for test results at the crack width of 0.035 inch can be provided using the University of Illinois research findings as well as observations made in this research. The Illinois aggregate interlock research proposed two mechanisms that contribute to the mobilization of friction at a PCC joint and which are directly related to crack width. The first mechanism occurs in joints with larger crack widths in which the surface-to-surface contact is largely by coarse aggregate contact. During shearing the interface surfaces will have a greater tendency to dilate, or override the roughness of the surfaces. When dilation occurs, normal stresses develop at the interface due to the restraining action of the concrete slabs. Conversely, the development of normal stresses indicates that the joint is mobilizing shear resistance by dilation. It is the development of normal stresses that also cause significant damage (degradation) to the interface by the crushing and wearing of the aggregate-to-aggregate contacts. The second mechanism occurs in joints at smaller crack widths and with smoother surfaces. At a smaller crack width, joints mobile shear resistance by shearing through the interface roughness and developing frictional resistance and to a lesser degree by dilation, i.e., developing normal stresses at the interface. A result of mobilizing frictional resistance as opposed to dilation is that smaller normal stresses develop at the interface. This concept is illustrated in Figure 4.16 where the smoother surface (block A) has a smaller normal force developed as opposed to the rougher surface (block B) with a larger normal force developing.

Again, the development of the normal forces is a result of the two slabs being restrained from movement as the surfaces attempt to push past each other apart during shear loading.

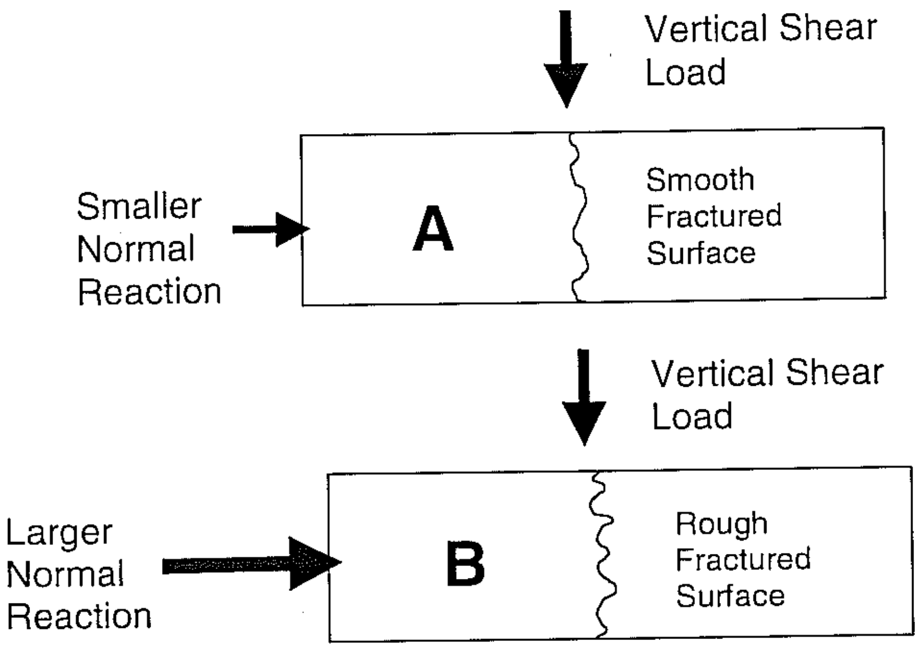

Figure 4.16 Rough versus smooth fracture surface and the development of normal stresses.

In considering these two mechanisms coupled with the higher shear stress levels used in this research, it is possible that the shear stresses were too high. At the 0.0350 inch crack width, coupled with a high interface shear stress of approximately 49 psi, the stronger coarse aggregates may have sheared through the weaker cement paste as well as dislodging embedded coarse aggregate. This would explain the large amount of material generated from the interface of the igneous samples. This was also seen in the Illinois research where the shear stress level on basalt coarse aggregate concrete (traprock) was increased by a factor of 1.6 with the resulting interface degradation increasing by 3.7. As shown in Figure 4.2, the difference in strength for the Bruce Mines concrete between the coarse aggregate (both dynamic and static strength) and the concrete is significantly large. On the other hand, for the slag concrete, the strength of the concrete is somewhat greater than the strength of the slag coarse aggregate. When the difference in strength between the coarse aggregate and concrete is large, such as for the Bruce Mines concrete, the possibility of the stronger coarse aggregate gouging the cement paste appears plausible for higher shear stresses. When the strength of coarse aggregate and the cement paste are similar, however, it is equally plausible that this would diminish the damaging effects of protruding stronger aggregates and would enhance the mobilization of friction with smaller normal stresses developing at the interface and consequently less interface damage. Thus, at a crack width of 0.0350 inches and the shear mobilization through friction as opposed to dilation the lower strength coarse aggregate may produce better aggregate interlock at high shear stresses. However, a number of other factors must also be considered in evaluating the results of these tests.

4.5.3 Joint Surface Morphology

Another significant factor involved in joint efficiency is the morphology or roughness of the concrete surfaces as noted above. In general, for any shape concrete surface, i.e., smooth or rough, the smaller the crack opening the greater number of surface-to-surface contacts there will be as opposed to larger crack widths. The larger number of surface-to-surface contacts during shear loading would then reduce the shear stress level at the contact points for a given surface load. The roughness or shape of the concrete surface also plays an important role in the shear stress transfer. For surfaces that are relatively flat or smooth the contact area will dramatically reduce as the crack opening increases. For rough surfaces the displacement that the surface may have to undergo to achieve shear resistance may be larger but at some point the surfaces will come into contact.

The difference in the morphology of the surfaces can be seen in Table 4.2 in the measurement of maximum roughness. Maximum roughness was defined as the maximum distance from the lowest point on the concrete surface (as defined by the four corners of the concrete specimen) to the highest point as illustrated in Figure 4.17. While visually the Bruce Mines concrete had the roughest surface and the slag the least rough, the measurements in Table 4.2 confirm this observation with a maximum roughness of 1.35 and 1.40 for the Bruce Mines concrete, 1.20 for the Presque Isle concrete and 1.05 for the slag concrete. The topographic mapping of the surfaces also suggest that the Bruce Mines had the roughest surface followed by the Presque Isle then the slag concrete as seen in Figures 4.6 through 4.9.

Although only two tests were conducted at a crack width of 0.05 inches, there was a large drop off of loading cycles for the slag concrete compared to the Presque Isle concrete as shown in Figure 4.10. This result would suggest that for smoother surfaces a larger crack width would result in a reduced interlocking capability. This can be seen in Figure 4.18 where the loading cycles for the slag concrete, at a crack width of 0.024, 0.035 and 0.05 inches, are compared. It should also be noted that a 4.5 kip load was used in the 0.024 crack width tests. Although insufficient tests were conducted to confirm that aggregate type plays a role in joint efficiency, the data does suggest that if aggregate type influences the shape of a joint's fracture surface (morphology), then the crack width opening can strongly influence joint efficiency with rougher surfaces performing better at larger crack widths. Conversely, the smoother surfaces will perform poorly at larger crack width compared to the rougher surfaces. In contrast to this, the data also suggest, although again not enough tests were conducted to confirm this, that smoother joint surface may perform better at smaller crack widths than the rougher surfaces, depending on the level of stress induced at the interface.

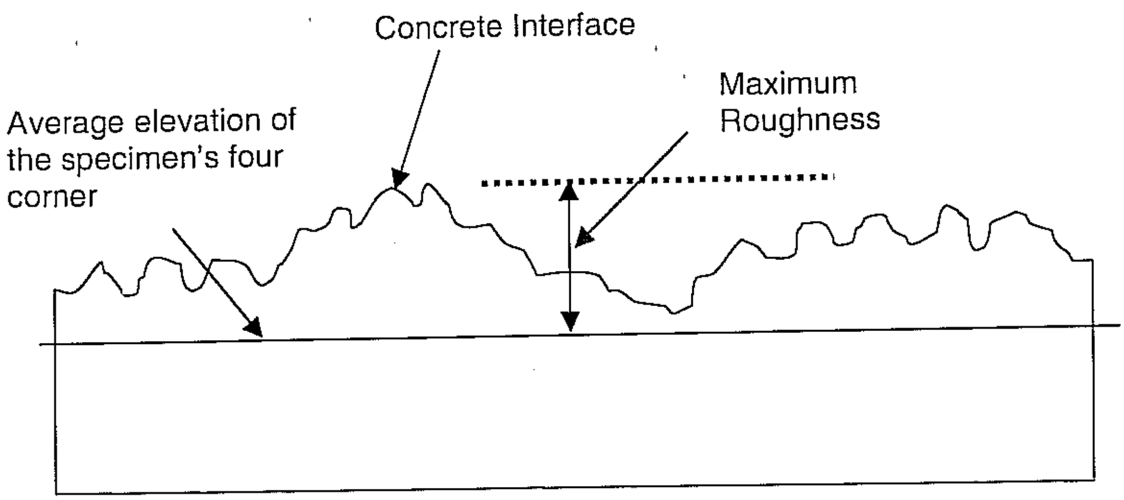

Figure 4.17 Definition of maximum roughness.

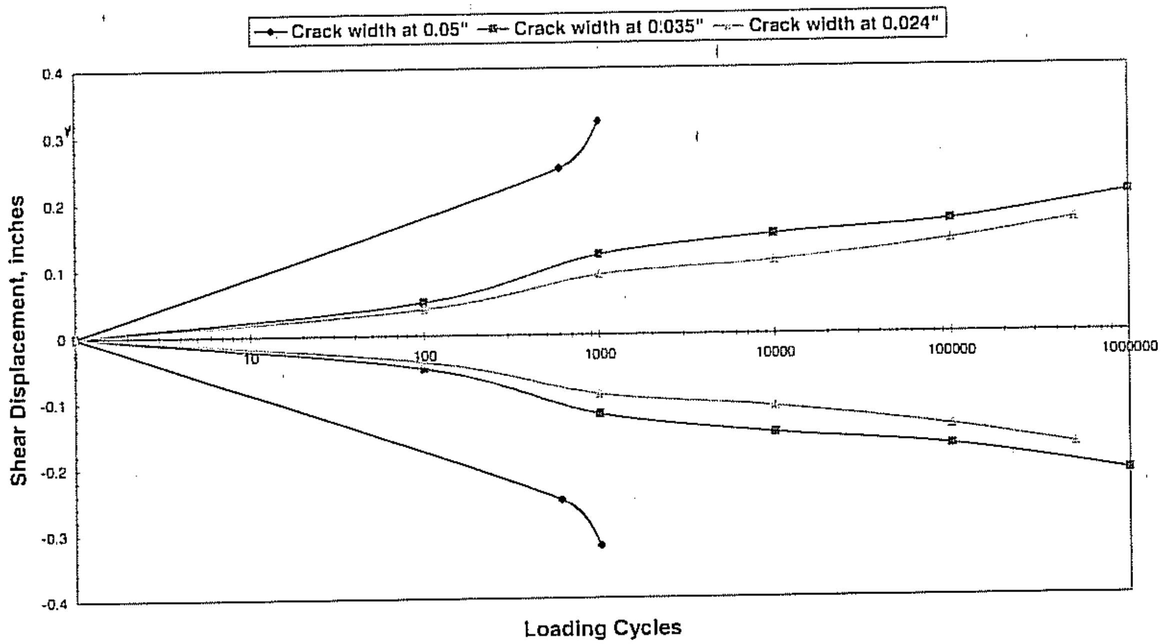

Figure 4.18 Comparison of shear displacement versus loading cycles for slag concrete at cracks widths of 0.024, 0.035, and 0.050 inches.

4.5.4 *Initial Shear Loading Degradation*

In all of the aggregate interlock tests conducted in this research as well as the research reported by Illinois, the majority of interface degradation occurs in the in the first 1000 loading cycles followed by degradation between 1000 and 10,000 cycles. As noted previously, all of the degradation plots in this chapter have the loading cycles plotted in a log scale. In viewing these plots, then, the change in degradation up to 1000 and between 1000 and 10,000 loading cycles is relatively apparent. Interestingly, the degradation in the Bruce Mines concrete has a significant change in the rate of degradation at 1000 cycles, the slag concrete also at 1000 cycles while the Presque Isle concrete has a change at 10,000 loading cycles. In the Illinois research, the change in rate of degradation was noted to be a function of crack width. For example, for crack widths at 0.01 inches (0.254 mm) the change in rate of degradation was at 1000 loading cycles while for a crack width of 0.030 inches (0.76 mm) the number of loading cycles increases to 10,000 cycles. A reason for this change in degradation behavior between

1000 and 10,000 was not discussed but appears to be relatively consistent throughout the aggregate interlock research.

An additional consideration concerning interface degradation is the initial crack width. At small crack widths the shear displacement on the first cycle should be less than for larger crack widths. That is, as the crack opening increases it should take more shear displacement to resist the shear loading. This means that at a fixed shear displacement limit of 0.5 inches, the larger crack openings should reach this limit at a lower number of cycles than at smaller crack widths. However, this was not evaluated in this research but should be a factor in considering the amount of displacement between the two concrete blocks during future aggregate interlock testing.

4.5.5 *Effect of Concrete Strength*

As reported earlier research on the effect of concrete strength on aggregate interlock was inconclusive with some research indicating that it is important while others indicated that it had a minimal effect. While not enough tests were successfully conducted in this research, it is interesting to compare the strength of the concrete for the specimens tested at 0.035 inches. As shown in Figure 4.14 the slag concrete, which had the largest number of loading cycles, had a 28-day unconfined compressive strength of 4,704 psi, followed by the Presque Isle concrete at strength of 6,838 psi and the Bruce Mines concrete with strength of 4,456 psi. While the Bruce Mines concrete had the lowest concrete strength and load cycles to failure, the slag concrete had the largest but its strength was significantly closer to the Bruce Mine concrete strength. Consequently, this data did not support the research that shows that concrete strength is an important parameter in aggregate interlock. This collaborates the Illinois research that state "The strength of intact concrete alone, as measured in a 28-day unconfined concrete compression test, does not have a significant impact on joint performance. Other factors such as aggregate size, aggregate quality, and roughness have a more dominant role on joint performance under cyclic shear than concrete strength." However, more testing would have to be conducted before this issue can be resolved.

4.5.6 Hydraulic System Performance

A significant factor in the dynamic testing of materials is the ability of the servo-hydraulic closed loop control system to conduct the required test. That is, can the testing system perform what the control system is requiring? Since the aggregate interlock tests were conducted in load control at a 2 Hz frequency, the ability of the system to consistently provide this load must be considered. In addition to these factors, a more critical factor is the stiffness of the material being tested; in this case the aggregate interlock stiffness. This issue was addressed in chapter three of this section, which discussed the PID control settings of the MTS 407 controller (for the vertical actuator) and the adjustment of the PID to account for the stiffness of a given test material. In general, the stiffness of the material being tested determines how much displacement will occur for a given load. For highly deformable materials there will be significant displacement at a given load. In dynamic testing this becomes a problem since the hydraulic actuators will need to travel further to obtain the desired load. This in turn requires a higher flow rate of hydraulic fluid from the pump. For many dynamic tests the size of the hydraulic pump limits the speed at which a test can be performed. A major consideration of testing aggregate interlock of concrete specimens is not only the initial stiffness of the concrete interface but, as shown by the results in this research, the change in stiffness as degradation occurs. That is, the amount of displacement (degradation) increases for each 3 kip load applied. This is a fundamental consideration in examining the results of this research as well as other research where cyclical loads are applied to a degrading interface.

The aggregate interlock research using hydraulic actuators that was similar to this research, was the Colley and Humphrey (1967) and the Illinois research (Abdel-maksoud, 2000). In the Colley and Humphrey testing two hydraulic actuators were used, one on each side of the joint. However, no discussion was provided concerning the performance of the hydraulic system. Since both actuators were in compression and were simply offset by a time delay to simulate traffic loading, though, it is highly likely that they performed adequately. The difficulty in dynamic testing is when a loading sequence requires both compressive and tension loading in the same cycle, which was required in this research and also in the Illinois work. In the Illinois work, however, the testing frequency was significantly longer. According to Abdel-maksoud (2000) the majority of tests were conducted at a loading rate of 0.05 Hz and some at 0.10 Hz. However, no mention of the waveform type used in the testing was provided. It is assumed from the experimental discussion that a triangular waveform was in fact used. This means that the tests were conducted at a 20 second and ten second loading cycle, which is longer than the 2 Hz frequency i.e., 0.5 second loading cycle, used in this research. In the Illinois work a 25 kip actuator was used with a 20 gpm hydraulic pump and an 8500 Instron controller. Based on previous research conducted by the author this system should be adequate for testing the aggregate interlock based on two assumptions. First, the 8500 Instron controller[2] is an excellent controller with the ability to use auto-adapting loop shaping to change the PID setting as the system stiffness changes during testing. However, there is no discussion in the Illinois research concerning the use of the auto-adapting capability of the Instron unit or if not available how the system response to changing stiffness was handled. However, the following statement concerning changing stiffness during aggregate interlock testing was provided: "The stiffness of the ram needed to be adjusted because of the reduction in the stiffness at the crack interface as testing progressed." This is the only statement concerning changing aggregate interlock stiffness in the Illinois research. However, the statement is somewhat confusing since the stiffness of the actuator should not change. It is the stiffness of the aggregate interlock interface that is changing and the only way to respond to the stiffness change is to adjust the control response of the system through the PID control settings. The second reason that the Illinois test system should have functioned adequately is that a 25 kip actuator with a three inch stroke and a 20 gpm pump should not have any difficulty conducting a 20 second loading cycle in both compression and tension. As a comparison, in this research two 55 kip actuators with ten-inch strokes were used with a 35-gpm pump.

In this research two MTS 407 digital controllers were used to independently control both the horizontal (to maintain a constant crack width in displacement control) and the vertical (shear loading in load control) actuators. The PID settings of the 407

[2] A 8500 Instron controller was used to test the 28-day unconfined compressive strength of the concrete test in Section Four.

controllers were set using a Levy slag concrete specimen. This control setting was used throughout all of the testing, since it was believed that the Levy slag concrete would have a lower joint stiffness than the Presque Isle or Bruce Mines concrete and require the most sensitive settings, e.g., highest gain setting. Accordingly, testing concrete specimens with higher stiffness (it was believed) would not require as sensitive a control setting, i.e., if the system response works adequately for the lower stiffness material it should function equally well for the higher stiffness material.

An example of the load and displacement versus time record for the Levy slag concrete specimen #5 (for which the control setting for all of the aggregate interlock testing was set) is shown in Figure 4.19. The displacement axis in Figure 4.19 is the total movement of the hydraulic actuator and not the LVDT's, which were measuring the displacement between the two concrete specimens, i.e., the relative displacement or shear displacement (degradation). It can be seen from this figure that the 3 kip compressive (positive) and tensile (negative) load was well maintained over the test[3]. The corresponding movement of the hydraulic actuator was also relatively consistent indicating that the test functioned well.

Figure 4.20 illustrates the load and displacement versus time for the Presque Isle (limestone) #4 concrete specimen. In this figure it can be seen that the start of loading was at 3.5 kips although the controller was programmed for 3 kips. The larger shear load may have resulted from the controller overreacting to the stiffer interface. However, between 40,000 and 50,000 loading cycles a change in the stiffness of the specimen occurs resulting in a change the shear load being applied. This change, at about 45,000 cycles, can also be seen in Figure 4.12 where there is a change in the degradation rate of the specimen, i.e., an increase in shear displacement. In addition, the ability of the control system to produce equal 3 kip compression and tension loads is changing with the system producing a slightly decreasing in compressive load while the tension load decreasing rather rapidly. As speculated above, it is believed that the primary reason for this happening is that the control settings (PID) were set too high to allow the limestone concrete test to run properly. In addition, as noted in the experimental setup discussion,

[3] The Levy #5 test run for 500,000 cycle which was 250,000 seconds.

the hydraulic system was also experiencing cavitation of the hydraulic fluid in the return lines, which may have also been a factor in the poorer response.

Figure 4.21 illustrates the load and displacement versus time for the Bruce Mines (basalt) #4 concrete specimen. This response is fundamentally different than the slag or limestone concrete. First, note that the vertical displacement of the hydraulic actuator is very small at about 0.1 inches. As a comparison, the initial vertical displacement of the limestone concrete is about 0.28 inches and the slag concrete is approximately 0.30 inches. This indicates that relatively little displacement was required to reach the 3 kip load in either compression or tension for the basalt concrete. Basically, the load was relatively consistent up to approximately 11,000 loading cycles, with a gradual increase in actuator displacement (degradation). However, at approximately 11,000 cycles the system became erratic and essentially unstable. This response occurred at 11,000 loading cycles for both basalt samples tested. After 11,000 loading cycles the hydraulic system was unable to apply equal compression and tension loads on the concrete. In effect, the hydraulic system was only able to apply the 3 kip compression load and limited tension load. This resulted in the hydraulic actuator continuously pushing down on the specimen with only a small tension load being applied during each cycle to relieve the compression load. The continuous downward movement of the actuator is seen as positive movement in Figure 4.20. As with the limestone concrete the cavitation in the return line may have played a role in this erratic behavior. However, it is strongly believed that the basic reason for this response is the inability of the MTS 407 controllers to adequately control the test due to the changing interface stiffness. Although the MTS 407 controller has PID control capability, it is made for relatively straightforward testing. It appears that a different PID setting should have been used for each aggregate type tested. It is believed that this would have resulted in better test data and an elimination of the erratic behavior of the system.

In reviewing Figure 4.14 it can also be clearly seen that both the limestone and basalt concrete had far less degradation between 1000 and 10,000 cycles than did the slag concrete. If the testing system had not become unstable it is likely that the test results would have been reversed with the basalt and limestone tests producing less degradation than the slag concrete for a given number of loading cycles. It is also likely that the large amount of damage (as measured by the amount of fragments collected after the test) as seen in Figure 4.15 can be explained by the hydraulic system becoming unstable. Therefore, it is strongly believed that the inability of the 407 controller to control the Bruce Mines test played a significant role in the low number of loading cycles to failure. In future aggregate interlock testing it is recommended that either an individual test should be conducted to set the PID control setting tests for each aggregate type tested or a more advanced controller such as the MTS TestStar controller, which can better handle changing system stiffness, should be used.

4.6 Aggregate Interlock Summary

Based on the research conducted in this report as well as existing aggregate interlock research the following summary is provided:

1. In reviewing aggregate interlock test systems used by other researchers, it is believed that the aggregate interlock test system developed and used in this research can be an effective system for testing aggregate interlock provided the following changes are made. First, the cavitation problem with the hydraulic return line must be eliminated. This can be accomplished by reducing the length of the supply and return hoses as well as slowing down the test frequency to one hertz (as opposed to two hertz). While changing the frequency will double the time for testing, it should also improve the test results. Second, a different controller must be used to control the vertical (shear loading) actuator. A MTS TestStar controller (or equivalent) is recommended to accomplish this task. Third, even with a better controller the PID control setting should be set based on the aggregate type concrete being tested. That is, one concrete specimen per coarse aggregate type should be used to determine the system response and PID control settings. It should be noted, however, that this specimen once used for control setting would probably not be useful for further testing. The main reason for this is that significant degradation occurs in the early stages of loading.

Consequently, it is likely that during the control setting that erratic behavior may occur, which will render the specimens as unusable.

2. It was apparent in the test results that aggregate interlock stiffness varies significantly between aggregate concrete types. The variation in stiffness is a function of the degradation of the interface.

3. The aggregate interlock test set is relatively easier to use and can be set up in a short period of time. It has been estimated that a test specimen (cured and ready for testing) can be set up in approximately two hours. As a comparison, in personal communications with the personnel at the University of Illinois it was stated that it took them approximately two days to set up a test sample.

4. Another feature that significantly improves aggregate interlock testing is the ability to maintain a constant crack width during testing. Since the horizontal actuator is used to accomplish this, it is relatively straightforward to adjust the crack width for any width desired. In addition, it would be possible to vary the crack width to simulate warm (small crack width) and cold weather (large crack widths) effects during a single test if desired.

5. While not enough successful aggregate interlock tests were conducted, the data that was obtained suggests that for small crack widths the coarse aggregate type may not significantly affect aggregate interlock. This is especially true for crack widths at 0.024 inches. However, for large crack widths the strength of the coarse aggregate may play an important role. This was demonstrated in the Illinois research and in the two tests conducted at 0.05 inches in this research. However, it is unclear as to whether the concrete surface morphology plays a more critical role or the strength and deformation properties of the coarse aggregate in maintaining aggregate interlock.

6. However, it appears that the coarse aggregate type does affect the morphology of the concrete fracture surface. While the method used to quantify surface morphology was not as successful as anticipated, it did reveal to some extent that the stronger aggregate (Bruce Mines) generated a rougher surface than the weaker aggregate (Levy slag). However, additional testing will have to be conducted to verify this observation. Newer technologies are now available that may be

provide a better means of quantifying the surface morphology, such as the use of digital imaging systems.

7. The sample fracture device worked well producing consistent concrete specimens. It is recommended that future testing monitor the strength of fracture as well as the deformation to failure. In fracturing the concrete it was apparent that coarse aggregate types play a role in the strength at fracture. For example, the Levy slag concrete always required higher pressure to fracture the concrete. It is possible that this higher pressure required for fracture might generate smoother fractured surfaces with a high percent of coarse aggregate fractures. Lower pressure fracture appeared to produce rougher surfaces with less coarse aggregate fracture.
8. Concrete strength does not appear to be a significant factor in aggregate interlock performance at large crack widths. This may be an important fact for future testing since it suggests that testing specimens at significantly different times in relation to their 28-day strength may not be important. That is, concrete may be tested anytime after a 28-day cure.
9. The stress level used in aggregate interlock testing should be no greater than 49 psi and preferably less.
10. The aggregate interlock test was conducted under pure aggregate interlock since no base reaction was provided.

Levy #5 Displacement

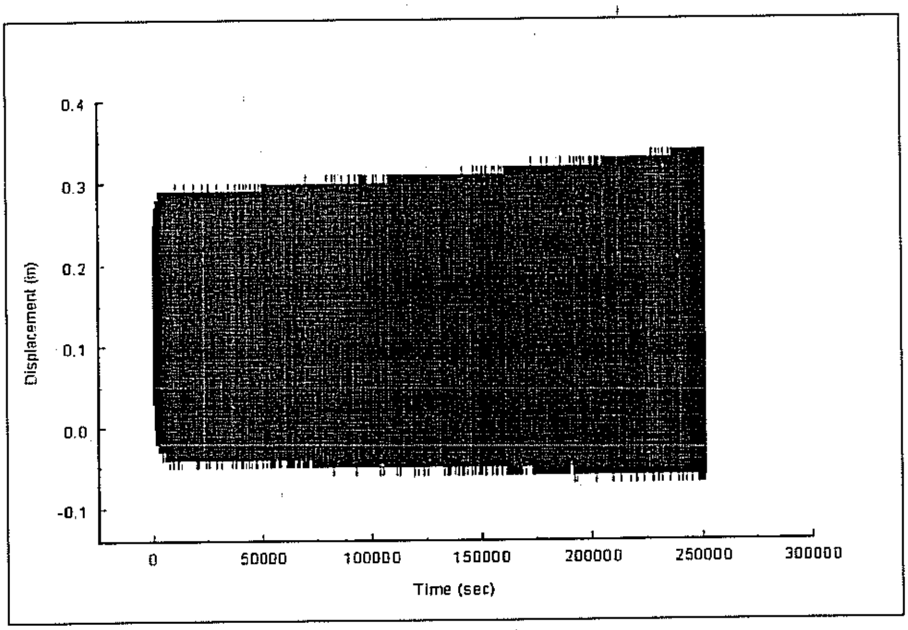

Levy #5 Load

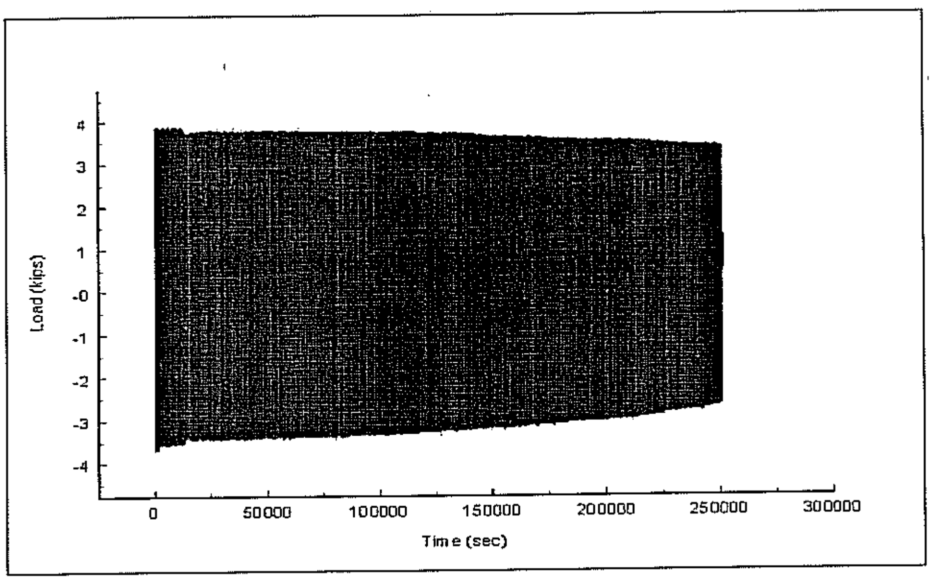

Figure 4.19 Load and displacement response versus time for slag concrete.

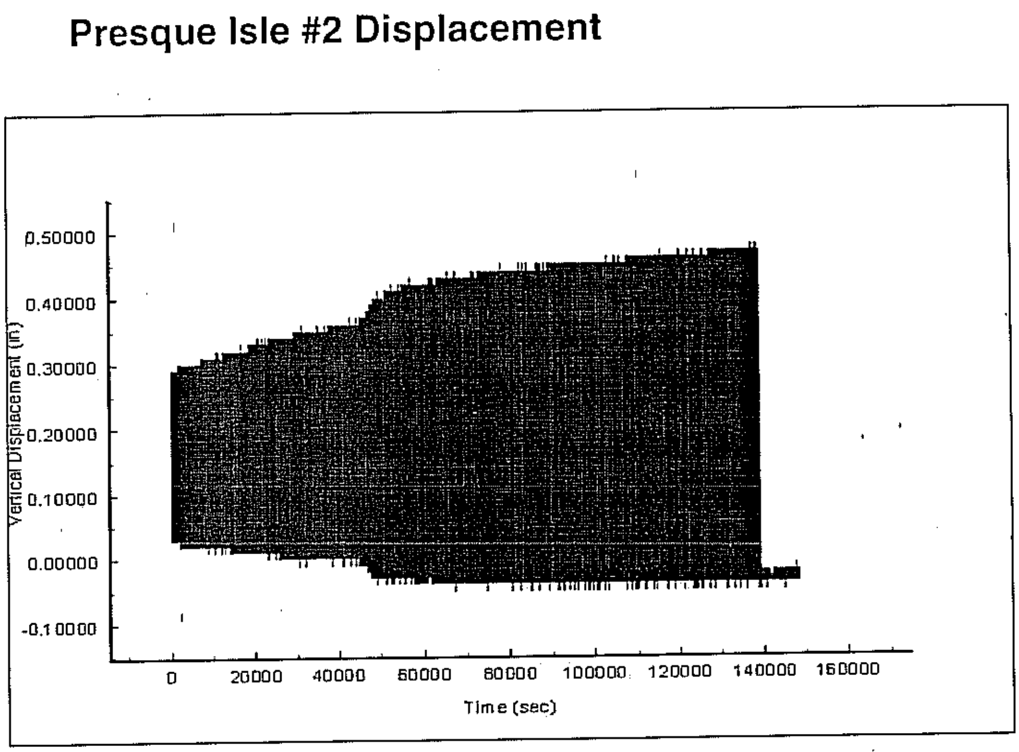

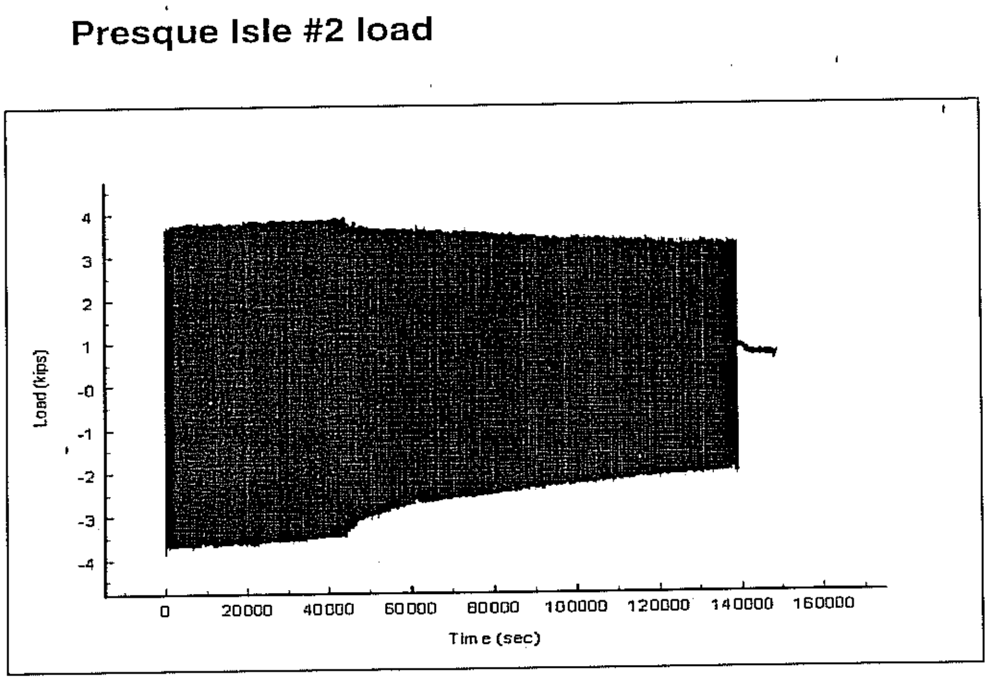

Figure 4.20 Load and displacement response versus time for Presque Isle concrete.

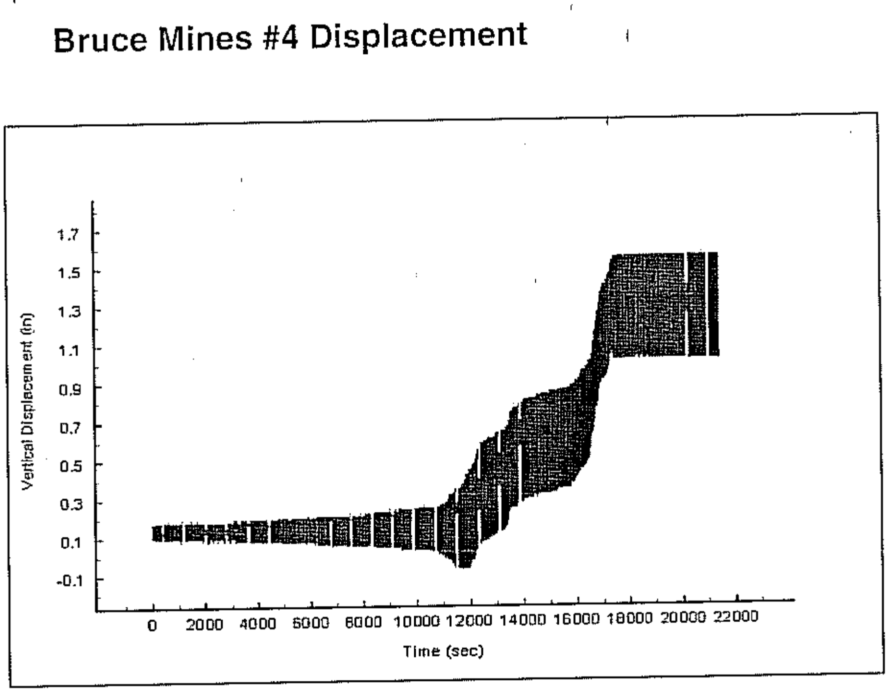

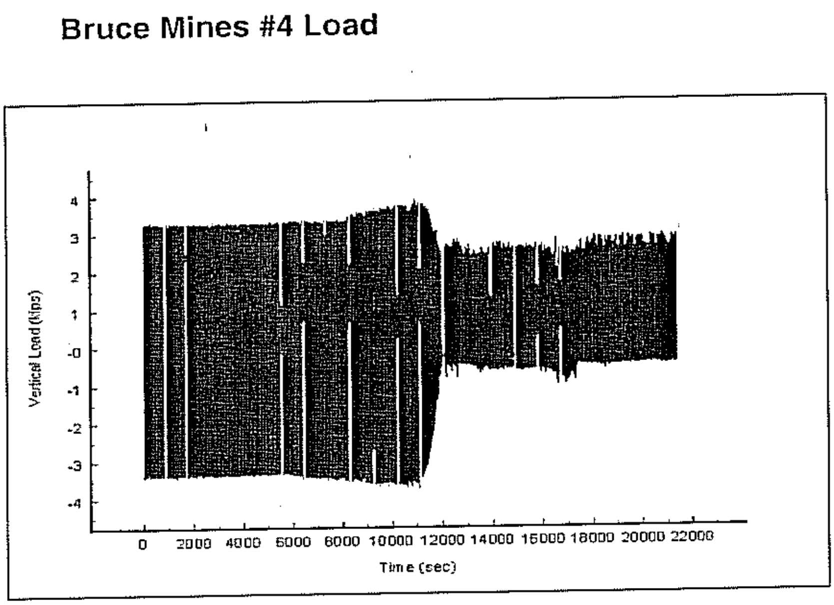

Figure 4.20 Load and displacement response versus time for Bruce Mine concrete.

5 Conclusions and Recommendations

There were five objectives for the research presented in this section. The first objective was to make improvements in the aggregate interlock test system to better replicate field conditions. The second objective was to prepare consistent concrete samples for testing with only the coarse aggregate as a variable. The third objective was to improve the ability of the sample fracture device to better split the concrete test blocks. The fourth objective was to develop a method to characterize the fracture surface of the concrete. The fifth and final objective was to conduct aggregate interlock tests on concrete made from different coarse aggregate types. This chapter provides the conclusions and recommendations from this aggregate interlock research.

1) The test and control system used was reprogrammed from a purely compressive loading to both a compressive and tensile load on the concrete sample interface with a 0.9 second constant minimum load. However, due to system limitations, the system was not able to produce a cyclical wave followed by a rest period. The main reasons for this was that firstly the hydraulic system was not able to maintain the loading throughout the 48 hour test period due to caviation in the hydraulic return lines. Secondly, the system control unit (MTS 407) was unable to change its PID control settings to adequately handle the changing stiffness of the interface as degradation occurred.

2) The same concrete mixing procedures as in prior projects at Michigan Tech were used, but less consistency in the concrete mixes occurred based on the 28-day compressive strength testing. One possible explanation may be in the mixing and rodding operations.

3) A torque wrench was used to place a constant load on all of the threaded rod secured in the concrete, prior and during sample fracture. In addition, anchor nuts were repositioned to the ends of the embedded threaded rods to provide better anchorage.

These changes improved the performance of the sample fracture device, produced accurate data, and effectively produced cracks in all of the test blocks except but one.

4) With the improvements of the sample fracture device and more consistent fracture surface development, the concrete with stronger coarse aggregate had rougher surfaces, with more aggregate pullout, while the weaker coarse aggregate, had less rough surfaces, with more aggregate fracture.

5) The method of using a CNC mill with an LVDT displacement gauge, only proved to be partly successful. The main obstacle was in collection and analysis of the data. However, surfaces analyzed indicated, both visually and numerically, the difference in roughness, but not in an overly convincing way.

6) The aggregate interlock tests were only partly successful. Both system and hydraulic pump failures prevented the majority of the concrete samples from being tested. The samples that were tested indicated that at a 0.035 inch crack width, the weaker coarse aggregate concrete appeared more efficient than the stronger coarse aggregate concrete. However, it is believed that due to the higher stiffness of the stronger aggregate concrete coupled with problems with the control system, the loading system become unstable resulting in early failure of the stiffer aggregate concrete. The research suggests that future aggregate interlock testing should be conducted for crack width openings from 0.035 to 0.06 inches to study the effectiveness of different types of coarse aggregate.

7) The aggregate interlock tests at a crack width of 0.024 inches indicated that this is an effective crack width regardless of the aggregate type. However, it is possible that stronger coarse aggregate concrete under very high vehicle loading may experience more degradation due to the gouging of the cement paste by the coarse aggregate.

The following recommendations are presented for future research an aggregate interlock testing:

1) Due to a continuous, non-linear change in the stiffness of the interface of the concrete samples, a MTS Test-Star controller (or equivalent) should be used to generate the desired load wave and control ability. The advantage of the Test-Star controller (or an equivalent) is that it can continuously adjust the PID (Proportional gain, Integral gain, and Derivative gain) to compensate for the ever-changing interface stiffness during testing.

2) The effect of aggregate base and subgrade support for PCC pavements in aggregate interlock was not studied in this research. However, further research should be conducted to investigate the interaction of base and the aggregate interlock load transfer mechanism. This has been anticipated with the addition of the threaded rod to the fixed end holder. Within the range of the fixed end holder stiffness, an additional set of plate steel may be fabricated that will add stiffness at a given level. It is possible that the test system can be modified to produce a load transfer mechanism that represents the sub-base material load transfer capabilities.

3) Surface morphology of the concrete interface surfaces should be measured using stereographic imagery, which would allow a better characterization of the concrete surfaces to be investigated. This would be very important in investigating the change in surface morphology with variations in crack width. This information could be entered into a mathematical model to determine a relationship of surface texture to crack width.. This is important to show that on larger crack widths, there is less surface area to generate the required load transfer. It could also be used to develop guidelines for crack width in the field.

4) The MTS 30 gpm pump used for testing did not perform as expected. It was assumed that the system could keep up with most dynamic loads since it was designed for earthquake loading. Initially, the PID was adjusted every 10 minutes, or if the load dropped below 80% of the design load. This would turn into continuous adjustment and eventual destruction of the sample as the rate of loading continued to increase. Comparison of tests would be impossible as would

running a test for 48 hours. After testing and failing samples without the proper loads being maintained, it was determined that the PID control had to be manually changed for the test wave to keep up. This was a trial and error approach, since it was assured by MTS that the system could keep up, the test wave was adjusted until it was working well without excessive need for PID adjustment. The system could be adjusted in size as required per the following equation;

$$g = \frac{2 * d * A}{f} \qquad \textbf{5.1}$$

Where: g = gallon per minute pump required for test. (gpm)
d = total displacement of test in one direction (required) (in)
A = cross sectional area of actuator piston (19.6 in^2 for our 55 kip actuator.) (in^2)
f = length of full sine wave (sec)

For example, calculations show that the system needs a 102 gpm or larger pump in order to be capable of the one inch total displacement.

5) The concrete made and tested in this test was not subjected to any sort of environmental conditions. In-situ concrete has to undergo many conditions that can be replicated in the lab to more fully understand the effects that coarse aggregate type has on this load transfer durability.

6) During pull-apart, debris fell from most samples. The material, which was of concern, was the material larger than ¼ inch cube. Since the crack width was decided upon as 0.035 inches, a piece of debris this large could be significant. This is being suggested since the in-situ concrete does not open 4-6 inches when the crack forms like the pull-apart test does, thus keeping this debris contained within the crack surface.

7) As shown on the "Bruce Mines #3 Before Testing" Plot, there is a possibility for the aggregate in the concrete to assume a parallel nature that is most likely not

present in the field. It is believed that this may be due to the rodding conducted on the samples during preparations. A concrete vibrating screen should be used in place of rodding to better represent field conditions.

Appendix 7A

Levy Slag
(82-019)

BATCH COMPUTATIONS WORKSHEET

WEIGHT IN kg

Coarse Aggregate

68.07 Coarse Agg (a)

Pail tare	1.74	1.74	3.48 + pails
			71.55 = total
25.0 - 19.0mm	17.01	0.00	
19.0 - 12.5mm	0.00	17.02	
12.5 - 9.5mm	0.00	17.02	
9.5 - 4.75mm	17.02	0.00	
Sub total	35.77	35.78	71.55 Total

Fine Aggregate

62.62 Fine Agg (b)

Moisture content

wet	dry
345.94	334.84
0.0332	MC

0.0332 MC

2.08 Moisture

Dry weight 62.62

\+

Moisture 2.08

Total 64.69

Cement

26.12 Cement (C)

Pail ID A' , B'

Tare weight 0.85 — 1.70 tare

Tare weight 0.85 — 27.82 Pail + cement

Total tare 1.70

Air Entraining Admixture 22 ml

Batch Summary

(a)	Coarse Aggregate as Designed	68.07	kg
(b)	Fine Aggregate as Designed	62.62	kg
(c)	Cement as Designed	26.12	kg
(D)	Total Water of Batch	15.15	kg
(e)	**Total Weight of Batch**	171.96	kg

BATCH NO. LS

COARSE AGG CA-S (Slag)

DATE: 3/9/00

Batch Made Thurs. @ 3:00

WATER MEASUREMENT

Coarse Agg +pail	35.77		
Coarse Agg +pail	35.78		
Total	71.55		
+ Total Batch Water	14.11	(d)	14.11
- Reserve Water	3.00		3.00
= Pails, Agg&Water	82.66	H_2O	11.11

RESERVE WATER

Res water	3.00	1.33	surplus & Tare
+ Tare	0.29	0.29	- tare
= Total	3.29	1.04	= surplus

Reserve Water	3.00		
- Surplus Water	1.04		
=	1.96	H_2O +	11.11
Subtotal of water in batch		=	13.07
+ Moisture in Fine Aggregate		+	2.08
Total Water in Batch		**(D) =**	**15.15**

UNIT WEIGHT

Weight of Concrete & Bucket	39.44	
- Weight of Bucket	8.15	
= Weight of Concrete in Bucket	31.29	(f)

SLUMP = 2 " 50.8 mm

AIR CONTENT

- Factor of Aggregate Porosity

= Percent Air 4

CONCRETE TEMPERATURE, C 19

Note: a,b,C,d come from mix proportions worksheet

BATCH COMPUTATIONS WORKSHEET **WEIGHT IN kg**

Coarse Aggregate

68.07 Coarse Agg (a)

Pail tare	1.72	1.72	3.44 + pails
			71.51 = total
25.0 - 19.0mm	17.01	0.00	
19.0 - 12.5mm	0.00	17.02	
12.5 - 9.5mm	0.00	17.02	
9.5 - 4.75mm	17.02	0.00	
Sub total	35.75	35.76	71.51 Total

Fine Aggregate

62.62 Fine Agg (b)

Moisture content

wet	dry
236.36	227.48
0.0390	MC

0.0390 MC

2.44 Moisture

Dry weight 62.62

\+ Moisture 2.44

Total 65.06

Cement

26.12 Cement (C)

Pail ID A', B'

Tare weight 0.85

Tare weight 0.85

Total tare 1.70

1.70 tare

27.82 Pail + cement

Air Entraining Admixture 20 ml

Batch Summary

(a)	Coarse Aggregate as Designed	68.07 kg
(b)	Fine Aggregate as Designed	62.62 kg
(c)	Cement as Designed	26.12 kg
(D)	Total Water of Batch	16.38 kg
(e)	**Total Weight of Batch**	**173.19** kg

BATCH NO. LS

COARSE AGG CA-S (Slag)

DATE: 6/29/00

Batch Made Thurs. @ 3:00

WATER MEASUREMENT

Coarse Agg +pail	35.75		
Coarse Agg +pail	35.76		
Total	71.51		
+ Total Batch Water	14.11	(d)	14.11
- Reserve Water	3.00		3.00
= Pails, Agg&Water	**82.62**	H_2O	11.11

RESERVE WATER

Res water	3.00	1.70 surplus & Tare
+ Tare	0.29	0.29 - tare
= Total	3.29	1.41 = surplus

Reserve Water	3.00		
- Surplus Water	1.41		
=	2.82	H_2O +	11.11
Subtotal of water in batch		=	13.93
+ Moisture in Fine Aggregate		+	2.44
Total Water in Batch		**(D) =**	**16.38**

UNIT WEIGHT

Weight of Concrete & Bucket	38.80	
- Weight of Bucket	8.15	
= Weight of Concrete in Bucket	**30.65**	**(f)**

SLUMP = 2.5 " **63.5** mm

AIR CONTENT

- Factor of Aggregate Porosity

= Percent Air **5.5**

CONCRETE TEMPERATURE, C 22

Note: a,b,C,d come from mix proportions worksheet

BATCH COMPUTATIONS WORKSHEET — **WEIGHT IN kg**

Coarse Aggregate

68.07 Coarse Agg (a)

Pail tare	1.72	1.72	3.44 + pails
			71.51 = total
25.0 - 19.0mm	17.01	0.00	
19.0 - 12.5mm	0.00	17.02	
12.5 - 9.5mm	0.00	17.02	
9.5 - 4.75mm	17.02	0.00	
Sub total	35.75	35.76	71.51 Total

BATCH NO.	LS
COARSE AGG	CA-S (Slag)
DATE:	7/7/00
Batch Made	Tues. @ 3:00

Fine Aggregate

62.62 Fine Agg (b)

Moisture content

wet	dry
177.92	171.64
0.0366	MC

0.0366 MC

2.29 Moisture

Dry weight	62.62
+ Moisture	2.29
Total	**64.91**

WATER MEASUREMENT

Coarse Agg +pail	35.75		
Coarse Agg +pail	35.76		
Total	71.51		
+ Total Batch Water	14.11	(d)	14.11
- Reserve Water	3.00		3.00
= Pails, Agg&Water	**82.62**	H_2O	11.11

RESERVE WATER

Res water	3.00	1.55 surplus & Tare
+ Tare	0.29	0.29 - tare
= Total	3.29	1.26 = surplus

Reserve Water	3.00	
- Surplus Water	1.26	
=	2.97	H_2O + 11.11
Subtotal of water in batch		= 14.09
+ Moisture in Fine Aggregate		+ 2.29
Total Water in Batch		**(D) = 16.38**

Cement

26.12 Cement (C)

Pail ID	A', B'	
Tare weight	0.85	1.70 tare
Tare weight	0.85	27.82 Pail + cement
Total tare	1.70	

UNIT WEIGHT

Weight of Concrete & Bucket	38.04	
- Weight of Bucket	8.15	
= Weight of Concrete in Bucket	**29.89**	(f)

Air Entraining Admixture 20 ml

SLUMP = 4 " **101.6** mm

Batch Summary

(a)	Coarse Aggregate as Designed	68.07 kg
(b)	Fine Aggregate as Designed	62.62 kg
(c)	Cement as Designed	26.12 kg
(D)	Total Water of Batch	16.38 kg
(e)	**Total Weight of Batch**	**173.19** kg

AIR CONTENT

- Factor of Aggregate Porosity	
= Percent Air	**6.25**

CONCRETE TEMPERATURE, C 24

Note: a,b,C,d come from mix proportions worksheet

Levy #5 Displacement

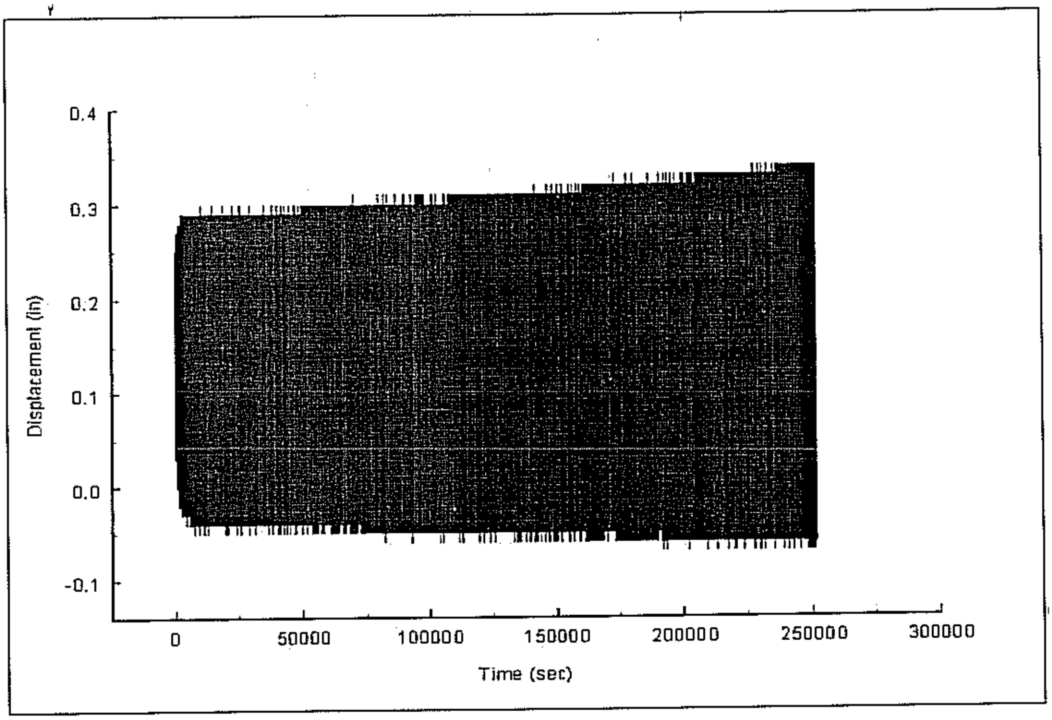

Levy #5 Load

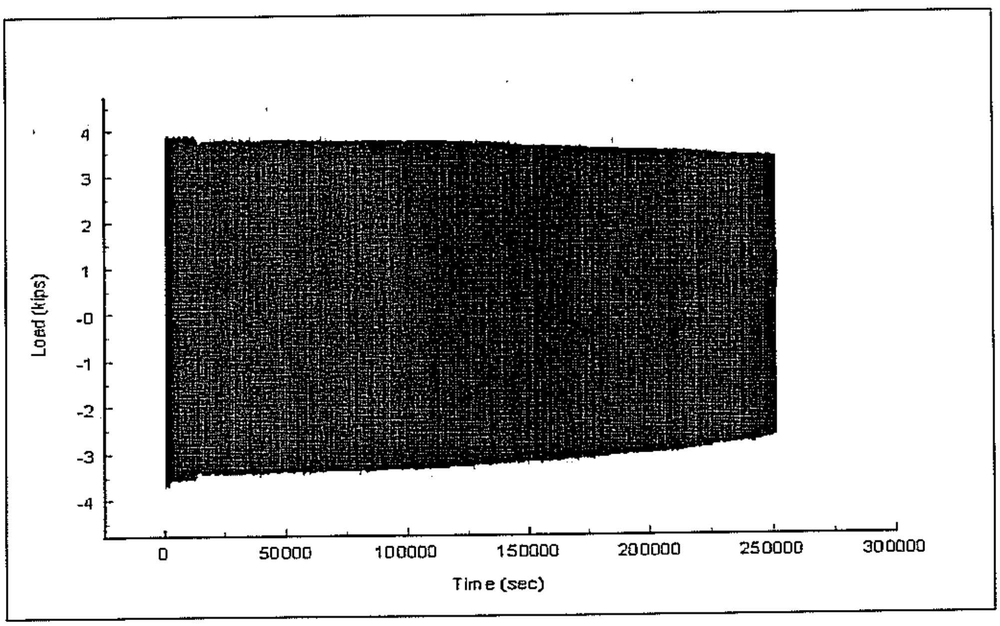

Appendix 7B

Bruce Mines
(95-010)

BATCH COMPUTATIONS WORKSHEET

WEIGHT IN kg

Coarse Aggregate

84.53 Coarse Agg (a)

Pail tare	1.75	1.75	3.50 + pails
			88.03 = total
25.0 - 19.0mm	21.13	0.00	
19.0 - 12.5mm	0.00	21.14	
12.5 - 9.5mm	0.00	21.13	
9.5 - 4.75mm	21.13	0.00	
Sub total	44.01	44.02	88.03 Total

Fine Aggregate

63.79 Fine Agg (b)

Moisture content

wet	dry
302.51	295.55
0.0235	MC

0.0235 **MC**

1.50 **Moisture**

Dry weight 63.79

\+

Moisture 1.50

Total 65.29

Cement

26.12 Cement (C)

Pail ID A' , B'

Tare weight 0.85

Tare weight 0.85

Total tare 1.70

1.70 tare

27.82 Pail + cement

Air Entraining Admixture 29 ml

Batch Summary

(a)	Coarse Aggregate as Designed	84.53 kg
(b)	Fine Aggregate as Designed	63.79 kg
(c)	Cement as Designed	26.12 kg
(D)	Total Water of Batch	13.05 kg
(e)	**Total Weight of Batch**	**187.48** kg

BATCH NO. **BM**

COARSE AGG **CA-B (Bruce M.)**

DATE: **3/8/00**

Batch Made **Wed @ 1:00**

WATER MEASUREMENT

Coarse Agg +pail	44.01		
Coarse Agg +pail	44.02		
Total	88.03		
+ Total Batch Water	12.32	(d)	12.32
- Reserve Water	3.00		3.00
= Pails, Agg&Water	**97.35**	H_2O	9.32

RESERVE WATER

Res water	3.00	1.06 surplus & Tare
+ Tare	0.29	0.29 - tare
= Total	3.29	0.77 = surplus

Reserve Water	3.00		
- Surplus Water	0.77		
=	2.23	H_2O +	9.32
Subtotal of water in batch		=	11.55
+ Moisture in Fine Aggregate		+	1.50
Total Water in Batch		**(D) =**	**13.05**

UNIT WEIGHT

Weight of Concrete & Bucket	41.80	
- Weight of Bucket	8.15	
= Weight of Concrete in Bucket	**33.65**	**(f)**

SLUMP = 1.75 " **44.5** mm

AIR CONTENT

- Factor of Aggregate Porosity

= Percent Air **4.5**

CONCRETE TEMPERATURE, C 20

Note: a,b,C,d come from mix proportions worksheet

BATCH COMPUTATIONS WORKSHEET

WEIGHT IN kg

Coarse Aggregate

84.53 Coarse Agg (a)

Pail tare	1.72	1.72	3.44 + pails
			87.97 = total
25.0 - 19.0mm	21.13	0.00	
19.0 - 12.5mm	0.00	21.14	
12.5 - 9.5mm	0.00	21.13	
9.5 - 4.75mm	21.13	0.00	
Sub total	43.98	43.99	87.97 Total

BATCH NO. BM

COARSE AGG CA-B (Bruce M.)

DATE: 6/20/00

Batch Made Tues @ 3:00

Fine Aggregate

63.79 Fine Agg (b)

Moisture content

wet	dry
464.01	451.3
0.0282	MC

0.0282 MC

1.80 Moisture

Dry weight 63.79
\+
Moisture 1.80
Total 65.58

WATER MEASUREMENT

Coarse Agg +pail 43.98
Coarse Agg +pail 43.99

Total 87.97
\+ Total Batch Water 12.32 **(d)** 12.32
\- Reserve Water 3.00 3.00
= Pails, Agg&Water 97.29 H_2O 9.32

Cement

26.12 Cement (C)

Pail ID A', B'

Tare weight 0.85 1.70 tare

Tare weight 0.85 27.82 Pail + cement

Total tare 1.70

RESERVE WATER

Res water	3.00	1.36 surplus & Tare
+ Tare	0.29	0.29 - tare
= Total	3.29	1.07 = surplus

Reserve Water 3.00
\- Surplus Water 1.07
= 1.93 H_2O + 9.32
Subtotal of water in batch = 11.25
\+ Moisture in Fine Aggregate + 1.80
Total Water in Batch (D) = 13.05

Air Entraining Admixture 29 ml

UNIT WEIGHT

Weight of Concrete & Bucket 41.31
\- Weight of Bucket 8.15
= Weight of Concrete in Bucket **33.16** **(f)**

Batch Summary

(a)	Coarse Aggregate as Designed	84.53 kg
(b)	Fine Aggregate as Designed	63.79 kg
(c)	Cement as Designed	26.12 kg
(D)	Total Water of Batch	13.05 kg
(e)	**Total Weight of Batch**	**187.48** kg

SLUMP = 3.25 " **82.6** mm

AIR CONTENT

\- Factor of Aggregate Porosity
= Percent Air **6.0**

CONCRETE TEMPERATURE, C 23

Note: a,b,C,d come from mix proportions worksheet

BATCH COMPUTATIONS WORKSHEET

WEIGHT IN kg

Coarse Aggregate

84.53 Coarse Agg (a)

Pail tare	1.72	1.72	3.44 + pails
			87.97 = total
25.0 - 19.0mm	21.13	0.00	
19.0 - 12.5mm	0.00	21.14	
12.5 - 9.5mm	0.00	21.13	
9.5 - 4.75mm	21.13	0.00	
Sub total	43.98	43.99	87.97 Total

Fine Aggregate

63.79 Fine Agg (b)

Moisture content

wet	dry
448.11	436.69
0.0262	MC

0.0262 MC

1.67 Moisture

Dry weight 63.79

\+

Moisture 1.67

Total 65.45

Cement

26.12 Cement (C)

Pail ID A' , B'

Tare weight 0.85

Tare weight 0.85

Total tare 1.70

1.70 tare

27.82 Pail + cement

Air Entraining Admixture 24 ml

Batch Summary

(a)	Coarse Aggregate as Designed	84.53 kg
(b)	Fine Aggregate as Designed	63.79 kg
(c)	Cement as Designed	26.12 kg
(D)	Total Water of Batch	13.05 kg
(e)	**Total Weight of Batch**	187.48 kg

BATCH NO. BM

COARSE AGG CA-B (Bruce M.)

DATE: 6/21/00

Batch Made Wed @ 3:00

WATER MEASUREMENT

Coarse Agg +pail	43.98		
Coarse Agg +pail	43.99		
Total	87.97		
+ Total Batch Water	12.32	(d)	12.32
- Reserve Water	3.00		3.00
= Pails, Agg&Water	97.29	H_2O	9.32

RESERVE WATER

Res water	3.00	1.23	surplus & Tare
+ Tare	0.29	0.29	- tare
= Total	3.29	0.94	= surplus

Reserve Water	3.00		
- Surplus Water	0.94		
=	2.06	H_2O +	9.32
Subtotal of water in batch		=	11.38
+ Moisture in Fine Aggregate		+	1.67
Total Water in Batch		(D) =	13.05

UNIT WEIGHT

Weight of Concrete & Bucket	40.19	
- Weight of Bucket	8.15	
= Weight of Concrete in Bucket	32.04	(f)

SLUMP = 3 " 76.2 mm

AIR CONTENT

- Factor of Aggregate Porosity
= Percent Air 6.5

CONCRETE TEMPERATURE, C 23

Note: a,b,C,d come from mix proportions worksheet

Bruce Mines #3 Displacement

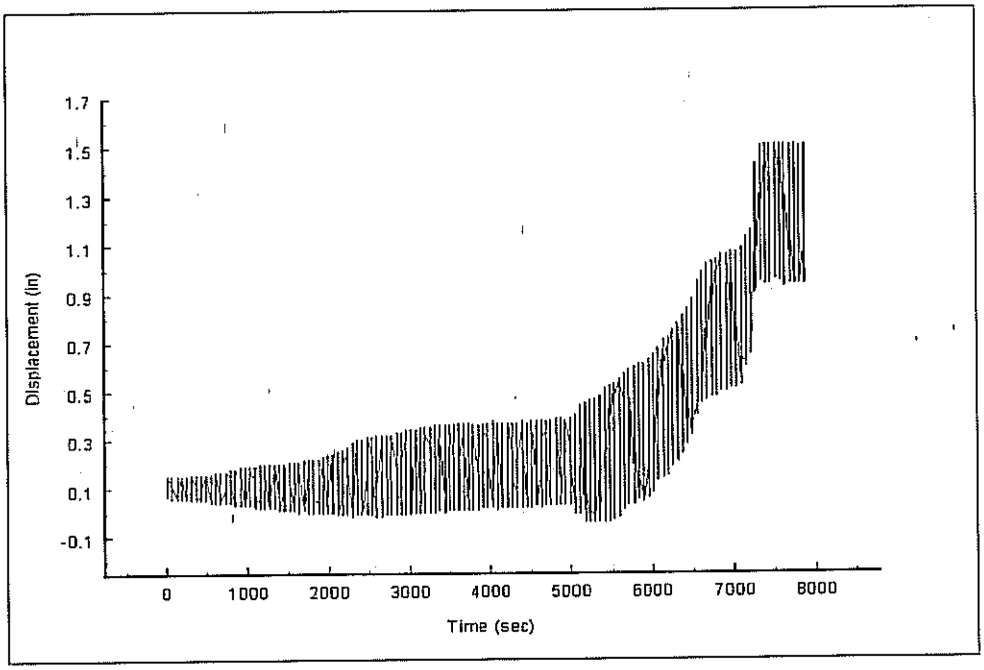

Bruce Mines #3 Load

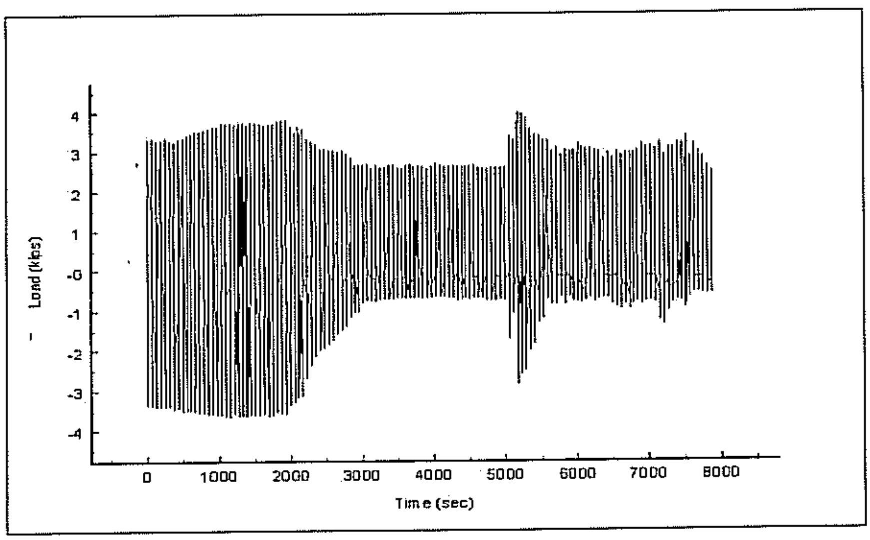

Bruce Mines #4 Displacement

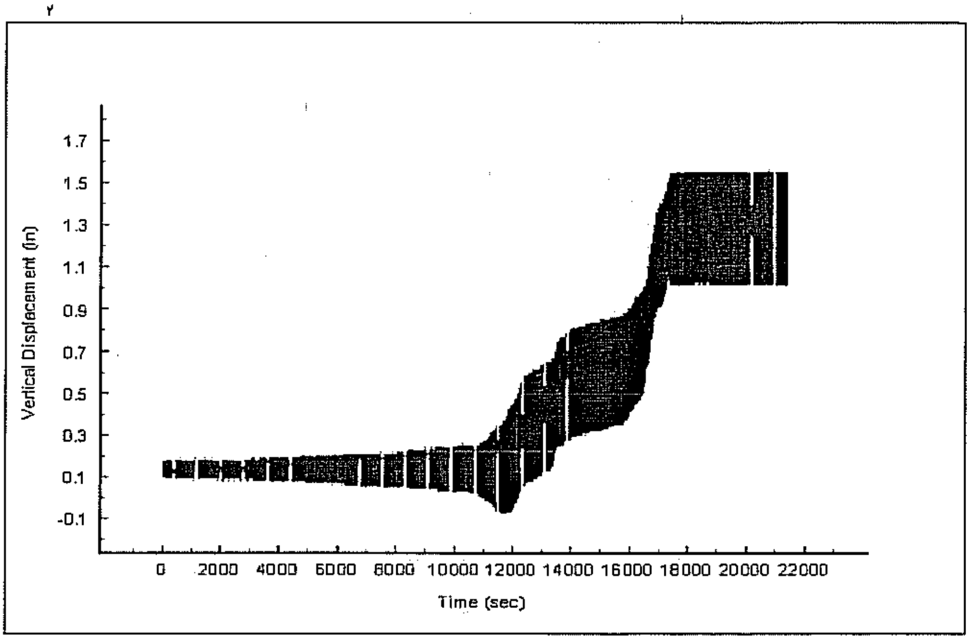

Bruce Mines #4 Load

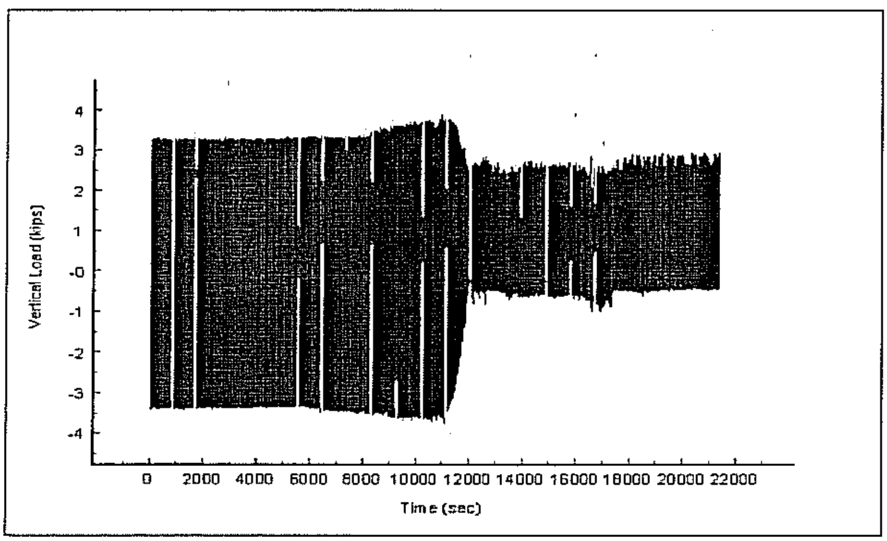

Appendix 7C

Port Inland
(75-005)

BATCH COMPUTATIONS WORKSHEET

WEIGHT IN kg

Coarse Aggregate

83.67 Coarse Agg (a)

Pail tare	1.75	1.75	3.50 + pails
			87.17 = total
25.0 - 19.0mm	20.92	0.00	
19.0 - 12.5mm	0.00	20.91	
12.5 - 9.5mm	0.00	20.92	
9.5 - 4.75mm	20.92	0.00	
Sub total	43.59	43.58	87.17 Total

Fine Aggregate

59.26 Fine Agg (b)

Moisture content

wet	dry
357.26	345.07
0.0353	MC

0.0353 MC

2.09 Moisture

Dry weight 59.26

\+

Moisture 2.09

Total **61.36**

9.16

Cement

26.12 Cement (C)

Pail ID A', B'

Tare weight 0.85

1.70 tare

Tare weight 0.85

27.82 Pail + cement

Total tare 1.70

Air Entraining Admixture

25 ml

Batch Summary

(a)	Coarse Aggregate as Designed	83.67 kg
(b)	Fine Aggregate as Designed	59.26 kg
(c)	Cement as Designed	26.12 kg
(D)	Total Water of Batch	13.16 kg
(e)	**Total Weight of Batch**	**182.22** kg

BATCH NO. Po.In.

COARSE AGG CA-P (Port In.)

DATE: 3/10/00

Batch Made Fri. @ 3:00

WATER MEASUREMENT

Coarse Agg +pail	43.59		
Coarse Agg +pail	43.58		
Total	87.17		
+ Total Batch Water	12.16	(d)	12.16
- Reserve Water	3.00		3.00
= Pails, Agg&Water	**96.33**	H_2O	9.16

RESERVE WATER

Res water	3.00	1.39	surplus & Tare
+ Tare	0.29	0.29	- tare
= Total	3.29	1.10	= surplus

Reserve Water	3.00		
- Surplus Water	1.10		
=	1.90	H_2O +	9.16
Subtotal of water in batch		=	11.07
+ Moisture in Fine Aggregate		+	2.09
Total Water in Batch		**(D) =**	**13.16**

UNIT WEIGHT

Weight of Concrete & Bucket	39.82	
- Weight of Bucket	8.15	
= Weight of Concrete in Bucket	**31.67**	**(f)**

SLUMP = 3.25 " 82.6 mm

AIR CONTENT

- Factor of Aggregate Porosity

= Percent Air **5.25**

CONCRETE TEMPERATURE, C 19

Note: a,b,C,d come from mix proportions worksheet

BATCH COMPUTATIONS WORKSHEET

WEIGHT IN kg

Coarse Aggregate

83.67 Coarse Agg (a)

Pail tare	1.72	1.72	3.44 + pails
			87.11 = total
25.0 - 19.0mm	20.92	0.00	
19.0 - 12.5mm	0.00	20.91	
12.5 - 9.5mm	0.00	20.92	
9.5 - 4.75mm	20.92	0.00	
Sub total	43.56	43.55	87.11 Total

Fine Aggregate

59.26 Fine Agg (b)

Moisture content

wet	dry
457.29	446.61
0.0239	MC

0.0239 MC

1.42 Moisture

Dry weight 59.26

\+

Moisture 1.42

Total 60.68

9.16

Cement

26.12 Cement (C)

Pail ID	A' , B'	
Tare weight	0.85	1.70 tare
Tare weight	0.85	27.82 Pail + cement
Total tare	1.70	

Air Entraining Admixture 21 ml

Batch Summary

(a) Coarse Aggregate as Designed	83.67	kg
(b) Fine Aggregate as Designed	59.26	kg
(c) Cement as Designed	26.12	kg
(D) Total Water of Batch	13.16	kg
(e) Total Weight of Batch	182.22	kg

BATCH NO.	Po.In.
COARSE AGG	CA-P (Port In.)
DATE:	6/23/00
Batch Made	Fri. @ 3:00

WATER MEASUREMENT

Coarse Agg +pail	43.56		
Coarse Agg +pail	43.55		
Total	87.11		
+ Total Batch Water	12.16	(d)	12.16
- Reserve Water	3.00		3.00
= Pails, Agg&Water	96.27	H_20	9.16

RESERVE WATER

Res water	3.00	0.71 surplus & Tare
+ Tare	0.29	0.29 - tare
= Total	3.29	0.42 = surplus

Reserve Water	3.00		
- Surplus Water	0.42		
=	2.58	H_2O +	9.16
Subtotal of water in batch		=	11.74
+ Moisture in Fine Aggregate		+	1.42
Total Water in Batch		(D) =	13.16

UNIT WEIGHT

Weight of Concrete & Bucket	38.93	
- Weight of Bucket	8.15	
= Weight of Concrete in Bucket	30.78	(f)

SLUMP = 3.5 " 88.9 mm

AIR CONTENT

- Factor of Aggregate Porosity	
= Percent Air	6.25

CONCRETE TEMPERATURE, C 24

Note: a,b,C,d come from mix proportions worksheet

BATCH COMPUTATIONS WORKSHEET

WEIGHT IN kg

Coarse Aggregate

83.67 Coarse Agg (a)

Pail tare	1.72	1.72	3.44 + pails
			87.11 = total
25.0 - 19.0mm	20.92	0.00	
19.0 - 12.5mm	0.00	20.91	
12.5 - 9.5mm	0.00	20.92	
9.5 - 4.75mm	20.92	0.00	
Sub total	43.56	43.55	87.11 Total

Fine Aggregate

59.26 Fine Agg (b)

Moisture content

wet	dry
163.62	157.81
0.0368	MC

0.0368 MC

2.18 Moisture

Dry weight 59.26

\+

Moisture 2.18

Total 61.45

9.16

Cement

26.12 Cement (C)

Pail ID A' , B'

Tare weight 0.85

1.70 tare

Tare weight 0.85

27.82 Pail + cement

Total tare 1.70

Air Entraining Admixture

19.75 ml

Batch Summary

(a)	Coarse Aggregate as Designed	83.67	kg
(b)	Fine Aggregate as Designed	59.26	kg
(c)	Cement as Designed	26.12	kg
(D)	Total Water of Batch	13.16	kg
(e)	**Total Weight of Batch**	**182.22**	kg

BATCH NO. Po.In.

COARSE AGG CA-P (Port In.)

DATE: 6/27/00

Batch Made Tues. @ 3:00

WATER MEASUREMENT

Coarse Agg +pail	43.56		
Coarse Agg +pail	43.55		
Total	87.11		
+ Total Batch Water	12.16	(d)	12.16
- Reserve Water	3.00		3.00
= Pails, Agg&Water	**96.27**	H_20	9.16

RESERVE WATER

Res water	3.00	1.48 surplus & Tare
+ Tare	0.29	0.29 - tare
= Total	3.29	1.19 = surplus

Reserve Water	3.00		
- Surplus Water	1.19		
=	1.81	H_2O +	9.16
Subtotal of water in batch		=	10.98
+ Moisture in Fine Aggregate		+	2.18
Total Water in Batch		**(D) =**	**13.16**

UNIT WEIGHT

Weight of Concrete & Bucket	39.75	
- Weight of Bucket	8.15	
= Weight of Concrete in Bucket	**31.60**	**(f)**

SLUMP = 2.75 " **69.9** mm

AIR CONTENT

- Factor of Aggregate Porosity	
= Percent Air	**5.5**

CONCRETE TEMPERATURE, C 22

Note: a,b,C,d come from mix proportions worksheet

Appendix D

Presque Isle
(71-047)

BATCH COMPUTATIONS WORKSHEET

WEIGHT IN kg

Coarse Aggregate

77.35 Coarse Agg (a)

Pail tare	1.75	1.75	3.50	+ pails
			80.85	= total
25.0 - 19.0mm	19.34	0.00		
19.0 - 12.5mm	0.00	19.33		
12.5 - 9.5mm	0.00	19.34		
9.5 - 4.75mm	19.34	0.00		
Sub total	40.43	40.42	80.85	Total

Fine Aggregate

61.52 Fine Agg (b)

Moisture content

wet	dry
350.81	339.42
0.0336	MC

0.0336 MC

2.06 Moisture

Dry weight 61.52

\+

Moisture 2.06

Total 63.59

Cement

26.12 Cement (C)

Pail ID A' , B'

Tare weight 0.85

Tare weight 0.85

Total tare 1.70

1.70 tare

27.82 Pail + cement

Air Entraining Admixture

21 ml

Batch Summary

(a)	Coarse Aggregate as Designed	77.35 kg
(b)	Fine Aggregate as Designed	61.52 kg
(c)	Cement as Designed	26.12 kg
(D)	Total Water of Batch	13.76 kg
(e)	**Total Weight of Batch**	**178.76** kg

BATCH NO.	Pr.Is.
COARSE AGG	CA-I (Pres. Isle)
DATE:	3/15/00
Batch Made	Wed. @ 12:30

WATER MEASUREMENT

Coarse Agg +pail	40.43		
Coarse Agg +pail	40.42		
Total	80.85		
+ Total Batch Water	12.87	(d)	12.87
- Reserve Water	3.00		3.00
= Pails, Agg&Water	**90.72**	H_2O	9.87

RESERVE WATER

Res water	3.00	1.46	surplus & Tare
+ Tare	0.29	0.29	- tare
= Total	3.29	1.17	= surplus

Reserve Water	3.00		
- Surplus Water	1.17		
=	1.83	H_2O +	9.87
Subtotal of water in batch		=	11.70
+ Moisture in Fine Aggregate		+	2.06
Total Water in Batch		**(D) =**	**13.76**

UNIT WEIGHT

Weight of Concrete & Bucket	39.84	
- Weight of Bucket	8.15	
= Weight of Concrete in Bucket	**31.69**	**(f)**

SLUMP = 3.25 " **82.6** mm

AIR CONTENT

- Factor of Aggregate Porosity
= Percent Air **5**

CONCRETE TEMPERATURE, C 18

Note: a,b,C,d come from mix proportions worksheet

BATCH COMPUTATIONS WORKSHEET **WEIGHT IN kg**

Coarse Aggregate 77.35 Coarse Agg (a)

Pail tare	1.71	1.71	3.42	+ pails
			80.77	= total
25.0 - 19.0mm	19.34	0.00		
19.0 - 12.5mm	0.00	19.33		
12.5 - 9.5mm	0.00	19.34		
9.5 - 4.75mm	19.34	0.00		
Sub total	40.39	40.38	80.77	Total

Fine Aggregate 61.52 Fine Agg (b)

Moisture content

wet	dry
322.7	316.01
0.0212	MC

0.0212 MC

1.30 Moisture

Dry weight 61.52

\+

Moisture 1.30

Total 62.83

Cement 26.12 Cement (C)

Pail ID A', B'

Tare weight 0.85

Tare weight 0.85

Total tare 1.70

1.70 tare

27.82 Pail + cement

Air Entraining Admixture 21 ml

Batch Summary

(a)	Coarse Aggregate as Designed	77.35	kg
(b)	Fine Aggregate as Designed	61.52	kg
(c)	Cement as Designed	26.12	kg
(D)	Total Water of Batch	13.76	kg
(e)	**Total Weight of Batch**	**178.76**	kg

BATCH NO.	Pr.Is.
COARSE AGG	CA-I (Pres. Isle)
DATE:	6/14/00
Batch Made	Wed. @ 3:00

WATER MEASUREMENT

Coarse Agg +pail	40.39		
Coarse Agg +pail	40.38		
Total	80.77		
+ Total Batch Water	12.87	(d)	12.87
- Reserve Water	3.00		3.00
= Pails, Agg&Water	**90.64**	H_2O	9.87

RESERVE WATER

Res water	3.00	0.70	surplus & Tare
+ Tare	0.29	0.29	- tare
= Total	3.29	0.41	= surplus

Reserve Water	3.00		
- Surplus Water	0.41		
=	2.59	H_2O +	9.87
Subtotal of water in batch		=	12.46
+ Moisture in Fine Aggregate		+	1.30
Total Water in Batch		**(D) =**	**13.76**

UNIT WEIGHT

Weight of Concrete & Bucket	40.18	
- Weight of Bucket	8.15	
= Weight of Concrete in Bucket	**32.03**	**(f)**

SLUMP = 2.25 " **57.2** mm

AIR CONTENT

- Factor of Aggregate Porosity
= Percent Air **4.5**

CONCRETE TEMPERATURE, C 22

Note: a,b,C,d come from mix proportions worksheet

BATCH COMPUTATIONS WORKSHEET

WEIGHT IN kg

BATCH NO.	Pr.Is.
COARSE AGG	CA-I (Pres. Isle)
DATE:	6/15/00
Batch Made	Thurs. @ 3:00

Coarse Aggregate

77.35 Coarse Agg (a)

Pail tare	1.71	1.71	3.42 + pails
			80.77 = total
25.0 - 19.0mm	19.34	0.00	
19.0 - 12.5mm	0.00	19.33	
12.5 - 9.5mm	0.00	19.34	
9.5 - 4.75mm	19.34	0.00	
Sub total	40.39	40.38	80.77 Total

Fine Aggregate

61.52 Fine Agg (b)

Moisture content

wet	dry
352.78	345.91
0.0199	MC

0.0199 MC

1.22 Moisture

Dry weight 61.52

\+

Moisture 1.22

Total 62.75

Cement

26.12 Cement (C)

Pail ID A' , B'

Tare weight 0.85

1.70 tare

Tare weight 0.85

27.82 Pail + cement

Total tare 1.70

Air Entraining Admixture

21 ml

Batch Summary

(a)	Coarse Aggregate as Designed	77.35 kg
(b)	Fine Aggregate as Designed	61.52 kg
(c)	Cement as Designed	26.12 kg
(D)	Total Water of Batch	13.76 kg
(e)	**Total Weight of Batch**	**178.76** kg

WATER MEASUREMENT

Coarse Agg +pail	40.39		
Coarse Agg +pail	40.38		
Total	80.77		
+ Total Batch Water	12.87	(d)	12.87
- Reserve Water	3.00		3.00
= Pails, Agg&Water	90.64	H_20	9.87

RESERVE WATER

Res water	3.00	0.62 surplus & Tare
+ Tare	0.29	0.29 - tare
= Total	3.29	0.33 = surplus

Reserve Water	3.00		
- Surplus Water	0.33		
=	2.67	H_2O +	9.87
Subtotal of water in batch		=	12.54
+ Moisture in Fine Aggregate		+	1.22
Total Water in Batch		**(D) =**	**13.76**

UNIT WEIGHT

Weight of Concrete & Bucket	40.37	
- Weight of Bucket	8.15	
= Weight of Concrete in Bucket	32.22	(f)

SLUMP = 1 " 25.4 mm

AIR CONTENT

- Factor of Aggregate Porosity
= Percent Air 4.75

CONCRETE TEMPERATURE, C 22

Note: a,b,C,d come from mix proportions worksheet

Presque Isle #2 Displacement

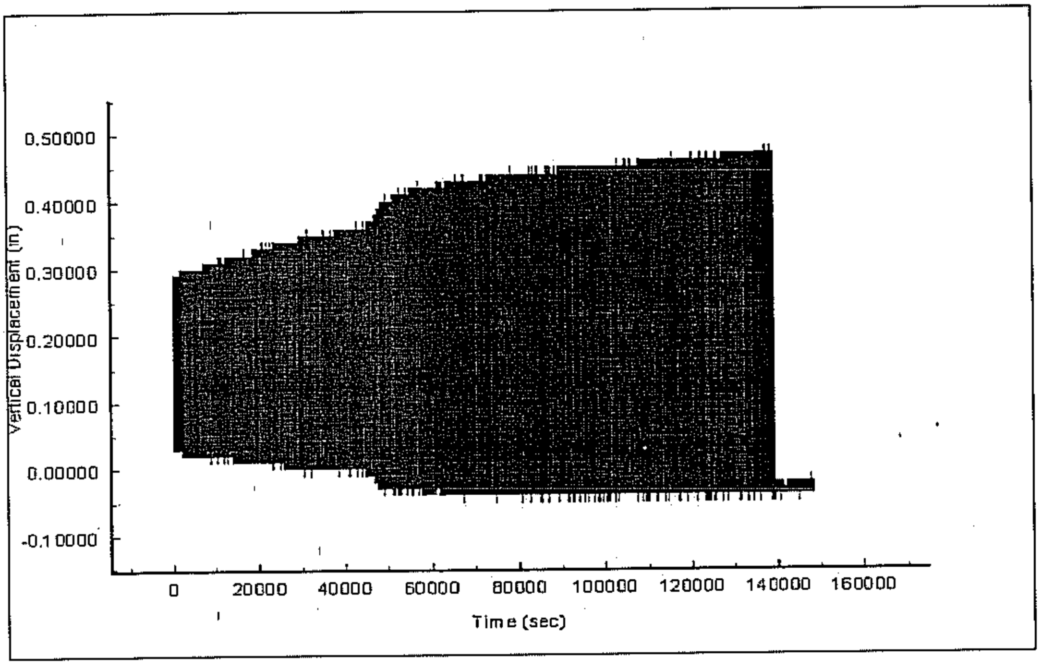

Presque Isle #2 load

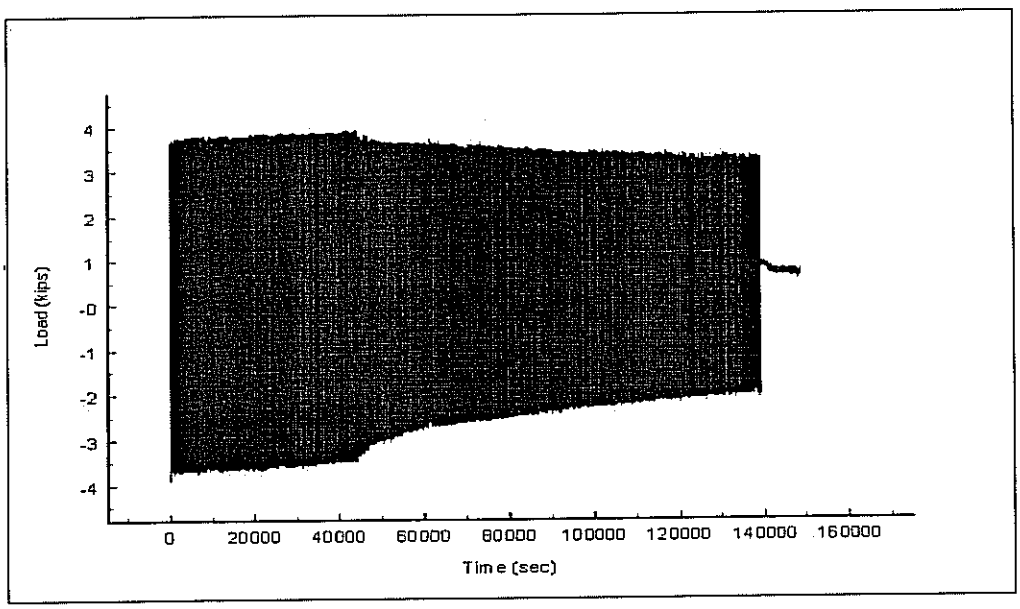

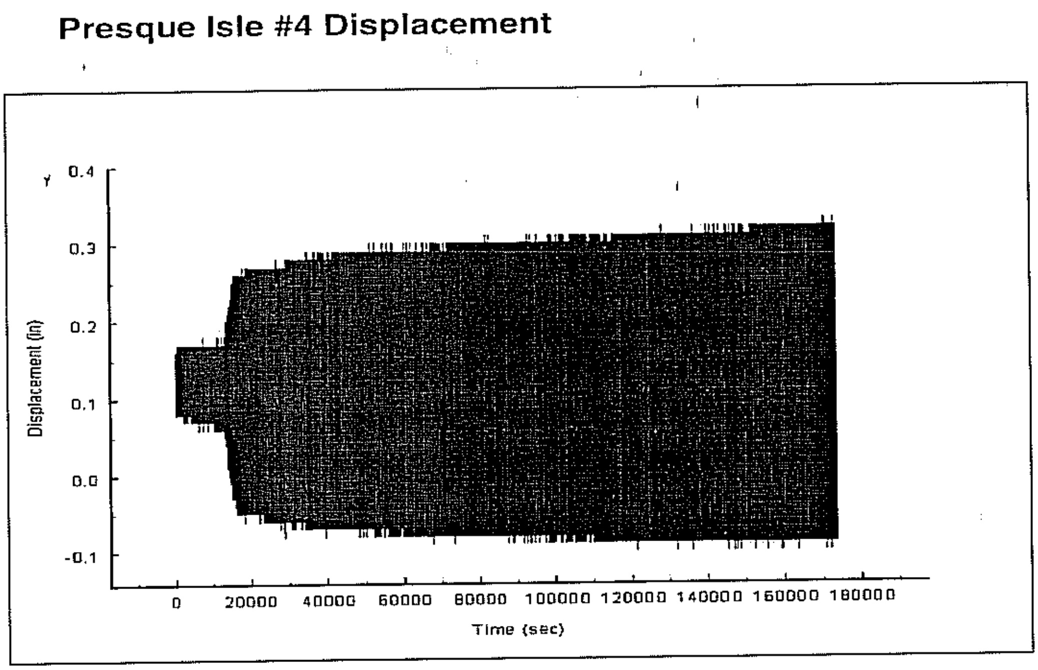
Presque Isle #4 Displacement
0.4
0.3
0.2
0.1
0.0
-0.1
Displacement (in)
0
20000
40000
60000
80000
100000
120000
140000
160000
180000
Time (sec)

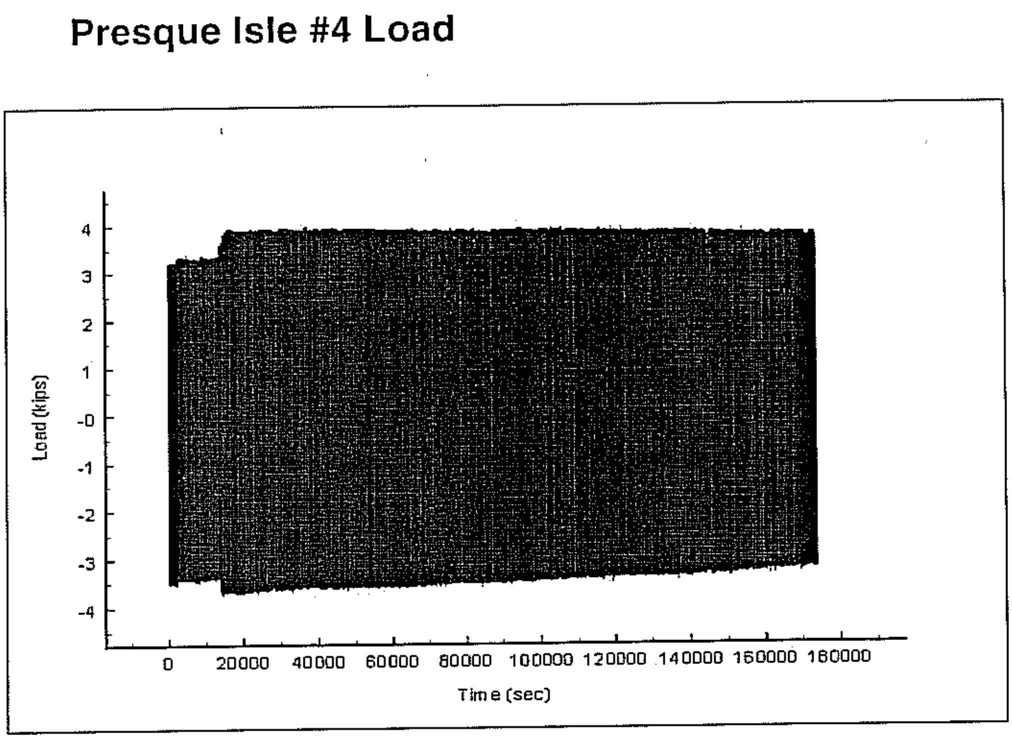
Presque Isle #4 Load
4
3
2
1
-0
-1
-2
-3
-4
Load (kips)
0
20000
40000
60000
80000
100000
120000
140000
160000
180000
Time (sec)

Appendix E

Batch properties and six inch static compressive cylinders

Complete sample crack test debris data

Comparison of static compressive strength of 3 X 6 inch cored cylinders

Test setup, truck configuration

Aggregate type/sample ID #	Slump (inch)	Air (%)	Temp (C)	Strength (psi)
Levy 1/2	0.75	4.25	23	7197.34
Levy 3/4	4	6.25	24	5812.11
Levy 5/6	2.5	5.5	21	4703.92
Presque Isle 1/2	2.25	4.5	22	
Presque Isle 3/4	1	4.75	22	6837.77
Port Inland 1/2	3.5	6.25	24	4049.61
Port Inland 3/4	2.75	5.5	22	4939.7
Bruce Mines 1/2	3.25	6	23	5470.22
Bruce Mines 3/4	3	6.5	23	4456.34

Date Cast	Date tested	Sample I.D.	Break Type	Load at failure (average)	Stress at failure	Comments
6/15/00	7/18/00	Pres 3/4	Double cone	193333.3333	6837.773701	Heavy aggregate fracture
6/20/00	7/18/00	BM 1/2	Single cone/Planer	154666.6667	5470.218961	No aggregate fracture
6/21/00	7/21/00	BM 3/4	Crush	126000	4456.342171	
6/23/00	7/21/00	Port 1/2	Crush	114500	4049.612528	
6/27/00	7/28/00	Port 2/3	Plane/Crush	139666.6667	4939.702036	
6/28/00	7/28/00	Levy 1/2	Double cone	203500	7197.346284	Low Slump, heavy aggregate fracture
6/29/00	7/28/00	Levy 3/4	Cone/Planer	164333.3333	5812.107646	Partical pull-out
7/5/00	8/7/00	Levy 5/6	Crush	133000	4703.916736	

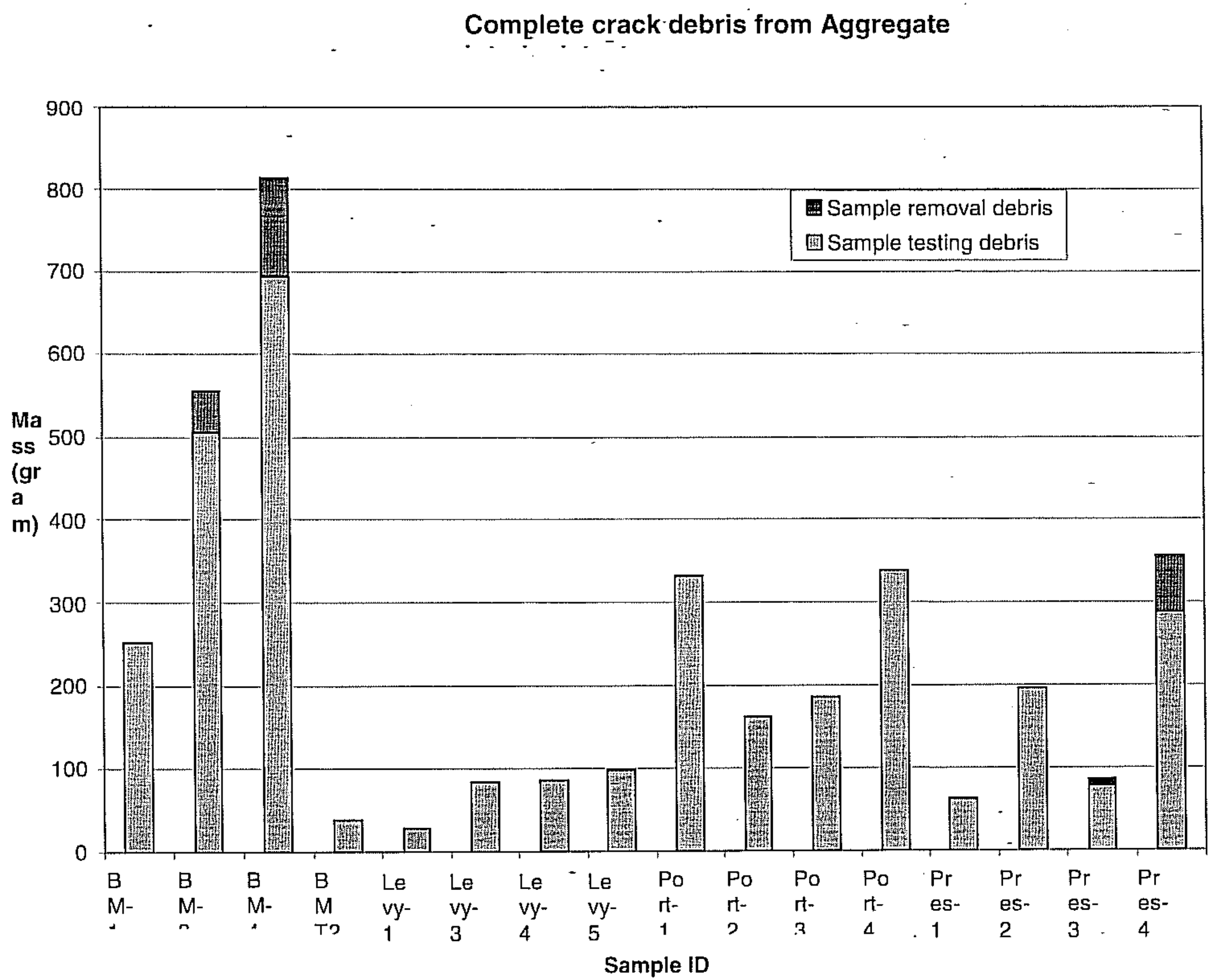
Complete crack debris from Aggregate
Sample removal debris
Sample testing debris
Mass (gram)
900
800
700
600
500
400
300
200
100
0
BM-1
BM-2
BM-4
BMT2
Levy-1
Levy-3
Levy-4
Levy-5
Port-1
Port-2
Port-3
Port-4
Pres-1
Pres-2
Pres-3
Pres-4
Sample ID

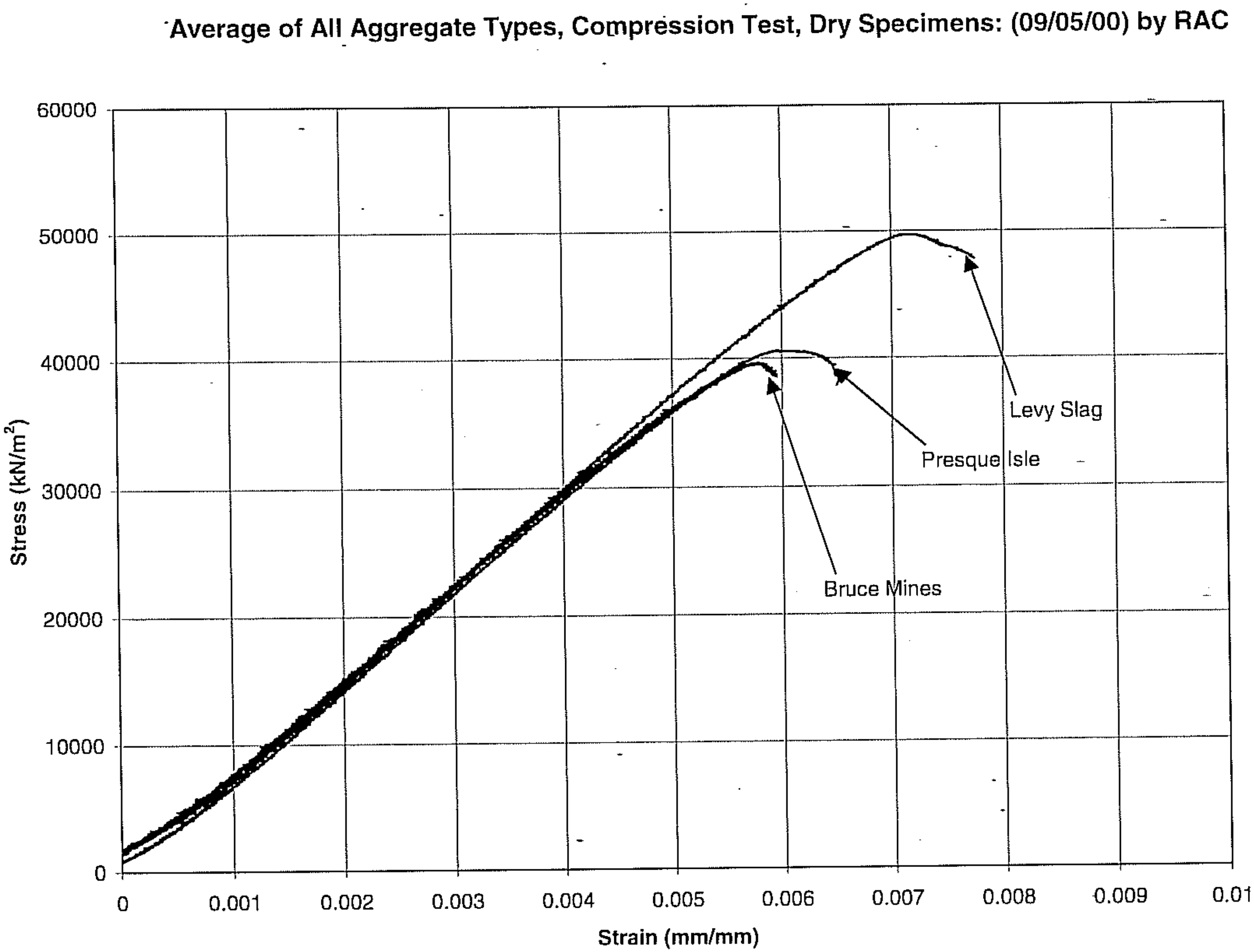
Average of All Aggregate Types, Compression Test, Dry Specimens: (09/05/00) by RAC
60000
50000
40000
30000
20000
10000
0
Stress (kN/m²)
0
0.001
0.002
0.003
0.004
0.005
0.006
0.007
0.008
0.009
0.01
Strain (mm/mm)
Levy Slag
Presque Isle
Bruce Mines

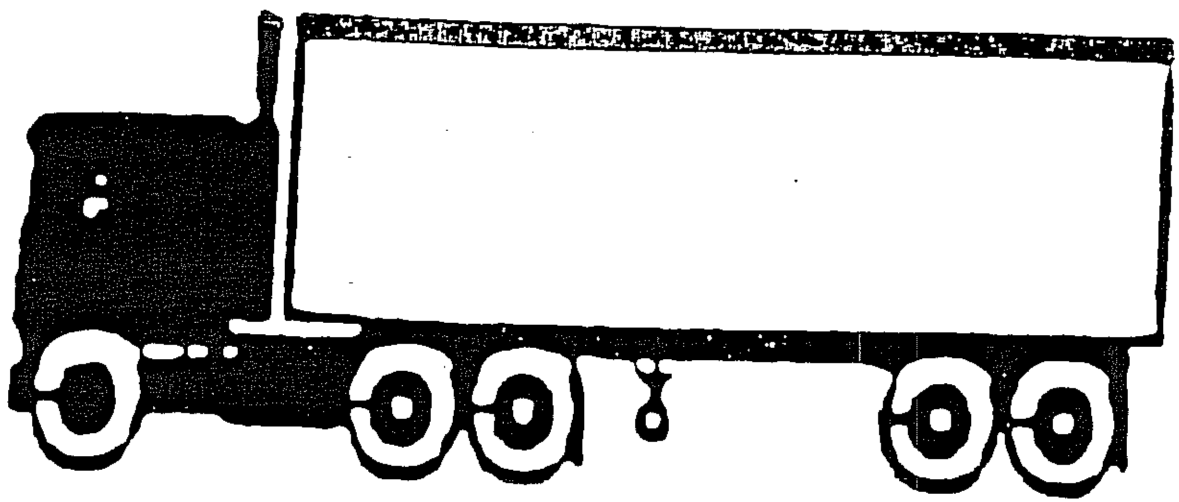

Test setup, truck configuration

References

Abdel-maksoud, M., G, "Relationship Between Joint Performance and Geometrical and Mechanical Properties of Concrete Joints Subject to Cyclic Shear, Doctoral Dissertation, University of Illinois, Department of Civil Engineering, April 2000.

Abdel-maksoud, M., G., Hawkins, N., Barenberg E., "Behavior of Concrete Joints under Cyclic Shear", ASCE Conference on Aircraft Pavement Technology, Seattle, Washington, 1997.

Abdel-maksoud, M., G., Hawkins, N., Barenberg E., "Effect of Geometric and Mechanical Properties of Concrete Joints on their Cyclic Shear Response", Federal Aviation Administration, Technology Transfer Conference, September 1998.

Bruinsma, J.E., Raja, Z.I., and Snyder, M.B., "Factors Affecting the Deterioration of Transverse Cracks in JRCP", Michigan Department of Transportation, Lansing Michigan, 1995.

Colley, B. E., and Humphrey, H. A., "Aggregate Interlock at Joints in Concrete Pavements", Highway Research Record, No. 189, Highway Research Board, Washington, D.C., 1967.

Federal Highway Administration, "Concrete Pavement Joints," Technical Advisory T 5040.30 Federal Highway Administration, Washington, D.C., November 1990.

Holtz, R. and Kovacs, "*An Introduction to Geotechnical Engineering*," Prentice-Hall, 1980.

Jimenez, R. White, R.N. and P. Gergley, "Cyclic Shear and Dowel Action Models in R/C. American Society of Civil Engineers, Structural Division, Vol. 108, No. ST5, pp. 1106-1123.

Martin-Perez, B and S.J. Pantazopoulou, "Effect of Bond, Aggregate Interlock and Dowel Action on the Shear Strength Degradation of Reinforced Concrete, "Engineering Structures, Vol. 23, pp. 214-227, January, 2001.

Laible, J.P, White, R.N. and P. Gergely, "Experimental Investigation of Seismic Shear Transfer Across Cracks in Concrete Nuclear Containment Vessels," American Concrete Institute, Special Publication pp. 203-226.

Mattock, A., H., "Cyclic Shear Transfer and Type of Interface", Journal of Structural Engineering, ASCE, vol. 107, NO. ST10, October 1981.

Nowlen, W.J., "Influence of Aggregate Properties on Effectiveness of Interlock Joints in Concrete Pavements, "Development Department Bulletin D139, Journal of the PCA Research and Development Laboratories, Portland Cement Association, Skokie, Illinois, May, 1968.

Reinhardt, H.W. and J.C. Walraven, "Cracks in Concrete Subject to Shear", ASCE, Journal of Structural Engineering, Vol. 108, No. ST1, pp. 492-442, 1982.

Sutherland, E., C., "Joint Spacing in Concrete Pavements", Highway Research Board, Research Report 17-B, Washington D.C., 1956.

Tassios, T., P., Vintzeleou, E., N., "Concrete-to-Concrete Friction", Journal of Structural Engineering, ASCE, vol. 113, April 1987.

Walraven, J., C., "Aggregate Interlock: A Theoretical and Experimental Analysis", Dissertation, Delft University of Technology, The Netherlands, October 1980.

Wattar, S., W., Hawkins, N., Barenberg, E., "Aggregate Interlock Behavior of Large Crack Width Concrete Joints", Federal Aviation Administration, Technology Transfer Conference, September 1998.